Cellular redox responses under standard oxygen cell culture conditions compared with physioxia

By

Jack Jordan

Of

The University of Exeter Medical School

Submitted by Jack Jordan, to the University of Exeter as a thesis for the degree of *Doctor of Philosophy* in Medical Studies, May 2022.

I certify that all material in this thesis which is not my own work has been identified and that any material that has previously been submitted and approved for the award of a degree by this or any other University has been acknowledged.

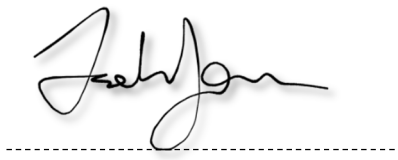

ABSTRACT

The physiological oxygen environment *in vivo* (physioxia) typically ranges from 1.0-12.5% O_2. However, *in vitro* mammalian cell culture largely utilises an O_2 concentration ([O_2]) of 18.6% O_2 (which accounts for the partial pressure of water in the incubator) during the growth stage. As such, most mammalian cells are grown in a non-physiological [O_2] during *in vitro* cell culture. The effect of growing mammalian cells long term in 18.6% O_2 on the subsequent cellular response to redox-active compounds compared to cells grown in physioxia is not well understood. It was shown that human non-melanoma squamous cell carcinoma cells (A431) cultured long term under 18.6% O_2 were resistant to auranofin (thioredoxin reductase inhibitor), and H_2O_2-induced cell death compared to A431 cells grown in 3.0% O_2 (physioxia in human skin). A431 cells grown in 18.6% O_2 were also resistant to H_2O_2, mercaptosuccinic acid, and cumene hydroperoxide-induced lipid peroxidation compared to A431 cells grown in 3.0% O_2. Auranofin-induced ROS generation and oxidative stress was lower in A431 cells grown in 18.6% O_2 compared to A431 cells grown in 3.0% O_2 for 96 h under the same treatment conditions. Catalase and glutathione reductase enzyme activities were higher in A431 cells grown in 18.6% O_2 compared to A431 cells grown in 3.0% O_2 for 96 h. Additionally, the expression levels of nuclear Nrf-2 protein, and NAD(P)H quinone oxidoreductase (NQO-1) protein, were about two-fold higher in A431 cells grown in 18.6% O_2 compared to the levels in A431 cells grown in 3.0% O_2 for 96 h. Auranofin treatment did not induce NQO-1 protein expression in A431 cells grown in 18.6% O_2 whilst A431 cells grown in 3.0% O_2 for 96 h showed higher auranofin-induced NQO-1 protein expression levels. These data showed that A431 grown in 18.6% O_2 exhibited resistance to auranofin and H_2O_2-induced cell death compared to A431 cells grown in physioxia under the same treatment conditions. This resistance involves, in part, higher levels and activities of certain antioxidant proteins and enzymes as conferred by long term growth in standard cell culture [O_2] compared to physioxia. It is concluded that the *in vitro* testing of redox-active compounds on squamous cell carcinoma cells grown in 18.6% O_2 may yield artefactual *in vitro* data compared to such *in vitro* testing on A431 cells grown in physioxia. It is advised that the *in vitro* testing of redox-active compounds on human non-melanoma squamous cell carcinoma cells should be performed on such cells grown in physioxia for at least four days prior and not on such cells grown chronically in a standard cell culture [O_2].

Acknowledgements

I would first like to thank my supervisors Paul Winyard, Gary Smerdon, and Miranda Smallwood. I learned a lot during my time in Exeter, and that was down to their excellent supervision. I appreciate very much the time and effort they put into me over the years. I would also like to thank the UEMS and the DDRC Healthcare for funding my research project, the staff at the St. Luke's lab (Annie and colleagues) who kept the lab running during COVID restrictions, and Susan Westoby for her administrative help.

Gabhaim buíochas le mo theaghlach Jenny, Dad, Luke, Emily, Kitty, agus mo sheantuismitheoirí, Nana/Paul O'Shea agus Fintan/Berry Jordan. A Kitty, a dúirt liom buíochas a ghabháil le Wally an coinín, go raibh maith agat Wally. Ní déarfaidh mé ach 'go raibh maith agaibh as gach rud', agus fágfaidh mé ansin é.

TABLE OF CONTENTS

LIST OF TABLES

LIST OF FIGURES

LIST OF ABBREVIATIONS

ΔΨm	Change in mitochondrial membrane potential
ΔA	Change in absorbance
2-OG	2-oxoglutarate
2-OH-E$^+$	2-hydroxy-ethidium
3-AT	3-amino-1,2,4-triazole
3-NT	3-nitrotyrosine
A	Absorbance
A431	Human non-melanoma squamous cell carcinoma
AIF	Apoptosis inducing factor
Ang	Angiopoietin
ANT	Adenine nuclear transporter
Apaf	Apoptosis protease activating factor
ARE	Antioxidant response element
ARNT	Aryl hydrocarbon receptor nuclear transporter
Bach-1	BTB domain and CNC homolog 1
Bad	Bcl-2-associated death promoter
Bax	Bcl-2-associated X protein
Bcl-2	B-cell lymphoma 2
BCA	Bicinchoninic acid
BH3$^\bullet$	Trihydrobiopterin radical
BH4	Tetrahydrobiopterin
Bid	BH3 interacting-domain death agonist
BSA	Bovine serum albumin
BTB	Broad-complex, tramtrack, bric-a-brac domain
BCC	Basal cell carcinoma
bHLH	Basic helix-loop-helix
CBP	CREB binding protein
CCCP	Carbonyl cyanide m-chlorophenyl hydrazine
C•H	Alkyl radical
CNC	Cap ‘n’ collar
CO_2	Carbon dioxide
COH-BR1	Human breast cancer cell line
CSCC	Cutaneous squamous cell carcinoma
Cul	Cullin
CuOOH	Cumene hydroperoxide
DCFHDA	2’, 7’-dichlorodihydrofluorescein diacetate
DCFH	2’, 7’-dichlorodihydrofluorescein
DCF	2’, 7’-dichlorofluorescein
DHE	Dihydroethidium
DISC	Death inducing signalling complex
UH_2O	Ultrapure water
DEM	Diethylmaleate
DMEM	Dulbecco‘s modified Eagle’s medium
DMSO	Dimethyl sulfoxide
DMF	Dimethyl fumarate
DNA	Deoxyribonucleic acid
CDNB	1-chloro-2,4-dinitrobenzene
DT40	Human diploid cell line
DTNB	5,5′-dithiobis(2-nitrobenzoic acid)
DTT	Dithiothreitol
E$^+$	Ethidium
EDTA	Ethylenediaminetetraacetic acid
EGTA	Egtazic acid

EPO	Erythropoietin
ER	Endoplasmic reticulum
ETC	Electron transport chain
FAD	Flavin adenine dinucleotide
FADD	Fas-associated death domain
FBS	Fetal bovine serum
FIH	Factor inhibiting hypoxia-inducible factor
FITC	Fluorescein isothiocyanate
FLIP	FLICE-inhibitory protein
FSC	Forward scatter
G6PD	Glucose-6-phosphate dehydrogenase
GR	Glutathione reductase
GS	Glutathione synthetase
Gpx	Glutathione peroxidase
GSH/GSSG	Glutathione reduced/oxidised
GST	Glutathione S-transferase
HIF-1α	Hypoxia-inducible factor 1 α
HIV	Human immunodeficiency virus
H_2O	Water
H_2O_2	Hydrogen peroxide
HELA	Cervical cancer cell line
HO-1	Haem oxygenase-1
HOCl	Hypochlorous acid
HNE	4-hydroxynonenal
HPLC	High performance liquid chromatography
HRE	Hypoxia response element
HRP	Horseradish peroxidase
HTS	High throughput screening
HUVEC	Human umbilical vessel endothelial cell
ICAD	Inhibitor of caspase-activated DNase
IGF	Insulin-like growth factor
IL	Interleukin
IVF	Intervening region
JC-1	Tetraethylbenzimidazolylcarbocyanine iodide
L-BSO	L-buthionine sulfoximine
LOOH	Lipid hydroperoxide
LO•	Lipid alkoxyl radical
LO_2•	Lipid peroxyl radical
MEF	Mouse embryonic fibroblast
MFI	Mean fluorescence intensity
MSA	Mercaptosuccinic acid
NADPH	Nicotinamide adenine dinucleotide phosphate
NADH	Nicotinamide adenine dinucleotide
NES	Nuclear export signal
NF-κB	Nuclear factor kappa-light-chain-enhancer of activated B cells
NLS	Nuclear localisation signal
NMSC	Non-melanoma skin cancer
N_2	Nitrogen
NO_2	Nitrogen dioxide
NO_2^-	Nitrite
NO_3^-	Nitrate
•NO	Nitric oxide radical
NOS	Nitric oxide synthase
NOX	NADPH oxidase
Nrf-2	Nuclear factor erythroid-2-related factor 2
NQO-1	NAD(P)H quinone oxidoreductase-1

•OH	Hydroxyl radical
O_2	Molecular oxygen
[O_2]	Molecular oxygen concentration
$O_2•^-$	Superoxide radical anion
$ONOO^-$	Peroxynitrite
PAGE	Polyacrylamide gel electrophoresis
PAS	PER-ARNT-SIM domain family
PBS	Phosphate buffered saline
PBST	Protein blocking buffer with tween-20
PHD	Prolyl hydroxylase
Physioxia	Physiological oxygen
PI	Propidium iodide
PPIX	Protoporphyrin IX
Prx	Peroxiredoxin
PS	Phosphatidylserine
PUFA	Polyunsaturated fatty acids
pVHL	pVHL
RCF	Relative centrifugal force
RFU	Relative fluorescence units
RH	Relative humidity
RIPA	Radio immunoprecipitation
RNS	Reactive nitrogen species
$RO_2•$	Peroxyl radical
ROS	Reactive oxygen species
SD	Standard deviation
SDS	Sodium dodecyl sulfate
Se^-	Selenol
SeOH	Selenic acid
SOD	Superoxide dismutase
TCA	Tricarboxylic acid cycle
Trx	Thioredoxin
TrxR	Thioredoxin reductase
TNF	Tumor necrosis factor
UV	Ultraviolet light
VEGF	Vascular endothelial growth factor
WST-1	4-[3-(4-Iodophenyl)-2-(4-nitro-phenyl)-2H-5-tetrazolio] -1, 3-benzene sulfonate)
X	Xanthine
XO	Xanthine oxidase

CHAPTER 1: GENERAL INTRODUCTION

1.1. Oxygen concentration in mammalian cell culture: an underappreciated problem in redox biology?

1.1.1. Cell culture

In the late 19th century, the English physiologist Sidney Ringer discovered that animal hearts could be maintained in an isotonic solution (later known as Ringer's buffer solution). Wilhelm Roux continued this *in vitro* (in glass) work by culturing mammalian tissue within a warm saline solution [1]. Roux's work established the early principals of *in vitro* tissue culture [1]. However, the credit for modern cell culture practise is often attributed to Ross Harrison and his seminal embryonic cell culture work in the early 20th century [2]. Around the same time, the effects of molecular oxygen (O_2) toxicity in animals were first described, followed by the discovery of the first organic free radical by Moses Gomberg **(section 1.1.4)** [3, 4].

Generally speaking, two types of cells are grown in cell culture today: cell lines and primary cells. Primary cells are derived directly from the target tissue [5]. However, they are prone to cellular senescence which prevents a somatic cell dividing beyond 40-60 cell divisions [6]. This is known as the Hayflick limit [7]. Beyond this limit, a cell may execute programmed cell death **(section 1.2.5.2)** [6]. This makes it harder to experiment with primary cells. Cell lines were developed to overcome this problem. In the 1960's, the first human cell line was cloned by George Otto Gey from the tissue of Henrietta Lacks who had died from cervical cancer in 1951 [8]. These cells were 'immortalised', meaning they could divide indefinitely in appropriate conditions [8].

Generally speaking, mammalian cells may be grown either as adherent or suspension cell cultures [9]. In adherent cell culture, cells adhere to a treated sterile growth surface made of materials such as hydrophobic polystyrene. Cell culture surfaces may be coated with biological materials such as extracellular matrix, collagen, fibrin and laminin to promote cellular attachment. Mammalian cells are normally grown in growth media of many different types containing an energy source (e.g. glucose) [10]. Fetal bovine serum (FBS) is often used as a growth supplement which provides critical growth factors needed for cellular propagation. Many of these growth media contain a bicarbonate buffer system that maintains a stable pH during *in vitro* growth [10].

Whether a primary cell or a cell line, mammalian cells are most often manipulated in atmospheric O_2 (20.9% O_2) [11]. Mammalian cells are often incubated at 37°C in an incubator which is usually set at 5.0% v/v carbon dioxide (CO_2) [11]. Cell culture incubators are humidified to a relative humidity (RH) of 95% using (usually) a tray of water (H_2O). The O_2 concentration ([O_2]) within an incubator (set at 37°C, 5% CO_2, and 95% RH) at sea level is actually about 18.6% O_2 [11]. This value is slightly lower than atmospheric [O_2] (20.9% O_2). This difference is due to the added gas pressures of H_2O vapour and CO_2 which decreases the [O_2] from 20.9% O_2 to 18.6% O_2 as per Henry's gas law [11]. Mammalian cells in the human body are not normally resident in an [O_2] as high as 18.6% O_2 [12]. For example, the [O_2] is about 3.0% O_2 in human skin **(section 1.1.2.1)**. The term used in this thesis to describe the physiological [O_2] *in vivo* is 'physioxia' **(section 1.1.2)**. Research into the effects of long term mammalian cell culture in 18.6% O_2 on cellular phenotype is surprisingly limited (**section 1.3.1.1.1)**.

The issue of [O_2] in cell culture is the current focus of this work. It is not suggested that [O_2] is the most important issue (or the only issue) associated with standard *in vitro* cell culture practise. Other concerns include: monoculture [13], intracellular signalling [13], cell line genetic drift and authentication [14], cell line cross contamination [15], FBS batch variation [13, 14], pro-oxidant status of cell culture media [18], O_2 gradients in cell culture medium [12], [glucose] in growth medium [19], lack of extracellular matrices [13], and two-dimensional vs three-dimensional cell culture [20]. Most (if not all) cell biologists are aware of the limitations of *in vitro* work. In fact, many would argue that *in vitro* models should not be expected to predict *in vivo* effects. Based on current technology, this argument is absolutely valid. However, it is the responsibility of research scientists to reduce the number of animals used in pre-clinical testing. This requires replacing *in vivo* testing with alternative methods which can replicate aspects of *in vivo* systems. One such alternative method is *in vitro* cell culture. To this end, the limiting factors of *in vitro* research must be addressed. [O_2] in cell culture is one of these limitations.

Of the many fields of biological research, redox biology is one of the most at risk of data generation that is artefactually affected by *in vitro* cell culture [O_2] **(section 1.1.4)**. This present work investigated whether epidermoid squamous cell

carcinoma cells (A431; **section 2.2.1**) grown in 18.6% O_2 long term were resistant to redox-active compound-induced cell death compared to A431 cells adapted to 3.0% O_2. The impetus for this investigation was based on the observation that A431 cells grown in 18.6% O_2 were resistant to photodynamic irradiation-induced cell death compared to A431 cells adapted to 3.0% O_2 **(section 3.1)** [21]. This resistance was associated with the increased transcription and activity of the anti-oxidant defence master regulator nuclear factor erythroid-2-related factor 2 **(Nrf-2; section 1.2.7.3.1)** target gene and enzyme (respectively) in A431 cells grown in 18.6% O_2 compared to A431 cells adapted to 3.0% O_2 **(section 3.1).** The term 'adaptation' used just now is explained in further detail in **section 1.1.2.2.**

The aims of this introduction are fourfold: first, to define the terms that will be used to discuss *in vivo* [O_2] and the [O_2] used in standard cell culture practice **(section 1.1.2)** and to distinguish such terms from hypoxia **(section 1.1.3)**; second, to discuss the [O_2] often utilised *in vitro* cell culture and its relationship to redox biology **(section 1.1.4)**; third, to introduce the basic components of redox biochemistry including free radicals (and their detection by fluorescent probes) **(section 1.2.1-1.2.3)**, oxidative stress **(section 1.2.4)**, cell death **(section 1.2.5)**, induction of oxidative stress by redox-active compounds used in this work **(section 1.2.6)**, antioxidant defence and its regulation **(section 1.2.7);** and fourth, to introduce the drug discovery process **(section 1.3)** and the potential effects of growing mammalian cells grown in 18.6% O_2 on the *in vitro* development of novel redox-active compounds **(section 1.3.1.1.1).**

First, *in vivo* [O_2] will be discussed, a condition which is almost always under-represented in modern *in vitro* cell culture practises.

1.1.2. O_2 transport *in vivo* and the definition of physioxia

Multicellular life has evolved to maximise the efficiency of O_2 delivery to respiring cells. Most mammalian cells are found no more than a few microns from the nearest blood vessel [12]. The atmospheric [O_2] at sea level (at standard temperature and pressure) is about 20.9% O_2, and falls to about 19% O_2 in the trachea upon inspiration. This fall in [O_2] is due to the introduction of H_2O vapour pressure within the trachea [12]. As air enters the bronchus and bronchiole, the

[O_2] falls to about 12-15% O_2. This is due to the mixing of inspired air with expired air containing gaseous H_2O and CO_2 (about 5.0%) [12]. O_2 then crosses the alveolar membrane into the blood vessel where it binds reversibly to haem forming oxy-haemoglobin through simple diffusion. Some of the deoxygenated blood from the surrounding lung adventitia drains into the pulmonary vein (carrying oxygenated blood) rather than the bronchial vein. This phenomenon is known as venous admixing **(Figure 1.1)**, which results in a further decrease in [O_2] within the blood [12]. The average arterial blood [O_2] is about 12.0% due to venous admixing, and the alveolar shunt [12]. This represents an [O_2] differential of about 9% when compared to atmospheric [O_2]. Once in the blood, O_2 binds haemoglobin, an iron-containing O_2-transporting metalloprotein, which transports O_2 around the body in the blood [22].

In general, the [O_2] within a given tissue will depend on two main criteria: first, distance of a tissue is from an O_2 supply; and second, the rate of O_2 consumption by the respiring tissue. An example of [O_2] distribution within a single organ is found in human skin **(section 1.1.2.1)**.

In summary, the transport of O_2 to respiring tissues is critical for the removal of metabolic by-products such as CO_2. Any failure in this process can cause hypoxia in organs and tissues **(Section 1.1.3).**

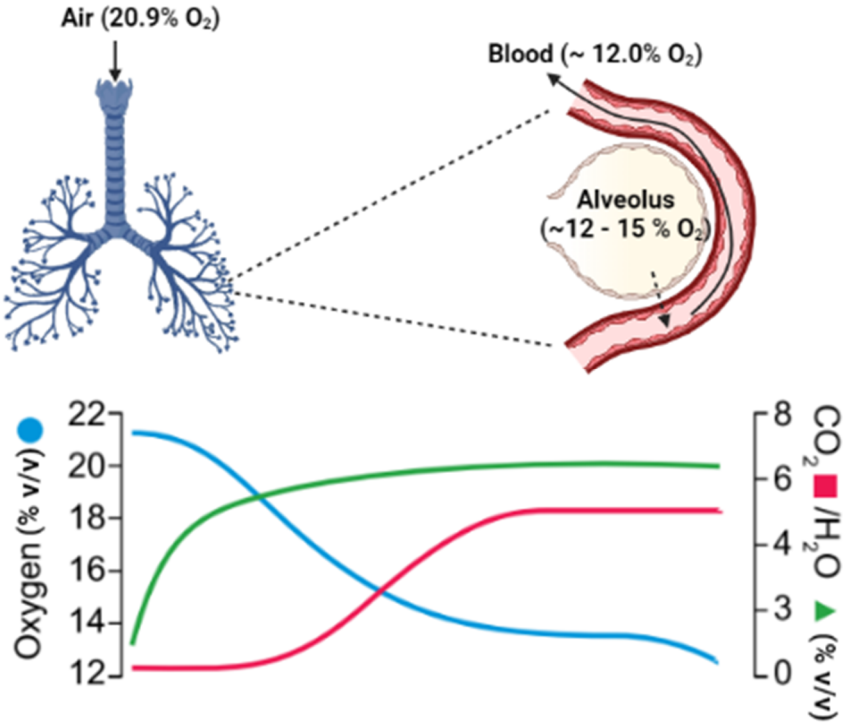

Figure 1.1. The change in O_2 concentration in air after inspiration into the lung and diffusion into the bloodstream. The left axis represents the [O_2] in % (v/v) where the decrease in [O_2] is indicated by the blue line moving from left to right as air passes through the trachea, bronchus and bronchioles. Air then enters alveolus where it diffuses into the blood stream. The increases in [CO_2] (right axis, red line) and [H_2O] (right axis, green line) further decrease [O_2]. Venous admixture, which mixes shunted non-oxygenated and re-oxygenated blood, causing a further decrease in [O_2] to about 12.5 % (v/v) in the arterial blood supply. Figure adapted from [12] using www.Biorender.com.

1.1.2.1. Rational for choosing 3.0% O_2 as the set point for mimicking the *in vivo* [O_2] conditions for *in vitro* squamous cell carcinoma growth

Human skin is made of three layers: the epidermis, the dermis and the transcutaneous layer. The epidermal layer is divided further into three main parts from most superficial to deep: stratum corneum (corneocytes), stratum spinosum (keratinocytes), and the stratum basale (basal cells**; Figure 1.2 a)**. The dermis is inferior to the epidermis, and is made up of the papillary dermis (papillary vasculature, oil glands) and the reticular dermis (hair follicles, nerves, blood vessels and connective tissue**; Figure 1.2 a)**. Finally, the most inferior layer is the trans-cutaneous layer which is made up mostly of protective adipose tissue, the vascular network, and nervous tissue **(Figure 1.2 a)**.

The skin has two distinct sources of O_2, the atmosphere and the microvasculature. The [O_2] within the skin is proportional to cutaneous blood flow and inversely proportional to cutaneous depth [9, 19]. The stratum corneum

receives a substantial amount of its O_2 supply from the atmosphere. As such, the [O_2] in the most superficial layer of the stratum corneum can be quite high (about 20.9% O_2; **Figure 1.2 b**). However, [O_2] decreases as a function of depth to around 4 ± 2% O_2 in the stratum spinosum **(Figure 1.2 b)** [19, 20]. The reason for this steep fall in [O_2] is due two factors: first, the rapidly dividing keratinocyte in the stratum spinosum have a high O_2 consumption rate; second, the stratum spinosum relies on O_2 supply from the atmosphere and the papillary loops in the proximal dermal layer [23]. The dermal layer contains the local papillary vasculature and has an [O_2] of 5 ± 3.5% O_2 **(Figure 1.2 b)** [11, 22, 23].

A431 cells were used for this work. The rationale for this choice is explained in **section 3.1**. A431 cells model non-melanoma cutaneous squamous cell carcinoma (CSCC) whose pathogenesis generally begins within the epidermal layer [25]. CSCC can originate from keratinocyte, first identifiable by actinic keratosis [25]. This is the first identifiable step in CSCC and is associated with the loss of keratinocyte polarity, and irregular nuclei volume [25]. The next stage of CSCC is CSCC *in-situ* which involves the entire thickness of the epidermis with no evidence of invasion into the dermis [25]. The next stage is invasive CSCC where the carcinoma invades the dermis with the potential to invade further into fat, muscle and bone tissues [25].

As shown in **Figure 1.2 b**, the [O_2] in the surface of the skin decreases sharply when measured across the stratum corneum and stratum spinosum. CSCC can occupy multiple strata in human skin, all of which possess different *in vivo* [O_2]. Choosing the correct *in vivo* [O_2] for growing for squamous cell carcinoma *in vitro* is therefore not simple. A431 cells growing in monolayer during *in vitro* growth may reflect aspects of actinic keratosis stage which develops in the stratum spinosum. As such, the average [O_2] within the stratum spinosum (3.0% O_2) was chosen to mimic the [O_2] present in the early stages of CSCC development.

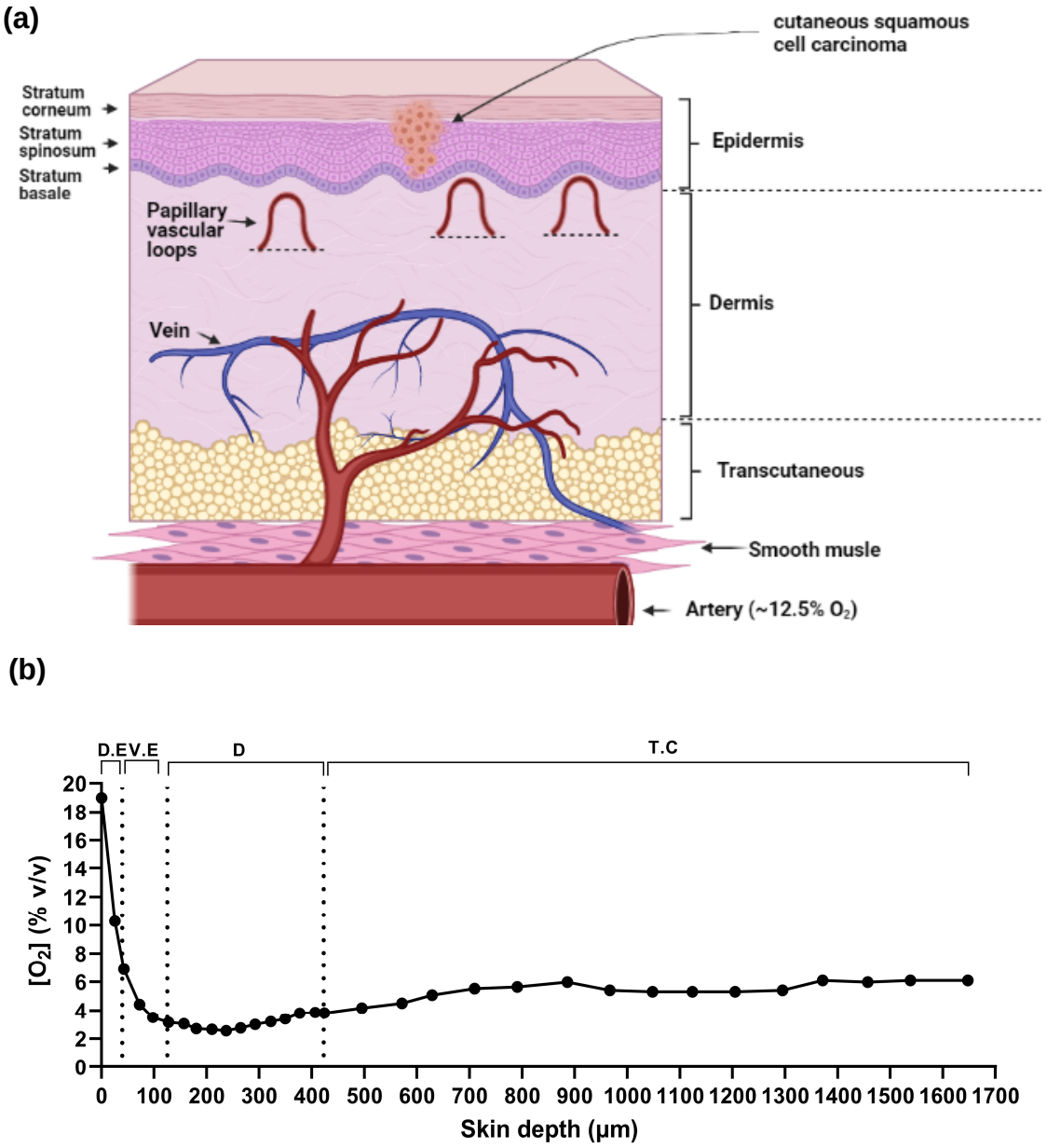

Figure 1.2. The layers of human skin and their associated O_2 concentration. Panel (a), the strata of human skin (not to scale). Cutaneous squamous cell carcinoma is believed to originate in the stratum spinosum in rapidly dividing keratinocyte. Panel **(b),** the $[O_2]$ in each layer of human skin measured by Clark electrode. The Image in panel (a) was made with www.biorender.com. **D:** dermis; **D.E:** dead epidermis; **T.C:** trans cutaneous; **V.E:** viable epidermis. The image in panel **(b)** was adapted from data derived from [24].

1.1.2.2. Nomenclature used to describe *in vivo* O_2 concentration, and its distinction from hypoxia

What should one call an $[O_2]$ *in vitro* which mimics *in vivo* $[O_2]$? Unfortunately there is no consensus regarding the most appropriate naming scheme for such a condition [25, 26]. One camp of thought considers the $[O_2]$ *in vivo* as 'normal' for cells (and is sometimes termed as 'normoxia') and that the $[O_2]$ used in standard

CO_2 incubators (18.6% O_2) should be termed 'hyperoxia' as it is higher than *in vivo* [O_2] [27, 20]. However, cells *in vitro* (especially cell lines) are not normally grown in an [O_2] that mimics *in vivo* conditions, but instead are most often grown in about 18.6% O_2 **(section 1.1)**. As such, a second camp of thought regards 18.6% O_2 as the normal [O_2] for these cells (and is termed 'normoxia'), with *in vivo* [O_2] often described using a variety of names ranging from 'physioxia', 'sub-oxia', '*in-situ* normoxia', and 'physiological hypoxia' to 'physiological chronic normoxia' [25, 28–30]. Such a list of nomenclature may cause confusion for those who may not have considered the issue of *in vitro* [O_2] before.

In this work, 18.6% O_2 is not defined as normal for the A431 cell line which models non-melanoma squamous cell carcinoma. If a disease is to be modelled *in vitro*, the [O_2] of the disease niche should be replicated even if the cell line is not normally grown in such [O_2] conditions. As such, the [O_2] *in vivo* is defined as 'physioxia'. The [O_2] commonly used in standard CO_2 incubators will be termed simply as '18.6% O_2' to avoid confusion from this point onwards. However, the terms used in this thesis may not be accepted by some to be the most appropriate. There is an argument that 18.6% O_2 is 'normal' for some cell lines which have, most likely, adapted to growing in a non-physiological [O_2] over many cellular generations (e.g. HeLa).

One point that must be made clear, physioxia describes an oxygenation condition which is different to hypoxia **(section 1.1.3)**. A low culture [O_2], relative to room air, does not always equate to hypoxia. There are a continuum of [O_2] niches lower than room air in human tissue (1-16.5 % O_2), but this does not indicate that these [O_2] niches are hypoxic to cells [12]. Hypoxia-related transcription factors such as hypoxia-inducible factor (HIF)-1α are usually activated at an [O_2] of < 1% (v/v) **(section 1.1.3.1)**. The activation of HIF-1α has a very steep half-maximal inhibitory concentration (IC_{50}) that is not normally relevant over an *in vivo* [O_2] range in healthy oxygenated tissue [32].

Finally, one aspect of the nomenclature surrounding physioxia cell culture may lead to some confusion. O_2 can have both an acute affect, and a chronic effect on the cellular responses to compound treatment.

Regarding the acute effect: the presence of O_2 itself, solely during treatment, may affect the mechanism of action of a compound. Photodynamic therapy for

example requires O_2 in order to form singlet oxygen during photodynamic irradiation [33]. Another example is the 'oxygen effect' in radiotherapy, where an acute decrease in [O_2] below 1.0% O_2 increases the radio resistance of some cancer cells to radiotherapy [34].

Regarding the chronic effect: the long term growth of cells under a particular [O_2], prior to compound treatment, may slowly affect the phenotype of the cell thus affecting their response to further treatment. For example, it is well known that cancer cells exposed to chronic hypoxia conditions are resistant to the effects of some chemotherapeutics [34, 35]. This is believed to involve an adaptation of such cells to this hypoxic environment leading to changes to the cellular phenotype over time. However, there is evidence that long term growth in physioxia also changes the cellular response to oxidative stress-induced cell killing. For example, the growth of squamous cell carcinoma cells in 3.0% O_2 for 48 h causes changes in the cellular phenotype which sensitises these cells to the subsequent killing effects of photodynamic irradiation compared to A431 cells grown in 18.6% O_2 for 48 h [21]. This change takes time to emerge, and has been termed as an 'adaptation' response to the 'new' [O_2] condition. In A431 cells, this adaptation appears to involve changes to the expression levels and activities of Nrf-2 related genes and enzymes, respectively [21]. Such changes may affect the *in vitro* development of Nrf-2-activating compounds **(section 1.3.1.1.1)**.

These described effects of *in vitro* cell culture [O_2] on the cellular responses to compound treatment may seem similar, but there is one important difference. One requires a particular [O_2] during treatment alone, the other requires that a cell is *adapted* to a particular [O_2] prior to treatment. This nuance is very important as it highlights a consideration. How long should one adapt a cell to physioxia for before measuring the appropriate endpoints?

In this work, the responses of A431 cells grown in 18.6% O_2 are compared to the responses of A431 cells 'adapted' to physioxia for a particular length of time. Cell lines, such as A431 cells, have likely adapted to growth in 18.6% O_2, and will likely not adapt any further. As such, using the term 'adaptation' to describe the growth of A431 cells in 18.6% O_2 is not useful in this context. Cells switched from 18.6% O_2 to physioxia now have a 'new' [O_2] to grow in and may begin to adapt their phenotype relative to the phenotype exhibited by A431 cells grown

chronically in 18.6% O_2. However, using the term ‘adapted’ in the relevant results sections assumes a response before any evidence is presented. As such the term ‘growth in’ is used in the relevant results sections to describe how cells were grown in both [O_2] conditions over the culture period. In the relevant discussion sections of chapter 3 and 4, the term ‘adapted’ is used after evidence is presented that A431 cells do in fact adapt elements of their phenotype. This term was also used to describe evidence presented in the literature where mammalian cells exhibited an adaptation response to physioxia.

1.1.3. Hypoxia

Hypoxia describes an [O_2] which is insufficient to meet the demands of oxidative phosphorylation [37]. Hypoxia can be described as being either acute, or chronic [10, 38, 39].

Hypoxia causes numerous physiological changes within the cell. Calcium ion homeostasis changes during hypoxia [39]. For example, Na^+/K^+-ATPase and Ca^{2+}-ATPase ion channel activities are altered during acute hypoxia [39]. The activity of these ion channels decreases during acute hypoxia due to, in part, a decrease in adenosine triphosphate (ATP) production by oxidative phosphorylation [40]. This leads to an efflux of K^+ and an influx of Na^+ and Ca^{2+} ions. Release of K^+ causes membrane de-polarisation further increasing Ca^{2+} influx through activation of voltage-dependent Ca^{2+} channels [41]. This change in ion homeostasis activates lipases and proteases which can increase the generation of reactive oxygen species (ROS) [41].

Metabolism is also affected under hypoxia. Due to the limited supply of O_2, a cell may switch from oxidative phosphorylation to glycolysis. This is known as the glycolytic switch. This process involves the upregulation of genes encoding proteins involved in glycolysis **(Figure 1.3)**.

Acute hypoxia also affects the therapeutic effectiveness of xenobiotics. This may occur by affecting xenobiotic clearance from the body. For example, hypoxia increases the toxicity of acetaminophen by increasing the levels of oxidised glutathione (GSSG) [42]. Reduced glutathione (GSH) is needed for glutathione S-transferase (GST)-mediated xenobiotic conjugation. As such, hypoxia can result in acetaminophen toxicity as the cell fails to clear it via xenobiotic

metabolism [43]. In addition, depletion of ATP during hypoxia may inhibit crucial ATP-dependent transporters such as members of the multi-drug resistance protein family [44].

1.1.3.1. Activation of hypoxia-inducible factor-1α

HIF 1-α is a heterodimeric transcription factor protein made up of two subunits, HIF-1α and HIF-1β. Both of these subunits are members of the basic helix-loop-helix (bHLH) containing PER-ARNT-SIM (PAS) domain family. HIF-1β, originally described by Ratcliffe et al. [45] as the aryl hydrocarbon receptor nuclear translocator (ARNT), contains the nuclear localisation signal. The HIF-1α subunit is O_2-sensitive, whereas the β subunit is O_2-insensitive. HIF-1α and HIF-1β heterodimerise through their bHLH and PAS domains.

The alpha subunit of HIF has three isoforms: HIF-1α, HIF-2α and HIF-3α. HIF-1α is expressed in most cells within the human body whereas HIF-2α and HIF3-α are mostly found in vascular endothelial cells, type II pneumocytes, renal interstitial cells, and liver parenchymal cells [36]. In physioxia **(section 1.1.3.1)**, HIF-1α is hydroxylated at proline residues by the enzyme prolyl hydroxylase (PHD). The activity of PHD is dependent on O_2 also. PHD require a high [O_2] to reach a half maximal reaction velocity (Michaelis-Menten constant (K_m))[46].

HIF-1α is then targeted for ubiquitination by the von-Hippel Lindau tumour suppressor gene product (pVHL) leading to its degradation by the proteasome **(Figure 1.3)** [32]. HIF-1α can also be inhibited by hydroxylation of Asp803 by factor inhibiting hypoxia-inducible factor (FIH). This prevents the binding of the HIF cofactor CBP-p300, thus preventing transcription factor function **(Figure 1.3)** [47].

Under hypoxia (< 1% O_2), PHD is inactivated due to the low [O_2] as it prevents HIF-1α proline-targeted hydroxylation [32]. This de-targets HIF-1α for degradation and allows translocation of the HIF-1α/HIF-1β hetero-dimer to the nucleus. The hetero-dimer then binds the hypoxia response element (HRE) along with the CREB-binding protein (CBP)-p300 [32]. HIF-1α stabilisation results in the transcription of genes which encode proteins involved in angiogenesis (vascular endothelial growth factor (VEGF)), erythropoietin (EPO), proliferation (transforming growth factor–α and –β), insulin-like growth factor, and platelet-

derived growth factor), glycolysis (glucose transporter 1 and -3), and apoptosis (Bcl-2, Nip3, Nix, Bax, Bid, p53 upregulated modulator of apoptosis, and Apaf-1). These changes augment O_2 delivery, increase cellular proliferation, and switch cellular energy production from oxidative phosphorylation to glycolysis. Additionally, HIF-1α signalling increases pro-survival signals through upregulation of both anti- and pro-apoptotic proteins **(Figure 1.3)** [48–51].

ROS production is also increased under hypoxia [51]. Inhibition of the electron transport chain (ETC) at complex III under hypoxia may generate ROS [51]. In addition, the activity of PHD depends on the Fe^{2+} catalytic site. ROS, such as H_2O_2, may inactivate PHD activity by oxidising the Fe^{2+} active site [51, 52] Chelation of Fe^{2+} from PHD results in enzyme inactivation [53]. Additionally, 2-oxoglutarate (2OG), an intermediary metabolite of the tricarboxylic acid (TCA) cycle, is thought to mediate HIF-1α hydroxylation and degradation. [2OG] may be decreased by ROS [54]. HIF-1α can also be activated through the Ca^{2+}-dependent phosphorylation of CBP-p300 by CaM kinase II **(Figure 1.3)**.

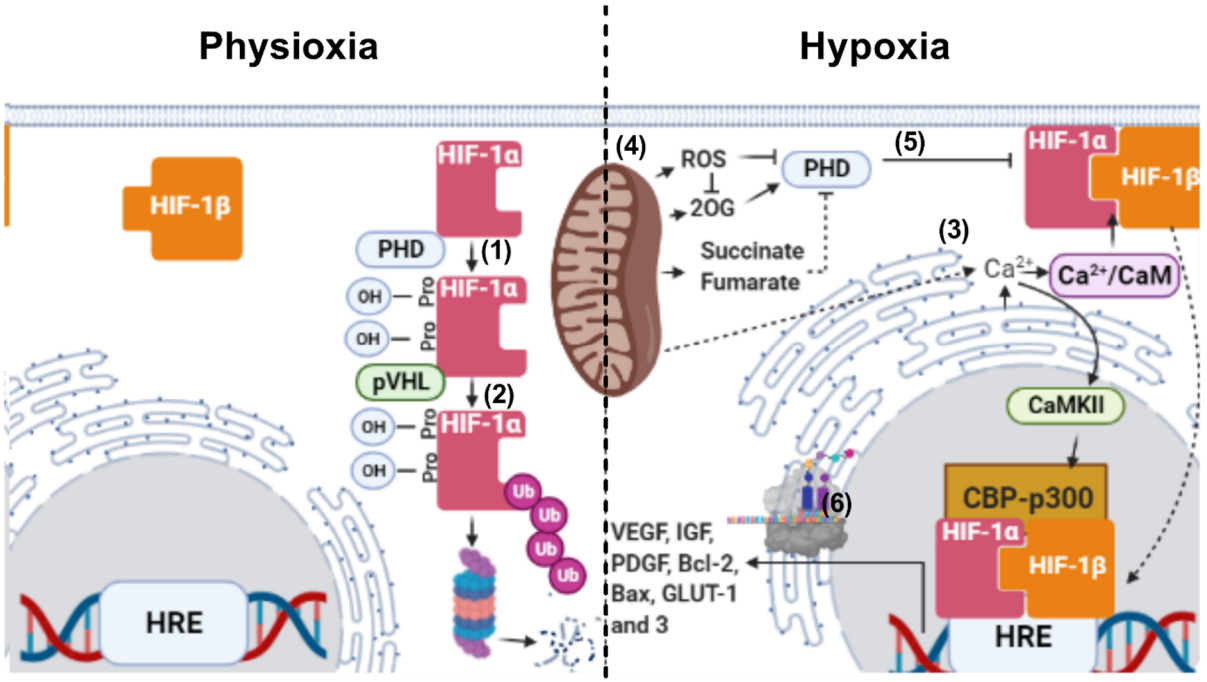

Figure 1.3. Hypoxia-inducible factor-1α activation under hypoxia. **(1)** In physioxia (left of dashed line), HIF-1α is hydroxylated at proline residues by PHD prior to **(2)** ubiquitination and proteasomal degradation facilitated by pVHL. PHD requires O_2 for HIF hydroxylation, and as such its activity is higher in physioxia than in hypoxia. In this state, HIF does not translocate to the nucleus or induce transcription of HIF targeted genes. In hypoxia (right of dashed line), **(3)** calcium homeostasis is affected, with increased calcium leakage from the ER and mitochondria. Ca^{2+}can bind with CAM to form the Ca^{2+}/CaM complex which facilitates stabilisation of the HIF heterodimer. In addition, Ca^{2+} can also activate CaMKII which promotes activation of the CBP-p300 co-activator complex. **(4)** From the mitochondria, increased ROS production can inhibit PHD which is required for HIF-1α hydroxylation. 2-OG production, which aids in the hydroxylation and degradation of HIF-1α, is decreased by ROS. Succinate and fumarate, products of the TCA cycle, inhibit PHD also. Primarily, the decrease in [O_2] during hypoxia also inhibits PHD. **(5)** Together, this results in the promotion of HIF stabilisation and nuclear translocation where it binds to the HRE and **(6)** initiates the transcription of a variety of target genes. **2-OG:** 2-oxoglutarate; **Bcl:** B-cell lymphoma 2; **Bax:** bcl-2 like protein 4; **CaM:** calmodulin; **CaMKII:** calmodulin kinase II; **CBP-p300:** CREB binding protein; **HIF:** hypoxia-inducible factor; **HRE:** hypoxia regulatory element; **GLUT:** glucose transporter; **IGF:** Insulin growth factor; **PDGF:** platelet-derived growth factor; **PHD:** proline hydroxylase; **Physioxia:** physiological oxygen concentration; **VEGF:** vascular endothelial cell growth factor. Image made with www.Biorender.com.

1.1.4. Oxygen concentration, cell culture and redox biology

As mentioned earlier in **section 1.1.1**, free radicals **(section 1.2.1)** were first identified in the late 19th century by Moses Gomberg. Upon his attempt to synthesise the compound hexaphenylethane, he inadvertently synthesised triphenylethane. In doing so he made the landmark discovery that carbon was not always tetravalent, and could exist as an organic free radical [55]. Around the same time, O_2 toxicity was also first described in mice by Paul Bert [56]. It was another 50 years before the mechanism of O_2 toxicity was solved by Rebecca Gerschman's landmark observation that hyperbaric oxygen toxicity and ionising radiation toxicity shared the same underlying mechanism of action, the formation of the oxygen free radical [4]. This led to the concern that O_2 could have a 'dark-side'. Various societies concerned with such phenomena were then formed, such as the Society for Free Radical Research in 1982 (originally called the Antioxidant Society). The generation of ROS is now widely accepted to be involved in the pathogenesis of diseases such as Alzheimer's disease, Parkinson's diseases, and rheumatoid arthritis **(section 1.2.4)**.

O_2 is a fundamentally important molecule in redox biochemistry. O_2, and its associated O_2 free radical species **(section 1.2.1)**, form the basis of biological free-radical research. As a molecule, O_2 is indispensable for energy production via oxidative phosphorylation [57]. O_2 can be generated via the catalase-mediated decomposition of hydrogen peroxide (H_2O_2) **(section 1.2.7.2.3)**, or utilised as a substrate by nicotinamide adenine dinucleotide phosphate (NADPH) oxidase, D-amino acid oxidase, xanthine oxidase (XO), and tyrosine hydroxylase [58–61]. Cellular biomolecules (e.g. deoxyribonucleic acid (DNA), protein and lipids) are directly damaged by ROS **(section 1.2.4)**. Some enzymes, such as pyruvate-formate lysase and ribonuclease reductase type III, utilise glycyl radicals as reactionary intermediates. However, glycyl radicals react readily with O_2 leading to the rapid inactivation of glycyl radical enzymes [62]. There is growing evidence that cellular ROS production by O_2-dependent enzymes is heightened in atmospheric O_2 compared to physioxia **(section 3.4.3.2 and 3.4.3.3)**. NADPH oxidase 4 (NOX-4) has a high K_m (O_2%) and has been described as an [O_2] sensor **(section 3.4.3.3)**. The [O_2] niches that cells reside in can affect cellular antioxidant defences **(section 4.4.1 and 4.4.2)**. For example, the levels

of GSH, a critical antioxidant defence peptide **(section 1.2.7.2.4)**, is reported to be about 8 times higher in the fluid lining the respiratory tract compared to that of blood plasma (5 vs 40-200 µM) [10, 63].

Minimising exposure to O_2 is a primitive mechanism which bacteria use to protect against O_2 toxicity and oxidative stress [64]. Human physiology has evolved similar strategies. For example, mammalian mitochondria can operate under low O_2, possibly to diminish the formation of ROS [46]. Cytochrome oxidases have a very low K_m (O_2%) possibly allowing optimal energy production even in low [O_2] [46]. Some stem cells, such as haematopoietic stem cells, are found in low [O_2] anatomical sites such as the bone marrow (about 5% O_2) [12]. The low [O_2] environment of bone marrow may diminish ROS-induced alteration of stem cell phenotype *in vivo* [65–67]. ROS is reported to affect stem cell differentiation, proliferation and instances of gene mutations [66, 67].

As discussed previously, most mammalian cells are grown *in vitro* in 18.6% O_2 and not physioxia **(section 1.1.1)**. Additionally, the vast majority of cell-lines used today are selected for based (partly) on their ability to grow in 18.6% O_2 [68, 69]. Cell lines that fail to propagate under high [O_2] are discarded in favour of clones with more favourable growth kinetics [68, 69]. Selection of desirable cell phenotypes (such as growth rate) are crucial for the primary selection phase in cell-line development, performed largely in 18.6% O_2 [68, 69]. It has led to the bizarre (yet necessary) discussion surrounding the ‘adaptation’ of mammalian cells to physioxia rather than their ‘adaptation’ to 18.6% O_2 [70].

Of the four most cited journals in cellular biology (Cell, Nature, Science, and Nature Biotechnology), none require that mammalian cell culture be performed under physioxia [71]. However, some fields of research are more likely to be affected by such publishing requirements, redox biology being one [20, 46, 72–77]. Knowing the importance of O_2 in redox reactions, one would expect research journals publishing under the umbrella term of ‘free radical research’ to be most concerned with redox-related biological experimentation under high *in vitro* cell culture [O_2]. However, none of the leading journals in redox biology require a physioxia-related [O_2] to be used during *in vitro* cell culture. But what evidence warrants the need for such a concern?

One of the first reported papers on this subject was in 1972 by Alan Richter who discovered that the plating efficiency of some murine neoplastic and non-neoplastic cells were sensitive to [O_2] [78]. Later, mouse embryonic fibroblasts (MEF) were shown to senesce when grown in 18.6% O_2 but not when adapted to 3.0% O_2 [79]. MEF grown in 18.6% O_2 also showed heightened levels of oxidative stress-induced DNA damage compared to those adapted to 3.0% O_2 [79]. Primary cells grown in 18.6% O_2 also exhibited an altered cellular phenotype compared to those adapted to physioxia [67, 72, 80–83]. For example, peripheral blood mononuclear cells grown in 18.6% O_2 exhibited higher levels of GSSG **(section 1.2.7.2.4)** compared to such cells adapted to physioxia [81]. This has led some to suggest that primary mononuclear cells should be adapted to physioxia to more accurately recapitulate the *in vivo* cellular phenotype for these cells [81].

The testing of redox-active compounds on mammalian cells grown chronically in 18.6% O_2 produces artefactual cellular responses compared to when said compounds are tested on mammalian cells adapted to physioxia [36, 72, 73, 75, 78, 82, 84]. For example, the induction of Nrf-2 **(section 1.2.7.3)** target protein by electrophilic activation is sensitive to the [O_2] that a cell is adapted to prior to assay [72]. With the transcription factor Nrf-2 now spotlighted as a promising target for pharmaceutical development [85–87], this raises a question: should redox-active compounds be tested on cells grown chronically under 18.6% O_2, or should they be tested on cells adapted to physioxia? This will be discussed further in **section 1.3.1.1.1.** First however, the basic elements of redox biochemistry (i.e. free radicals, oxidative stress, and antioxidant defence) will be introduced.

1.2. Important concepts in redox biology.

1.2.1. What is a free radical?

A free radical is a chemical species which contains one or more unpaired electrons that is capable of existing on its own [89].

Free radicals can be formed when a covalent bond is broken, either caused by heat, or radiation [90]. Once a covalent bond is broken, electrons can be shared equally amongst the atoms through homolytic fission. Alternatively, the electrons can go to just one of the atoms through heterolytic fission. For example, H_2O can undergo both homolytic fission and heterolytic fission [90]. Homolytic fission of

H_2O results in the formation of a hydrogen radical ($H^{\bullet}$) and a hydroxyl radical ($^{\bullet}OH$). Heterolytic fission results in the formation of a hydrogen ion (H^+) and the hydroxide ion (OH^-).

The unpaired electrons in free radicals render them highly reactive. Due to this characteristic, free radicals are generally unselective in their reactivity with cellular biomolecules.

1.2.1.1. How do free radicals react?

Free radicals react in different ways: some free radicals can react with each other, or with biomolecules, causing a chain reactions. This can lead to the production of more free radicals capable of causing cellular damage.

The simplest radical, the hydrogen radical ($H^{\bullet}$), can react with itself to form molecular hydrogen (H_2).

$$H^{\bullet} + H^{\bullet} \rightarrow H_2 \qquad \textbf{(Eq. 1.01)}$$

However, chain reactions can also occur. $^{\bullet}OH$ can attack the hydrogen atom in a C-H bond in lipid side chains [91]. This results in the formation of a carbon centred radical which can react with O_2 to form a peroxyl radical ($RO_2^{\bullet}$) [91]. This reaction is important for the initiation of lipid peroxidation **(section 1.2.4.1).**

Radicals may donate an electron to a non-radical. This is a reduction reaction.

$$X^{\bullet} + Y \rightarrow X^{+} + Y^{\bullet -} \qquad \textbf{(Eq. 1.02)}$$

In other cases, radicals can accept an electron from non-radicals. This is an oxidation reaction.

$$X^{\bullet} + Y \rightarrow X^{-} + Y^{\bullet +} \qquad \textbf{(Eq. 1.03)}$$

Generally speaking, radicals can react with other radicals to form non-radicals. Radicals can also react with non-radicals to form a new free radical species [92].

1.2.2. The chemistry of biologically important free radicals and transition metal ions.

1.2.2.1. Transition metal ions

Transition metal ions can accept and donate single electrons making them important reactants in redox biochemistry [90]. Most transition metal ions in the d-block of the periodic table, other than the zinc ion, have unpaired electrons. This renders transition metal ions, such as iron (Fe) ions and copper (Cu) ions, as tentative free radicals [93]. However, rarely are Fe ions and Cu ions found freely existing in mammalian systems. Their distribution and availability is carefully controlled in mammalian systems by proteins such as ferritin **(section 3.4.5)**. Fe ion are purposefully added to some cell culture growth medium in the form of ferric nitrate, such as in the Dulbecco's modified Eagle's medium used in this work **(section 2.2)**. Fe and Cu ions are also common contaminants in culture media also, which together warrants a discussion of their biochemistry here.

The transition metal Fe^{2+} catalyses the generation of $^{\bullet}OH$ from H_2O_2 **(Eq. 1.11)** [93], a highly reactive free radical species **(section 1.2.2.2)**.

Cu ions are another type of transition metal that are found in cellular systems. Cu ions have two common oxidation states, Cu^{+} and Cu^{2+}. They are involved in numerous redox reactions:

$$Cu^{+} + O_2 \rightarrow Cu^{2+} + O_2^{\bullet-} \quad \textbf{(Eq. 1.04)}$$

$$Cu^{2+} + O_2^{\bullet-} \rightarrow Cu^{+} + O_2 \quad \textbf{(Eq. 1.05)}$$

$$Cu^{+} + O_2^{\bullet-} \xrightarrow{2H^{+}} H_2O_2 + Cu^{2+} \quad \textbf{(Eq. 1.06)}$$

$$Cu^{3+} + Cu^{+} \rightarrow 2Cu^{2+} \quad \textbf{(Eq. 1.07)}$$

$$Cu^{2+} + H_2O_2 \xrightarrow{-2H^{+}} Cu^{+} + O_2 \quad \textbf{(Eq. 1.08)}$$

$$Cu^{+} + H_2O_2 \xrightarrow{-2OH^{+}} Cu^{3+} \quad \textbf{(Eq. 1.09)}$$

The reaction between $O_2^{\bullet-}$ and Cu^{+} **(Eq. 1.06)** has a high rate constant ($k = 1.98 \pm 0.05 \times 10^9\ M^{-1}\ s^{-1}$) which forms H_2O_2 [94]. $^{\bullet}OH$, the breakdown product of H_2O_2, is much more reactive than $O_2^{\bullet-}$ [90]. Cu^{+} can be regenerated from Cu^{2+} by reacting with H_2O_2 **(Eq. 1.08)**. Therefore, Cu^{+} can initiate a series of deleterious

reactions which can generate the most highly reactive free radical in living systems, $^{\bullet}OH$.

1.2.2.2. Hydroxyl radical

In most biological settings, $^{\bullet}OH$ is one of the most highly reactive free radical species [90]. It can be formed through a number of different reactions.

Homolytic fission of H_2O_2 by ultraviolet light (UV) can form $^{\bullet}OH$ [95]. However, this is not usually biologically relevant.

$^{\bullet}OH$ is also formed through the reaction of hypochlorous acid (HOCl) and $O_2^{\bullet-}$ **(Eq. 1.10).** HOCl is formed *in vivo* through the peroxidation of chloride ions by myeloperoxidase in macrophage, for example.

$$HOCl + O_2^{\bullet-} \rightarrow O_2 + Cl^- + {}^{\bullet}OH \qquad \textbf{(Eq. 1.10)}$$

The Fenton reaction is another way in which $^{\bullet}OH$ can be formed *in vivo* [96]. This reaction is based on the availability of transition metal ions such as Fe^{2+}, and their subsequent reaction with H_2O_2 [96]. H_2O_2 is not a free radical, nor is it very reactive on its own. The oxidising potential of H_2O_2, and the resulting cellular damage, is mostly due to $^{\bullet}OH$.

$$Fe^{2+} + H_2O_2 \rightarrow \text{Intermediate complex} \rightarrow Fe^{3+} + {}^{\bullet}OH + OH^- \qquad \textbf{(Eq. 1.11)}$$

$^{\bullet}OH$ is involved in the initiation of lipid peroxidation **(section 1.2.4.1)** [97]. $^{\bullet}OH$ can react with aromatic compounds such as deoxyguanosine in DNA forming 8-hydroxy-2'-deoxyguanosine for example [98].

1.2.2.3. Superoxide radical anion

The superoxide radical anion ($O_2^{\bullet-}$) is less reactive than $^{\bullet}OH$ [90]. The main difference in electronic configuration between O_2 and $O_2^{\bullet-}$ is a single electron added into the π* antibonding orbital **(Table 1.1)**. Compared to O_2, $O_2^{\bullet-}$ has fewer unpaired electrons. Because of the single unpaired electron in the antibonding orbital of $O_2^{\bullet-}$, and the associated direction of electron spin, $O_2^{\bullet-}$ is more reactive than O_2.

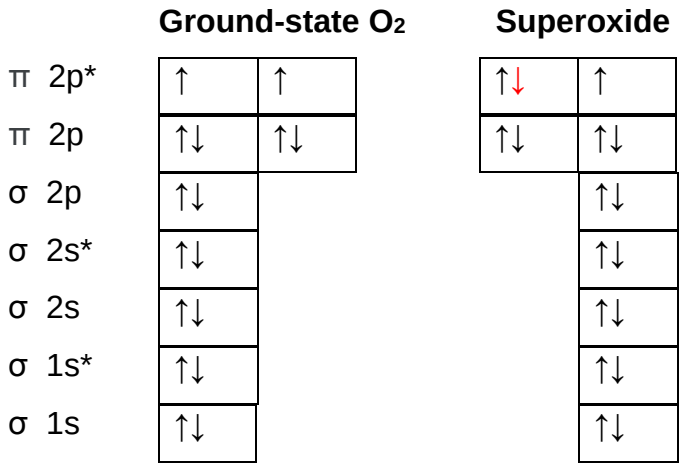

Table 1.1. Molecular electronic configurations of ground state molecular oxygen and the superoxide free radical. Antibonding orbitals are indicated by the ***** symbol. Arrows are representative of electrons, and their direction of spin. The difference in the electronic configuration between ground state oxygen and superoxide is the single electron (red arrow; right) in the π* antibonding orbital.

$O_2^{\bullet-}$ is formed through a number of biological processes, including by the ETC [99]. O_2 is utilised as a reducing equivalent to reduce NADH to NAD^+ at complex I and III of the ETC. $O_2^{\bullet-}$ can undergo a dismutation reaction **(section 1.2.7.2.1)**, mediated by superoxide dismutase (SOD), forming H_2O_2 and O_2. The dismutation of $O_2^{\bullet-}$ prevents its reaction with biomolecules such as NADH, cytochrome c, DNA, lipids, iron-sulphur (Fe-S) clusters, and amino acids.

$O_2^{\bullet-}$ can also be produced through enzymatic reactions such as XO-mediated oxidation of xanthine/hypoxanthine to uric acid [59].

$O_2^{\bullet-}$ can destroy Fe-S containing proteins causing the release of Fe^{2+}, and can reduce Fe^{3+} **(Eq. 1.12)**.

$$Fe^{3+} + O_2^{\bullet-} \rightarrow Fe^{2+} + O_2 \qquad \textbf{(Eq. 1.12)}$$

In fact, this reaction forms a part of what is now known as the Haber-Weiss reaction. Initially, it was first thought that $O_2^{\bullet-}$ reacts directly with H_2O_2 to form $^{\bullet}OH$ [100]. However, such a reaction has a rate constant of almost zero. The formation of $^{\bullet}OH$, from a system containing $O_2^{\bullet-}$ and H_2O_2, requires catalysis by Fe^{3+}. The Haber-Weiss net reaction is shown below.

Net Reaction: $O_2^{\bullet-} + H_2O_2 \xrightarrow{\text{Fe (III)}} O_2 + {}^{\bullet}OH + OH^-$ **(Eq. 1.13)**

$O_2^{\bullet-}$ also reacts with reactive nitrogen species (RNS) such as nitric oxide ($^{\bullet}NO$) to form peroxynitrite ($ONOO^-$), a non-radical that can destroy Fe-S-containing proteins, or directly modify proteins (e.g. the 3-nitrotyrosine (3-NT) protein modification, **section 1.2.4.2**)[101]**.**

1.2.2.4. Peroxynitrite

As mentioned previously, $ONOO^-$ is formed when $^{\bullet}NO$ reacts with $O_2^{\bullet-}$ [92]. This reaction has a high rate constant ($k = 7 \times 10^9\ M^{-1}\ s^{-1}$) [92]. Addition of SOD to a system containing $O_2^{\bullet-}$, can attenuate the formation of $ONOO^-$. As $^{\bullet}NO$ has a relatively long half-life (about 1s), $ONOO^-$ formation is generally formed near sites of $O_2^{\bullet-}$ production [102].

$$^{\bullet}NO + O_2^{\bullet-} \rightarrow ONOO^- \ (k \approx 7 \times 10^9\ M^{-1}\ s^{-1}) \qquad \textbf{(Eq. 1.14)}$$

$ONOO^-$ reacts with Tyr protein residues forming 3-NT **(section 1.2.4.2)**. Such nitration reactions can affect the activity of antioxidant enzymes such as glutamine synthetase [103], and gluthathione reductase **(section 1.2.4.2, Figure 4.19)** [104]**.** In addition, $ONOO^-$ can attack Cu transport proteins such as ceruloplasmin, thus releasing Cu ions [105]. Later in chapter 4, $ONOO^-$ was synthesised and used to nitrate BSA prior to its use as a positive control in the 3-nitrotyrosine western blotting studies **(section 4.2.7.1)**.

1.2.3. Detection of reactive oxygen species and free radicals by fluorescent probes

Generally speaking, free radical species have short half-lives as they can react rapidly with biomolecules or other free radicals **(section 1.2.1.1)**. As such, free radicals and ROS can be difficult to detect. For example, detection of $O_2^{\bullet-}$ can be challenging due to its rapid dismutation by SOD 1 **(section 1.2.7.2.1)**. SOD 2 is abundant near sites where $O_2^{\bullet-}$ is produced (i.e. mitochondria; **section 1.2.7.2.2**). Fluorescence detection, used in conjunction with suitable probes, can be used to measure ROS such as H_2O_2 and $O_2^{\bullet-}$ [106]. These probes have been used in conjunction with flow cytometry [108, 109]. A discussion of the fluorescent probes used in this work, and their limitations, will be discussed presently.

1.2.3.1. Amplex Red

N-Acetyl-3,7-dihydroxyphenoxazine (Amplex Red) is a fluorescent probe utilised for the detection of H_2O_2 [109]. Amplex Red was used in this work for the detection of extracellular [H_2O_2] produced from cellular systems in chapter 3 **(section 3.3.1.5)**. In the presence of horseradish peroxidase (HRP) and H_2O_2, Amplex Red forms resorufin (λ ex/em 563/587 nm; **Figure 1.4**) [110]. Amplex Red reacts with H_2O_2 in the presence of HRP [111].

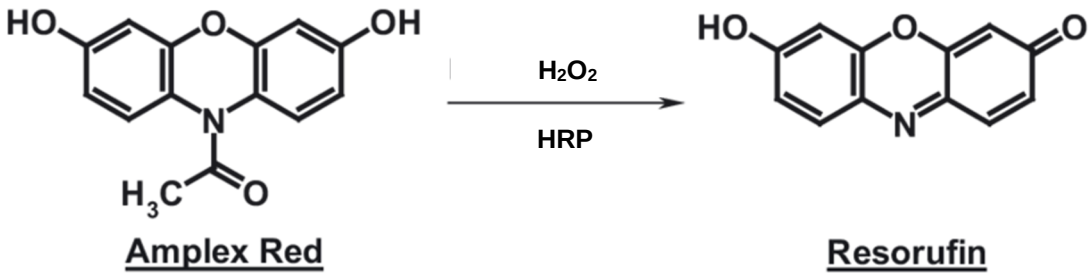

Figure 1.4. Horseradish peroxidase-catalysed oxidation of Amplex Red to resorufin by H_2O_2. Amplex Red is oxidised to resorufin by H_2O_2 in a HRP catalysed reaction**.** Amplex red is non fluorescent, whilst resorufin is fluorescent (λ ex/em 563/587 nm).

Addition of catalase **(section 1.2.7.2.3)** to a reaction mixture of HRP and H_2O_2 prevents the formation of resorufin from Amplex Red [110]. $O_2^{\bullet-}$ does not oxidise Amplex Red to resorufin [110]. However, HOCl may react with Amplex Red to form resorufin, but only at very high concentrations (1 mM) [110]. Other methods for the detection of H_2O_2, such as the HRP-catalysed oxidation of scopoletin, are about 10 times less sensitive than the Amplex Red detection method under the same conditions. The Amplex Red detection method has a lower detection limit of about 50 nmol H_2O_2 [109].

1.2.3.2. Dihydroethidium and MitoSOX

Dihydroethidium (DHE) (also known as hydroethidine) is a fluorescent probe utilised for $O_2^{\bullet-}$ detection. DHE was used in this work for the detection of cellular ROS generation in chapter 3 **(section 3.3.5)**. The reaction between DHE and $O_2^{\bullet-}$ generates 2-hydroxy ethidium (2-OH-E^+; λ ex/em of 520/590 nm; **Figure 1.5)**. This is the only product formed when $O_2^{\bullet-}$ reacts with DHE [112]. However, ethidium (E^+) can also be formed from DHE in a non-$O_2^{\bullet-}$ dependent reaction **(Figure 1.5)**.

In addition, there is a mitochondria-targeted version of DHE known as Mito-DHE (commercially sold as MitoSOX). MitoSOX Red was used in chapter 3 to detect mitochondrial ROS **(section 3.3.4).** The chemical structure of MitoSox Red is modified by conjugating DHE to a triphenylphosphonium cation (TPP^+) moiety. This allows MitoSOX to accumulate rapidly into mitochondria due to the positive charge on the TPP^+ moiety. The reaction between $O_2^{\bullet-}$ and MitoSOX forms 2-OH-Mito-E^+, a product very similar in structure, and in fluorescence characteristics, to 2-OH-E^+.

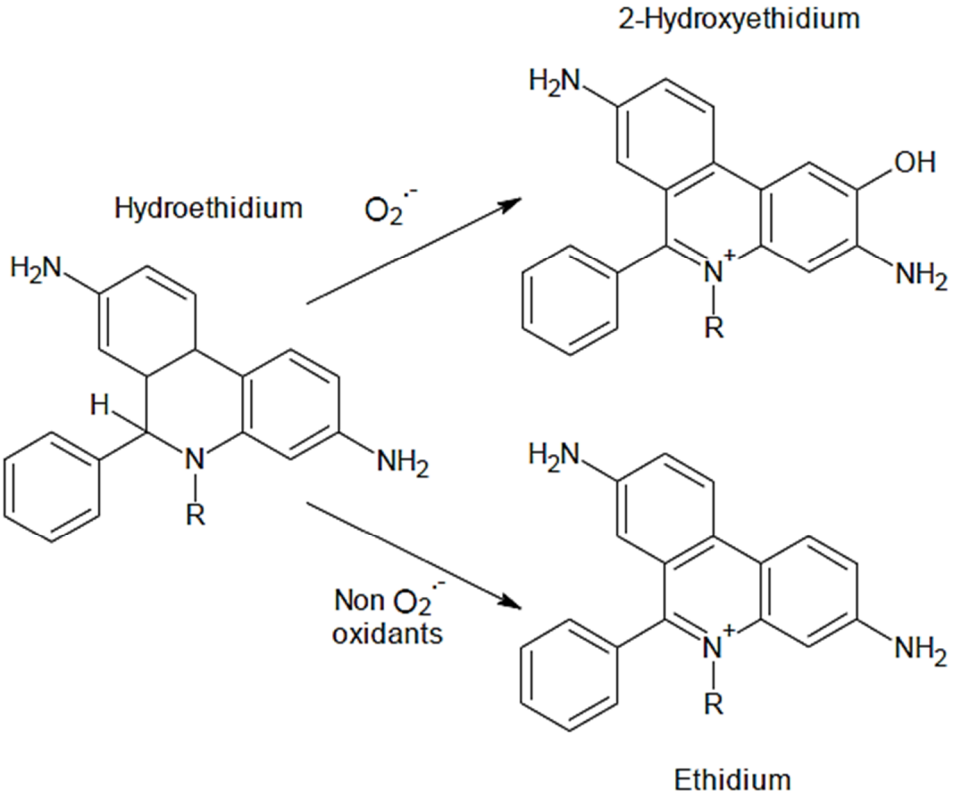

Figure 1.5. The oxidation of dihydroethidium to 2-hydroxy-ethidium or ethidium. Hydroethidium (left) can be oxidised by either non-$O_2^{\bullet-}$ oxidants or $O_2^{\bullet-}$. When reacting with $O_2^{\bullet-}$, 2-hydroxy-ethidium is formed (top right). When reacting with non-$O_2^{\bullet-}$, ethidium is formed (bottom right).

Unfortunately, both 2-OH-E^+ and E^+ share very similar emission profiles when excited at 488 nm (λ ex/em 488/590 nm vs 488/610 nm). As such, the emission signal of 2-OH-E^+ and E^+ cannot be easily distinguished by fluorescence detection alone [112]. About 40% of the 2-OH-E^+ signal measured at 488/567nm overlaps with the E^+ emission under the same conditions [112]. Separation of the DHE and MitoSOX end products by high-performance liquid chromatography (HPLC) is necessary in order to determine the specificity of these probes for $O_2^{\bullet-}$

.As such, the data generated in this thesis using DHE and MitoSOX are discussed in context of ROS detection and not $O_2^{\bullet-}$ specifically.

1.2.3.3. 2', 7'-dichloro-dihydro-fluorescein diacetate

2',7'-dichloro-dihydro-fluorescein diacetate (DCFHDA) is a fluorescent probe often utilised for the measurement of ROS in cellular systems [106]. DCFHDA is converted to 2', 7'-dichloro-dihydro-fluorescein (DCFH) by cellular esterase where it accumulates within the cytoplasm. When DCFH reacts with ROS, it can form 2', 7'-dichloro-fluorescein (DCF; λ ex/em 488/525) [106].

Neither peroxides, nor $O_2^{\bullet-}$ oxidise DCFH rapidly [113]. However, other ROS such as $RO_2^{\bullet}$, $RO^{\bullet}$, $NO_2^{\bullet}$, $RS^{\bullet}$, and $^{\bullet}OH$ radicals can do so [113]. The formation of these radicals (the $^{\bullet}OH$ radical especially) requires transition metal ions for their generation **(section 1.2.2.1)**. The fluorescence of DCF therefore depends on multiple inputs: esterase activity, transition metal ion availability and [ROS]. Additionally, it has been reported that DCFH can be oxidised by cytochrome c [113]. DCFH can also undergo one-electron oxidation by various ROS to produce the DCF phenoxyl radical [113]. This can cause further ROS generation through reactions with GSH, ascorbate, and NADH [113]. For example, the DCF phenoxyl radical can react with GSH to form the glutathione thiyl radical [114]. Additionally, the DCFH radical can reduce O_2 to $O_2^{\bullet-}$. As such, DCFHDA cannot be employed to measure individual ROS specifically [114]. In chapter 3, DCFHDA was utilised to measure general cellular oxidative stress **(section 1.2.4)** in chapter 3 **(section 3.3.6)**.

1.2.4. Oxidative stress

Oxidative stress is an imbalance between the production and removal of free radicals/ROS/RNS resulting in damage to biological systems [115]. Cellular antioxidant defences defend against oxidative stress **(section 1.2.7).** The major targets of oxidative stress-induced damage are lipids, DNA and proteins [116]. However, lipid peroxidation will be discussed in detail as it is most relevant to the present work.

1.2.4.1. Lipid peroxidation

The membranes of sub-cellular organelles (e.g. mitochondria and peroxisomes), in addition to the cellular plasma membrane itself, contain large quantities of polyunsaturated fatty acid (PUFA) lipid side chains [117]. The most common lipids found in cell membranes are glycerol based phospholipids [118].

Cellular membranes also contain variable amounts of protein, depending on the type of membrane and its function [118]. As such, membranes that are susceptible to lipid peroxidation are also susceptible to protein damage. The end result of lipid peroxidation is a decrease in membrane fluidity. This makes it easier for substances to cross that would normally be impeded due to charge or size (e.g. Ca^{2+}). Additionally, fragmentation of the subcellular and cellular membranes can also occur. This can result in the release of toxic hydrolytic enzymes which can amplify cellular damage [91].

Lipid peroxidation occurs in three main stages: initiation, propagation and termination [118]. Initiation of lipid peroxidation occurs via the abstraction of the allylic hydrogen atom from the methylene group ($-CH_2-$) of a PUFA by an oxidising agent [91]. PUFAs are susceptible to lipid peroxidation due to being unsaturated i.e. in possession of carbon-carbon double bonds. For example, PUFA can be readily oxidised by free radicals such as $^{\bullet}OH$, $HO_2^{\bullet}$, $RO^{\bullet}$ and $RO_2^{\bullet}$ [119]. $^{\bullet}OH$ scavengers, such as mannitol and formate, inhibit the induction of lipid peroxidation by $^{\bullet}OH$ [118]. Hydrogen abstraction results in the formation of an alkyl radical ($-C^{\bullet}H$) [118].

$$-CH_2- + {}^{\bullet}OH \rightarrow -C^{\bullet}H- + H_2O \qquad \textbf{(Eq. 1.15)}$$

Once $-C^{\bullet}H$ is formed, molecular re-arrangement (known as isomerisation) occurs. During this process, the carbon centred radical stabilises by changing the position of its free electron along the carbon chain. This forms an unsaturated hydrocarbon containing a carbon-carbon double bond i.e. a conjugated diene [91].

O_2 is critical for the propagation step of lipid peroxidation **(Figure 1.6)**. O_2 reacts with carbon centred radicals forming the lipid peroxyl radical ($LO_2^{\bullet}$). $LO_2^{\bullet}$ then propagates the lipid peroxidation reaction by abstracting a hydrogen atom from the adjacent carbon forming a lipid hydroperoxide (L-OOH) **(Figure 1.6)**. The

number of L-OOH formed depends on the type of fatty acid. Linolenic acid yields four L-OOH, and docosahexaenoic acid yields ten L-OOH per chain [120].

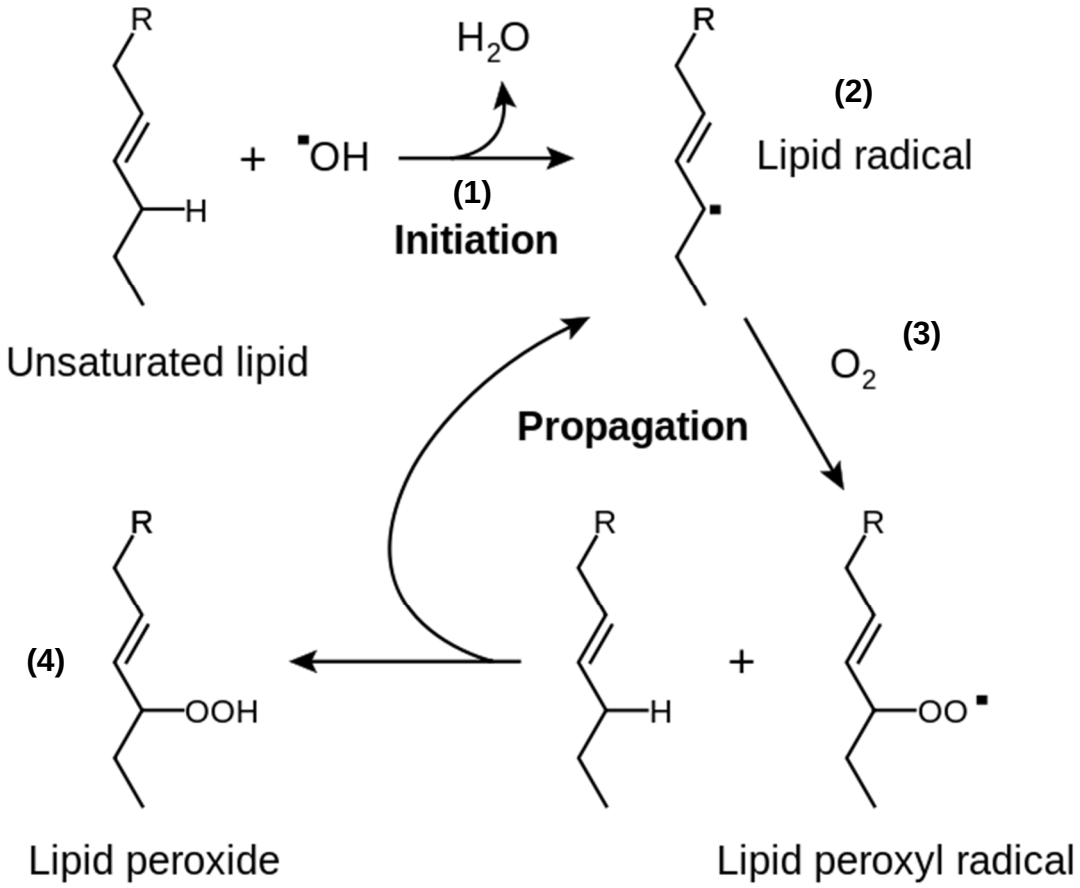

Figure 1.6. The stages of lipid peroxidation. (1) The abstraction of a hydrogen atom from an allylic carbon results in the formation of an alkyl radical. **(2)** The free electron changes position along the lipid chain (isomerisation). **(3)** O_2 then reacts with the alkyl radical to form a lipid peroxyl radical. **(4)** Lipid hydroperoxide are formed when the peroxyl radical abstracts a hydrogen from the adjacent carbon. Lipid hydroperoxide are unstable and are prone to degradation, β scission of a lipid hydroperoxide results in the formation of fatty acid alcohols, ketones and aldehydes. Adapted from [121].

L-OOH decompose into lipid alkoxyl radical ($LO^{\bullet}$), in the presence of transition metal ions such as Fe^{2+}, which splits the O-O bond **(Eq. 1.16)**.

$$L\text{-}OOH + Fe^{2+} \rightarrow Fe^{3+} + OH^{-} + L\text{-}O^{\bullet} \qquad \textbf{(Eq. 1.16)}$$

L-OOH can also undergo β-scission to form fatty acid alcohols, ketones and aldehydes [122].

The termination of lipid peroxidation occurs when two $-C^{\bullet}H$ react forming a non-radical product.

Lipid peroxidation can produces toxic end products which can have further deleterious effects. Malondialdehyde (MDA) and 4-hydroxynonenal (HNE) are

produced from L-OOH leading to mutagenic and cytotoxic effects within the cell [123]. MDA can cause DNA/protein crosslinking and frameshift/point mutations in DNA [91]. HNE at high concentrations (20–100 µM) can inhibit protein synthesis and stimulate cell death via glutathione depletion [123].

1.2.4.2. Protein modifications induced by nitrative stress

Oxidative stress can cause protein damage in biomolecules such as receptors, and enzymes. Protein modification by free radicals can occur via carbonylation and nitration reactions. Carbonylation arises from the oxidation of amino acid side chains. Lysine, arginine and proline residues can be carbonylated either by H_2O_2, whilst HNE **(section 1.2.4.1)** carbonylates cysteine, histidine and lysine residues. Carbonylation reactions can inactivate key antioxidant enzymes such as catalase and SOD 1 [124]. Although protein damage is a key consequence of oxidative stress, it is not relevant to the present work. The most relevant protein modification is the 3-NT protein modification which is discussed in the following section.

1.2.4.2.1. 3-Nitrotyrosine

3-NT is formed when $ONOO^-$ (**section 1.2.2.4**) reacts with Tyr residues found in protein or free in solution [125]. Only about 15% of Tyr residues face inward toward the protein core [125]. This renders many proteins with outward facing Tyr residues susceptible to protein nitration [125].

The nitration of Tyr has been reported to be a measure of $ONOO^-$-mediated cellular damage [126]. $ONOO^-$-mediated damage has been detected in blood plasma in disease states such as rheumatoid arthritis, atherosclerosis, multiple sclerosis, and asthma [126]. $ONOO^-$-mediated damage is associated with higher expression levels of protein exhibiting the 3-NT protein modification [126]. SOD and NOS inhibitors attenuate the formation of 3-NT [127]. This suggested that $ONOO^-$ mediates the formation of 3-NT protein modifications [127]. Although the formation of 3-NT in protein is believed to be correlated with $ONOO^-$-mediated damage, it may also be formed through reactions involving HOCl, nitrogen dioxide ($NO_2^\bullet$), H_2O_2, and peroxidase enzymes *in vivo* [127, 128]. As such 3-NT has been described more accurately as an indicator of ROS damage, rather than $ONOO^-$-mediated damage specifically [127].

The majority of nitrated protein within the cell is found within the mitochondria where $O_2^{\bullet-}$ is produced **(section 1.2.2.4)** [128]. As $O_2^{\bullet-}$ is required for $ONOO^-$ production, this may contribute to 3-NT formation in proteins present within the mitochondria [128].

Immunohistochemistry has been used to detect 3-NT in lung from cystic fibrosis, in bone from osteoarthritis, and in brain from Parkinson's disease [128, 130]. In addition, western blotting has been used to detect 3-NT in liver protein after acetaminophen-induced hepatotoxicity treatment, and in cardiac protein after cardiac arrest [126, 131]. In chapter 4, the expression levels of proteins containing the 3-NT modification were assessed by western blotting.

1.2.5. Programmed and non-programmed cell death

In order to maintain normal physiological function, damaged cells initiate programmed cell death. *In vivo*, this targets these cells for clearance by phagocytic cells such as macrophage. Two of the most well understood modes of cell death are programmed cell death (i.e. apoptosis), and non-programmed cell death (i.e. necrosis). These two modes of death are biologically distinct from one another and will be described presently.

However, the field of cell death has developed significantly in recent years. There are now at least 12 major cell death subroutines including anoikis (loss of integrin dependent anchorage), parthanatos (poly-ADP-ribose polymerase 1 hyper activation and DNA degradation), and pyroptosis (gasderdin-dependent plasma membrane pore formation)[131]. Additionally, another form of iron-dependent cell death known as ferroptosis has been identified which differs morphologically from necrosis and apoptosis [124].

However, for the purposes of relevancy, only apoptosis, and necrosis will be discussed in detail. Apoptosis and necrosis were measured in chapter 3 using annexin V-FITC and PI staining in conjunction with flow cytometry **(section 2.4)**.

1.2.5.1. Morphological distinctions between apoptosis and necrosis

Kerr et al. [132] described an energy-dependent form of cell death known as apoptosis that was morphologically distinct from necrosis. In the early stage of apoptosis, the cell shrinks exhibiting a dense cytoplasm with compacted organelles [133]. The nucleus also shrinks and the chromatin condenses

(pyknosis). The apoptotic cell has a dark eosinophilic cytoplasm with dense purple chromatin fragments. Following this, the plasma membrane 'blebs' followed by nuclear fragmentation (karyorrhexis; **Figure 1.7)**. Eventually, membrane bound cellular fragments, known as apoptotic bodies, form **(Figure 1.7)**. Phosphatidylserine (PS) is normally kept in equilibrium across the inner and outer membrane by the Ca^{2+}-dependent enzyme phosphatidylserine scramblase [133]. During apoptosis, PS externalisation predominates over internalisation. PS acts as a phagocytic signal for macrophage [133]. Alteration of the PS equilibrium is utilised for the detection of apoptotic cells by annexin V-FITC **(section 2.4.1).**

During this time, the plasma membrane is still intact [133]. *In vivo,* these cells would normally be phagocytosed by macrophage **(Figure 1.7)**. At no point does the apoptotic cell, or the associated apoptotic bodies, rupture [133]. As such, apoptosis *in vivo* generally does not cause inflammation or secondary necrosis in the surrounding tissue. The engulfing cells also do not, in general, produce an inflammatory reaction [134].

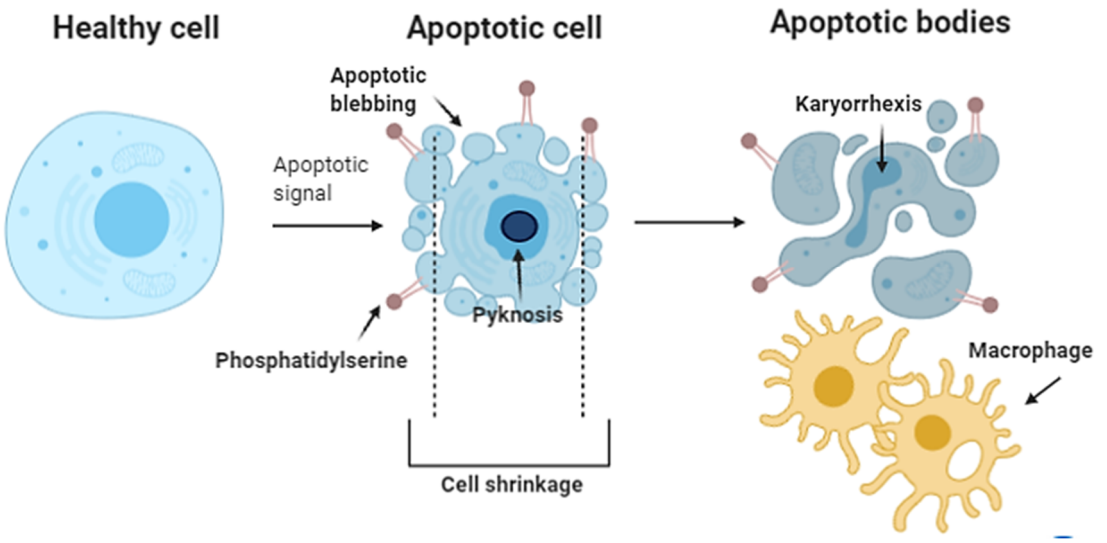

Figure 1.7. Morphological changes that occur during apoptosis. Cells exposed to cytotoxic agents exhibit apoptotic blebbing. Phosphatidylserine equilibrium is affected resulting in phosphatidylserine externalisation. Chromatin also irreversibly condenses in a process called pyknosis. The cell also shrinks. After this, the apoptotic bodies break away from the membrane to form independent apoptotic bodies which also express external phosphatidylserine residues. The nuclear membrane fragments in a process known as karyorrhexis. *In vivo*, these apoptotic bodies are phagocytosed by macrophage. Image made using www.Biorender.com.

While apoptosis is programmed and energy-dependent, necrosis is an un-programmed process that is energy-independent. Necrosis is initiated by physical trauma, blood vessel damage or ischaemia [135]. Necrosis is also characterised by large numbers of cells dying at once, whereas apoptosis can select single cells from a population to initiate the cell death pathway.

Necrosis has a few morphological distinctions from apoptosis including karyorrlysis (dissolution of nuclear compartment), disruption of the cellular plasma membrane, and the membranes of organelles. This leads to the release of cytoplasmic components into the extracellular milieu causing an inflammatory response *in vivo* **(Figure 1.8)** [136]. The loss of membrane integrity occurs in necrosis, but not in apoptosis.

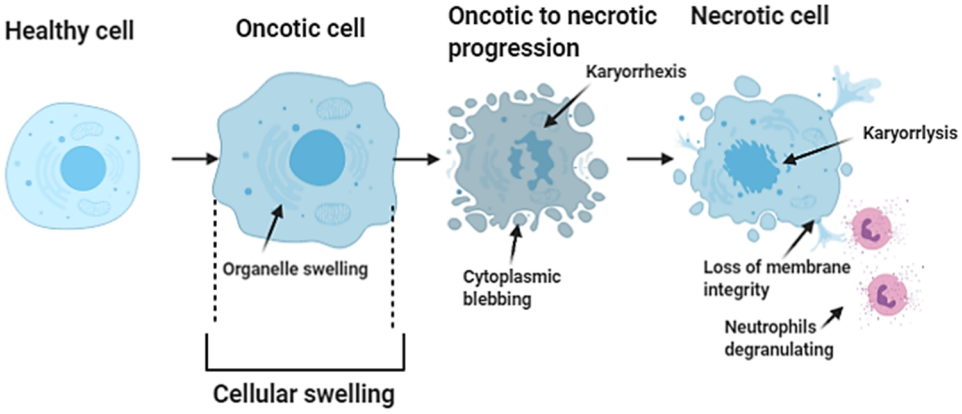

Figure 1.8. Morphological changes that occur during necrosis. A healthy cell is hit by a sudden shock signal or stimulus that results in swelling of the cytoplasm and sub cellular organelles. Necrosis is characterised by cytoplasmic blebbing, loss of nuclear and cytoplasmic integrity and release of the constituents of these internal compartments into the extracellular environment. This results in an inflammatory response *in vivo*, recruiting cells such as neutrophil to the site of damage. Image made using www.Biorender.com.

1.2.5.2. Apoptotic pathways

There are two main pathways leading to the induction of apoptosis. The intrinsic pathway **(section 1.2.5.2.1)**, and the extrinsic pathway **(section 1.2.5.2.2)**.

1.2.5.2.1. Intrinsic apoptosis

The intrinsic pathway is initiated in the mitochondria which contains compartments separated by internal lipid membranes. The inner mitochondrial membrane contains the mitochondrial matrix, and the outer mitochondrial membrane separates the extracellular space from the internal matrix. The space between these two membranes is known as the inter-membrane space.

Apoptotic insult results in the permeabilisation of the mitochondrial membrane. This causes a loss of mitochondrial membrane potential (ψ_m) [137]. Ψ_m is an electrochemical potential that is maintained across the inner mitochondrial membrane to facilitate oxidative phosphorylation [137]. The mitochondrial membrane potential (with the interior of the organelle being electronegative), under normal conditions, facilitates an inward transport of cations and outward transport of anions. As such, cations accumulate in the interior of the mitochondria. This electrochemical gradient facilitates ATP synthesis. However, during apoptosis, ψ_m decreases due to the opening of permeability transition pores [137]. As the mitochondria loses ψ_m, H_2O diffuses into the mitochondria

resulting in mitochondrial swelling. Ψ_m is measured in chapter 3 using flow cytometry in conjunction with JC-1 **(section 3.2.7)**.

$\Delta\psi_m$ initiates intrinsic apoptosis by facilitating the release of apoptotic factors from the inner mitochondrial space. These factors include cytochrome c, apoptosis inducing factor (AIF), endonuclease G, the mitochondrial serine protease Omi/HtrA2, and second mitochondria-derived activator of caspases (smac) /DIABLO **(Figure 1.9)**. When cytochrome c is released it binds to apoptotic peptidase-activating factor 1 (Apaf-1) forming the apoptosome [131]. Procaspase-9 then binds to the 'apoptosome' and becomes activated **(Figure 1.9)**. The apoptosome then cleaves pro-caspase 3 into active caspase 3. Bcl-2, an important regulator of apoptosis, induces and inhibits apoptosis. Bcl-2 can regulate the release of cytochrome c from the inner mitochondrial space by inhibiting the pro-apoptotic proteins Bax and Bak **(Figure 1.9)**. Another important pro-apoptotic molecule is p53, which is normally regulated and targeted for ubiquitination via mouse double minute 2 [138]. p53 promotes the release of pro-apoptotic factors such as Bax [138]. Omi/HtrA2 and Smac/DIABLO inhibit the initiation of apoptosis by preventing procaspase-9 activation.

This end-point of the intrinsic pathway is the activation of caspase 3, and the initiation of the execution pathway. The execution pathway involves the cleavage of substrates such as the nuclear protein NuMA, the plasma membrane cytoskeletal protein alpha fodrin, poly (ADP-ribose) polymerase, as well as the inhibitor of caspase–activated DNase (ICAD).

1.2.5.2.2. Extrinsic apoptosis

The extrinsic pathway involves the activation of transmembrane 'death' receptors which are part of the tumour necrosis factor (TNF) receptor gene superfamily. TNF death receptors have conserved cysteine-rich domains known as "death domains" **(Figure 1.9)**. This domain transmits a 'death signal' through a number of different pathways [133]. Described below is the extrinsic apoptotic pathway for FasL/FasR.

Binding of FasL to its receptor FasR results in the recruitment of the adaptor molecule Fas-associated death domain (FADD) and caspase 8 to the intracellular portion of the FasR receptor [133]. This complex is known as the death-inducing

signalling complex (DISC) **(Figure 1.9)**. Upon recruitment, caspase 8 is activated and initiates apoptosis by cleaving pro-caspase 3 into its active form [133]. The caspase 8 modulatory protein FLICE-inhibitory protein (FLIP) inhibits activation of pro-caspase 8 by DISC [133]. Activated caspase 3 then induces the execution pathway. This results in changes to cellular morphology including cell shrinkage, karyorrhexis and the formation of apoptotic bodies [133]. Caspase-8 also cleaves the pro-apoptotic protein Bid to truncated (Bid). tBid inhibits Bcl-2 and Bcl-xl. This allows Bax and Bak, normally inhibited by Bcl-2 and Bcl-xl, to translocate to the OMM where they promote cytochrome c release [133]. The signalling of tBID represents a cross-over between the extrinsic and intrinsic pathway **(Figure 1.9)**.

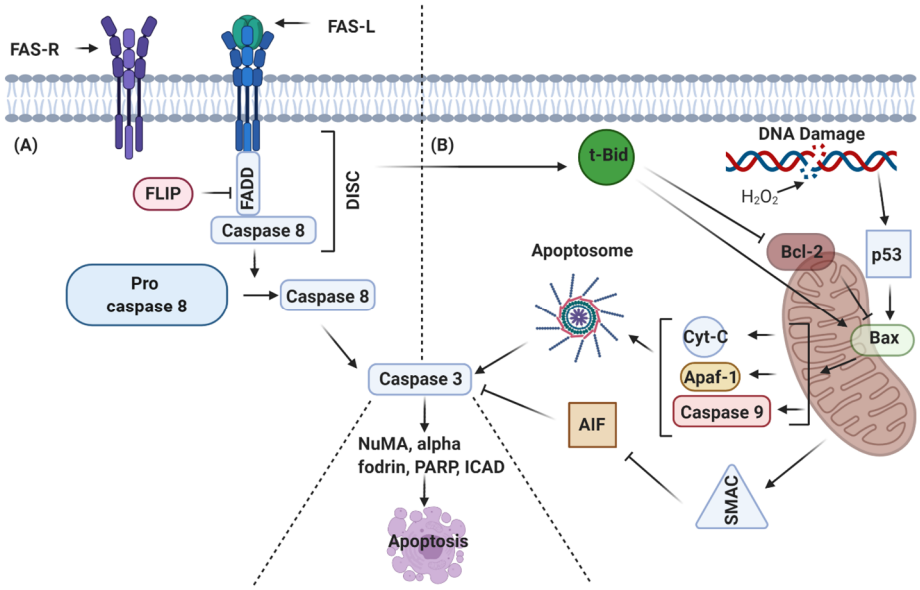

Figure 1.9. Intrinsic and extrinsic apoptotic signalling pathways. Panel (a), Extrinsic apoptosis. Stimulation of the FAS-R receptor by its ligand FAS-L results in the recruitment of adaptor molecules such as FADD and caspase 8 to the intracellular domain. This complex is known as DISC which cleaves pro-caspase 8 into active caspase 8. This complex can be inhibited by FLIP. Caspase 8 then activates caspase 3 and initiates the execution pathway. **Panel (b), Intrinsic apoptosis**: DNA damage by ROS induces p53 which activates Bax. Bax promotes mitochondrial permeabilisation and the subsequent release of cytochrome c, Apaf-1, and caspase-9 which form the apoptosome. The apoptosome then cleaves pro-caspase 3 into caspase 3. Smac acts as a pro-apoptotic molecule by inhibiting the anti-apoptotic action of AIF on caspase 3. There is cross-talk between these two pathways. t-Bid, which is first cleaved into its truncated form by the DISC complex, can promote cytochrome c release by inhibiting the anti-apoptotic protein Bcl-2. The endpoint of both pathways is the execution pathway wherein caspase-3 cleaves the nuclear protein NuMA, the plasma membrane cytoskeletal protein alpha fodrin, PARP as well as caspase activated endonuclease. **AIF:** Apoptosis inhibiting factor; **Apaf:** Apoptotic peptidase-activating factor 1; **Bax:** Bcl-2 like protein; **Bcl-2:** B cell lymphoma 2; **Cyt-C:** Cytochrome C; **DISC:** Death inducing signalling complex; **FADD.** Fas-associated protein with death domain; **Fas R/L.** Fas ligand/receptor; **FLIP:** FLICE inhibitory protein; **ICAD:** Inhibitor of caspase activated DNase; **NuMA:** Nuclear mitotic apparatus; **PARP:** Poly (ADP-ribose) polymerase; **t-BID:** Truncated p15 BID; **SMAC:** Second mitochondria-derived activator of caspase. Image made using www.Biorender.com.

1.2.5.2.3. Caspase

Cysteine-dependent aspartate-specific protease (caspase) are hydrolytic enzymes involves in both the intrinsic and extrinsic pathways of apoptosis **(Figure 1.9)**. Caspases are normally found in healthy cells in their zymogen form (procaspase) and are cleaved into an active form prior to the initiation of apoptosis. Caspase-3 has essentially no activity in a healthy cell until cleaved into its active form. This prevents unintentional activation of the apoptotic execution pathway **(section 1.2.5.2)** [139]. 14 different caspases have been found in humans, each of which contain the amino acid sequence Ala-Gln-Cys-X-Gly (where X represents one of the amino acids Arg, Gln or Asp) in the active site. Caspases specifically act after aspartic acid residues on their substrates.

There are two types of caspase: initiator caspases (2, 8, 9, and 10) and effector caspases (3, 6 and 7). Pro-caspases have three domains which include an N-terminal pro-domain, a large P-20 domain, and a smaller P-10 domain. The active forms of caspases are composed of heterodimers of the P-20/P-10 domains.

Pro-caspase activation occurs via proteolytic cleavage through autocatalytic activation. Effector pro-caspases such as pro-caspases 3, 6 and 7, are cleaved at aspartic acid residues between the N terminal pro-domain and the P-20 domain, and between the P-20 domain and the P-10 domain [140].

1.2.6. Induction of oxidative stress by redox-active compounds

Oxidative stress can be induced in at least two ways. First: exogenous treatment with ROS (i.e. H_2O_2); second: inhibition of key antioxidant enzymes or proteins. In this work, oxidative stress was induced by inhibiting TrxR using auranofin **(section 1.2.6.1.1)**, H_2O_2 treatment **(section 1.2.6.2)**, inhibiting catalase using 3-AT **(section 1.2.6.2.1)** depleting GSH using L-BSO **(section 1.2.6.3.1)**, and by inducing lipid peroxidation using CuOOH or MSA **(section 1.2.6.4.1 and 1.2.6.4.2).**

1.2.6.1. Inhibition of thioredoxin reductase

As discussed previously, TrxR is an enzyme involved in the Trx antioxidant defence system **(Figure 1.18, section 1.2.7.2.7)**.

The Trx system is implicated in cancer pathogenesis [141]. For example, Trx expression is reported to be increased in various human cancers such as in lung, cervix, pancreas, colon, liver, stomach and breast cancer tissue [141]. Inoculation of mice with a transformed MCF-7 breast cancer cell line with a redox inactive Trx construct showed inhibition of tumour growth [142]. High expression levels of Trx protein is associated with resistance to anti-cancer chemotherapeutic compounds such as doxorubicin, cisplatin, docetaxel and tamoxifen [167–169]. Inhibition of TrxR may represent a promising avenue for adjunctive treatments in certain cancers.

1.2.6.1.1. Auranofin

Auranofin (2,3,4,6-tetra-*o*-acetyl-L-thio-β-D-glycopyranp-sato-*S*-(triethyl-phosphine)-gold) is a gold I thiolate which was approved for use in rheumatoid arthritis in 1985 [146]. It decreases blood IgG levels in rheumatoid arthritis patients with associated improvements in joint swelling [146]. Auranofin also inhibits selenium-dependent enzymes such as TrxR due to its high affinity for inorganic selenide (HSe^-) [146]. Displacement of the sulfur in the thiol of auranofin with the Se atom in selenide results in the inhibition of TrxR and the formation of an auranofin-selenium adduct and a hydrogen sulfide by-product [147]. Auranofin inhibits both the cytosolic and mitochondrial forms of TrxR [147]. Auranofin may also inhibit the ubiquitin proteasome system through inhibition of the 19S proteasome-associated deubiquitinase [148]. New and more specific inhibitors of TrxR are currently in development [149].

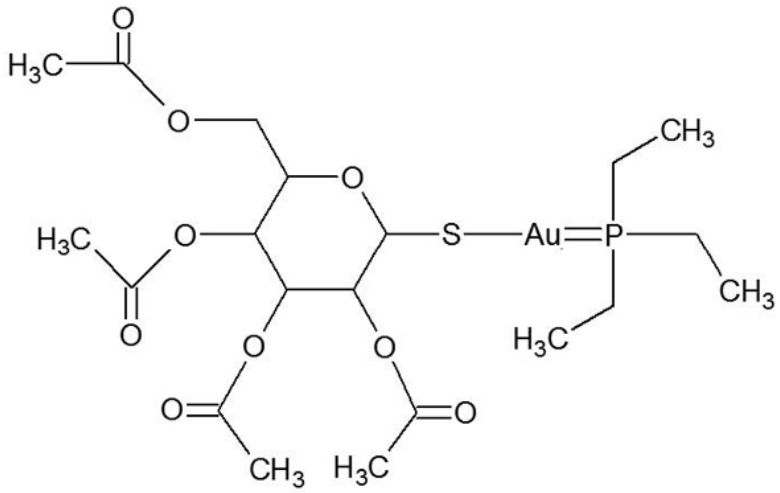

Figure 1.10 Chemical structure of auranofin.

Auranofin has been shown to induce the expression of the Nrf-2-target protein HO-1 in human primary astrocyte and U-373 MG astrocytic cells [150]. The cytotoxicity of auranofin can be augmented through co-treatment with selenocysteine which competes for the active site of TrxR with Trx [151]. Auranofin is currently being investigated in a phase II clinical trial for the treatment of ovarian cancer [152]. In chapter 3, auranofin-induced cell death was measured in A431 cells grown in 18.6% O_2 or 3.0% O_2 **(section 3.3.2).**

1.2.6.2. Hydrogen peroxide

As discussed in **section 1.2.2.2**, H_2O_2 is a ROS which is not very reactive [90]. Much of the damaging effects of H_2O_2 are due to $^{\bullet}OH$ radical.

H_2O_2 readily diffuses down its concentration gradient across the cellular membrane. This makes it more suitable a signalling molecule compared to $^{\bullet}OH$ which has a short half-life (10^{-9} s) under normal physiological conditions [153]. H_2O_2 is thought to be involved in the modification of proteins such as the mitochondrial enzyme aconitase (TCA cycle), α-ketoglutarate dehydrogenase (Kreb's cycle) and complex I in the ETC [154]. The regulation of protein modifications by ROS is controlled by enzymes such as glutaredoxin and sulfiredoxin. These enzymes catalyse the reduction of proteins subject to glutathionylation or cysteine oxidation, respectively [154]. H_2O_2 also activates Nrf-2 [155] and is a classical inducer of oxidative stress-induced cell death [156]. In chapter 3, H_2O_2-induced cell death was measured in A431 cells grown in 18.6% O_2 or 3.0% O_2 **(section 3.3.1).**

1.2.6.2.1. Inhibition of catalase by 3-amino-1, 2, 4-triazole

As discussed in **section 1.2.7.2.3**, catalase is an antioxidant enzyme which catalyses the dismutation of two molecules of H_2O_2 into H_2O or O_2.

Catalase is inhibited by azide, cyanide, $ONOO^-$, and HOCl [157]. However, these are non-specific inhibitors of catalase. A more specific inhibitor of catalase is 3-AT [157]. 3-AT is a heterocyclic organic compound with a 1, 2, 4 triazole substituted to an amino group **(Figure 1.11)** [158]. 3-AT actually inhibits catalase complex I which is formed when catalase reacts with H_2O_2 **(Eq.1.26)**. H_2O_2 is therefore required for 3-AT-mediated inactivation of catalase [158]. The

mechanism of this inactivation involves a modification of His74 in the catalase active site.

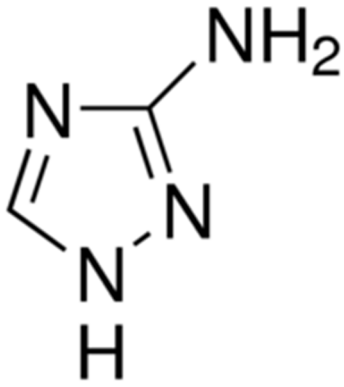

Figure 1.11. Chemical structure of 3-amino-1, 2, 4-triazole

Inhibition of catalase with 3-AT induces oxidative stress. *In-vivo* studies in goldfish showed a decrease in brain catalase activity when administered 1 mg 3-AT per gram of body tissue [159]. Rabbits injected intravenously with 4 mL of 3-AT (from a 3 M stock solution) per kilogram of body tissue, followed by an intracameral injection of H_2O_2 showed evidence of swollen ciliary processes, vessel dilation, alteration of the pigment epithelium and corneal endothelial damage after 24 h [160]. H_2O_2 treatment alone, however, resulted in only minor morphological changes [160]. This indicated that catalase played a key protective role *in-vivo* against peroxide mediated cellular damage.

The rate to which 3-AT inhibits catalase is dependent on [H_2O_2] [157]. Due to this particular nuance, 3-AT has been used to selectively assay for H_2O_2 generation in mammalian cells and organs [161]. In chapter 3, 3-AT was used to sensitise A431 cells to H_2O_2-induced cell death **(section 3.3.1.2).**

1.2.6.3. GSH depletion

As discussed in **section 1.2.7.2.4**, GSH is an important antioxidant protein which participates in ROS detoxification. The depletion of GSH is thought to sensitise some cancer cells to chemotherapeutic/ionising radiation approaches making it a promising adjunctive therapeutic avenue [162]. However, the selective depletion of GSH within cancer tissue is a significant technical issue due to the deleterious effects of GSH depletion on surrounding healthy tissue [163].

1.2.6.3.1. L-buthionine sulfoximine

L-BSO **(Figure 1.12)** is a synthetic amino acid which inhibits γGCS, an enzyme involved in GSH synthesis **(Figure 1.15)**. Inhibition of γGCS depletes cellular GSH. L-BSO–mediated depletion of GSH sensitised cells to further oxidant treatment [181, 182].

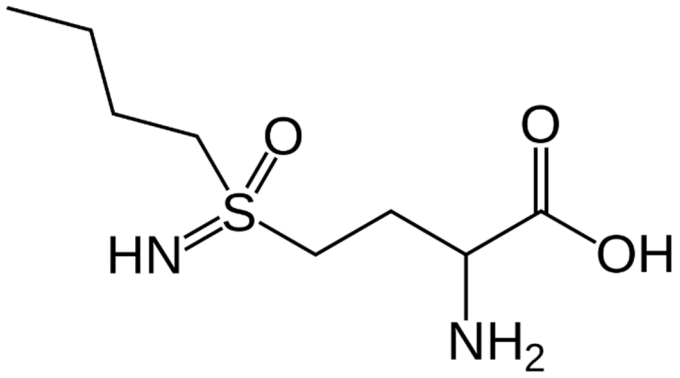

Figure 1.12. Chemical structure of L-BSO

L-BSO depleted intracellular GSH in the B16 mouse melanoma cell line [166]. Mice treated with L-BSO after inoculation with melanoma cells, showed improved survival and decreased evidence of tumour metastasis [166]. L-BSO may represent a particularly promising therapeutic avenue for the treatment of multiple myeloma also [167]. Depletion of GSH by L-BSO enhanced the efficacy of the chemotherapeutic agent melphalan in a pre-clinical model of multiple myeloma [167]. The depletion of GSH however has been shown to severely alter cellular redox homeostasis within mammalian cells, rendering cellular systems susceptible to further oxidant treatment [167]. There are numerous reports detailing the protective effects of glutathione against oxidative-stress induced cell death [184, 237–239]. For example, porcine intestinal endothelial cells pre-treated with N-acetyl cysteine (NAC; GSH precursor) prior to zearalenone treatment (a nonsteroidal estrogenic mycotoxin) were protected from oxidative-stress-induced cell death [168]. Depletion of GSH by L-BSO sensitised mammalian cells to oxidative-stress induced cell injury and induced ROS generation [181,240]. L-BSO also potentiated the efficacy of redox-active treatments such as photodynamic irradiation in a cell culture model of skin cancer [172]. In chapter 3, L-BSO was used to sensitise cells grown in 18.6% or 3.0% O_2 to H_2O_2-induced cell death through GSH depletion **(section 3.3.1.3 and 3.3.1.4).**

1.2.6.4. Induction of lipid peroxidation

As discussed in **section 1.2.4.1**, lipid peroxidation occurs as a result of oxidative damage to lipid membranes. Unlike apoptosis, which is a response of the cell to overwhelming cell damage, lipid peroxidation is a direct consequence of oxidative damage and not a response to it.

1.2.6.4.1. Cumene hydroperoxide

Cumene hydroperoxide (CuOOH) is an organic hydroperoxide which induces lipid peroxidation [118]. CuOOH forms a cumoxyl radical in the presence of transition metal ions. The cumoxyl radical can then react with PUFA to form α-cumyl alcohol and lipid radical **(Figure 1.13)** [118]. In addition, the cumoxyl radical can react with CuOOH to form a cumoperoxyl radical which can readily oxidise PUFA. The cumoperoxyl radical can also react with O_2 to reform the cumoxyl radical thereby propagating lipid peroxidation via a chain reaction**.**

CuOOH induces lipid peroxidation in a variety of cell types and subcellular compartments, such as A431 cells, cervical cancer cells (HeLa), C6 glioma cells, and rat liver microsomes [36, 185, 186]. Progression of lipid peroxidation is controlled by the activity of antioxidant enzymes. Gpx **(section 1.2.7.2.5)** defends against lipid peroxidation by detoxifying hydroperoxide through the oxidation of GSH to GSSG [91]. The detoxification of hydroperoxide by Gpx therefore requires a ready supply of GSH. GR resupplies GSH from GSSG through a reduction reaction **(section 1.2.7.2.5).** Conversely, the inhibition of Gpx by compounds such as MSA **(section 1.2.6.4.2)** may attenuate cellular defence against lipid peroxidation [175]. In chapter 3, CuOOH was used to induce lipid peroxidation in A431 cells grown in 18.6% or 3.0% O_2 **(section 3.3.16).**

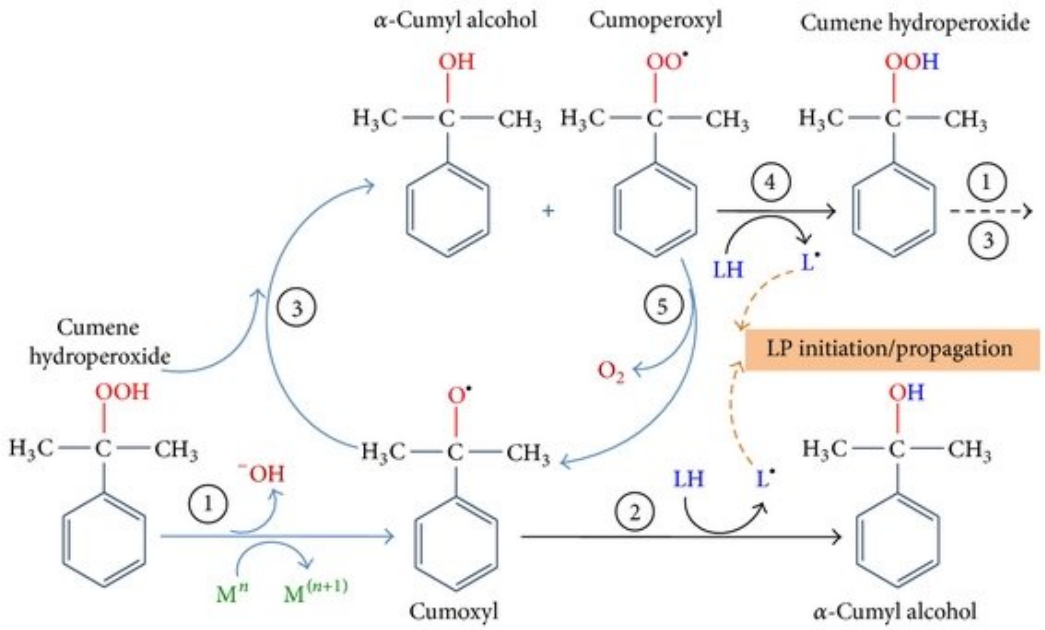

Figure 1.13. Mechanism of CuOOH-induced lipid peroxidation. (1) CuOOH, in presence of transition metal ions, produce cumoxyl radical, which oxidises LH through hydrogen abstraction resulting in the generation of **(2)** cumyl alcohol and L•. These products react readily with O_2 promoting the initiation or propagation of lipid peroxidation. **(3)** Cumoxyl radical react with another CuOOH molecule to yield cumyl alcohol and a cumoperoxyl radical. **(4)** Finally, cumoperoxyl radical may oxidise lipids through hydrogen abstraction to reform CuOOH and produce L•. L• can further propagate lipid peroxidation through chain reaction. **(5)** Cumoperoxyl radical can react with O_2 to yield a new cumoxyl radical thereby restarting the reaction. **CuOOH:** cumene hydroperoxide; **L•:** lipid radical; **LH:** lipid side chain; **LP:** Lipid peroxidation; **M:** transition metal ions (i.e. Fe^{2+} or Cu^{2+}). Image taken from [118].

1.2.6.4.2. Mercaptosuccinic acid

Mercaptosuccinic acid (MSA), also known as thiomalic acid, is a dicarboxylic acid containing a thiol functional group **(Figure 1.14)** [90]. MSA inactivates Gpx by reacting with the selenium atom in the selenocysteine active site in Gpx [176]. Inactivation of Gpx is thought to sensitise mammalian cells to lipid peroxidation [177].

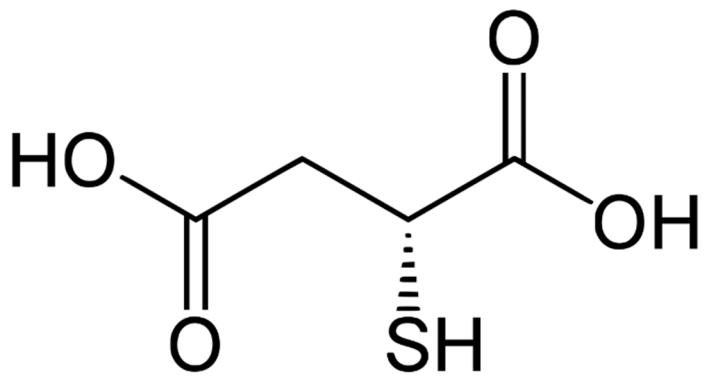

Figure 1.14. Chemical structure of mercaptosuccinic acid.

The inactivation of Gpx by MSA has been utilised for the treatment of rheumatoid arthritis [176]. Sodium gold MSA and sodium MSA supressed lymphocyte activation in rheumatoid arthritis [178]. MSA-mediated inhibition of Gpx decreased brain infarct damage produced by transient middle cerebral artery occlusion in rats [179]. This was attenuated by co-treatment with 3-AT indicating the requirement for catalase in MSA-mediated neuroprotection [179]. In chapter 3, MSA was used to sensitise cells to CuOOH-induced lipid peroxidation **(section 3.3.17 and 3.3.18).**

1.2.6.5. Carmustine

1,3-Bis(2-chloroethyl)-1-nitrosourea (carmustine) is currently the only FDA-approved intracerebral chemo-therapeutic agent for the treatment of newly diagnosed and recurrent malignant glioma [180]. Carmustine is an alkylating agent which interferes in cellular DNA replication [180]. Additionally, carmustine is also known to carbamylate lysine residues on proteins leading to their inactivation. For example, carmustine inhibits GR and therefore part of its mechanism of action can be described as being redox-related [193–195].

Unfortunately, the efficacy of carmustine is severely limited by oncogene such as Nrf-2. High Nrf-2 expression levels are associated with tumour resistance to cisplatin and temozolomide [196–200]. Human malignant glioma cells (U87MG) overexpressing Nrf-2 resisted carmustine-induced cell death compared to U87MG cells expressing normal expression levels of Nrf-2 protein [189]. Pre-treatment of U87MG cells with NAC attenuated carmustine-induced cell death suggesting a ROS-mediated mechanism of action [189]. Nrf-2 may therefore contribute toward the resistance of glioma cells to alkylating agents such as carmustine. In chapter 3, carmustine was used to induce cell death in A431 cells grown in 18.6% O_2 or 3.0% O_2 **(section 3.3.8).**

1.2.7. Antioxidant defence

1.2.7.1. What is an antioxidant?

Gutteridge and Halliwell et al. [92] have defined an antioxidant as “any substance that delays, prevents or removes oxidative damage to its target molecule”.

Although there are many antioxidants which can detoxify free radicals and ROS in mammalian systems (e.g. non-enzymatic ‘quenching’ of ROS and free radicals via ascorbate, pyruvate and α-tocopherol) antioxidant enzyme-mediated decomposition of ROS will be discussed in detail.

1.2.7.2. Antioxidant enzymes

1.2.7.2.1. Cu/Zn superoxide dismutase

Human Cu/Zn superoxide dismutase (SOD 1) has a molecular mass of 16 kDa and contains two protein subunits [190]. The active site contains one Cu^{+}, and one Zn^{2+} ion. SOD 1 is cytosolic and is found in almost all eukaryotic cells [190]. SOD catalyses the dismutation of $O_2^{\bullet-}$, where one $O_2^{\bullet-}$ molecule is oxidised to O_2 and another molecule of $O_2^{\bullet-}$ is reduced to H_2O_2. The dismutation of $O_2^{\bullet-}$ by SOD proceeds as follows:

$$\text{SOD 1-}Cu^{2+} + O_2^{\bullet-} \rightarrow \text{SOD 1-}Cu^{+} + O_2 \qquad \textbf{(Eq. 1.18)}$$

$$\text{SOD 1-}Cu^{+} + O_2^{\bullet-} + 2H^{+} \rightarrow \text{SOD 1-}Cu^{2+} + H_2O_2 \qquad \textbf{(Eq. 1.19)}$$

The rate constant of this reaction is at least $k = 1.5 \times 10^9\ M^{-1}s^{-1}$, which is almost three orders of magnitude greater than the un-catalysed reaction at pH 7 [190].

1.2.7.2.2. Mn/Zn superoxide dismutase

Human Mn/Zn (SOD 2) has a molecular weight of 25 kDa. Unlike SOD 1, SOD 2 is not inhibited by Cu ion chelators like diethyldithiocarbamate. This is because SOD 2 does not contain a copper ion in its active site. Instead, Mn^{2+} is found in the active site of SOD 2 [191]. As such, SOD 2 is often referred to as Mn/Zn SOD. However, SOD 2 is more susceptible to heat inactivation compared to SOD 1 [190].

SOD 2 contains four protein subunits that have either one Mn ion, or half an ion (two subunits share a Mn ion) [190]. The active site lies between the N terminal and the C terminal [190].

Human SOD 2 is found in the mitochondrial matrix [191]. Compared to SOD 1, SOD 2 appears to be much more responsive to stressors such as cytokines, growth factors, and p53. SOD 2 protein levels can change rapidly in response to changes in cell physiology [192].

SOD 2 catalyses a similar dismutation reaction to SOD 1:

Mn^{3+} SOD-OH^- + $O_2^{\bullet-}$ + H^+ → Mn^{2+}SOD (H_2O) + O_2 **(Eq. 1.20)**

Mn^{2+}SOD (H_2O) + $O_2^{\bullet-}$ + H^+ → Mn^{3+} SOD-OH^- + H_2O_2 **(Eq. 1.21)**

The rate of this reaction is similar to that of SOD 1 (1.8×10^9 M^{-1} s^{-1}) at pH 7.8 [92].

1.2.7.2.3. Catalase

Human catalase is composed of four subunits, each with a molecule of NADPH. Fe^{3+}-haem is found within the active site. Fe ion chelators such as desferrioxamine inhibit catalase [193]. Fe^{3+}-haem is bound to Tyr358, His74 and Asp174 ligands within the active site [194]. His74 is modified by the catalase inhibitor 3-amino-1,2,4-triazole (3-AT; used in chapter 3) in the presence of H_2O_2 resulting in the irreversible inhibition of catalase compound I **(section 1.2.6.2.1)** [194].

Human catalase decomposes H_2O_2 to H_2O and O_2 **(Eq. 1.22–1.23)**. The rate constant of the reaction between H_2O_2 and catalase is 1.7×10^7 M^{-1} s^{-1} at pH 7.0 [194]. This reaction is actually a dismutation reaction where one molecule of H_2O_2 is reduced to H_2O and the other is oxidised to O_2.

Catalase-Fe^{3+} haem + H_2O_2 → catalase compound I + H_2O **(Eq. 1.22)**

Catalase compound I + H_2O_2 → catalase-Fe^{3+} haem + O_2 + H_2O **(Eq. 1.23)**

Human catalase is generally found in membrane bound organelles such as peroxisomes [194]. The peroxisome is a site of major H_2O_2 generation by enzymes such as glycolate oxidase, urate oxidase, and flavoprotein dehydrogenase [194].

1.2.7.2.4. Glutathione synthesis and reaction chemistry

GSH is a tri-peptide molecule made up of Glu, Cys and Gly and is involved in antioxidant defence [92]. GSH forms a disulphide bond with another molecule of GSH when oxidised forming GSSG. GSH is synthesised in the cytoplasm by two enzymes. First, glutamylcysteine is formed from L-glutamate and L-cysteine by γ-glutamate-cysteinyl ligase (γGCS) **(Figure 1.15)**:

$$\text{L-glutamate} + \text{L-cysteine} + \text{ATP} \xrightarrow{\gamma\mathbf{GCS}} \text{L-}\gamma\text{ glutamylcysteine} + \text{ADP} + P_i \quad \textbf{(Eq. 1.24)}$$

Second, glutathione synthetase (GS) binds the di-peptide to Gly yielding GSH:

$$\text{L-}\gamma\text{-glutamylcysteine} + \text{glycine} + \text{ATP} \xrightarrow{\mathbf{GS}} \text{GSH} + \text{ADP} + P_i \quad \textbf{(Eq. 1.25)}$$

L-buthionine sulfoximine (L-BSO) inhibits GS **(section 1.2.6.3.1)** and was used in chapter 3 to deplete GSH.

GSH is involved in ascorbate metabolism, maintenance of gap junctions and prevention of protein thiol oxidation. GSH is normally found at mM concentrations within the human cell [92]. However, it exists in a constant flux between its reduced and oxidised form [92]. This equilibrium is most commonly referred to as the GSH:GSSG ratio [195]. This ratio was measured in A431 cells in chapter 4.

GSH can react with free radicals (e.g. $^{\bullet}$OH, RO$^{\bullet}$, and RO2$^{\bullet}$) and lipid peroxidation end products such as HNE [196]. GSH does not however react rapidly with $O_2^{\bullet-}$ [197]. However, $ONOO^-$ can react with GSH to form nitrosothiol. GSH is also involved in the metabolism of xenobiotics via conjugation reactions catalysed by GST, a phase II detoxification enzyme [198]. The conjugation of the xenobiotic to GSH facilitates xenobiotic detoxification [198]. The activity of GST was measured in chapter 4 in A431 cells grown in 18.6% or 3.0% O_2 **(section 4.3.6)**.

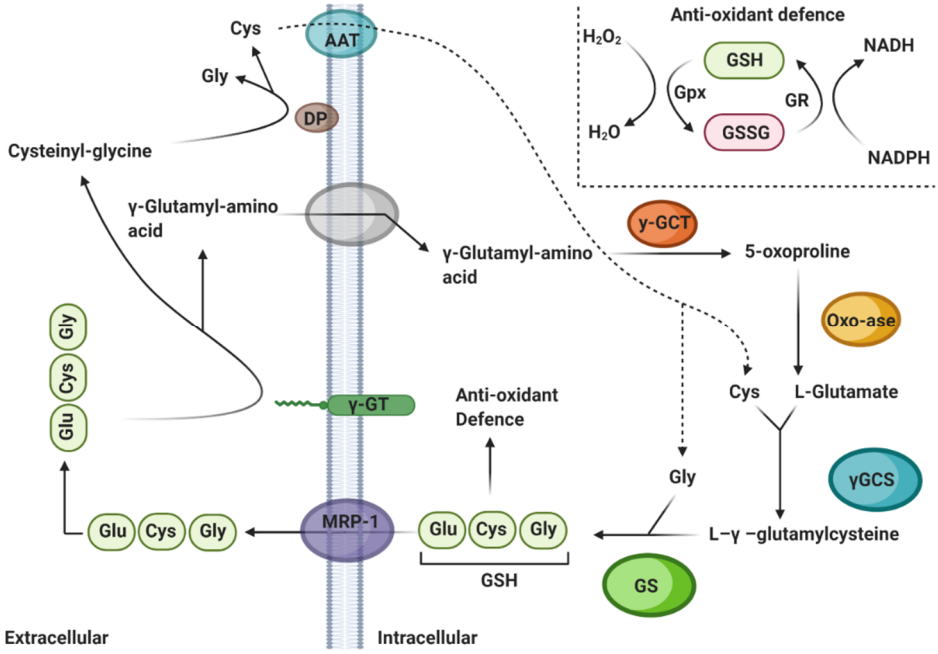

Figure 1.15. Glutathione biosynthesis pathway. GSH is exported from the cell by the protein MRP-1 across the cell membrane. GSH is broken down by γ –GT into cysteinyl-glycine and a γ-glutamyl residue. The γ-glutamyl residue is bound to an amino acid (such as cysteine, or methionine). Cysteinyl-glycine is broken down into glycine and cysteine by DP found on the outer membrane. Cysteine and glycine can then be transported into the cell via AAT. γ-glutamyl-amino acid is transported into the cell by amino acid transporters where it is converted to 5-oxoproline by γ-GCT. Oxo-ase then converts 5-oxoproline into L-glutamate, which binds with cysteine through the action of γGCS to form L- γ-glutamylcysteine. This di-peptide then binds with glycine through the action of GS to form the tri-peptide GSH. GSH can then quench ROS such as H_2O_2 through disulfide exchange reactions catalysed by Gpx. GSSG can be reduced back to GSH by GR. **AAT:** Amino acid transporter; **DP:** Di-peptidase; **Gpx:** Glutathione peroxidase; **GR:** Glutathione reductase; **GSH:** Reduced glutathione (γ-glutamyl-cysteinyl-glycine); **GSSG:** Oxidised glutathione; **MRP-1:** Multi drug resistant protein-1; **Oxo-ase:** 5-oxoprolinease; **γGCS:** γ-glutamylcysteine synthetase; **γ-GCT:** γ-glutamyl cyclo transferase; **γ –GT:** γ- glutamyl transferase. Image made with www.Biorender.com.

1.2.7.2.5. Glutathione reductase and peroxidase

Two enzymes are involved in maintaining GSH:GSSG. Glutathione peroxidase (Gpx) catalyses the peroxidation of ROS via GSH oxidation. Glutathione reductase (GR) reduces GSSG into GSH.

Human GR contains two subunits, including an NADPH binding domain. Its active site contains a molecule of flavin adenine dinucleotide (FAD). The GR-mediated reduction reaction of GSSG proceeds in two phases: the reductive phase and the oxidative phase.

In the reductive phase, the electron donor NADPH binds to the NADPH binding domain and transfers its electrons to FAD. This results in the formation of an $FADH^-$ anion. The Cys58-Cys63 disulfide is then reduced, breaking the disulfide

bond. $NADP^+$ is then released and replaced by a second molecule of NADPH. In the oxidative half of the reaction, GSSG then binds to the reduced GR enzyme near the active site. His467 promotes the nucleophilic attack of Cys63 on the sulfide unit in GSSG. This forms a mixed disulfide (GS-Cys58) and a GS^- anion. The GS^- anion is protonated by His467 releasing the first GSH peptide. Finally, nucleophilic attack by Cys63 on Cys58 releases another GS^- anion, which is then protonated by a solvent proton, releasing a second molecule of GSH. The mechanism is generalised in **Figure 1.16**.

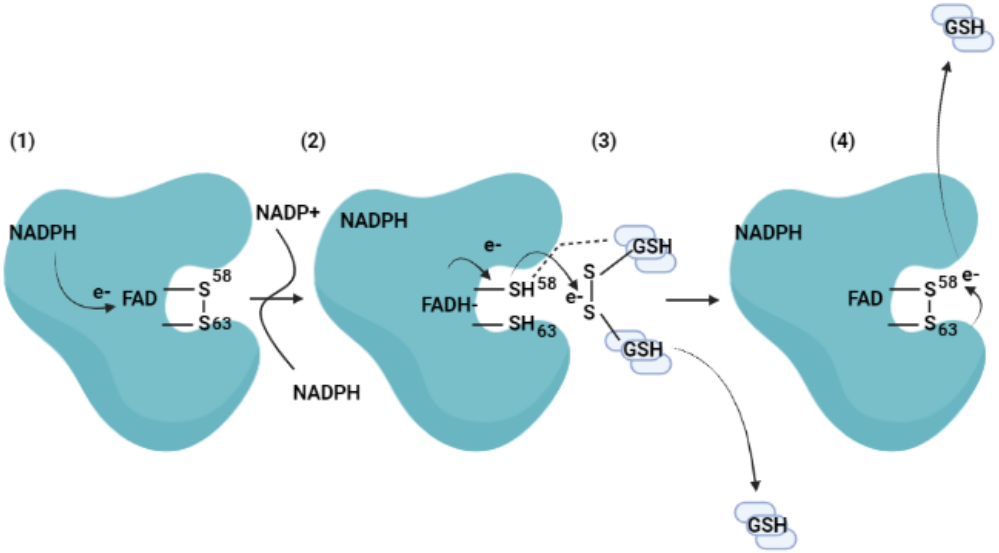

Figure 1.16. The reduction of oxidised glutathione by glutathione reductase. **(1)** NADPH binds to the oxidized enzyme which results in the reduction of FAD to $FADH^-$. **(2)** $FADH^-$ then reduces the Cys58-Cys63 disulfide. **(3)** GSSG binds to the reduced enzyme and forms a mixed disulfide with Cys58 (dashed line) and releases one GSH molecule. **(4)** Cys63 attacks the mixed disulfide on Cys58 to release another molecule of GSH to reform the disulfide. **GR:** glutathione reductase; **GSH:** reduced glutathione; **GSSG:** oxidised glutathione. Image made using www.Biorender.com.

The ratio of GSH to GSSG is kept high through the rapid reduction of GSSG to GSH by GR **(Figure 1.16)**. The simplified net reduction reaction proceeds as follows:

$$GSSG + NADPH + H^+ \xrightarrow{GR} 2GSH + NADP^+ \qquad \textbf{(Eq. 1.26)}$$

Gpx catalyses the reverse peroxidation reaction i.e. the oxidation of two molecules of GSH into GSSG resulting in the reduction of H_2O_2 into H_2O.

There are a number of Gpx isoforms: Gpx1 (cytosolic), Gpx2 (intestinal), Gpx3 (extracellular fluid and blood plasma), Gpx4 (Liver) and Gpx 7, 8 (endoplasmic reticulum (ER)). Gpx1, 2 and 3 contain four protein subunits, each with an atom of selenium (Se) in the form of selenocysteine within the active site [199]. However, Gpx4 is a monomer of molecular weight 19 kDa and contains only one atom of Se. Gpx 7 and 8 do not contain selenocysteine, and are thought to play a role in protein folding by assisting peroxiredoxin (Prx)-4-mediated H_2O_2 detoxification within the ER [199].

The reaction of Gpx proceeds by the reaction of selenol (Se^-) within the active site, with a peroxide (ROOH) to yield selenic acid (SeOH). In this reaction, Gln 83 is the proton acceptor [200].

$Gpx\text{-}Se^- + ROOH + H^+ \rightarrow ROH + Gpx\text{-}SeOH$ **(Eq. 1.27)**

GSH then binds to the active site, resulting in the formation of H_2O and glutathiolated selenol (Gpx-Se-SG) [201].

$Gpx\text{-}SeOH\text{-}GSH \rightarrow H_2O + Gpx\text{-}Se\text{-}SG$ **(Eq. 1.28)**

The second molecule of GSH then binds, forms a disulfide with the first GSH molecule and is released as GSSG thereby reforming $Gpx\text{-}Se^-$.

$Gpx\text{-}Se\text{-}SG\text{-}GSH \rightarrow Gpx\text{-}SeH\text{-}GSSG \rightarrow Gpx\text{-}Se^- + H^+ + GSSG$ **(Eq. 1.29)**

The reaction results in the formation of GSSG from GSH, and the associated detoxification of the peroxide **(Figure 1.15)**.

1.2.7.2.6. Peroxiredoxin family of antioxidant enzymes.

H_2O_2 can be produced through a number of different mechanisms such as through the dismutation of $O_2^{\bullet -}$ by SOD. Although H_2O_2 is an important signalling molecule, it is a potentially dangerous ROS. As such, cellular [H_2O_2] is carefully controlled. Prx play a key role in maintaining this equilibrium by catalysing the peroxidation of H_2O_2 **(Eq. 1.30)**

$$SH_2 + H_2O_2 \xrightarrow{\mathbf{Prx}} S + 2H_2O \qquad \textbf{(Eq. 1.30)}$$

Of most relevance to this work are thioredoxin (Trx) and thioredoxin reductase (TrxR), co-factors of the Prx family of proteins.

1.2.7.2.7. Thioredoxin and thioredoxin reductase

Human Trx has a molecular weight of 16 kDa. Trx is found mostly within the cytosol, with Trx2 being found mostly within mitochondria [202]. Trx proteins have a Cys-Gly-Pro-Cys catalytic motif which is highly conserved amongst the Trx protein family [202]. Trx utilise the Cys residue within the catalytic motif to reduce disulfide bonds on target proteins **(Figure 1.17).**

Trx can exists in either a reduced or oxidised form. A family of enzymes known as TrxR utilise NADPH as a reducing equivalent to reduce the disulfide on oxidised Trx **(Figure 1.17)**. Human TrxR1 is about 54.6 kDa in molecular weight, and its structure consists of a C terminal selenium containing catalytic site (Gly-

Cys-Se/Cys-Gly), an interface domain, an FAD domain, and an NADPH domain where another catalytic site (Cys-Val-Asn-Val-Gly-Cys) is found.

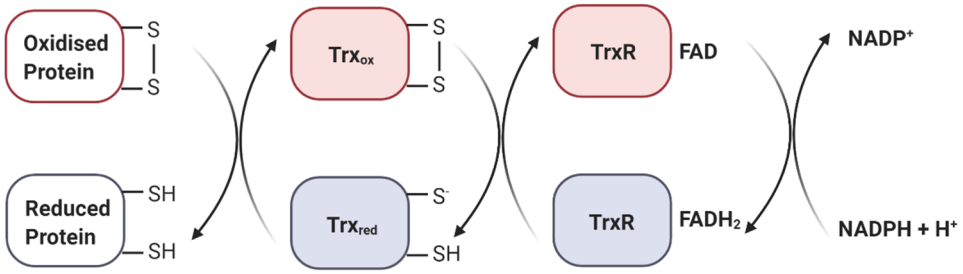

Figure 1.17. Thioredoxin-mediated reduction of oxidised thiols. Trx in its reduced state (Trx_{red}) attacks the disulfide on oxidised proteins and is itself oxidised (Trx_{ox}) resulting in the reduction of the target protein. Trx_{ox} is reduced back into Trx_{red} by the flavo enzyme thioredoxin reductase (TrxR) which uses NADPH as a reducing equivalent. Image made using www.Biorender.com.

TrxR2 contains a mitochondrial import sequence adjacent to the NADPH domain [203]. The function of TrxR2 is not very well understood. The presence of TrxR2 in the mitochondria however suggests that it may protect the mitochondria from ROS generated during oxidative phosphorylation [204].

The reduction of Trx by TrxR proceeds as shown in **Figure 1.18.** NADPH binds to the NADPH-binding domain of TrxR. Electrons are transferred to FAD resulting in the reduction of the disulfide bond in the Cys-Val-Asn-Val-Gly-Cys catalytic site in TrxR. The C terminal catalytic site (Gly-Cys-Se-Cys-Gly) remains oxidised at this point **(Figure 1.18)**. When TrxR comes in contact with the disulfide on its substrate Trx, the Cys-Val-Asn-Val-Gly-Cys catalytic site is oxidised, and the C terminal catalytic site is reduced. The selenocysteine catalytic site then transfers electrons to the substrate resulting in the reduction of the disulfide bond on Trx **(Figure 1.18)** [204]. This results in the oxidation of the C terminal catalytic site in TrxR thereby reforming the disulfide prior to the next catalytic reaction.

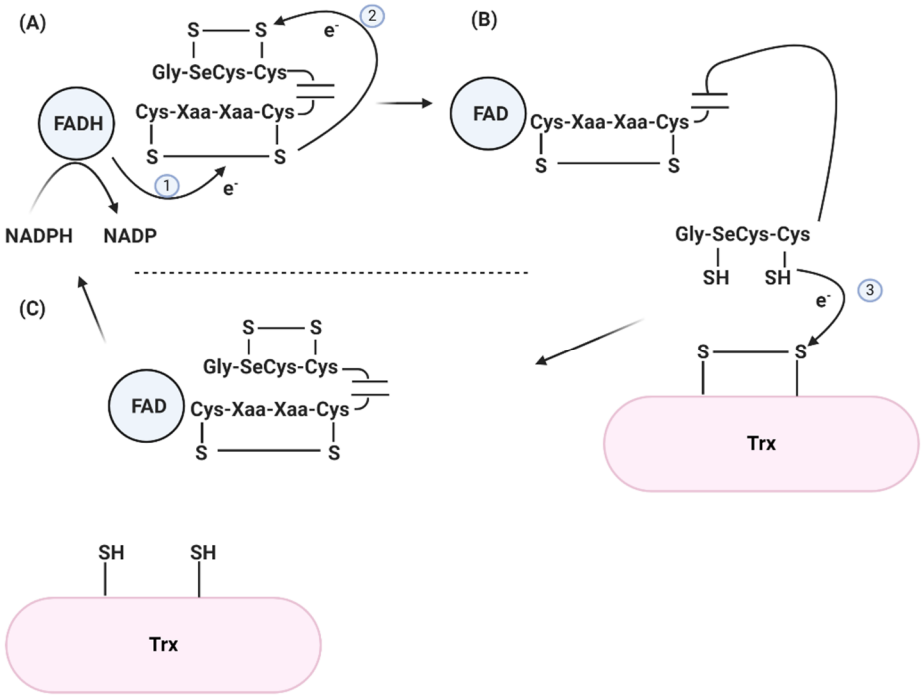

Figure 1.18. Reduction of thioredoxin by thioredoxin reductase. Panel (a), NADPH transfers an electron to FAD resulting in the formation of $FADH^-$. (1) $FADH^-$ reduces the disulfide on the Cys-Xaa-Xaa-Cys catalytic site followed by (2) reduction of the Gly-Se/Cys-Cys catalytic site. **Panel (b),** a conformational change in the protein structure due to the reduction of the Gly-Se/Cys-Cys moves the catalytic site away from the Cys-Xaa-Xaa-Cys catalytic site. The Gly-Se/Cys-Cys catalytic site then reduces the disulfide on oxidised Trx (3). **(c)** The Gly-Se/Cys-Cys catalytic site resolves and moves back to its previous position. FAD can then receive another electron from NADPH to restart the reaction. A reduced Trx protein is then formed which can then participate in the reaction shown in Figure 1.17. **Trx:** thioredoxin. Adapted from [204] using www.Biorender.com.

1.2.7.3. Regulation and control of antioxidant defence

Although antioxidant defence is needed to protect the cell against oxidative stress-induced by ROS, regulation of this system is also needed so that the cell can return its antioxidant defence levels back to normal after oxidative stress has subsided. This is needed so that the reactions of ROS, which may be involved in critical cell signalling pathways, are not completely quenched.

For the purpose of relevancy, the Nrf-2 transcription factor will be discussed in detail.

1.2.7.3.1. Nuclear factor erythroid-2-related factor 2

The antioxidant response element (ARE) is an enhancer sequence found in the promoters of many genes encoding antioxidant and cyto-protective protein and enzyme. Binding of the Nrf-2 transcription factor to the ARE results in increased transcription of genes encoding NQO-1, UDP-glucuronosyltransferases,

CYP2A5, P-glycoprotein, and multidrug resistance associated proteins [198]. In addition, Nrf-2 promotes the transcription of genes encoding anti-oxidant proteins and enzymes such as haem oxygenase-1 (HO-1), SOD 1, SOD 2, catalase, ferritin, Gpx, Trx, TrxR, and γ-GCS [36, 72].

Inter alia, Nrf-2 activation protects the cell against oxidative stress-related cellular damage.

1.2.7.3.1.1. Molecular mechanism of nuclear factor-erythroid factor 2-related factor 2 activation

The Keap-1 dimer prevents Nrf-2 stabilisation by promoting Nrf-2 ubiquitination and degradation by the proteasome [198]. The Keap-1 dimer is made up three domains, the intervening domain (IVF), the broad complex/tramtrac/bric-a-brac (BTB) and the Kelch domain [198]. BTB binds Cullin-3 (Cul-3), which aids in dimerization of the Keap-1 dimer **(Figure 1.19).**

The Kelch domain is needed for the binding of Keap-1 to actin and myosin in the cytoskeleton. This immobilises the Keap-1 dimer in the cytoplasm [198]. In addition, the Kelch domain is critical for the binding of keap-1 to the amino-terminal Nrf-2-ECH homology-2 (Neh2) domain of Nrf-2. Nrf-2 has 6 of these Neh domains. Neh1 contains the nuclear localisation signal (NLS) motif, a basic leucine zipper (bZIP) motif, a cap 'n' collar region (CNC) and a nuclear export signal. Neh3 contains the C terminal critical for transactivation. Neh4 and 5 contains transactivation sites and a nuclear export signal (NES), believed to be important for interaction between Nrf-2 and CBP-p300 in the nucleus. Finally, Neh6 contains a linker domain thought to be important for the degradation of Nrf-2 [198].

There are two domains within Neh-2 to which Kelch can bind. The first is a high affinity binding motif called ETGE, which acts functionally as a 'hinge'. The second binding motif is DLG which functions as a 'latch' [205]. When both are bound to the Kelch domain, Lys residues within the Neh-2 domain are ubiquitinated [205]. Upon ubiquitination, Nrf-2 is targeted for degradation by the proteasome **(Figure 1.19)**.

Exposure of the cell to ROS such as H_2O_2, or RNS such as $ONOO^-$, results in modification of Cys272 and Cys288 on the IVF. This leads to the release of Kelch

from DLG. The binding of ETGE remains unaffected, due to its high affinity binding, resembling a 'hinge' like mechanism [205]. Binding of P21 to DLG possibly promotes further dissociation of Nrf-2 from Keap-1 [198].

Once free in the cytoplasm, Nrf-2 translocates to the nucleus where it binds to the ARE. Before this can occur, it is phosphorylated by PKCδ at Ser40 **(Figure 1.19)**. This has a number of functions: first, it prevents re-binding of Keap-1 to Nrf-2; second, it also allows Nrf-2 to be imported into the nucleus via importin proteins present in the nuclear membrane [205].

Within the nucleus, Nrf-2 dimerises with small muscular-aponeurotic fibro sarcoma (Maf) proteins and bZIP. Maf is thought to mask the NES domain, preventing Nrf-2 export from the nucleus [198]. Negative regulators of Nrf-2 activation, such as BTB domain and CNC homolog 1 (Bach-1), block Nrf-2 and Maf binding. Further prevention of nuclear export of Nrf-2 is achieved by oxidation of Cys183 in the NES, which is highly redox sensitive [206]. This Nrf-2/bZIP complex binds to the ARE sequence in the promoter regions of the target gene and recruits the CBP-p300 complex. Transcription of Nrf-2-target genes then commences, including *de-novo* transcription of the gene *NFE2L2* encoding *de novo* Nrf-2 protein. *De-novo* synthesised Nrf-2 protein is exported from the nucleus via exportin proteins and is phosphorylated in the same way as before by PKCδ. This further propagates the signal generated by Nrf-2 **(Figure 1.19**; [205]).

Nuclear export of Nrf-2 is regulated by protein kinases such as Fyn which phosphorylates Nrf-2 at Tyr568. This is believed to contribute toward the signal termination of Nrf-2 [205]. Expression of Nrf-2-targets such as Trx, TrxR and Ɣ-GCS terminate Nrf-2 signalling through oxidant detoxification. When ROS levels decrease as antioxidant levels rise, Nrf-2 dissociation from the Keap-1 complex also decreases.

The extent to which Nrf-2 is activated in cells growing *in vitro* may be artefactually affected by the [O_2] that the cell is adapted to growing in prior to assay [20, 72]. This is particularly problematic for the *in vitro* testing of Nrf-2-activating agents. This will be discussed in **section 1.3.1.1.1.** First, there will be a brief introduction to the drug discovery pipeline which will provide context for the involvement of *in vitro* cell culture in the testing of novel compounds.

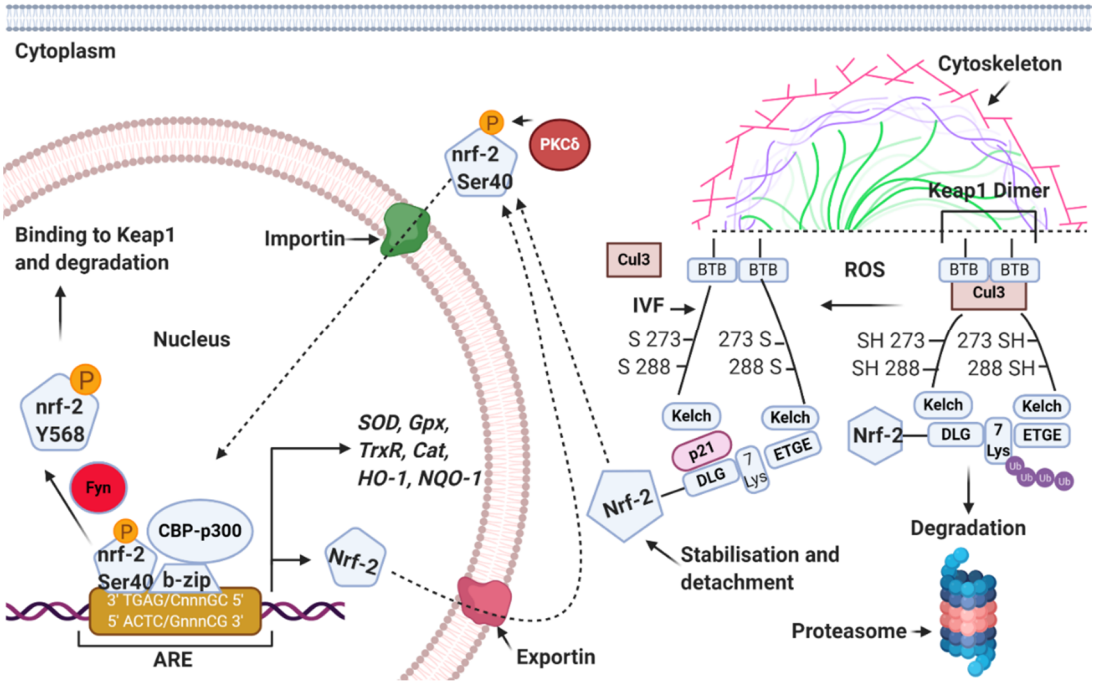

Figure 1.19. Molecular mechanism of Nrf-2 activation. ROS react with Cys residues on the Keap1 dimer (see text) releasing Nrf-2. Nrf-2 is no longer targeted for proteasomal degradation. For nuclear translocation, Nrf-2 requires phosphorylation at Ser_{40} by PKCδ. Nrf-2, phosphorylated at Ser_{40}, enters the nucleus via importin proteins. It then binds to the ARE by forming a complex with bZIP and CBP-p300. Nrf-2 activates gene expression by binding to the ARE in the promoter regions of various anti-oxidant and cyto-protective genes (see text). Phosphorylation at Tyr568 by the Tyr kinase Fyn leads to nuclear export of Nrf-2. Exported Nrf-2 can bind Keap-1 is subsequently targeted for ubiquitination. **ARE:** antioxidant response element; **BTB:** broad complex/tramtrac/bric-a-brac; **bZIP:** basic leucine zipper; **Cat:** catalase; **Cul3:** Cullin 3; **CBP-p300:** CREB binding protein p300; **Gpx:** glutathione peroxidase; **HO-1:** haem oxygenase-1; **NQO-1:** NADPH quinone oxidoreductase-1; **TrxR:** thioredoxin reductase; **PKC:** protein kinase C; **SOD:** superoxide dismutase. Image made using www.biorender.com.

1.3. On the use of standard *in vitro* cell culture oxygenation conditions during the discovery and development of novel nuclear factor erythroid-2-related factor 2-activating compounds.

1.3.1. The drug discovery process

In the fields of medicine, biotechnology and pharmacology, drug discovery is the process by which new candidate medications are discovered. Drug discovery usually begins by identifying a target (such as a protein, gene, pathway etc.) with disease modifying potential; and by identifying a compound which can affect said target. This is known as lead target/lead compound identification. *In vitro* cell culture methods can be used in the early stages of the drug discovery pathway to identify disease targets and to run preliminary cell-based testing **(section 1.3.1.1)**.

A description of the drug discovery pathway beyond these simple *in vitro* assays will not be provided as it is not the focus of this present work. However, an illustration of the general drug discovery pathway is shown in **Figure 1.20** so as to provide context for the involvement of *in vitro* cell-based systems in drug discovery [207]. It takes a long time for a drug to reach the market, and unfortunately the failure rate of potential drug candidates markedly exceeds the success rate **(Figure 1.21)**. Although there are many reasons which contribute toward this problem, one of these may involve issues with the ways *in vitro* cell-based testing is performed. This will be discussed in the following section.

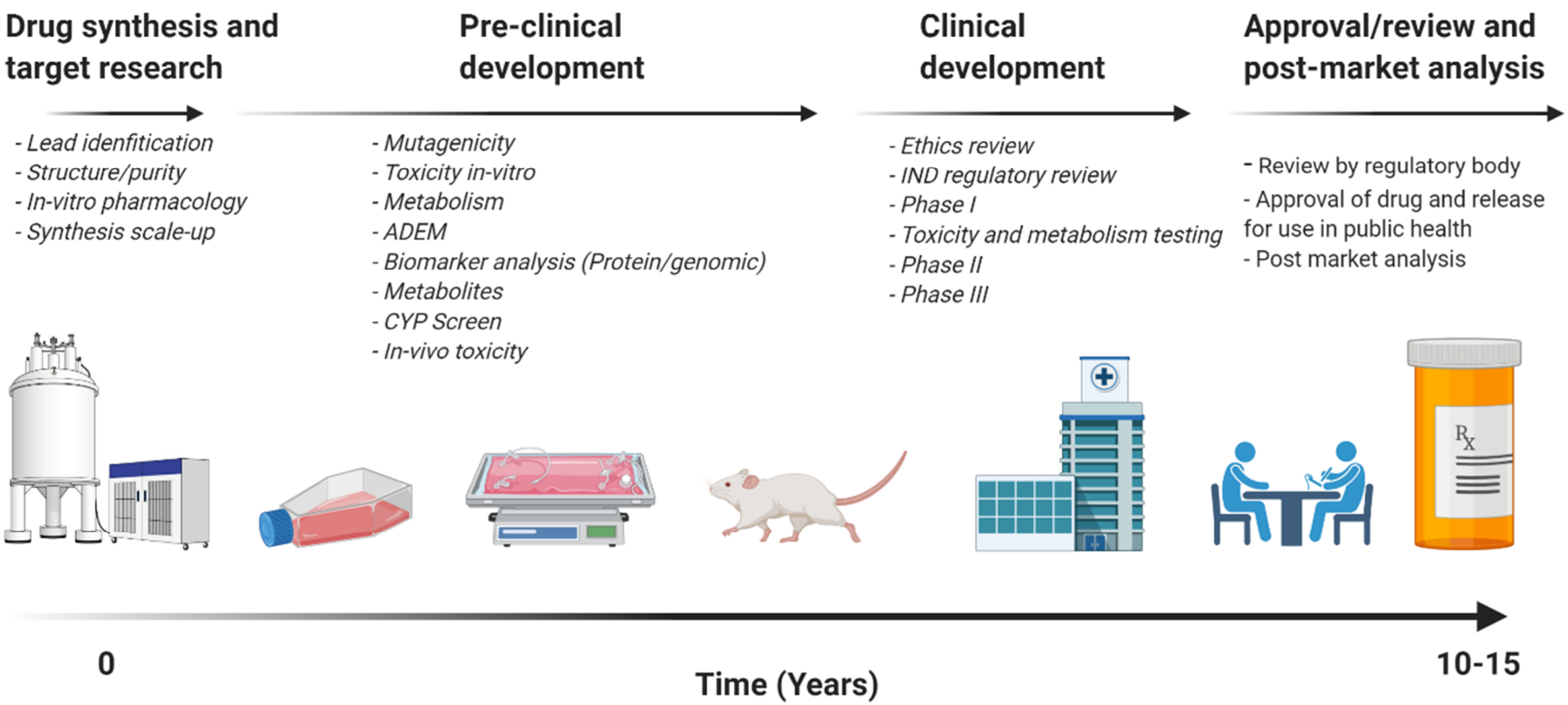

Figure 1.20. The drug discovery pathway timescale. ADEM: Absorption, digestion, excretion and metabolism; **CYP:** cytochrome p450; **IND:** Investigational new drug. Figure made in www.Biorender.com.

1.3.1.1. Lead compound attrition in drug discovery

In 2015, an analysis of the drug attrition rates from AstraZeneca, Eli Lilly, GlaxoSmithKline and Pfizer showed that the primary cause for compound attrition during the compound nomination phase was due to non-clinical toxicology (n=240 compounds) [208]. This attrition is often planned for by bio-pharmaceutical companies. Multiple projects are run at each stage of the drug discovery process to increase the chance of a drug reaching the market **(Figure 1.21)** [209]. If a compound fails in the non-clinical stage, this still represents a significant loss of time and money [210].

One of the purposes of non-clinical toxicology is to filter out compounds incompatible with human physiology. For example, the cardiac potassium ion channel hERG has been identified as a primary anti-target in safety pharmacology. Only 1 in 5 projects pass through the pre-clinical testing phase, with less than 1 in 10 passing through clinical trials [209]. What could explain the large attrition rate of compounds during discovery and development? There exist some possible explanations: biological issues include target selection/ validation, and chemistry-related issue concern lead optimisation and toxicity profiling. The ability to identify lead targets in a disease pathway, and to design compounds that target those pathways with favourable pharmacokinetics and dynamics are current limitations in the drug discovery process [209].

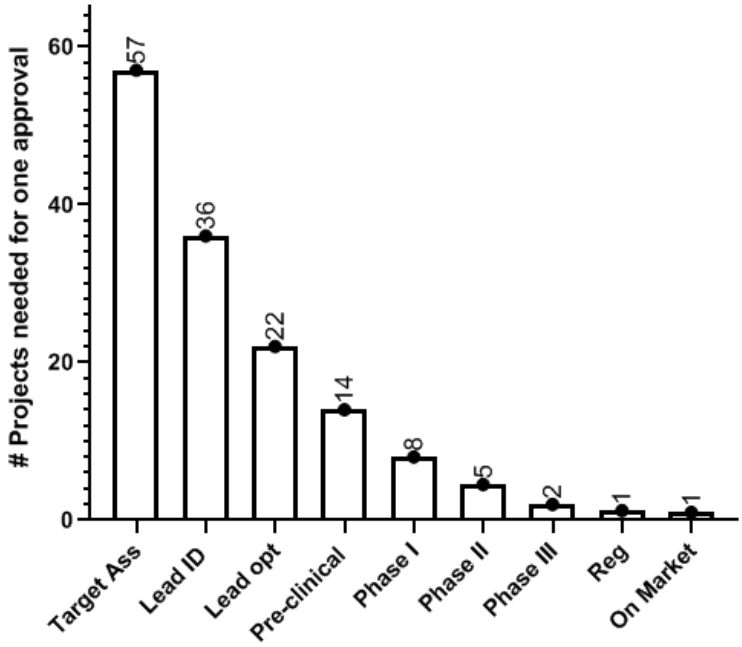

Figure 1.21. Compound attrition in research and development. The data represented here shows the number of projects statistically needed at each stage of the drug discovery process in order for one compound to reach the market the accumulated experience of several leading pharmaceutical companies. **Ass:** assessment; **ID:** identification; **Opt:** optimization; **Reg:** regulatory. Graph adapted from [209].

Cell culture is a relatively minor part of the drug discovery process. However, it represents a key starting point used in lead target/compound development. *In vitro* cell culture is used for the generation of sub cellular fractions during drug pulldown, and for the assessment of compound toxicity prior to pre-clinical work in animals. *In vitro* potency is an important parameter used to select hits during high-throughput screening (HTS) in lead generation campaigns [210]. The low-throughput *in vivo* pharmacology-based screening has been largely replaced in favour of 'omics'-informed approaches to target disease pathways using *in vitro* screening cascades [210]. Front loading attrition of compounds onto the *in vitro* stage is a financially advisable strategy as it is generally less expensive than *in vivo work*, as well as being higher throughput [210]. The pharmaceutical industry has invested heavily in designing these HTS procedures to test thousands of compounds using cell based *in vitro* assays [209]. *In vitro* compound potency testing against a target is used to predict which compounds can achieve *in vivo* efficacy at low microgram doses [202, 205]

However, Gleeson et al. [210] showed that *in vitro* potency against the target does not correlate strongly with therapeutic dose in the clinic. This is not surprising, as drugs *in vivo* have quite complicated pharmacokinetics and

pharmacodynamics that are not reflected in simplistic *in vitro* assays. However, only 10% of drugs deemed 'potent' by *in vitro* assays end up on the market [210]. The very high drug attrition rates at this early stage in drug discovery may be an artefact caused by the potency filters put in place during *in vitro* HTS campaigns. If the potency of a drug is affected by the environmental conditions used during the *in vitro* screening assay, artefactual efficacy (or lack thereof) may lead to downstream drug attrition.

The [O_2] used during the *in vitro* cell culture growth phase is unlikely to affect the efficacy of all lead compounds **(section 1.1.4)**. However, O_2 is a fundamentally important molecule in redox biology which may render this field of study susceptible to artefacts caused (in part) by the use of standard cell culture [O_2] during the *in vitro* drug development of redox active compounds. There is now considerable emphasis placed on the role of redox-related mechanisms in human health, both in ageing and in cancer [87, 164, 172, 206–209]. For example, biopharmaceutical companies are targeting Nrf-2-activating agents, such as dimethyl fumarate (DMF), for the treatment of multiple sclerosis and psoriasis [210–212]. Many of these compounds are in the preclinical or the 'investigational new drug' stages of development. Additionally, Nrf-2 expression is associated with chemo resistance to 5- fluorouracil, carboplatin, cisplatin and temozolomide rendering Nrf-2 a promising target for adjunctive anti-cancer therapeutic approaches [196–200]. The next section will discuss the potential risk of testing Nrf-2-activating compounds *in vitro* on mammalian cells grown chronically in standard cell culture conditions compared to such cells grown in physioxia.

1.3.1.1.1. Lead series development: nuclear factor erythroid-2-related factor 2-activating compounds.

Nrf-2 activating compounds are utilised for the treatment of multiple sclerosis and psoriasis [155]. The mechanism of action is believed to involve induction of antioxidant defence and cyto-protective-related proteins **(section 1.2.7.3.1.1)**. There are numerous classes of Nrf-2 activators. These are classified based on the amino acid residue targeted on the Keap-1 homodimer: class I inducers preferentially target Cys151 on the BTB domain of the Keap-1 complex (Diethylmaleate (DEM), DMF, sulforaphane, and tert-butylhydrquinone); class II and III inducers (nitro-oleic acid, 4-HNE) target Cys151, Cys273 and Cys288;

class IV inducers (H_2O_2, Cd^{2+}, prostaglandin A2) are Cys-independent inducers **(Figure 4.18)**.

Pharmaceutical development of novel therapeutics targeting Nrf-2 has been slow [155]. Currently, Biogen is the only pharmaceutical company in the world marketing a Food and Drug Administration-approved Nrf-2-targeting drug for the treatment of multiple relapsing multiple sclerosis and psoriasis (i.e. DMF) [155].

In recent years, the interest in Nrf-2 as a potential therapeutic target for human disease has increased [155]. Nrf-2-activating agents are being considered for the treatment of connective tissue disease (phase III), pulmonary hypertension (phase III), Alport syndrome (phase II), Friedrich's ataxia (phase II), subarachnoid haemorrhage (phase II), oestrogen receptor positive metastatic breast cancer (phase II), and Parkinson's disease (preclinical), and Alzheimer's disease (Preclinical) [86, 87].

How are compounds targeting Nrf-2 generally tested *in vitro*? The most common ways involve measuring the activation of Nrf-2, induction of Nrf-2-target proteins, and the activity of Nrf-2-target enzymes.

Daiichi Sankyo's Nrf-2-activating compound known as RS9 was developed for the treatment of retinovascular disease [218]. RS9 efficacy was evaluated by measuring NQO-1 protein expression (Nrf-2-target protein) in Hepa1c1c7 cells. Intravitreal administration of RS9 was shown to improve retinopathy in rats [218]. CX4 Discovery's ML334 was developed for the treatment of type-2 diabetes mellitus and chronic obstructive pulmonary disorder [219]. ML334 is not a direct activator of Nrf-2, but instead impedes the binding of the inhibitor (Keap-1) to Nrf-2. ML334 efficacy was tested using an ARE gene reporter assay and an Nrf-2 translocation assay [219]. Mochida's TFM725 was identified using a hit-to-lead approach followed by high-throughput screening utilising an Nrf-2 degron-LacZ reporter system to monitor Nrf-2 activation [220]. TFM725 was efficacious in a mouse model of autoimmune encephalomyelitis through the activation of Nrf-2 and the inhibition of the inflammatory response [220]. Compound A developed by GlaxoSmithKline is a Keap-1/Nrf-2 inhibitor currently being investigated for the treatment of chronic obstructive pulmonary disorder [221]. Compound A efficacy was measured by quantifying the expression levels of nuclear Nrf-2 protein by western blotting [221]. vTv Therapeutics' Bach-1 repressor GPP971 activates

Nrf-2 by inhibiting the inhibitor of Nrf-2 binding to the ARE [222]. Unlike other Nrf-2 activators, HPP971 is not an electrophile, does not modulate directly the Keap-1 complex and is unaffected by treatment with antioxidants such as ascorbic acid or NAC. HPP971 efficacy was measured by assaying the expression levels of NQO-1 and HO-1 protein by western blotting, and by measuring the extent of Nrf-2 binding to the *HMOX1* ARE promoter via chromatin immunoprecipitation [222].

Nrf-2 directly controls the expression of antioxidant proteins as previously mentioned in **section 1.2.7.3.1**. As such, measuring the expression of these target proteins is a rational approach to assess the efficacy of potential Nrf-2 activating compounds. However, the testing of Nrf-2 activating compounds on mammalian cells grown chronically under standard cell culture [O_2] **(section 1.1)** may yield artefactual results compared to such testing on mammalian cells adapted to physioxia.

Tert-butyl hydroquinone (tBHQ) is a commonly used Nrf-2 activator. *Inter alia*, it induces the expression of HO-1 and NQO-1 [223]. tBHQ reacts with Cys151 in Keap-1 causing Nrf-2 release [223]. In 2010, Wang et al. [223] showed that Nrf-2 was not directly activated by tBHQ, but instead by its metabolite tert butyl quinone (tBQ). The formation of tBQ from tBHQ requires Cu^{2+} as a catalyst. Addition of $CuCl_2$ to the human mammary ARE-reporter cell line (AREc32) resulted in a 10 fold increase in tBHQ-mediated ARE induction compared to conditions where no $CuCl_2$ was added. Addition of metal chelators such as DFX and EDTA attenuated this effect [223]. The activation of tBHQ by $CuCl_2$ requires O_2 in order to form tBQ. In the presence of O_2, Cu^{2+} catalyses the one electron oxidation of tBHQ to the semiquinone radical (tBsQ). The tBsQ species then reacts with a second molecule of O_2 to yield $O_2^{\bullet-}$ and tBQ [223]. The induction of Nrf-2-target genes by Cu^{2+}-mediated tBHQ-induced Nrf-2 activation in AREc32 was 30 fold lower in 1% O_2 compared to atmospheric O_2 conditions [223]. Further to this, addition of Cu^{2+} to AREc32 treated with tBQ further amplified Nrf-2 induction [223]. This implicates the actions of NQO-1 in tBHQ-mediated activation of Nrf-2 as NQO-1 catalyses the reduction of tBQ to yield Cu^{2+}-labile tBHQ. H_2O_2 can also act as an electron donor in the Cu^{2+}-catalysed oxidation of tBHQ to tBQ [223]. As such, there are numerous factors which are important for the activation of Nrf-2 by quinone: the presence of an electron donor (O_2, H_2O_2), transition metal ion availability (e.g. Cu^{2+}, Mn^{2+}), and NQO-1 activity. As O_2 was needed for tBHQ-

mediated Nrf-2 activation, Wang et al. [223] demonstrated an acute effect of [O_2] on the cellular response to tBHQ. However, O_2 can also have a chronic effect on the cellular responses to redox-active compounds. This may involve a phenomenon known as O_2 adaptation **(section 1.1.2.2)**.

In 2018, Chapple et al. [72] showed that the growth of human umbilical vessel endothelial cells (HUVEC) in 18.6% O_2 resulted in a 5 fold increase in DEM-induced expression of the Nrf-2-target genes NQO-1 and HO-1 compared to HUVEC adapted to physioxia (5.0% O_2) for 5 days under the same conditions. The Nrf-2 inhibitory regulator Bach-1 was downregulated in HUVEC grown in 18.6% O_2 compared to those adapted to 5.0% O_2. As such, the effects of DEM on Nrf-2 activation were increased in HUVEC grown in 18.6% O_2 compared to HUVEC adapted to 5.0% O_2 for 5 days under the same treatment conditions. DEM differentially induced the expression of TrxR, GR, and the multidrug resistance member 4 in DEM-treated HUVEC grown in 18.6% O_2 compared to HUVEC adapted to 5.0% O_2 for 5 days under the same treatment conditions [72]. However, knockdown of Bach-1 restored DEM-induced expression of HO-1 and NQO-1 in HUVEC adapted to 5.0% O_2 [72]. 5.0% O_2 represents a physiologically 'normal' [O_2] for HUVEC, and as such the upregulation of Bach-1 in HUVEC grown in such [O_2] conditions may also be deemed a 'normal' cellular phenotype for these cells. Alternatively, the augmented DEM-induced induction of Nrf-2-target protein in HUVEC grown in 18.6% O_2 could be viewed as an artefactual effect compared to such an induction in HUVEC adapted to 5.0% O_2 under the same treatment conditions.

The impetus for the work in this thesis is based on the findings of Ferguson et al. [21]. A431 cells grown in 18.6% O_2 showed increased transcription of Nrf-2-target genes encoding SOD 1, PRDX1, NQO-1, HMOX1, GPX1, and catalase when compared to A431 cells adapted to 2.0% O_2 for 48 h [21]. Additionally, A431 cells grown in 18.6% O_2 also exhibited heightened transcription of *NFE2L2* compared to A431 cells adapted to 2.0% O_2 for 48 h **(section 1.2.7.3.1.1)** [21]. This increase in the expression of Nrf-2-target genes was associated with a resistance to photodynamic irradiation **(section 3.1)**, auranofin **(section 1.2.6.1.1)** and H_2O_2- **(section 1.2.6.2)** induced cytotoxicity. A431 cells therefore represent another cell line in which Nrf-2 signalling is altered when grown in standard cell culture [O_2] compared to physioxia.

The main question this thesis set out to answer was whether A431 cells grown *in vitro* long term under 18.6% O_2 were resistant to the effects of redox active compounds compared to A431 cells adapted to 3.0% O_2. Secondarily, this thesis set out to answer whether any such resistance involved changes to the activity or levels of Nrf-2-regulated antioxidant defence systems. These questions form the basis for the research hypothesis and associated research objectives outlined in **section 1.4.** The main endpoints investigated in chapter 3 were cell death, Δψm, ROS generation and lipid peroxidation as these are redox-related endpoints and often used to measure redox-active compound efficacy using *in vitro* cell culture systems. In chapter 4, the molecular mechanism of any such resistance was investigated by measuring the activity of Nrf-2-target antioxidant enzymes, and by measuring the protein expression levels and activity of Nrf-2-target protein to build on the Nrf-2-target gene expression studies by Ferguson et al in A431 cells [21]**.**

1.4. Hypothesis, aims and objectives

Hypothesis: A431 cells grown in 18.6% O_2 are resistant to oxidative stress-induced cell death compared to A431 cells grown in physioxia.

Aims:

1. To grow A431 cells in 3.0% O_2 over the required culture period without inducing hypoxia.
2. To determine whether A431 cells grown in 18.6% O_2 are resistant to auranofin and H_2O_2-induced cell death compared to A431 cells grown in 3.0% O_2.
3. To determine how long A431 cells should be grown in physioxia for so that any such responses to redox-active compounds no longer change relative to A431 cells grown in 18.6% O_2 under the same treatment conditions.
4. To determine the molecular mechanisms behind any observed resistance of A431 cells grown in 18.6% O_2 to oxidative stress-induced cell death/damage compared to A431 cells grown in 3.0% O_2.

Objectives:

1. To maintain various crucial cell culture environmental parameters, such [O_2] and humidity, whilst A431 grow in 3.0% O_2.
2. To determine whether A431 cells grown in 3.0% O_2 express HIF 1-α protein (a known indicator of hypoxic response) using western blotting.
3. To measure H_2O_2 and auranofin-induced cell death in A431 cells grown in 18.6% O_2 or 3.0% O_2 using flow cytometry.
4. To determine the appropriate physioxia growth period for further investigations by growing A431 cells in 3.0% O_2 or 18.6% O_2 for 24, 48, 72 or 96 h.
5. To test the effect of changing the [O_2] *during treatment* on auranofin-induced cell death in A431 cells previously grown in 3.0% or 18.6% O_2, for 48 h. This is necessary in order to determine any observed resistance of A431 cells grown in 18.6% O_2 to auranofin-induced cell death can be reversed by lowering the [O_2] during auranofin treatment.
6. To test whether any such resistance of A431 cells grown in 18.6% O_2 (compared to physioxia) to H_2O_2/auranofin-induced cell death compared

to A431 cells grown in 3.0% O_2 extends to other redox-active compounds including 3-AT, L-BSO, carmustine, MSA, and CuOOH.

7. To identify the key molecular mechanisms through which A431 cells grown in 18.6% O_2 may acquire resistance to the effects of redox-active compounds compared to physioxia. A number of endpoints were assayed: $\Delta\psi_m$ (JC-1), ROS generation (MitoSOX, DHE, Amplex Red and DCFHDA), lipid peroxidation (C_{11} BODIPY$^{581/591}$), antioxidant enzymatic activity (e.g. catalase, SOD, GR, Gpx, and GST), protein nitration modifications (e.g. 3-nitrotyrosine residue), nuclear Nrf-2 protein expression level, and the expression levels of Nrf-2-target protein (i.e. NQO-1 and catalase). These endpoints were assessed in A431 grown in 18.6% O_2 or 3.0% O_2 for a culture period based on the outcome from objective 4.

CHAPTER 2: MATERIALS AND METHODS

2.1. Materials

Cell culture: Dulbecco's Modified Eagle's Medium (DMEM; 4.5 g/L glucose); fetal bovine serum (FBS; Batch #SH30070.03, # HYC23, US Origin), 2% L-glutamine (#LZBE17-605E) and 2% penicillin/streptomycin (pen/strep; #P4458-100 mL) were all sourced from Lonza; trypan blue (#T8154-100 mL) from Merck; T75 cell culture flasks from Greiner Bio-One; inert silicon grease (MolyKote 1102 grease; Dow Corning, Berry, Wales); and an O_2 clip single gas detector (#Clip SGD) from Crowden, Scunthorpe, England, UK.

Toxicity testing: Annexin V-FITC (#640905), and annexin V-FITC binding buffer (#422201) from BioLegend; propidium iodide (PI; #537059, Merck), JC-1 (#420200), H_2O_2 (#H1009), auranofin (#A6733), MSA (#820763), $_L$-BSO (#508228), CuOOH (#820502) from Merck.

Detection of reactive oxygen species and lipid peroxidation: DHE (#309800), DCFHDA (#D6883), and MitoTracker Red (#M7512) from Merck; MitoSOX (#M36008), C_{11} BODIPY$^{581/591}$ (#D3861), and Amplex Red (#A22188) from ThermoFisher.

Enzyme activity: GR from baker's yeast (#G3664), NADPH (#481973), catalase from bovine liver (#C9322), SOD from bovine erythrocyte (#574594), Gpx from bovine erythrocyte (#G6137), Ellman's Reagent (#322123), XO (#X4376), Diethylenetriaminepentaacetic acid (#D6518-5G), reduced glutathione (#104090), oxidised glutathione (#3542), 2-vinyl-pyridine (#132292) were sourced from Merck; 4-[3-(4-Iodophenyl)-2-(4-nitro-phenyl)-2H-5-tetrazolio]-1,3-benzene sulfonate (WST-1; #W201) from Dojindo Molecular Technologies, Maryland, USA.

Western blotting: protein blocking buffer (#927-60001) from LICOR, Nebraska, USA; 8–16% Mini-PROTEAN® TGX™ Precast Protein Gels (#4561105) pre-stained molecular weight protein ladder (#1610373), Trans-Blot Turbo RTA Mini 0.2 µm PVDF Transfer Kit (#1704272) from BioRad, Hemel Hemstead, UK; recombinant human NQO-1 protein (#ab87692), NQO-1 primary antibody (#ab264434) from Abcam; recombinant human Nrf-2 protein (#H00004780), Nrf-2 primary antibody (#NBP1-32822), catalase primary antibody (#NBP2-24916), glyceraldehyde-3-phosphate dehydrogenase primary antibody (GAPDH;

#NB300-221) from BioTechne, Abington, Oxford, UK; HIF-1α primary antibody from Thermofisher (#17-7528-82); β-cytoskeletal actin primary antibody (#A300-485A) from Bethyl laboratories, Montgomery, TX, USA.

2.2. Routines for *in vitro* cell culture

2.2.1. Use of the laminar flow hood

All cell culture work was carried out under aseptic conditions in a class-II laminar flow hood (HerasafeHS-15, Fisher Scientific; Loughborough, UK) to prevent bacterial or fungal contamination. Tissue culture-clean laboratory coats and latex/nitrile gloves were worn at all times. Prior to cell culture, the hood was sprayed and wiped internally on all surfaces with 70% v/v ethanol made up with ultrapure water (UH_2O). This included the sterilisation of any items used within the hood. Pipette tips were sterilised in an autoclave at 121°C prior to use inside the laminar flow hood (Priorclave EV100; Priorclave, London, UK).

2.2.1. A431 cells as a model cell line for non-melanoma skin cancer research

A431 cells are a squamous cell carcinoma human cell line which model aspects of non-melanoma squamous cell carcinoma (NMSC) [224]. The cells were isolated from an epidermoid carcinoma in the skin of an 85 year old female patient [225]. A431 cells possess no functional p53 and are highly sensitive to mitogenic stimuli such as epidermal growth factor [225]. The mutations present in p53 in the A431 cell line contain C to T, and CC to TT transitions at dipyrimidine sequences which are known UV signature mutations [226]. UV radiation in sunlight is believed to be responsible for the induction of NMSC [227]. UV mutations in p53 precede the progression of skin cancer tumour growth in mice [227].

2.2.2. Receipt of frozen ampoule

The laminar flow cabinet which was run for 10 min before use to stabilise the air flow. The A431 cell growth medium was DMEM containing 10% v/v FBS, 2% v/v L-glutamine, and 2% v/v penicillin/streptomycin (pen/strep). Upon receipt of the frozen A431 cell ampule from the European Collection of Authenticated Cell Cultures (ECACC) at passage 5+, the vial was thawed quickly in a 37°C bead bath. The contents were subsequently transferred into a 15 mL tube containing 5

mL of pre-warmed growth medium. The Falcon tube was centrifuged for 2 min at a relative centrifugal force (RCF) of 200 x g. The supernatant was vacuum aspirated and the pellet was re-suspended in 10 mL of pre-warmed growth medium. The resulting cell suspension was transferred into T75 (surface area 75 cm^2) vented flasks. The cells were then monitored under an inverted light microscope (Nikon Eclipse, TS100, Nikon, and Surrey, UK) to ensure even distribution. The flasks were then transferred to an incubator set at 37°C and 5% CO_2 for 24 h. After 24 h, the old growth medium was aspirated and replaced with fresh pre-warmed growth medium. The flasks were then transferred to the incubator (37°C/5% CO_2). Due to the fast growth kinetics of A431 cells **(section 2.3.4)**, the growth medium was replaced every 24 h and A431 cells were sub-cultured every 3-4 days (or when the cells were about 70-80% confluent). Cellular confluence was monitored using inverted light microscopy **(Figure 2.1)**.

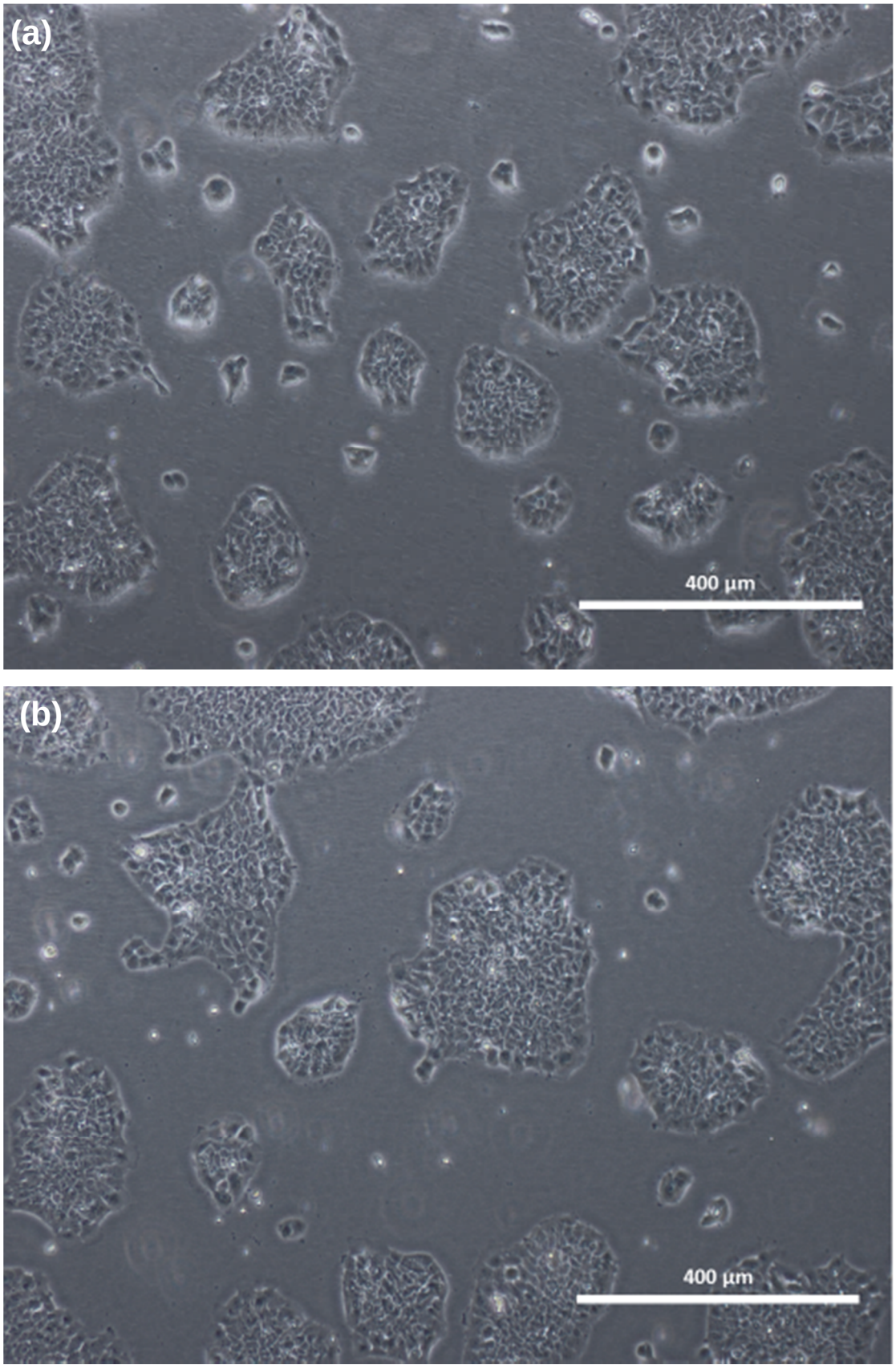

Figure 2.1. A431 cells growing in cell culture in either 18.6% O_2 or 3.0% O_2. A431 cells form colonies in their sub-confluent growth phase with irregular borders during the initial stages of cell culture (< 20 h). However, these borders eventually (>20 h) become more regular in appearance and form oblong/oval shaped colonies. Microscope images taken at x10 magnification using a Nikon inverted light microscope. **Panel (a),** A431 cells grown in 18.6% O_2 for 48 h. **Panel (b),** A431 cells grown in 3.0% O_2 for 48 h.

2.2.3. Subculture of A431 cells

At 70-80% cellular confluence, the growth medium was aspirated and the cell monolayer was washed two times with pre-warmed, sterile filtered, PBS without calcium or magnesium (137 mM NaCl, 2.7 mM KCL, 10 mM Na_2HPO_4, and 1.8 mM KH_2PO_4 with a pH buffering range of 7.0–7.6; # F151278, Lonza). This PBS concentration was used in all flow cytometry preparations, and cell culture washing procedures. PBS was then aspirated into 10% v/v Virkon (Fisher Scientific). 3 mL of pre-warmed 0.25% v/v trypsin-(ethylenediaminetetraacetic acid; EDTA) with phenol red was then added. The flasks were then incubated at 37°C for no more than 5 min. For optimal activity, Trypsin–EDTA was frozen down into single use aliquots and was used at 300 µL per 1.0 x 10^6 cells.

The flasks were gently tapped to aid cellular detachment. Cellular dissociation from the culture flasks was monitored by light microscopy. Once the cells had detached, the trypsin was inactivated by adding an equal volume of pre-warmed growth medium. The resulting cell suspension was transferred into a 15 mL Falcon tube and centrifuged at 200 RCF for 2 min. The supernatant was then aspirated and the cell pellet was washed two times with pre-warmed PBS. The pellet was then re-suspended in pre-warmed growth medium. A 10 µL sample of this solution was then collected for cell counting **(section 2.2.4)**. A431 cells were split into varying numbers of T75 flasks (depending on the number of flasks required for experimentation) at a density of 9.5 x 10^3 cells/cm^2.

2.2.4. Cell counting

10 µL of the sample cell suspension was mixed with 10 µL of trypan blue (1:1 dilution). 10 µL of this solution was added in duplicate to each chamber of an automated cell counting slides (#1450015, Bio-Rad Laboratories Ltd, Watford, Hertfordshire, UK). The slides were then inserted into the counting chamber of a TC20™ automated cell counter (Bio-Rad). The automated cell counter automatically detected the presence of trypan blue and determined the concentrations of viable cells per mL based on trypan blue exclusion [228]. The resulting cell concentration was used to determine the appropriate volume of sample needed in order to achieve the required seeding density for experimentation.

2.2.5. Measuring the time required for A431 cells to attach to a cell culture plate prior to a medium change

Moving A431 cells into 3.0% O_2 **(section 2.3)** required replacing the growth medium with 3.0% O_2-equilibrated growth medium. In order to avoid losing cells during the medium change, it was necessary to determine how long A431 cells required to adhere to cell culture plastic prior to replacing the growth medium. To this end, A431 cells were seeded in 24 well plates at 9.5 x 10^3 cells/cm^2 and were incubated at 37°C/5% CO_2 for 0–3 h. The number of cells detached after pipette aspiration was measured by cell counting **(section 2.2.4).** A 1.5 h incubation prior to pipette aspiration resulted in a lower number of A431 cells detaching from the plate compared to the time 0 control, with means of 2300 ± 860 cells vs 19,653 ± 620 cells ($P < 0.0001$; **Figure 2.2**). Cell counts at further time points (i.e. 2 h) was not measured due to the lower detection limit of the automated cell counter.

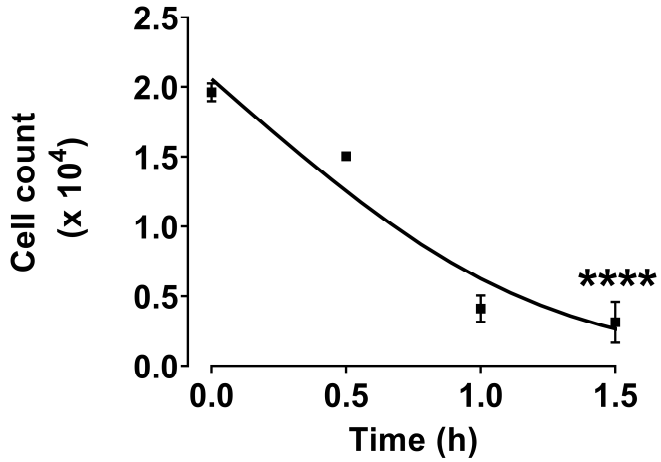

Figure 2.2. The length of time required for A431 cells to adhere to cell culture treated plastic. A431 cells were seeded at a density of 9.5 x 10^3 cells/cm^2 in 24 well plates. A431 cells were incubated for 0, 0.5, 1, or 1.5 h (37°C/5% CO_2). For the 0 h time point, cells were kept suspended in growth medium in a 15 mL Falcon tube. After the end of each respective incubation period, the growth medium was pipette aspirated from each well and was transferred into a 15 mL tube. The well was also washed once with PBS (see section 2.2.3 for concentration) to mimic the routine protocol for changing cell growth medium. The PBS used for this purpose was also transferred into the respective 15 mL tubes. The cell suspension was centrifuged at 200 RCF for 1 min and re-suspended in 0.5 mL of growth medium. A cell count was performed using a TC20™ automated cell counter. **** = $P < 0.0001$ versus time 0 control utilising a paired two-tailed Student's t-test. Data are presented as the mean ± 1 SD. n = 3. Where error bars are not visible, this is because the error bar is smaller than the size of the data point.

2.3. Culturing cells under physioxia

To mimic the [O_2] in human skin, A431 cells were grown at an [O_2] of 3.0% O_2 **(section 1.1.2.1)**.

To this end, all 'physioxia' cell culture were performed in a low O_2 workstation (Sci-Tive Stem Cell Investigations Total in Vitro Environment advanced hypoxia workstation, The Baker Company, 175 Gatehouse Road, Sanford, Maine, 04073 USA) set at 3.0% O_2, 5% CO_2, and 37°C **(Figure 2.3 and Figure 2.4)**. This is referred to in the text as a 'physioxia hood'. A 3.0% O_2 gas environment refers to a total gas mixture of 3.0% O_2, 5% CO_2 and 92% N_2 at 95% RH. The issue of RH in the physioxia hood is addressed in **section 2.3.2.** An illustration of how A431 cells were grown in physioxia for different lengths of time is shown in **Figure 2.17**.

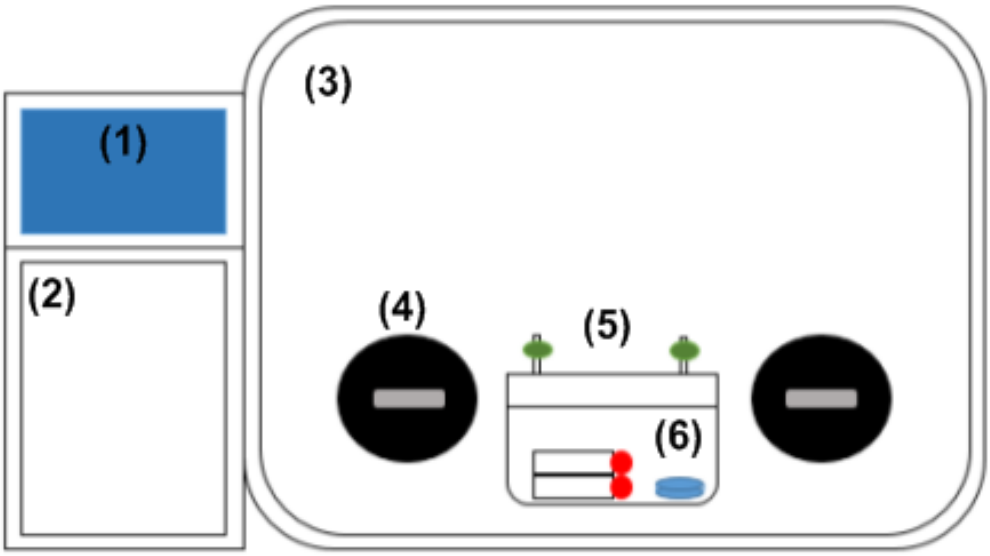

Figure 2.3. Illustration of the Sci-Tive Total In-Vitro Environment hood. (1), control panel. **(2),** chamber interlock. **(3),** plexiglass front. **(4),** chamber glove ports. **(5),** 'Klip-lock' container. **(6),** T75 flasks and petri dish of water sealed inside the 'Klip-lock' container.

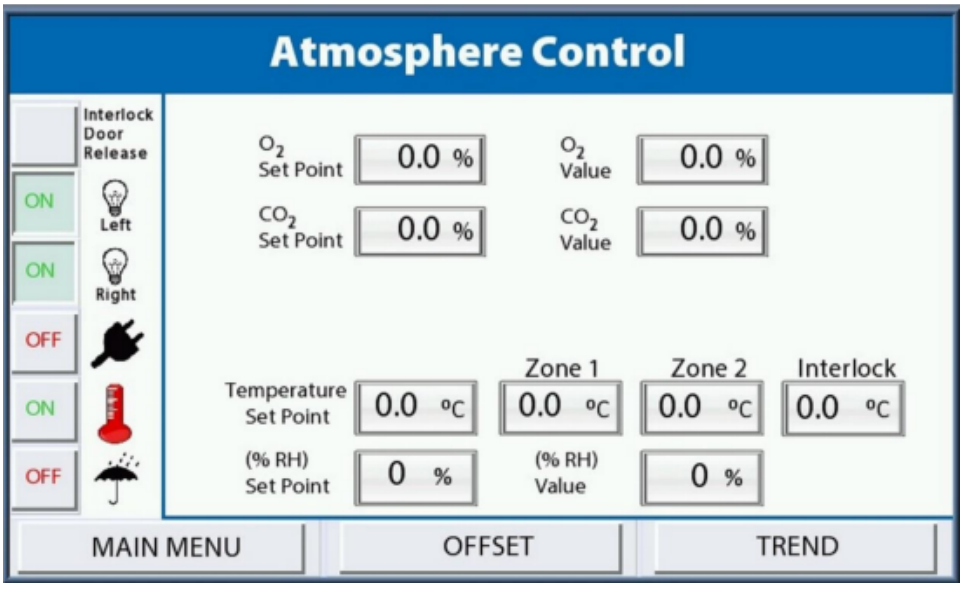

Figure 2.4. Sci-Tive Total *in vitro* Environment hood control screen. From this screen, [O_2], [CO_2], and temperature were set at the desired values. The actual values detected by the electrochemical and paramagnetic detectors are designated as the O_2 and CO_2 'Value', respectively. **[CO_2]:** carbon dioxide concentration; **[O_2]**: molecular oxygen concentration.

2.3.1. Routine for using the physioxia hood

All cell culture manipulations under physioxia were performed through the glove ports set into the gas tight screen of the physioxia hood **(Figure 2.3)**. Equipment such as a micro-centrifuge, and a 'pipette-boy' were powered within the hood allowing general cell culture procedures to be performed in physioxia. Microscopes were not used inside the hood due to voltage limitations. Instead, gas-tight screw-cap lids (#658170, Greiner) were used to seal the flasks prior to removal from the physioxia hood **(Figure 2.5)**. Microscopy could then be performed outside the physioxia hood without changing the [O_2] in the flasks.

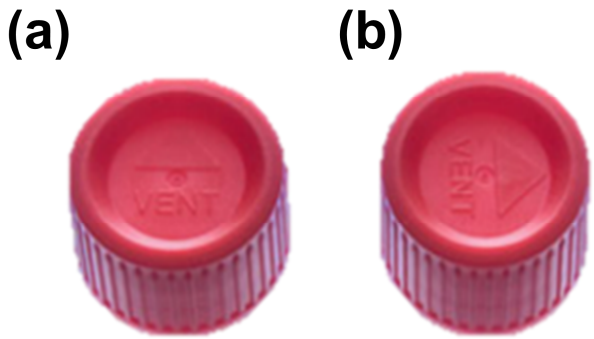

Figure 2.5. Screw caps used for physioxia cell culture. Panel (a), in this position, the flask lid is vented to allow oxygenation of the flasks. **Panel (b),** by screwing the lid clockwise, an airtight seal is created, and the oxygenation condition within the flasks was maintained. A431 cells could then by viewed under a microscope without changing the [O_2]. **[O_2]**: molecular oxygen concentration.

All cell culture equipment was sprayed with 70% ethanol. Routine cleaning of the hood was performed daily (or after use) with 70% ethanol. A deep clean was performed with detergent and Virkon every month.

Generally, A431 cells were seeded as required into T75 or 24 well plate at a density of 9.5 x 10^3 cells/cm^2 and were allowed to adhere to the plates/flasks for at least 3 h at 37 °C/5% CO_2 prior to transfer to the physioxia hood. The medium was then removed, the monolayer was washed once with PBS (see **section 2.2.3** for concentration) and was replaced with 3.0% O_2-equilibrated growth medium **(section 2.3.3.1)**. The flasks/plates were then placed into a 'Klip-lock' container with a 150 x 15 mm petri dish filled halfway containing H_2O **(section 2.3.2)**. The box was then sealed inside the physioxia hood and the cells were allowed to incubate for the required length of time in 3.0% O_2. Growth medium was changed every 24 h with O_2-equilibrated growth medium.

2.3.1.1. Calibration of Ruskinn Environmental chamber O_2 sensor

The O_2 sensor in the physioxia hood was calibrated once a month. **Figure 2.6** shows the O_2 auto-calibration screen. Once initiated, the [O_2] within an external bladder decreased from atmospheric (20.9%) to anoxia (0%). As the calibration was performed using this external bladder, the internal partial pressures of the main chamber were not affected. Once completed, the software indicated whether the sensor has passed or failed the calibration.

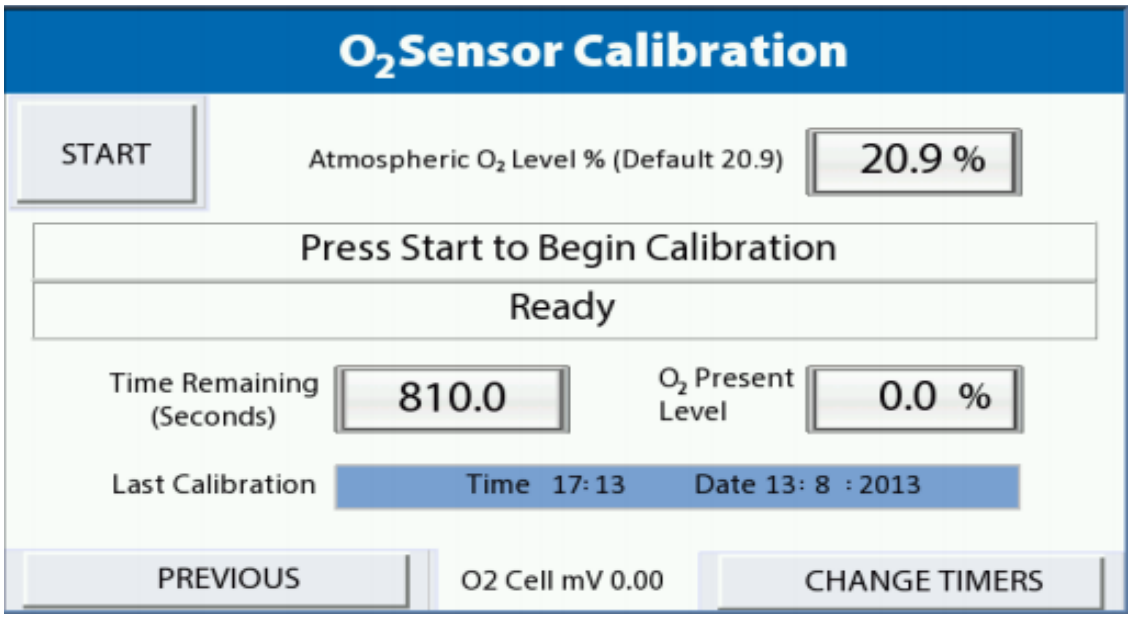

Figure 2.6. O_2 sensor calibration screen for the Sci-Tive Total in vitro Environment hood.

2.3.2. Method development: maintaining relative humidity 'physioxia' cell culture

Mammalian cells grown in standard CO_2 incubators at 37°C are usually grown at 95% RH. Humidity is usually generated through the evaporation of H_2O from a tray kept at the base of the incubator unit. This parameter was also replicated for growing cells in 3.0% O_2.

Unfortunately, humidification of the physioxia hood using the built in humidification system made it difficult to control the growth of contaminants. This was despite rigorous sterilisation of the components inserted into the hood, and weekly cleaning of the hood itself using 70% ethanol and Virkon. A standard CO_2 incubator can be cleaned relatively easily as the shelves are usually removable. However, cleaning the physioxia hood required removal of the Plexiglas front and the plastic base **(Figure 2.3)**. Doing so required flushing the gas environment inside the physioxia hood to atmospheric conditions. These issues significantly increased the cost of running the physioxia hood per month. An entire 150 L pressurised nitrogen gas cylinder was needed to re-gas the physioxia hood to 3.0% O_2 after cleaning. Based on the incidence of contamination, the physioxia hood required cleaning once to twice per week when the built-in humidification system was used.

To overcome this, a bisphenol A free plastic lunchbox container ('Klip-Lock' Sainsbury's; **Figure 2.7)** was used as a scaled-down growth environment for physioxia cell culture. This provided two advantages: First, the boxes were much easier to clean as they boxes could be washed in a dishwasher or wiped down with 70% ethanol; secondly, the boxes could be easily humidified without exposing the rest of the physioxia hood to humidity that would otherwise encourage microbial or fungal growth. The use of the boxes therefore kept the physioxia hood clean and contamination free whilst also providing a suitable [O_2] growth environment for the cells **(Figure 2.3)**.

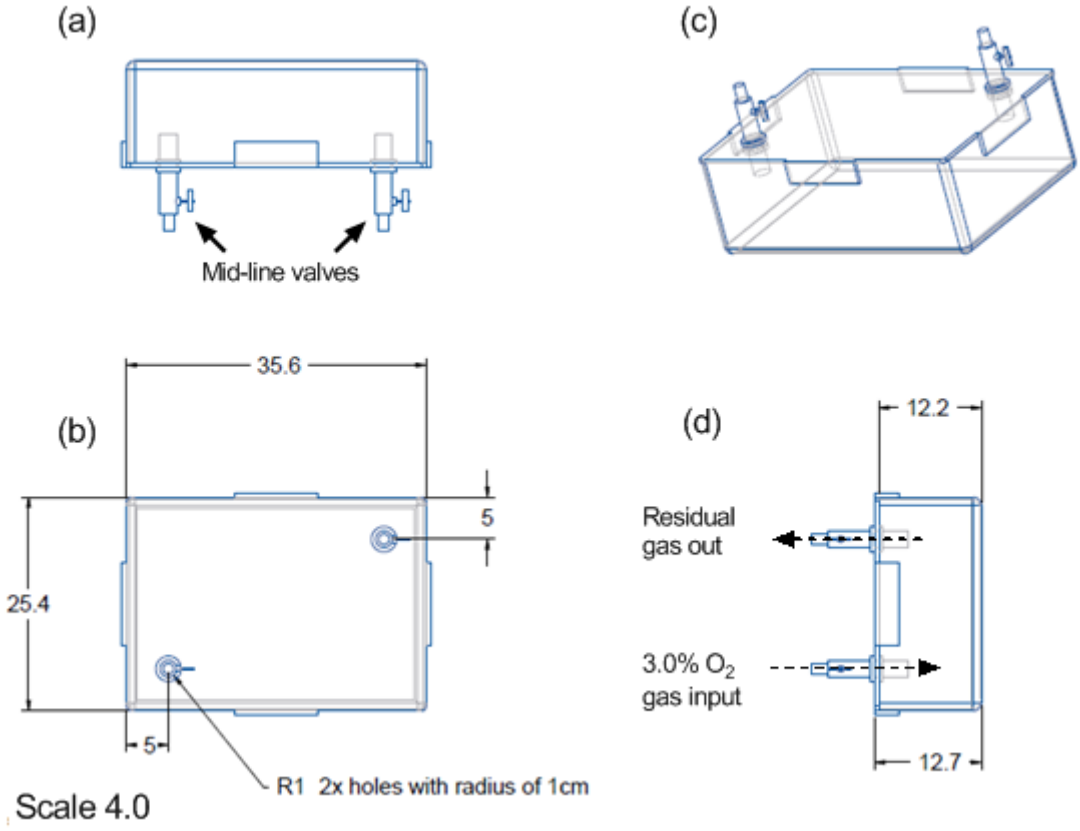

Figure 2.7. 'Klip-lock' lunch box container used for the growth of A431 cells under 3.0% O_2. The 'Klip-lock' containers were augmented with midline valves to allow the internal gas environment in the box to be purged using a pre-mixed gas canister (3.0% O_2, 5% CO_2, 92% N_2; DDRC Healthcare). **Panel (a),** side view. **Panel (b),** top view. **Panel (c),** isometric view. **Panel (d),** demonstration of gas flow using an attached pre-mixed gas cylinder. All measurements are in centimetre. Image kindly produced in CREO CAD parametric by L. Jordan.

The ability of the Klip-lock containers to maintain the appropriate RH % (v/v) value was measured. First however, the normal RH% in a standard cell culture incubator was measured.

Using a hygrometer (T2041, Merck), RH% was determined by filling a standard cell culture water tray (35 cm x 35 cm x 15 cm) with 1 L of autoclaved H_2O. Once filled, the hygrometer was placed inside the incubator. The incubator was then closed. The RH % (v/v) value was recorded at intervals of 5 min for 50 min by viewing the value on the hygrometer through the interior glass door without purging the chamber to air **(Figure 2.8)**. At 40 min when the reading had stabilised, the hygrometer was removed from the incubator and the RH% (v/v) was read for an additional 15 min.

A similar experiment was also performed in the plastic 'Klip-lock' containers to determine whether a 95% (v/v) humidity could be generated. The volume of the boxes was about 30 times lower than the standard CO_2 incubators. As such, a scaled down version of the incubator water tray was required. To this end, a 150 x 15mm petri dish of water was filled halfway with autoclaved H_2O and placed inside the 'Klip-lock' box with the hygrometer. The 'Klip-lock' box was then sealed within the physioxia hood set at 3.0% O_2. The RH% (v/v) value was recorded at intervals of 5 min for 50 min by viewing the value on the hygrometer through the plastic without opening it to the physoxia hood **(Figure 2.8)**. At 40 min, when the reading had stabilised, the box was removed from the physioxia hood and opened to air. The RH% (v/v) was then read for an additional 15 min. Both the CO_2 incubator and the 'Klip-lock' box showed statistically significant increases in RH% (v/v) after 20 min compared to respective 0 time-points ($P < 0.0001$). There was no statistically significant differences in the RH% value at 20 mins between the two groups.

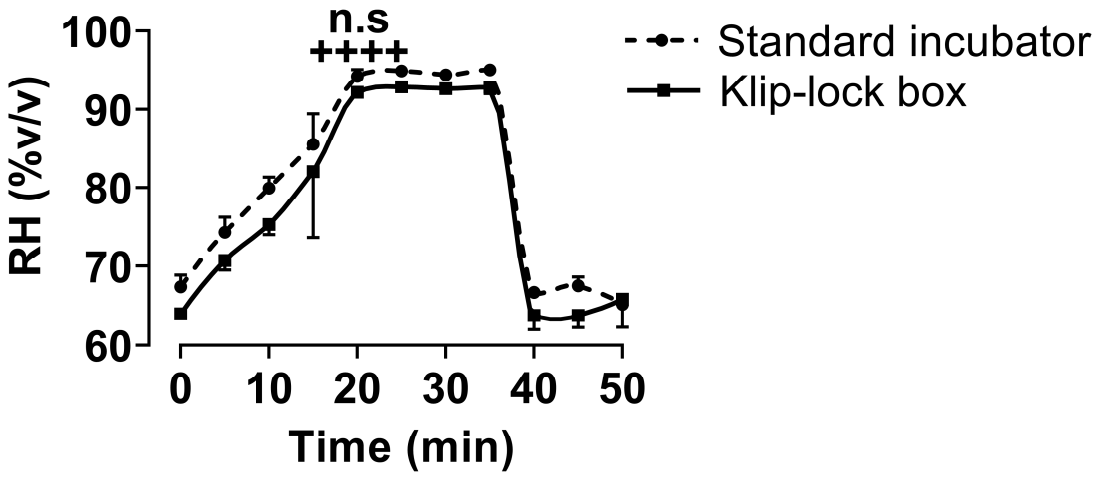

Figure 2.8. Relative humidity generation in a standard CO_2 incubator compared to a 'Klip-lock' box. RH generation at 37°C was measured at intervals of 5 min for 40 min inside either a standard CO_2 incubator or inside a 'Klip-lock' box sealed within the physioxia hood sealed set at 3.0% O_2. The source of humidification in the standard CO_2 incubator was 35 cm x 35 cm x 10 cm metal water tray half filled with autoclaved water. The source of humidification for the 'Klip-lock' box was a 150 x 15mm petri dish half filled with autoclaved water. At 0 min, the RH% (v/v) value on the hygrometer was recorded before placing the hygrometer into the incubator or plastic box. For RH% measurements in the CO_2 incubator, the hygrometer was placed inside the incubator and the internal and external doors were closed. For the plastic box measurements, the hygrometer was placed into the 'Klip-lock' box and sealed inside the physioxia hood. The RH% (v/v) was measured at intervals of 5 min for 40 min. The hygrometer was then removed from the incubator or 'Klip-lock' box at 40 min. The resulting RH% (v/v) value was recorded for an additional 15 min at 5 minute intervals. n.s = not significant versus standard incubator, ++++ = $P < 0.0001$ versus respective 0 time-point utilising a two-way ANOVA with multiple comparison and Šidák correction. Data are presented as the mean ± 1 SD. n = 3, where error bars are not visible, this is because the error bar is smaller than the size of the data point. **RH:** relative humidity.

2.3.3. Method development: testing the airtightness of 'Klip-lock' boxes for reagent equilibration

Reagents used for experimentation (e.g. PBS, DMEM, and UH_2O) were equilibrated to 3.0% O_2 prior to use. The physioxia hood was not used for [O_2] equilibration. This is explained in **section 2.3.3.1.** Gassed 'Klip-lock' containers were used instead. It was first necessary to test the airtightness of these containers when used outside of the physioxia hood.

The containers were designed to be gas-tight, but to further ensure the internal [O_2] environment was maintained, the rubberised seals on the lid were greased with an inert silicon grease (MolyKote 1102 grease; Dow Corning, Berry, Wales). The 'Klip-lock' containers were designed to allow the displacement of O_2 utilising pre-mixed gas **(Figure 2.9 a)**. The 3.0% O_2 gas mixture was made up in 10 L, 150 bar cylinders (Diving Diseases Research Centre Healthcare, Plymouth, UK). To displace the gas within the container, the pre-mixed gas canister was affixed to the inlet valve of the 'Klip-lock' container. Both the inlet and outlet midline valves were opened and the gas flow was initiated. This resulted in the displacement of the existing gas (20.9% O_2) to 3.0% O_2 within the container. The pre-mixed gas canister had a gas flow rate of about 4 L/min. Gassing a 4L container to 3.0% O_2 with a pre-mixed gas cylinders took about 2 mins. This was initially verified using an O_2 clip single gas detector (#Clip SGD, Crowden, Scunthorpe, England, UK, **Figure 2.9 b**). Closure of both of the valves after the test [O_2] was reached produced a gas-tight environment that was stable for up to 48 h **(Figure 2.10)**. Therefore, the 'klip-lock' boxes were utilised for overnight equilibration of test reagents to 3.0% O_2.

Although no change in the [O_2] in the 'Klip-lock' containers over 48 h was noted **(Figure 2.10)**, the detector used in these experiments measured [O_2] to an accuracy of a single decimal place. Minor changes in [O_2] smaller than the detection limit for the O_2 detector (< 0.05% O_2) may have occurred **(Figure 2.10)**. 'Klip-lock' containers were tested for airtightness at least once a month. The lip seals were re-greased with an inert silicone grease every fortnight.

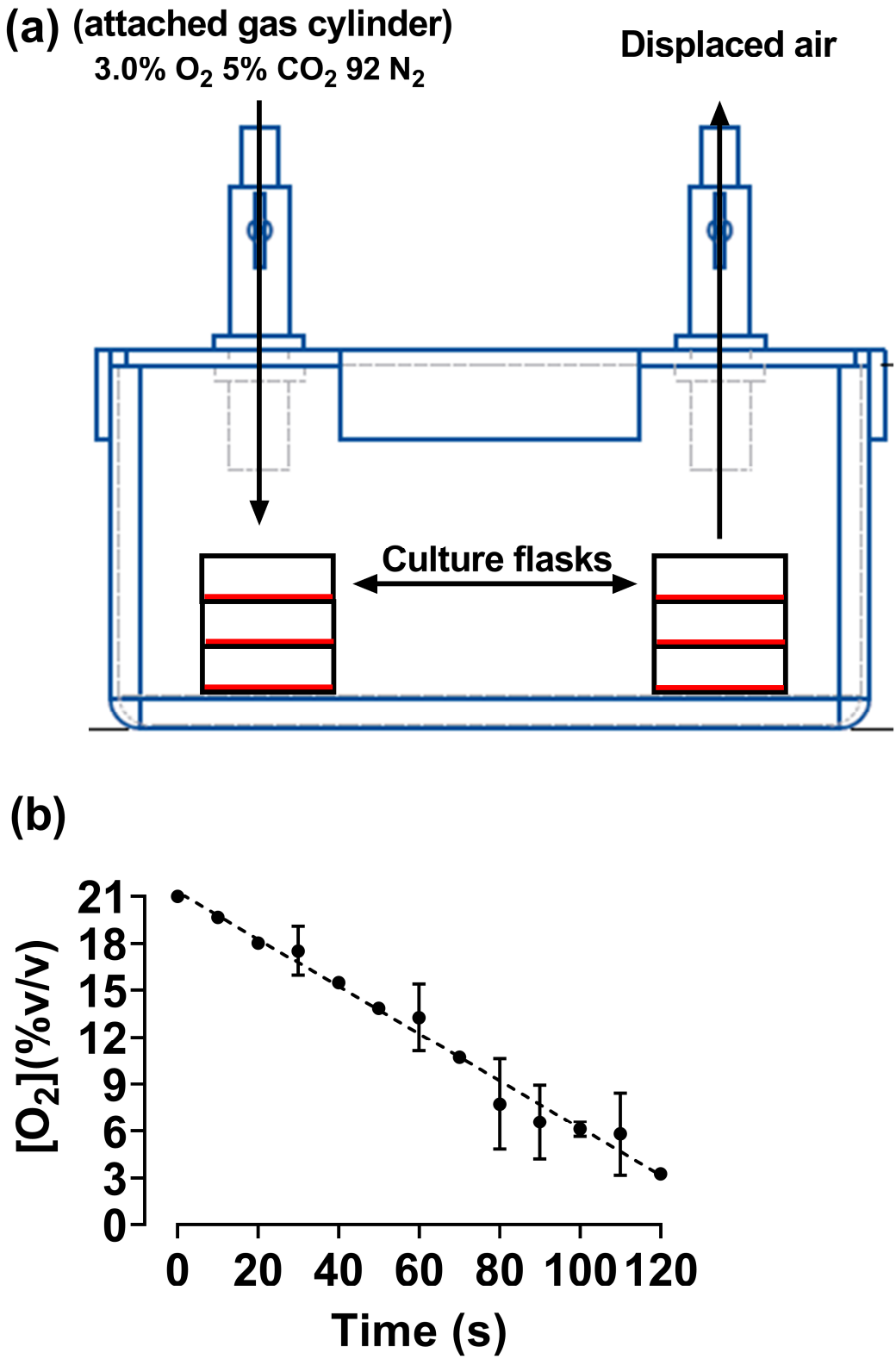

Figure 2.9. Illustration of a 'Klip-lock' container and a representative graph depicting the decay in O_2 concentration in these containers during gassing. Panel (a), A 'Klip-lock' box containing medium undergoing equilibration to 3.0% O_2 using a pre-mixed gas cylinder (3.0% O_2, 5% CO_2, 92% N_2; DDRC Healthcare). **Panel (b),** gas displacement by pre-mixed gas in the 'Klip-lock' container representative of a single experiment. The dashed line represents the best fit line generated by simple linear regression (R_2= 0.94).

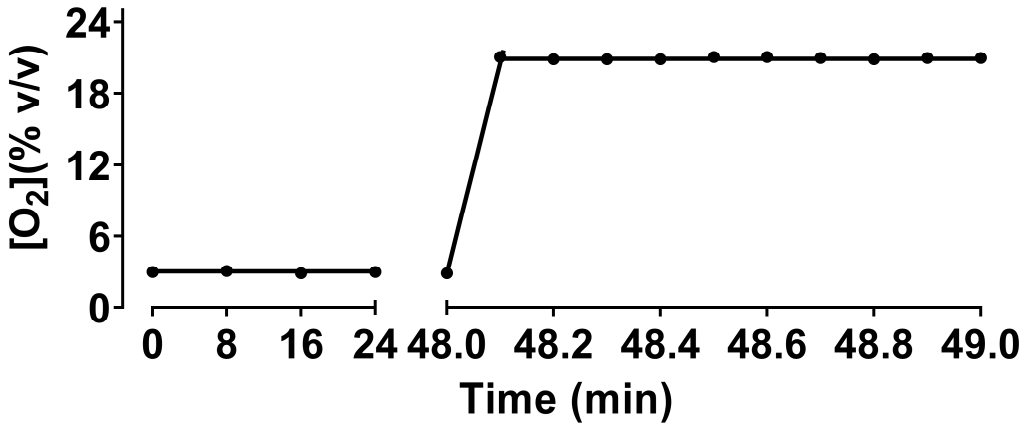

Figure 2.10. Testing the airtightness of a 'Klip-lock' container. An O_2 gas detector probe was placed into a 'Klip-lock' container which was subsequently purged to 3.0% O_2 with pre-mixed gas (DDRC Healthcare). Once the [O_2] had reached 3.0% O_2, the box was sealed by closing the inlet and outlet valves. The [O_2] was monitored at intervals of 8 h for a total of 48 h by recording the reading on the O_2 single gas detector (Crowden) through the transparent plastic. The box was then opened to air (after x axis break) and [O_2] was monitored at intervals of 10 min for an additional 1 h. n=1.

2.3.3.1. Method development: measuring [O_2] in growth medium using a blood gas analyser

The physioxia hood was not used to equilibrate growth media/ liquid test reagents to 3.0% O_2. This was because it was in constant use at 37°C and could not be cooled below room temperature. Growth medium required at least 8 h to reach 3.0% O_2 **(Figure 2.11)**. Storage of growth medium in 37°C for long periods of time added an experimental variable not recapitulated in the 18.6% O_2 growth medium. Most 18.6% O_2 reagents were warmed for only 15-30 minutes in a bead bath prior to use. As such, medium/reagents were equilibrated to 3.0% O_2 at 4°C in klip-lock boxes.

Initial experiments set out to measure the time taken for growth medium to equilibrate to 3.0% O_2 from 20.9% O_2. Additionally, the effect of agitation on the time taken for [O_2] equilibration was also determined.

To this end, T75 cm^2 flasks were filled with 40 mL of growth medium and were placed into 'Klip-lock' boxes. The boxes were then gassed as described previously **(section 2.3.3)**. To test the effect of agitation on equilibration time, a small magnetic stirrer was added to one of the T75 cm^2 flasks. Once the container had been gassed to 3.0% O_2, the box was moved into the cold room (4°C). The

box with the magnetic stir bar was placed on top of a magnetic stirrer and was set to stir at 60 RPM.

A blood gas analyser (ABL9, Radiometer Ireland Limited, Lismeehan, O'Callaghan's Mills, Clare, Ireland) was used to measure [O_2] in growth medium. Prior to analysing the sample, an instrument calibration was performed. The purpose of calibration was to evaluate the accuracy to which the analyser measured [O_2]. The ALB-9 utilises a basic amperometric based method to measure [O_2] using a Clark electrode. A three point calibration was performed using solutions of known [O_2] (0, 10 and 20.9% O_2).

To avoid re-oxygenation of the test reagents, gas tight vials (#1172A68, Thomas Scientific) were used to collect the sample to prevent re-oxygenation. Sample collection was performed inside the physioxia hood. 5 mL of the growth medium from the stirred and unstirred group was then transferred into a gas tight glass vial prior to sealing the cap closed. The medium was sampled by the analyser through the airtight rubber septum in the gas tight vial.

Measurement of sample [O_2] was performed by initiating the analysis software to detect pO_2. The sample gasket needle was inserted into the vial through the rubber septum. The ABL-9 analyser measured [O_2] in the units of partial pressure with the SI unit kilo pascal (kPa). kPa was then converted into O_2% (v/v) using the formula in **Eq.2.1**.

$$\frac{\textbf{Pressure of O2 within solution (kPa)}}{\textbf{Atmospheric pressure (kPa)}} \textbf{ x } 100\% = \%\,O_2 \qquad \textbf{(Eq. 2.1)}$$

The effect of medium agitation on [O_2] equilibration is shown in **Figure 2.11**. Although stirred medium equilibrated to 3.0% O_2 faster compared to unstirred medium, unstirred overnight equilibration (about 16 h) was sufficient for our purposes **(Figure 2.11)**. Stirring also caused frothing even at quite low RPM (30 RPM). This risked the loss of key growth supplements in growth medium and so it was not performed.

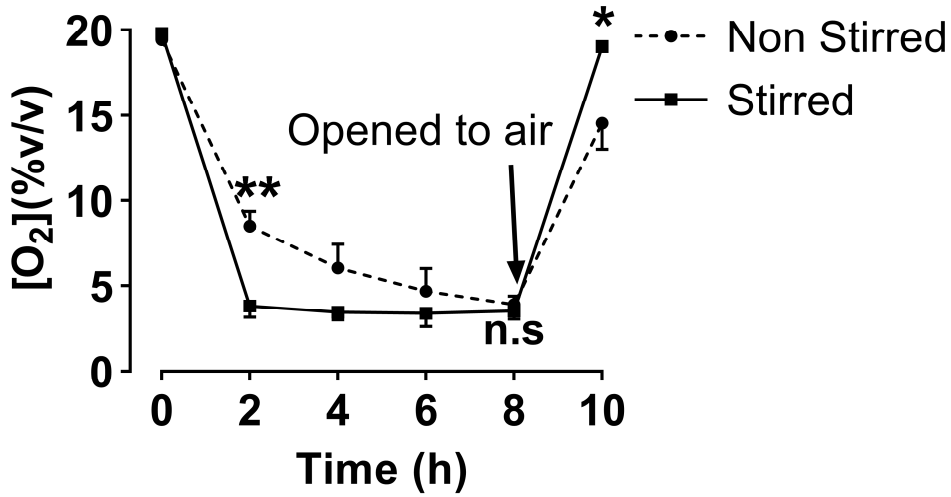

Figure 2.11. The time taken for growth medium to equilibrate to 3.0% O_2 with or without stirring. Two 75 cm^2 flasks were filled with 40 mL of growth medium and were placed into a 'Klip-lock' container. In order to determine the effect of agitation on [O_2] equilibration time, a magnetic stirring bar (36 x 9mm) was added to one of the flasks and the other was left un-stirred. A total of 4 boxes, each representing the 2, 4, 6, or 8 h time-point, were used with separate flasks. This was needed as measurement of [O_2] required removal of the flasks from the stirrer in order to sample the medium. The boxes were then closed and gassed to 3.0% O_2 utilising pre-mixed gas (section 2.3.3). The boxes were then sealed by closing the inlet and outlet valve before placing the appropriate containers onto a magnetic stirrer set at 60 RPM in a cold room at 4°C. The medium was allowed to equilibrate for a total of 10 h, and the [O_2] was measured at intervals of 2 h from the appropriate box. To measure [O_2], a 5 mL sample of liquid from each flask was transferred into a gas tight glass vial performed within a physioxia hood set at 3.0% O_2. The [O_2] within the sample was measured using an ABL-9 blood gas analyser. After 8 h, the box containing the 8 h group was analysed for [O_2] and was subsequently allowed to equilibrate to atmospheric O_2 at 4°C by opening the box to air. After an additional 2 h the [O_2] from this group was measured as before. n.s = not significant, * = $P < 0.05$ versus non-stirred, ** = $P < 0.01$ versus stirred utilising a two-way ANOVA with multiple comparisons and Dunn-Šidák correction. Data are presented as the mean ± 1 SD. n = 3, where error bars are not visible, this is because the error bar is smaller than the size of the data point.

2.3.4. The effect of growing A431 cells in 18.6% O_2 on cellular growth kinetics versus 3.0% O_2

Prior to toxicity testing with redox-active compounds **(Chapter 3)**, the growth kinetics of A431 cells grown in 18.6% O_2 or 3.0% O_2 were measured. This was to ensure that [O_2]-dependent differences in the cellular response to compound treatment was not due to [O_2]-dependent differences in growth rate. To this end, A431 cells were grown in 3.0% O_2 or 18.6% O_2 for 24, 48, 72 or 96 h and then a cell count was performed **(Figure 2.12)**. There was no statistically significant differences in the total cell count between the two [O_2] groups at any of the indicated time points. Therefore, it was concluded that the growth of A431 cells in 3.0% O_2 did not affect growth rate compared to A431 cells grown in 18.6% O_2.

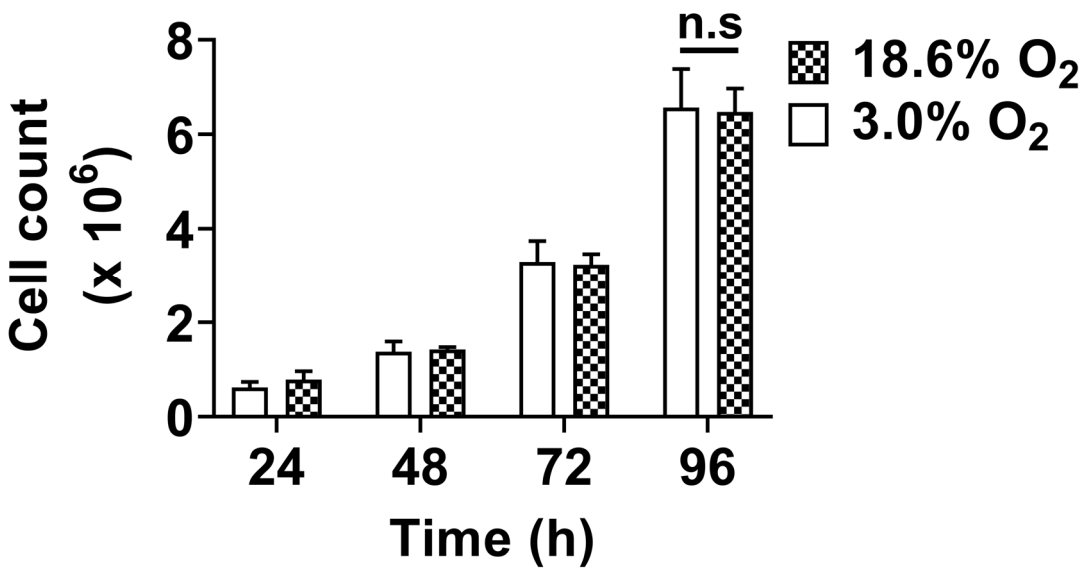

Figure 2.12. Effect of growing A431 cells in 18.6% O_2 on cellular growth kinetics compared to A431 cells grown in 3.0% O_2. A431 cells were seeded at a density of 9.5 x 10^3 cells/cm^2 in T75 flasks and were grown for 24-96 h in 3.0% or 18.6% O_2 at 37°C / 5% CO_2. After the indicated incubation times, cells were detached with 0.25% trypsin-EDTA and counted with a TC20™ automated cell counter. n.s = not significant compared to 3.0% O_2 utilising a two-tailed Student's t-test. Data are presented as the mean ± 1 SD. n=3.

2.3.5. Measuring the induction of hypoxia: Hypoxia-inducible factor-1α

Growth of cells under < 1% O_2 may induce a hypoxia response **(section 1.1.3)**. The test [O_2] used in this work was 3.0% O_2. This replicates physioxia in skin **(section 1.1.2.1)**. [O_2] gradients may form in cell culture medium due to the O_2 demands of oxidative phosphorylation [11]. This may have resulted in a difference between the [O_2] set point on the gas controller **(Figure 2.4)** and the [O_2] at the peri-cellular layer *in vitro*. As such the growth of mammalian cells at 3.0% O_2 may have activate HIF-1α.

A bio-reactor system would solve this issue by preventing the formation of O_2 gradients through growth medium agitation. Simple disposable plastic bioreactors can be used and are readily available. However, medium agitation may introduce liquid shear stress forces. As this laboratory did not possess the means to measure these types of bio-physical phenomena, it was decided that regular cell culture techniques would be used instead. The use of a basic *in vitro* cell culture technique had the benefit of expanding the application of this project to researchers who utilise 2D monoculture for their *in vitro* modelling systems.

The induction of a cellular hypoxia response is associated with higher expression levels of HIF-1α protein **(section 1.1.3.1)**. As previously discussed **(section 1.1.3.1)**, HIF-1α is a transcription factor which is continuously degraded in the presence of O_2 by the VHL ubiquitin ligase complex **(Figure 1.3)**. Under hypoxic conditions, HIF-1α accumulates in the nucleus and induces the expression of genes involved in the hypoxia survival response (e.g. VEGF, Ang4, and EPO).

In order to determine whether HIF-1α was activated in A431 cells grown in 3.0% O_2, nuclear HIF-1α protein expression levels were measured by western blotting using lysate from A431 cells grown in 18.6% O_2 or 3.0% O_2 for 96 h.

2.3.5.1. Detection of hypoxia-inducible factor-1α by western blotting

A431 cells were seeded at a density of 9.5 x 10^3 cells/cm^2 in T75 cm^2 flasks and were grown in 18.6% O_2 or 3.0% O_2 **(section 2.3.1)** for 96 h (5%CO_2/37°C). As a positive control for HIF-1α activation, one flask of cells growing in 18.6% O_2 for 92 h was switched into 0.5% O_2 for 4 h in order to allow HIF-1α protein to accumulate. As the switch from 18.6% O_2 to 0.5% O_2 required changing the 18.6% O_2-equilibrated medium with 0.5% O_2-equilibrated medium, the decrease

in [O_2] from 18.6% to 3.0% O_2 was immediate and not gradual. After the growth period, A431 cells then underwent nuclear protein extraction **(section 2.12.2)**. The [protein] was determined by the BCA assay **(section 2.12.3)**. The cells in 3.0% and 0.5% O_2 underwent nuclear lysis inside the physioxia hood (set at 3.0 or 0.5% O_2, respectively) to prevent re-oxygenation and potential degradation of the HIF-1α protein. Additionally, HIF-1α can be targeted for degradation in cellular lysate if allowed to reach a high enough [O_2] [11, 229]. As such, the preparation of the lysates for western blotting were also performed inside the physioxia hood on ice. The cells grown in 18.6% were lysed under atmospheric O_2 conditions on ice. Preparation of the lysates for western blotting is described in **section 2.12.2**.

After sample preparation, 50 µg of protein was loaded onto a pre-made 8-16% polyacrylamide gel (Bio-Rad). Protein electrophoresis and transfer was then performed **(section 2.12.5)**. The protein was then transferred onto a nitrocellulose membrane (**section 2.12.6)**. The membrane was then stained with a total protein stain for normalisation purposes **(section 2.12.8)**, which was then imaged on an azure Biosystems gel imaging system. The total protein stain was then washed off and the membrane was blocked with protein free blocking buffer (PBS) overnight at 4°C **(section 2.12.7)**.

Anti-HIF-1α primary antibody was diluted 1:500 in PBS containing 0.1% v/v Tween-20 and 0.3% v/v BSA (PBST). The nitrocellulose membrane was incubated with the antibody solution overnight on a rocker at 4°C. After primary antibody incubation, the membrane was washed three times with PBST and one time with PBS. IR DYE® 800CW anti-mouse IgG secondary antibody (LI-COR) was diluted 1:10000 in PBS containing 0.3% v/v BSA. The secondary antibody solution was then added to the membrane which was then incubated in a black box for 1 h at room temperature on a rocker. The membrane was then washed two times with PBST and one time with PBS prior to imaging on the Odyssey CLx near-infrared system (LI-COR; **section 2.12.9**).

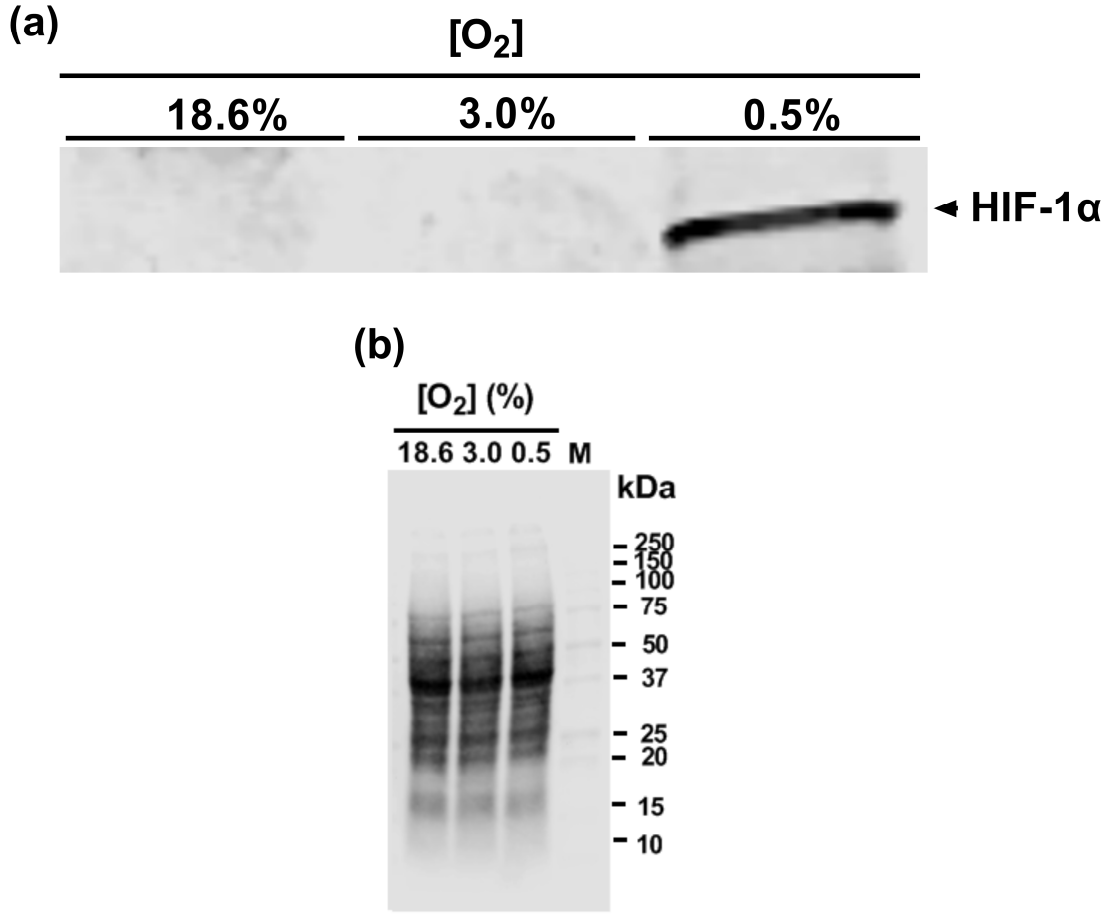

Figure 2.13. The effect of adapting A431 cells to 3.0% O_2 on hypoxia-inducible factor-1α expression compared to A431 cells grown in 18.6% O_2. The expression levels of HIF-1α protein were measured in A431 cells grown in 18.6% or 3.0% O_2 for 96 h (37 °C/5% CO_2) by western blotting. For positive expression of HIF-1α, A431 cells were grown in 0.5% O_2 for 4 h prior to lysis. A431 cells were then prepared for nuclear extraction (section 2.12.2). [Protein] was quantified by BCA assay. Proteins were then separated by reducing SDS PAGE, transferred onto a nitrocellulose membrane, stained for total protein (section 2.12.8) and analysed for HIF-1α expression by probing with an anti-HIF-1α primary antibody and an anti-mouse Infrared dye-conjugated secondary antibody (section 2.12.7). The immunoblot was then imaged using a LI-COR Odyssey CLx imaging system (section 2.12.9). **Panel (a),** representative immunoblot from one experiment showing the 93 kDa HIF-1α band from lysates derived from A431 cells grown in 18.6%, 3.0%, or 0.5% O_2. The full length anti-HIF-1α immunoblots are in Figure A.1 **Panel (b),** representative example from one experiment showing the associated total protein stain for data normalisation. Densitometry analysis was not performed due to the absence of visible bands in the 18.6% and 3.0% O_2 sample lanes. **HIF:** hypoxia inducible factor.

Densitometry analysis was not performed due to the absence of visible bands in the 18.6% and 3.0% O_2 sample lanes. However, A431 cells exposed to 0.5% O_2 for 4 h showed induction of nuclear HIF-1α protein expression **(Figure 2.13 a)**. The molecular weight of this band in the 0.5% sample land closely corresponded to the predicted molecular weight of unmodified HIF-1α (93 kDa) [230]. The strong [O_2]-dependent 93 kDa band in the 0.5% O_2 sample is strong evidence that this protein is HIF-1α **(Figure 2.13 a)**. It was concluded that the absence of a HIF-1 α band in the 18.6% and 3.0% O_2 sample lanes indicated that these cells were not

hypoxic. The full length immunoblot images of the entire blot are shown in the Appendix **(Figure A.1).**

2.4. Cell death analysis: annexin V-fluorescein isothiocyanate and propidium iodide

Annexin V conjugated to fluorescein isothiocyanate (annexin V-FITC) and PI staining was used to measure cell death in conjunction with flow cytometry in chapter 3. Annexin V binds to PS, a marker of apoptosis **(section 1.2.5.2)**. When used in association with the DNA intercalating stain PI, the stages of apoptosis (e.g. early apoptosis, and late apoptosis) can be differentiated from one another. Apoptosis can also be distinguished from necrosis using this method **(section 1.2.5.2)**. Positive cellular staining for annexin V-FITC alone indicates a cell in early apoptosis whereas positive cellular staining with PI alone indicates a necrotic cell. Dual cellular staining for both annexin V-FITC and PI indicates that a cell is in late apoptosis **(Figure 2.16).**

2.4.1. Staining: annexin V-fluorescein isothiocyanate and propidium iodide

After treatment with the compound of interest, the medium was collected and transferred into a 15 mL conical tube. To prevent the cells from drying out, 1 mL of equilibrated PBS (see **section 2.2.3** for concentration) was added to the well immediately after medium removal. A431 cells were then detached by 0.25% v/v trypsin-EDTA. After a 5 min incubation (37°C/5% CO_2), the trypsin was inactivated by adding an equal volume of appropriate [O_2]-equilibrated growth medium. This solution was transferred into a conical tube prior to centrifugation at 200 RCF for 2min. The supernatant was then aspirated, and the pellet was washed with 5 mL of [O_2]-equilibrated PBS. This centrifugation/wash procedure was repeated a further two times.

After the last wash cycle, the PBS was aspirated and the pellet was re-suspended in 95 µL of ice-cold annexin V-FITC binding buffer (50 mM HEPES, 700 mM NaCl, 12.5 mM $CaCl_2$, pH 7.4). To this cell suspension, 5 µL of 12.5 µg/mL annexin V-FITC was added (final concentration of annexin V-FITC = 0.63 µg/mL) under low light. The cells were then placed on ice in the dark for 15 min. 860 µL of ice cold annexin V-FITC was then added to each tube, followed by 40 µL of 1 mg/mL PI

(final concentration of 40 µg/mL). The samples were then agitated manually by gently flicking the bottom of the tube. The samples were then immediately analysed by flow cytometry. The emission spectra of annexin V-FITC and PI are shown in **Figure 2.14 (a and b)**.

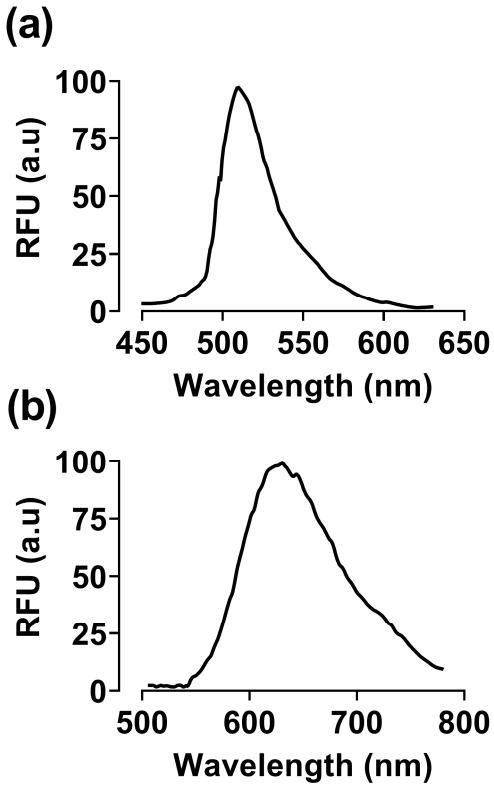

Figure 2.14. Representative emission wavelength scans of annexin V-fluorescein isothiocyanate and propidium iodide both at an excitation wavelength of 488nm. Annexin V-FITC (a) or PI (b) was diluted to a final concentration of 1.25 µg/mL or 0.04 mg/mL in annexin V-FITC binding buffer in a 1 mL quartz cuvette. Emission spectra were measured at an excitation wavelength 488 nm using a SpectraMax M2e spectrophotometer. **Panel (a),** emission spectrum of annexin V-FITC at 488 nm excitation. **Panel (b),** emission spectrum of PI at 488 nm excitation. n=1. **a.u:** arbitrary units; **RFU:** relative fluorescence intensity.

2.4.2. Flow cytometry gating set-up and colour compensation

For measurement of cell death, a Guava 'Easy Cyte' benchtop flow cytometer was used (Luminex, Austin, TX, USA). Laser alignment and particle size measurements were determined and calibrated using fluorobeads (Beckman Coulter) either on a daily basis or prior to use. These fluorobeads had a fixed diameter of 20 µM with specific fluorescence characteristics allowing accurate calibration.

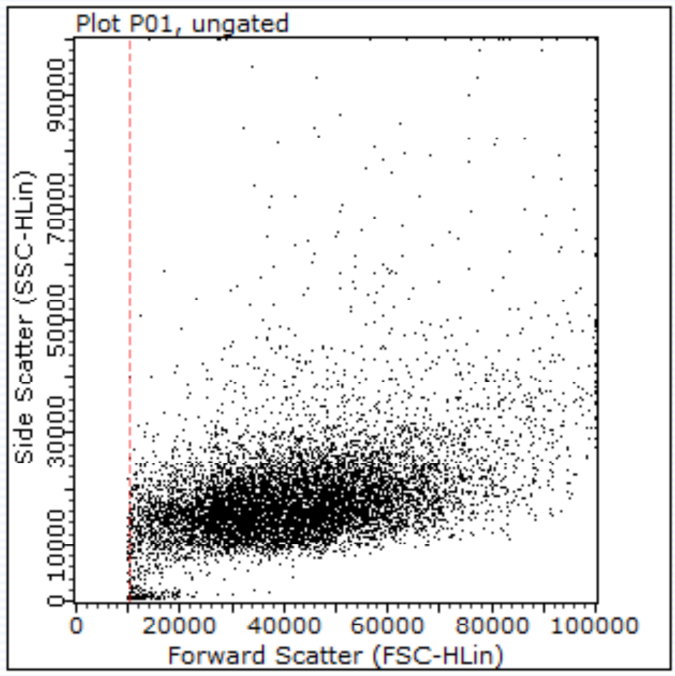

Figure 2.15. Representative dot plot histogram showing forward scatter graphed against side scatter using an untreated A431 cell sample. The dashed red line shows the forward scatter threshold selected to gate out cell debris.

Gating was then performed. For the purposes of this project, a single cell type was used. The only 'populations' were A431 cells and the cell debris. To this end, an unstained untreated cell sample was processed by flow cytometry. Side scatter (SSC, indicates cell granularity) was plotted against forward scatter (FSC, indicates cell size) **(Figure 2.15)**. A threshold (10'000 FSC, **Figure 2.15**) was then set which 'gated' out cell debris from the subsequent analysis.

The photomultiplier tube (PMT) voltages were then set for each detector in order to ensure that the unstained and untreated cells were situated in the 1st decade of a 4-decade logarithmic-scale dot plot histogram **(Figure 2.16 a and b)**. Logarithmic dot plot histogram were used to determine the percentage of cells

staining positively or negatively for each chosen fluorophore. The stains used were annexin V-FITC and PI. As such, the detectors chosen for analysis were the FL1 and FL3 detectors, respectively. These detectors are bandpass filters meaning light within a specific emission wavelength range was detected. For example, the FL1 detector detects emitted light at 520 ± 17.5 nm when excited at 488 nm and is abbreviated as 520/35 nm. The FL3 detector detects emitted light at 670 ± 10 nm when excited at 488 nm and is abbreviated as 670/20 nm. The 488 nm argon laser was utilised for fluorophore excitation. The generated 4-decade logarithmic-scale dot plot histogram indicates unstained cells in the bottom left quadrant (viable cells), single staining for annexin V-FITC in the bottom right quadrant (early apoptotic), dual staining for annexin V-FITC and PI in the top right (late apoptotic), and single staining for PI in the top left (necrotic, **Figure 2.16 a and b)**.

Colour compensation was then carried out. This was necessary as there is an emission wavelength spectral overlap between annexin V-FITC and PI fluorophores of about 15%. In general, a population of cells staining positively or negatively for annexin V-FITC should have minimal emission in the PI channel (FL3 detector). Any such emitted light detected by the FL3 detector is ‘spill-over’ emitted light from the annexin V-FITC stained cells. If not compensated for, this ‘spill-over’ light would be calculated as being due to PI fluorescence. Single stained samples for each fluorophores, in addition to a no stain control, were run to correct for ‘spill-over’ light. Adjustments were made to the software to compensate for emission light ‘spill-over’ using the built-in automatic compensation software.

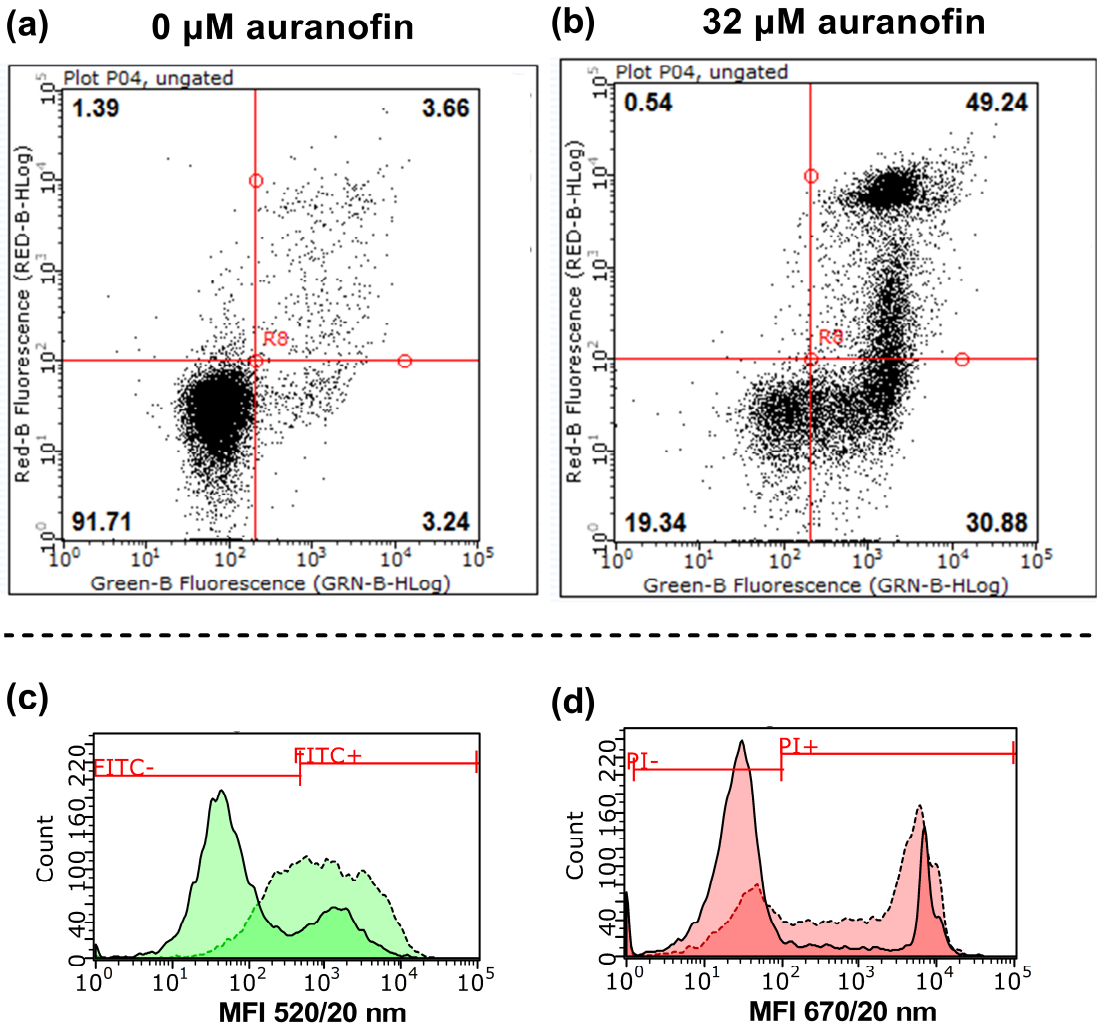

Figure 2.16. Representative flow cytometry dot plots and fluorescence histograms for A431 cells stained with annexin V-fluorescein isothiocyanate and propidium iodide. Panel (a), 4-decade logarithmic scale histograms showing untreated A431 cells stained with annexin V-FITC and PI: viable (FITC-/PI-, bottom left quadrant), early apoptotic (FITC+/PI-, bottom right quadrant), late apoptotic (FITC+/PI+, top right quadrant) and necrotic (FITC-/PI+, top left quadrant). **Panel (b),** 4-decade logarithmic scale histograms showing A431 cells treated with 32 µM auranofin and stained with annexin V-FITC and PI: The numbers in bold within each of the quadrants represents the percentage of events detected in each respective quadrant. **Panel (c),** representative annexin V-FITC fluorescence histogram using the FL1 channel (520/35 nm band-pass filter) in untreated (solid trace) or 32 µM auranofin (dashed trace) A431 cells. **Panel (d),** representative PI fluorescence histogram using the FL3 channel (670/20 nm band-pass filter) in untreated (solid trace) or 32 µM auranofin treated (dashed trace) A431 cells. The y axis label (count) indicates the number of events (cells) detected at the respective MFI. n = 1. **FITC:** fluorescein isothiocyanate; **MFI:** mean fluorescence intensity; **PI:** propidium iodide.

2.5. General experimental design for concentration response testing with redox-active compounds

Various compounds were used for toxicity testing in this work including auranofin, H_2O_2, L-BSO, 3-AT, MSA, and carmustine. Various endpoints were tested including: cell death **(section 3.3.1-3.3.3 and 3.3.8)**, ROS generation **(section 3.3.4-3.3.6),** $\psi\Delta_m$ **(section 3.3.12 and 3.3.13)**, and lipid peroxidation **(section 3.3.14-3.3.18)**. Although different endpoints were investigated, the general preparatory cell culture set up was the same.

A431 cells were seeded at a density of 9.5 x 10^3 cells/cm^2 in 24 well plates and grown in 18.6% or 3.0% O_2 **(section 2.3.1)** for the required amount of time (37°C/5% CO_2). The total culture time in all cases was 96 h. This ensured that A431 cells grown in 18.6% or 3.0% O_2 were at the same level of confluence when treated with the test compound. This particular aspect of the experimental design was used throughout this work and is illustrated for clarity in **Figure 2.17**. Growth medium was changed every 24 h with the appropriate [O_2]-equilibrated growth medium. Although this removed medium in which the cells had likely conditioned with growth factors (i.e. conditioned medium), it was a necessary experimental decision as it ensured that the cells were at the same level of confluence, and received the same number of medium changes, prior to compound treatment **(Figure 2.17)**. After the required growth period, A431 cells were then treated with the compound of interest for the required amount of time in either 18.6% O_2 or 3.0% O_2 (37°C/5% CO_2).

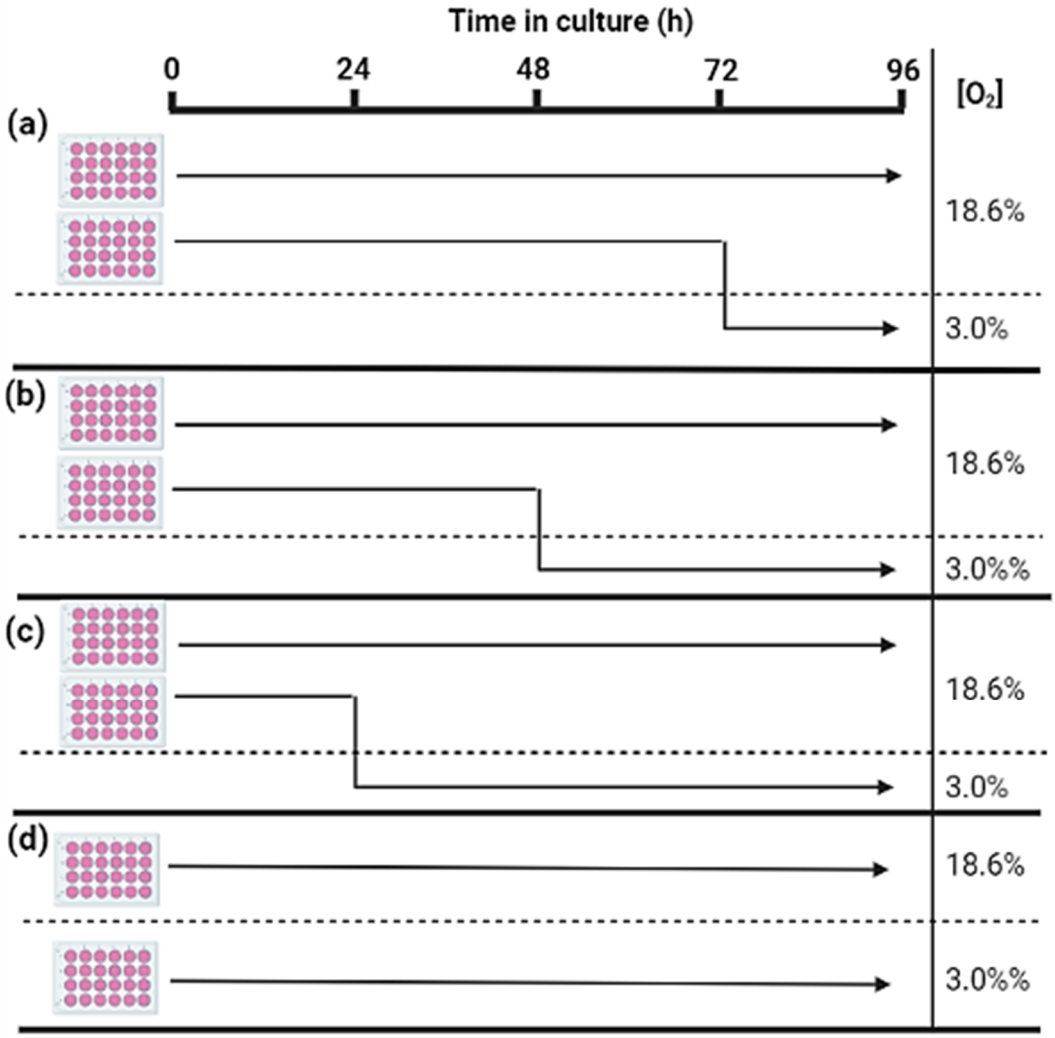

Figure 2.17. General experimental design for growing A431 cells for different lengths of time in physioxia. Two 24 well plate were seeded at a density of 9.5 x 10^3 cells/cm^2. **Panel (a),** one seeded 24 well plate was grown and maintained in 18.6% O_2 (37°C/5% CO_2 above dashed line) for 96 h and the other was switched into 3.0% O_2 (37°C/5% CO_2; below dashed line) after 72 h for the remaining 24 h of the culture period. This was performed by moving the plate into a physioxia hood (section 2.3; set at 3.0% O_2/5% CO_2), changing the media with 3.0% O_2-equilibrated growth medium, and sealing the plate inside a 'klip-lock' container with a petri dish of water for humidification. In this case, the cells have grown in 3.0% O_2 for 24 h prior to experimentation and is designated as the 24 h 3.0% O_2 group. The responses of this group to compound treatment were compared to the responses of cells maintained in 18.6% O_2. **Panel (b),** one seeded 24 well plate was grown and maintained in 18.6% O_2 (37°C/5% CO_2 above dashed line) for 96 h and the other was switched into 3.0% O_2 (37°C/5% CO_2; below dashed line) after 48 h for the remaining 48 h of the culture period. This 3.0% O_2 group represents the 48 h time point group. **Panel (c),** one seeded 24 well plate was grown and maintained in 18.6% O_2 (37°C/5% CO_2 above dashed line) for 96 h and the other was switched into 3.0% O_2 (37°C/5% CO_2; below dashed line) after 24 h for the remaining 72 h of the culture period. This 3.0% O_2 group represents the 72 h time point group. **Panel (d),** one seeded 24 well plate was grown and maintained in 18.6% O_2 (37°C/5% CO_2 above dashed line) for 96 h and the other was grown and maintained in 3.0% O_2 (37°C/5% CO_2; below dashed line) for 96 h. This 3.0% O_2 group represents the 96 h time point group. Each group was fed with appropriate [O_2]-equilibrated growth medium every 24 h. Image was made using www.BioRender.com.

2.5.1. Measuring the H_2O_2 concentration in a stock solution by spectrophotometry

A Spectramax M_2e spectrophotometer (Molecular Devices, San Jose, California, USA) was used to measure the absorbance of various products in solution. This was used for the BCA assay **(section 2.12.3)**, and enzyme activity assays **(section 4.2.1-4.2.5).**

H_2O_2 was used in chapter 3. It was necessary to measure [H_2O_2] from a stock solution from week to week. This is because H_2O_2 may degrade over time. [H_2O_2] was estimated by measuring the absorbance (A) of H_2O_2 at 240 nm **(Figure 2.18)**. The Spectramax M_2e spectrophotometer was used to measure absorbance from both cuvette and microplate setups. These investigations were performed at room temperature. To measure [H_2O_2], H_2O_2 was dissolved 1:500 in UH_2O to a final volume of 1 mL inside a laminar flow hood. A_{240} was then measured using a spectramax M_2e spectrophotometer. Of note, the absorbance of H_2O_2 is without a clearly defined peak **(Figure 2.18)** [231].

The Beer Lambert equation **(Eq. 2.2)** was used to estimate [H_2O_2] in the stock solution, where A = absorbance (O.D), ε = extinction coefficient (M^{-1} cm^{-1}), and l = path length (cm). In the representative example in **Figure 2.18**, a 1:500 dilution of 30% v/v H_2O_2 in UH_2O had an absorbance of 0.781 at 240 nm after blank correction. The molar extinction coefficient of H_2O_2 was 43.6 M^{-1} cm^{-1}. This corresponded to a stock concentration of 8.95 M H_2O_2 after dilution correction.

$$A = \varepsilon c l \qquad \textbf{(Eq. 2.2).}$$

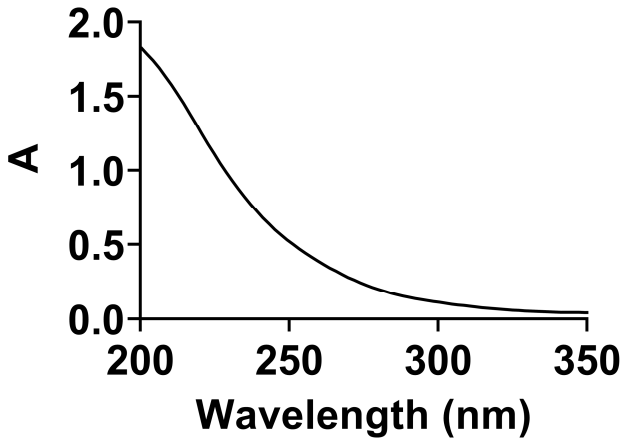

Figure 2.18. Representative absorbance spectrum of H_2O_2. H_2O_2 was diluted 1:500 in UH_2O and was transferred into a quartz cuvette. An absorbance spectrum scan was performed using a Spectramax M_2e spectrophotometer. In this representative example, an absorbance reading of 0.812 was obtained at 240 nm. However, H_2O_2 does not have a clearly defined absorbance peak. Using the absorbance of H_2O_2 at 240 nm, the extinction coefficient of H_2O_2 at 240 nM (43.6 $M^{-1}cm^{-1}$), and the path length (1 cm), [H_2O_2] from a stock solution was estimated. n=1. **A:** absorbance

2.5.2. Measuring O_2 release from A431 cells treated with H_2O_2.

As mentioned previously, H_2O_2 was utilised to induce cell death in A431 cells in chapter 3. Mammalian cells with functional catalase decompose H_2O_2 into H_2O and O_2 **(section 1.2.7.2.3)**. The O_2 release due to H_2O_2 was an experimental concern. Treatment of A431 cells grown in 18.6% O_2 or 3.0% O_2 with H_2O_2 may have resulted in a catalase-mediated increase in [O_2]. The [O_2] during the treatment phase may therefore have been different to the [O_2] during the growth phase. To measure the H_2O_2-mediated increase in [O_2] in the A431 cell system, four different experimental groups were utilised: First, 8.0 x 10^4 A431 cells placed into a gas tight vial in growth medium and treated with 1mM H_2O_2 (A431 cell group); second, 8.0 x 10^4 cells placed into a gas tight vial in growth medium and treated with 0.1% v/v H_2O (vehicle control group); third, growth medium with H_2O_2 (negative control group); fourth, as a positive control for O_2 generation, catalase was added to the growth medium containing H_2O_2. The resulting [O_2] increase was measured using an ABL-9 blood gas analyser **(section 2.3.3.1)**.

The time 0 [O_2] reading in the vials containing A431 cells was 20.3 ± 0.23% O_2 **(Figure 2.19 a.0)**. Addition of 1 mM H_2O_2 at the 15 min timepoint to the vials containing A431 cells resulted in an increase in [O_2] at the 20 min timepoint compared to time 0 ($P < 0.0001$), with means of 20.8 ± 0.23 vs 22.7 ± 0.31% O_2.

There was no increase in [O_2] after addition of H_2O_2 to growth medium alone when compared to time 0 **(Figure 2.19 b)**.

However, addition of 100 U/mL of catalase at the 55 min timepoint to the vials containing H_2O_2 disolved in DMEM resulted in an increase in [O_2] compared to the A431 cell group ($P < 0.0001$, **Figure 2.19 a.2)**, with means of 55 ± 2.37% vs 28.77 ± 1.54% O_2, respectively. There was no increase in [O_2] when 100 U/mL catalase was added at 55 min to the vehicle control group when compared to time 0 **(Figure 2.19 a.2)**.

As the treatment of A431 cells with 1 mM H_2O_2 caused an increase in [O_2], H_2O_2 was not chosen to test the effect of changing the [O_2] during treatment on the subsequent cellular responses of A431 cells previously grown in 18.6% or 3.0% O_2 to treatment-induced cell death. It was decided that auranofin should be used instead for this purpose **(section 3.3.3)**. However, the small increase in [O_2] after A431 cell treatment with 1 mM H_2O_2 compared to the time 0 baseline (around a 2% increase; **Figure 2.19 b**), represents a limitation to the H_2O_2 cell death studies **(section 3.3.1)**. This is discussed further in **section 3.4.1.**

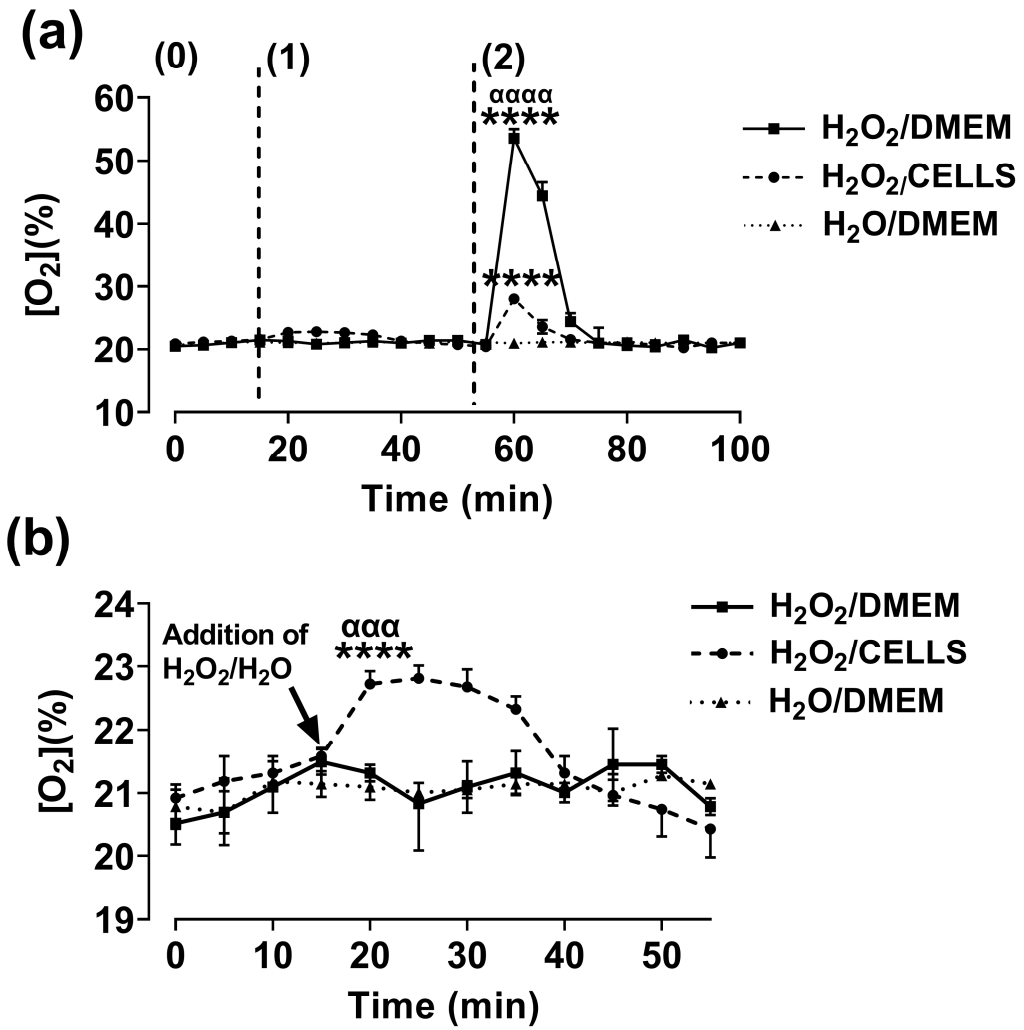

Figure 2.19. Effect of H_2O_2 treatment on the generation of O_2 from A431 cells. A431 cells were seeded at a density of 9.5 x 10^3 cells/cm^2 into 24 well plates and were incubated at 37°C/5% CO_2 for 96 h. After 96 h, A431 cells were detached with 0.25% trypsin-EDTA. 8.0 x 10^4 cells were transferred into a gas tight vial containing pre-warmed DMEM. Two other groups were also included, a vehicle control (DMEM and H_2O) and a positive control (H_2O_2, DMEM and catalase). **Panel (a. 0),** [O_2] measured in growth medium containing, or not containing, A431 cells using an ABL-9 blood gas analyser (section 2.3.3.1). **Panel (a. 1),** [O_2] after addition of 1 mM H_2O_2 to a vial containing A431 cells in growth medium or to a vial containing only growth medium, or the [O_2] after the addition of 0.1% (v/v) UH_2O to a vial containing only growth medium. **Panel (a. 2),** [O_2] after addition of 100U/mL catalase to a vial containing A431 cells treated with 1 mM H_2O_2, growth medium with 1 mM H_2O_2 added, or growth medium with 0.1% v/v UH_2O added. **Panel (b),** data from panel (a. 1) (time-point 10–55 min) expanded into a separate graph for clarity. **** = $P < 0.0001$ versus baseline; ααα = $P < 0.001$ versus H_2O_2/DMEM, αααα = $P < 0.0001$ versus H_2O_2/cells utilising a two-tailed Student's t-test. Data are presented as the mean ± 1 SD. n = 3. Where error bars are not visible, this is because the error bar is smaller than the size of the data point.

2.5.3. Determining an appropriate H_2O_2 treatment time for future testing

Prior to testing with H_2O_2 in chapter 3, the optimal H_2O_2 treatment time for cell death analysis was investigated. To this end, A431 cells were treated with H_2O_2 for 1, 4 or 24 h. Cell death was measured by annexin V-FITC and PI staining in conjunction with flow cytometry **(section 2.4.1)**.

A two-way ANOVA was performed to analyse the effects of treatment time and [H_2O_2] on cellular viability. A *post-hoc* multiple comparison analysis showed that A431 cells treated with 1mM H_2O_2 for 1 h exhibited heightened viability compared to A431 cells treated with 1 mM H_2O_2 for 24 h ($P < 0.0001$, **Figure 2.20 a**), with means of 62.9 ± 12.98% vs 3.03 ± 2.42%, respectively.

The interaction between the effects of H_2O_2 treatment time and [H_2O_2] on cellular viability was statistically significant (F (4, 25) = 4.441, $P = 0.007$).

There was also an increase in the percentage of late apoptotic cells after H_2O_2 treatment in the 24 h treatment group compared to the 4 h ($P < 0.05$) and 1 h ($P < 0.01$) treatment groups **(Figure 2.20 c)**. There was no statistically significant effect of treatment time on the percentage of necrotic cells, or when compared to within-group untreated control **(Figure 2.20 d)**.

The 1 h H_2O_2 treatment time was chosen for future experimentation, as it represented the treatment time where potential [O_2]-dependent changes to the concentration response curve could be observed.

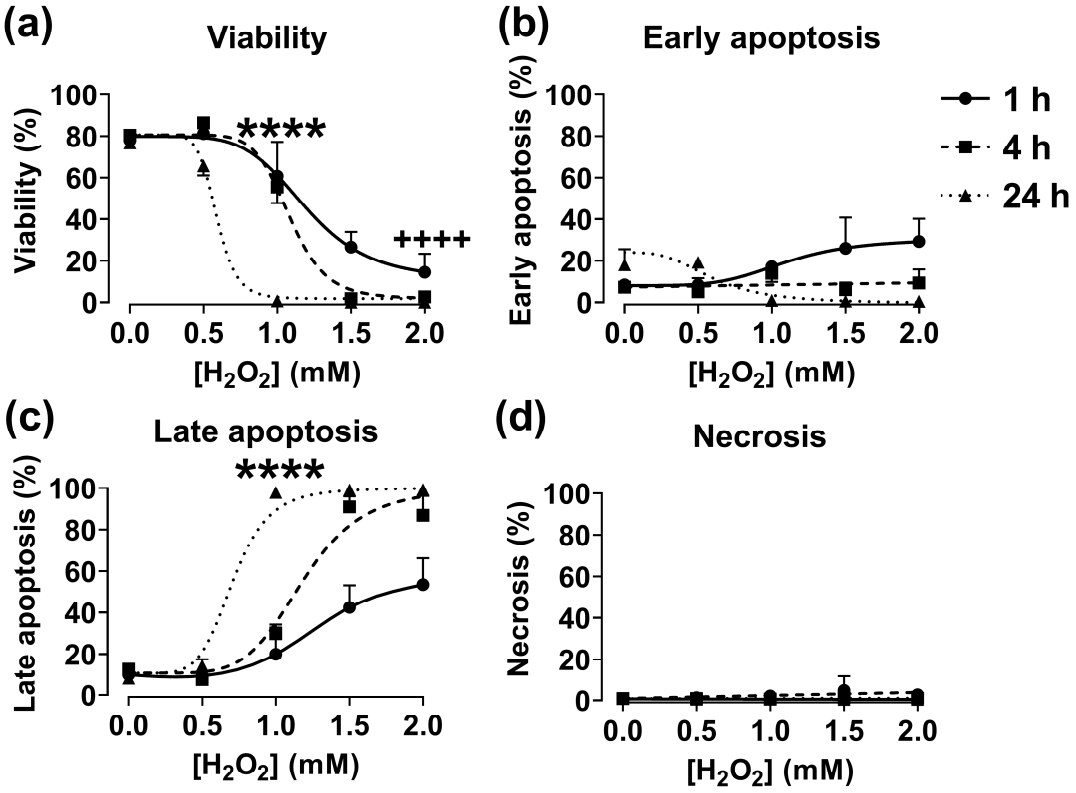

Figure 2.20. Determining an appropriate H_2O_2 treatment time for further testing. A431 cells were seeded at a density of 9.5 x 10^4 cells/cm^2 in 24 well plates and grown in 18.6% O_2 (37°C / 5% CO_2) for 96 h. After 96 h, A431 cells were treated with 0.5-2 mM H_2O_2 or vehicle (0.1% v/v UH_2O) for 1, 4 or 24 h (37°C / 5% CO_2). After the treatment period, A431 cells were detached, washed with PBS (see section 2.2.3 for concentration), and subsequently stained with annexin V-FITC and PI prior to cell death analysis by flow cytometry (section 2.4.1). **Panel (a),** cell viability. **Panel (b),** early apoptosis. **Panel (c),** late apoptosis. **Panel (d),** necrosis. **** = $P < 0.0001$ versus 24 h in panel (a) or 1h in panel (c)**,** ++++ = $P < 0.0001$ versus respective untreated control utilising a two-way ANOVA with multiple comparison and Dunn-Šidák correction. Data are presented as the mean ± 1 SD. n=3. Where error bars are not visible, this is because the error bar is smaller than the size of the data point.

2.5.4. Determining an appropriate carmustine concentration range for further testing

Prior to toxicity testing with carmustine, the appropriate carmustine concentration range was determined by treating A431 cells grown in 18.6% O_2 for 96 h with 0–1000 µM carmustine for 24 h. Cell death was then measured by annexin V-FITC and PI staining in conjunction with flow cytometry **(section 2.4)**.

Treatment of A431 cells with 0–100 µM did not affect cellular viability, early apoptosis or late apoptosis compared to untreated control cells (**Figure 2.21 a and c)**. However, treatment with 1000 µM carmustine caused a decrease in viability, with an associated increase in the percentage of late apoptotic cells compared to untreated control cells ($P < 0.0001$, **Figure 2.21 a and c)**. Treatment

with carmustine did not affect the percentage of cells in early apoptosis, or in necrosis (**Figure 2.21 b and d)**. Therefore, the carmustine concentration range of 200-1000 uM was utilised for cytotoxicity testing in chapter 3 **(section 3.3.8)**. The 0–200 uM carmustine concentration range was used for sensitisation experiments in chapter 3 **(section 3.3.9).**

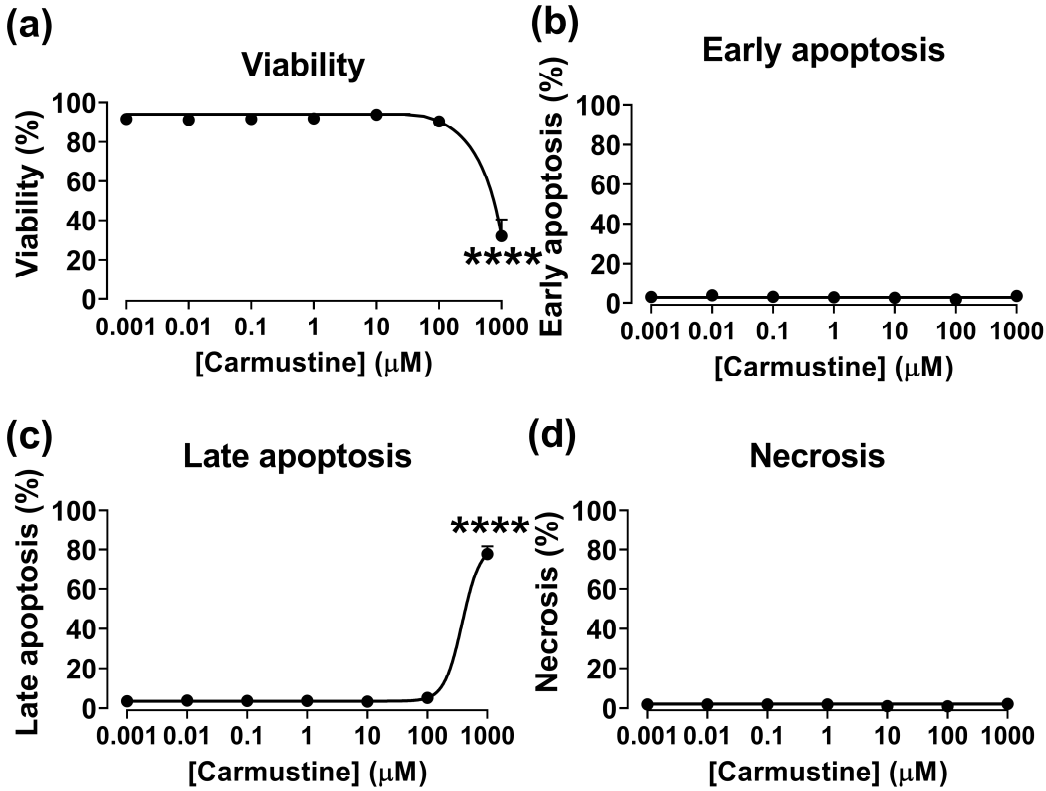

Figure 2.21. Determination of the appropriate carmustine concentration range for further testing. A431 cells were seeded at a density of 9.5 x 10^3 cells/cm^2 in 24 well plates and grown in 18.6% O_2 for 96 h (37°C / 5% CO_2). Growth medium was changed every 24 h. After 96 h of growth, cells were treated with 0–1000 µM carmustine for 24 h in 18.6% or 3.0% O_2 (37°C / 5% CO_2). A431 cells were then detached, washed with PBS (see section 2.2.3 for concentration), and subsequently stained with annexin V-FITC and PI prior to cell death analysis by flow cytometry. **Panel (a),** viability**. Panel (b),** early apoptosis. **Panel (c),** late apoptosis. **Panel (d),** necrosis. **** = P < 0.0001 versus untreated control utilising a paired two-tailed Student's t-test. Data are presented as the mean ± 1 SD. n = 4. Where error bars are not visible, this is because the error bar is smaller than the size of the data point.

2.5.5. Determining a non-cytotoxic mercaptosuccinic acid concentration range for sensitisation testing

MSA was used in the lipid peroxidation studies in chapter 3 **(section 3.3.17 and 3.3.18)**. Prior to this, an appropriate MSA concentration range was determined. To this end, A431 cells were grown in 18.6% or 3.0% O_2 for 96 h prior to treatment with MSA for 24 h. Cell death was measured by annexin V-FITC and PI staining in conjunction with flow cytometry **(section 2.4)**.

A two-way ANOVA was used to analyse the effects of [MSA], and the [O_2] cells were grown in, on cell viability. A *post-hoc* multiple comparison test showed that treatment with 0–1000 µM MSA did not affect cellular viability in either [O_2] group compared to respective untreated control (**Figure 2.22 a**). Additionally, there was no effect of MSA treatment on the percentage of cells in early apoptosis, late apoptosis or those in necrosis compared to respective untreated control (**Figure 2.22 a**). Detection of cell death was functional as treatment with 2 mM H_2O_2 alone resulted in a statistically significant decrease in cell viability compared to respective untreated controls in both [O_2] groups.

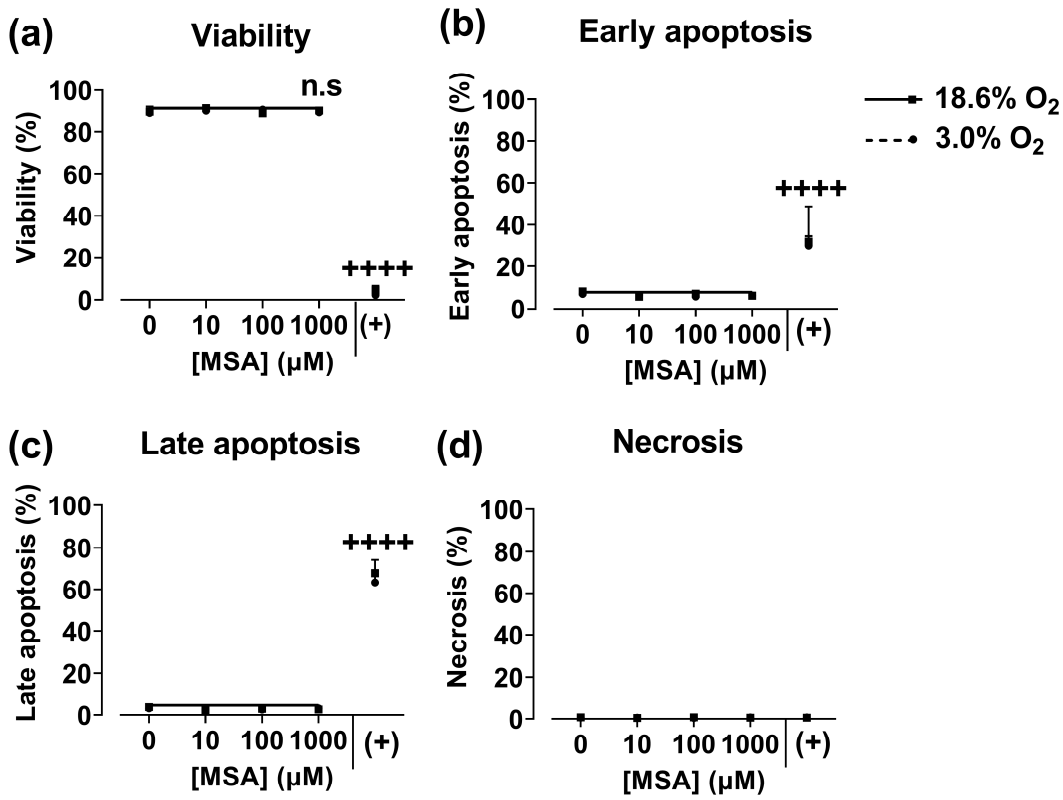

Figure 2.22. Determining the appropriate mercaptosuccinic acid concentration range for further testing. A431 cells were seeded at a density of 9.5 x 10^3 cells/cm^2 in 24 well plates and grown in either 3.0% O_2 or 18.6% O_2 for 96 h (37°C / 5% CO_2). The growth medium was changed every 24 h. After the required growth period, A431 cells were treated with the indicated concentrations of MSA, or vehicle (0.1% v/v UH_2O) for an additional 24 h in 18.6% or 3.0% O_2 (37°C / 5% CO_2). Positive control wells (+) were treated with 2.0 mM H_2O_2 alone for 1 h in 18.6% or 3.0% O_2 (37°C / 5% CO_2). A431 cells were then detached, washed with PBS (see section 2.2.3 for concentration), and stained with annexin V-FITC and PI prior to cell death analysis by flow cytometry. **Panel (a),** viability. **Panel (b),** early apoptosis. **Panel (c),** late apoptosis. **Panel (d),** necrosis. n.s = not significant, ++++ = $P < 0.0001$ versus respective untreated control utilising a two way ANOVA and a *post-hoc* multiple comparison test with Dunn-Šidák correction. Data are presented as the mean ± 1 SD. n = 3. Where error bars are not visible, this is because the error bar is smaller than the size of the data point.

2.6. Measuring mitochondrial membrane potential

$\Delta\psi_m$ occurs during apoptosis **(section 1.2.5.2.1)**. 1, 1', 3, 3'-tetraethyl-5, 5', 6, 6'-tetrachloroimidacarbocyanine iodide dye (JC-1; **Figure 2.23 a)** is a ratiometric dye used to measure $\Delta\psi_m$. This probe was used in chapter 3 to measure $\Delta\psi_m$ **(section 3.3.12 and section 3.3.13)**. JC-1 is a lipophilic cationic dye that forms a monomer (J-monomer; ex/em 515/527 nm) when in the cytoplasm. JC-1 accumulates in healthy mitochondria forming reversible aggregates (J-aggregates; ex/em 585/590 nm) in a concentration and charge-dependent manner **(Figure 2.23 b)** [232]. Loss of electrochemical potential in mitochondria (e.g. by apoptosis) affects the generation of these J-aggregates. JC-1 data were reported as the fluorescence ratio of the JC-1 monomer (detected by the FL1 detector) to the JC-1 aggregate (FL2 detector; 590/20 nm). This is abbreviated as F520:F590 throughout the text. An increase to F520:F590 indicates a decrease in ψ_m (**Figure 2.24 a and b)**. Where the data from F520:F590 is described in the text, the data were reported without units as F520:F590 is a ratio of two fluorescence readings.

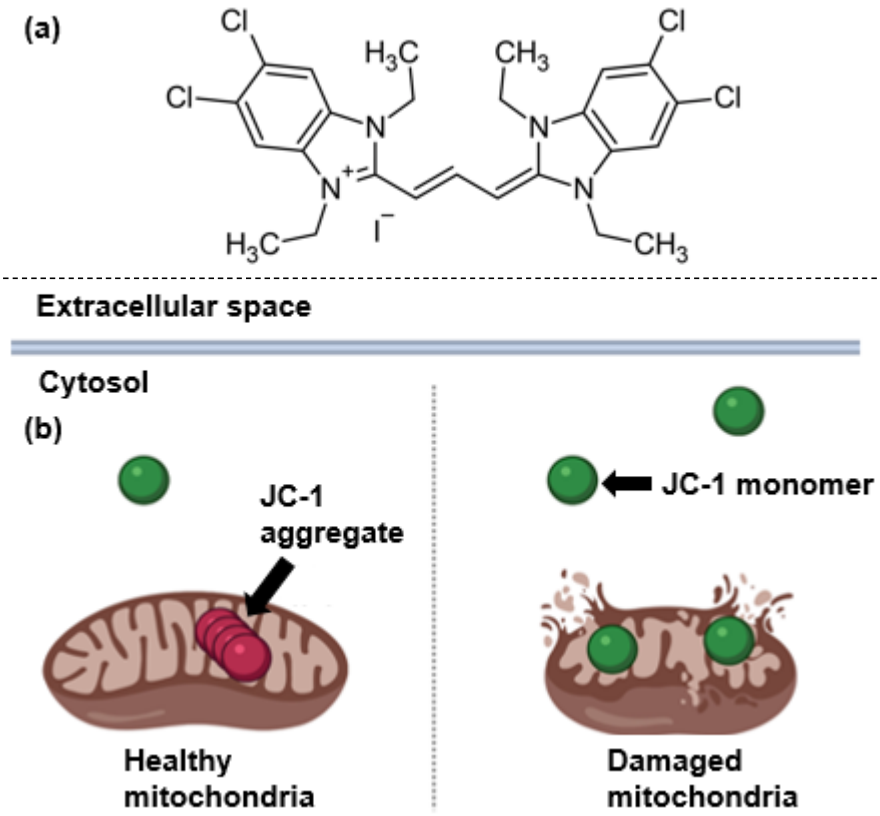

Figure 2.23. Skeletal structure of the JC-1 probe and illustration of JC-1 J-aggregate and J-monomer formation. Panel (a), chemical structure of the JC-1 cationic probe. **Panel (b),** illustration of JC-1 aggregation in mitochondria. JC-1 is a membrane permeable cationic dye used to measure $\Delta\psi_m$. In the cellular cytosol, JC-1 exists as a J-monomer (ex/em 515/527 nm). However, it accumulates in energized healthy mitochondria forming J-aggregates (ex/em 514/590 nm) in a concentration and charge dependent manner. Active mitochondria stained with JC-1 dye exhibit a higher ratio of red fluorescence signal (J-aggregate) to green fluorescence signal (J-monomer) compared to depolarised mitochondria which exhibit a lower ratio of red fluorescence signal to green fluorescence signal. Image made using www.BioRender.com. **$\Delta\psi_m$:** change in mitochondrial electrochemical membrane potential.

2.6.1. Validating carbonyl cyanide *m*-chlorophenyl hydrazine as a positive control for inducing mitochondrial de-polarisation

Carbonyl cyanide *m*-chlorophenyl hydrazine (CCCP) is a protonophore which inhibits oxidative phosphorylation [233]. More specifically, CCCP is a competitive inhibitor of complex IV (cytochrome c oxidase) of the ETC which causes a loss of Ψ_m in mitochondria. In order to ensure that JC-1 detection of $\Delta\psi_m$ was functional in A431 cells, CCCP was used as a positive control for $\Delta\psi_m$ in chapter 3 **(section 3.3.12 and 3.3.13)**. First, it was necessary to determine the appropriate [CCCP] to induce $\Delta\psi_m$ in A431 cells.

To this end, A431 cells were seeded at a density of 9.5 x 10^3 cells/cm^2 in 24 well plates and incubated for 96 h (37°C/5% CO2). A431 cells were treated with CCCP to final concentrations of 3–100 µM for 1 h (37°C/5% CO2). Vehicle control cells were treated with 0.1% (v/v) dimethyl sulfoxide (DMSO). After 1 h, the medium was removed and, under low light, replaced with fresh growth medium containing 2 µM JC-1. The plate was incubated for 1 h prior to cellular detachment with 0.25% v/v trypsin-EDTA. F520:F590 was then measured by flow cytometry using the FL1 and FL2 detectors **(Figure 2.24)**. Treatment with CCCP increased F520:F590 **(Figure 2.24 a)**. Therefore, 100 µM CCCP was chosen as the appropriate concentration to induce $\Delta\psi_m$ in A431 cells.

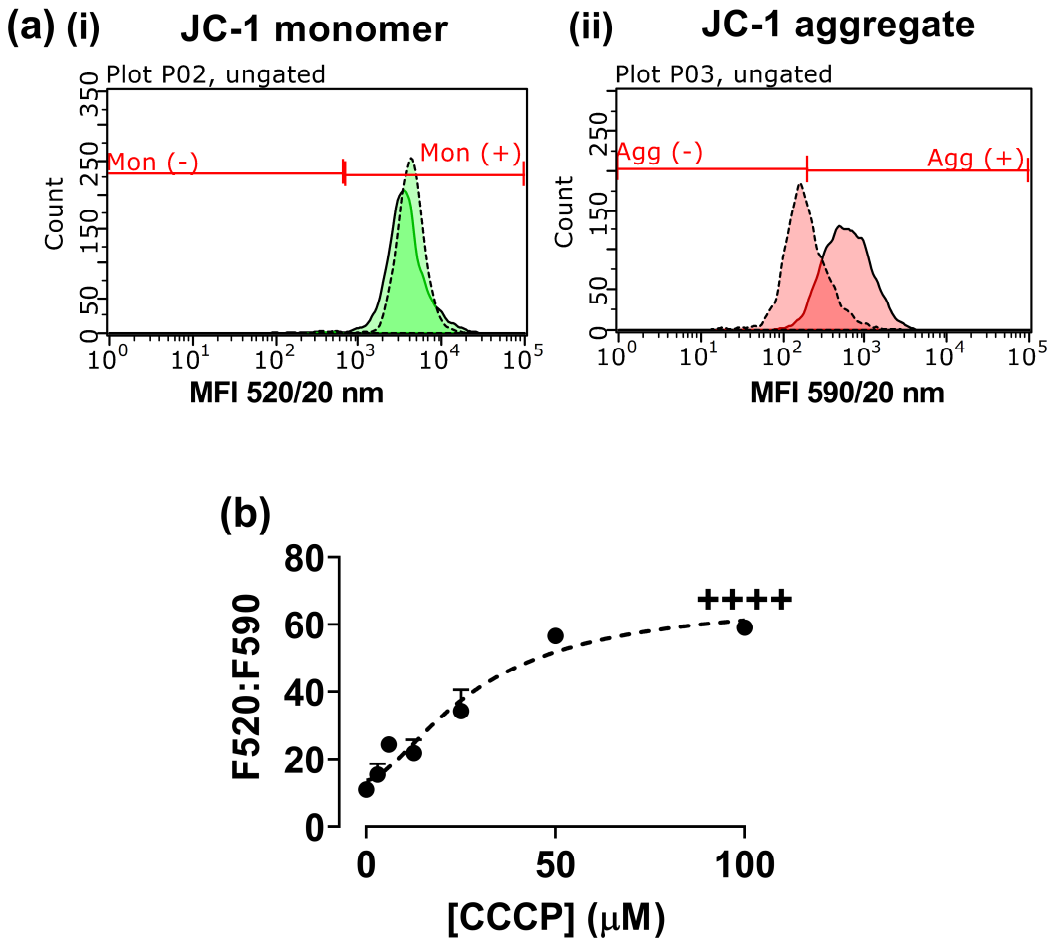

Figure 2.24. Representative flow cytometry fluorescence histograms showing carbonyl cyanide *m*-chlorophenyl hydrazine-induced changes to mitochondrial membrane potential in JC-1 stained A431 cells. A431 cells were seeded at a density of 9.5 x 10^3 cells/cm^2 in 24 well plates and grown in 18.6% O_2 for 96 h (37°C/5% CO_2). Growth medium was changed every 24 h. After 96 h of growth, cells were treated with 3–100 µM CCCP, or vehicle (0.1% (v/v) DMSO), for 1 h (37°C/5% CO_2). Under low light, cells were stained with 2 µM JC-1 for 1 h (37°C/5% CO_2). A431 cells were then detached, washed with PBS (see section 2.2.3 for concentration), and the fluorescence intensity of the JC-1 stain was analysed by flow cytometry. **Panel (a),** representative flow cytometry fluorescence histograms showing **(i)** J-monomer (Mon +/-) and **(ii)** J-aggregate (Agg +/-) formation as detected by the FL1 or FL2 detector (respectively) in untreated (solid trace) or 25 µM CCCP treated (dashed trace) A431 cells. The y axis label (count) indicates the number of events (cells) detected at the respective MFI. **Panel (b),** F520:F590 in CCCP-treated A431 cells. ++++ = $P < 0.0001$ versus 0 µM CCCP utilising a two-tailed Student's t-test. Data in panel (b) is presented as the mean ± 1 SD. n = 3. Where error bars are not visible, this is because the error bar is smaller than the size of the data point. **Agg (-/+):** JC-1 aggregate negative or positive regions**; CCCP:** carbonyl cyanide *m*-chlorophenyl hydrazine; **F520:F590:** mean fluorescence intensity ratio of the emission light at wavelength 520 nm to the emission light at 590 nm when both excited at 488 nm; **MFI:** mean fluorescence intensity; **Mon (-/+):** JC-1 monomer negative or positive regions.

2.7. Measuring lipid peroxidation using C_{11} BODIPY$^{581/591}$

Lipid peroxidation occurs as a result of oxidative stress **(section 1.2.4.1)**. C_{11} BODIPY$^{581/591}$ is used to detect lipid peroxidation in conjunction with flow cytometry [117]. This probe was used in chapter 3 **(section 3.3.15-3.3.18)**. The phenyl group of BODIPY is conjugated to a fluorophore through a

polyunsaturated dienyl linker which is oxidised by $LO_2^{\bullet}$. Oxidation of the dienyl linker results in the fluorescence shift of the C_{11} BODIPY$^{581/591}$ molecule from red (595 nm) to green (520 nm) which can be measured at excitation 488 nm. Both the oxidised and reduced forms of C_{11} BODIPY$^{581/591}$ are highly lipophilic and accumulate into membranes containing PUFAs. As the C_{11} BODIPY$^{581/591}$ probe enters cellular membranes indiscriminately it is used as a measure of total cellular lipid peroxidation rather than being a measure of lipid peroxidation within specific cellular compartments.

C_{11} BODIPY$^{581/591}$ data were expressed as a ratio of the green oxidised form (FL1 detector) to the red reduced form (FL2 detector) [21]. This is abbreviated as F520:F590 throughout the text. An increased in F520:F590 indicates an increase in cellular lipid peroxidation. Where the data from F520:F590 is described in the text, the data were reported without units as this comparison is a ratio of two fluorescence readings.

2.7.1. Validating cumene hydroperoxide as a positive control for lipid peroxidation

CuOOH induces lipid peroxidation in mammalian cells **(Figure 1.13)** [173]. CuOOH was utilised to confirm that C_{11} BODIPY$^{581/591}$ detection of lipid peroxidation was functional in A431 cellular samples in chapter 3 **(section 3.3.15-3.3.18)**. First, the appropriate [CuOOH] to induce lipid peroxidation was determined.

To this end, A431 cells were seeded at a density of 9.5 x 10^3 cells/cm^2 in 24 well plate prior to incubation for 96 h (37°C/5% CO_2). After the growth period, cells were then treated with vehicle (0.1% v/v DMSO) or 6-200 µM CuOOH for 1 h (37°C/5% CO_2). Under low light, A431 cells were then stained with 2 µM C_{11} BODIPY$^{581/591}$ and were incubated for an additional 1 h (37°C/5% CO2). The MFI of the C_{11} BODIPY$^{581/591}$ dye was analysed by flow cytometry using the FL1 and FL2 detectors. The effect of [CuOOH] on the oxidation of the C_{11} BODIPY$^{581/591}$ dye is shown in **Figure 2.25 a and b**. As [CuOOH] was increased, F520:F590 increased relative to the untreated control cells. This indicated an increase in cellular lipid peroxidation. Based on concentration response testing, 100 µM

CuOOH was chosen as the appropriate positive control concentration for inducing lipid peroxidation in A431 cells **(Figure 2.25 b)**.

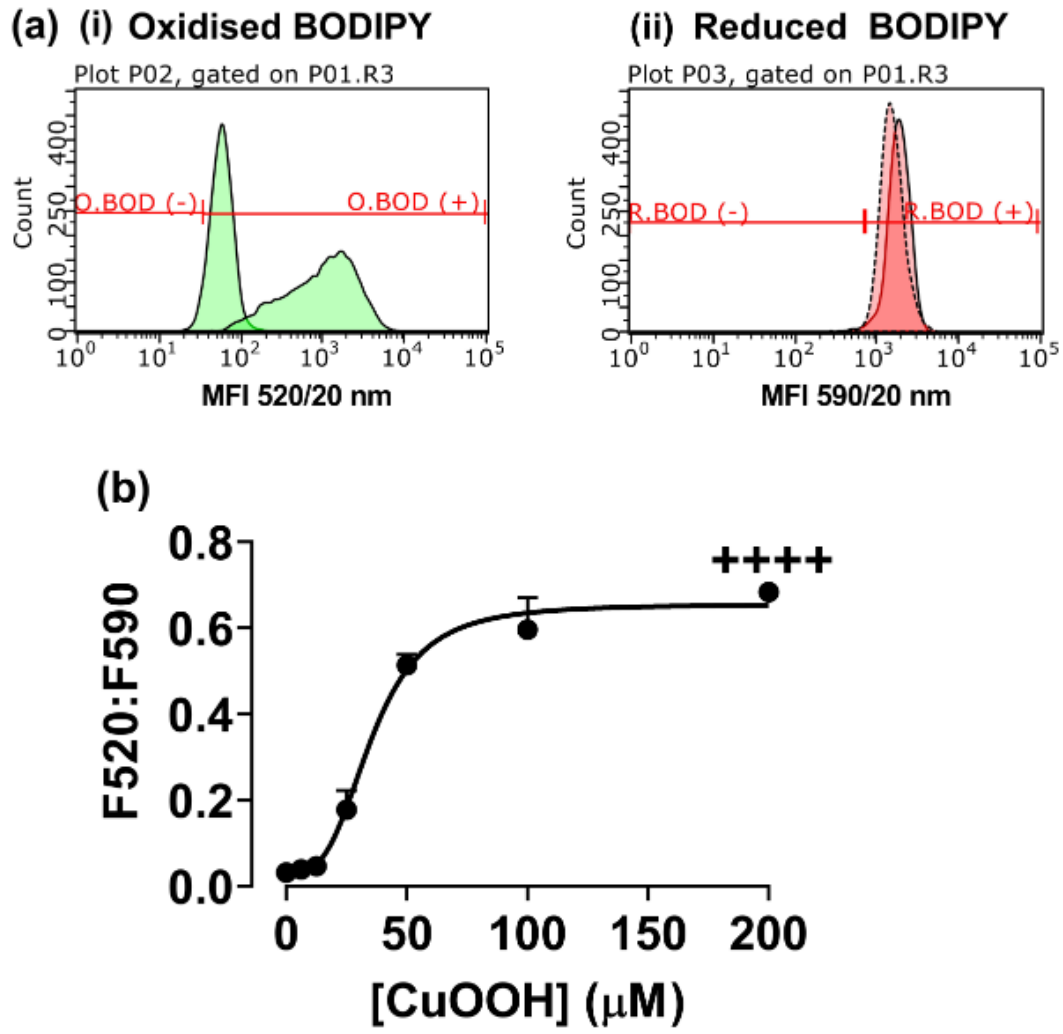

Figure 2.25. Representative flow cytometry fluorescence histograms showing cumene hydroperoxide-induced lipid peroxidation in C_{11} BODIPY$^{581/591}$-stained A431 cells. A431 cells were seeded at 9.5 x 10^3 cells/cm^2 and grown for 96 h in 18.6% O_2 (37°C/5% CO_2). After the incubation period, A431 cells were treated with 6–200 µM CuOOH, or vehicle (0.1% (v/v) DMSO) for 1 h (37°C/5% CO_2). A431 cells were then stained with 2 µM C_{11} BODIPY$^{581/591}$ for an additional 1 h (37°C/5% CO2). A431 cells were then detached with 0.25% (v/v) Trypsin-EDTA and washed with PBS (see section 2.2.3 for concentration). The emission of C_{11} BODIPY$^{581/591}$ was measured by flow cytometry utilising the FL1 and FL2 detector. **Panel (a),** representative flow cytometry histograms showing the effect of [CuOOH] on the MFI of (i) oxidised BODIPY (O.BOD -/+) and (ii) reduced BODIPY (R.BOD -/+) in untreated (solid trace) or 50 µM CuOOH treated (dashed trace) A431 cells. The y axis label (count) indicates the number of events (cells) detected at the respective MFI. **Panel (b),** F520:F590 in CuOOH-treated A431 cells. ++++ = $P < 0.0001$ versus 0 µM CCCP utilising a two-tailed Student's t-test. Data in panel (b) is presented as the mean ± 1 SD. n = 3. Where error bars are not visible, this is because the error bar is smaller than the size of the data point. **CuOOH:** cumene hydroperoxide; **F520:F590:** mean fluorescence intensity ratio of the emission light at wavelength 520 nm to the emission light at 590 nm when both excited at 488 nm; **MFI:** mean fluorescence intensity; **O.BOD (-/+):** oxidised BODIPY negative and positive regions; **R.BOD (-/+):** reduced BODIPY negative and positive regions.

2.8. Measuring cellular reactive oxygen species generation.

2.8.1. Dihydroethidium and MitoSOX Red

MitoSOX Red and DHE were utilised for the detection of mitochondrial-derived, and total cellular, ROS generation (respectively) in chapter 3 **(section 3.3.4 and 3.3.5)**. These probes were described previously in **section 1.2.3.2.** Prior to testing with DHE and MitoSOX, a number of preliminary tests were performed. First, the emission spectra of DHE and MitoSOX red were measured; second: the optimal [DHE] for cellular staining was determined; third: the ability of DHE to detect $O_2^{\bullet -}$ was investigated.

2.8.1.1. Validating carbonyl cyanide *m*-chlorophenyl hydrazine as a positive control for reactive oxygen species generation

As described previously **(section 2.6.1)**, CCCP is an uncoupler of the ETC which induces $O_2^{\bullet -}$ generation. CCCP was utilised as a positive control for cellular ROS generation in the DHE and MitoSOX Red studies in chapter 4 **(section 3.3.4 and 3.3.5)**. First however, CCCP induction of ROS generation in A431 cells was verified.

To this end, A431 cells were seeded at a density of 9.5 x 10^3 cells/cm^2 into 24 well plates and grown for 96 h in 18.6% O_2 (37°C/5% CO_2). The growth medium was replaced every 24 h. After the growth period, A431 cells were then treated with CCCP for 1 h (37°C/5% CO_2). Treatment of A431 cells with 50 µM CCCP increased the MFI detected in DHE and MitoSOX-stained A431 cells **(Figure 2.26 a and b)**. Based on the data from **section 2.6.1**, 50 µM CCCP was used as a positive control for ROS generation in the DHE and MitoSOX studies in chapter 3.

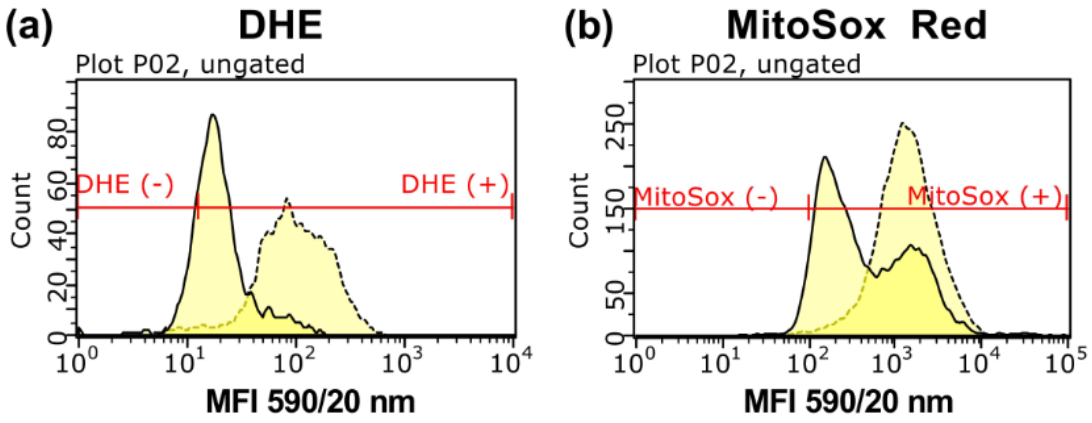

Figure 2.26. Effect of carbonyl cyanide *m*-chlorophenyl hydrazine on cellular reactive oxygen species generation in dihydroethidium or MitoSOX Red-stained A431 cells. Representative flow cytometry fluorescence histograms showing **(a)** DHE fluorescence (DHE -/+) or **(b)** MitoSOX fluorescence (MitoSOX -/+) in untreated (solid trace) or CCCP treated (dashed trace) A431 cells as detected by the FL2 channel whilst excited by a 488 nm argon laser. The y axis label (count) indicates the number of events (cells) detected at the respective MFI. n=1. **CCCP:** carbonyl cyanide *m*-chlorophenyl hydrazine; **DHE:** dihydroethidium; **MFI:** mean fluorescence intensity.

2.8.1.2. Determining the optimal dihydroethidium concentration for the detection of reactive oxygen species

The appropriate [DHE] for staining was first verified prior to assay in chapter 3. To this end, A431 cells were seeded at a density of 9.5 x 10^3 cells/cm^2 into 24 well plates and grown for 96 h in 18.6% O_2 (37°C/5% CO_2). The growth medium was replaced every 24 h. After the growth period, A431 cells were then treated with 50 µM CCCP for 1 h (37°C/5% CO_2). A431 cells were then stained under low light with vehicle (0.1% v/v DMSO) or 0.5-10 µM DHE for an additional 1 h (37°C/5% CO_2). Increasing [DHE] led to an associated increase in the fluorescence of DHE-stained A431 cells **(Figure 2.27 a)**. However, 10 µM DHE was chosen as the appropriate DHE staining concentration for further work as this lead to the largest increase in MFI relative to the unstained control cells **(Figure 2.27 b)**. The staining concentrations utilised for MitoSOX Red and DCFHDA were 2 µM and 10 µM (respectively) based on personal communication with Ferguson et al.

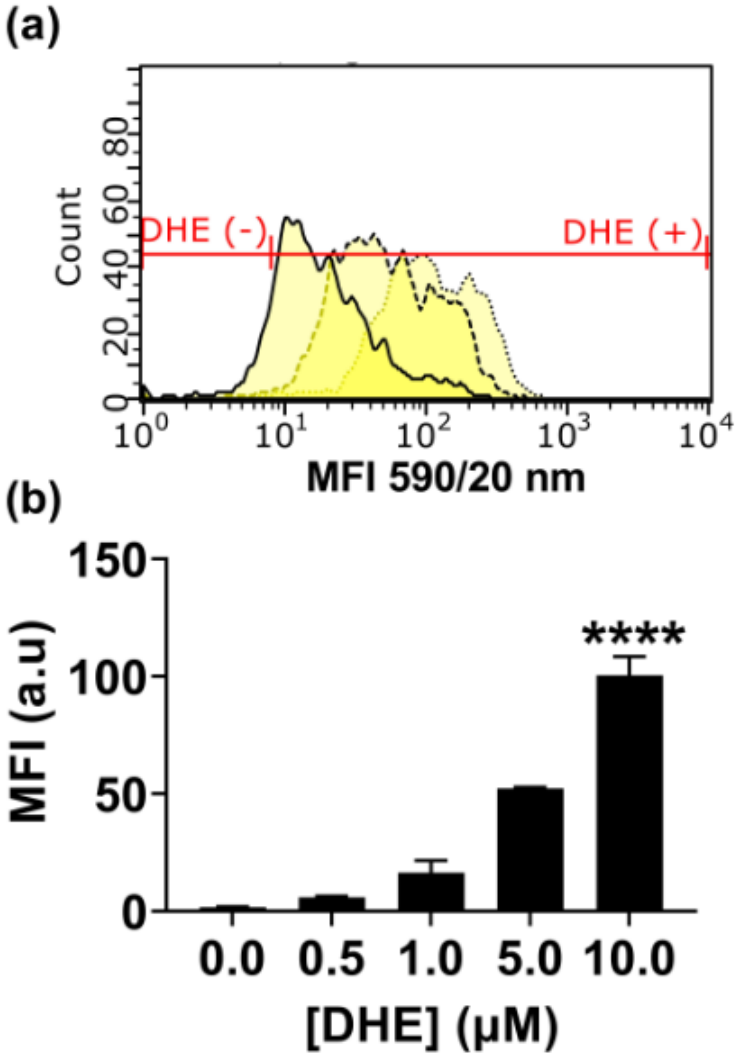

Figure 2.27. Effect of dihydroethidium concentration on cyanide *m*-chlorophenylhydrazone-induced reactive oxygen species detection. A431 cells were seeded at a density of 9.5 x 10^3 cells/cm^2 in 24 well plates and grown in 18.6% O_2 for 96 h (37°C / 5% CO_2). Growth medium was changed every 24 h. After 96 h of growth, A431 cells were treated with 50 µM CCCP for 1 h. Under low light, A431 cells were then stained with 0.5-10 µM DHE or vehicle (0.1% v/v DMSO) for an additional 1 h (37°C / 5% CO_2) prior to quantification of ROS generation by flow cytometry using the FL2 detector whilst excited by a 488 nm argon laser. **Panel (a),** representative DHE fluorescence histogram of A431 cells treated with 50 µM CCCP after staining with 1 µM (solid trace), 5 µM (dashed trace), or 10 µM DHE (dotted trace). The y axis label (count) indicates the number of events (cells) detected at the respective MFI. **Panel (b),** the effect of [DHE] on detected CCCP-induced ROS generation. **** = $P < 0.0001$, versus 0 µM DHE utilising a paired two-tailed student's t-test. Data in panel (b) is presented as the mean ± 1 SD. n=3. **a.u:** arbitrary units; **MFI:** mean fluorescence intensity.

2.8.2. 2′, 7′-dichloro-dihydro-fluorescin diacetate

DCFHDA was used to estimate treatment-induced oxidative stress. As discussed previously discussed **(section 1.2.3.3),** DCFHDA cannot be employed to measure individual ROS specifically. This is because DCFHDA-mediated detection of ROS relies on numerous inputs including [Fe^{2+}], and esterase

activity. FBS may contain free Fe^{2+} which may interfere with the oxidation of DCHFDA by ROS. This potential interference was tested in the following section.

2.8.2.1. Measuring whether the presence of fetal bovine serum in cell culture growth medium interfered with 2', 7'-dichloro-dihydro-fluorescein diacetate-mediated detection of oxidative stress

A431 were seeded as described previously in **section 2.4** and grown in 18.6% O_2 for 96 h. A431 cells were then treated with vehicle (0.1% v/v DMSO) or 1–32 µM auranofin for 1 h. A431 cells were then stained with 10 µM DCFHDA in growth medium containing, or not containing, 10% v/v FBS for 1 h (37°C/5% CO_2). ROS generation was then measured by flow cytometry utilising the FL1 detector whilst excited at 488 nm. Example DCFHDA fluorescence histogram are shown in **Figure 2.28 a.**

A two-way ANOVA was performed to analyse the effect of treatment and FBS on DCFHDA-mediated detection of oxidative stress. A *post-hoc* analysis showed that the treatment of A431 cells with 16 uM and 32 uM auranofin in DMEM without FBS resulted in a statistically significant increase in the MFI detected by the FL1 channel compared to the FBS containing group under the same treatment conditions **(Figure 2.28 b),** with means of 308.9 ± 17.8 MFI vs 247.3 ± 5.4 MFI ($P < 0.01$), and 450.4 ± 34.3 MFI vs 328.8 ± 1.6 MFI ($P < 0.001$), respectively.

The interaction between the effects of [auranofin] and FBS on DCFHDA-detected oxidative stress was statistically significant (F (3, 24) = 5.603, P=0.0047).

As such, FBS was not included in the growth medium during the analyses using DCFHDA in chapter 3.

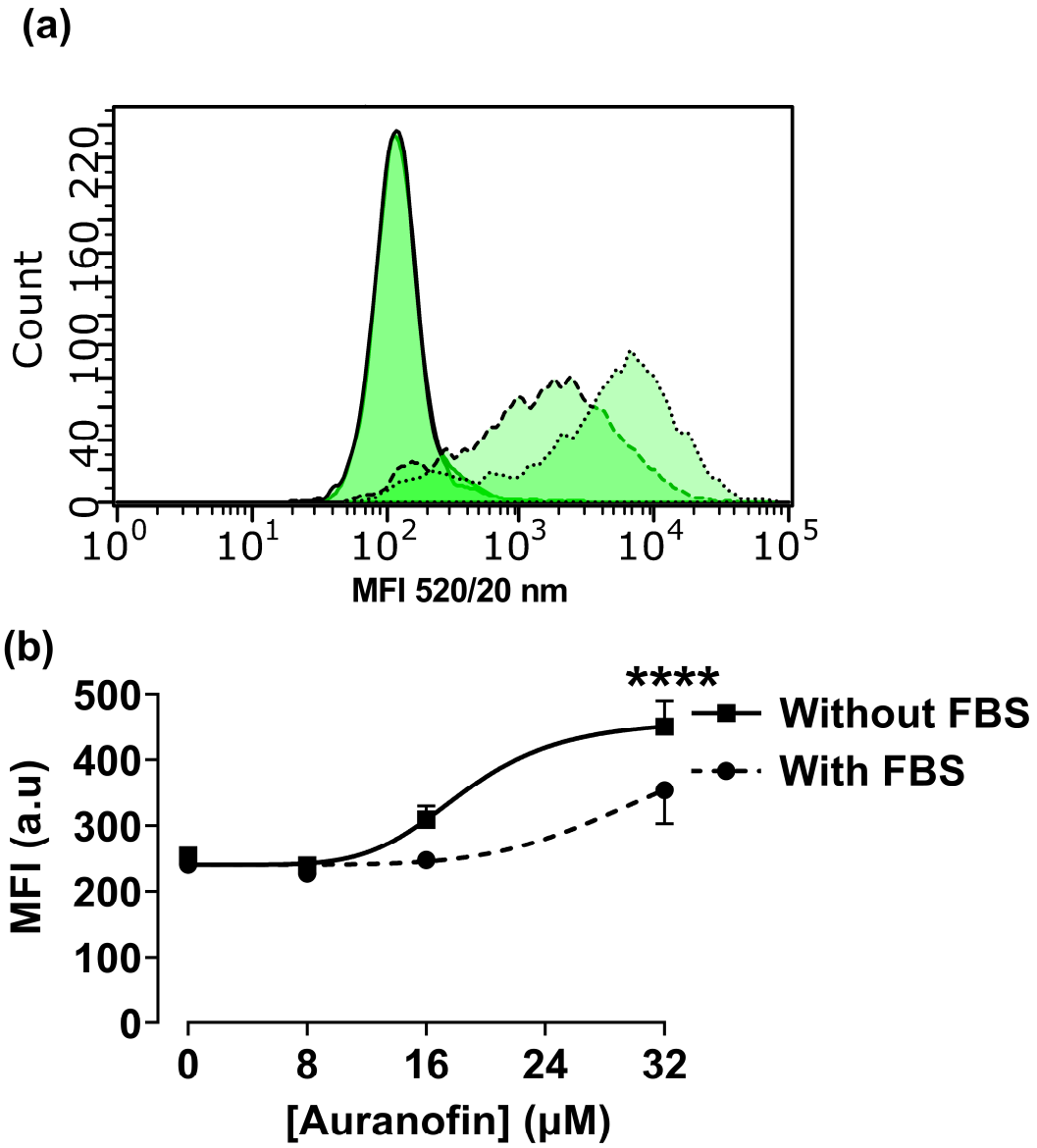

Figure 2.28. Effect of fetal bovine serum on auranofin-induced oxidative stress in 2', 7'-dichloro-dihydro-fluorescein diacetate-stained A431 cells. A431 cells were seeded at a density of 9.5 x 10^3 cells/cm^2 in 24 well plates and were grown for 96 h in 18.6% O_2 for 96 h (37°C/5% CO_2). A431 cells were fed with fresh growth medium every 24 h. After the incubation period, cells were treated with 1-32 µM auranofin or vehicle (0.1% v/v DMSO) for 1 h in 18.6% (37°C/5% CO_2). After the treatment period, A431 cells were stained with DCFHDA at a final concentration of 10 µM for 1 h in culture medium with/without 10% FBS supplementation (37°C/5% CO_2). A431 cells were subsequently washed with PBS (see section 2.2.3 for concentration), detached with 0.25% v/v trypsin-EDTA, and oxidative stress was analysed by flow cytometry as detected by the FL1 detector whilst excited by a 488 nm argon laser. **Panel (a),** representative DCFHDA fluorescence histogram of untreated (solid trace) or 32 µM auranofin-treated A431 cells with FBS (dashed line) or without FBS (dotted trace). The y axis label (count) indicates the number of events (cells) detected at the respective MFI. **Panel (b),** the effect of FBS in growth medium on the detection of auranofin-induced oxidative stress in A431 cells by DCFHDA. **** = $P < 0.0001$ versus 'with FBS' group utilising a two-way ANOVA and a *post-hoc* multiple comparison test and Dunn-Šidák correction. Data in panel (b) is presented as the mean ± 1 SD. n = 3. Where error bars are not visible, this is because the error bar is smaller than the size of the data point. **a.u:** arbitrary units; **FBS:** fetal bovine serum; **MFI:** mean fluorescence intensity.

2.8.3. Amplex Red

Extracellular H_2O_2 generation was measured by Amplex Red **(section 1.2.3.1)** in chapter 3 **(section 3.3.7)**. Phenol red has been shown to interfere with the detection of H_2O_2 [234]. This is because phenol red is a substrate for HRP which was used in the Amplex red assay in this work **(section 1.2.3.1)**. Additionally, phenol red was in the A431 cell growth medium. As such, the effect of phenol red on Amplex Red-mediated detection of H_2O_2 was determined prior to further testing with Amplex Red.

2.8.3.1. Determining whether phenol red interferes with Amplex red-mediated detection of H_2O_2

Amplex Red and HRP were added to growth medium with or without phenol red. To this solution, H_2O_2 was added to achieve a final concentration of 0–20 µM. The fluorescence emission of the resorufin end product was then measured at an excitation wavelength of 570 nm and an emission wavelength of 585 nm. Statistical significance was not calculated due to an insufficient number of experimental repeats (n = 1). However, the presence of phenol red resulted in a standard curve with a smaller slope compared to the standard curve generated in the absence of phenol red, with means of 722.6 vs 819.6 respectively. The presence of phenol red did not affect the linearity of the standard curve compared to the group stained in the absence of phenol red, with R^2 = 0.99 vs 0.99, respectively **(Figure 2.29)**. Although the effect of phenol red on Amplex red-mediated detection of H_2O_2 was minimal, phenol red was not included in the growth medium during the Amplex Red analyses in chapter 3.

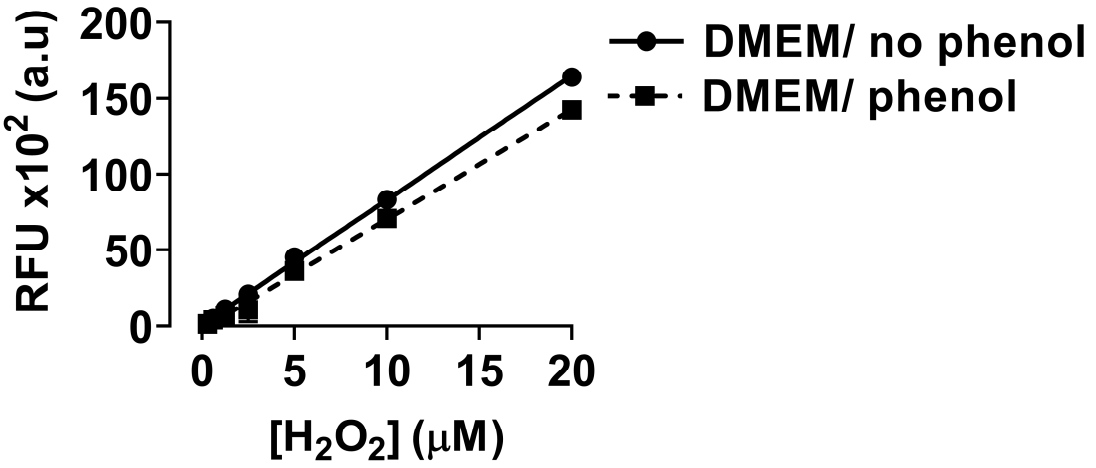

Figure 2.29. The effect of phenol red on the detection of H_2O_2 by Amplex Red. Under low light, a reaction mixture of Amplex Red (100 μM) and horseradish peroxidase (0.2 U/mL) was made up in DMEM with or without phenol red. 50 μL of this reaction mixture was added to black walled plastic 96 well plates. A 20 mM H_2O_2 working stock was made up in UH_2O. To the reaction mixture, 1 μL of H_2O_2 was added to achieve H_2O_2 final concentrations of 0–20 μM. The plate was then agitated on an orbital shaker for 10 s. The fluorescence emission of the resorufin end product was then measured on a Spectramax M_2e spectrophotometer at an excitation wavelength of 570 nm and an emission wavelength of 585 nm. Simple linear regression was used to generate the slopes of the standard lines (reported in the text). n = 1. Where error bars are not visible, this is because the error bar is smaller than the size of the data point. **a.u:** arbitrary units; **DMEM:** Dulbecco's modified Eagle's medium.

2.9. Mitochondrial staining with MitoTracker Red

MitoTracker Red is a fluorescent dye used to stain mitochondria. This stain was used in chapter 3 to quantify mitochondrial mass by flow cytometry and fluorescence microscopy **(section 3.3.10 and 3.3.11)**. Unlike other mitochondria-targeted probes (e.g. tetramethylrhodamine methyl ester, and rhodamine 123) the chloromethyl group present in MitoTracker dyes forms a covalent bond with thiols on proteins and peptides. As MitoTracker is a cationic probe, it selectively accumulates in mitochondria due to the negative electrochemical potential in healthy mitochondrial [235]. The accumulation of MitoTracker Red into mitochondria is therefore dependent on ψ_m [235].

2.10. Measuring antioxidant enzyme activity and the levels of reduced and oxidised glutathione

In chapter 4, the activities of key Nrf-2-target antioxidant enzymes was measured **(section 4.3.1 and 4.3.3-4.3.6)**. The general cell culture set up for these analysis was as follows. A431 cells were seeded at a density of 9.5 x 10^3 cells/cm^2 in T75 flasks and were grown in 18.6% O_2 or 3.0% O_2 **(section 2.3)** for 24, 48, 72 or 96

h (5% CO_2/37°C). Growth medium was changed every 24 h with appropriate [O_2]-equilibrated growth medium. A431 cells were then lysed under the appropriate [O_2] condition and [protein] was determined by the BCA assay **(section 2.12.3)**. The methods used for measuring the enzyme activity of catalase, SOD, GR, Gpx, and GST are described in detail in **section 4.2.1-4.2.5.** The method used for the measurement of GSH and GSSG is described in **section 4.2.6.**

In chapter 3, antioxidant enzyme inhibitors were used. For example, the catalase inhibitor 3-amino-1, 2, 4-triazole **(section 3.3.1.1 and 3.3.1.2)**, and the GS inhibitor L-BSO **(section 3.3.1.3 and 3.3.1.4)**. It was first necessary to confirm that these compounds inhibited their respective enzyme/protein systems.

2.10.1. Validation of catalase inhibition by 3-amino-1, 2, 4-triazole

3-AT was utilised to inhibit catalase in chapter 3 **(section 3.3.1.1 and 3.3.1.2)**. 3-AT-mediated inhibition of catalase was first verified in A431 cells. Catalase activity was measured by monitoring the decomposition of H_2O_2 at 240 nm in the presence of whole-cell lysates **(section 4.2.1)**. A431 cells were seeded at a density of 9.5 x 10^3 cells/cm^2 into 6 well plates and were incubated for 96 h at 37°C /5% CO_2. A431 cells were then treated with 8 or 16 mM 3-AT or vehicle (0.1% v/v UH_2O) for 24 h at 37°C /5% CO_2. A431 cells were also treated with 1 mM sodium azide (NaN_3) for 1 h at 37°C /5% CO_2 to serve as a positive control for catalase inhibition. As [3-AT] increased, there was an associated decrease in catalase activity **(Figure 2.30 b)**. For example, treatment of A431 cells with 16 mM 3-AT for 24 h resulted in a statistically significant decrease in catalase activity compared to untreated control cells ($P < 0.0001$, **Figure 2.30 b**), with means of 52.55 ± 15.37 U vs 81.48 ± 14.69 U, respectively. However, there was no statistically significant difference in catalase activity when comparing the 8 mM 3-AT-treated group to the 16 mM 3-AT-treated group **(Figure 2.30 b)**. Of note, treatment with 1 mM sodium azide resulted in a further decrease in catalase activity when compared to the 16 mM 3-AT treated group ($P < 0.05$), with means of 20.82 ± 10.72 U vs 52.55 ± 15.37 U. Although 3-AT was confirmed to inhibit catalase, the decomposition of H_2O_2 (and its subsequent detection at A_{240}) likely involved other enzymes capable of decomposing H_2O_2 due to the additive inhibitory effect of sodium azide on detected enzymatic activity in A431 cell lysate already treated with 3-AT. This is discussed in further detail in **section 4.4.1.**

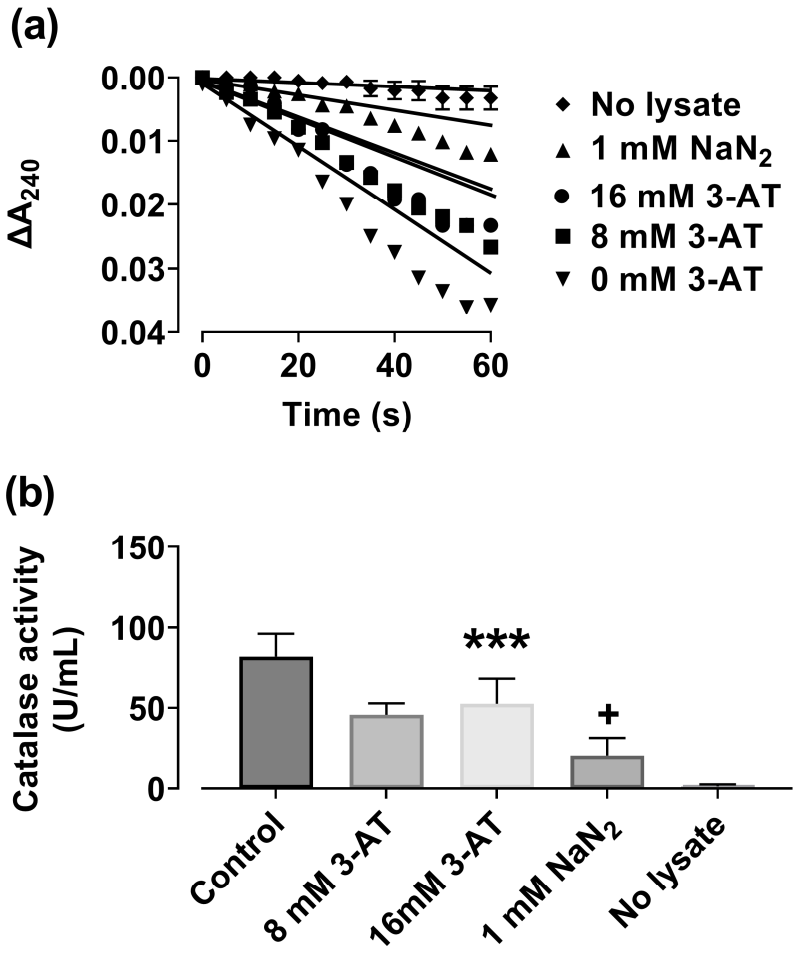

Figure 2.30. 3-amino-1, 2, 4-triazole-mediated inhibition of cellular catalase. A431 cells were seeded at a density of 9.5 x 10^3 cells/cm^2 into 6 well plate and incubated for 96 h at 37°C /5% CO_2. A431 cells were then treated with 8 or 16 mM 3-AT or vehicle control (0.1% v/v UH_2O) for an additional 24 h. A431 cells were also treated with 1 mM sodium azide for 1 h as a positive control for enzyme inhibition. After treatment, cells were lysed and [protein] was determined by the BCA assay (section 2.12.3). In a quartz cuvette, 100 µg of sample protein or standard (0–200 U/mL catalase from bovine liver) was added to 900 µL of 50 mM phosphate buffer (28.9 mM Na_2HPO_4, 21.1 mM NaH_2PO_4, pH 7.0). To this solution, H_2O_2 was added to a final concentration of 5 mM. To one reaction mixture, no lysate was added (negative control). **Panel (a),** ΔA_{240} of H_2O_2 in the presence of cellular lysates, derived from A431 cells previously treated with 8 or 16 mM 3-AT, or 1 mM NaN_3, measured at intervals of 5 s for 1 min using a Spectramax M_2e spectrophotometer. **Panel (b),** catalase activity per mg of protein in 3-AT or NaN_3-treated A431 cells. **** = $P < 0.0001$ versus untreated control utilising a paired two-tailed Student's t-test. Data in panel (a) is representative of one experiment. Data in panel (b) is presented as the mean ± 1 SD. n=3. Where error bars are not visible, this is because the error bar is smaller than the size of the data point. **ΔA:** change in absorbance; **3-AT:** 3-amino-1, 2, 4-triazole; **NaN_3:** sodium azide.

2.10.2. Validating glutathione depletion by L-buthionine sulfoximine

L-BSO was used in chapter 3 for H_2O_2 sensitisation experiments **(section 3.3.1.3 and 3.3.1.4)**. First, L-BSO-mediated depletion of GSH in A431 cells was verified. To this end, A431 cells were grown in 18.6% or 3.0% O_2 **(section 2.3)** for 96 h (37°C/5% CO_2). A431 cells were then treated with L-BSO for an additional 24 h.

A431 cells were then lysed under the appropriate [O_2] conditions **(section 2.12.1)**. For the purposes of normalisation, [protein] from the cellular lysate was measured using the BCA assay **(section 2.12.3)**.

[GSH] was measured utilising the method by Rahman et al [236]. 20 µL of GSH standards (0-200 µM) or cell lysate samples were added to a clear bottom plastic 96 well plates in assay buffer (0.1M potassium phosphate buffer with 5 mM EDTA disodium salt, pH 7.5). 5,5′-Dithiobis(2-nitrobenzoic acid)(DTNB) and GR enzyme from baker's yeast were added together in equal volumes to achieve a final concentration of 1 mM and an activity of 2 U (respectively). 120 µL of the DTNB and GR mixture was then added to the sample. After 30 s, NADPH (from a stock solution made up in assay buffer) was added to a final concentration of 240 µM. The plate was shaken for 10 s on an orbital shaker prior to measuring A_{412} of the TNB product at intervals of 10 s for 1 min using a SpectraMax M_2e spectrophotometer. Known concentrations of GSH (0–200 µM) were also assayed, allowing interpolation of sample [GSH] against a standard curve, where the slope of the initial linear reaction (A_{412} 0–1 min) was plotted against [GSH] **(Figure 4.6)**. The resulting activity was then normalised to sample [protein].

A two-way ANOVA was performed to analyse the effects of the [O_2] cells were grown in, and [L-BSO], on [GSH]. The effect of L-BSO on [GSH] was statistically significant ($P < 0.0001$), however, the effect of [O_2] was not statistically significant. Treatment with 1 mM L-BSO resulted in a decrease in [GSH] compared to respective untreated control in both [O_2] groups ($P < 0.0001$, **Figure 2.31 d**), with means of 98.7 ± 11.5 µM vs 9.0 ± 0.8 µM and 78.5 ± 18.5 µM vs 11.1 ± 0.4 µM, respectively. This decrease was maximal at 1 mM in both [O_2] groups, with no further decrease noted at 4 mM or 8 mM L-BSO compared to the 1 mM L-BSO treatment. As such, L-BSO was confirmed to deplete GSH in A431 cells.

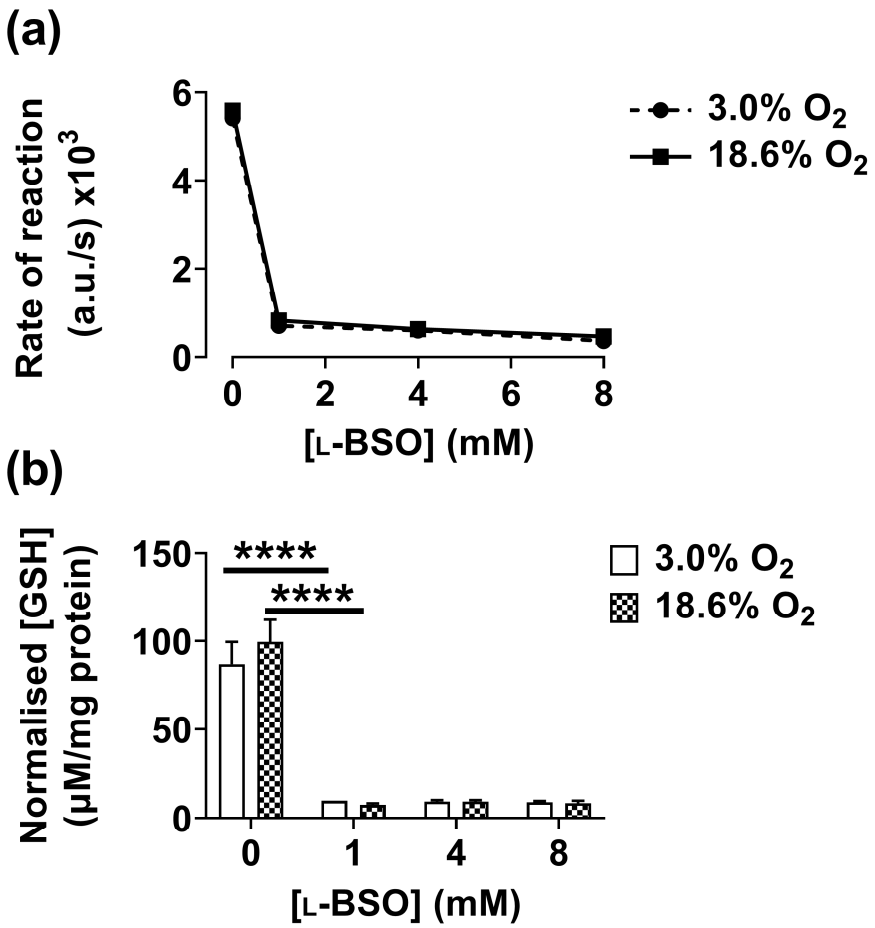

Figure 2.31. L-BSO-mediated depletion of cellular GSH. A431 cells were grown for 96 h in 18.6% O_2 or 3.0% O_2 for 96 h prior to treatment with 1-8 mM L-BSO, or vehicle (0.1 % v/v UH_2O), for 24 h (37°C/5% CO_2). A431 cells were then lysed under 18.6% or 3.0% O_2 and [protein] was determined using the BCA assay**.** [GSH] was then assayed using the GR enzyme recycling method as described by Rahman et al [236]. In brief, 100 µg of sample protein was added to a clear bottom plastic 96 well plates containing DTNB (1mM) and GR (2 U/mL). After 30 s, NADPH was added to a final concentration of 240 µM. The plate was then shaken for 10 s. A_{412} of TNB was then measured at intervals of 10 s for 1 minute. **Panel (a),** the slope of the initial linear reaction (ΔA_{412} 0–1 min) plotted against [L-BSO] from treated A431 cellular lysates. This is labelled as the rate of reaction (a.u./s) on the y axis. **Panel (b),** the effect of L-BSO treatment on cellular [GSH]. **** = P < 0.0001 versus untreated control utilising a two-way ANOVA and a *post-hoc* multiple comparison test and Dunn-Šidák correction. Data are presented as the mean ± 1 SD. n = 3. Where error bars are not visible, this is because the error bar is smaller than the size of the data point. **ΔA:** change in absorbance; **DTNB:** 5,5′-Dithiobis(2-nitrobenzoic acid); **L-BSO:** L-buthionine sulfoximine; **TNB:** 5'-thio-2-nitrobenzoic acid.

2.11. Nuclear staining with Hoechst 33342

In chapter 3, mitochondrial mass was estimated using MitoTracker Red **(section 3.3.10)**. To this end, it was also necessary to counterstain cellular nuclei. The Hoechst 33342 stain was used for these purposes. A431 cells were seeded at a density of 9.5 x 10^3 cells/cm^2 in tissue culture-treated glass bottom cell culture slides and incubated for 96 h in 18.6% O_2 (37°C /5% CO_2). The growth medium was then replaced with growth medium containing 2 µM Hoechst 33342 from a

stock solution made up in UH_2O. A431 cells were then left to stain for 15 min (37°C /5% CO_2). A431 cells were then washed three times with pre-warmed PBS (see section 2.2.3 for concentration) prior to addition of Dulbecco's modified phosphate buffered saline (PBS) containing 4.5 g/L glucose without phenol red (DPBS; #D8662, Merck). A431 cells were imaged at random fields of view using an EVOS™ live cell imaging microscope with an EVOS™ LED cube v2 DAPI at x20 magnification.

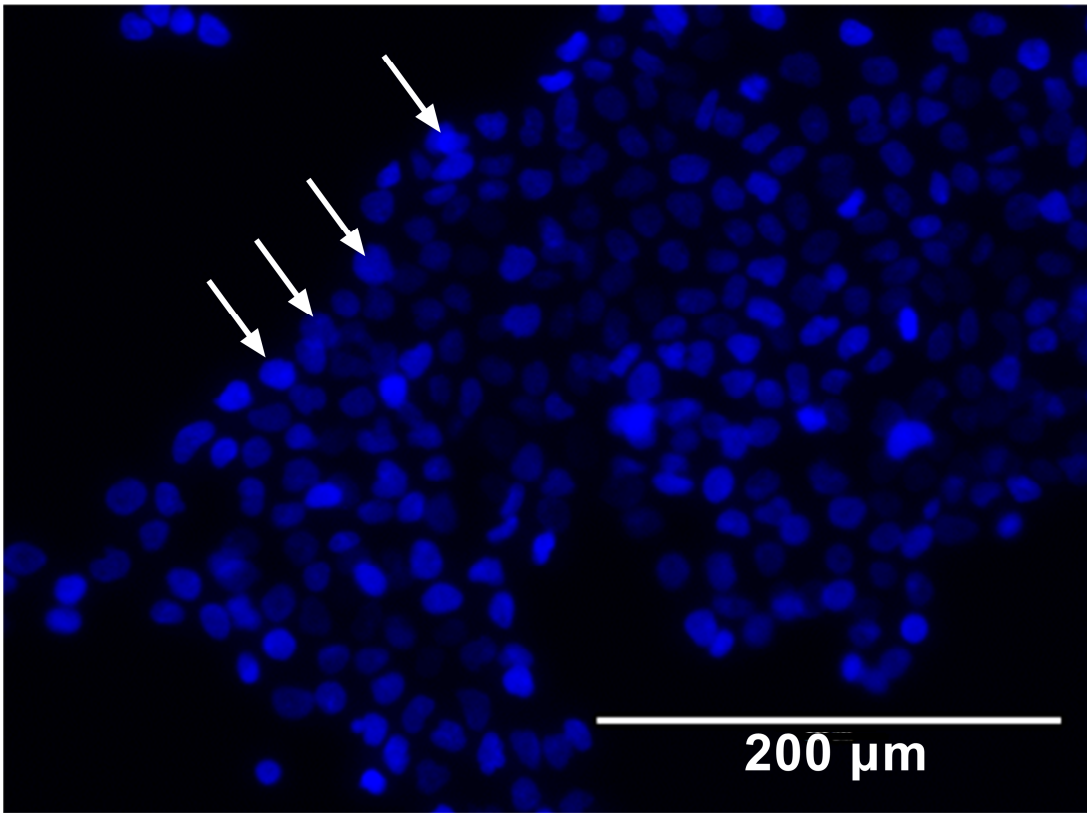

Figure 2.32. Representative image of A431 cells stained with Hoechst 33342. Arrows indicate examples of cellular nuclei imaged using an EVOS™ live cell imaging microscope with an EVOS™ LED cube v2 DAPI at 20 x magnification.

2.12. Western blotting

The expression levels of key anti-oxidant enzymes and transcription factor were determined by western blotting in chapter 5 **(section 4.3.8 and 4.3.9).** Both nuclear and whole-cell lysates were required for analysis. The protocols for whole-cell and nuclear lysis will be described first **(section 2.12.1 and 2.12.2)** before detailing the western blotting method.

2.12.1. Whole-cell lysis

For whole-cell lysis, cells were washed three times with cold PBS (see **section 2.2.3** for concentration). Lysis for 3.0% O_2 samples was performed in the physioxia hood, or on the lab bench for the 18.6% O_2 samples. In both cases, lysis was performed on ice. Lysis buffer was prepared by adding one protease inhibitor tablet (#A32963, Thermofisher) to 10 mL of radio immunoprecipitation assay (RIPA) buffer (10 mM Tris-HCl, 1 mM EDTA, 0.5 mM egtazic acid (EGTA), 1 mM phenylmethylsulfonyl fluoride (PMSF), 140 mM NaCl, 1% Triton X-100, 0.1% sodium deoxycholate, and 0.1% sodium dodecyl sulfate (SDS); pH 8). Once the tablet was fully dissolved, the buffer was then kept on ice. 100 µL of RIPA buffer was added per 1.0 x 10^6 cells (i.e. 1 mL of RIPA buffer was added to a T75 cm^2 plate at about 80% confluence). The plate was then transferred onto a rocker in a cold room and left to agitate for 2 min at 4°C. The lysate was then collected into a 1.5 mL Eppendorf tube by scraping the bottom of the flasks with a cell scraper (Corning). The lysates were then kept on ice for 15 min with vortexing every 3 min to ensure optimal lysis. A 40 µL sample was also kept aside for [protein] measurement using the Pierce™ BCA protein assay kit **(section 2.12.3).**

2.12.2. Nuclear lysis

Nuclear extraction was performed according to the method described by Schreiber et al. [237]. Nuclear extracts were used for semi-quantifying the expression levels of HIF-1α **(section 2.3.5.1)** and Nrf-2 protein **(section 4.3.8)**. As described previously **(section 2.12.1)**, cells were lysed under the appropriate [O_2]. A431 cells were washed with appropriate [O_2]-equilibrated PBS (see **section 2.2.3** for concentration), detached with 0.25% v/v Trypsin-EDTA, and pelleted by centrifugation at 200 RCF for 2mins. The cells were then re-suspended in ice cold cell lysis buffer (10 mM HEPES; pH 7.5, 10 mM KCl, 0.1 mM EDTA, 1 mM dithiothreitol (DTT), 0.5% Nonidet-40, 0.5 mM PMSF) and protease inhibitor cocktail (#ab65621, Abcam). The cells were left to swell on ice for 15-20 min with intermittent mixing every 3 min using a vortex set at 200 rpm. The sample was then centrifuged at 12,000 g at 4°C for 1 min. The supernatant constituted the cytoplasmic fraction.

The pellet was then re-suspended in nuclear extraction buffer (20 mM HEPES (pH 7.5), 400 mM NaCl, 1 mM EDTA, 1 mM DTT, 1 mM PMSF, and protease inhibitor cocktail (Abcam)). The pellet was then incubated on ice for 30 min with intermittent mixing at intervals of 5 min using a vortex set at 200 rpm. This lysate was then pelleted again by centrifugation at 14,000 g for 15 min at 4°C. The supernatant constituted the nuclear fraction and was stored at -80°C. [Protein] in the nuclear extract was estimated using the Pierce™ BCA protein assay kit.

As the expression levels of transcription factors are quite low within the cell, ≥ 40-50 µg of protein was loaded into each well of the gel to attain a visible band on the resulting immunoblot. To do this, ultracentrifugation was performed to concentrate the protein sample. A 10 kDa molecular weight cut off filter (Amicon®, Sigma) was used to concentrate the nuclear lysate. This was done by adding the nuclear lysate sample to the filter reservoir before centrifugation at 14,000 g for 15 min using a 40° fixed angle rotor. The filtrate was then discarded and the filter was placed into a new sample tube. After this initial spin step, a volume of about 20 µL remained in the reservoir. In order to recover the sample, the filter was inverted into a new sample collection tube and centrifuged again at 14,000 g for 5 min.

2.12.3. Bicinchoninic acid protein assay

The BCA protein assay is a colorimetric assay used to estimate [protein], and was used to normalise various endpoints measurements in this work such as the enzyme activity analyses in chapter 4. 20 µL of sample cellular lysate was added to a plastic 96 well plates. A 6 point protein standard curve **(Figure 2.33)** was made by diluting bovine serum albumin (BSA) to 0-2 µg/µL in UH_2O. 20 µL of each standard was added to plastic 96 well plates. 180 µL of a BCA/copper sulfate solution (200 µL copper sulfate for every 10 mL BCA) was added. The plate was then incubated in the dark at 37°C for 30 min. Some wells were set aside to measure blank absorbance (i.e. BCA/Copper sulfate and 20 µL of RIPA buffer). Following incubation, sample absorbance was measured at 562 nm using a Spectramax M_2e spectrophotometer. Sample [protein] was then interpolated from a standard curve.

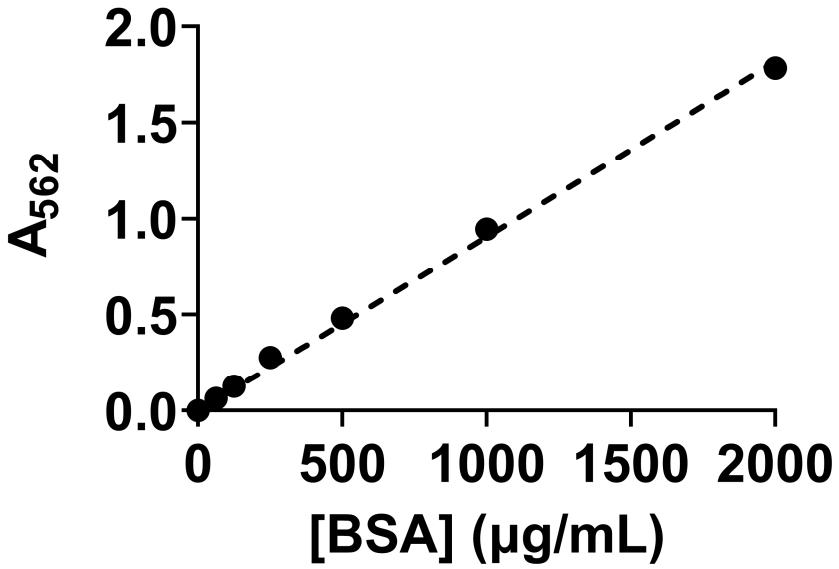

Figure 2.33. Representative bicinchoninic acid assay standard curve. To plastic 96 well plates, 20 µL of respective BSA standard (0–2000 µg/mL) was added followed by 180 µL of BCA/copper sulfate solution. The plate was mixed on an orbital shaker briefly for 1 min followed by a 30 min incubation at 37°C. Following incubation, A_{562} was measured using a SpectraMax M_2e spectrophotometer. The dashed line represents the best fit line generated by simple linear regression (R^2 = 0.99), n=1. **A:** absorbance; **BSA:** bovine serum albumin.

2.12.4. Preparation of samples for sodium dodecyl sulphate polyacrylamide gel electrophoresis

Pre-made 8-16% polyacrylamide gradient gels held a volume of 30 µL per well. To avoid sample spill over into the adjacent wells, 15 µL of sample (Made up to 22.5 µL with sample buffer) was used. Using the concentrations of protein determined by the BCA assay, 15 µg of whole-cell lysate samples (or 50 µg for nuclear samples) were transferred into 500 µL Eppendorf tubes and made up to 15 µL with UH_2O where necessary. A 4x solution of Laemmli buffer (62.5 mM Tris-HCl pH 6.8, 10% glycerol, 1% SDS, 0.005% Bromophenol Blue) was prepared. To 300 µL of this solution, 100 µL of DTT was added (DTT final concentration 50 mM; 3x Laemmli buffer solution). 7.5 µL of the Laemmli sample buffer was then added to each 15 µL sample solution before vortexing briefly. The sample was then centrifuged for 5 s to concentrate the sample at the bottom of the tube. The samples were then incubated at 95°C for 5 min and then left to cool on ice for 5 min.

2.12.5. Preparation of gels and loading of samples

Pre-made 8-16% polyacrylamide gradient gels were placed inside the gasket of a western blotting electrophoresis tank. To the gasket chamber, SDS buffer (30.3 g Tris base, 144.2 g glycine, 10 g SDS in 1 L of UH_2O) was added until it covered the wells of the pre-made gels. The internal chamber was then checked for leaks. The rest of the tank was then filled up to the required level depending on the number of gels being run.

22.5 µL of the prepared sample **(section 2.12.4)** was then loaded using gel loading tips (FisherBrand™). For molecular weight referencing, 2 µL of pre-stained protein standards (#1610773, Bio-Rad) were added to one well. The tank was then attached to a power source and electrophoresis was performed at 75 V for 15 min followed by 100 V for 45-60 min.

2.12.6. Transfer of protein to membrane

Transfer of protein to the nitrocellulose membrane was performed using a TransBlot Turbo transfer system kit. The nitrocellulose membrane was placed onto the bottom reservoir ion stack. The bottom reservoir ion stack and membrane were then placed into the bottom Turbo-Blot tray (anode). The gel cassette was opened using a metal insert key and the gel was placed onto the nitrocellulose membrane. The remaining reservoir ion stack was then placed on top of the gel. Bubbles were removed using a soft rolling pin. The tray was then sealed and placed into the Turbo-Blot system. The system was set to run using the ‘mixed molecular weight’ protocol which allows the transfer of proteins 5-150 kDa in weight. The protocol transferred at 1.3 A and up to 25 V.

Once the transfer was complete, the membrane was removed from the tray and was stored in a black plastic box with 5 mL of REVERT™ 700 total protein stain (#926-11011, LI-COR, Lincoln, Nebraska, USA). The LI-COR total protein stain allowed transferred protein to be stained for the purposes of data normalisation. The membrane was left to stain on a rocker for 5 min. Excess protein stain was then removed by washing the membrane three times with 5 mL of REVERT™700 wash solution (#926-11015, LI-COR) on a rocker at 5 min intervals. The membrane was then imaged at 700 nm using an Azure Biosystems gel imaging system (Azure Biosystems, Dublin, Ireland). The stain was then removed by

washing three times with 5 mL of REVERT™ 700 reversal solution (#926-11015, LI-COR) on a rocker at 5 min intervals. Removal of the stain was verified by imaging the membrane again at 700 nm after the reversal step. The membrane was then washed five times with UH_2O and placed into a new black plastic box.

The membrane was then blocked by adding 5 mL of Pierce™ protein free blocking buffer. The membrane was then left to block overnight at 4 °C on a rocker.

2.12.7. Incubation with primary and secondary antibody

Most primary antibodies were diluted 1:1,000 (anti Nrf-2, and NQO-1 were diluted 1:500) in PBS containing 0.1% Tween-20 (PBST) and 0.3% BSA (w/v). The membrane was then incubated with the primary antibody for 1 h at room temperature on a rocker. An anti-cytoskeletal β actin antibody from rabbit (#A300-485A, Bethyl Laboratories, Montgomery, TX, USA) diluted 1:10,000 in PBS (containing 0.3% BSA) was used to control for loading error **(section 2.12.8)**. After primary antibody incubation, the antibody solution was removed and the membranes were washed three times with PBST and one time with PBS at 5 min intervals on a rocker. The appropriate conjugated fluorescent secondary antibodies (LI-COR) were then diluted 1:10,000 in PBS. The secondary antibodies were then incubated with the membrane for an additional 1 h at room temperature on a rocker. The membrane was then washed three times with PBST and one time with PBS on a rocker at 5 min intervals.

2.12.8. Loading control: cytoskeletal actin and total protein

Although effort was made to load the same amount of protein into the gel wells, small inconsistencies in protein loading, transfer efficiency, and sample preparation can result in minor changes to the levels of protein detected on the immunoblot. As such, a normalisation step was needed to ensure that relative changes to the target protein levels were not due to systematic experimental error. For these purposes, whole-cell lysate samples were normalised to cytoskeletal actin or glyceraldehyde 3-phosphate dehydrogenase (GAPDH), and nuclear protein lysates were normalised to total protein. This decision was based on the cost of buying an antibody for the nuclear fraction (i.e. lamin B1).

The relationship between loaded [protein] and detected cytoskeletal β actin or total protein is shown in **Figure 2.34 (a and b)** and **Figure 2.35 (a and b),** respectively. In both cases, the relationship between the weight of loaded protein and the relative fluorescence units (RFU) of the associated detection fluorophore was linear with, $R^2 = 0.96$ and $R^2 = 0.98$, respectively.

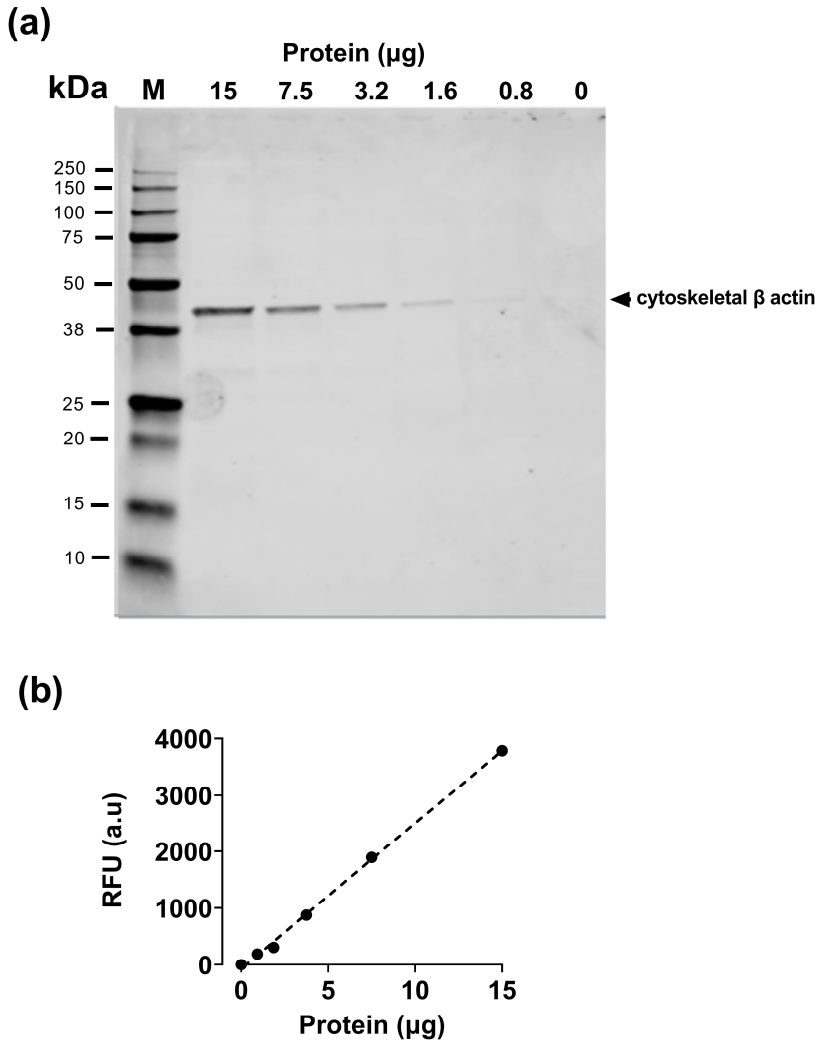

Figure 2.34. The effect of loaded protein weight on the expression levels of cytoskeletal β actin as assessed by western blotting. Protein lysates from A431 cells were analysed for [protein] using the BCA assay. 0–15 µg of protein at a volume of 15 µL was added to 7.5 µL of 3x Laemmli buffer containing 50 mM DTT. Samples were then boiled at 95°C/5 mins, centrifuged at 14,000 g at 4°C/5 mins, and then loaded into pre-made 8-16% gradient polyacrylamide gel. Protein electrophoresis was then performed (stacking phase 75 V/15 min, followed by 100 V/60 min). Protein was transferred at 25 V and 1.3 A to a nitrocellulose membrane using a TurboBlot transfer kit. The membrane was then subsequently probed with an anti-cytoskeletal β actin primary antibody and an anti-rabbit secondary antibody. The fluorescence intensity of the target bands (42 kDa) were analysed with an Odyssey Clx near infrared imaging system (LI-COR). **Panel (a),** anti-cytoskeletal actin (42 kDa) immunoblot. **Panel (b),** the effect of loaded protein weight on the expression levels of cytoskeletal actin. The dotted line represents the best fit line generated from simple linear regression, $R^2 = 0.96$, n=1. **a.u:** arbitrary units; **kDa:** kilo Daltons; **M:** molecular weight marker lane.

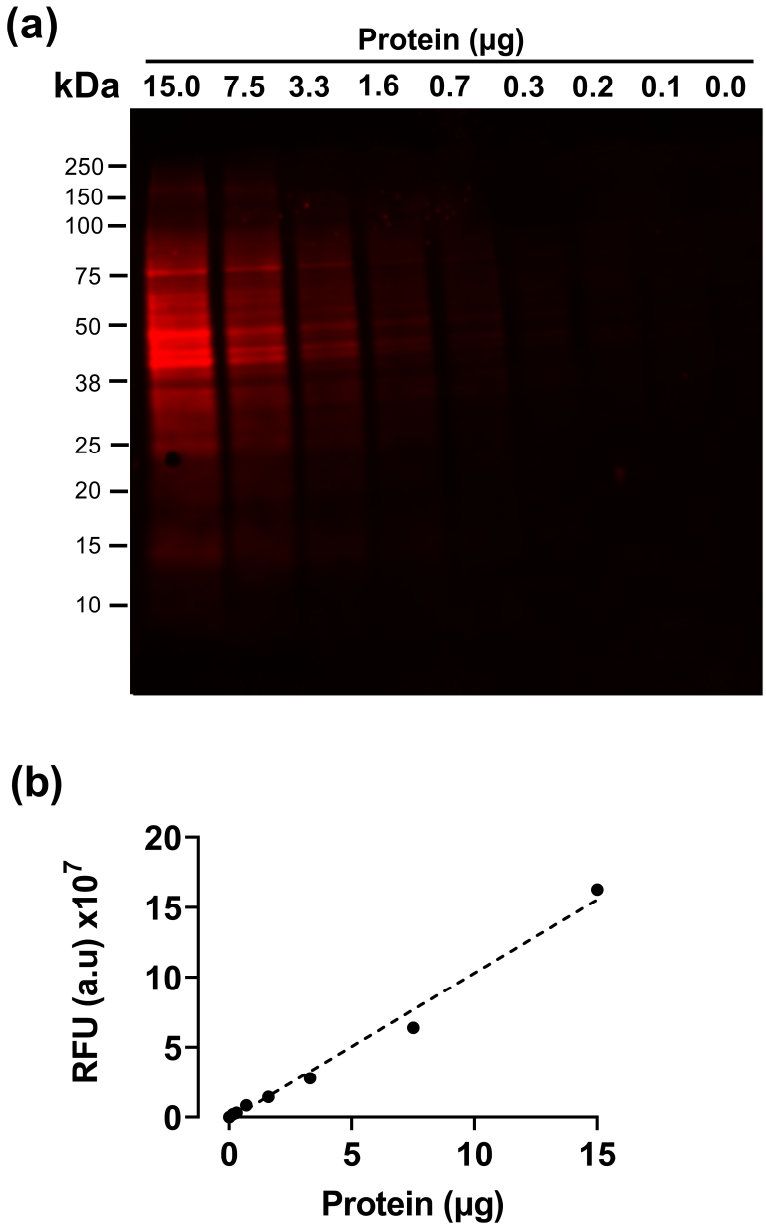

Figure 2.35. The effect of loaded protein weight on total protein as assessed by western blotting and total protein staining. Protein lysates from A431 cells were analysed for [protein] using the BCA assay. 0–15 µg of protein, in a volume of 15 µL, was added to 7.5 µL of 3x Laemmli buffer containing 50 mM DTT. Samples were then boiled at 95°C/5 mins, centrifuged at 14,000 g at 4°C/5 mins, and then loaded into pre-made 8-16% gradient polyacrylamide gel. Protein electrophoresis was then performed (stacking phase 75 V/15 min, followed by 100 V/60 min). Protein was transferred at 25 V and 1.3 A to a nitrocellulose membrane using a TurboBlot transfer kit. The membrane was then subsequently probed with 5 mL of REVERT^{TM}700 total protein stain (LI-COR) for 5 mins on a rocker at room temperature prior to washing three times with 5 mL of REVERT^{TM}700 wash solution for 3 min on a rocker. The fluorescence intensity of the LI-COR total protein stain was then measured using an Azure Biosystems gel imaging system (Azure Biosystems, Dublin, Ireland). **Panel (a),** total protein stain image. **Panel (b),** total protein stain fluorescence (RFU) versus loaded protein weight. The dotted line represents the best fit line (R^2= 0.98) generated by simple linear regression, n=1. **a.u:** arbitrary units; **kDa:** kilodalton; **RFU:** relative fluorescence units.

2.12.9. Imaging of the membrane

An Odyssey CLx near infra-red imaging system (LI-COR) was used to image the immunoblot membrane. The Odyssey CLx imaging system utilised a set of solid state diode lasers that provide excitation light at 685 nm and 785 nm. Although the Odyssey system is capable of a number of different modes to accommodate for dynamic range, the system was always set to 'automatic' mode in which the system would attempt to acquire an image devoid of saturated pixels.

The surface of the scanning area was wiped clean with ethanol and a lint free cloth. The membrane was placed face-down onto the scanning surface using a clean forceps. To remove bubbles, a silicone mat was placed over the membrane and the bubbles were removed using a 4" soft roller.

The Odyssey CLx imaging software was initiated, 'Western blot' was selected in the 'Analysis' tab, and 'Auto' was selected in the 'Channels' tab. A resolution of '169 µM' and a focus offset of '0.0 µM' was selected in the 'Scan Controls' tab. A work area was drawn around the membrane by selecting the 'Draw New' option from the 'Scan Area' tab. In the 'Scanner' tab, the run was initiated by selecting 'Start'.

Once the imaging was complete, the image was checked for saturation. If the image contained saturated pixels, the blot was run again blocking out the saturated region using a piece of black felt paper. Blots were stored dry in re-sealable zip-lock bags and were protected from light.

2.12.10. Data analysis

ImageStudio Lite Ver5.2 was used to analyse and normalise protein levels from the bands of interest. An immunoblot imaged using both the 685 nm and 785 nm excitation lasers generated two separate acquisition files. Display settings (i.e. brightness, contrast) could be adjusted on the acquisition file. This was performed by selecting either the 700 nm or 800 nm channel in the 'adjust' setting within the 'image' tab. Changing the contrast/brightness only modifies the visual appearance of the blot and does not alter the original acquisition file.

The fluorescence emission detected by the photodiode was converted into a digital signal. The fluorescence intensity of the target bands is presented in

arbitrary units. The fluorescence intensity emitted by the secondary antibody (when bound to the target-bound primary antibody) was used to estimate *relative* changes to the levels of a target protein expression compared to a chosen control.

In order to measure relative changes in protein expression, the fluorescence intensity of the bands of interest were collected. First, the median background fluorescence was subtracted from the acquisition. Median background fluorescence was subtracted when the background fluorescence present on the blot was not uniform. The average background fluorescence was subtracted when the background fluorescence was uniform. To measure the signal from the target bands, non-intersecting rectangles were drawn around both the target bands and the loading control bands. Once done, the signal from each band was recorded using the Clx imaging suite software.

The following formula was used to determine the lane normalisation factor:

$$\text{Lane normalisation factor} = \frac{\text{Fluorescence signal from each band/lane}}{\text{Band/lane with the highest fluorescence signal}}$$

A normalised signal for each target band was then generated using the following formula:

$$\text{Normalised signal for target band} = \frac{\text{Target band signal}}{\text{Lane normalisation factor}}$$

This normalised signal was utilised to semi-quantify relative changes to target protein expression levels.

2.13. Statistical analysis

The effect of [O_2] and treatment on the subsequent cellular response was a frequently used statistical comparison. The null hypothesis proposed that the differences between the cellular responses to treatment were the same in both [O_2] groups (i.e. the concentration response curves were parallel). To reject the null hypothesis, a two-way ANOVA was chosen to test the interaction between the effects of [O_2] cells were grown in and treatment on the appropriate cellular responses/endpoints. A statistically significant interaction indicated that the effect of treatment between [O_2] groups was not the same at each concentration (i.e. the concentration response curves were non-parallel). Whenever a statistically

significant interaction effect was reported, it was followed by the P value, F ratio, degree of freedom of the numerator (DFn), and the degrees of freedom of the denominator (DFd). When such an interaction was not significant, this was not reported in the text.

In certain cases, a multiple comparison *post-hoc* was performed to determine at which treatment concentration cells exhibited statistically significant differences in their cellular response. The result of (usually) one representative two-way ANOVA *post-hoc* multiple comparison test was reported in the text at the concentration of largest difference between the two [O_2] groups. When a *post-hoc* comparison was made, the P value was reported in brackets directly after. A P value of less than 0.05 indicated that an effect was statistically significant.

In cases where the means of two separate treatments were compared, a paired two-tailed Student's t-test was used.

CHAPTER 3: SQUAMOUS CELL CARCINOMA CELLS GROWN IN STANDARD CELL CULTURE OXYGEN CONCENTRATIONS ARE RESISTANT TO OXIDATIVE-STRESS-INDUCED CELL DEATH, COMPARED TO CELLS ADAPTED TO PHYSIOXIA

3.1. Introduction

As mentioned previously, redox-active therapeutics are currently in development for the treatment of human diseases such as cancer **(section 1.3.1.1.1)**. However, the *in vitro* testing of such compounds on mammalian cells grown long term under 18.6% O_2 may lead to artefactual cellular responses compared to cells adapted to physioxia **(section 1.3.1.1.1)**. For example, mammalian cells grown in 18.6% O_2 exhibited resistance to copper oxide nanoparticles, rotenone, acetaminophen and the human immunodeficiency virus (HIV) virotoxin Tat compared to mammalian cells adapted to physioxia [73, 75, 82, 84]. As discussed previously, the induction of Nrf-2-target protein by DMF was increased in HUVEC grown in 18.6% O_2 compared to physioxia **(section 1.3.1.1.1)**. Of most relevancy to this present work, A431 cells grown in 18.6% O_2 were resistant to photodynamic irradiation-induced cell death compared to those adapted to physioxia [21].

Photodynamic irradiation is a redox-active treatment used for the treatment of CSCC (which A431 cells model). This approach uses a photosensitiser (e.g. protoporphyrin IX (PPIX)) to induce oxidative stress-induced cell death via singlet oxygen generation when excited by red light (λ_{max} 635 nm). As such, photodynamic therapy is dependent on three main factors: the energy of the photo irradiation, [photosensitiser], and [O_2].

Ferguson et al. [21] demonstrated that A431 cells grown in 18.6% O_2 accumulated more of the photosensitiser PPIX, and generated more photodynamic irradiation-induced ROS, than A431 cells adapted to 2.0% O_2 for 48 h. As the energy of the irradiation was the same in both [O_2] conditions, it was surprising that the levels of photodynamic irradiation-induced cell death was also the same in both [O_2] groups despite the differences in [O_2], PPIX cellular accumulation, and ROS generation [21]. This phenotype was not due to an acute effect of O_2 during treatment. Changing A431 cells previously grown in 3.0% O_2 for 48 h into 18.6% O_2 during photo irradiation did not confer cellular resistance to photodynamic irradiation-induced cell death. The authors concluded that the growth of A431 cells in 18.6% O_2 conferred a phenotype that rendered these cells resistant to photodynamic irradiation-induced cell death compared to A431 cells adapted to 2.0% O_2 for 48 h. What were these phenotypic changes? A431 cells

grown in 18.6% O_2 exhibited increased expression and activity of Nrf-2-target protein and enzyme compared to A431 cells grown in physioxia. These included the upregulated transcription of the antioxidant genes *TrxR1, SOD 1, PRDX1, NQO-1, HO-1, GPX1*, *CAT,* and *NFE2L2*. Of interest, the upregulated transcription of *TrxR1* (the molecular target of auranofin; **section 1.2.7.2.7**) in A431 cells grown in 18.6% O_2 was associated with a resistance to auranofin-induced cell death compared to A431 cells adapted to 2.0% O_2 for 48 h [21].

This present chapter set out to answer the following questions: Are A431 cells grown in 18.6% O_2 resistant to H_2O_2 and/or auranofin-induced cell death compared to A431 cells grown in 3.0% O_2? How long should A431 cells be grown in physioxia for such that H_2O_2 and auranofin-induced cell death no longer changes relative to cell death in A431 cells grown in 18.6% O_2 under the same treatment conditions? Does any such resistance of A431 cells grown in 18.6% O_2 toward H_2O_2/auranofin-induced cell death extend to other redox-active compounds such as 3-AT **(section 1.2.6.2.1)**, L-BSO **(section 1.2.6.3.1)**, CuOOH **(section 1.2.6.4.1)**, MSA **(section 1.2.6.4.2)**, and carmustine **(section 1.2.6.5)**? These research questions addressed aims 2–3, and objectives 2–6 outlined previously **(section 1.4).** To this end, A431 cells were grown in 18.6% O_2 or 3.0% O_2 for 24-96 h prior to treatment with these previously mentioned compounds. The endpoints investigated were cell death, ROS production, $\psi\Delta_m$ and lipid peroxidation.

3.2. Methods

3.2.1. Cell culture setup for concentration response testing using redox-active compounds

A431 cells were seeded at a density of 9.5 x 10^3 cells/cm^2 in 24 well plates and incubated in 18.6% O_2 or 3.0% O_2 (37°C/5% CO_2) for the required length of time **(Figure 2.17)**. The culture medium was replaced every 24 h with respective (18.6% or 3.0% O_2) [O_2]-equilibrated medium. The cells were then incubated under their respective O_2 conditions (37°C/5% CO_2). Following this incubation period, the culture medium was then removed and the plates were washed with warm [O_2]-equilibrated PBS (see **section 2.2.3** for concentration). The cells were then treated with the compound of interest reconstituted in growth medium in 18.6% or 3.0% O_2 for the required treatment time (37°C/5% CO_2). After treatment, a number of different endpoints were analysed: cell death as measured using annexin V-FITC and PI **(section 3.2.2)**; ROS production as measured using DHE, MitoSOX Red and DCFHDA **(section 3.2.3)**, $\psi\Delta_m$ as measured using JC-1 **(section 3.2.7)**; and lipid peroxidation as measured using C_{11} BODIPY$^{581/591}$ **(section 3.2.8)**.

3.2.2. Measuring apoptosis and necrosis by annexin V-FITC and propidium iodide in conjunction with flow cytometry

Cell death was measured using annexin V-FITC and PI staining in conjunction with flow cytometry **(section 2.4)**. A431 cells were seeded and cultured as before **(section 3.2.1)**. A431 cells were then treated with the compound of interest under the appropriate [O_2], detached with 0.25% (v/v) trypsin-EDTA, washed three times with warm [O_2]-equilibrated PBS (see **section 2.2.3** for concentration) and re-suspended in ice cold 95 µL annexin V-FITC binding buffer **(section 2.4.1)**. To this solution, annexin V-FITC was added to a final concentration of 1.25 µg/mL. A431 cells were incubated at 4°C in the dark for 15 min. 860 µL of annexin V-FITC binding buffer was then added prior to addition of 40 µL of 1 mg/mL PI (final concentration 0.04 mg/mL). A431 cells were then analysed by flow cytometry **(section 2.4)**. Annexin V-FITC and PI fluorescence were monitored using the FL1 and FL3 channels of a Guava EasyCyte™ flow cytometer using the 488 nm excitation laser **(section 2.4)**.

3.2.3. Measuring the flux of reactive oxygen species by dihydroethidium and MitoSOX red, and estimating the levels of oxidative stress with 2′, 7′-dichloro-dihydro-fluorescein diacetate

Treatment-induced ROS generation was measured using two different fluorescent probes: DHE for the measurement of total cellular ROS, and MitoSOX Red for the measurement of Mitochondria-derived ROS. DCFHDA was utilised to estimate treatment-induced oxidative stress.

To this end, A431 cells were seeded at a density of 9.5 x 10^3 cells/cm^2 in 24 well plates and incubated in 18.6% O_2 or 3.0% for 96 h (37°C/5% CO_2). A431 cells were fed every 24 h with fresh respective (18.6% or 3.0% O_2) [O_2]-equilibrated growth medium. After 96 h of growth, A431 cells were treated with 0–32 µM auranofin or vehicle (0.1% v/v DMSO) for 1 h in 18.6% O_2 or 3.0% O_2 (37°C/5% CO_2). A431 cells were treated with 100 µM CCCP **(section 2.8.1.1)** for 1 h (37°C/5% CO2) served as the positive control. After 1 h, A431 cells were stained with 10 µM DHE **(section 1.2.3.2)**, 1 µM MitoSOX **(section 1.2.3.2)**, or 10 µM DCHFDA **(section 1.2.3.3)** for a further 1 h (37°C/5% CO_2) in the appropriate [O_2]. After staining, the culture medium was collected into 15 mL tubes. A431 cells were then detached with 0.25% (v/v) trypsin before washing three times with PBS (see **section 2.2.3** for concentration) with centrifugation at 200 RCF for 1 min in between washes. ROS generation, as detected by DHE and MitoSOX Red, was then measured by flow cytometry using the FL2 detector whilst being excited at 488 nm using an argon laser. Oxidative stress, as detected by DCFHDA, was measured by flow cytometry using the FL1 detector whilst excited by a 488 nm argon laser.

3.2.4. Measuring H_2O_2 generation using Amplex Red

Amplex Red **(section 1.2.3.1)** was utilised to measure extracellular H_2O_2 generation. A431 cells were seeded at a density of 9.5 x 10^3 cells/cm^2 in black plastic 96 well plates and incubated in 18.6% O_2 or 3.0% O_2 **(section 2.3)** for 96 h (37°C / 5% CO_2). A431 cells were fed every 24 h with fresh respective (18.6% or 3.0% O_2) [O_2]-equilibrated growth medium. After the growth period, the medium was removed and replaced with 100 µL of respective (18.6% or 3.0% O_2) [O_2]-equilibrated growth medium without phenol red. To this, 100 µL of an Amplex Red reaction mixture (100 µM Amplex Red and 0.2 U/mL HRP made up

in fresh [O_2]-equilibrated growth medium without phenol red) was added (1:1 dilution). H_2O_2 standards (0–20 µM H_2O_2) were made up in DMEM without phenol red. Plates in both [O_2] conditions were sealed with gas-impermeable cellophane tape to maintain the gas environment during analysis. A kinetic time-course fluorescence scan was performed at an excitation wavelength of 570 nm and an emission wavelength of 585 nm at intervals of 30 min for 2 h using a Spectramax M_2e spectrophotometer. After analysis, a cell count was performed for data normalisation purposes **(section 2.2.4)**. [H_2O_2] was determined by interpolating sample fluorescence against a H_2O_2 standard curve **(Figure 3.1).**

Cellular-mediated degradation of H_2O_2 was also measured in this chapter **(section 3.3.1.5)** using Amplex Red. To this end, A431 cells were seeded and fed as previously described and grown in 18.6% O_2 or 3.0% O_2 for 96 h (37°C/5% CO_2). After 96 h, the growth medium was replaced with respective (18.6% or 3.0% O_2) [O_2]-equilibrated growth medium without phenol red containing 10 µM H_2O_2. For the time 0 data point, 100 µL of the Amplex Red reaction mixture was added (1:1 dilution) to each well immediately after cellular exposure to 10 µM H_2O_2. The plate was then agitated for 5 s on an orbital shaker and the fluorescence of the resorufin end product was measured immediately at an excitation wavelength of 570nm and an emission wavelength of 585 nm using a Spectramax M_2e spectrophotometer. For the remaining time-points, the reaction mixture was added to the appropriate wells at 125 s intervals after cellular exposure to 10 µM H_2O_2 in DMEM without phenol red (1:1 dilution). The plates were sealed with gas impermeable tape as outlined before. The [H_2O_2] remaining at each of the time points was determined by interpolation of sample fluorescence against H_2O_2 standards (0–20 µM H_2O_2, **Figure 3.1)**.

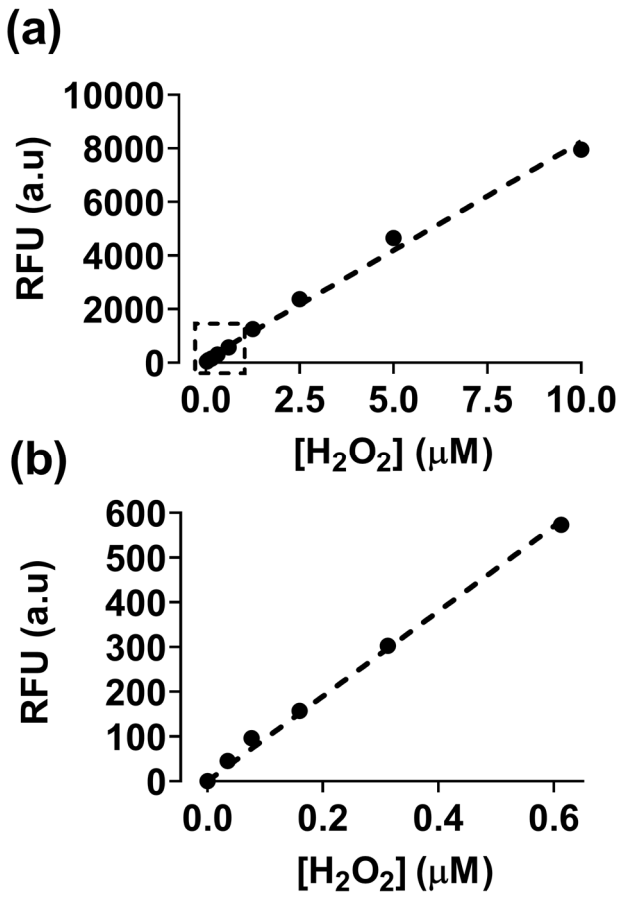

Figure 3.1. Representative Amplex Red standard curve. Under low light, a reaction mixture of Amplex Red (100 µM) and horseradish peroxidase (0.2 U/mL) was made up in DMEM without phenol red. 100 µL of this reaction mixture was added to black plastic 96 well plates containing 0–10 µM H_2O_2 made up in DMEM without phenol red (1:1 dilution). The plate was then agitated on an orbital shaker for 5 s. The fluorescence emission of resorufin was measured immediately after agitation utilising a SpectraMax M_2e spectrophotometer at an excitation wavelength of 570 nm and an emission wavelength of 585 nm. **Panel (a),** Amplex Red standard curve (0-10 µM H_2O_2). **Panel (b),** shows the data-points from within the dashed line box (0–0.6 µM) from panel (a) in a separate graph. n=1. R_2=0.99. **a.u:** arbitrary units; **RFU:** relative fluorescence units.

3.2.5. Visualisation of mitochondrial mass by fluorescence microscopy using MitoTracker Red and Hoechst 33342

Mitochondrial mass was estimated with MitoTracker Red **(section 2.9)** in conjunction with fluorescence microscopy. This was later quantified by flow cytometry **(section 3.3.11)**. To this end, A431 cells were seeded at a density of 9.5 x 10^3 cells/cm^2 in tissue culture treated glass bottom cell culture slides (#4221098, Thermofisher) and were incubated in 18.6% O_2 or 3.0% O_2 for 96 h (37°C/5% CO_2). A431 cells were fed every 24 h with respective (18.6% or 3.0% O_2) [O_2]-equilibrated growth medium. After the incubation period, the growth medium in each well was replaced with growth medium containing 2 µM Hoechst 33342 (from a stock solution made up in UH_2O) and 1 µM MitoTracker Red (from a stock solution made up in DMSO). A431 cells were stained for 20 min in 18.6% or 3.0% O_2 (37°C /5% CO_2). A431 cells were then washed three times with PBS (see section 2.2.3 for concentration). 200 µL of Dulbecco's phosphate buffered saline (DPBS; #D8537, Merck) was then added. To avoid re-oxygenation, A431 cells were imaged through the slide cap using slide cap-adjusted focusing. A431 cells were then imaged at random fields of view using an EVOS™ live cell imaging microscope (Thermofisher) with an EVOS™ LED cube, v2, DAPI and EVOS™ LED cube, v2, Texas Red at x10, x20, or x40 magnification.

3.2.6. Quantification of mitochondrial mass with MitoTracker red staining in conjunction with flow cytometry

A431 cells were seeded and cultured as detailed before **(section 3.2.1)**. The growth medium was replaced with [O_2]-equilibrated DPBS containing 1 µM MitoTracker Red (from a stock solution made up in DMSO). The cells were then left to stain for 20 min in 3.0% or 18.6% O_2 (37°C /5% CO_2). After the staining period, A431 cells were prepared for flow cytometry as detailed previously **(section 2.4.1)**. The fluorescence of the MitoTracker red dye was analysed using the FL3 detector of a Guava EasyCyte™ flow cytometer whilst excited by a 488 nm argon laser.

3.2.7. Measuring changes to mitochondrial membrane potential using JC-1 in conjunction with flow cytometry

A431 cells were seeded and cultured as before **(section 3.2.1)**. A431 cells were then treated with the compound of interest in 18.6% or 3.0% O_2 (37°C/5% CO_2). A431 cells were also treated with 100 µM CCCP for 1 h in 18.6% or 3.0% O_2 (37°C/5% CO_2) as a positive control for Δψm **(section 2.6.1)**. Under low light, JC-1 was reconstituted in [O_2]-equilibrated growth medium to a final concentration of 2 µM and was added to the cells. The cells were then incubated in 3.0% or 18.6% O_2 for an additional 1 h (37°C/5% CO_2). After 1 h, the growth medium was collected into 15 mL Falcon tubes, and the cells were detached with 0.25% (v/v) trypsin-EDTA. The cells were then washed three times with PBS (see **section 2.2.3** for concentration) prior with centrifugation at 200 RCF for 1 min in between washes. The fluorescence of the JC-1 monomer and aggregate was then measured by flow cytometry using the FL1 and FL2 detectors, respectively **(section 2.6.)**. The F520:F590 units were calculated by dividing the Mon (+) green fluorescent signal detected by the FL-1 channel by the Agg (+) red signal detected by the FL-2 channel.

3.2.8. Detection of lipid peroxidation using BODIPY $C_{11}^{581/591}$ in conjunction with flow cytometry.

A431 cells were seeded and cultured as before **(section 3.2.1)**. A431 cells were then treated with the compound of interest for the required amount of time in 18.6% or 3.0% O_2 (37°C/5% CO_2). A431 cells were also treated with CuOOH at a final concentration of 100 µM for 1 h in 3.0% or 18.6% O_2 (37°C/5% CO_2) to serve as a positive control for induction of lipid peroxidation **(section 2.7.1).** Under low light, C_{11} BODIPY$^{581/591}$ was reconstituted in [O_2]-equilibrated growth medium to a final concentration of 2 µM and was then added to the cells. The cells were then incubated in 3.0% or 18.6% O_2 for an additional 1 h (37°C/5% CO_2). The fluorescence of oxidised C_{11} BODIPY$^{581/591}$ (O.BOD) and reduced C_{11} BODIPY$^{581/591}$ (R.BOD) was analysed by flow cytometry using the FL1 and FL2 detectors, respectively **(section 2.7)**. The F520:F590 units were calculated by dividing the O.BOD (+) green fluorescent signal detected by the FL-1 channel by the R.BOD (+) red signal detected by the FL-2 channel.

3.3. Results

3.3.1. The effect of growing A431 cells in 18.6% on H_2O_2-induced cell death compared to A431 cells grown in 3.0% O_2

H_2O_2-induced cell death was assessed by annexin V-FITC and PI staining **(section 2.4)** in conjunction with flow cytometry in A431 cells grown in 18.6% O_2 or 3.0% O_2 for 24-96 h. Representative dot plot histograms are shown in **Figure 3.2**.

A two-way ANOVA was performed to analyse the effects of [H_2O_2], and the [O_2] cells were grown in, on cellular viability. A *post-hoc* test showed that A431 cells grown in 18.6% O_2 treated with 1 mM H_2O_2 exhibited heightened viability compared to A431 cells grown in 3.0% O_2 for 96 h under the same treatment conditions ($P < 0.01$), with means of 57.1 ± 7.1% vs 7.1 ± 3.6% **(Figure 3.3 a iv)**. The interaction between the effects of [H_2O_2], and the [O_2] cells were grown in, on cell viability was statistically significant (F (16, 80) = 11.05, $P < 0.0001$). However there was no statistically significant difference in viability in A431 cells grown in 18.6% O_2 for 24–72 h treated with 1 mM H_2O_2 compared to A431 cells grown in 3.0% O_2 for 24-72 h under the same treatment conditions **(Figure 3.3 a i-iii)**.

A two-way ANOVA was performed to analyse the effects of [H_2O_2], and the [O_2] cells were grown in, on early apoptosis. A *post-hoc* test showed that A431 cells grown in 18.6% O_2 treated with 1 mM H_2O_2 showed a decrease in the percentage of early apoptotic cells compared to A431 cells grown in 3.0% O_2 for 96 h under the same treatment conditions ($P < 0.0001$, **Figure 3.3 b iv), with means of** 18.0 ± 1.6% vs 70.2 ± 3.0%, respectively.

There was no statistically significant difference in H_2O_2-induced late apoptosis or necrosis when comparing A431 cells grown in 18.6% O_2 to A431 cells grown in 3.0% O_2 for 24-96 h under the same treatment conditions (**Figure 3.3 c and d i–iv)**.

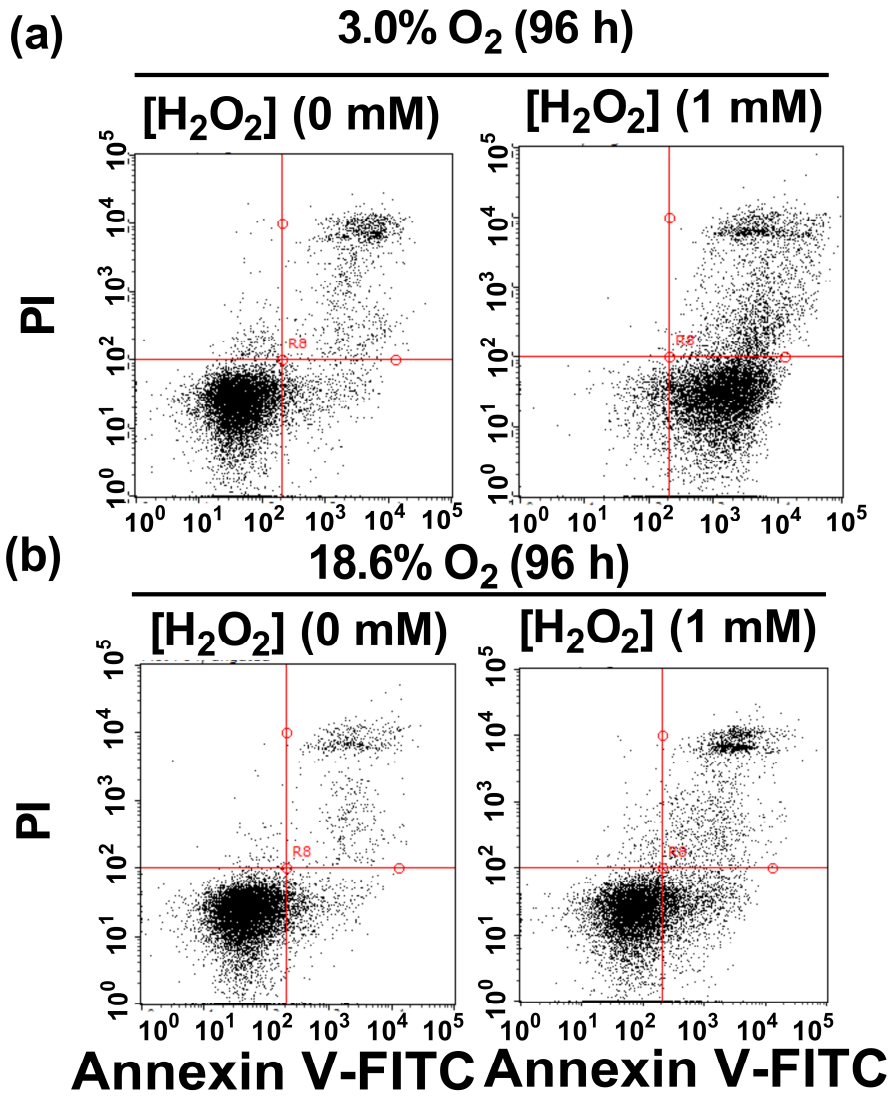

Figure 3.2. Representative dot plot histograms showing H_2O_2-induced cell death in A431 cells grown in 18.6% O_2 or 3.0% O_2 for 96 h. A431 cells were grown in 18.6% or 3.0% O_2 for 96 h prior to treatment with vehicle (0.1 v/v dH_2O) or 1 mM H_2O_2 for 1 h. Cells were then stained with annexin V-FITC and PI and cell death was then analysed by flow cytometry using the FL1 and FL3 detectors whilst excited by a 488 nm argon excitation laser (section 2.4). The 4-quadrant scatter plots represents 4 groups of differently stained cells: viable (unstained, bottom left), early apoptotic (+AnnV/-PI, bottom right), late apoptotic (+AnnV/+PI, top right) and necrotic (-AnnV/+PI, top left). The intersecting lines show the separation of the quadrants. **Panel (a),** dot plot histograms of H_2O_2-treated A431 cells grown in 3.0% O_2 for 96 h. **Panel (b),** dot plot histograms of H_2O_2-treated A431 cells grown in 18.6% O_2 for 96 h. **FITC:** fluorescein isothiocyanate**; PI:** propidium iodide.

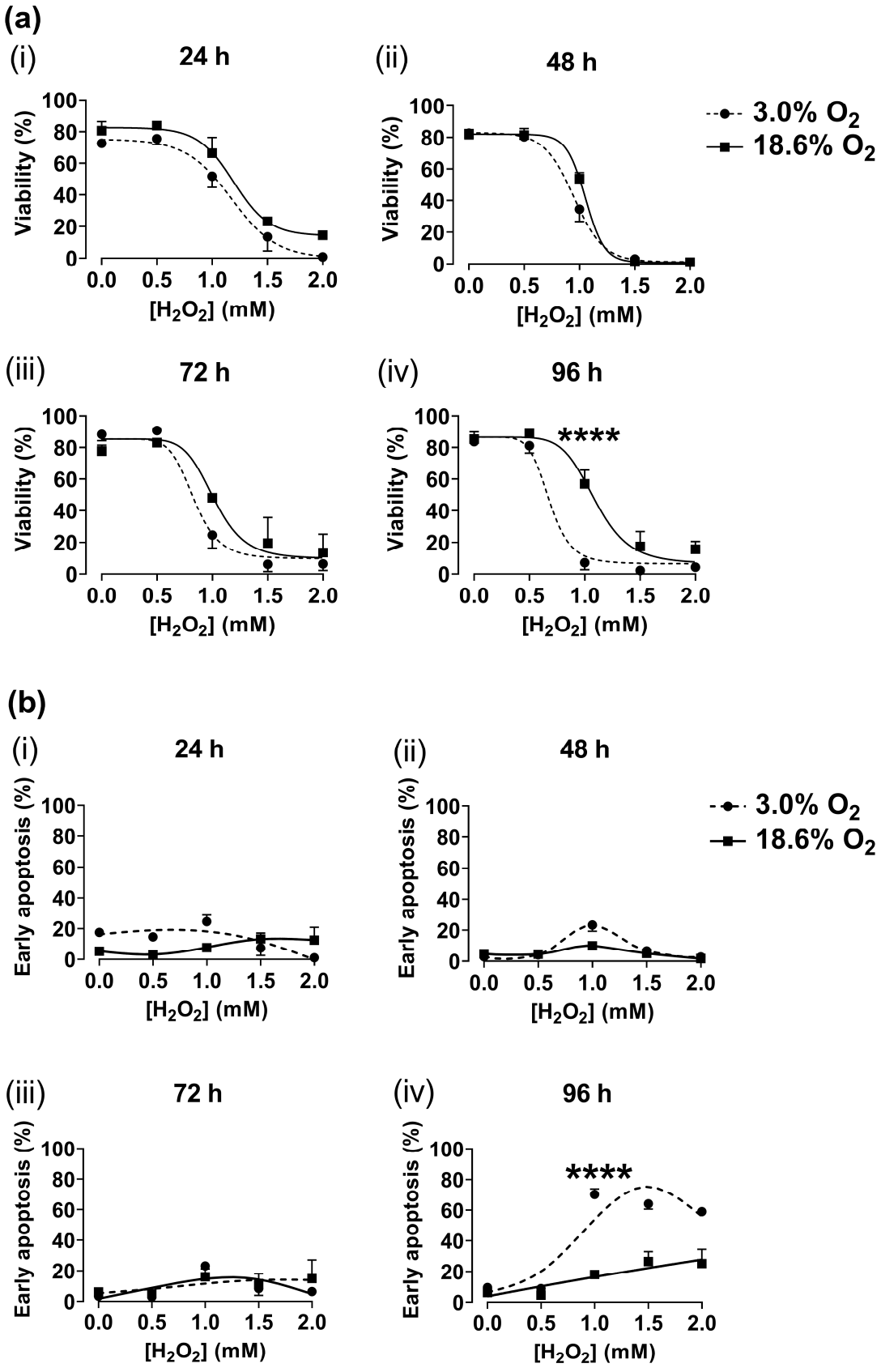
(a)
(i)
24 h
(ii)
48 h
(iii)
72 h
(iv)
96 h
Viability (%)
[H2O2] (mM)
3.0% O2
18.6% O2
****
(b)
Early apoptosis (%)
****

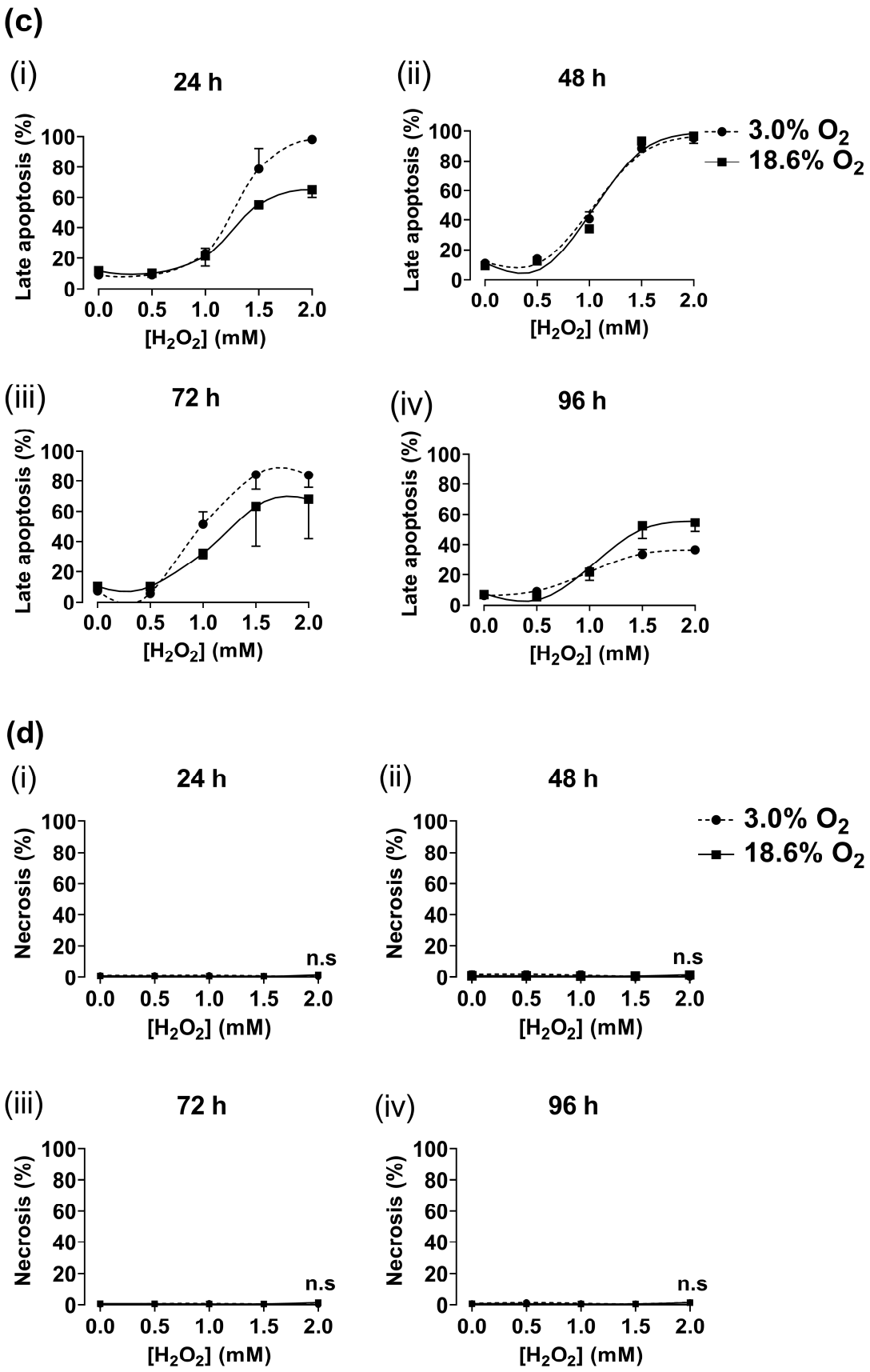
(c)
(i)
24 h
(ii)
48 h
(iii)
72 h
(iv)
96 h
Late apoptosis (%)
[H2O2] (mM)
3.0% O2
18.6% O2
(d)
Necrosis (%)
n.s

Figure 3.3. The effect of growing A431 cells in 18.6% O_2 on H_2O_2-induced cell death compared to A431 cells grown in 3.0% O_2 for 24-96 h. A431 cells were seeded at a density of 9.5 x 10^3 cells/cm^2 in 24 well plates and were grown in 18.6% O_2 or 3.0% O_2 for 24-96 h (37°C /5% CO_2). The total growth period in culture for all time-points was 96 h, with cells being switched into 3.0% O_2 at the indicated time points throughout the culture period (Figure 2.17)**.** Growth medium was replaced every 24 h with respective O_2-equilibrated growth medium. After the required period, A431 cells were treated with vehicle (0.1% v/v UH_2O) or 0.5-2 mM H_2O_2 for 1 h in 18.6% or 3.0% O_2 (37°C/5% CO_2). After the treatment period, A431 cells were then detached with 0.25% v/v trypsin-EDTA, washed with PBS (see section 2.2.3 for concentration), and subsequently stained with annexin V-FITC and PI prior to cell death analysis by flow cytometry (section 2.4). **Panel (a),** viability in H_2O_2-treated A431 cells grown in 18.6% or grown in 3.0% O_2 for 24-96 h (i–iv). **Panel (b),** early apoptosis in H_2O_2-treated A431 cells grown in 18.6% or 3.0% O_2 for 24-96 h (i–iv). **Panel (c),** late apoptosis in H_2O_2-treated A431 cells grown in 18.6% or 3.0% O_2 for 24-96 h (i–iv). **Panel (d),** necrosis in H_2O_2-treated A431 cells grown in 18.6% or 3.0% O_2 for 24-96 h (i–iv). n.s = not significant, **** = $P < 0.0001$ versus 3.0% O_2 utilising a two-way ANOVA and a *post-hoc* multiple comparison test with Dunn-Šidák correction. Data are presented as the mean ± 1 SD. n = 3. Where error bars are not visible, this is because the error bar is smaller than the size of the data point. **FITC:** fluorescein isothiocyanate**; PI:** propidium iodide.

3.3.1.1. The effect of growing A431 cells in 18.6% O_2 on 3-amino-1, 2, 4-triazole-induced cell death compared to A431 cells grown in 3.0% O_2

3-AT-induced cell death was measured by annexin V-FITC and PI staining in conjunction with flow cytometry in A431 cells grown in 18.6% O_2 or 3.0% O_2 for 96 h **(section 2.4)**. Representative dot plot histograms are shown in **Figure 3.4**.

A two-way ANOVA was performed to analyse the effects of [3-AT], and the [O_2] cells were grown in, on cellular viability. Detection of cell death was functional as treatment with 1 mM H_2O_2 alone resulted in a decrease in cell viability in both [O_2] groups relative to untreated control cells ($P < 0.001$, **Figure 3.5 a**). A *post-hoc* test showed no statistically significant effect of [3-AT] on cellular viability in A431 cells grown in 18.6% or 3.0% O_2 for 96 h compared to respective untreated control cells **(Figure 3.5 b)**.

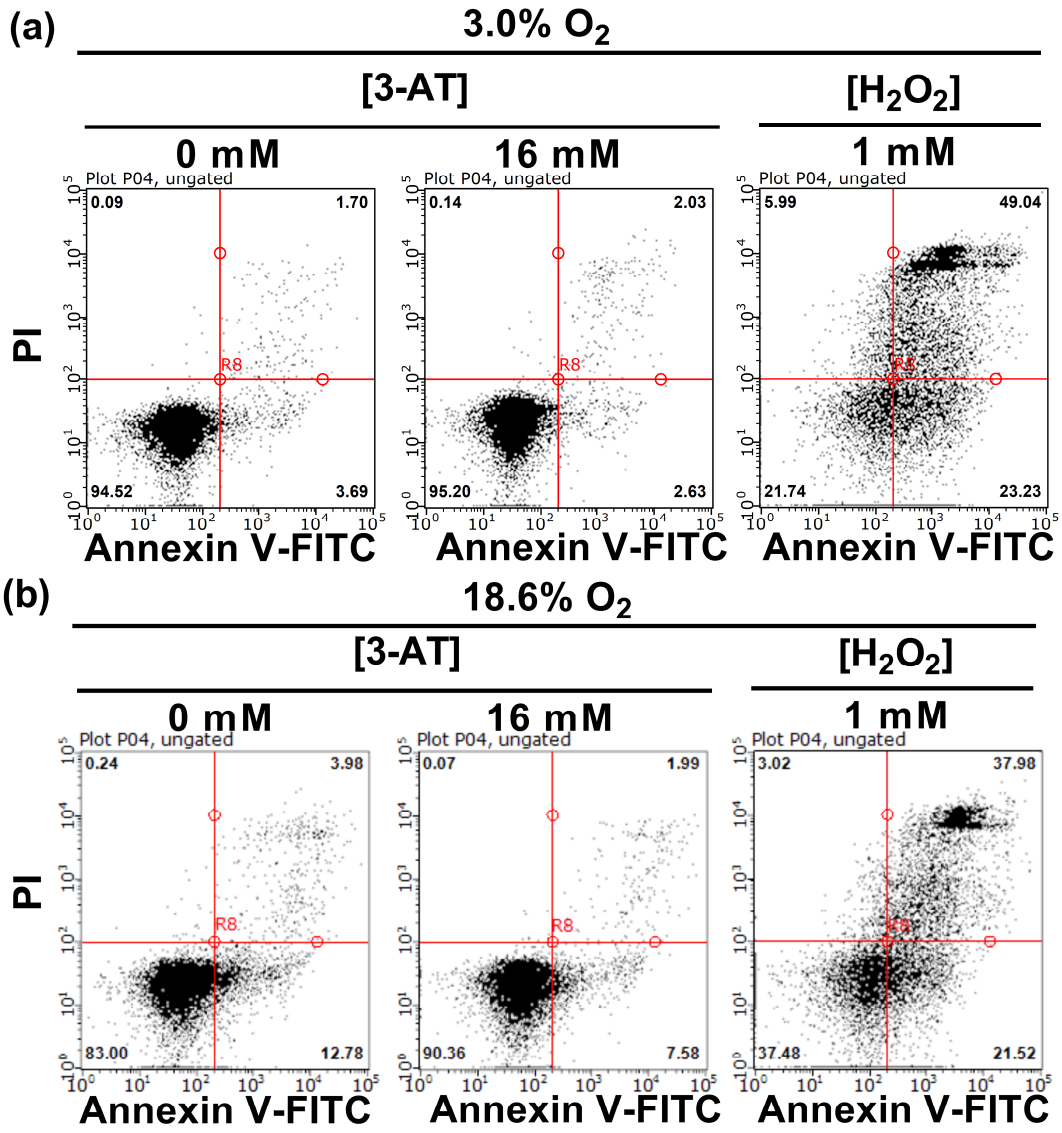

Figure 3.4. Representative dot plot histograms showing 3-amino-1, 2, 4-triazole-induced cell death in A431 cells grown in 18.6% O_2 or 3.0% O_2 for 96 h. A431 cells were grown in 18.6% or 3.0% O_2 for 96 h prior to treatment with vehicle (0.1% v/v dH_2O) or 16 mM 3-AT for 24 h in 18.6% or 3.0% O_2 (37°C / 5% CO_2). A431 cells were also treated with 1 mM H_2O_2 for 1 h (37°C / 5% CO_2) as a positive inducer of cell death. Cell death was then analysed by flow cytometry using the FL1 and FL3 detectors whilst excited by a 488 nm argon excitation laser (section 2.4). The 4-quadrant scatter plots represents 4 groups of differently stained cells: viable (unstained, bottom left), early apoptotic (+AnnV/-PI, bottom right), late apoptotic (+AnnV/+PI, top right) and necrotic (-AnnV/+PI, top left). The intersecting lines show the separation of the quadrants. The numbers in each quadrant represent the percentage of cells in each respective stage of apoptosis or necrosis. **Panel (a),** dot plot histogram of 3-AT-treated A431 cells previously grown in 3.0% O_2 and subsequently stained with annexin V-FITC and PI. **Panel (b),** dot plot histograms of 3-AT-treated A431 cells previously grown in 18.6% O_2 and subsequently stained with annexin V-FITC and PI. **3-AT:** 3-amino-1, 2, 4-triazole; **FITC:** fluorescein isothiocyanate**; PI:** propidium iodide.

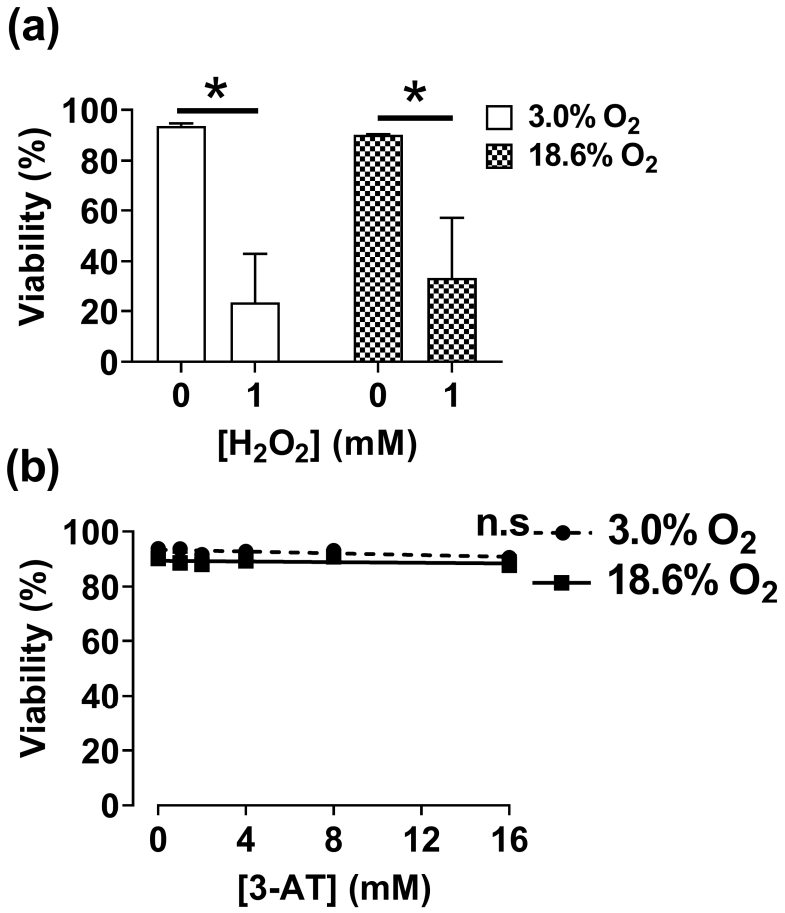

Figure 3.5. Effect of growing A431 cells in 18.6% O_2 on 3-amino-1, 2, 4-triazole-induced cell death compared to A431 cells grown in 3.0% O_2 for 96 h. A431 cells were seeded at a density of 9.5 x 10^3 cells/cm^2 in 24 well plates and grown in either 18.6% O_2 or 3.0% O_2 for 96 h (37°C /5% CO_2). Growth medium was changed every 24 h with respective (18.6% or 3.0% O_2) [O_2]-equilibrated growth medium. After the incubation period, A431 cells were treated with vehicle (0.1 v/v UH_2O), 1-16 mM 3-AT for 24 h or positive control (+; 1 mM H_2O_2) for 1 h in 18.6% or 3.0% O_2 (37°C / 5% CO_2). A431 cells were then detached with 0.25% v/v trypsin-EDTA, washed with PBS (see section 2.2.3 for concentration), and subsequently stained with annexin V-FITC and PI prior to cell death analysis by flow cytometry (section 2.4). **Panel (a),** viability in untreated A431 cells versus A431 cells treated with 1 mM H_2O_2. **Panel (b),** the effect of growing A431 cells in 18.6% or 3.0% O_2 for 96 h on 3-AT-induced cell death. n.s = not significant versus 3.0% O_2, * = $P < 0.05$ versus respective untreated control utilising a two-way ANOVA with multiple comparison and Dunn-Šidák correction. Data are presented as the mean ± 1 SD. n = 3. Where error bars are not visible, this is because the error bar is smaller than the size of the data point. **3-AT:** 3-amino- 1, 2, 4- triazole.

3.3.1.2. The effect of growing A431 cells in 18.6% O_2 on 3-amino-1, 2, 4-triazole-mediated sensitisation to H_2O_2-induced cell death compared to A431 cells grown in 3.0% O_2.

3-AT-mediated sensitisation to H_2O_2-induced cell death was measured by annexin V-FITC and PI staining in conjunction with flow cytometry in A431 cells grown in 18.6% O_2 or 3.0% O_2 for 96 h **(section 2.4)**. Representative dot plot histograms are shown in **Figure 3.6**.

A two-way ANOVA was performed to analyse the effects of [3-AT/H_2O_2], and the [O_2] cells were grown in, on cell viability. Treatment with 0.5 mM H_2O_2 alone did not decrease viability compared to respective untreated control in either [O_2] group **(Figure 3.7 a)**. The detection of cell death was functional, as A431 cells grown in 18.6% O_2 or 3.0% O_2 for 96 h treated with 1 mM H_2O_2 exhibited a decrease in viability compared to respective untreated control cells ($p < 0.0001$, **Figure 3.7 a**), with means of 91.1 ± 2.6% vs 36.5 ± 8.5% and 88.8 ± 3.6% vs 20.3 ± 12.2%. A *post-hoc* analysis showed that pre-treatment of A431 cells previously grown in 18.6% O_2 or 3.0% O_2 for 96 h with 3-AT did not sensitise either [O_2] group to H_2O_2-induced cell death when compared to respective untreated control cells **(Figure 3.7 b)**.

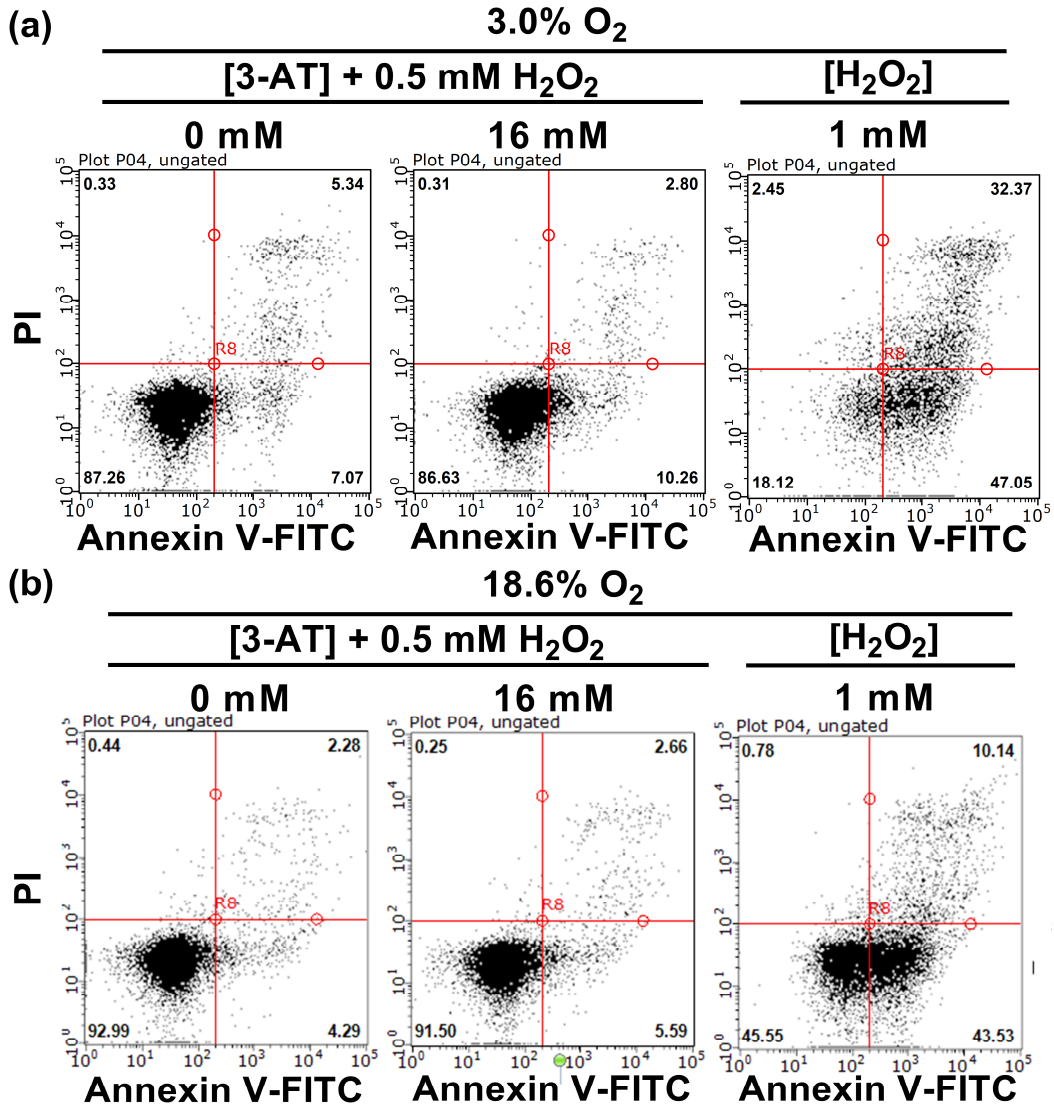

Figure 3.6. Representative dot plot histograms showing the effect of 3-amino-1, 2, 4-triazole pre-treatment on H_2O_2-induced cell death in A431 cells grown in 18.6% O_2 or 3.0% O_2 for 96 h. A431 cells were grown in 18.6% or 3.0% O_2 for 96 h prior to treatment with vehicle (0.1% v/v uH_2O) or 16 mM 3-AT for a further 24 h in 18.6% or 3.0% O_2 (37°C / 5% CO_2). A431 cells were also treated with 1 mM H_2O_2 for 1 h (37°C / 5% CO_2) as a positive inducer of cell death. Cell death was then analysed by flow cytometry using the FL1 and FL3 detectors whilst excited by a 488 nm argon excitation laser (section 2.4). The 4-quadrant scatter plots represents 4 groups of differently stained cells: viable (unstained, bottom left), early apoptotic (+AnnV/-PI, bottom right), late apoptotic (+AnnV/+PI, top right) and necrotic (-AnnV/+PI, top left). The intersecting lines show the separation of the quadrants. The numbers in each quadrant represent the percentage of cells in each respective stage of apoptosis or necrosis. **Panel (a),** dot plot histograms for 3-AT/H_2O_2-treated A431 cells previously grown in 3.0% O_2 for 96 h and subsequently stained with annexin V-FITC and PI. **Panel (b),** dot plot histograms for 3-AT/H_2O_2-treated A431 cells previously grown in 18.6% O_2 for 96 h and subsequently stained with annexin V-FITC and PI. **3-AT:** 3-amino-1, 2, 4-triazole; **FITC:** fluorescein isothiocyanate**; PI:** propidium iodide.

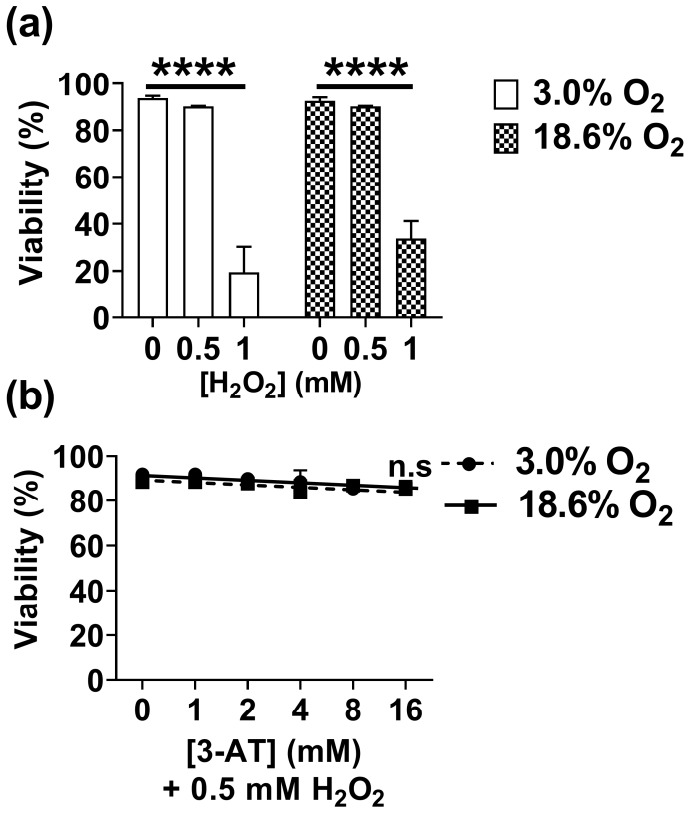

Figure 3.7. Effect of growing A431 cells in 18.6% O_2 on 3-amino-1, 2, 4-triazole-mediated sensitisation to H_2O_2-induced cell death compared to A431 cells grown in 3.0% O_2 for 96 h. A431 cells were seeded at a density of 9.5 x 10^3 cells/cm^2 in 24 well plates and grown in 18.6% O_2 or 3.0% O_2 for 96 h (37°C/5% CO_2). Growth medium was changed every 24 h. After 96 h of growth, cells were treated with vehicle (0.1% v/v UH_2O), or 1-16 mM AT for 24 h. After 24 h, A431 cells were then treated with 0.5 mM H_2O_2 for 1 h in 18.6% or 3.0% O_2 (37°C / 5% CO_2). Positive control wells were treated with 1 mM H_2O_2 alone for 1 h as a positive control for cell death. A431 cells were then detached, washed with PBS (see section 2.2.3 for concentration), and subsequently stained with annexin V-FITC and PI prior to cell death analysis by flow cytometry (section 2.4). **Panel (a),** comparison of cell death in untreated A431 cells versus A431 cells treated with 0.5 mM or 1 mM H_2O_2 alone for 1 h. **Panel (b),** the effect of growing A431 cells in 18.6% or 3.0% O_2 for 96 h on 3-AT-mediated sensitisation to H_2O_2-induced cell death. n.s = not significant, **** = $P < 0.0001$, versus respective untreated control utilising a two-way ANOVA with multiple comparison and Dunn-Šidák correction. Data are presented as the mean ± 1 SD. n=3. Where error bars are not visible, this is because the error bar is smaller than the size of the data point. **3-AT**: 3-amino-1, 2, 4-triazole.

3.3.1.3. The effect of growing A431 cells in 18.6% O_2 on L-buthionine sulfoximine-induced cell death compared to A431 cells grown in 3.0% O_2

L-BSO-induced cell death was measured by annexin V-FITC and PI staining in conjunction with flow cytometry in A431 cells grown in 18.6% O_2 or 3.0% O_2 for 96 h **(section 2.3)**. Representative dot plot histograms are shown in **Figure 3.8**.

A two-way ANOVA was performed to analyse the effects of [L-BSO], and the [O_2] cells are grown in, and on cell viability. The detection of cell death was functional, as A431 cells grown in 18.6% and 3.0% O_2 for 96 h treated with 1 mM H_2O_2 showed a decrease in viability compared to respective untreated control cells ($p < 0.01$, **Figure 3.9 a**), with means of 86.5 ± 3.3% vs 42.9 ± 9.0% and 89.5 ± 4.9% vs 37.9 ± 7.4%. A *post-hoc* test showed no effect of [L-BSO] on cell viability in A431 cells grown in 18.6% O_2 or 3.0% O_2 for 96 h when compared to respective untreated control cells **(Figure 3.9 b)**.

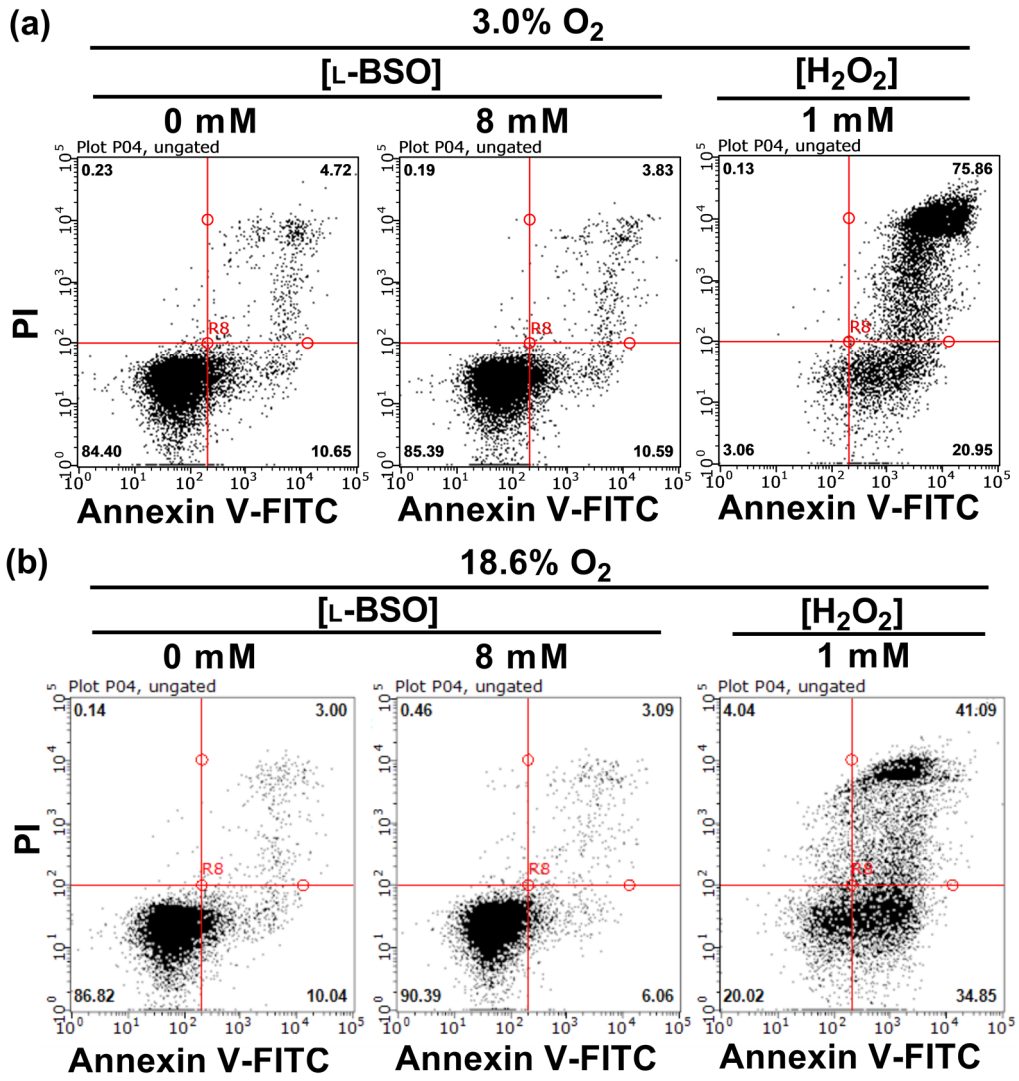

Figure 3.8. Representative dot plot histograms showing L-buthionine sulfoximine-induced cell death in A431 cells grown in 18.6% O_2 or 3.0% O_2 for 96 h. A431 cells were grown in 18.6% or 3.0% O_2 for 96 h prior to treatment with vehicle (0.1% UH_2O) or 8 mM L-BSO for 24 h. A431 cells were also treated with 1 mM H_2O_2 alone for 1 h as a positive inducer of cell death. Cell death was then analysed by flow cytometry using the FL1 and FL3 detectors whilst excited by a 488 nm argon excitation laser (section 2.4). The 4-quadrant scatter plots represents 4 groups of differently stained cells: viable (unstained, bottom left), early apoptotic (+AnnV/-PI, bottom right), late apoptotic (+AnnV/+PI, top right) and necrotic (-AnnV/+PI, top left). The intersecting lines show the separation of the quadrants. The numbers in each quadrant represent the percentage of cells in each respective stage of apoptosis or necrosis. **Panel (a),** dot plot histograms of L-BSO-treated A431 cells previously grown in 3.0% O_2 for 96 h and subsequently stained with annexin V-FITC and PI. **Panel (b),** dot plot histograms of L-BSO-treated A431 cells previously grown in 18.6% O_2 for 96 h and subsequently stained with annexin V-FITC and PI. **L-BSO:** L-buthionine sulfoximine; **FITC:** fluorescein isothiocyanate; **PI:** propidium iodide.

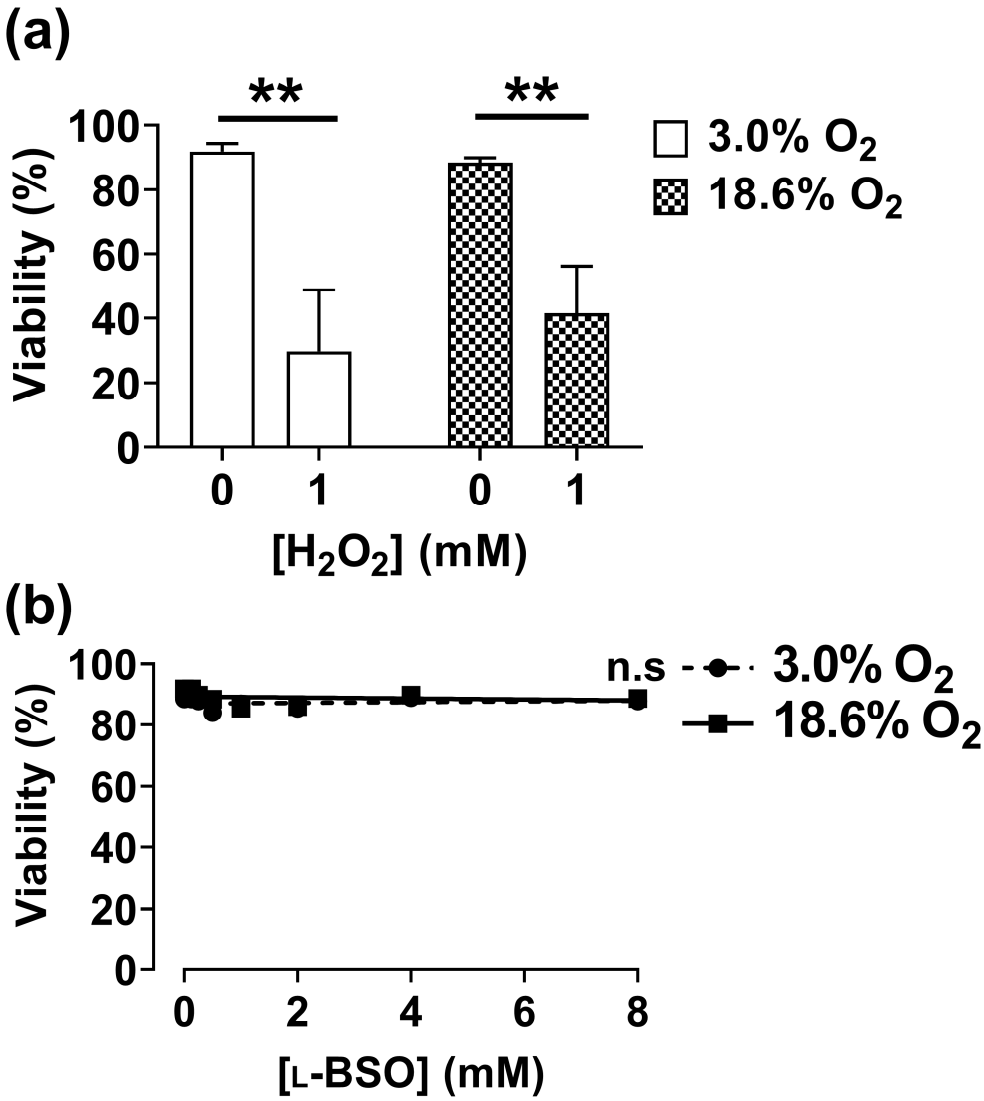

Figure 3.9. The effect of growing A431 cells in 18.6% O_2 on L-buthionine sulfoximine-induced cell death compared to A431 cells grown in 3.0% O_2 for 96 h. A431 cells were seeded at a density of 9.5 x 10^3 cells/cm^2 in 24 well plates and grown in 18.6% O_2 or 3.0% O_2 for 96 h (37°C / 5% CO_2). Growth medium was changed every 24 h with respective (18.6% or 3.0% O_2) [O_2]-equilibrated growth medium. After 96 h of growth, A431 cells were pre-treated with vehicle (0.1% v/v UH_2O) or 1–8 mM L-BSO for 24 h in 18.6% or 3.0% O_2 (37°C / 5% CO_2). A431 cells were also treated with 1 mM H_2O_2 alone for 1 h in 18.6% or 3.0% O_2 (37°C / 5% CO_2) which served as a positive control for cell death. After 24 h of treatment, the cells were then detached, washed with PBS (see section 2.2.3 for concentration), and subsequently stained with annexin V-FITC and PI prior to cell death analysis by flow cytometry (section 2.4). **Panel (a),** viability of untreated A431 cells versus A431 cells treated with 1 mM H_2O_2 for 1 h. **Panel (b),** the effect of growing A431 cells in 18.6% or 3.0% O_2 for 96 h on L-BSO-induced cell death. n.s = not significant, ** = $P < 0.01$ versus respective untreated controls utilising a two-way ANOVA and a *post-hoc* multiple comparison test with Dunn-Šidák correction. Data are presented as the mean ± 1 SD. n=3. Where error bars are not visible, this is because the error bar is smaller than the size of the data point. **L-BSO:** L-buthionine sulfoximine.

3.3.1.4. The effect of growing A431 cells in 18.6% O_2 on L-buthionine sulfoximine-mediated sensitisation to H_2O_2-induced cell death compared to A431 cells grown in 3.0% O_2.

L-BSO-mediated sensitisation to H_2O_2-induced cell death was measured by annexin V-FITC and PI staining in conjunction with flow cytometry in A431 cells grown in 18.6% O_2 or 3.0% O_2 for 96 h **(section 2.3).** Representative dot plot histograms are shown in **Figure 3.10.**

A two-way ANOVA was performed to analyse the effects of [L-BSO/H_2O_2], and the [O_2] cells were grown in, on cellular viability. The detection of cell death was functional, as A431 cells grown in 18.6% and 3.0% O_2 for 96 h treated with 1 mM H_2O_2 showed a decrease in viability compared to respective untreated control cells ($p < 0.0001$), whilst treatment with 0.5 mM did not **(Figure 3.11 a)**. Pre-treatment of A431 cells grown in 3.0% O_2 for 96 h with 8 mM L-BSO prior to treatment with 0.5 mM H_2O_2 decreased cellular viability compared to respective untreated control cells **(Figure 3.11 b i)**, with means of 85.0 ± 7.1% vs 63.5 ± 2.7%. However, a *post-hoc* multiple comparison test showed that this decrease was not statistically significant. Pre-treatment of A431 cells grown in 18.6% for 96 h with 8 mM L-BSO prior to treatment with 0.5 mM H_2O_2 did not affect cellular viability compared to untreated control cells (**Figure 3.11 b i**), with means of 83.1 ± 3.5% vs 81.0% ± 2.0%. A431 cells grown in 18.6% O_2 pre-treated with 8 mM L-BSO prior to treatment with 0.5 mM H_2O_2 exhibited an apparent higher viability compared to A431 cells grown in 3.0% O_2 for 96 h under the same treatment conditions (**Figure 3.11 b i**), with means of 81.0% ± 2.0% vs 63.5 ± 2.7% respectively. However a *post-hoc* multiple comparison test showed that this apparent decrease was not statistically significant.

Pre-treatment of A431 cells grown in 18.6% O_2 with 8mM L-BSO prior to treatment 0.5 mM H_2O_2 showed an apparent decrease in the percentage of early apoptotic and late apoptotic cells compared to A431 cells grown in 3.0% O_2 for 96 h under the same treatment conditions (**Figure 3.11 b ii and iii**), with means of 5.2 ± 0.9% vs 14.3 ± 2.1% and 10.8 ± 1.9% vs 19.1% ± 2.0%, respectively. However a *post-hoc* multiple comparison test showed that this apparent decrease was not statistically significant. L-BSO pre-treatment had no statistically significant effect on H_2O_2-induced necrosis in A431 cells grown in either [O_2] condition for 96 h compared to respective untreated control cells **(Figure 3.11 b iv)**.

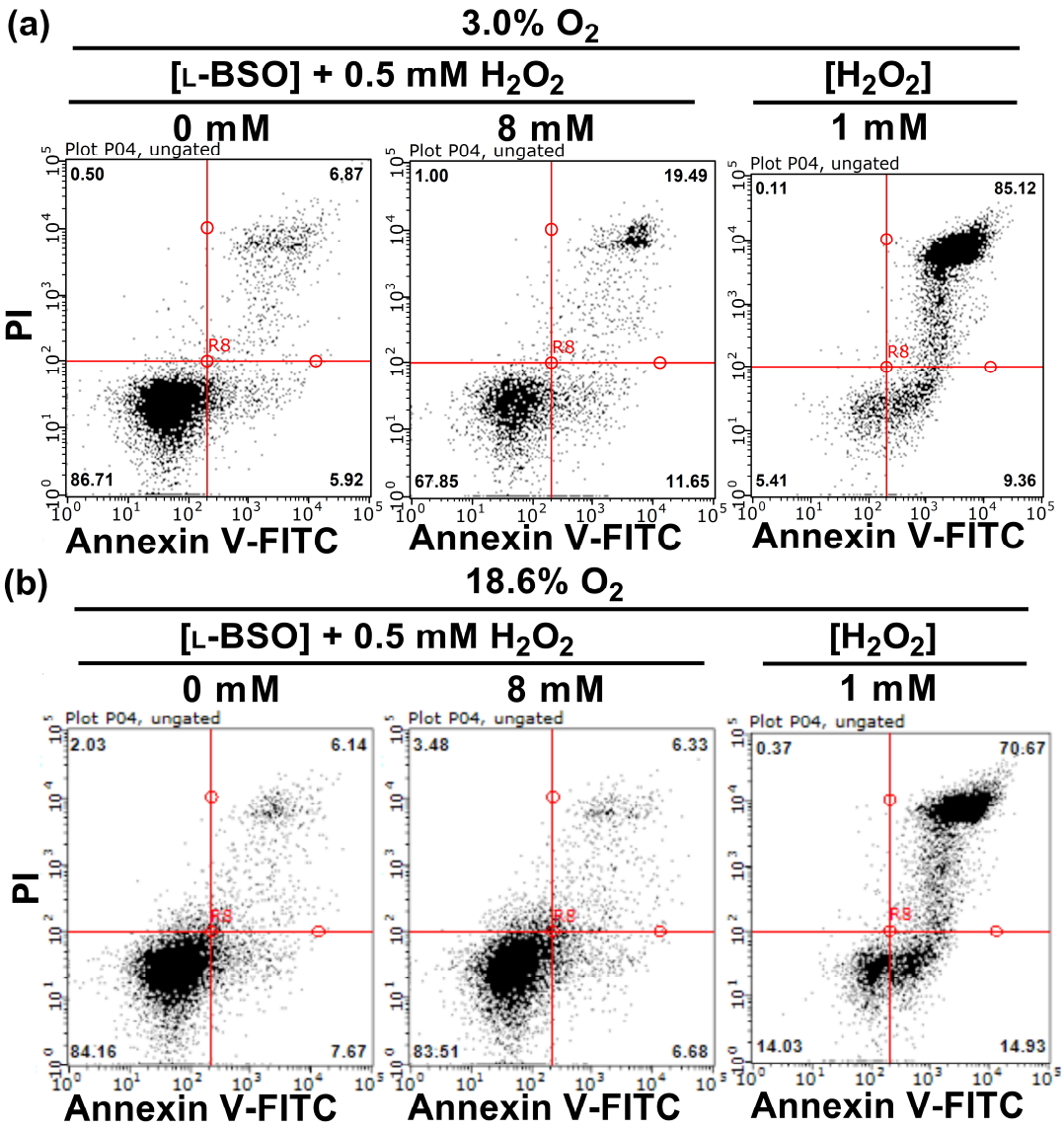

Figure 3.10. Representative dot plot histograms showing L-buthionine sulfoximine-mediated sensitisation to H_2O_2-induced cell death in A431 cells grown in 18.6% O_2 or 3.0% O_2 for 96 h. A431 cells were grown in 18.6% or 3.0% O_2 for 96 h prior to pre-treatment with 0–8 mM L-BSO for 24 h in 18.6% or 3.0% O_2 prior to subsequent treatment with 0.5 mM H_2O_2 for 1 h (37°C / 5% CO_2). A431 cells were also treated with 1 mM H_2O_2 alone for 1 h (37°C / 5% CO_2) which was a positive control for cell death. Cell death was then analysed by flow cytometry using the FL1 and FL3 detectors whilst excited by a 488 nm argon excitation laser (section 2.4). The 4-quadrant scatter plots represents 4 groups of differently stained cells: viable (unstained, bottom left), early apoptotic (+AnnV/-PI, bottom right), late apoptotic (+AnnV/+PI, top right) and necrotic (-AnnV/+PI, top left). The intersecting lines show the separation of the quadrants. The numbers in each quadrant represent the percentage of cells in each respective stage of apoptosis or necrosis. **Panel (a),** dot plot histograms for L-BSO/H_2O_2-treated A431 cells previously grown in 3.0% O_2 for 96 h and subsequently stained with annexin V-FITC and PI. **Panel (b),** dot plot histograms for L-BSO/H_2O_2-treated A431 cells previously grown in 18.6% O_2 and subsequently stained with annexin V-FITC and PI. **L-BSO:** L-buthionine sulfoximine; **FITC:** fluorescein isothiocyanate**; PI:** propidium iodide.

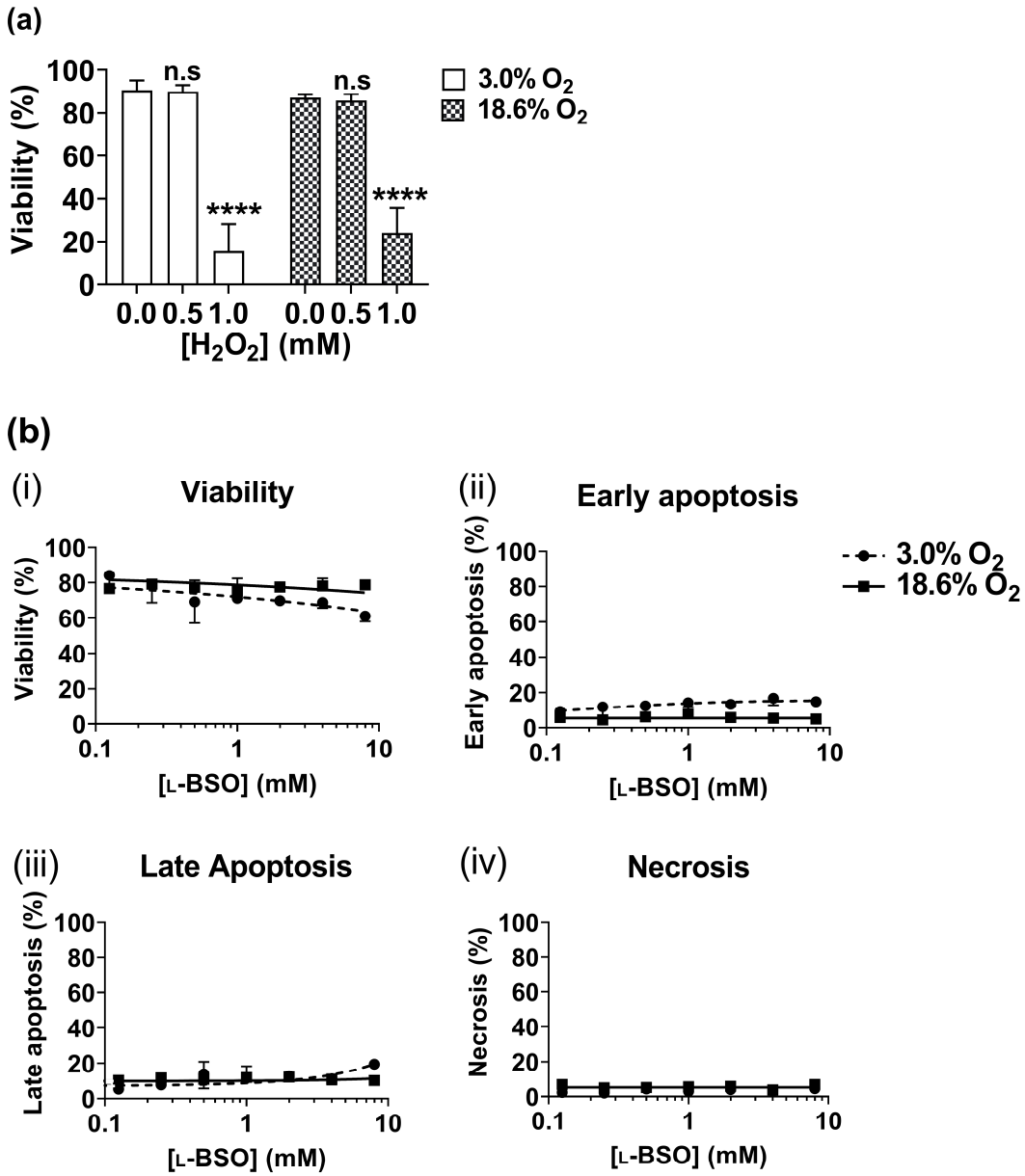

Figure 3.11. The effect of growing A431 cells in 18.6% O_2 on L-buthionine sulfoximine-mediated sensitisation to H_2O_2-induced cell death compared to 3.0% O_2 for 96 h. A431 cells were seeded at a density of 9.5 x 10^3 cells/cm^2 in 24 well plates and grown in 18.6% O_2 or 3.0% O_2 for 96 h (37°C / 5% CO_2). Growth medium was changed every 24 h with respective (18.6% or 3.0% O_2) [O_2]-equilibrated growth medium. After 96 h of growth, A431 cells were pre-treated with vehicle (0.1 % v/v UH_2O) or 1-8 mM L-BSO for 24 h in 18.6% or 3.0% O_2 (37°C / 5% CO_2). After 24 h, A431 cells were subsequently treated with 0.5 mM H_2O_2 for 1 h (37°C / 5% CO_2) in 18.6% or 3.0% O_2. A431 cells were also treated with 1 mM H_2O_2 for 1 h (37°C / 5% CO_2) which was a positive control for cell death. A431 cells were then detached, washed with PBS (see section 2.2.3 for concentration), and subsequently stained with annexin V-FITC and PI prior to cell death analysis by flow cytometry (section 2.4). The x axis was transformed to a log scale to allow visualisation of the data. Panel **(a),** viability of untreated A431 cells and A431 cells treated with 0.5 mM or 2mM H_2O_2 alone for 1 h. **Panel (b),** L-BSO-mediated sensitisation to H_2O_2-induced cell death in A431 cells grown in 18.6% O_2 or 3.0% O_2 for 96 h which included analysis of **(i)** viability, **(ii)** early apoptosis, **(iii)** late apoptosis, and **(iv)** necrosis. n.s = not significant, **** = $P < 0.0001$ versus respective untreated control utilising a two-way ANOVA with multiple comparison and Dunn-Šidák correction. Data are presented as the mean ± 1 SD. n=3. Where error bars are not visible, this is because the error bar is smaller than the size of the data point. **L-BSO:** L-buthionine sulfoximine.

3.3.1.5. The effect of growing A431 cells in 18.6% O_2 on the cellular decomposition of H_2O_2 compared to A431 cells grown in 3.0% O_2

The decomposition of H_2O_2 by A431 cells was measured in A431 cells previously grown in 18.6% O_2 or 3.0% O_2 for 96 h using Amplex Red **(section 3.2.4)**.

The difference in H_2O_2 decomposition in A431 cells grown in 18.6% O_2 or 3.0% O_2 for 96 h was measured by comparing the slopes (representing H_2O_2 decomposition) by simple linear regression analysis. A431 cells grown in 18.6% O_2 showed an apparent increase in the rate of H_2O_2 decomposition compared to A431 cells grown in 3.0% O_2 for 96 h, with means of 6.46 ± 0.03 µM/s vs 5.66 ± 0.04 µM/s ($P < 0.05$, **Figure 3.12**), respectively. However this apparent increase was not statistically significant. Detection of H_2O_2 was functional as addition of 50 U/mL catalase to 10 µM H_2O_2 caused a statistically significant decrease in [H_2O_2] compared to the 0 timepoint in the 18.6% O_2 group ($P < 0.0001$, **Figure 3.12**).

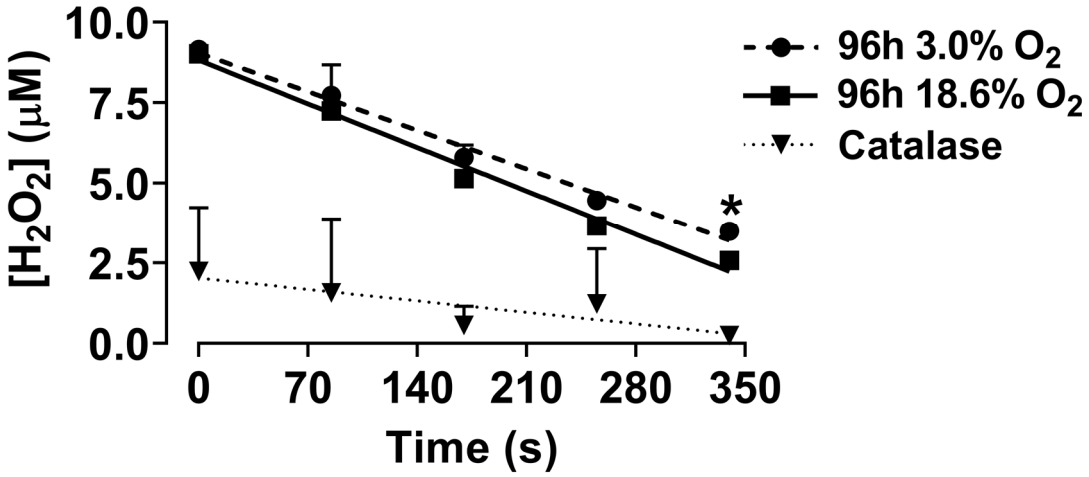

Figure 3.12. Effect of growing A431 cells in 18.6% O_2 on the cellular-mediated breakdown of H_2O_2 compared to A431 cells grown in 3.0% O_2 for 96 h. A431 cells were seeded at a density of 9.5 x 10^3 cells/cm^2 into black plastic 96 well plates and incubated in 18.6% O_2 or 3.0% for 96 h (37°C / 5% CO_2). A431 cells were fed every 24 h with fresh-equilibrated growth medium. After 96 h, H_2O_2 was added to a final concentration of 10 µM to each well. The reaction mix (100 µM Amplex Red and 0.2 U/mL HRP) was added immediately to the time 0 group (1:1 dilution) after addition of H_2O_2, and was added at 85 s intervals after addition of H_2O_2 to achieve the remaining time-points. The fluorescence of resorufin was measured at an excitation wavelength of 570 nm and an emission wavelength of 585 nm utilising a Spectramax M_2e spectrophotometer. The [H_2O_2] remaining in each well after the appropriate time had passed was determined through standard curve interpolation (Figure 3.1). After analysis, a cell count was performed for data normalisation. The decomposition of [H_2O_2] was normalised to cell number ([H_2O_2] per 10^4 cells). n.s = not significant, versus the slope of the 3.0% O_2 group utilising simple linear regression analysis. Data are presented as the mean ± 1 SD, with error bars smaller than the symbol removed. n=3. Where error bars are not visible, this is because the error bar is smaller than the size of the data point.

3.3.2. The effect of growing A431 cells in 18.6% O_2 on auranofin-induced cell death compared to A431 cells grown in 3.0% O_2

Auranofin-induced cell death was assessed by annexin V-FITC and PI staining **(section 2.4)** in conjunction with flow cytometry in A431 cells grown in 18.6% O_2 or 3.0% O_2 for 24-96 h.

A two-way ANOVA was performed to analyse the effects of [auranofin], and the [O_2] cells were grown in, on cellular viability. A *post-hoc* analysis showed that A431 cells grown in 18.6% O_2 exhibited higher viability when treated with 16 µM auranofin compared to A431 cells grown in 3.0% O_2 for 96 h ($P < 0.0001$, **Figure 3.14 a iv**), with means of 42.1 ± 8.8 vs 11.0 ± 5.6%, respectively. The interaction between the effects of [auranofin], and the [O_2] cells were grown in, on cell viability was statistically significant (F (15, 72) = 11.55, $P < 0.0001$).

A431 cells grown in 18.6% O_2 for 96 h and treated with 32 µM auranofin exhibited increased early apoptosis compared to A431 cells grown in 3.0% O_2 for 96 h under the same treatment conditions ($P < 0.0001$, **Figure 3.14 b iv**). However,

A431 cells grown in 3.0% O_2 for 96 h and treated with 32 µM auranofin exhibited increased late apoptosis compared to A431 cells grown in 18.6% O_2 under the same treatment conditions ($P < 0.0001$, **Figure 3.14 c iv**), with means of 91.8 ± 2.1% vs 29.2 ± 12.9%, respectively.

Auranofin treatment did not induce necrosis in either [O_2] group when compared to respective untreated control cells (**Figure 3.14 d i-iv)**.

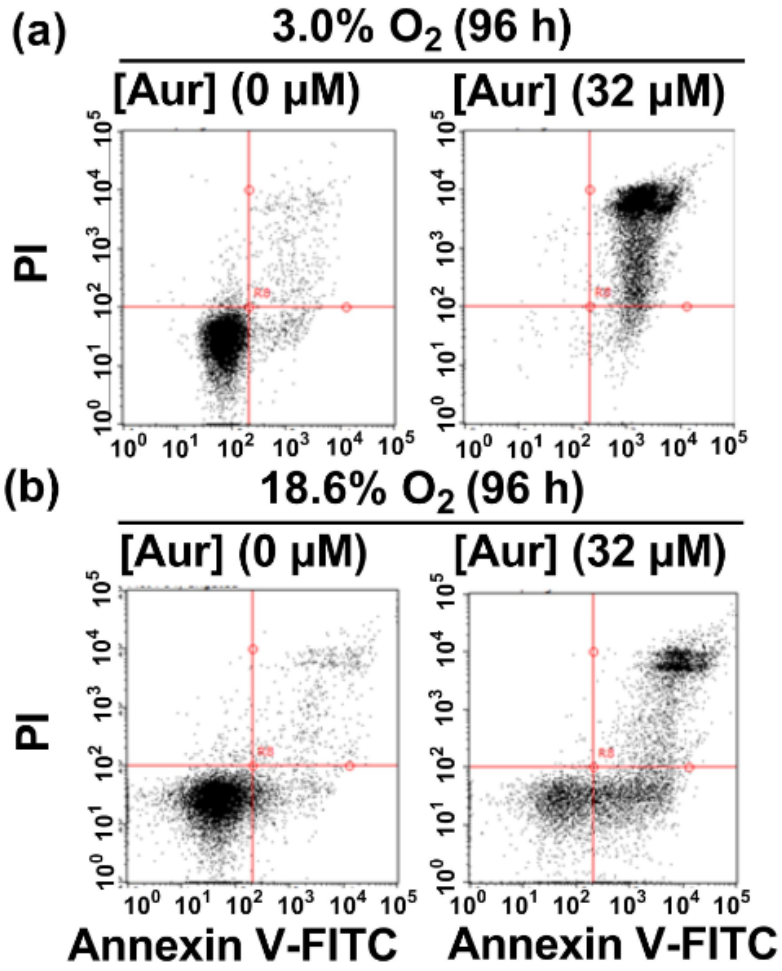

Figure 3.13. Representative dot plot histograms showing auranofin-induced cell death in A431 cells grown in 18.6% O_2 or 3.0% O_2 for 96 h. A431 cells were grown in 18.6% or 3.0% O_2 for 96 h (37°C/5% CO_2) prior to a 1h treatment with vehicle (0.1% v/v DMSO) or 1–32 µM auranofin in 18.6% or 3.0% O_2 (37°C/5% CO_2). Cell death was then analysed by flow cytometry using the FL1 and FL3 detectors whilst excited by a 488 nm argon excitation laser (section 2.4). The 4-quadrant scatter plots represents 4 groups of differently stained cells: viable (unstained, bottom left), early apoptotic (+AnnV/-PI, bottom right), late apoptotic (+AnnV/+PI, top right) and necrotic (-AnnV/+PI, top left). The intersecting lines show the separation of the quadrants. The numbers in each quadrant represent the percentage of cells in each respective stage of apoptosis or necrosis. **Panel (a),** dot plot histograms of auranofin-treated A431 cells previously grown in 3.0% O_2 and subsequently stained with annexin V-FITC and PI. **Panel (b),** dot plot histograms of auranofin-treated A431 cells grown in 18.6% O_2 and subsequently stained with annexin V-FITC and PI. **FITC:** fluorescein isothiocyanate; **PI:** propidium iodide.

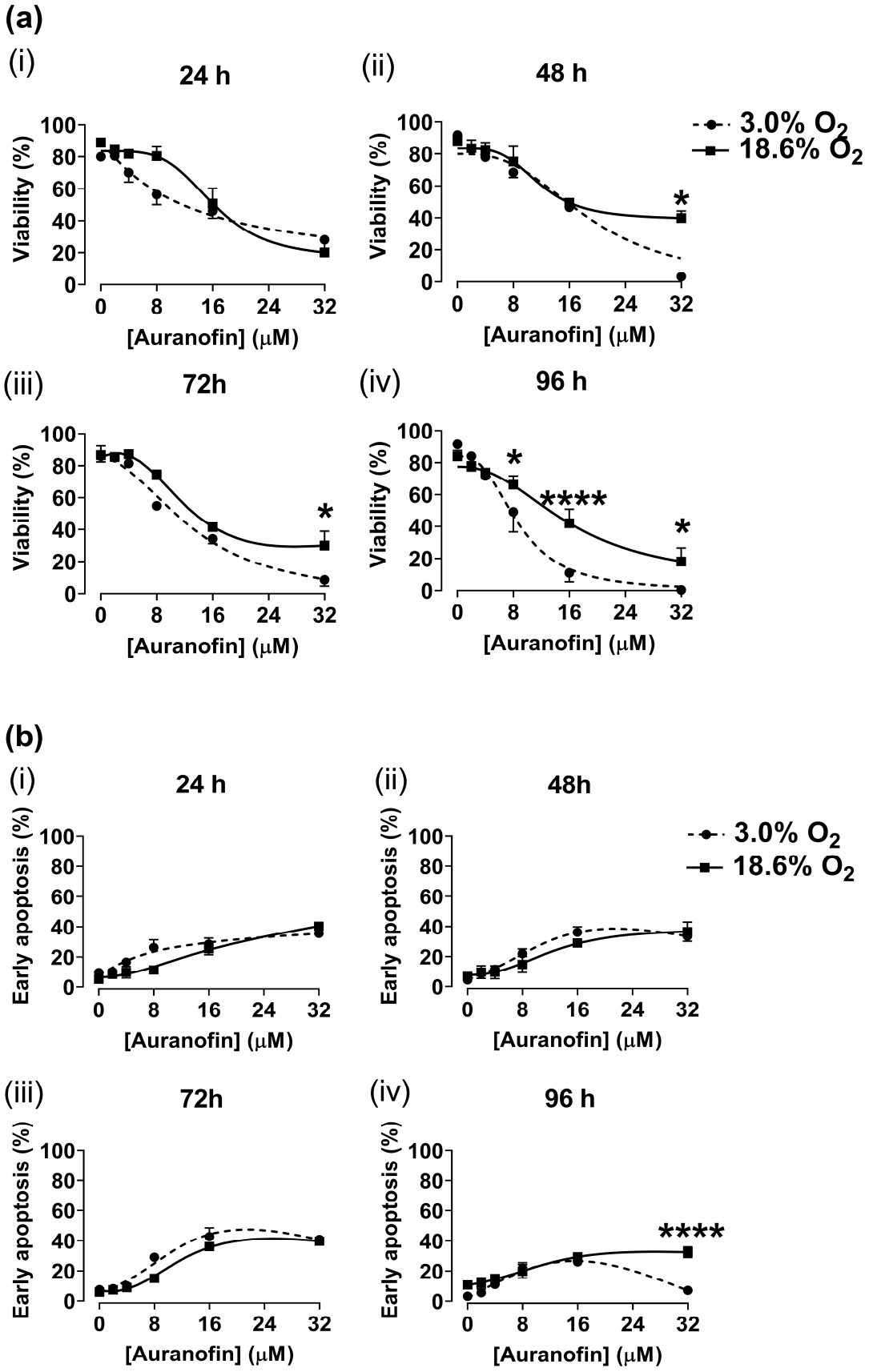
(a)
(i)
24 h
(ii)
48 h
3.0% O2
18.6% O2
Viability (%)
[Auranofin] (μM)
(iii)
72h
(iv)
96 h
*
****
(b)
Early apoptosis (%)

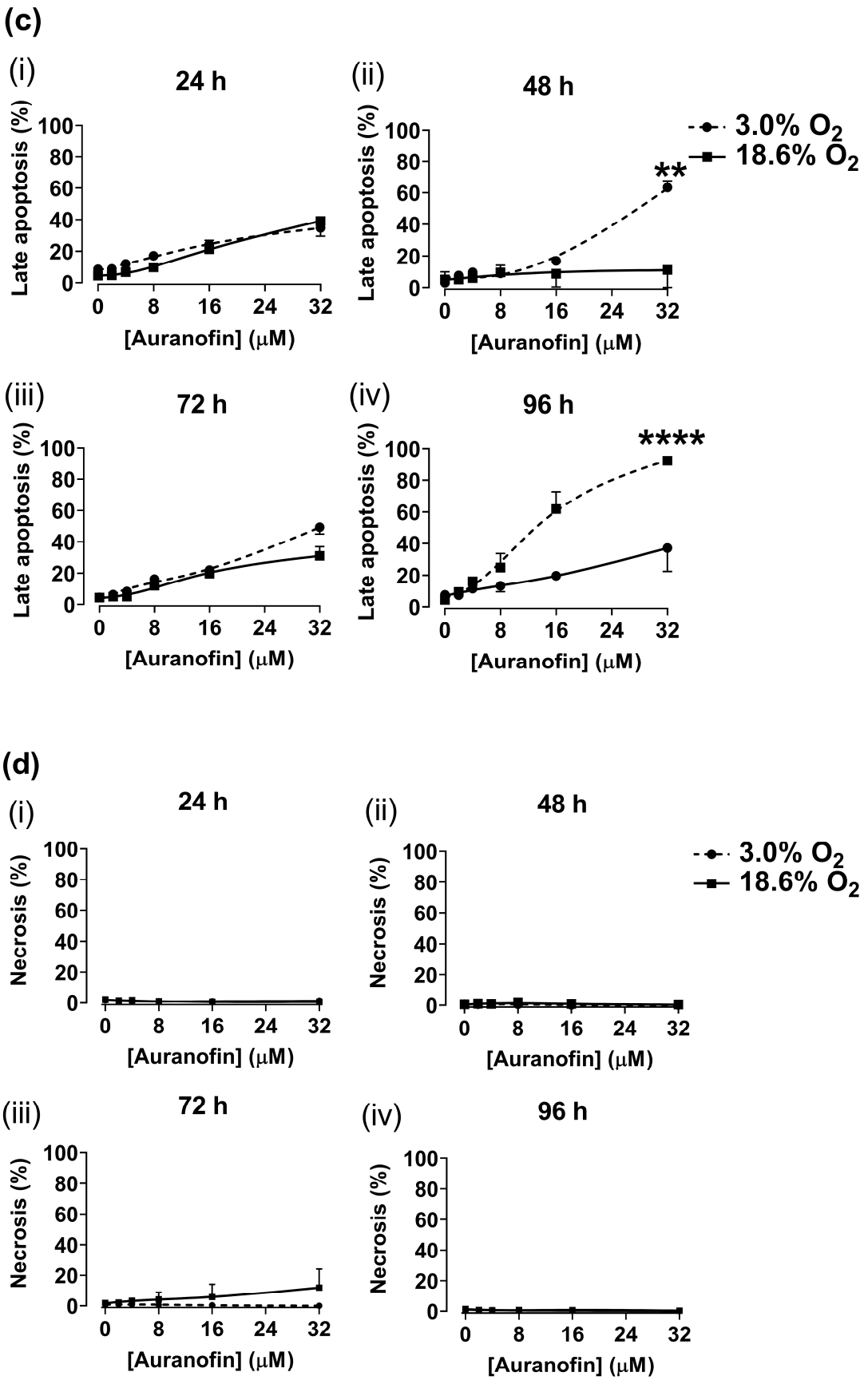
(c)
(i)
24 h
Late apoptosis (%)
[Auranofin] (μM)
(ii)
48 h
**
3.0% O2
18.6% O2
(iii)
72 h
(iv)
96 h
****
(d)
Necrosis (%)

Figure 3.14. The effect of growing A431 cells in 18.6% O_2 on auranofin-induced cell death compared to A431 cells grown in 3.0% O_2 for 24-96 h. A431 cells were seeded at a density of 9.5 x 10^3 cells/cm^2 in 24 well plates and grown in 18.6% O_2 or 3.0% O_2 for 24-96 h (37°C / 5% CO_2). Growth medium was changed every 24 h with respective (18.6% or 3.0% O_2) [O_2]-equilibrated growth medium. After the incubation period, A431 cells were treated with vehicle (0.1% v/v DMSO) or 1–32 µM auranofin for 1 h in 18.6% or 3.0% O_2 (37°C / 5% CO_2). A431 cells were then detached, washed with PBS (see section 2.2.3 for concentration) , and subsequently stained with annexin V-FITC and PI prior to cell death analysis by flow cytometry (section 2.4) using the FL1 and FL3 detectors whilst excited by a 488 nm argon excitation laser which included analysis of viability**,** early apoptosis, late apoptosis, and necrosis. **Panel (a),** viability in auranofin-treated A431 cells grown in 18.6% or 3.0% O_2 for 24-96 h (i–iv). **Panel (b),** early apoptosis in auranofin-treated A431 cells grown in 18.6% or 3.0% O_2 for 24-96 h (i–iv). **Panel (c),** late apoptosis in auranofin-treated A431 cells grown in 18.6% or 3.0% O_2 for 24-96 h (i–iv). **Panel (d),** necrosis in auranofin-treated A431 cells grown in 18.6% or 3.0% O_2 for 24-96 h (i–iv). n.s = not significant, * = $P < 0.05$, **** = $P < 0.0001$, versus 3.0% O_2 utilising a two-way ANOVA and a *post-hoc* multiple comparison test with Dunn-Šidák correction. Data are presented as the mean ± 1 SD. n=4. Where error bars are not visible, this is because the error bar is smaller than the size of the data point. **FITC:** fluorescein isothiocyanate**; PI:** propidium iodide.

3.3.3. The effect of changing the [O_2] during treatment on auranofin-induced cell death

The effect of changing the [O_2] during treatment on auranofin-induced cell death was assessed by annexin V-FITC and PI staining **(section 2.4)** in conjunction with flow cytometry. Four groups were analysed, A431 cells grown in 18.6% O_2 for 48 h and subsequently treated with auranofin in 18.6% O_2 (18.6% O_2 group), A431 cells grown in 3.0% O_2 for 48 h and treated with auranofin in 3.0% O_2 (3.0% O_2 group), A431 cells grown in 18.6% O_2 for 48 h and switched into 3.0% O_2 during auranofin treatment (18.6% → 3.0% group) O_2) and A431 cells grown in 3.0% O_2 for 48 h and switched into 18.6% O_2 during auranofin treatment (3.0% → 18.6% group). Representative dot plot histograms are shown in **Figure 3.15**.

A two-way ANOVA was performed to analyse the effects of [auranofin], and the [O_2] during auranofin treatment, on cell viability. A *post-hoc* analysis showed that the 18.6% group exhibited higher viability after treatment with 32 µM auranofin compared to the 3.0% group, the 18.6% → 3.0% O_2 group and the 3.0% → 18.6% O_2 group ($P < 0.0001$, **Figure 3.16 a)**, with means of 33.6 ± 10.7% vs 8.5% ± 3.3%, 33.6 ± 10.7% vs 8.1 ± 2.4%, and 33.6 ± 10.7% vs 6.2 ± 3.7%, respectively.

Additionally, the 3.0% → 18.6% O_2 group exhibited heightened viability after treatment with 16 µM auranofin compared to the 3.0% group (**Figure 3.16 a**), with means of 45.0 ± 2.40% vs 35.75 ± 2.50%. The interaction between the effects of [auranofin], and the [O_2] during auranofin treatment, on cell viability was statistically significant ($F (15, 72) = 11.55$, $P<0.0001$, **Figure 3.16 a**).

There was a statistically significant effect of [auranofin], and [O_2] during treatment, on late apoptosis ($P < 0.0001$, **Figure 3.16 c**). A *post-hoc* test showed that the percentage of late apoptotic cells was higher in the 18 % → 3.0% O_2 group after treatment with 32 µM auranofin compared to all other [O_2] groups ($p < 0.0001$, **Figure 3.16 c**), with means of 85.1 ± 6.7% vs 34.5 ± 11.4%, 85.1 ± 6.7% vs 47.6 ± 7.1%, and 85.1 ± 6.7% vs 52.1 ± 5.7%, respectively. The interactions between the effects of [auranofin], and the [O_2] during treatment, on late apoptosis was statistically significant ($F (15, 72) = 14.8$, $P < 0.0001$, **Figure 3.16 c**).

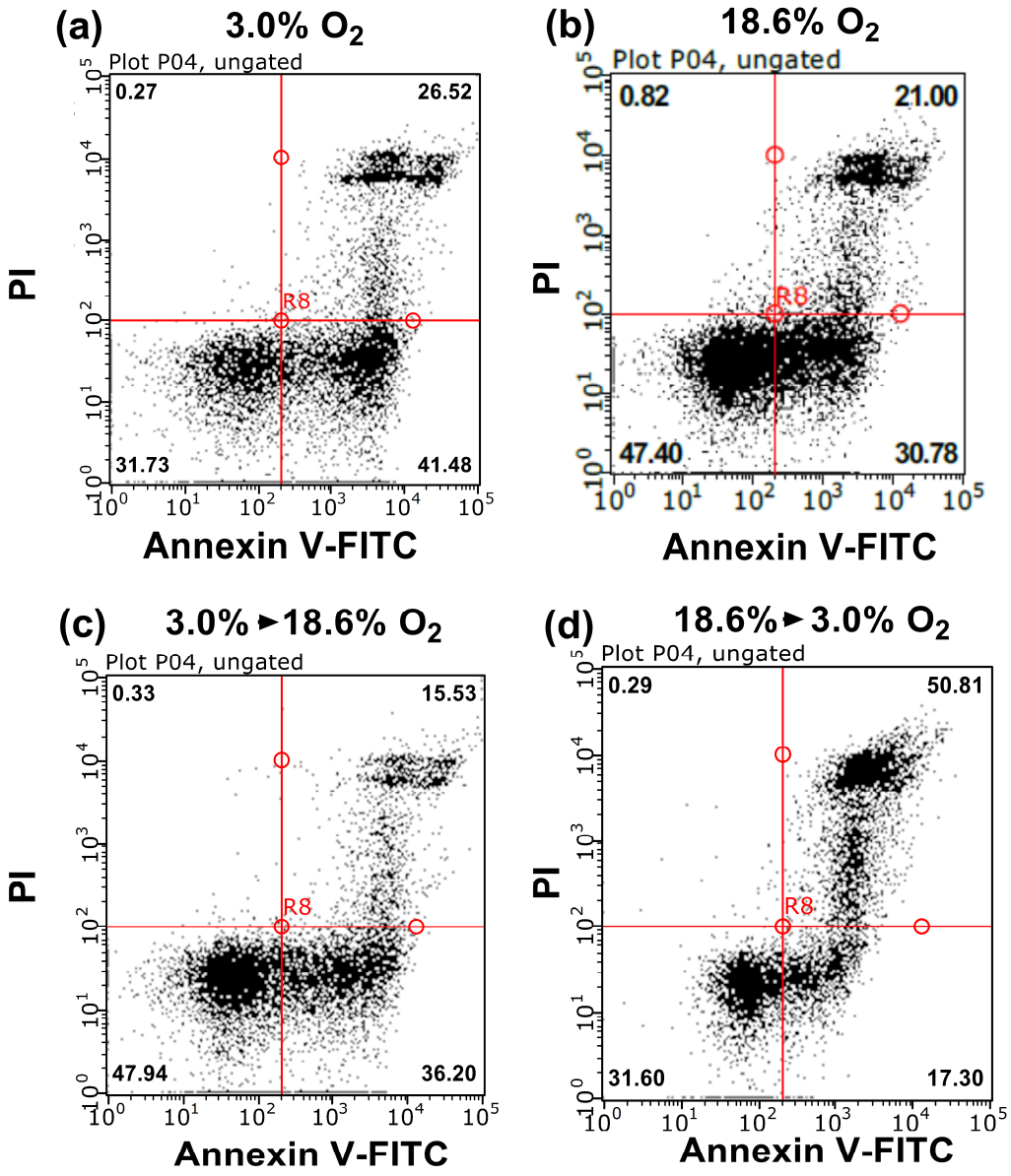

Figure 3.15. Representative dot plot histograms showing the effect of changing the oxygen concentration during auranofin treatment on auranofin-induced cell death in A431 cells grown in 18.6% O_2 or 3.0% O_2 for 96 h. A431 cells were grown in 18.6% or 3.0% O_2 for 96 h (37°C/5% CO_2). After 48 h, A431 cells were switched into 18.6% O_2 or 3.0% O_2 or maintained in 18.6% O_2 or 3.0% O_2 (37°C/5% CO_2). A431 cells were then treated with vehicle (0.1% v/v DMSO) or 1–32 µM auranofin for 1 h (37°C/5% CO_2) under the appropriate [O_2]. A431 cells were then stained with PI and annexin V-FITC and cell death was analysed by flow cytometry (section 2.4) using the FL1 and FL3 detectors whilst excited by a 488 nm argon excitation laser. **Panel (a),** A431 grown in 3.0% O_2 for 48 h, treated with 16 µM auranofin in 3.0% O_2, and subsequently stained with annexin V-FITC and PI. **Panel (b),** A431 cells grown in 18.6% O_2, treated with 16 µM auranofin in 18.6% O_2, and subsequently stained with annexin V-FITC and PI. **Panel (c),** A431 cells grown in 3.0% O_2 for 48 h, switched into 18.6% O_2 during treatment with 16 µM auranofin, and subsequently stained with annexin V-FITC and PI. **Panel (d),** A431 cells grown in 18.6 % O_2 for 48 h, switched into 3.0% O_2 during treatment with 16 µM auranofin and subsequently stained with annexin V-FITC and PI. **FITC:** fluorescein isothiocyanate; **PI:** propidium iodide.

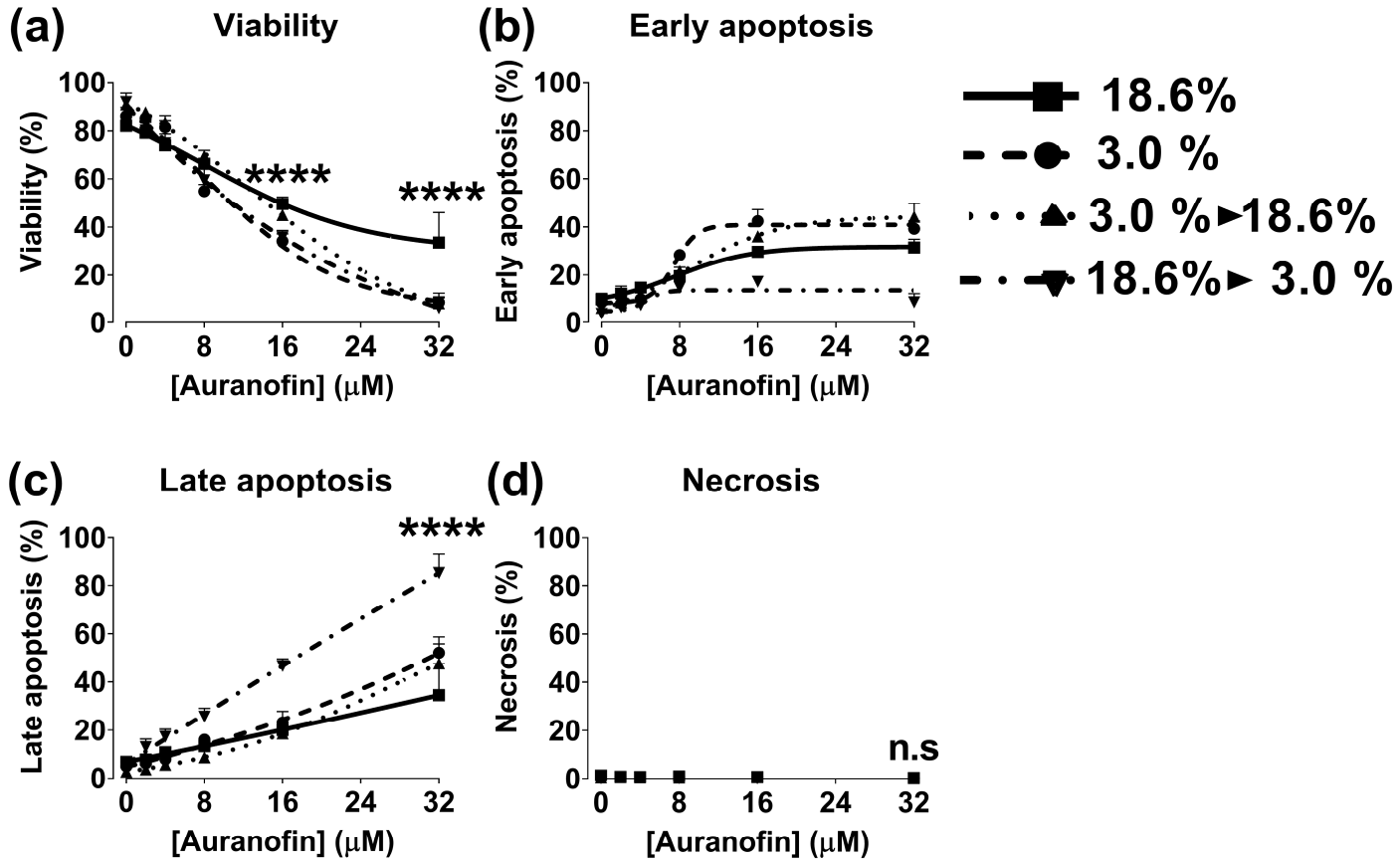

Figure 3.16. The effect of changing the O_2 concentration during treatment on auranofin-induced cell death in A431 cells previously grown in 18.6% or 3.0% O_2 for 48 h. A431 cells were seeded at a density of 9.5 x 10^3 cells/cm^2 in 24 well plates and grown in 18.6% O_2 or 3.0% O_2 for 48 h (37°C / 5% CO_2). Growth medium was changed every 24 h with respective (18.6% or 3.0% O_2) [O_2]-equilibrated growth medium. After 48 h, A431 cells were switched into 18.6% O_2 or 3.0% O_2 or maintained in 18.6% O_2 or 3.0% O_2. A431 cells were then immediately treated with vehicle (0.1% v/v DMSO) or 1-32 µM auranofin for 1 h (37°C / 5% CO_2). A431 cells were then detached, washed with PBS (see section 2.2.3 for concentration), and subsequently stained with annexin V-FITC and PI prior to cell death analysis by flow cytometry (section 2.4). **Panel (a),** viability in auranofin-treated A431 cells. **Panel (b),** early apoptosis in auranofin-treated A431 cells. **Panel (c),** late apoptosis in auranofin-treated A431 cells. **Panel (d),** necrosis in auranofin-treated A431 cells. n.s = not significant, **** = $P < 0.0001$ versus 3.0% O_2 utilising a two-way ANOVA and a *post-hoc* multiple comparison test with Dunn-Šidák correction. Data are presented as the mean ± 1 SD. n = 3. Where error bars are not visible, this is because the error bar is smaller than the size of the data point. **FITC:** fluorescein isothiocyanate**; PI:** propidium iodide.

3.3.4. The effect of growing A431 cells in 18.6% O_2 on auranofin-induced mitochondria-derived reactive oxygen species generation compared to A431 cells grown in 3.0% O_2

Auranofin-induced mitochondria-derived ROS generation was measured using MitoSOX Red **(section 1.2.3.2)** staining in conjunction with flow cytometry **(section 3.2.3)** in A431 cells grown in 18.6% O_2 or 3.0% O_2 for 96 h. Example fluorescence histograms are shown in **Figure 3.17**.

A two-way ANOVA was performed to analyse the effects of [auranofin], and the [O_2] cells were grown in, on mitochondrial ROS generation. Detection of mitochondrial ROS was functional as treatment with 100 µM CCCP increased ROS generation in both [O_2] groups when compared to respective untreated control cells ($P < 0.0001$, **Figure 3.18 a**). A *post-hoc* test showed no significant differences in mitochondrial ROS production when comparing the untreated control cells in both [O_2] conditions (**Figure 3.18 a**). A431 cells grown in 18.6% O_2 for 96 h exhibited a decrease in mitochondrial ROS generation after treatment with 8 µM, and 16 µM auranofin when compared to A431 cells grown in 3.0% O_2 for 96 h under the same treatment conditions, with means of 282.5 ± 54.0 MFI vs 407.7 ± 69.2 MFI ($P < 0.05$), and 444.1 ± 35.5 MFI vs 543.4 ± 24.2 MFI ($P < 0.01$, **Figure 3.18 b**), respectively.

The interaction between the effects of [auranofin], and the [O_2] cells were grown in, on mitochondrial-derived ROS production was statistically significant (F (6, 42) = 6.720, $P < 0.01$).

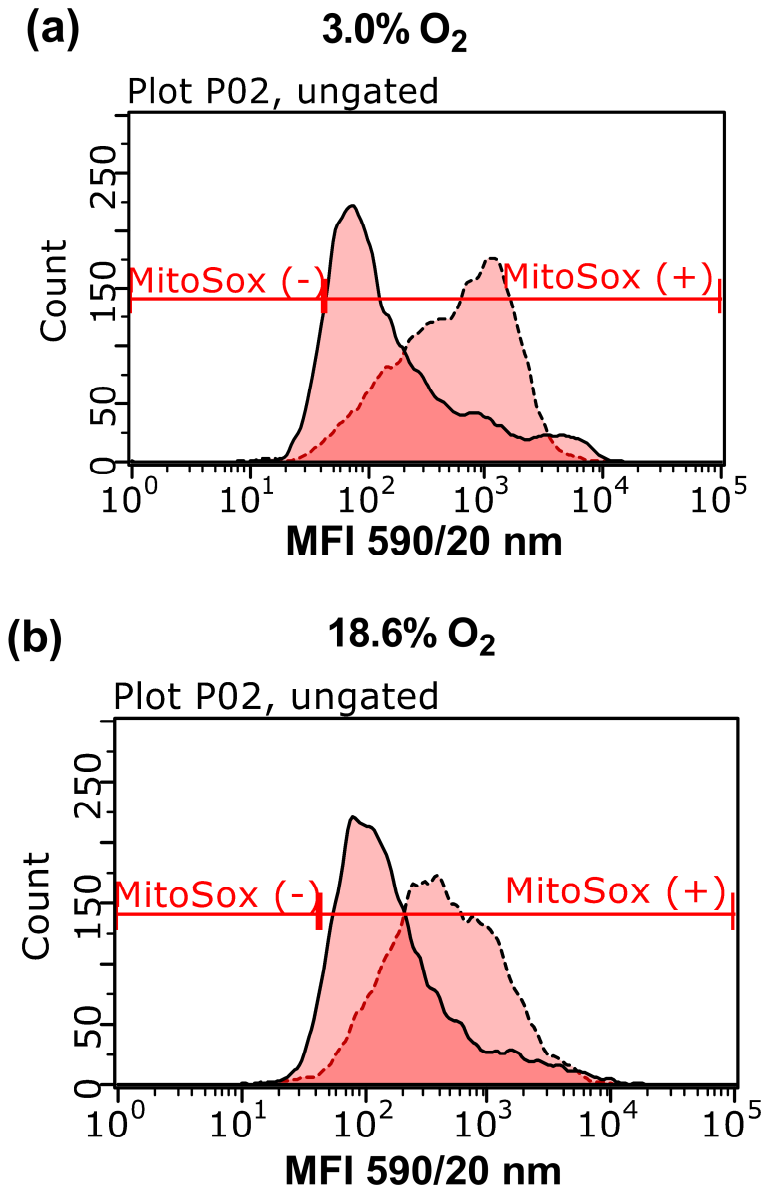

Figure 3.17. Representative MitoSOX Red flow cytometry fluorescence histograms showing auranofin-induced reactive oxygen species generation in A431 cells grown in 18.6% O_2 or 3.0% O_2. A431 cells were grown in 18.6% O_2 or 3.0% O_2 for 96 h prior to treatment with vehicle (0.1% v/v DMSO) or 1–32 µM auranofin for 1h (37°C/5% CO_2) and subsequent staining with 2 µM MitoSOX Red for 1 h (37°C/5% CO_2). Auranofin-induced mitochondrial ROS generation was then measured by flow cytometry utilising the FL2 detector whilst excited by a 488 nm argon laser. In this example, untreated controls are indicated by the solid trace, and auranofin treated cells are indicated by the dashed trace. **Panel (a),** fluorescence histogram of auranofin-induced ROS generation in A431 cells grown in 3.0% O_2 for 96 h subsequently stained with MitoSox Red. **Panel (b),** fluorescence histogram of auranofin-induced ROS generation in A431 cells grown in 18.6% O_2 subsequently stained with MitoSox red. The y axis label (count) indicates the number of events (cells) detected at the respective MFI. **MFI:** mean fluorescence intensity; **MitoSOX: (-/+)**: MitoSOX Red negative/positive region.

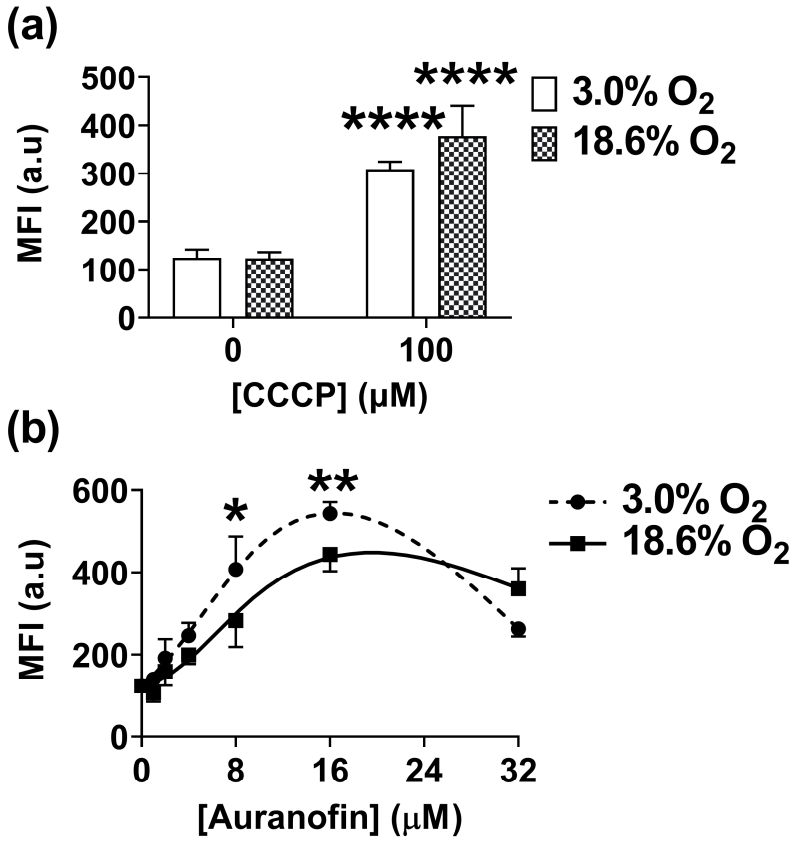

Figure 3.18. Effect of growing A431 cells in 18.6% O_2 on auranofin-induced mitochondrial reactive oxygen species generation compared to A431 cells grown in 3.0% O_2 for 96 h. A431 cells were seeded at a density of 9.5 x 10^3 cells/cm^2 in 24 well plates and were grown in 18.6% O_2 or 3.0% O_2 for 24 or 96 h (37°C/5% CO_2). A431 cells were fed with fresh respective (18.6% or 3.0% O_2) [O_2]-equilibrated growth medium every 24 h. After the incubation period, A431 cells were treated with vehicle (0.1% (v/v) DMSO), 1-32 µM auranofin, or 100 µM CCCP (positive control for ROS generation) for 1 h in 18.6% or 3.0% O_2 (37°C/5% CO_2). After the treatment period, under low light, the cells were stained with 1 µM MitoSOX Red for 30 min (37°C/5% CO_2) in 18.6% or 3.0% O_2. A431 cells were subsequently washed with PBS (see section 2.2.3 for concentration), detached with 0.25% v/v trypsin-EDTA, and the fluorescence intensity of MitoSOX Red-stained A431 cells were analysed by flow cytometry utilising the FL-2 detector whilst being excited by a 488 nm argon laser (section 3.2.3). **Panel (a),** ROS generation in untreated A431cells or A431 cells treated with 100 µM CCCP for 1 h. **Panel (b),** ROS generation in A431 cells grown in 18.6% or 3.0% O_2 for 96 h treated with 1–32 µM auranofin. * = $P < 0.05$, ** = $P < 0.01$ versus 18.6% O_2, **** = $P < 0.0001$ versus untreated control utilising a two-way ANOVA with a *post-hoc* multiple comparison test with Dunn-Šidák correction. Data are presented as the mean ± 1 SD. n=4. Where error bars are not visible, this is because the error bar is smaller than the size of the data point. **a.u**: arbitrary units; **CCCP:** carbonyl cyanide m-chlorophenyl hydrazine; **MFI:** mean fluorescence intensity.

3.3.5. The effect of growing A431 cells in 18.6% O_2 on auranofin-induced reactive oxygen species generation compared to A431 cells grown in 3.0% O_2.

Auranofin-induced cellular ROS generation was measured using DHE **(section 1.2.3.2)** staining in conjunction with flow cytometry **(section 3.2.3)** in A431 cells grown in 18.6% O_2 or 3.0% O_2 for 24 h or 96 h. Example fluorescence histograms are shown in **Figure 3.19**.

A two-way ANOVA was performed to analyse the effects of [auranofin], and the [O_2] cells were grown in, on ROS generation. A *post-hoc* test showed no significant differences in ROS generation when comparing the untreated control cells in both [O_2] groups **(Figure 3.20 a)**.

A431 cells grown in 18.6% O_2 and treated with 32 µM auranofin showed no statistically significant change in ROS production when compared to respective untreated control cells **(Figure 3.20 b)**. However, A431 cells grown in 3.0% O_2 for 24 h, and treated with 32 µM auranofin, exhibited a decrease in auranofin-induced ROS generation compared to untreated control ($P < 0.0001$; **Figure 3.20 a)**, with means of 26.7 ± 1.4 MFI vs 13.1 ± 0.9 MFI. Additionally, A431 cells grown in 3.0% O_2 for 24 h, and treated with 32 µM auranofin, exhibited higher ROS generation compared to A431 cells grown in 3.0% O_2 for 96 h under the same treatment conditions ($P < 0.0001$, **Figure 3.20 b**), with means of 3.8 ± 0.3 MFI vs 13.1 ± 0.9 MFI, respectively.

The interaction between the effects of [auranofin], and the [O_2] cells were grown in, on ROS production was statistically significant (F (12, 42) = 16.65, $P<0.0001$).

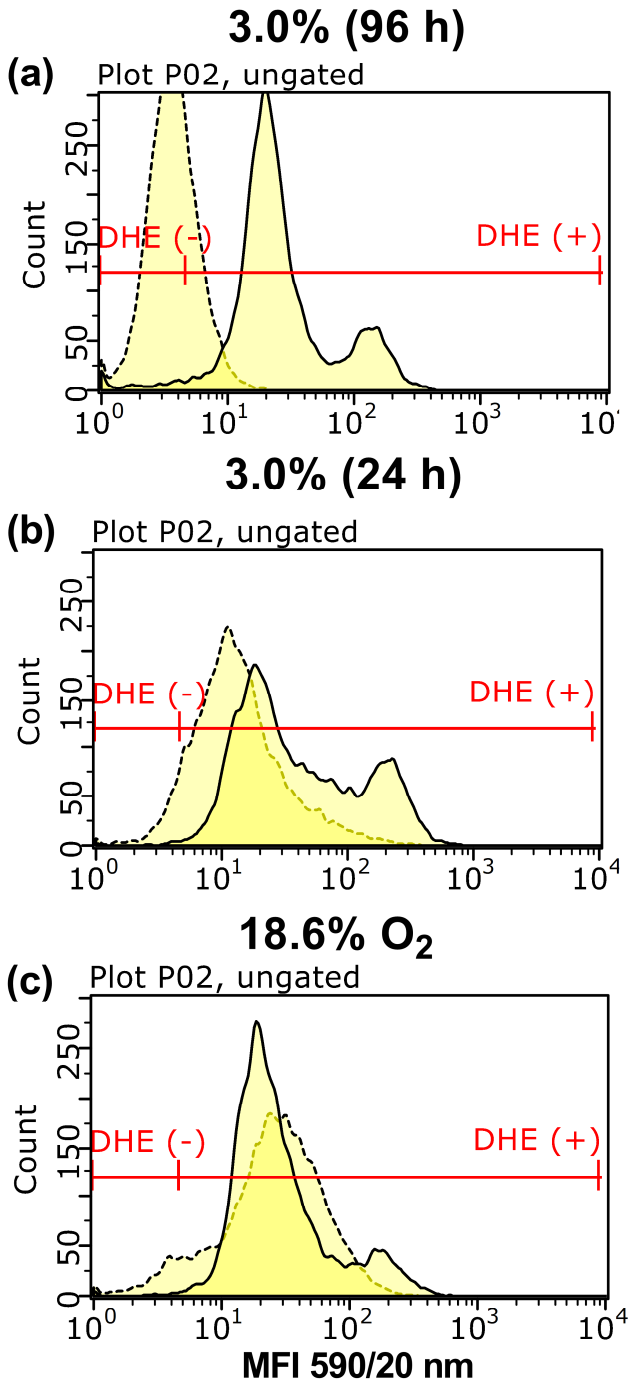

Figure 3.19. Representative dihydroethidium flow cytometry fluorescence histograms showing auranofin-induced ROS generation in A431 cells grown in 18.6% O_2 or 3.0% O_2 for 96 h. A431 cells were grown in 18.6% O_2 or 3.0% O_2 for 24 or 96 h prior to treatment with vehicle (0.1% v/v DMSO) or 1–32 µM auranofin for 1h. A431 cells were then stained with 10 µM DHE for 1 h. Auranofin-induced ROS generation was then measured by flow cytometry utilising the FL2 detector whilst excited by a 488 nm argon laser. In this example, A431 cells were grown in 18.6% O_2 or 3.0% O_2 for 24 or 96 h prior to treatment with vehicle (0.1% v/v DMSO; solid trace) or 32 µM auranofin (dashed trace). **Panel (a),** auranofin-induced ROS generation in A431 cells grown in 18.6% O_2 subsequently stained with DHE. **Panel (b),** auranofin-induced ROS generation in A431 cells grown in 3.0% O_2 for 24 h subsequently stained with DHE. **Panel (c),** auranofin-induced ROS generation in A431 cells grown in 3.0% O_2 for 96 h subsequently stained with DHE. The y axis label (count) indicates the number of events (cells) detected at the respective MFI. **DHE: (-/+):** dihydroethidium negative/positive region; **MFI:** mean fluorescence intensity.

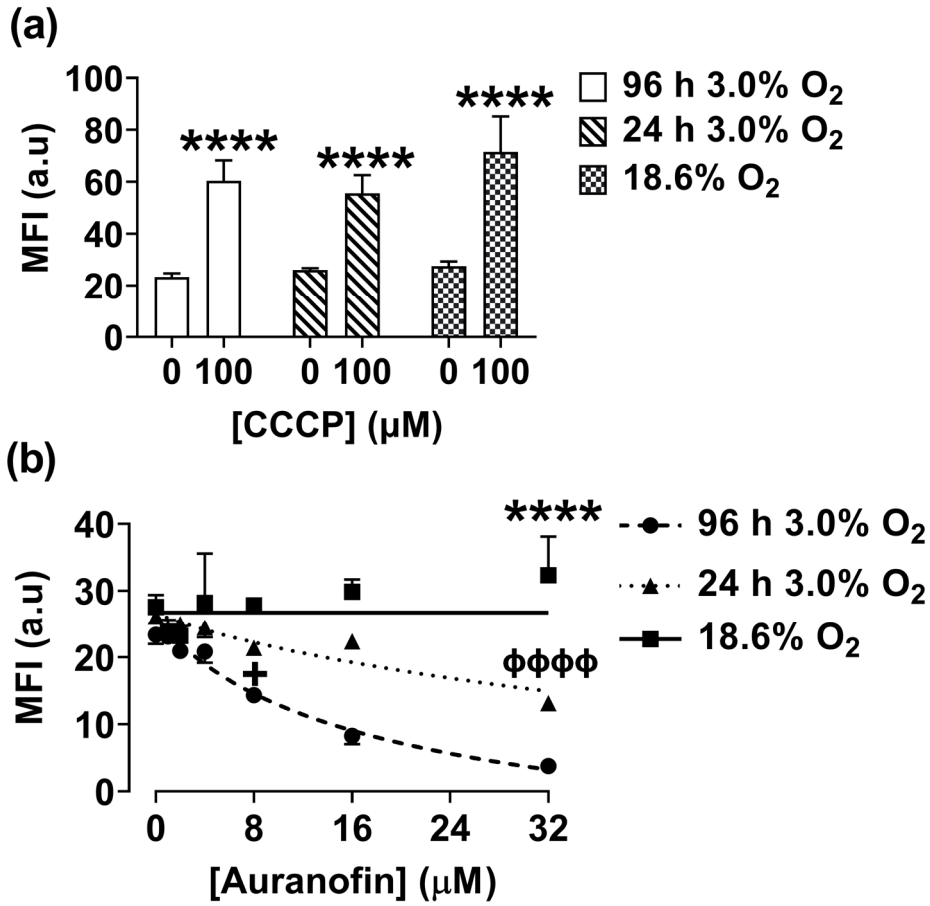

Figure 3.20. The effect of growing A431 cells in 18.6% O_2 on auranofin-induced reactive oxygen species generation compared to A431 cells grown in 3.0% O_2 for 24 or 96 h. A431 cells were seeded at a density of 9.5 x 10^3 cells/cm^2 in 24 well plates and grown in 18.6% O_2 or 3.0% O_2 for 24 or 96 h (37°C / 5% CO_2). Growth medium was changed every 24 h with respective (18.6% or 3.0% O_2) [O_2]-equilibrated growth medium. After 96 h of growth, A431 cells were treated with vehicle (0.1% v/v DMSO) or 1-32 µM auranofin for 1 h in 18.6% or 3.0% O_2 (37°C / 5% CO_2). A431 cells were also treated with 100 µM CCCP which served as a positive control for ROS generation. Under low light, A431 cells were incubated with 10 µM DHE for an additional 1 h (37°C / 5% CO_2) prior to measuring the fluorescence of DHE-stained A431 cells by flow cytometry using the FL-2 detector whilst being excited at 488 nm using an argon laser. **Panel (a),** ROS generation in untreated A431 cells or A431 cells treated with 100 µM CCCP. **Panel (b),** auranofin-induced ROS generation in A431 cells grown in 18.6% or 3.0% O_2 for 24 or 96h. **** = P < 0.0001 versus untreated control in panel (a) and versus 24 and 96 h 3.0% O_2 in panel (b), ϕϕϕϕ = P < 0.0001 versus 3.0% O_2 96 h utilising a two-way ANOVA and a *post-hoc* multiple comparison test with Dunn–Šidák correction. Data are presented as the mean ± 1 SD. n=3. Where error bars are not visible, this is because the error bar is smaller than the size of the data point. **a.u:** arbitrary units; **CCCP:** carbonyl cyanide m-chlorophenyl hydrazine; **MFI:** mean fluorescence intensity.

3.3.6. The effect of growing A431 cells in 18.6% O_2 auranofin-induced oxidative stress compared to A431 cells grown in 3.0% O_2

Auranofin-induced oxidative stress was estimated using DCFHDA **(section 1.2.3.3)** staining in conjunction with flow cytometry **(section 3.2.3)** in A431 cells grown in 18.6% O_2 or 3.0% O_2 for 96 h. Example fluorescence histograms are shown in **Figure 3.21**.

A two-way ANOVA was performed to analyse the effect of [auranofin], and the [O_2] cells were grown in, on ROS generation. A *post-hoc* test showed no significant differences in ROS generation when comparing the untreated control cells in both [O_2] groups **(Figure 3.22 a)**. A *post-hoc* analysis showed that treatment of A431 cells grown in 18.6% O_2 with 16 µM auranofin exhibited a decrease in oxidative stress compared to A431 cells grown in 3.0% O_2 for 96 h under the same treatment conditions ($P < 0.0001$, **Figure 3.22 b**), with means of 354.5 ± 22.6 MFI vs 478.3 ± 12.0 MFI, respectively.

The interaction between the effects of [auranofin], and the [O_2] cells were grown in, on ROS generation was statistically significant ($F(3, 24) = 7.149$, $P = 0.0014$).

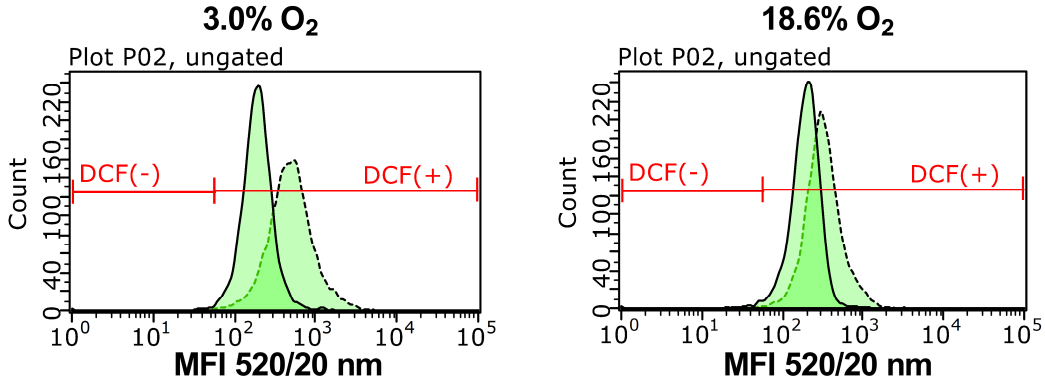

Figure 3.21. Representative 2′, 7′-dichlorofluorescin diacetate flow cytometry fluorescence histograms showing auranofin-induced oxidative stress in A431 cells grown in 18.6% O_2 or 3.0% O_2 for 96 h. A431 cells were grown in 18.6% O_2 or 3.0% O_2 for 96 h prior to treatment with vehicle (0.1% v/v DMSO) or 1–32 µM auranofin for 1h. A431 cells were subsequently stained with 10 µM DCFHDA for 1 h. Auranofin-induced oxidative stress was then estimated by flow cytometry utilising the FL1 detector whilst excited by a 488 nm argon laser. In this example, A431 cells were grown in 3.0% O_2 (left) or 18.6% O_2 (right) for 96 h and treated with vehicle (0.1% v/v DMSO; solid trace) or 32 µM auranofin (dashed trace) for 1 h. **Panel (a)** fluorescence histogram of auranofin-induced oxidative stress in A431 cells previously grown in 3.0% O_2 for 96 h and subsequently stained with DCFHDA. **Panel (b)** fluorescence histogram of auranofin-induced oxidative stress in A431 cells previously grown in 18.6% O_2 for 96 h and subsequently stained with DCFHDA. The y axis label (count) indicates the number of events (cells) detected at the respective MFI. **DCF (-/+):** 2', 7'–dichlorofluorescein negative/positive regions.

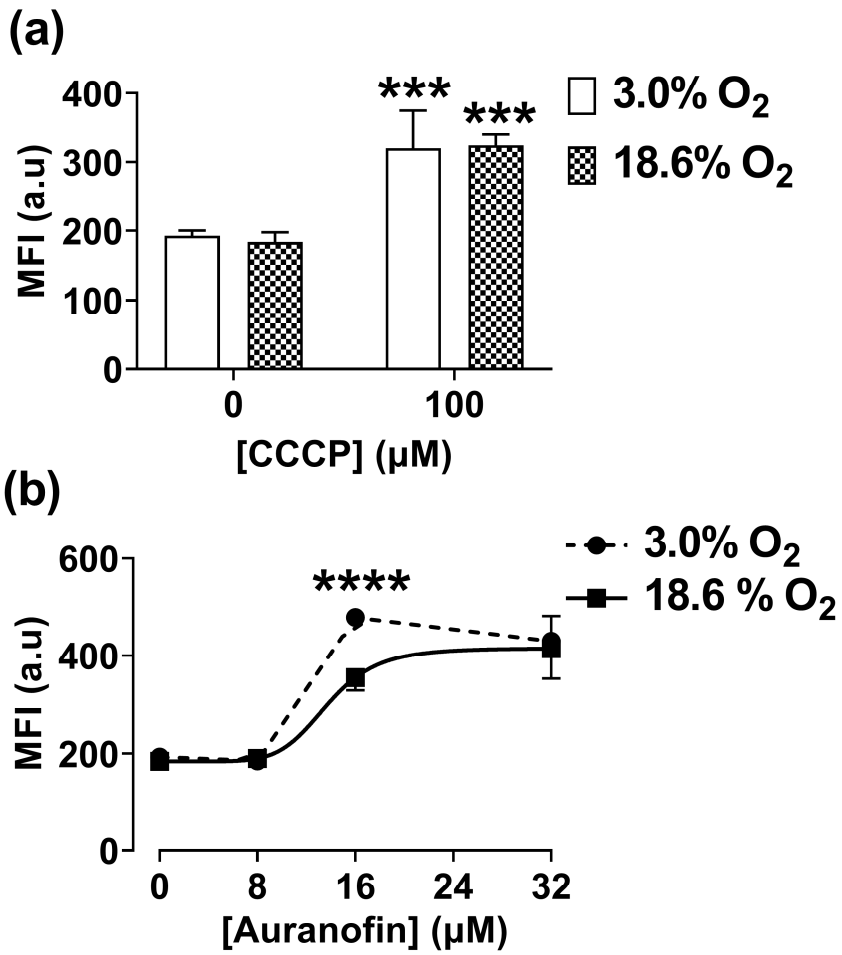

Figure 3.22. Effect of growing A431 cells in 18.6% O_2 on auranofin-induced oxidative stress compared to A431 cells grown in 3.0% O_2 for 96 h. A431 cells were seeded at a density of 9.5 x 10^3 cells/cm^2 in 24 well plates and were grown in 18.6% O_2 or 3.0% for 96 h (37°C/5% CO_2). A431 cells were fed with fresh respective (18.6% or 3.0% O_2) [O_2]-equilibrated growth medium every 24 h. After the incubation period, A431 cells were treated with vehicle (0.1% v/v DMSO) or 1-32 µM auranofin for 1 h in 18.6% or 3.0% O_2 (37°C/5% CO_2). A431 cells were treated with 100 µM CCCP for 1 h as a positive control for ROS generation. After the treatment period, A431 cells were stained with 10 µM DCFHDA for 1 h in 18.6% or 3.0% O_2 (37°C/5% CO_2). A431 cells were subsequently washed with PBS (see section 2.2.3 for concentration), detached with 0.25% v/v trypsin-EDTA, and the fluorescence of DCFHDA-stained cells was analysed by flow cytometry utilising the FL-1 detector whilst excited by a 488 nm argon laser. **Panel (a),** oxidative stress in untreated A431 cells and A431 cells treated with 100 µM for 1 h. **Panel (b),** auranofin-induced oxidative stress in A431 cells grown in 18.6% O_2 or 3.0% O_2 for 96 h. *** = $P < 0.001$ versus untreated control, **** = $P < 0.0001$ versus 18.6% O_2 utilising a two-way ANOVA and a *post-hoc* multiple comparison test with Dunn-Šidák correction. Data are presented as the mean ± 1 SD. n=4. Where error bars are not visible, this is because the error bar is smaller than the size of the data point. **a.u:** arbitrary units; **CCCP:** carbonyl cyanide *m*-chlorophenyl hydrazine; **MFI:** mean fluorescence intensity.

3.3.7. The effect of growing A431 cells in 18.6% O_2 on the cellular generation of H_2O_2 compared to A431 cells grown in 3.0% O_2

Cellular H_2O_2 generation was measured using Amplex Red **(section 1.2.3.1)** in A431 cells grown in 18.6% O_2 or 3.0% O_2 for 96 h.

A two-way ANOVA was performed to analyse the effects of time, and the [O_2] cells were grown in, on H_2O_2 generation. A *post-hoc* analysis showed that A431 cells grown in 18.6% O_2 for 96 h generated more H_2O_2 after 2 h compared to A431 cells grown in 3.0% O_2 for 96 h, with means of 2.8 ± 0.3 µM vs 1.7 ± 0.1 µM H_2O_2 ($P < 0.0001$, **Figure 3.23**). The interaction between the effects of time, and the [O_2] cells were grown in, on H_2O_2 generation was statistically significant ($F = 7.64$, DFn = 4, DFd = 20, $P = 0.0007$).

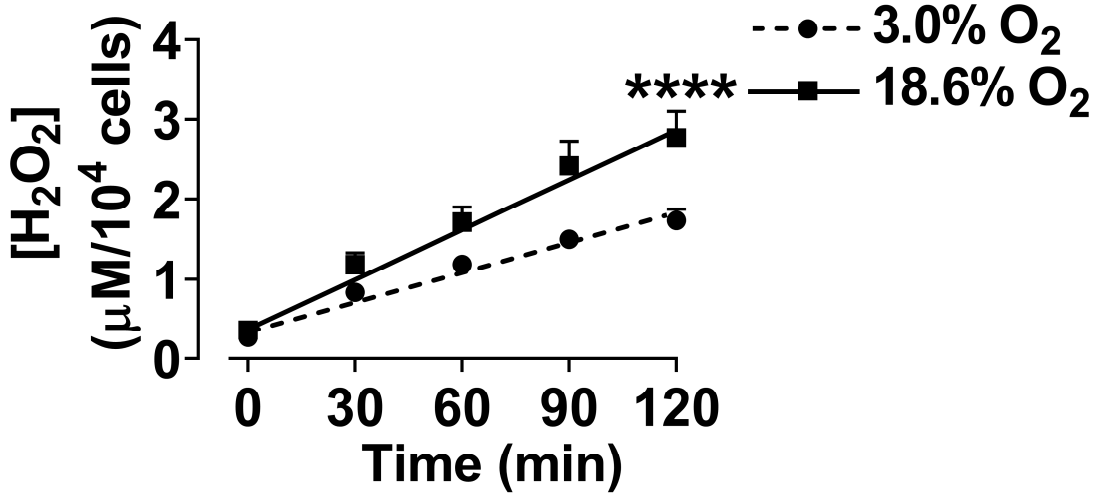

Figure 3.23. Effect of growing A431 cells in 18.6% O_2 on the generation of H_2O_2 compared to A431 cells grown in 3.0% O_2 for 96 h. A431 cells were seeded at a density of 9.5 x 10^3 cells/cm^2 into black plastic 96 well plates and were incubated in 18.6% O_2 or 3.0% O_2 for 96 h (37°C / 5% CO_2). A431 cells were fed every 24 h with fresh respective (18.6% or 3.0% O_2) [O_2]-equilibrated growth medium. After 96 h, a reaction mixture of Amplex Red (100 µM) and HRP (0.2 U/mL) was made up in [O_2]-equilibrated growth medium without phenol red and added to the appropriate wells under low light (1:1 dilution). Blank wells contained DMEM alone. Background signal wells contained a mixture of DMEM and the reaction mixture alone. Both 3.0% and 18.6% O_2 plates were sealed with cellophane tape to maintain the gas environment in both conditions during analysis. A kinetic fluorescence time-point scan was measured at an excitation wavelength of 570 nm and an emission wavelength of 585 nm at intervals of 30 min for 2 h utilising a Spectramax M_2e spectrophotometer. After analysis, a cell count was performed for data normalisation. Cellular H_2O_2 generation was determined through standard curve interpolation (Figure 3.1). **** = $P < 0.0001$ versus 3.0% O_2 utilising a two-way ANOVA and a *post-hoc* multiple comparison test with Šidák correction. Data are presented as the mean ± 1 SD. n=4. Where error bars are not visible, this is because the error bar is smaller than the size of the data point. **DMEM:** Dulbecco's modified Eagle's Medium.

3.3.8. The effect of growing A431 cells in 18.6% O_2 on carmustine-induced cell death compared to A431 cells grown in 3.0% O_2

Carmustine-induced cell death was measured using annexin V-FITC and PI staining **(section 2.4)** in A431 cells grown in 18.6% O_2 or 3.0% O_2 for 96 h. Example dot plot histograms are shown in **Figure 3.24**.

A two-way ANOVA was performed to analyse the effects of [carmustine], and the [O_2] cells were grown in, on cell death. A *post-hoc* analysis showed that A431 cells grown in 18.6%, and treated with 700 µM carmustine, exhibited heightened viability compared to A431 cells grown in 3.0% O_2 for 96 h under the same treatment conditions ($P < 0.0001$, **Figure 3.25 a)**, with means of 33.0 ± 5.1% vs 7.9 ± 0.8%, respectively.

The interaction between the effects of [carmustine], and the [O_2] cells were grown in, on cell viability was statistically significant (F (6, 38) = 10.08, $P<0.0001$).

Additionally, A431 cells grown in 18.6% O_2, and treated with 700 µM carmustine, showed a statistically significant decrease in the percentage of cells in late apoptosis ($P < 0.05$) and necrosis ($P < 0.01$) compared to A431 cells grown in 3.0% O_2 under the same treatment conditions **(Figure 3.25 c and d)**.

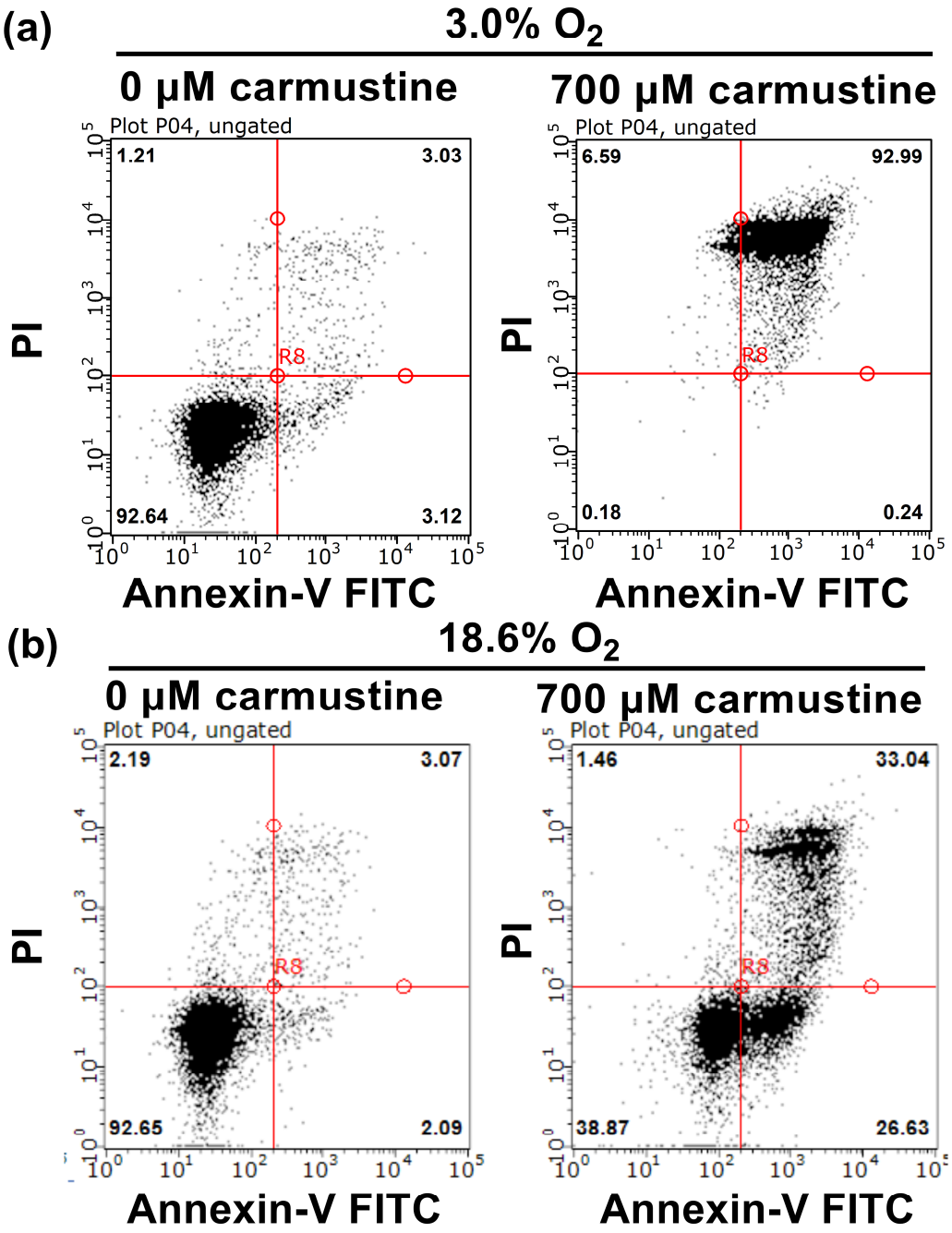

Figure 3.24. Representative dot plot histograms showing carmustine-induced cell death in A431 cells grown in 18.6% O_2 compared to A431 cells grown in 3.0% O_2 for 96 h. A431 cells were grown in 18.6% or 3.0% O_2 for 96 h prior to treatment with vehicle (0.1% v/v DMSO) or 700 µM carmustine for 1 h. A431 cells were then stained with annexin V-FITC and PI. Cell death was then analysed by flow cytometry using the FL1 and FL3 detectors whilst excited by a 488 nm argon excitation laser (section 2.4). The 4-quadrant scatter plots represents 4 groups of differently stained cells: viable (unstained, bottom left), apoptotic (+AnnV/-PI, bottom right), late apoptotic (+AnnV/+PI, top right) and necrotic (-AnnV/+PI, top left). The two lines show the separation of the quadrants. The numbers in bold in each quadrant represent the percentage of cells in each respective stage of apoptosis or necrosis. **Panel (a),** dot plot histograms of carmustine-treated A431 cells grown in 3.0% O_2 subsequently stained with annexin V-FITC and PI. **Panel (b),** dot plot histograms of carmustine-treated A431 cells grown in 18.6% O_2 subsequently stained with annexin V-FITC and PI. **FITC:** fluorescein isothiocyanate**; PI:** propidium iodide.

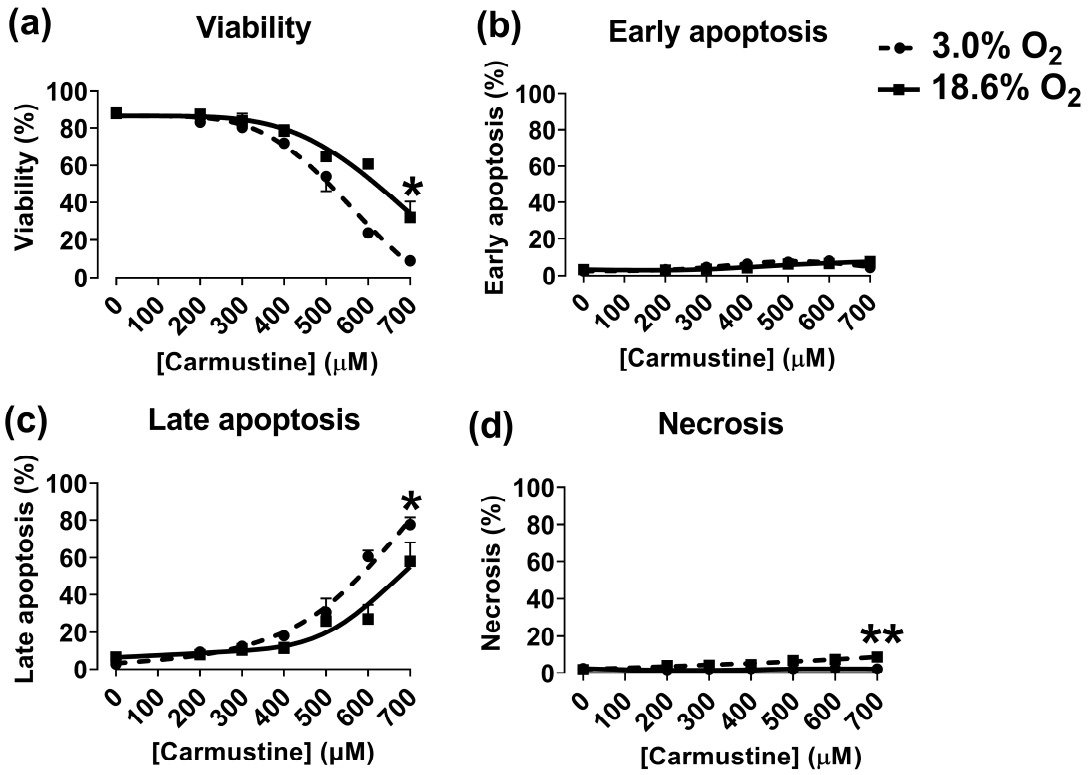

Figure 3.25. The effect of growing A431 cells in 18.6% O_2 on carmustine-induced cell death compared to A431 cells grown in 3.0% O_2 for 96 h. A431 cells were seeded at a density of 9.5 x 10^3 cells/cm^2 in 24 well plates and grown in either 18.6% O_2 or adapted 3.0% O_2 for 96 h (37°C / 5% CO_2). Growth medium was changed every 24 h with respective (18.6% or 3.0% O_2) [O_2]-equilibrated growth medium. After 96 h of growth, cells were treated with 0-700 µM carmustine for an additional 24 h. A431 cells were then detached, washed with PBS (see section 2.2.3 for concentration), and subsequently stained with annexin V-FITC and PI prior to cell death analysis by flow cytometry (section 2.4). **Panel (a),** cell viability. **Panel (b),** early apoptosis. **Panel (c),** late apoptosis. **Panel (d),** necrosis. ***** = $P < 0.05$ versus 3.0% O_2 in panel (a) and versus 18.6% O_2 in panel (b), ****** = $P < 0.01$ versus 18.6% O_2 utilising a two-way ANOVA with multiple comparison and Dunn-Šidák correction. Data are presented as the mean ± 1 SD. n=4. Where error bars are not visible, this is because the error bar is smaller than the size of the data point. **FITC:** fluorescein isothiocyanate; **PI:** propidium iodide.

3.3.9. The effect of growing A431 cells in 18.6% O_2 on carmustine-mediated sensitisation to H_2O_2-induced cell death compared to A431 cells grown in 3.0% O_2

Carmustine-mediated sensitisation to H_2O_2-induced cell death was measured in A431 cells grown in 18.6% O_2 or 3.0% O_2 for 96 h utilising annexin V-FITC and PI staining in conjunction with flow cytometry **(section 2.4).** A non-toxic carmustine concentration (100 µM) was determined from concentration response testing as shown in **section 2.5.4.** Example dot plot histograms are shown in **Figure 3.26**.

A two-way ANOVA was performed to analyse the effects of [carmustine], and the [O_2] cells were grown in, on cell viability. Treatment with A431 cells alone with 0.5 mM H_2O_2 did not decrease viability in either [O_2] group compared to respective untreated control cells **Figure 3.27 a**. A *post-hoc* test showed that pre-treatment of A431 cells with 100 µM carmustine for 24 h, prior to treatment with 0.5 mM H_2O_2, did not affect cellular viability, or the percentage of cells in early apoptotic, late apoptotic or necrosis when compared to respective untreated controls cells in either [O_2] condition **(Figure 3.27 b i-iv)**. However, detection of cell death was functional as treatment with 1000 µM carmustine alone resulted in a decrease in viability, and an increase in early apoptotic, late apoptotic and necrotic cells in both [O_2] conditions when compared to respective untreated control cells ($P < 0.05$, **Figure 3.27 b i-iv**).

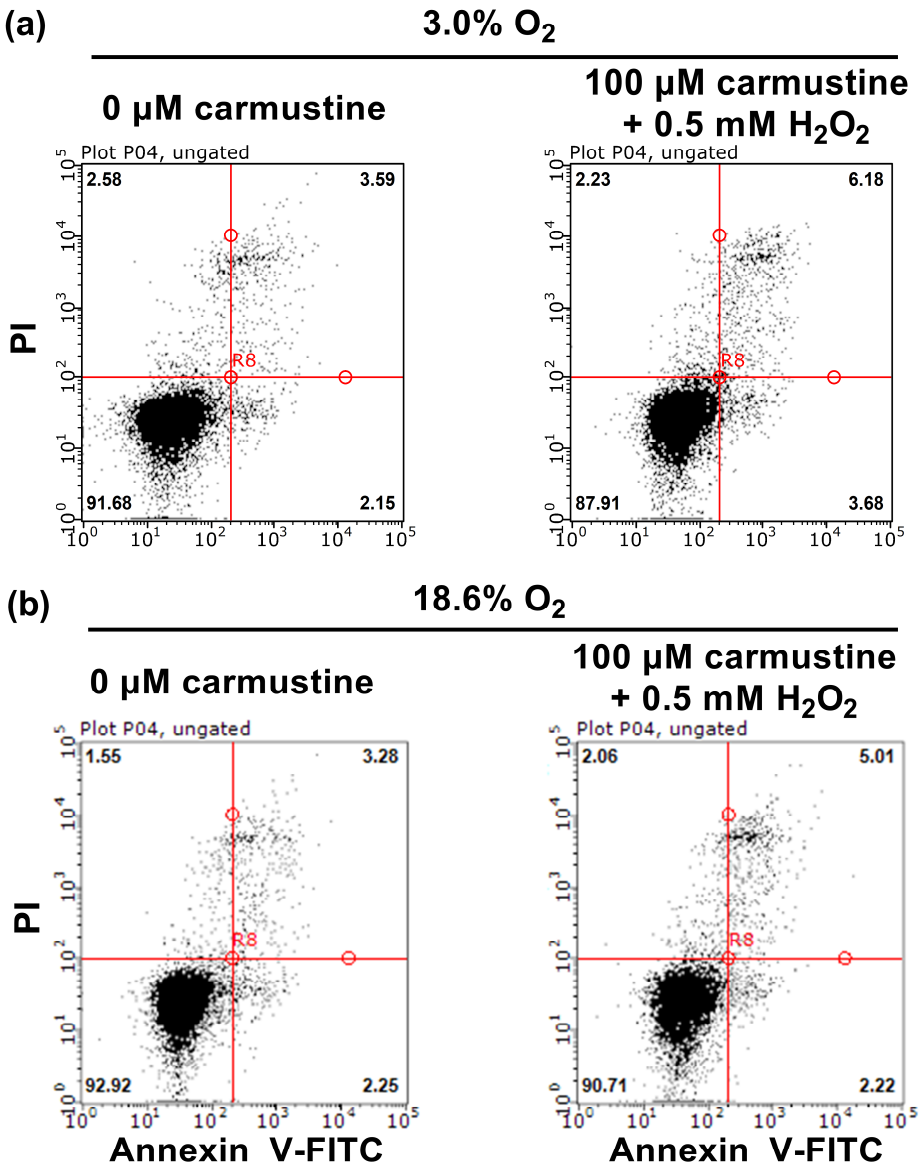

Figure 3.26. Representative dot plot histograms showing the effect of carmustine pre-treatment on H_2O_2-induced cell death in A431 cells grown in 18.6% O_2 or 3.0% O_2 for 96 h. A431 cells were grown in 18.6% or 3.0% O_2 for 96 h prior to treatment with vehicle (0.1% v/v DMSO) or 1–100 µM carmustine for 24 h. A431 cells were treated with 1000 µM carmustine for 1 h as a positive inducer of cell death. After 24 h, A431 cells were then treated with 0.5 mM H_2O_2 for an additional 1 h under the appropriate [O_2]. A431 cells were then stained with annexin V-FITC and PI. Cell death was then analysed by flow cytometry using the FL1 and FL3 detectors whilst excited by a 488 nm argon excitation laser (section 2.4). The 4-quadrant scatter plots represents 4 groups of differently stained cells: viable (unstained, bottom left), apoptotic (+AnnV/-PI, bottom right), late apoptotic (+AnnV/+PI, top right) and necrotic (-AnnV/+PI, top left). The two lines show the separation of the quadrants. The numbers in bold in each quadrant represent the percentage of cells in each respective stage of apoptosis or necrosis. **Panel (a),** dot plot histograms for carmustine-mediated sensitisation to H_2O_2-induced cell death in A431 cells previously grown in 3.0% O_2 for 96 h and subsequently stained with annexin V-FITC and PI. **Panel (b),** dot plot histograms for carmustine-mediated sensitisation to H_2O_2-induced cell death in A431 cells previously grown in 18.6% O_2 for 96 h and subsequently stained with annexin V-FITC and PI. **FITC:** fluorescein isothiocyanate**; PI:** propidium iodide.

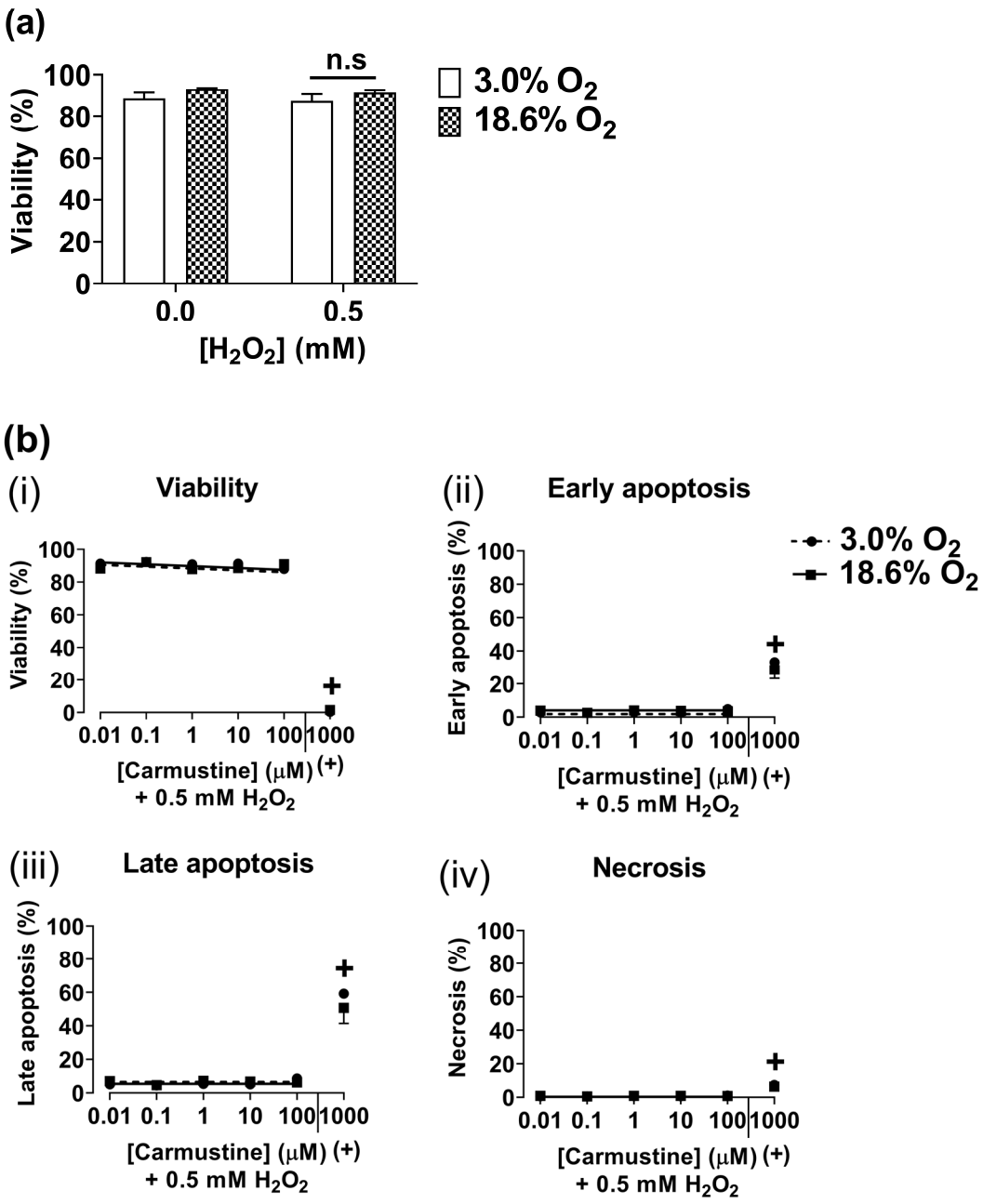

Figure 3.27. Effect of growing A431 cells in 18.6% O_2 on carmustine-mediated sensitisation to H_2O_2-induced cell death compared to A431 cells grown in 3.0% O_2 for 96 h. A431 cells were seeded at a density of 9.5 x 10^3 cells/cm^2 in 24 well plates and grown in 18.6% or 3.0% O_2 for 96 h (37°C / 5% CO_2). Growth medium was changed every 24 h with respective (18.6% or 3.0% O_2) [O_2]-equilibrated growth medium. After 96 h of growth, A431 cells were pre-treated with the indicated final concentrations of carmustine or 1000 μM carmustine alone (which served as a positive control (+) for cell death) for 24 h in 18.6% or 3.0% O_2 (37°C / 5% CO_2). After 24 h, A431 cells were then treated with 0.5 mM H_2O_2 for an additional 1 h in 18.6% or 3.0% O_2 (37°C / 5% CO_2). A431 cells were then detached, washed with PBS (see section 2.2.3 for concentration), and subsequently stained with annexin V-FITC and PI prior to cell death analysis by flow cytometry (section 2.4). **Panel (a),** viability of untreated or 0.5 mM H_2O_2-treated A431 cells. **Panel (b),** the effect of growing A431 cells in 18.6% O_2 or 3.0% O_2 for 96 h on carmustine-mediated sensitisation to H_2O_2-induced cell death with analysis of **(i)** viability, **(ii)** early apoptosis, **(iii)** late apoptosis, and **(iv)** necrosis. n.s = not significant versus 3.0% O_2, + = $P < 0.0001$ versus respective untreated control utilising a two-way ANOVA and a *post-hoc* multiple comparison test with Dunn-Šidák correction. Data are presented as the mean ± 1 SD. n=4. Where error bars are not visible, this is because the error bar is smaller than the size of the data point.

3.3.10. The effect of growing A431 cells in 18.6% O_2 on mitochondrial mass compared to A431 cells grown in 3.0% O_2

Mitochondria were imaged in A431 cells grown in 18.6% O_2 or 3.0% O_2 for 96 h using MitoTracker Red **(section 3.2.5)** in conjunction with fluorescence microscopy **(Figure 3.28)**. MitoTracker Red fluorescence was later quantified with flow cytometry **(section 3.3.11)**.

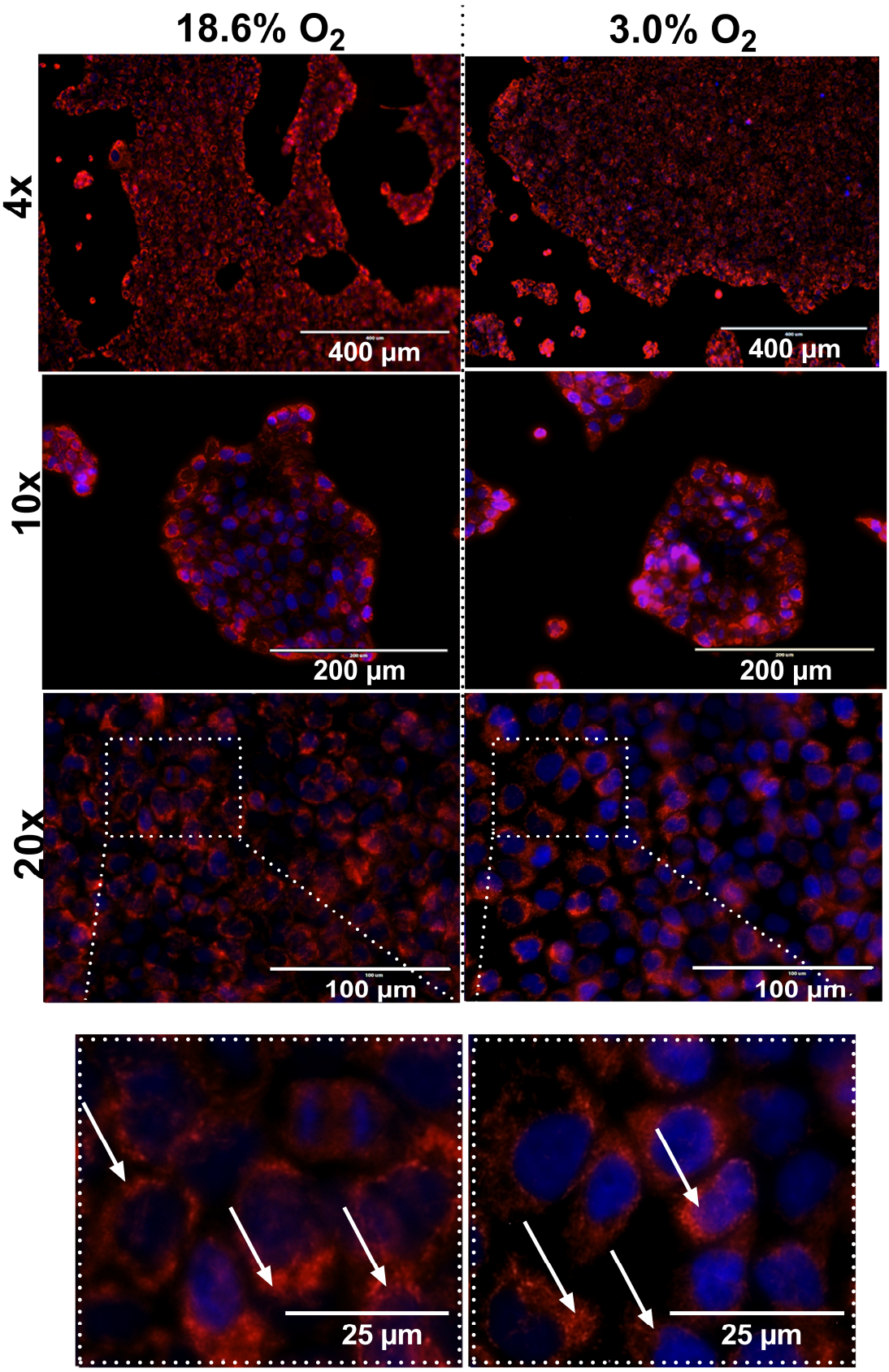
18.6% O2
3.0% O2
4x
10x
20x
400 µm
400 µm
200 µm
200 µm
100 µm
100 µm
25 µm
25 µm

Figure 3.28. Representative images of MitoTracker Red-stained A431 cells grown in 18.6% O_2 or 3.0% O_2 for 96 h. A431 cells were seeded at a density of 9.5 x 10^3 cells/cm^2 in tissue culture treated glass bottom chamber slides (#171080, Thermofisher). A431 cells were grown in 18.6% O_2 or 3.0% O_2 for 96 h (37°C /5% CO_2). A431 cells were fed every 24 h with fresh respective (18.6% or 3.0% O_2) [O_2]-equilibrated growth medium. After 96 h of growth, the growth medium was replaced with growth medium containing 2 µM Hoechst 33342 (from a stock solution made up in UH_2O; Sigma) and 1 µM MitoTracker Red (from a stock solution made up in DMSO; Thermofisher). The slides were left to stain for 15 min at 37°C /5% CO_2 at respective (18.6% or 3.0% O_2) [O_2]. After the staining period, A431 cells were washed three times with pre-warmed PBS (see section 2.2.3 for concentration) before pre-warmed DPBS (without phenol red) was added. To prevent re-oxygenation, the chamber slides were sealed by coating the outside edge of the plastic lid with an inert silicon grease and sealing with cellophane prior to removal from the physioxia hood. A431 cells were imaged at random fields of view using an EVOS™ live cell imaging microscope with an EVOS™ LED cube, v2, DAPI and EVOS™ LED cube, v2, Texas Red at x10, x20 and x40 magnification using slide cap-adjusted focusing. Images are presented as merged composites of the DAPI and Texas Red emission channels. The dashed boxes in the x40 images were enlarged manually into separate images below. The white arrows indicate possible instances of mitochondrial staining. Due to the low resolution of the acquired images at high magnification, these dots were hard to visualise in many of the individual cells. Manual sharpening of the image by +50% using image J was performed. In cases where image sharpening was performed, these manipulations were performed uniformly across all images.

3.3.11. Quantification of MitoTracker Red fluorescence in A431 cells grown in 18.6% and 3.0% O_2

The fluorescence of MitoTracker Red-stained A431 cells was quantified by flow cytometry **(section 3.2.6)**. Example fluorescence histograms are shown in **Figure 3.29 a.** A431 cells grown in 18.6% O_2 exhibited an apparent lower MitoTracker Red MFI compared to the MitoTracker Red MFI in A431 cells grown in 3.0% O_2 for 96 h. However, this apparent decrease in MFI was not statistically significant **(Figure 3.29 b).**

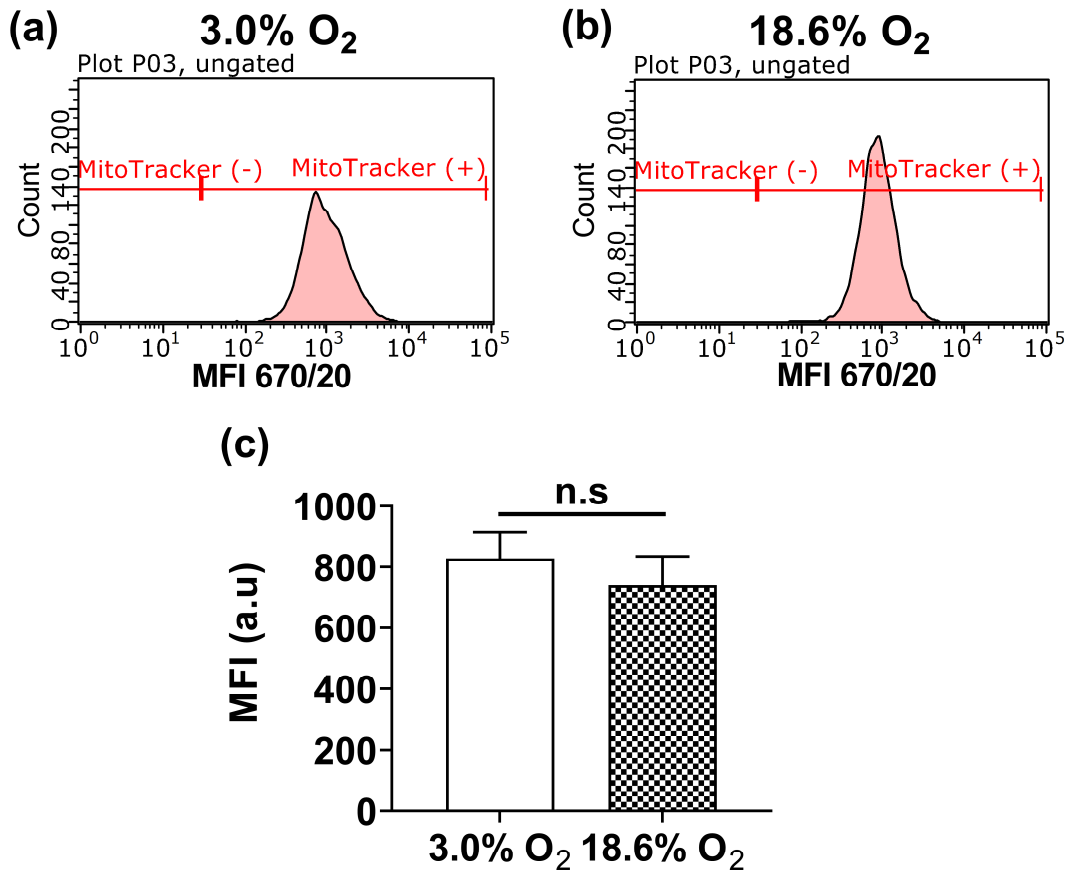

Figure 3.29. Quantification of MitoTracker Red fluorescence in A431 cells grown in 18.6% O_2 or 3.0% O_2 for 96 h. A431 cells stained with MitoTracker Red (Figure 3.28) were quantified for MitoTracker Red fluorescence utilising flow cytometry. A431 cells were stained with 1 µM MitoTracker Red for 1 h in respective (18.6% or 3.0% O_2) [O_2]-equilibrated growth medium. The cells were then detached with 0.25% (v/v) trypsin-EDTA, washed with PBS (see section 2.2.3 for concentration) and re-suspended in fresh PBS prior to measurement of MitoTracker Red fluorescence with flow cytometry whilst excited by a 488 nm argon laser. **Panel (a),** representative fluorescence histograms of MitoTracker Red-stained A431 cell grown in 3.0% O_2 (left) or 18.6% O_2 (right) for 96 h. **Panel (b),** representative fluorescence histograms of MitoTracker Red-stained A431 cell grown in 18.6% O_2 or 3.0% O_2 for 96 h. The y axis label (count) indicates the number of events (cells) detected at the respective MFI. **Panel (c),** quantitation of MitoTracker Red MFI from MitoTracker Red-stained A431 cells previously grown in 18.6% O_2 or 3.0% O_2 for 96 h. n.s = not significant versus 3.0% O_2 utilising a paired two-tailed Student's t-test. Data in panel (c) is presented as the mean ± 1 SD. n=3. Where error bars are not visible, this is because the error bar is smaller than the size of the data point. **a.u:** arbitrary units; **MFI:** mean fluorescence intensity; **MitoTracker (-/+):** MitoTracker Red negative or positive regions.

3.3.12. The effect of growing A431 cells in 18.6% O_2 on auranofin-induced changes to mitochondrial membrane potential compared to A431 cells grown in 3.0% O_2

Auranofin-induced $\Delta\psi_m$ was measured by JC-1 staining in conjunction with flow cytometry **(section 2.6)** in A431 cells grown in 18.6% O_2 or 3.0% O_2 for 96 h. Example JC-1 fluorescence histograms are shown in **Figure 3.30**

A two-way ANOVA was performed to analyse the effects of [auranofin], and the [O_2] cells were grown in, on $\Delta\psi_m$. A431 cells grown in 18.6% O_2 exhibited an apparent increase in basal ψ_m compared to A431 cells grown in 3.0% O_2 96 h. However, a *post-hoc* test showed that this apparent increase was not statistically significant (**Figure 3.31 a)**. Detection of $\Delta\psi_m$ was functional in both [O_2] conditions as treatment with 100 µM CCCP resulted in a statistically significant $\Delta\psi_m$ compared to respective untreated control cells in A431 cells grown in both [O_2] conditions **(Figure 3.31 a)**.

A *post-hoc* test showed that A431 cells grown in 18.6% O_2, and treated with 32 µM auranofin, exhibited attenuated auranofin-induced $\Delta\psi_m$ compared to A431 cells grown in 3.0% O_2 for 96 h under the same treatment conditions ($P < 0.0001$, **Figure 3.31 b**), with means of 41.8 ± 3.0 vs 126.6 ± 14.9, respectively. The interaction between the effects of [auranofin], and the [O_2] cells were grown in, on $\Delta\psi_m$ was statistically significant (F (7, 48) = 72.78, $P < 0.0001$).

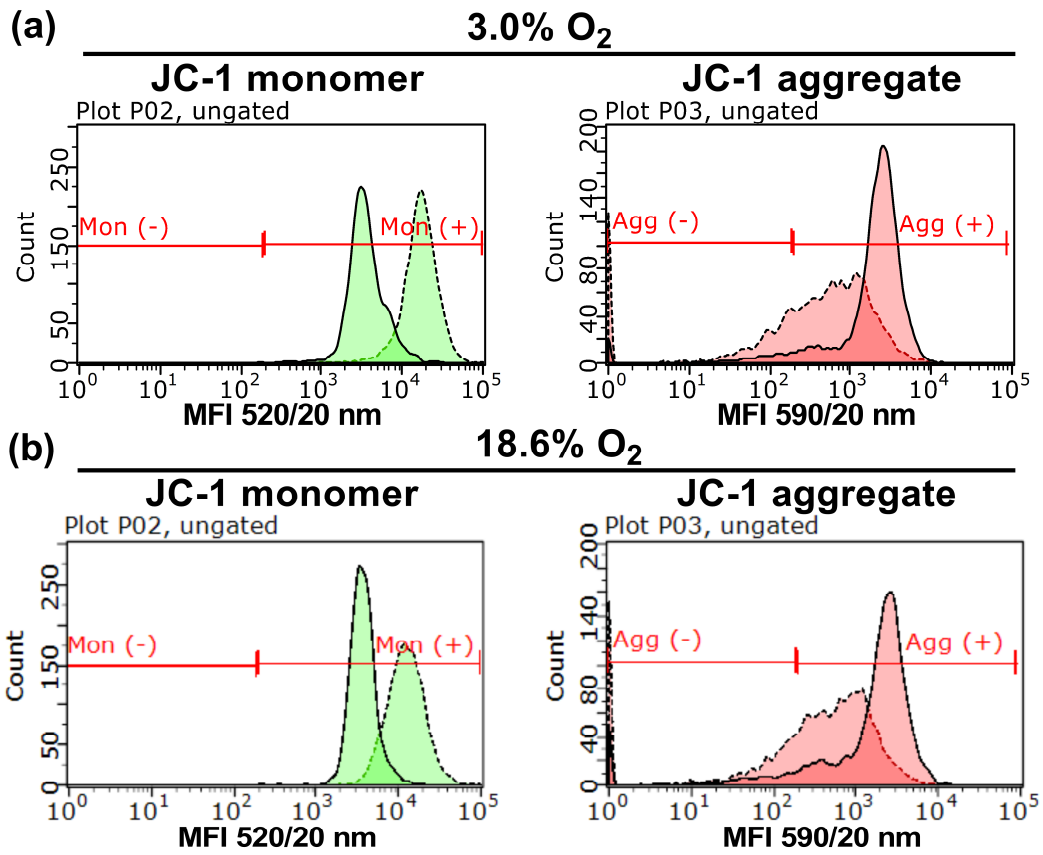

Figure 3.30. Representative JC-1 fluorescence histograms showing auranofin-induced changes to mitochondrial membrane potential in A431 cells grown in 18.6% O_2 or 3.0% O_2 for 96 h. A431 cells were grown in 18.6% or 3.0% O_2 for 96 h prior to treatment with vehicle (0.1% v/v DMSO) or 1–32 µM auranofin for 1 h. A431 cells were then stained with 2 µM JC-1. Δψm was then analysed by flow cytometry using the FL1 and FL2 detectors whilst excited by a 488 nm argon laser. **Panel (a),** representative fluorescence histograms of $\Delta\psi_m$ in A431 cells grown in 3.0% O_2 for 96 h treated with vehicle (0.1% v/v DMSO; solid trace) or 32 µM auranofin (dashed trace) and subsequently stained with JC-1. **Panel (b),** representative fluorescence histograms of $\Delta\psi_m$ in A431 cells grown in 18.6% O_2 for 96 h treated with vehicle (0.1% v/v DMSO; solid trace) or 32 µM auranofin (dashed trace) and subsequently stained with JC-1. The y axis label (count) indicates the number of events (cells) detected at the respective MFI. **ψm:** mitochondrial membrane potential; **Agg (-/+):** JC-1 aggregate negative or positive regions; **MFI:** mean fluorescence intensity; **Mon (-/+):** JC-1 monomer negative or positive regions.

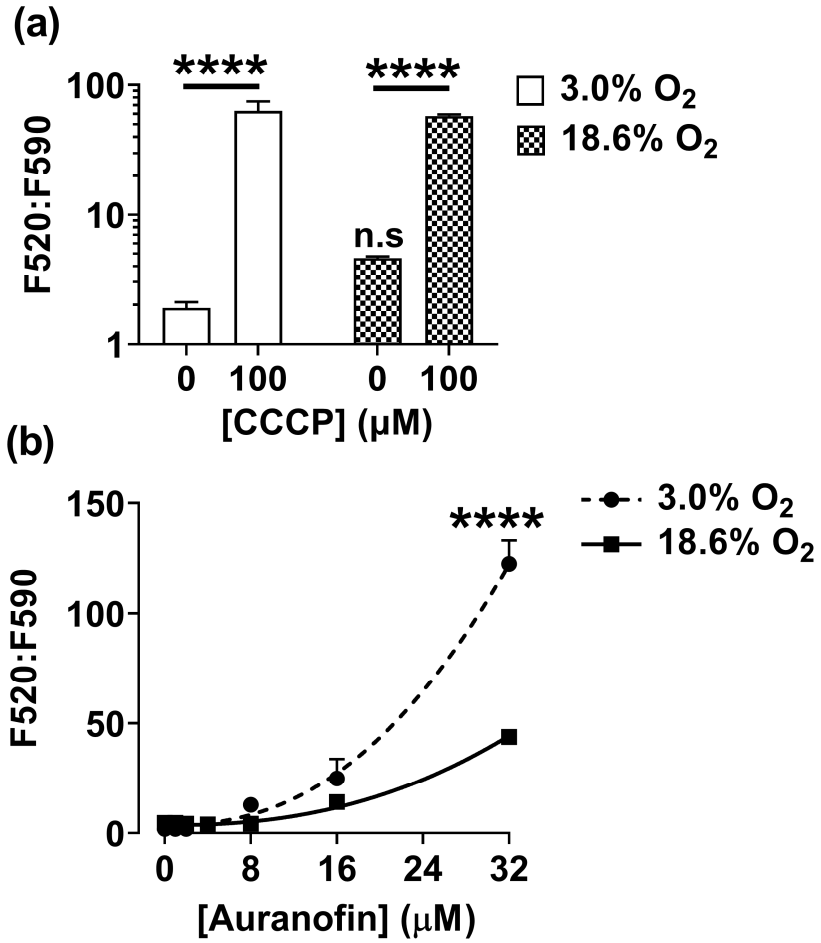

Figure 3.31. The effect of growing A431 cells in 18.6% O_2 on auranofin-induced changes to mitochondrial membrane potential compared to A431 cells grown in 3.0% O_2 for 96 h. A431 cells were seeded at a density of 9.5 x 10^3 cells/cm^2 in 24 well plates and grown in 18.6% O_2 or 3.0% O_2 for 96 h (37°C / 5% CO_2). Growth medium was changed every 24 h with respective (18.6% or 3.0% O_2) [O_2]-equilibrated growth medium. After 96 h of growth, A431 cells were treated with vehicle (0.1% v/v DMSO) or 1-32 µM auranofin for 1 h in 18.6% or 3.0% O_2 (37°C / 5% CO_2). A431 cells were also treated with 100 µM CCCP for 1 h which served as a positive control. Under low light, A431 cells were stained with 2 µM JC-1 for 1 h in 18.6% or 3.0% O_2 (37°C/5% CO_2). A431 cells were then detached, washed with PBS (see section 2.2.3 for concentration), and the MFI of the JC-1 monomer and aggregate were analysed by flow cytometry using the FL1 and FL2 detectors whilst excited by a 488 nm argon laser. **Panel (a),** $\Delta\psi_m$ in untreated A431 cells and A431 cells treated with 100 µM CCCP for 1 h. **Panel (b),** auranofin-induced $\Delta\psi_m$ in A431 cells previously grown in 18.6% or 3.0% O_2 for 96 h. The F520: F590 units were calculated by dividing the Mon (+) green fluorescent signal detected by the FL-1 channel by the Agg (+) red signal detected by the FL-2 channel. n.s = not significant versus 3.0% O_2 untreated control, **** = $P < 0.0001$ versus respective untreated controls in panel (a) and versus 18.6% O_2 in panel (b) utilising a two-way ANOVA and a *post-hoc* multiple comparison test with Dunn-Šidák correction. Data are presented as the mean ± 1 SD. n=4. Where error bars are not visible, this is because the error bar is smaller than the size of the data point. **Agg (-/+):** JC-1 aggregate negative or positive regions; **CCCP:** carbonyl cyanide *m*-chlorophenyl hydrazine; **F520:F590:** mean fluorescence intensity ratio of the emission light at wavelength 520 nm to the emission light at 590 nm when both excited at 488 nm; **MFI:** mean fluorescence intensity; **Mon (-/+):** JC-1 monomer negative or positive regions.

3.3.13. The effect of growing A431 cells in 18.6% O_2 on carmustine-induced changes to mitochondrial membrane potential compared to A431 cells grown in 3.0% O_2

Carmustine-induced Δψm was measured by JC-1 staining in conjunction with flow cytometry **(section 2.6)** in A431 cells grown in 18.6% O_2 or 3.0% O_2 for 96 h. Example JC-1 fluorescence histograms are shown in **Figure 3.32**.

A two-way ANOVA was performed to analyse the effects of [carmustine], and the [O_2] cells were grown in, on Δψm. JC-1 detection of $\Delta\psi_m$ was functional as treatment with 100 µM CCCP resulted in $\Delta\psi_m$ in both [O_2] groups when compared to respective untreated control cells ($P < 0.0001$, **Figure 3.33 a**). A *post-hoc* test showed that untreated A431 cells grown in 18.6% O_2 exhibited apparent increase in ψm compared to untreated A431 cells grown in 3.0% O_2 96 h. However, a *post-hoc* test showed that this apparent increase was not statistically significant (**Figure 3.33 a**). A431 cells grown in 18.6% O_2, and treated with 500 µM carmustine, exhibited decreased carmustine-induced $\Delta\psi_m$ compared to A431 cells grown in 3.0% O_2 for 96 h under the same treatment conditions ($P < 0.0001$, **Figure 3.33 b)**, with means of 3.2 ± 2.1 vs 11.5 ± 4.7. The interaction between the effects of [carmustine], and the [O_2] cells were grown in, on $\Delta\psi_m$ was statistically significant $F(6, 42) = 4.446$, $P = 0.0014$.

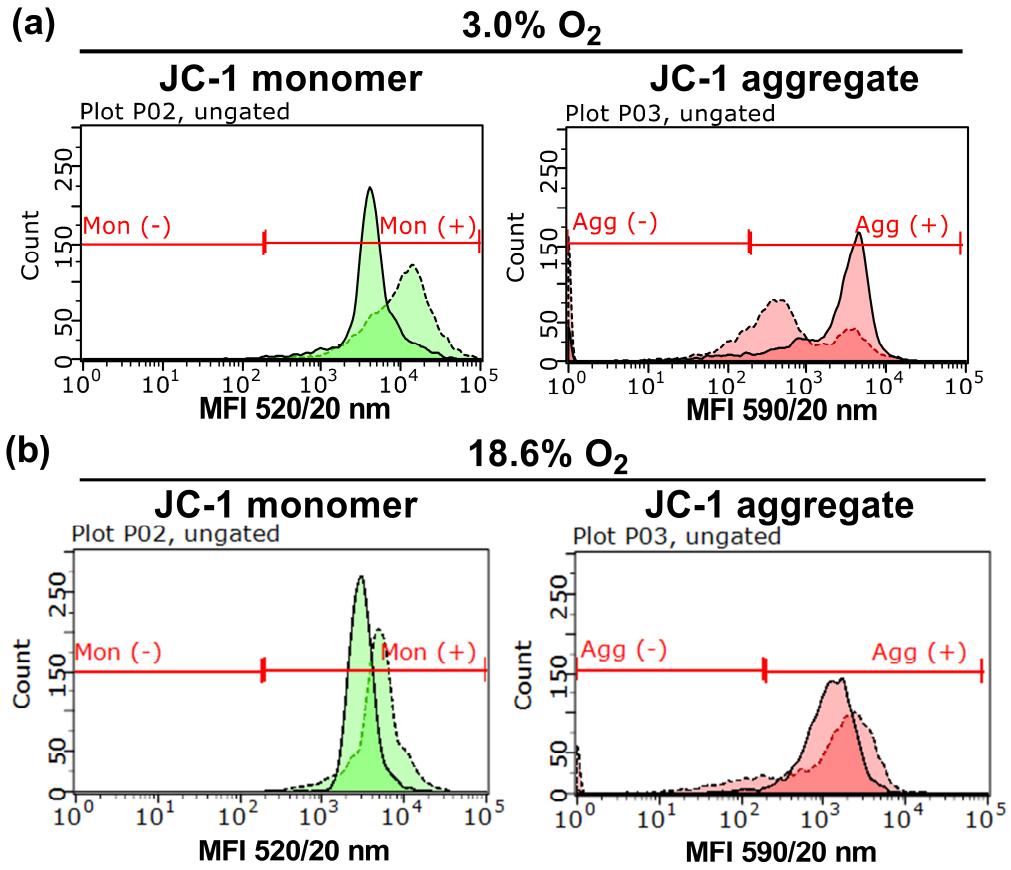

Figure 3.32. Representative JC-1 fluorescence histograms showing carmustine-induced changes to mitochondrial membrane potential in A431 cells grown in 18.6% O_2 or 3.0% O_2 for 96 h. A431 cells were grown in 18.6% O_2 or 3.0% O_2 for 96 h (37.0°C/5.0% CO_2). These cells were then treated with vehicle (0.1% v/v DMSO) or 100-700 µM carmustine for 1 h. A431 cells were then stained with 2 µM JC-1 for 1 h in 18.6% or 3.0% O_2 (37°C/5% CO_2). $\Delta\psi_m$ was subsequently analysed by flow cytometry using the FL1 and FL2 detectors whilst excited by a 488 nm argon laser. **Panel (a),** representative fluorescence histograms of $\Delta\psi_m$ in A431 cells previously grown in 3.0% O_2 for 96 h, treated with vehicle (0.1% v/v DMSO; solid trace) or 500 µM carmustine (dashed trace) and subsequently stained with JC-1. **Panel (b),** representative fluorescence histograms of $\Delta\psi_m$ in A431 cells previously grown in 18.6% O_2 for 96 h, treated with vehicle (0.1% v/v DMSO; solid trace) or 500 µM carmustine (dashed trace) and subsequently stained with JC-1. The y axis label (count) indicates the number of events (cells) detected at the respective MFI. **Ψm:** mitochondrial membrane potential; **Agg (-/+):** JC-1 aggregate negative or positive regions; **MFI:** mean fluorescence intensity; **Mon (-/+):** JC-1 monomer negative or positive regions.

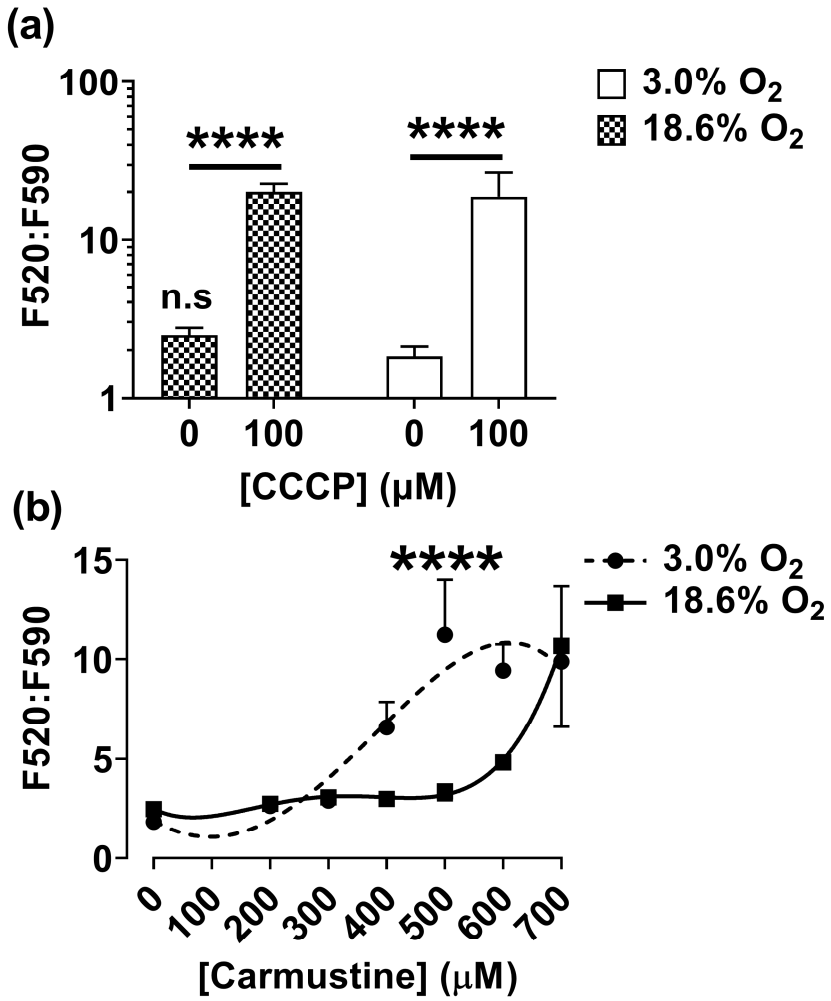

Figure 3.33. The effect of growing A431 cells in 18.6% O_2 on carmustine-induced changes to mitochondrial membrane potential compared to A431 cells grown in 3.0% O_2 for 96 h. A431 cells were seeded at a density of 9.5 x 10^3 cells/cm^2 in 24 well plates and grown in 18.6% O_2 or 3.0% O_2 for 96 h (37°C / 5% CO_2). Growth medium was changed every 24 h with respective (18.6% or 3.0% O_2) [O_2]-equilibrated growth medium. After 96 h of growth, A431 cells were treated with vehicle (0.1% v/v DMSO) or 100–700 µM carmustine for 1 h in 18.6% or 3.0% O_2 (37°C / 5% CO_2). A431 cells were also treated with 100 µM CCCP for 1 h which served as a positive control for $\Delta\psi_m$. Under low light, cells were stained with 2 µM JC-1 for 1 h in 18.6% or 3.0% O_2 (37°C/5% CO_2). A431 cells were then detached, washed with PBS (see section 2.2.3 for concentration), and JC-1 fluorescence was analysed by flow cytometry utilising the FL1 and FL3 detectors whilst excited by a 488 nm argon laser. **Panel (a),** $\Delta\psi_m$ in untreated A431 cells and A431 cells treated with 100 µM CCCP for 1 h. **Panel (b),** carmustine-induced $\Delta\psi_m$ in A431 cells previously grown in 18.6% or 3.0% O_2 for 96 h. F520:F590 was calculated by dividing the JC-1 Mon (+) green MFI detected using the FL-1 channel by the JC-1 Agg (+) red signal detected using the FL-2 channel. n.s = not significant versus 3.0% O_2 untreated control, **** = $P < 0.0001$ versus untreated control in panel (a) and versus 18.6% O_2 in panel (b) utilising a two-way ANOVA and a *post-hoc* multiple comparison test with Dunn-Šidák correction. Data are presented as the mean ± 1 SD. n=4. Where error bars are not visible, this is because the error bar is smaller than the size of the data point. **Agg (-/+):** JC-1 aggregate negative or positive regions; **CCCP:** carbonyl cyanide *m*-chlorophenyl hydrazine; **F520:F590:** mean fluorescence intensity ratio of the emission light at wavelength 520 nm to the emission light at 590 nm when both excited at 488 nm; **MFI:** mean fluorescence intensity; **Mon (-/+):** JC-1 monomer negative or positive regions.

3.3.14. The effect of growing A431 cells in 18.6% O_2 on auranofin-induced lipid peroxidation compared to A431 cells grown in 3.0% O_2

Auranofin-induced lipid peroxidation was measured by C_{11} BODIPY$^{581/591}$ staining in conjunction with flow cytometry **(section 2.7)** in A431 cells grown in 18.6% O_2 or 3.0% O_2 for 96 h. Example C_{11} BODIPY$^{581/591}$ fluorescence histograms are shown in **Figure 3.34.**

A two-way ANOVA was performed to analyse the effects of [auranofin], and the [O_2] cells were grown in, on lipid peroxidation. C_{11} BODIPY$^{581/591}$ detection of lipid peroxidation was functional, as CuOOH treatment induced lipid peroxidation in both [O_2] groups compared to respective untreated control cells ($P < 0.0001$ **Figure 3.35 a**) Treatment with 32 µM auranofin resulted in a statistically significant increase in lipid peroxidation in both A431 cells grown in 18.6% or 3.0% O_2 for 96 h when compared to respective untreated controls ($P < 0.0001$, **Figure 3.35 b**), with means of 0.03 ± 0.001 vs 0.1 ± 0.01 and 0.04 ± 0.002 vs 0.1 ± 0.004, respectively. However, a *post-hoc* test showed that there was no statistically significant difference when comparing auranofin-induced lipid peroxidation when comparing A431 cells grown in 18.6% O_2 to A431 cells grown in 3.0% O_2 for 96 h at any treatment concentration **(Figure 3.35 b)**.

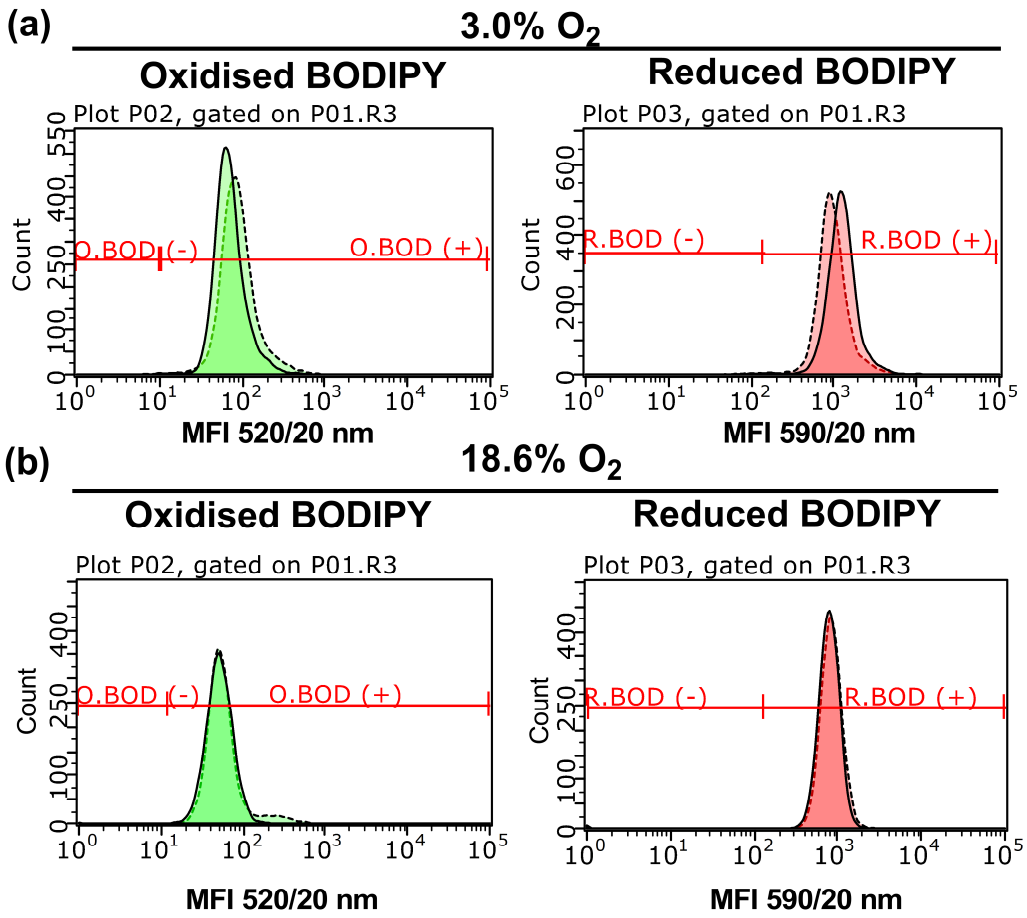

Figure 3.34. Representative C_{11} BODIPY$^{581/591}$ fluorescence histograms showing auranofin-induced lipid peroxidation in A431 cells grown in 18.6% O_2 or 3.0% O_2 for 96 h. A431 cells were grown in 18.6% or 3.0% O_2 for 96 h and were then treated with vehicle (0.1% v/v DMSO) or 1-32 µM auranofin for 1 h. A431 cells were then stained with C_{11} BODIPY$^{581/591}$. Lipid peroxidation was then analysed by flow cytometry using the FL1 and FL2 detectors whilst excited by a 488 nm argon laser. **Panel (a),** representative C_{11} BODIPY$^{581/591}$ fluorescence histograms of A431 cells previously grown in 3.0% O_2 for 96 h, treated with vehicle (0.1% v/v DMSO; solid trace) or 32 µM auranofin (dashed trace), and subsequently stained with C_{11} BODIPY$^{581/591}$. **Panel (b),** representative C_{11} BODIPY$^{581/591}$ fluorescence histograms of A431 cells previously grown in 18.6% O_2 for 96 h, treated with vehicle (0.1% v/v DMSO; solid trace) or 32 µM auranofin (dashed trace), and subsequently stained with C_{11} BODIPY$^{581/591}$. The y axis label (count) indicates the number of events (cells) detected at the respective MFI. **MFI:** mean fluorescence intensity; **O.BOD (-/+):** oxidised BODIPY negative and positive regions; **R.BOD (-/+):** reduced BODIPY negative and positive regions.

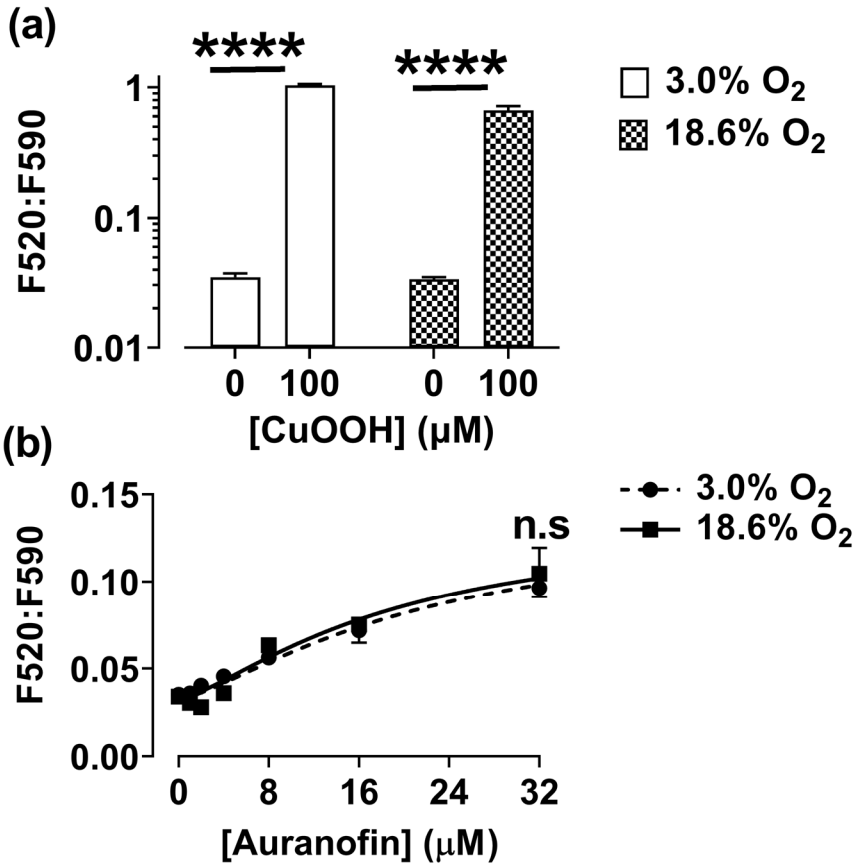

Figure 3.35. The effect of growing A431 cells in 18.6% O_2 on auranofin-induced lipid peroxidation compared to A431 cells grown in 3.0% O_2 for 96 h. A431 cells were seeded at a density of 9.5 x 10^3 cells/cm^2 in 24 well plates and grown in either 3.0% O_2 or 18.6% O_2 for 96 h (37°C / 5% CO_2). Growth medium was changed every 24 h with respective (18.6% or 3.0% O_2) [O_2]-equilibrated growth medium. After 96 h of growth, A431 cells were treated with vehicle (0.1% v/v DMSO) or 1–32 μM auranofin for 1 h in 18.6% or 3.0% O_2 (37°C / 5% CO_2). Under low light, A431 cells were stained with 2 μM C_{11} BODIPY$^{581/591}$ for an additional 1 h in 18.6% or 3.0% O_2 (37°C / 5% CO_2). A431 cells were then detached, washed with PBS (see section 2.2.3 for concentration), and C_{11} BODIPY$^{581/591}$ fluorescence was measured by flow cytometry (section 2.7). **Panel (a),** lipid peroxidation in untreated A431 cells and A431 cells treated with 100 μM CuOOH. **Panel (b),** auranofin-induced lipid peroxidation in A431 cells previously grown in 18.6% O_2 or 3.0% O_2 for 96 h. F520:F590 was calculated by dividing the O.BOD (+) red MFI detected using the FL-1 channel by the R.BOD (+) red MFI detected using the FL-2 channel. n.s = not significant versus 3.0% O_2, **** = P < 0.0001 versus respective untreated control utilising a two-way ANOVA and a *post-hoc* multiple comparison test with Dunn–Šidák correction. Data are presented as the mean ± 1 SD. n=4. Where error bars are not visible, this is because the error bar is smaller than the size of the data point. **CuOOH:** cumene hydroperoxide; **F520:F590:** mean fluorescence intensity ratio of the emission light at wavelength 520 nm to the emission light at 590 nm when both excited at 488 nm; **O.BOD (-/+):** oxidised BODIPY negative and positive regions; **R.BOD (-/+):** reduced BODIPY negative and positive regions.

3.3.15. The effect of growing A431 cells in 18.6% O_2 on H_2O_2-induced lipid peroxidation compared to A431 cells grown in 3.0% O_2

H_2O_2-induced lipid peroxidation was measured by C_{11} BODIPY$^{581/591}$ staining in conjunction with flow cytometry **(section 2.7)** in A431 cells grown in 18.6% O_2 or 3.0% O_2 for 96 h. Example C_{11} BODIPY$^{581/591}$ fluorescence histograms are shown in **Figure 3.36**.

A two-way ANOVA was performed to analyse the effects of [H_2O_2], and the [O_2] cells were grown in, on lipid peroxidation. Detection of lipid peroxidation with C_{11} BODIPY was functional however as treatment with 100 µM CuOOH resulted in an increase in lipid peroxidation in both [O_2] groups compared to respective untreated control cells ($P < 0.0001$, **Figure 3.37 a**). A *post-hoc* analysis showed that A431 cells grown in 18.6%, treated with 0.75 mM H_2O_2, exhibited a decrease in lipid peroxidation compared to A431 cells grown in 3.0% O_2 under the same treatment conditions ($P < 0.0001$, **Figure 3.37 b**), with means of 0.06 ± 0.01 vs 0.12 ± 0.002, respectively.

The interaction between the effects of [H_2O_2], and the [O_2] cells were grown in, on lipid peroxidation was statistically significant ($F (7, 48) = 21.35$, $P<0.0001$).

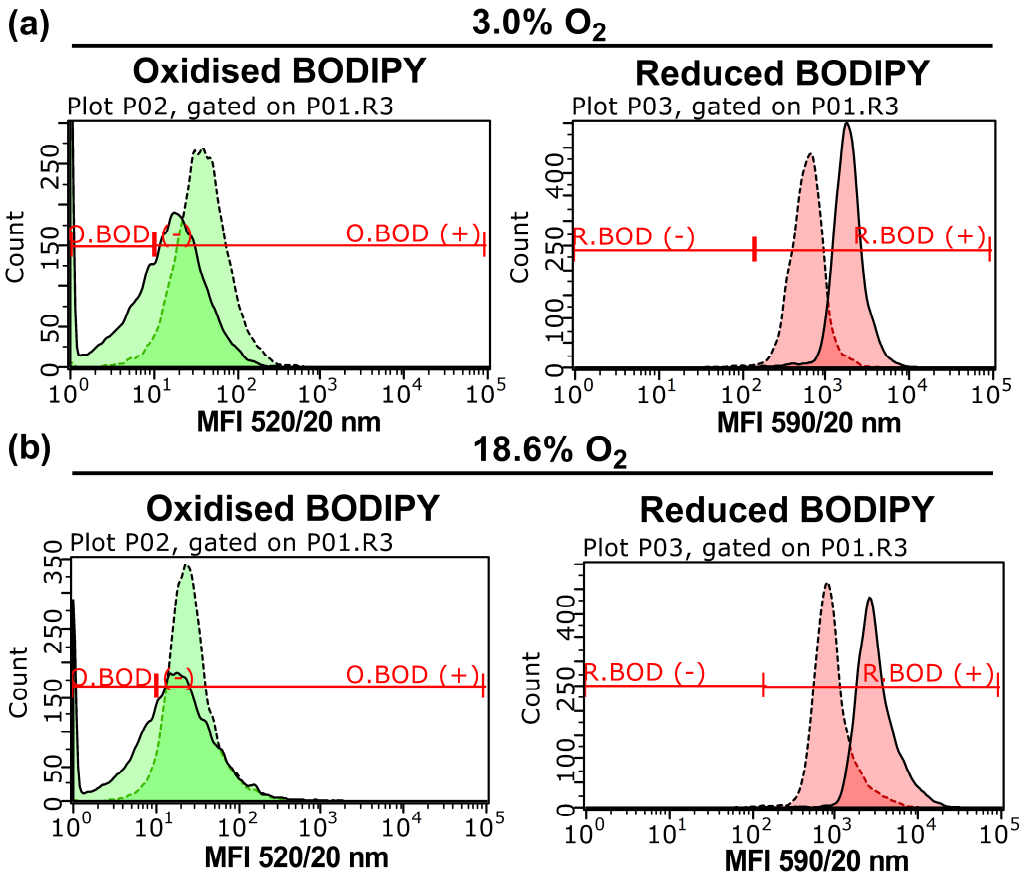

Figure 3.36. Representative C_{11} BODIPY$^{581/591}$ fluorescence histograms showing H_2O_2-induced lipid peroxidation in A431 cells grown in 18.6% O_2 or 3.0% O_2 for 96 h. A431 cells were grown in 18.6% O_2 or 3.0% O_2 for 96 h prior to treatment with vehicle (0.1% v/v UH_2O) or 0.5-2 mM H_2O_2 for 1 h under the appropriate [O_2]. A431 cells were then stained with 2 µM C_{11} BODIPY$^{581/591}$ for 1 h (37 °C/ 5% CO_2). Lipid peroxidation was then analysed by flow cytometry using the FL1 and FL2 detectors whilst excited by a 488 nm argon laser. **Panel (a),** representative C_{11} BODIPY$^{581/591}$ fluorescence histograms of A431 cells previously grown in 3.0% O_2 for 96 h, treated with vehicle (0.1% v/v H_2O; solid trace) or 0.75 mM H_2O_2 (dashed trace), and stained with C_{11} BODIPY$^{581/591}$. **Panel (b),** representative C_{11} BODIPY$^{581/591}$ fluorescence histograms of A431 cells previously grown in 18.6% O_2 for 96 h, treated with vehicle (0.1% v/v UH_2O; solid trace) or 0.75 mM H_2O_2 (dashed trace), and stained with C_{11} BODIPY$^{581/591}$. The y axis label (count) indicates the number of events (cells) detected at the respective MFI. **MFI:** mean fluorescence intensity; **O.BOD (-/+):** oxidised BODIPY negative and positive regions; **R.BOD (-/+):** reduced BODIPY negative and positive regions.

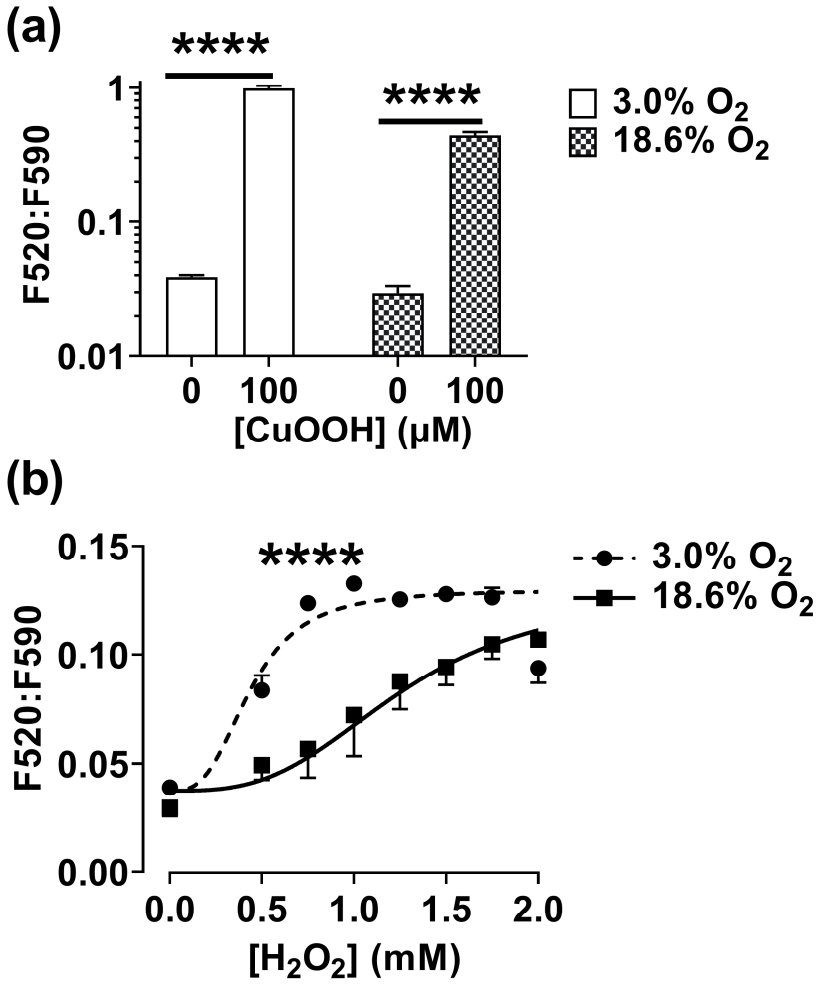

Figure 3.37. The effect of growing A431 cells in 18.6% O_2 on H_2O_2-induced lipid peroxidation compared to A431 cells grown in 3.0% O_2 for 96 h. A431 cells were seeded at a density of 9.5 x 10^3 cells/cm^2 in 24 well plates and grown in 18.6% O_2 or 3.0% O_2 for 96 h (37°C / 5% CO_2). Growth medium was changed every 24 h with respective (18.6% or 3.0% O_2) [O_2]-equilibrated growth medium. After 96 h, cells were treated with vehicle (0.1% v/v UH_2O) or 0.5-2 mM H_2O_2 for 1 h in 18.6% or 3.0% O_2 (37°C / 5% CO_2). A431 cells were treated with 100 µM CuOOH for 1 h as a positive control for lipid peroxidation. Under low light, cells were stained with 2 µM C_{11} BODIPY$^{581/591}$ for an additional 1 h in 18.6% or 3.0% O_2 (37°C/5% CO_2). A431 cells were then detached, washed with PBS (see section 2.2.3 for concentration), and lipid peroxidation was measured by C_{11} BODIPY$^{581/591}$ fluorescence in conjunction with flow cytometry (section 2.7). **Panel (a),** lipid peroxidation in untreated A431 cells and A431 cells treated with 100 µM CuOOH for 1 h. **Panel (b),** H_2O_2-induced lipid peroxidation in A431 cells previously grown in 18.6% or 3.0% O_2 for 96 h. F520:F590 was calculated by dividing the O.BOD (+) green fluorescent signal detected using the FL-1 channel by the R.BOD (+) red signal detected using the FL-2 channel. **** = $P < 0.0001$ versus untreated control in panel (a) and versus 18.6% O_2 in panel (b) utilising a two-way ANOVA and a *post-hoc* multiple comparison test with Dunn–Šidák correction. Data are presented as the mean ± 1 SD. n=4. Where error bars are not visible, this is because the error bar is smaller than the size of the data point. **CuOOH:** cumene hydroperoxide; **F520:F590:** mean fluorescence intensity ratio of the emission light at wavelength 520 nm to the emission light at 590 nm when both excited at 488 nm; **MFI:** mean fluorescence intensity; **O.BOD (-/+):** oxidised BODIPY negative and positive regions; **R.BOD (-/+):** reduced BODIPY negative and positive regions.

3.3.16. The effect of growing A431 cells in 18.6% O_2 on cumene hydroperoxide-induced lipid peroxidation compared to A431 cells grown in 3.0%

CuOOH-induced lipid peroxidation was measured in A431 cells grown in 18.6% O_2 or 3.0% O_2 for 24 or 96 h using C_{11} BODIPY$^{581/591}$ staining in conjunction with flow cytometry **(section 2.7)**. Example C_{11} BODIPY$^{581/591}$ fluorescence histograms are shown in **Figure 3.38**.

A two-way ANOVA was performed to analyse the effects of [CuOOH], and the [O_2] cells were grown in, on lipid peroxidation. A *post-hoc* analysis showed no statistically significant difference in lipid peroxidation when comparing the untreated controls of both [O_2] groups **(Figure 3.39 a)**. However, A431 cells grown in 18.6% O_2, and treated with 200 µM CuOOH, showed a decrease in lipid peroxidation compared to A431 cells grown in 3.0% O_2 for 24 h and 96 h under the same treatment conditions ($P < 0.0001$, **Figure 3.39 b**), with means of 0.7 ± 0.02 vs 1.0 ± 0.1 and 0.7 ± 0.02 vs 1.2 ± 0.03, respectively.

Additionally, A431 cells grown in 3.0% O_2 for 96 h exhibited an increase in lipid peroxidation when treated with 200 µM CuOOH compared to A431 cells grown in 3.0% O_2 for 24 h under the same treatment conditions ($P < 0.05$, **Figure 3.39 b**), with means of 1.2 ± 0.03 vs 1.0 ± 0.1, respectively. The interaction between the effects of [CuOOH], and the [O_2] cells were grown in, on lipid peroxidation was statistically significant (F (12, 63) = 40.03, $P < 0.0001$).

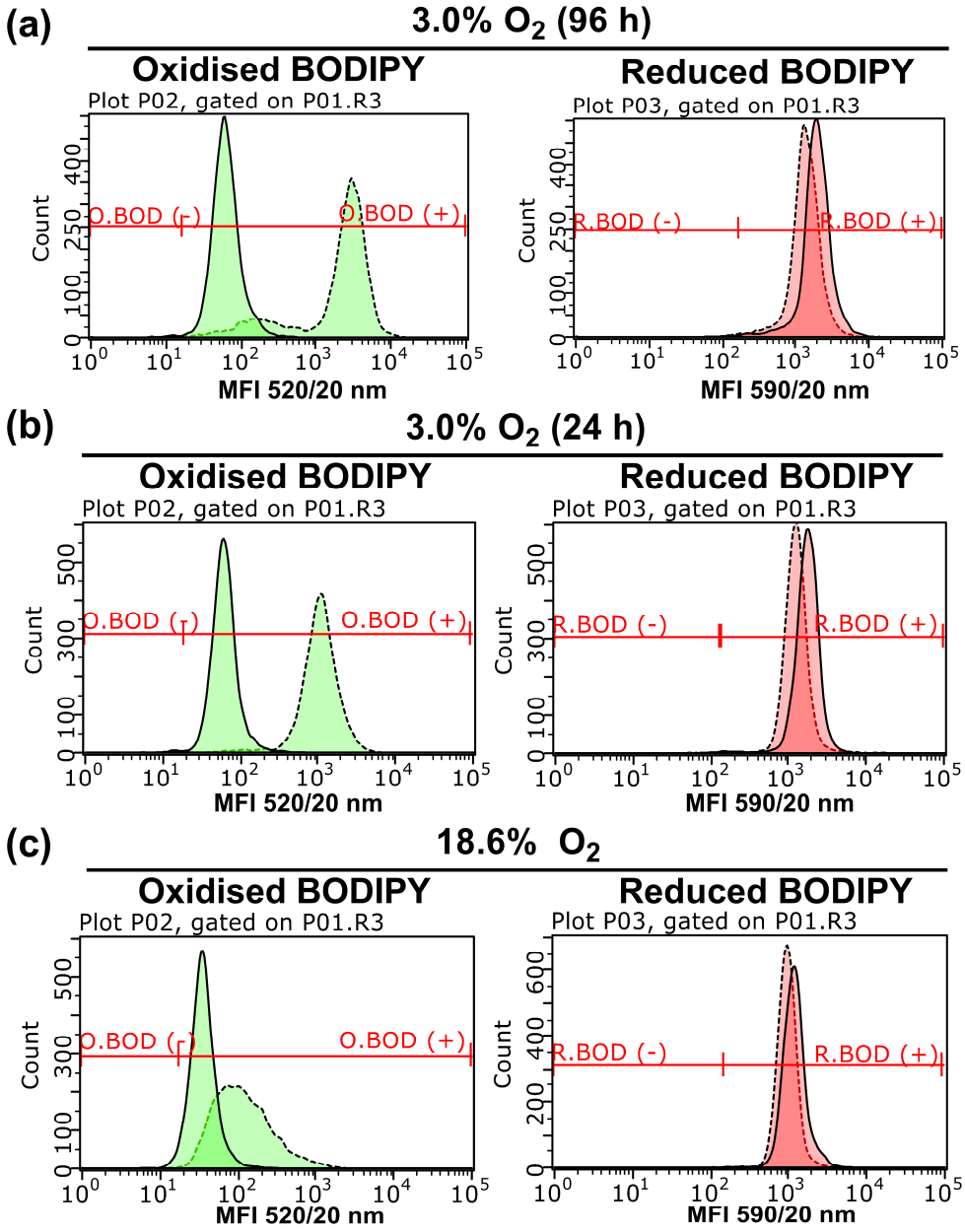

Figure 3.38. Representative C_{11} BODIPY$^{581/591}$ fluorescence histograms showing cumene hydroperoxide-induced lipid peroxidation in A431 cells grown in 18.6% O_2 or 3.0% O_2 for 96 h. A431 cells were grown in 18.6% O_2 or 3.0% O_2 for 24 h or 96 h prior to treatment with vehicle (0.1% v/v DMSO) or 6–200 µM CuOOH for 1 h under the appropriate [O_2]. A431 cells were then stained with 2 µM C_{11} BODIPY$^{581/591}$ for 1 h (37 °C/ 5% CO_2). Lipid peroxidation was then analysed by flow cytometry using the FL1 and FL2 detectors whilst excited by a 488 nm argon laser. **Panel (a),** representative C_{11} BODIPY$^{581/591}$ fluorescence histograms of A431 cells grown in 3.0% O_2 for 96 h treated with vehicle (0.1% v/v DMSO; solid trace) or 100 µM CuOOH (dashed trace), and stained with C_{11} BODIPY$^{581/591}$. **Panel (b),** representative C_{11} BODIPY$^{581/591}$ fluorescence histograms of A431 cells grown in 3.0% O_2 for 24 h, treated with vehicle (0.1% v/v DMSO; solid trace) or 100 µM CuOOH (dashed trace), and stained with C_{11} BODIPY$^{581/591}$. **Panel (c),** Representative C_{11} BODIPY$^{581/591}$ fluorescence histograms of A431 cells grown in 18.6% O_2 for 96 h, treated with vehicle (0.1% v/v DMSO; solid trace) or 100 µM CuOOH (dashed trace), and stained with C_{11} BODIPY$^{581/591}$. The y axis label (count) indicates the number of events (cells) detected at the respective MFI. **CuOOH:** cumene hydroperoxide; **MFI:** mean fluorescence intensity; **O.BOD (-/+):** oxidised BODIPY negative and positive regions; **R.BOD (-/+):** reduced BODIPY negative and positive regions.

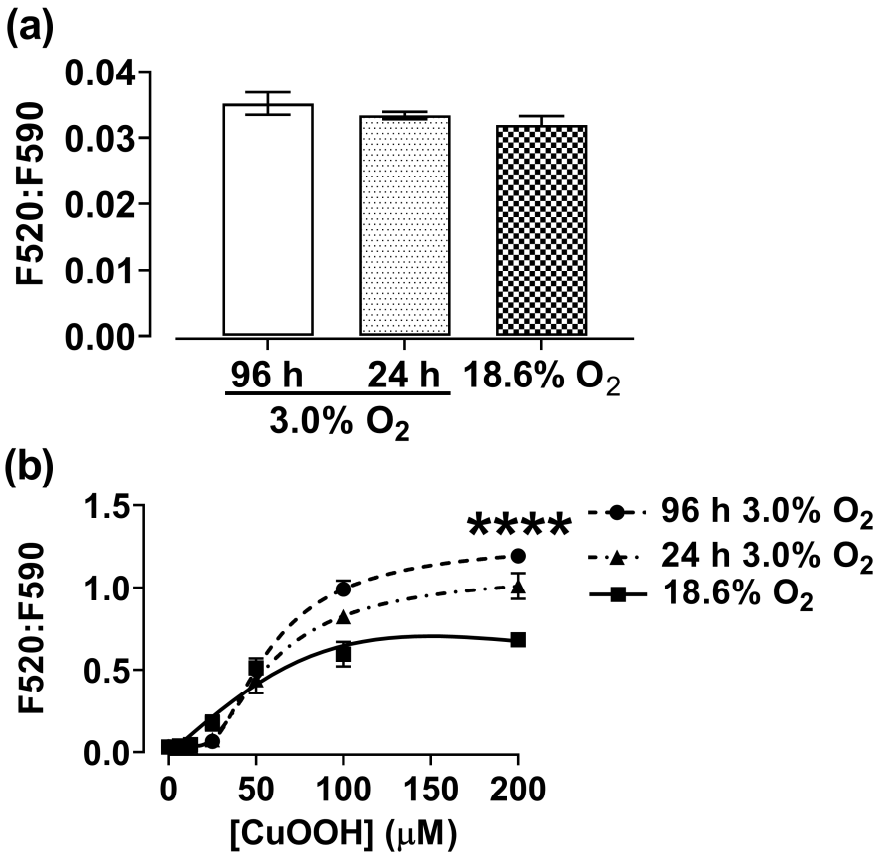

Figure 3.39. The effect of growing A431 cells in 18.6% O_2 on cumene hydroperoxide-induced lipid peroxidation compared to A431 cells grown in 3.0% O_2 for 96 h. A431 cells were seeded at a density of 9.5 x 10^3 cells/cm^2 in 24 well plates and grown in either 18.6% O_2 or 3.0% O_2 for 24 or 96 h (37°C / 5% CO_2). Growth medium was changed every 24 h with respective (18.6% or 3.0% O_2) [O_2]-equilibrated growth medium. After 96 h, A431 cells were treated with 6–200 µM CuOOH, or vehicle (0.1% v/v DMSO) for 24 h in 18.6% or 3.0% O_2 (37°C / 5% CO_2). Under low light, cells were stained with 2 µM C_{11} BODIPY$^{581/591}$ for an additional 1 h in 18.6% or 3.0% O_2 (37°C / 5% CO_2). A431 cells were then detached, washed with PBS, and lipid peroxidation was measured by C_{11} BODIPY$^{581/591}$ fluorescence in conjunction with flow cytometry (section 2.7). **Panel (a),** lipid peroxidation in untreated A431 cells. **Panel (b),** CuOOH-induced lipid peroxidation in A431 cells previously grown in 18.6% or 3.0% O_2 for 96 h. F520:F590 was calculated by dividing the O.BOD (+) MFI detected using the FL-1 channel by the R.BOD (+) MFI detected using the FL-2 channel. **** = $P < 0.0001$ versus 18.6% O_2 utilising a two-way ANOVA and a *post-hoc* multiple comparison test with Dunn–Šidák correction. Data are presented as the mean ± 1 SD. n=4. Where error bars are not visible, this is because the error bar is smaller than the size of the data point. **CuOOH:** cumene hydroperoxide; **F520:F590:** mean fluorescence intensity ratio of the emission light at wavelength 520 nm to the emission light at 590 nm when both excited at 488 nm; **MFI:** mean fluorescence intensity; **O.BOD (-/+):** oxidised BODIPY negative and positive regions; **R.BOD (-/+):** reduced BODIPY negative and positive regions.

3.3.17. The effect of growing A431 cells in 18.6% O_2 on mercaptosuccinic acid-induced lipid peroxidation compared to A431 cells grown in 3.0% O_2

MSA-induced lipid peroxidation was measured in A431 cells grown in 18.6% O_2 or 3.0% O_2 using C_{11} BODIPY$^{581/591}$ staining in conjunction with flow cytometry **(section 2.7).**

A two-way ANOVA was performed to analyse the effects of [MSA], and the [O_2] cells were grown in, on lipid peroxidation. The detection of lipid peroxidation was functional as treatment with 100 µM CuOOH induced lipid peroxidation in both [O_2] groups compared to respective untreated control cells ($P < 0.0001$, **Figure 3.41 a**). A *post-hoc* multiple comparison test showed no statistically significant differences in lipid peroxidation when comparing the untreated controls in the two [O_2] groups (**Figure 3.41 a**). A431 cells grown in 18.6% O_2 for 96 h treated with 1000 µM MSA showed no statistically significant increase in lipid peroxidation when compared to respective untreated control cells (**Figure 3.41 b**). However, A431 cells grown in 3.0% O_2 for 96 h, and treated with 62 µM MSA, showed a statistically significant increase in lipid peroxidation compared to untreated control cells ($P < 0.05$, **Figure 3.41 b**), with means of 0.028 ± 0.008 vs 0.036 ± 0.006, respectively. A431 cells grown in 18.6% O_2 for 96 h, and treated with 500 µM MSA, exhibited a decrease in MSA-induced lipid peroxidation compared to A431 cells grown in 3.0% O_2 for 96 h under the same treatment conditions ($P < 0.0001$, **Figure 3.41 b**), with means of 0.030 ± 0.001 vs 0.042 ± 0.002, respectively. The interaction between the effects of [MSA], and the [O_2] cells were grown in, on lipid peroxidation was statistically significant (F (6, 42) = 2.954, $P = 0.0170$).

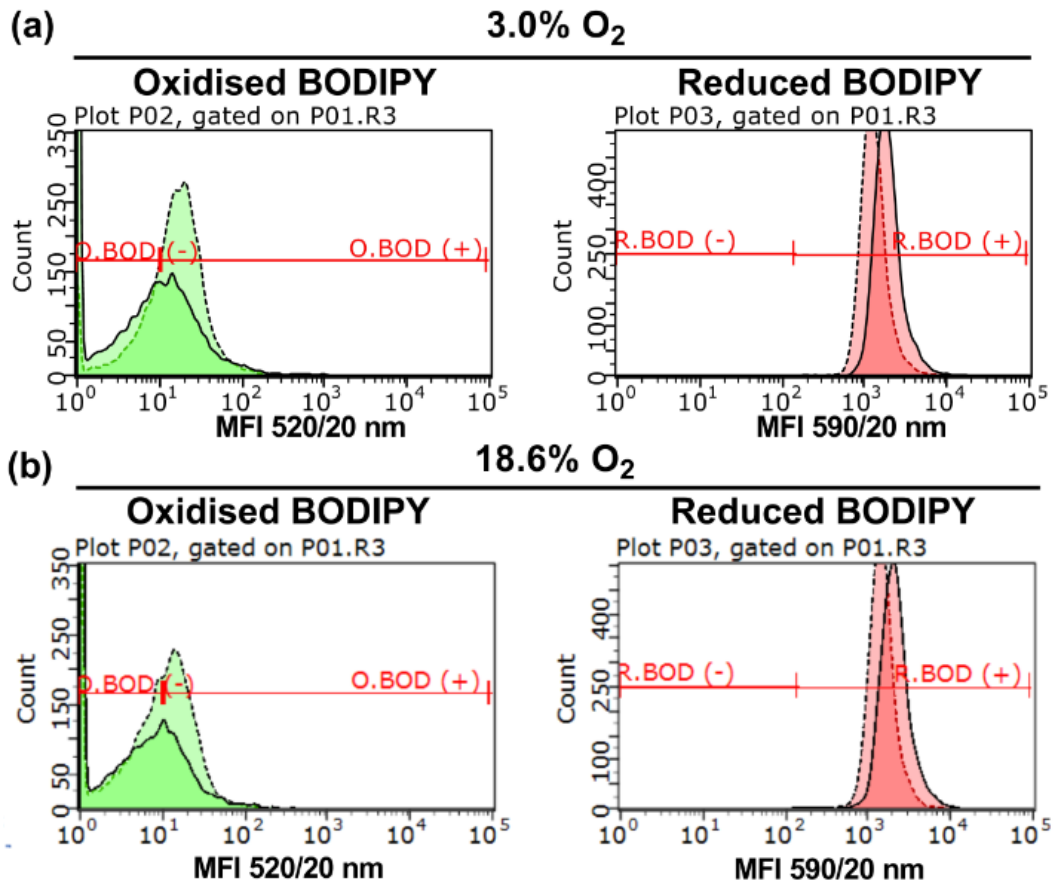

Figure 3.40. Representative C_{11} BODIPY$^{581/591}$ fluorescence histograms showing mercaptosuccinic acid-induced lipid peroxidation in A431 cells grown in 18.6% O_2 or 3.0% O_2 for 96 h. A431 cells were grown in 18.6% O_2 or 3.0% O_2 for 96 h. These cells were then treated with vehicle (0.1% v/v UH_2O) or 30–1000 µM MSA for 24 h in the appropriate [O_2]. A431 cells were then stained with 2 µM C_{11} BODIPY$^{581/591}$ for 1 h in the appropriate [O_2]. Lipid peroxidation was then analysed by flow cytometry using the FL1 and FL2 detectors whilst excited by a 488 nm argon laser. The MFI of oxidised C_{11} BODIPY$^{581/591}$ (O.BOD +/-) and reduced C_{11} BODIPY$^{581/591}$ (R.BOD -/+) was used to calculate F520:F590. **Panel (a),** representative C_{11} BODIPY$^{581/591}$ fluorescence histograms of A431 cells grown in 3.0% O_2 for 96 h, treated with vehicle (0.1% v/v UH_2O; solid trace) or 500 µM MSA (dashed trace) and subsequently stained with C_{11} BODIPY$^{581/591}$. **Panel (b),** representative C_{11} BODIPY$^{581/591}$ fluorescence histograms of A431 cells grown in 18.6% O_2 for 96 h, treated with vehicle (0.1% v/v H_2O; solid trace) or 500 µM MSA (dashed trace) and subsequently stained with C_{11} BODIPY$^{581/591}$. The y axis label (count) indicates the number of events (cells) detected at the respective MFI. **F520:F590:** mean fluorescence intensity ratio of the emission light at wavelength 520 nm to the emission light at 590 nm when both excited at 488 nm; **MFI:** mean fluorescence intensity; **O.BOD (-/+):** oxidised BODIPY negative and positive regions; **R.BOD (-/+):** reduced BODIPY negative and positive regions.

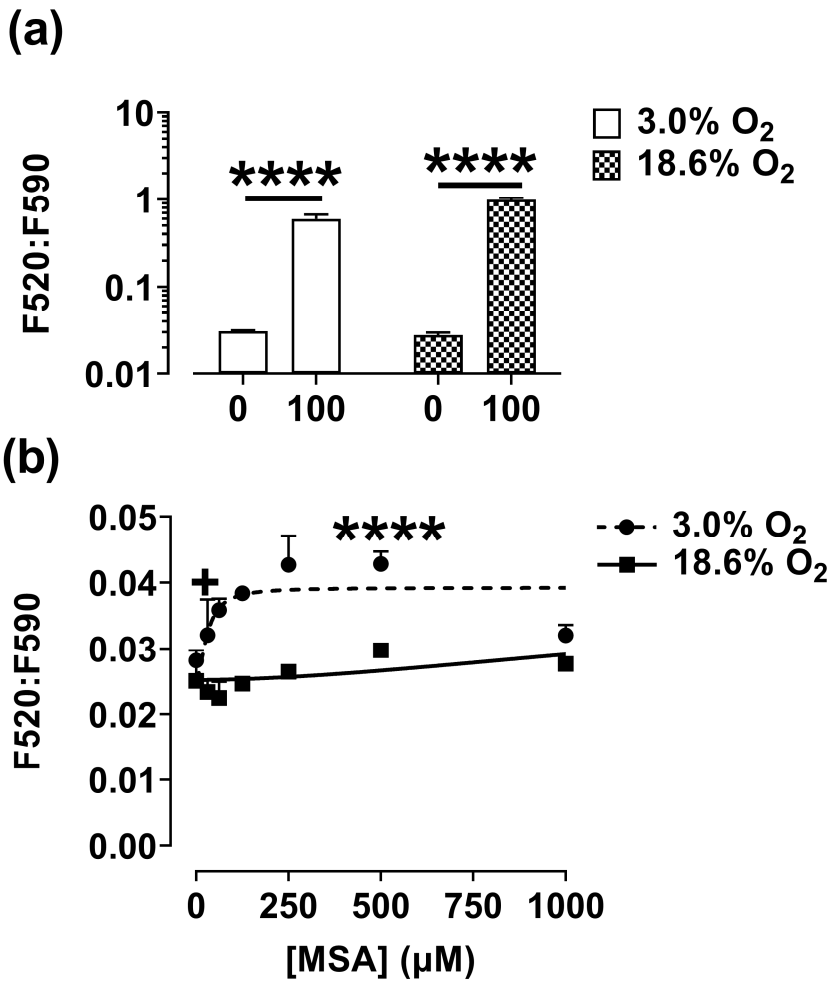

Figure 3.41. The effect of growing A431 cells in 18.6% O_2 on mercaptosuccinic acid-induced lipid peroxidation compared to A431 cells grown in 3.0% O_2 for 96 h. A431 cells were seeded at a density of 9.5 x 10^3 cells/cm^2 in 24 well plates and grown in either 3.0% O_2 or 18.6% O_2 for 96 h (37°C / 5% CO_2). Growth medium was changed every 24 h with respective (18.6% or 3.0% O_2) [O_2]-equilibrated growth medium. After 96 h of growth, A431 cells were treated with vehicle (0.1% v/v UH_2O) or 30–1000 µM MSA or for 24 h in 18.6% or 3.0% O_2 (37°C / 5% CO_2). Under low light, A431 cells were stained with 2 µM C_{11} BODIPY$^{581/591}$ for an additional 1 h in the appropriate [O_2]. A431 cells were then detached, washed with PBS, and lipid peroxidation was measured by C_{11} BODIPY$^{581/591}$ fluorescence in conjunction with flow cytometry (section 2.7). **Panel (a),** lipid peroxidation in untreated A431 cells and in A431 cells treated with 100 µM CuOOH for 1 h. **Panel (b),** MSA-induced lipid peroxidation in A431 cells previously grown in 18.6% O_2 or 3.0% O_2 for 96 h. The F520: F590 arbitrary units were calculated by dividing the O.BOD (+) green MFI detected using the FL-1 channel by the R.BOD (+) red MFI detected using the FL-2 channel. n.s = not significant, + = $P < 0.05$ versus respective untreated control, **** = $P < 0.0001$ versus untreated control in panel (a) and versus 18.6% O_2 in panel (b) utilising a two-way ANOVA and a *post-hoc* multiple comparison test with Dunn–Šidák correction. Data are presented as the mean ± 1 SD. n=4. Where error bars are not visible, this is because the error bar is smaller than the size of the data point. **CuOOH:** cumene hydroperoxide; **F520:F590:** mean fluorescence intensity ratio of the emission light at wavelength 520 nm to the emission light at 590 nm when both excited at 488 nm; **MSA:** mercaptosuccinic acid; **MFI:** mean fluorescence intensity; **O.BOD (-/+):** oxidised BODIPY negative and positive regions; **R.BOD (-/+):** reduced BODIPY negative and positive regions.

3.3.18. The effect of growing cells in 18.6% O_2 on mercaptosuccinic acid-mediated sensitisation to cumene hydroperoxide-induced lipid peroxidation compared to A431 cells grown in 3.0% O_2

MSA-mediated sensitisation to CuOOH-induced lipid peroxidation was measured in A431 cells grown in 18.6% O_2 or 3.0% O_2 for 96 h using C_{11} BODIPY$^{581/591}$ staining in conjunction with flow cytometry **(section 2.6)**. 50 µM CuOOH was chosen as the test concentration as it induced a similar level of lipid peroxidation in both [O_2] groups as previously shown in a concentration response study **(section 3.3.16)**. Example fluorescence histograms are shown in **Figure 3.42**.

A two-way ANOVA was performed to analyse the effects of [MSA], and the [O_2] cells were grown in, on lipid peroxidation. C_{11} BODIPY$^{581/591}$ detection of lipid peroxidation was functional groups as treatment with 100 µM CuOOH resulted in a statistically significant increase in lipid peroxidation **(Figure 3.43 a)**. A *post-hoc* multiple comparison test showed no statistically significant differences in lipid peroxidation when comparing the untreated control cells in both [O_2] groups (**Figure 3.43 a)**. However, A431 cells grown in 18.6% O_2, pre-treated with 60 µM MSA, and subsequently treated with 50 µM CuOOH, exhibited a decrease in lipid peroxidation compared to A431 cells grown in 3.0% O_2 for 96 h under the same treatment conditions ($P < 0.001$, **Figure 3.43 b**), with means of 0.17 ± 0.07 vs 0.44 ± 0.17. The interaction between the effects of [MSA/CuOOH], and the [O_2] cells were grown in, on lipid peroxidation was statistically significant (F (6, 42) = 2.027**,** P<0.0001).

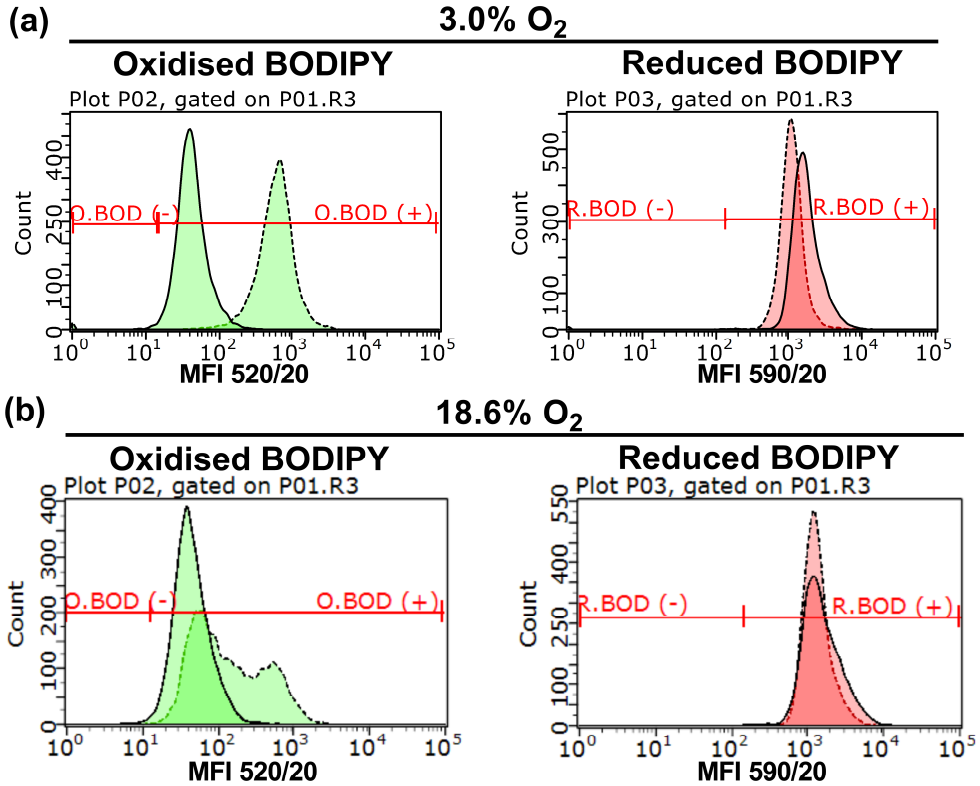

Figure 3.42. Representative C_{11} BODIPY$^{581/591}$ fluorescence histograms showing the effect of mercaptosuccinic acid-mediated sensitisation to cumene hydroperoxide-induced lipid peroxidation in A431 cells grown in 18.6% O_2 or 3.0% O_2 for 96 h. A431 cells were grown in 18.6% O_2 or 3.0% O_2 for 96 h. These cells were then pre-treated with vehicle (0.1% v/v DMSO) or 30–1000 µM MSA for an additional 24 h in the appropriate [O_2]. A431 cells were then treated with 50 µM CuOOH for an additional 1 h and were stained with C_{11} BODIPY$^{581/591}$ for 1 h. Lipid peroxidation was then analysed by flow cytometry using the FL1 and FL2 detectors whilst excited by a 488 nm argon laser. The MFI of oxidised C_{11} BODIPY$^{581/591}$ (O.BOD +/-) and reduced C_{11} BODIPY$^{581/591}$ (R.BOD -/+) was used to calculate F520:F590. **Panel (a),** representative C_{11} BODIPY$^{581/591}$ fluorescence histograms of A431 cells grown in 3.0% O_2 for 96 h, pre-treated with 30-1000 µM MSA, treated with vehicle (0.1% v/v DMSO; solid trace) or 50 µM CuOOH (dashed trace), and then stained with C_{11} BODIPY$^{581/591}$. **Panel (b),** representative C_{11} BODIPY$^{581/591}$ fluorescence histograms of A431 cells grown in 18.6% O_2 for 96 h, pre-treated with 30-1000 µM MSA, treated with vehicle (0.1% v/v DMSO; solid trace) or 50 µM CuOOH (dashed trace), and then stained with C_{11} BODIPY$^{581/591}$ The y axis label (count) indicates the number of events (cells) detected at the respective MFI. **F520:F590:** mean fluorescence intensity ratio of the emission light at wavelength 520 nm to the emission light at 590 nm when both excited at 488 nm **MFI:** mean fluorescence intensity; **O.BOD (-/+):** oxidised BODIPY negative and positive regions; **R.BOD (-/+):** reduced BODIPY negative and positive regions.

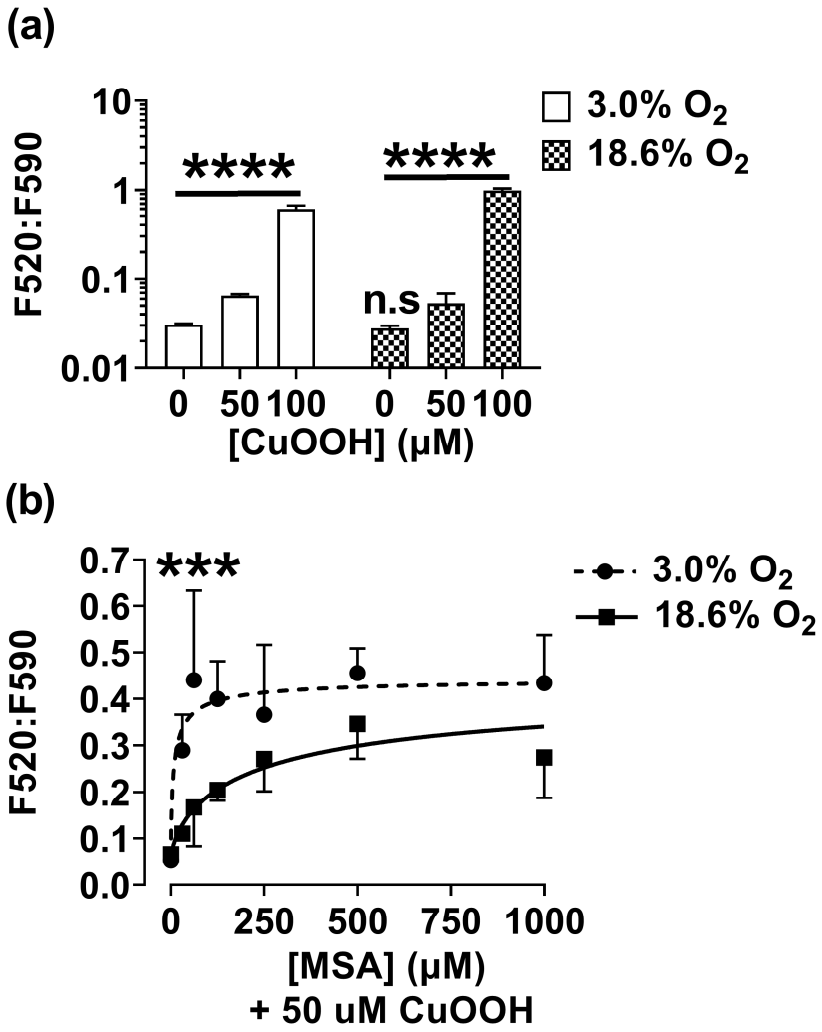

Figure 3.43. The effect of growing A431 cells in 18.6% O_2 on mercaptosuccinic acid-mediated sensitisation to cumene hydroperoxide-induced lipid peroxidation compared to 3.0% O_2 for 96 h. A431 cells were seeded at a density of 9.5 x 10^3 cells/cm^2 in 24 well plates and grown in 18.6% O_2 or 3.0% O_2 for 96 h (37°C / 5% CO_2). Growth medium was changed every 24 h with respective (18.6% or 3.0% O_2) [O_2]-equilibrated growth medium. After 96 h of growth, A431 cells were pre-treated with vehicle (0.1% v/v DMSO) or 30–1000 µM MSA or for 24 h in 18.6% or 3.0% O_2 (37°C / 5% CO_2). After pre-treatment, A431 cells were then treated with 50 µM CuOOH for an additional 1 h in 18.6% or 3.0% O_2 (37°C / 5% CO_2). Under low light, A431 cells were stained with 2 µM C_{11} BODIPY$^{581/591}$ for an additional 1 h in 18.6% or 3.0% O_2 (37°C / 5% CO_2). A431 cells were then detached, washed with PBS (see section 2.2.3 for concentration), and lipid peroxidation was measured by flow cytometry using the FL1 and FL2 detectors whilst excited by a 488 nm argon laser. **Panel (a),** lipid peroxidation in untreated A431 cells and in A431 cells treated with 50 or 100 µM CuOOH alone for 1 h. **Panel (b),** MSA-mediated sensitisation to CuOOH-induced lipid peroxidation in A431 cells grown in 18.6% O_2 or 3.0% O_2 for 96 h. F520: F590 was calculated by dividing the O.BOD (+) green MFI detected using the FL-1 channel by the R.BOD (+) red MFI detected using the FL-2 channel. n.s = not significant versus untreated control cells in 3.0% O_2, *** = $P < 0.001$ versus 18.6% O_2, **** = $P < 0.0001$ versus untreated control utilising a two-way ANOVA and a *post-hoc* multiple comparison test with Dunn–Šidák correction. Data are presented as the mean ± 1 SD. n=4. Where error bars are not visible, this is because the error bar is smaller than the size of the data point. **CuOOH:** cumene hydroperoxide; **F520:F590:** mean fluorescence intensity ratio of the emission light at wavelength 520 nm to the emission light at 590 nm when both excited at 488 nm; **MSA:** mercaptosuccinic acid; **MFI:** mean fluorescence intensity; **O.BOD (-/+):** oxidised BODIPY negative and positive regions; **R.BOD (-/+):** reduced BODIPY negative and positive regions.

3.4. Discussion

This chapter set out to answer three main questions: Are A431 cells grown in 18.6% O_2 resistant to H_2O_2 and/or auranofin-induced cell death compared to A431 cells grown in 3.0% O_2? How long should A431 cells be grown in physioxia for such that H_2O_2 or auranofin-induced cell death no longer changes relative to A431 cells grown in 18.6% O_2? Are A431 cells grown in 18.6% O_2 resistant to the effects of other types of redox-active compounds such as L-BSO, 3-AT, MSA, CuOOH and carmustine compared to A431 cells grown in physioxia? Such questions addressed aims 1–3, and objectives 1-6 outlined previously in **section 1.4.**

3.4.1. A431 cells grown in 18.6% O_2 are resistant to H_2O_2-induced cell death compared to 3.0% O_2 compared to A431 cells adapted to 3.0% O_2.

A431 cells grown in 18.6% O_2 were resistant to H_2O_2-induced cell death compared to A431 cells adapted to 3.0% O_2 for 96 h **(section 3.3.1)**. However, there was no statistically significant difference in H_2O_2-induced cell death when comparing A431 cells grown in 18.6% O_2 to A431 cells adapted to 3.0% O_2 for 24-72 h. These data suggest that A431 cells require at least a 96 h physioxia adaptation period in order to sensitise A431 cells to H_2O_2-induced cell death compared to A431 cells grown in 18.6% O_2 under the same treatment conditions.

It was originally thought that A431 cells adapted to 3.0% O_2 were more sensitive to H_2O_2-induced cell death if they exhibited a lower growth rate compared to A431 cells grown in 18.6% O_2. In essence, if there was a difference in the number of cells at the time of treatment between the [O_2] groups (due to differences in growth rate), this may have affected the ability of H_2O_2 to induce cell death. However, A431 cells adapted to 3.0% O_2 for 24 – 96 h showed no difference in growth rate when compared to A431 cells grown in 18.6% O_2. Therefore, the difference in H_2O_2-induced cell death when comparing cells grown in the two [O_2] conditions was not due to differences in the number of cells on the plate during H_2O_2 treatment **(section 2.3.4)**.

Additionally, it was also thought that A431 cells adapted to 3.0% O_2 for 96 h were hypoxic therefore increasing cellular sensitivity toward H_2O_2-induced cell death when compared to A431 cells grown in 18.6% O_2. However, A431 cells adapted

to 3.0% O_2 for 96 h showed no evidence of HIF-1α protein expression indicating that these cells were not hypoxic **(section 2.3.5.1)**. The full length HIF-1α western blots shown in the appendix **(Figure A.1 i-iii)** show an [O_2]-dependent band at about 93 kDa in the 0.5% O_2 sample lane which corresponds to the theoretical molecular weight of unmodified HIF-1α. This 93 kDa band was not detected in the other two samples (i.e. A431 cells grown in 18.6% or 3.0% O_2 for 96 h). However, the HIF-1 α antibody showed reactivity at other places on the western blot in A431 cell samples grown in 18.6%, 3.0% and 0.5% O_2. The most prominent of these being low molecular weight bands between 15-17 kDa and two bands at about 21 and 24 kDa. However, other bands at 50 kDa and 75 kDa were also observed but were detected only in the 0.5% O_2 sample lanes at these molecular weights. As previously stated, HIF-1α is very rapidly targeted for degradation in the presence of O_2 **(section 1.1.3.1)**. The nuclear fraction was utilised for HIF-1α western blotting in this work. As such, it is unlikely that these aforementioned bands represent HIF-1α targeted for proteolysis by pVHL as this process occurs within the cytoplasm **(section 1.1.3.1)**. Therefore, it cannot be ruled out that the bands at 15-17 kDa, 21 kDa, 24 kDa, 50 kDa and 75 kDa are non-specific bands for HIF1-α. A peptide blocking experiment should be performed in future using the #17-7528-82 HIF-1α antibody to determine its specificity for HIF-1α in A431 cell samples. However, this antibody was raised against a partial recombinant human HIF-1α protein (amino acids 530-826; Uniprot #Q16665). A sequence similarity search using a Basic Local Alignment Search Tool (BLAST) for this amino acid sequence identified no other known human proteins with this amino acid sequence other than HIF-1α. The [O_2]-dependent band at 93 kDa **(Figure A.1 i-iii)**, which corresponds to the predicted molecular weight for HIF-1α, suggested that this antibody was detecting HIF-1α protein at this position on the western blot. Therefore, the absence of such protein staining at this 93 kDa position, when analysing A431 cells grown in 18.6% or 3.0% O_2 for 96 h, indicates that these cells did not express HIF-1 α and were therefore not hypoxic.

What then explains the resistance of A431 cells grown in 18.6% O_2 to H_2O_2-induced cell death compared to A431 cells adapted to 3.0% O_2 for 96 h. Ferguson et al. [21] showed that A431 cells grown in 18.6% O_2 were resistant to H_2O_2-induced cell death compared to A431 cells adapted to 2.0% O_2 for 48 h. Ferguson

et al. showed that A431 cells grown in 18.6% O_2 exhibited heightened transcription of genes encoding catalase, TrxR, Trx, Prx, and Nrf-2 compared to A431 cells adapted to 2.0% O_2 for 48 h. If the growth of A431 cells in 18.6% O_2 augments cellular antioxidant defence, this may also have conferred resistance to H_2O_2-induced cell death compared to A431 cells adapted to physioxia. Later in this work, A431 cells grown in 18.6% O_2 showed higher protein expression levels and enzyme activity of catalase compared to A431 cells adapted to 3.0% O_2 **(section 4.3.1 and 4.3.2)**. The higher levels and activity of catalase protein in A431 cells grown in 18.6% O_2 represents a clear mechanism through which these cells resisted H_2O_2-induced cell death compared to A431 cells adapted to physioxia for 96 h.

It must be made clear however that the shift in the H_2O_2 concentration response curve, when comparing the two [O_2] groups, occurred almost exclusively around the 1 mM H_2O_2 concentration **(section 3.3.1)**. At high [H_2O_2] (i.e. 2 mM), A431 cells succumbed to apoptosis regardless of the [O_2] condition they were grown in during cell culture. 2 mM H_2O_2 was a high enough concentration to kill even A431 cells grown in 18.6% O_2 which had previously resisted H_2O_2-induced cell death at 1 mM H_2O_2 compared to A431 cells adapted to 3.0% O_2 for 96 h. At 1 mM, H_2O_2 was not entirely toxic to A431 cells grown in 18.6% O_2, but it was toxic to A431 cells adapted to 3.0% O_2 for 96 h. As such, the toxicity of H_2O_2 at a 1 mM concentration depended on the [O_2] the A431 cell was adapted to growing in prior to assay **(section 3.3.1)**. Of most interest, A431 cells only became sensitised to H_2O_2-induced cell death at 1 mM H_2O_2 when grown for 96 h in 3.0% O_2. 24-72 h adaptation periods in 3.0% O_2 were not sufficient to sensitise A431 cells to 1 mM H_2O_2. Future work should focus on the 1 mM H_2O_2 concentration in order to investigate further outputs such as protein carbonylation and sulfoxidation, in addition to investigating the activation of the antioxidant response (e.g. Nrf-2, Keap-1, Bach-1, HO-1, catalase).

Although H_2O_2-induced cell death was dependent on the [O_2] A431 cells were adapted to growing in prior to assay, H_2O_2-induced cell death was also dependent on the batch of FBS used. In **section 3.3.1**, it was observed that A431 cells grown in 18.6% O_2 were resistant to 1mM H_2O_2-induced cell death compared to A431 cells adapted to 3.0% O_2 for 96 h. The same batch of FBS was used for all experiments in this study **(section 3.3.1)**. However, in later studies **(section**

3.3.1.1-3.3.1.4), a different batch of FBS was utilised. In these studies **(section 3.3.1.1-3.3.1.4)**, A431 cells grown in 18.6% O_2 did not exhibit a statistically significant resistance to H_2O_2-induced cell death when compared to A431 cells adapted to 3.0% O_2 for 96 h. For example, there was no statistically significant difference in cell death when comparing A431 cells grown in 18.6% after treatment with 1 mM H_2O_2 compared to A431 cells adapted to 3.0% O_2 for 96 h as shown in **Figure 3.5 a**. However there was a large difference in cell death in A431 cells grown in 18.6% treated with 1 mM H_2O_2 compared to A431 cells adapted to 3.0% O_2 for 96 h as shown in **Figure 3.3 a iv.** Each of these studies utilised a different batch of FBS. The H_2O_2 concentration response testing in **section 3.3.1** used the FBS batch (#SH30070.03) from Hyclone, whilst the studies in sections **3.3.1.1-3.3.1.4** utilised the FBS batch (#SH30071.04) from Hyclone. It cannot therefore be ruled out that FBS batch-to-batch variation affected the cellular response to H_2O_2 across studies. Differences in the content of iron or ferritin for example may have resulted in differential Fenton reaction-mediated **(section 1.2.2.2)** $^{\bullet}OH$ production from H_2O_2 [238]. Hempel et al. [239] found that pre-treatment with Fe^{2+} protected mammalian cells from H_2O_2-induced cell death. This is not intuitive, as Fe^{2+} should catalyse the formation of the $^{\bullet}OH$ production from H_2O_2, the former being a highly reactive and dangerous free radical species **(section 1.2.2.2)**. However the half-life of $^{\bullet}OH$ is quite short (10^{-9} s). If exogenously added Fe^{2+} (present in FBS) catalysed the formation of $^{\bullet}OH$ from H_2O_2 outside the cell, rather than inside the cell, the distance of the $^{\bullet}OH$ radical from cellular biomolecules may have limited its toxicity due to its short half-life. For example the generated $^{\bullet}OH$ radical may have instead reacted with the thiols in FBS rather than cellular DNA, lipids or proteins. Differences in the iron content in the FBS batches used in this work may have acutely affected the cellular-response to H_2O_2.

A potential limitation to the study in **section 3.3.1** concerns how cell death was measured i.e. the detection of phosphatidyl serine externalisation (using annexin V-FITC), and cellular membrane permeability (using PI). Phosphatidyl serine detection by the annexin V-FITC antibody (used for the detection of early and late apoptosis) is dependent on the activity of the enzyme phospholipid scramblase **(section 1.2.5)**. Although there is currently no evidence that the adaptation of A431 cells to physioxia affects the activity of this enzyme, any alteration in this

regard would affect how the cell death studies presented in chapter 3 are interpreted. Future work should verify that the activity of phospholipid scramblase is not affected by cellular adaptation to physioxia relative to the activity in A431 cells grown in 18.6% O_2. Phospholipid scramblase is however a calcium-dependent enzyme [240]. There is some evidence that the adaptation of HUVEC cells to 5.0% O_2 for 5 days decreased histamine-induced Ca^+ mobilisation compared to HUVEC grown in 18.6% O_2 for 5 days [80]. Therefore, future work should also measure both basal calcium ion flux, and calcium ion flux after treatment with H_2O_2/auranofin in A431 cells grown in 18.6% O_2 compared to A431 cells adapted to 3.0% O_2 for 96 h.

Finally, treatment of A431 cells with 1 mM H_2O_2 caused about a 2.0% v/v increase in [O_2] compared to untreated control cells **(section 2.5.2).** The production of O_2 was likely due to the catalase-mediated decomposition of H_2O_2 **(section 1.2.7.2.3).** In a future section, it was shown that A431 cells grown in 18.6% exhibit higher expression levels of catalase protein compared to A431 cells adapted to 3.0% O_2 for 96 h **(section 4.3.2)**. As such, the amount of [O_2] generated during H_2O_2 treatment may be higher in A431 cells grown in 18.6% compared to A431 cells adapted to 3.0% O_2 for 96 h under the same treatment conditions. Previously reported [21], A431 cells adapted to 2.0% O_2 for 48 h, that were then exposed acutely to 18.6% O_2 for 1 h, exhibited increased gene expression of antioxidant genes encoding proteins such as TrxR1, SOD 1, SOD 2, NQO-1, Nrf-2, and HO-1 compared to A431 cells adapted to 2.0% O_2 for 48 h. As such, an acute change in [O_2] due to the catalase-dependent decomposition of H_2O_2 may affect the gene expression of these previously mentioned antioxidant genes. Future work should firstly determine whether there is a difference in [O_2] generated after H_2O_2 treatment when comparing A431 grown in 18.6% O_2 to A431 cells adapted to 3.0% O_2. Secondly, it should be determined whether these respective increases in [O_2] acutely affects the transcription of the antioxidant genes previously outlined.

3.4.2. A431 cells grown in 18.6% O_2 are not resistant to $_L$-buthionine sulfoximine-mediated sensitisation to H_2O_2-induced cell death compared to A431 cells adapted to 3.0% O_2

As previously outlined **(section 3.4.1)**, A431 cells grown in 18.6% O_2 were resistant to H_2O_2-induced cell death compared to A431 cells adapted to 3.0% O_2.

Inhibition of catalase was hypothesised to sensitise A431 cells toward H_2O_2 treatment in both [O_2] groups. This investigation utilised the catalase inhibitor 3-AT to test this hypothesis. 3-AT inhibited cellular catalase enzyme activity **(section 2.10.1)**. 3-AT pre-treatment did not however sensitise A431 cells grown in either [O_2] condition for 96 h to H_2O_2-induced cell death **(section 3.3.1.2**). This was an unexpected observation. Intuitively, the increased activity or higher expression level of catalase protein might have conferred the observed resistance of A431 cells grown in 18.6% O_2 for 96 h to H_2O_2-induced cell death compared to A431 cells adapted to 3.0% O_2 for 96 h under the same treatment conditions. The concentration of H_2O_2 that A431 cells were treated with after 3-AT pre-treatment was 0.5 mM. This concentration was chosen for this sensitisation study as it was non-toxic in both [O_2] groups based on the H_2O_2 concentration response studies **(section 3.3.1)**. However, this concentration may not have been high enough to elicit a cell death response even in the absence of functional catalase. Future work should utilise a higher concentration of H_2O_2 (i.e. 0.75 mM – 1 mM) in further sensitisation studies with 3-AT in A431 cells grown in 18.6% or 3.0% O_2 for 96 h.

Next, it was hypothesised that other antioxidant defence systems, such as GSH, may have been present at sufficient levels in A431 cells grown in both [O_2] conditions to protect against H_2O_2-induced cell death even in the absence of active catalase due to 3-AT-mediated inhibition. To this end, the GSH anti-oxidant defence arm was then investigated. L-BSO **(section 1.2.6.3.1)** was used to deplete GSH in A431 cells as demonstrated in **section 2.10.2**. Depletion of GSH alone did not induce apoptosis in either [O_2] group (**section 3.3.1.3**). This was not unexpected, as L-BSO is largely used as an adjunctive treatment used in combination with other chemicals **(section 1.2.6.3.1)** [241].

There was however no statistically significant difference in L-BSO-mediated sensitisation to H_2O_2-induced cell death when comparing A431 cells adapted to 3.0% O_2 for 96 h to A431 cells grown in 18.6% O_2 under the same treatment conditions **(section 3.3.1.4)**. Firstly, this data suggested that A431 cells are capable of resisting peroxide-induced cell death in the absence of GSH as L-BSO was shown to deplete GSH in both [O_2] conditions **(section 2.10.2)**. Second, it suggested that the ability of L-BSO to sensitise A431 cells to oxidative-stress-induced cell death was not dependent on the [O_2] A431 cells were adapted to

growing in prior to assay. Therefore, not all arms of the cellular antioxidant defence system (i.e. GSH) may change in cells grown in standard cell culture [O_2] compared to physioxia. This idea is supported by others. Chapple et al. [72] showed that the expression and transcription of genes encoding GSH-related enzymes (e.g. solute carrier family 7 anionic amino acid transporter light chain (cysteine transporter), and glutamate cysteine ligase modifier subunit) were not increased in HUVEC grown in 18.6% O_2 compared to HUVEC adapted to 5.0% O_2 for 5 days. However, Chapple et al. [72] found that the transcription of other antioxidant genes (i.e. NQO-1, HO-1) were increased in HUVEC grown in 18.6% O_2 compared to HUVEC adapted to 5.0% O_2 for 5 days when treated with an Nrf-2 activator (i.e. DEM **section 1.3.1.1.1**). Although it was not shown that the depletion of GSH by $_L$-BSO differentially sensitised A431 cells grown in 18.6% O_2 to H_2O_2-induced cell death compared to A431 cells adapted to 3.0% O_2 for 96 h under the same treatment conditions, it raised another question. Through what mechanism did A431 cells grown in 18.6% O_2 resist H_2O_2-induced cell death compared to A431 cells adapted to 3.0% O_2 for 96 h under the same treatment conditions? This is discussed in more detail in chapter 4 where the activities of certain antioxidant enzymes such as catalase **(section 4.3.1)**, and GR **(section 4.3.4),** as well as the expression levels of certain antioxidant proteins such as catalase **(section 4.3.2)** and NQO-1 **(section 4.3.9),** were found to be higher in A431 cells grown in 18.6% O_2 compared to A431 cells adapted to 3.0% O_2 for 96 h.

3.4.3. A431 cells grown in 18.6% O_2 were resistant to auranofin-induced cell death and reactive oxygen species generation compared to A431 cells adapted to 3.0% O_2

A431 cells grown in 18.6% O_2 were resistant to auranofin-induced cell death compared to A431 cells adapted to 3.0% O_2 for 96 h **(section 3.3.2)**. Auranofin-induced cell death continued to change with time until at least 96 h after placing the cells under 3.0% O_2 compared to auranofin-induced cell death in A431 cells grown in 18.6% O_2. Whilst A431 cells required a 96 h adaptation period in 3.0% O_2 to become sensitised to H_2O_2 compared to 18.6% O_2 **(section 3.3.1)**, the auranofin studies revealed a statistically significant change in auranofin-induced cell death after only a 48 h adaptation period in 3.0% O_2 when compared to auranofin-induced cell death in A431 cells grown in 18.6% O_2.

The resistance of A431 cells grown in 18.6% O_2 to auranofin-induced cell death was associated with a resistance to auranofin-induced $\Delta\psi_m$ compared to A431 cells adapted to 3.0% O_2 for 96 h under the same treatment conditions **(section 3.3.12)**. Although MitoTracker Red fluorescence detection of mitochondrial mass is affected by ψ_m [242], there was no statistically significant difference in basal ψ_m when comparing A431 cells grown in 18.6% O_2 to A431 cells adapted to 3.0% O_2 for 96 h. This suggests that the quantitation of mitochondrial mass was unaffected by the [O_2] conditions used in these experiments. As such, the resistance of A431 cells grown in 18.6% O_2 for 96 h to auranofin-induced $\Delta\psi_m$ compared to A431 cells adapted to 3.0% O_2 for 96 h was not due to differences in mitochondrial mass as quantified by MitoTracker Red **(section 3.3.11)**. A431 cells grown in 18.6% O_2 were also resistant to auranofin-induced ROS production as detected by the DCFHDA and MitoSOX red probes **(section 3.3.4 and section 3.3.6)**. This suggested that part of the mechanism through which A431 cells grown in 18.6% O_2 resisted auranofin-induced cell death was through lower treatment-induced ROS generation.

As discussed previously, the main molecular target of auranofin is TrxR **(section 1.2.6.1.1)**. The transcription of genes encoding TrxR and Trx was higher in A431 cells grown in 18.6% O_2 when compared A431 cells adapted to 2.0% O_2 for 48 h [21]. TrxR and Trx defend against O_2 toxicity [146]. For example, the inhalation of 100% O_2 by primates caused increased gene expression of *TRX* and *TRXR1*, and increased the expression levels of oxidised Trx protein compared to primates breathing room air [146]. The authors suggested that TrxR is key in the defence against hyperoxia-induced injury [146]. Mice possessing a dominant negative Trx (dnTrx) phenotype were hyper-sensitive to ambient air inhalation compared to wild type. Additionally, mice with a dnTrx phenotype exhibited a threefold increase in the levels of oxidised Trx compared to wild type [243]. A431 cells grown in 18.6% O_2 may have upregulated the levels of TrxR and Trx to protect against oxygen-mediated cell damage. Indirectly, this may confer resistance to compounds which target these proteins (i.e. auranofin). Of particular interest, TrxR2 (also a molecular target for auranofin) localises to the mitochondria [204], a compartment which produces a significant amount of cellular ROS. A431 cells grown in 18.6% O_2 upregulated the transcription of SOD 2, and the activity of SOD 1 compared to A431 cells adapted to 2.0% O_2 for 48 h [21]. This may have

supported the detoxification of auranofin-induced mitochondrial ROS generation even in the absence of functional TrxR2 due to auranofin-mediated inhibition. This may explain why A431 cells grown in 18.6% O_2 exhibited diminished auranofin-induced ROS generation compared to auranofin-treated A431 cells adapted to 3.0% O_2 for 96 h.

What implications does the above data hold for the *in vitro* testing of compounds like auranofin which target TrxR? Auranofin was once used to treat rheumatoid arthritis [244]. However its side effect profile (abdominal pain, incontinence, stomatitis and mouth ulcerations) led to its discontinuation [164, 244]. Auranofin is now a candidate for drug repurposing [164, 245–248]. For example, auranofin has shown potential utility for the treatment of parasitic infections, bacterial infections, HIV, and neurodegenerative disorders [164, 245–248]. Auranofin has also gained interest as a promising anti-cancer therapeutic [249–252]. For example, auranofin is currently in clinical trials for the treatment of fallopian tube cancer, ovarian epithelial cancer, primary peritoneal cavity cancer, ovarian serous tumor, and ovarian carcinoma (clinicaltrials.gov). Heightened TrxR expression also predicted poor prognosis in squamous cell carcinoma of the tongue [254]. Drug repurposing has at least two benefits: first, it is less expensive than designing a drug from scratch **(section 1.3)**; and second: the *in vivo* safety profile of the drug is already well understood [146]. If an old drug is repurposed, a significant amount of time and money may be saved [146].

If auranofin is to be re-purposed, it should not be re-tested on mammalian cells grown chronically in standard cell culture [O_2] as this may affect the expression levels of the lead target (i.e. TrxR1 and TrxR2). Specifically, A431 cells grown in 18.6% O_2 exhibit increased activity of TrxR and increased transcription of genes encoding TrxR and Trx compared to A431 cells adapted to 3.0% O_2 [21]. Additionally, the expression of these proteins is controlled by Nrf-2, a transcription factor which may also exhibit altered activity in mammalian cells grown in 18.6% O_2 compared to those adapted to physioxia **(section 1.3.1.1.1)**. Newly discovered selective inhibitors of TrxR are currently under development [149]. However, the *in vitro* testing of these compounds is being carried out on mammalian cells grown chronically in 18.6% O_2. The data from **section 3.3.2** suggested that TrxR targeting inhibitors should be tested on cells adapted to physioxia and not standard cell culture [O_2].

However, the cellular response of A431 cells to auranofin does not appear to be solely dependent on the [O_2] utilised during the cell culture growth period, but also partly on the [O_2] during the treatment phase also. This will be discussed in the following section.

3.4.3.1. An acute switch in [O_2] during the treatment phase alone was sufficient to affect the responses of A431 cells to auranofin

As shown in **section 3.3.2,** A431 cells grown in 18.6% O_2 were resistant to auranofin-induced cell death compared to A431 cells adapted to 3.0% O_2 for 48–96 h. The resistance of A431 to auranofin, conferred by cell culture in 18.6% O_2, can be partially reversed by changing the [O_2] from 18.6% to 3.0% O_2 during the treatment phase alone.

A431 cells that were grown in 18.6% O_2 for 48 h, and subsequently switched into 3.0% O_2 (18.6% → 3.0% O_2 group) during the 1 h auranofin treatment, exhibited decreased viability at 16 µM, and 32 µM auranofin compared to A431 cells that were cultured and treated in 18.6% O_2 (18.6% O_2 group; **section 3.3.3**). The extent of auranofin-induced cell death was similar when comparing A431 cells adapted to 3.0% O_2 for 48 h and treated with 32 µM auranofin in 3.0% O_2 (3.0% O_2 group) to the 18.6% → 3.0% O_2 group also treated with 32 µM auranofin. Conversely, A431 cells adapted to 3.0% for 48 h and treated with 16 µM auranofin in 18.6% O_2 (3.0% → 18.6% O_2 group) showed heightened viability compared to A431 cells adapted to the 3.0% O_2 group. However this protective effect was not sufficient to protect A431 cells at all concentrations of auranofin. For example, the extent of auranofin-induced cell death was similar in the 3.0% → 18.6% O_2 group treated with 32 µM auranofin compared to the 3.0% O_2 group treated with 32 µM auranofin. This indicated that increasing the [O_2] from 3.0% O_2 to 18.6% O_2 during treatment with auranofin can protect A431 cells previously adapted to 3.0% O_2 for 48 h against sub-lethal concentrations of auranofin (16 µM auranofin).

Of note, there was a large increase in the percentage of cells in late apoptosis in the 18.6% → 3.0% O_2 group when treated with 16 µM, and 32 µM auranofin compared to the 18.6% O_2 group treated with 16 µM, and 32 µM auranofin **(section 3.3.3)**. The percentage of late apoptotic cells was higher in the 3.0% O_2

group treated with 8–32 µM compared to the 18.6% O_2 group treated with 8–32 µM auranofin. However, this difference was even greater when comparing the 18.6% → 3.0% O_2 group to the 3.0% O_2 group. As it takes time for cells to progress through the stages of apoptosis, and all cells were treated at the same time across [O_2] conditions, this suggested that changing A431 cells from 18.6% to 3.0% O_2 during treatment shortened the time taken for A431 cells to succumb to auranofin-mediated cell death. In essence, by changing the cells from 18.6% O_2 to 3.0% O_2 during treatment, A431 cells became sensitised to auranofin-induced cell death which resulted in more cells being detected in late apoptosis as these same cells activated programmed cell death before other more resistant cells (i.e. A431 cells grown and treated in 18.6% O_2)

In summary, there appeared to be at least two mechanisms involved in the [O_2]-sensitive responses of A431 cells to auranofin. First: long term growth of A431 cells in 18.6% O_2 conferred resistance to auranofin-induced cell death. A431 cells adapted to 3.0% O_2 may lose this resistance over the course of days during physioxia adaptation compared to A431 cells grown in 18.6% O_2. This adaptation to physioxia may have involved a slow change to the levels of antioxidant defences within the cell. Currently, evidence has suggested that certain arms of the antioxidant response are altered in mammalian cells grown in 18.6% O_2 compared to physioxia [36, 72, 78]. For example, the expression levels of Nrf-2 protein, and the induction of Nrf-2-target protein by oxidative stress, may be sensitive to the [O_2] a cell is adapted to growing in [36, 72, 78] . Evidence for this statement from this present work is provided in chapter 4 **(section 4.3.1- 4.3.9)**. This may explain why there was no difference in auranofin-induced cell death until A431 cells had been adapted to 3.0% O_2 for at least 48 h when compared to A431 cells grown in 18.6% O_2 **(section 3.3.2)**. A 24 h adaptation to 3.0% O_2 may not have allowed sufficient time for A431 cells to adapt the expression of Nrf-2-target proteins compared to the expression levels of such proteins in A431 cells grown in 18.6% O_2 [155]. Nrf-2-target protein, such as HO-1 and NQO-1, may have been present at high expression levels even in A431 cells adapted to 3.0% O_2 for 24 h due to the long half-lives of these proteins [155]. At longer time-points in physioxia (e.g. 48 h), the mRNA or protein levels of pre-existing Nrf-2-targets (generated under 18.6% O_2) may have begun to fall as they approached their respective half-lives [21]. TrxR1 and Trx1 have mRNA half-lives of about 6.2

and 35 h respectively in mouse liver cells, with HO-1, Prx 1, and GR having mRNA half-lives of 2.6, 22, and 31 h, respectively [255]. Nrf-2 is an unstable protein, and is believed to have a half-life of about 15–20 min in HL-60 cells [255]. However the Nrf-2 half-life can increase to 100 min during oxidative stress [255]. The expression levels of Nrf-2-target protein (and de-novo production of Nrf-2 itself) may have decreased with time as A431 cells were adapted to physioxia compared to A431 cells grown in 18.6% O_2. This may in part have rendered A431 cell adapted to physioxia less resistant to oxidative stress compared to A431 cells grown in 18.6% O_2.

Second: despite the upregulation of Nrf-2-target genes, A431 cells grown in 18.6% O_2 can be rendered susceptible to auranofin-induced cell death by acutely lowering the [O_2] during auranofin-treatment alone. Although it is possible that the [O_2] switch from 18.6% to 3.0% O_2 may have affected the gene expression of some antioxidant proteins, it is unlikely to have affected the levels of mRNA or protein already transcribed or expressed (respectively) within the cell prior to the [O_2] switch. This indicates that high [O_2] may not only confer resistance to redox-active compounds by slowly altering cellular phenotype, but may represent an essential requirement *during treatment* in order to protect A431 cells against auranofin-induced cell death.

How might an acute switch of [O_2] from 18.6% O_2 to 3.0% O_2 during auranofin treatment alone sensitise A431 cells to auranofin-induced cell death compared to auranofin-induced cell death in A431 cells grown and treated in 18.6% O_2? Activation of HIF-1α may have occurred during the [O_2] switch from 18.6% to 3.0% O_2. HIF-1α expression levels have been shown to vary over a physiologically relevant O_2 range (1.5–2% O_2) [256]. Although our investigations showed no evidence of HIF-1α induction after 96 h of growth in 3.0% O_2 **(Figure 2.13)**, it was not determined whether an acute switch in [O_2] from 18.6% to 3.0% O_2 acutely activated HIF-1α [37]. Future work should determine whether HIF-1α is activated by changing the A431 cells from 18.6% O_2 to 3.0% O_2 during the 1 h treatment period with auranofin.

Enzymes with a high K_m (O_2%) may have been affected by an acute change in [O_2] during treatment. These enzymes may include NOX4 (K_m (O_2%) = 18-20), neuronal nitric oxide synthase (nNOS, K_m (O_2%) = 15–39.9), inducible nitric oxide

synthase (iNOS, K_m (O_2%) = 10.6–11), cyclooxygenase-1 (K_m (O_2%) = 1–3), monoamine oxidase (K_m (O_2%) = 3.4–28), PHD (K_m (O_2%) = 41-46) and FIH (K_m (O_2%) = 4–12) [46].

NOX-4 activity is sensitive to [O_2] due to its high K_m (O_2%). H_2O_2 generation by isolated NOX-4 doubled when tested at 12.0% O_2 compared to 3.0% O_2 [46, 257]. NOX-4-derived ROS is associated with the increased resistance of pancreatic cells, urothelial carcinoma cells, and human renal carcinoma cells to anticancer treatments such as etoposide, cisplatin and vincristine [259–262]. During a switch from 18.6% O_2 to 3.0% O_2, the production of H_2O_2 by NOX-4 may decrease based on its high K_m (O_2 %) [46]. This potential decrease in H_2O_2 production may have acutely sensitised A431 cells to auranofin-induced cell death when switched from 18.6% O_2 to 3.0% O_2.

NOS activity may also have been affected by the decrease in [O_2] from 18.6% O_2 to 3.0% O_2. Such a decrease may have decreased the production of $^{\bullet}$NO with possible effects on auranofin-induced cell death in A431 cells switched from 18.6% O_2 to 3.0% O_2 during treatment. As stated previously, some forms of NOS have a K_m (O_2%) that lies within the physioxia range. For example, RAW 246.7 macrophage produced $^{\bullet}$NO as a function of [O_2] [262]. A decrease in [O_2] from 18.6% to 3.0% O_2 may have acutely affected the production of NOS-derived $^{\bullet}$NO. NOS-derived $^{\bullet}$NO production protected mammalian cells against oxidative stress-induced cell death [264, 265, 266]. NOS-mediated $^{\bullet}$NO production may protect squamous cell carcinoma cells from radiation-induced cell death [263]. For example, inhibition of NOS by N(G)-nitro-L-arginine sensitised mice bearing A431 cell xenografts to ionizing radiation [263].

NOS-mediated $^{\bullet}$NO production also conferred resistance to photodynamic irradiation-mediated cell killing [264]. Photo-killing of lymphoblastoid cells by photodynamic irradiation was suppressed by pre-treatment with L-arginine (NO donor) [265]. Conversely, NO scavengers increased the efficacy of photodynamic irradiation-induced cell killing 2.5 fold over untreated control cells in human breast cancer cells (COH-BR1) [266]. COH-BR1 pre-treatment with spermine NONOate also conferred resistance to tert-butyl hydroquinone-induced lipid peroxidation compared to untreated control cells [267]. $^{\bullet}$NO-dependent resistance to photodynamic irradiation-induced cell death may involve the scavenging of $LO_2^{\bullet}$

by •NO [268]. Incubation of COH-BR1 with the •NO donor spermine NONOate increased the expression of both HO-1 and ferritin [268]. Therefore, NOS-mediated •NO production may protect cells against oxidant-induced damage by directly scavenging $LO_2^{\bullet}$, or by upregulating the expression levels of other Nrf-2-target antioxidant proteins (e.g. HO-1 or ferritin). A sudden decrease in [O_2] from 18.6% O_2 to 3.0% O_2 may acutely decrease NOS-derived •NO production thereby sensitising A431 cells to auranofin-induced cell death through an Nrf-2-related mechanism compared to A431 cells grown and treated with auranofin in 18.6% O_2.

NQO-1 may also have contributed to the acute effect of [O_2] on auranofin-induced cell death. As described in **section 1.3.1.1.1**, NQO-1 catalyses the 2 electron reduction of quinone to hydroquinone. Quinone can also undergo 1 electron reduction to the semiquinone radical via cytochrome p450 reductase **(Figure 3.44)**. Although NQO-1 does not utilise O_2 as a reducing equivalent, many of the quinone intermediate species, such as the semiquinone radical, are labile to O_2 **(Figure 3.44)** [269]. For example, semiquinone are oxidised by O_2 to quinone forming $O_2^{\bullet-}$ in the process [270].

Later in this work, A431 cells grown in 18.6% O_2 were shown to exhibit higher expression levels of NQO-1 protein compared to A431 cells adapted to 3.0% O_2 for 96 h **(section 4.3.2).** The NQO-1-mediated reduction of quinone to hydroquinone may therefore be increased in A431 cells grown in 18.6% O_2 compared to A431 cells adapted to 3.0% O_2 for 96 h. A lower expression level of NQO-1 protein in A431 cells adapted to 3.0% O_2 may allow CYP450 to compete for quinone reduction with NQO-1. The [O_2] is lower in 3.0% O_2 compared to 18.6% O_2 which may have limited the [O_2]-dependent oxidation of semiquinone to quinone in A431 cells adapted to 3.0% O_2 compared to the same reaction in A431 cells grown in 18.6% O_2. Acutely changing the [O_2] from 18.6% O_2 to 3.0% O_2 may have increased the steady state concentration of the semiquinone radical in A431 cells adapted to 3.0% O_2 compared to A431 cells grown in 18.6% O_2. The semiquinone radical is relatively stable relative to other more reactive free radicals [269, 270]. Conversely, in 18.6% O_2, the high [O_2] may have increased the O_2-mediated oxidation of the semiquinone radical thereby increasing the availability of quinone for NQO-1-mediated reduction to hydroquinone. Some hydroquinone can be oxidised to quinone by O_2 in the presence of Cu^+ [223]. As

such, the oxidation of hydroquinone to quinone may be sensitive to acute changes in [O_2]. These redox-active quinone species may participate in an [O_2]-dependent activation of Nrf-2 thereby acutely protecting A431 cells treated in 18.6% O_2 from further oxidative stress compared to A431 cells treated in 3.0% O_2 [273]. A sudden decrease in O_2 from 18.6% O_2 to 3.0% O_2 during auranofin treatment may have attenuated the [O_2]-dependent formation of such redox-active quinone species compared to A431 cells treated in 18.6% O_2. This may have acutely affected the [O_2]-dependent quinone-mediated activation of Nrf-2 and the subsequent Nrf-2-mediated cellular protection from auranofin-induced cell death. This proposed mechanism is summarised in **Figure 3.44**.

Finally, other non-redox active mechanisms may be involved. The levels of microRNA (MiRNA; 17 - 22 nucleotide noncoding single-stranded RNA molecules) may change in response to sudden changes in [O_2]. For example, MiRNA-93 was identified as a negative regulator of Nrf-2 protein expression [274]. The levels of MiRNA-93 has been shown to change in response to [O_2]. MiRNA-93 has been shown to regulate hypoxia-induced autophagy in MEF [275]. [O_2]-dependent changes to MiRNA may affect the levels of Nrf-2 which has a very short protein half-life. In theory, this may acutely affect the responses of A431 cells to oxidative stress-induced cell death.

Overall, a sudden switch in O_2 from 18.6% to 3.0% O_2 may have sensitised A431 cells to auranofin-induced cell death through redox-related pathways which utilise O_2 as a substrate. This mechanism may have involved changes to the activity of enzymes with high K_m (O_2 %), or by mediating the formation of redox-active hydroquinone species which may have directly activated the Nrf-2/Keap-1 complex.

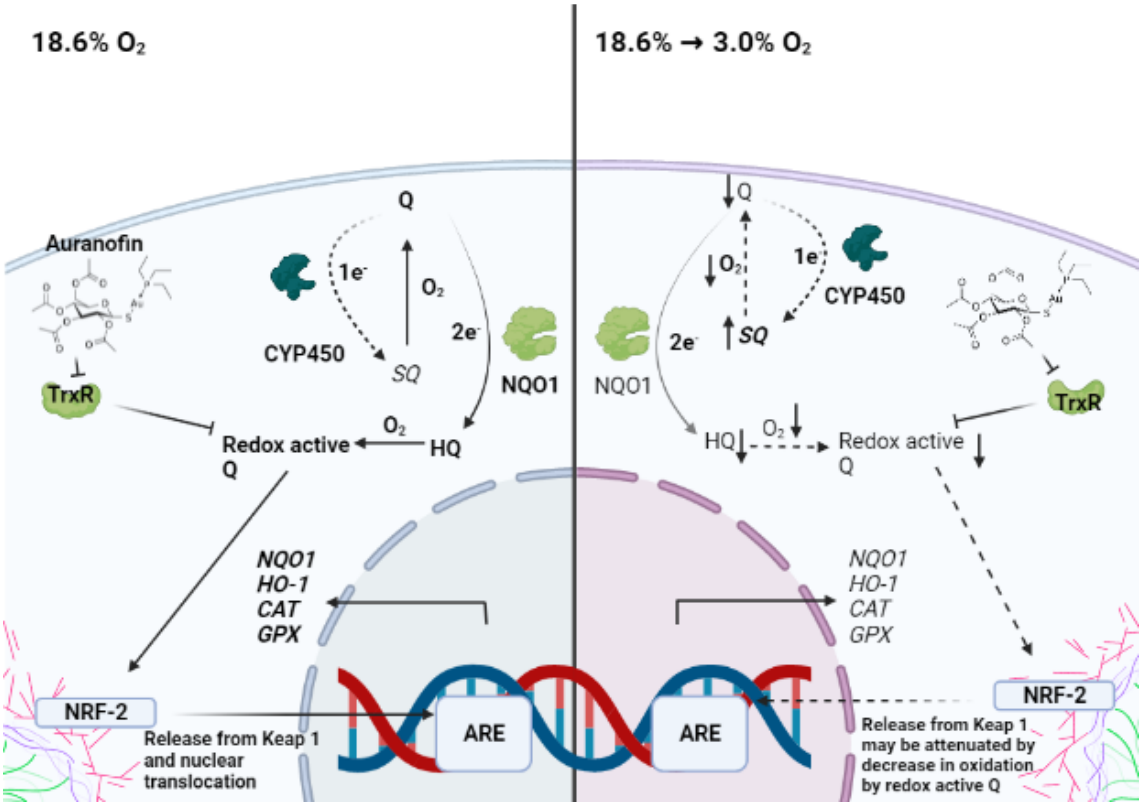

Figure 3.44. Proposed mechanism of oxygen-mediated cyto-protection from auranofin-induced cell death through NAD(P)H quinone oxidoreductase-1. Under 18.6% O_2, SQ is oxidised to Q. Q can then undergo two electron reduction to HQ by NQO-1. Some HQ generated by NQO-1 are labile to O_2 and can generate redox-active quinone which may activate the Nrf-2/Keap1 complex directly. Auranofin inhibits thioredoxin reductase which may allow redox-active Q to accumulate. When switched from high O_2 to low O_2, the O_2-mediated oxidation of SQ to Q may be slowed. This may decrease the pool of Q available for two electron reduction to HQ by NQO-1. The decrease in O_2 may also attenuate HQ autoxidation by O_2, resulting in decreased activation of Nrf-2 and subsequent transcription of Nrf-2-target genes. **ARE:** antioxidant response element; **CAT:** catalase; **CYP 450:** cytochrome P450; **e^-:** electron; **Gpx:** glutathione peroxidase; **HO-1:** haem oxygenase 1; **HQ:** hydroquinone; **NQO-1:** NADPH quinone oxidoreductase 1; **Nrf-2:** nuclear factor erythroid-2-related factor 2; **Q:** quinone; **SQ:** semiquinone radical; **TrxR:** thioredoxin reductase. Made with www.BioRender.com.

3.4.3.2. Auranofin-induced reactive oxygen species production was altered in A431 cells grown in 18.6% O_2 compared to A431 cells adapted to 3.0% O_2.

A431 cells grown in 18.6% O_2 exhibited decreased auranofin-induced mitochondrial ROS generation compared to A431 cells adapted to 3.0% O_2 **(section 3.3.4)**. The decreased in auranofin-induced ROS generation in A431 cells grown in 18.6% O_2 may in part explain why A431 cells, grown in standard cell culture [O_2], resisted auranofin-induced cell death compared to A431 cells adapted to 3.0% O_2 for 96 h under the same treatment conditions. Why might the growth of A431 cells in standard cell culture [O_2] cause these cells to produce

less mitochondrial ROS when treated with auranofin compared to A431 cells adapted to 3.0% O_2 for 96 h under the same treatment conditions?

As discussed previously **(section 1.2.6.1.1),** auranofin inhibits both TrxR1 and TrxR2, the latter of which is found in the mitochondria [204]. TrxR2 contains a mitochondria localisation signal in its N terminus [276]. TrxR2 is believed to be critical for the detoxification of ROS in mitochondria, and its overexpression protected HEK293 cells from oxidative stress-induced apoptosis by tert-butyl hydroperoxide [276]. TrxR protects the mitochondrial respiratory chain from ROS-mediated damage [277]. Deletion of TrxR2 in DT40 (chicken B lymphocyte cell line) increased mitochondrial ROS generation and induced cell death [277]. Depletion of GSH by L-BSO sensitised TrxR2$^{-/-}$ DT40 cells to oxidative stress-induced cell death compared to cells expressing normal expression levels of TrxR2 protein. This indicated that GSH may detoxify mitochondrial ROS in the absence of functional TrxR2 [277]. A GSH importer protein (SLC25A39) has been recently discovered in mitochondria which suggested that GSH plays a role in mitochondrial antioxidant defence [278]. Therefore, the attenuated auranofin-induced ROS generation in A431 cells grown in 18.6% O_2 compared to A431 cells adapted to 3.0% O_2 for 96 h may involve detoxification by GSH and GSH-related antioxidant defence systems such as GSH, Gpx and GR in the absence of functional TrxR1 and TrxR2. For example, the majority of mitochondrial ROS decomposition in TrxR2$^{-/-}$ DT40 cells was shown to be facilitated by GR and Gpx [277]. Later, A431 cells grown in 18.6% O_2 were shown to exhibit heightened GR activity compared to the GR activity in A431 cells adapted to 3.0% O_2 for 96 h **(section 4.3.4)**. The increased GR activity exhibited by A431 cells grown in 18.6% O_2 may have decreased auranofin-induced mitochondrial ROS generation compared to auranofin-induced ROS generation in A431 cells adapted to 3.0% O_2 for 96 h.

In contrast to the MitoSOX Red probe, the DHE probe detected a different cellular response to auranofin when comparing A431 cells grown in 18.6% or 3.0% O_2 for 96 h. When utilising DHE, A431 cells grown in 18.6% O_2 showed no statistically significant increase in auranofin-induced ROS generation compared to respective untreated control cells. However, A431 cells adapted to 3.0% O_2 for

96 h showed an auranofin-dependent decrease in auranofin-induced ROS generation compared to respective untreated control cells **(section 3.3.5)**.

In other work, auranofin induced ROS generation in HELA cells at low concentrations (2–5 µM) as detected by DHE [279]. This increase in ROS generation was associated with the depletion of cellular GSH [279]. Auranofin has also been shown to induce ROS generation in human chronic B-cell leukaemia cells and chronic lymphocytic leukaemia cells [276, 277]. As such, the observations noted in this work do not agree with other work investigating auranofin-induced ROS generation using the DHE probe. DHE measures total cellular ROS **(section 1.2.3.2)** including mitochondria-derived ROS which was shown to increase in the presence of auranofin in both [O_2] conditions **(section 3.3.4)**. Why then does auranofin treatment decrease DHE-detected ROS generation in A431 cells adapted to 3.0% O_2, but not in A431 cells grown in 18.6% O_2?

The auranofin-dependent decrease in DHE-detected ROS generation in A431 cells adapted to 3.0% O_2 may have involved $O_2^{\bullet-}$ oxidation by cytochrome c. Cytochrome c is reduced by $O_2^{\bullet-}$ forming O_2 [282]. The induction of intrinsic apoptosis is associated with the release of cytochrome c from the mitochondria **(Figure 1.9)**. A431 cells adapted to 3.0% O_2 for 96 h, and subsequently treated with auranofin, showed heightened levels of apoptosis compared to auranofin-treated A431 cells grown in 18.6% O_2 **(section 3.3.2)**. Cytochrome c-mediated oxidation of $O_2^{\bullet-}$ to O_2 may have been greater in auranofin-treated A431 cells adapted to 3.0% O_2 compared to auranofin-treated A431 cells grown in 18.6% O_2. This may have attenuated DHE-detected ROS generation in auranofin-treated A431 cells adapted to 3.0% O_2 for 96 h compared to DHE-detected ROS generation in auranofin-treated A431 cells grown in 18.6%. Despite the resistance of A431 cells grown in 18.6% O_2 toward auranofin-induced cell death compared to A431 cells adapted to 3.0% O_2 for 96 h, auranofin still induced apoptosis in A431 cells grown in 18.6% O_2 **(section 3.3.2)**. If cytochrome c release decreased DHE-detected ROS generation, then this phenomenon should have been observed in A431 cells grown in both [O_2] conditions. However, this was not observed. What then could explain the difference in auranofin-induced ROS formation when comparing auranofin-treated A431 cells grown in 18.6% O_2 to auranofin-treated A431 cells adapted to 3.0% O_2 for 96 h.

In chapter 4, it is shown that auranofin-mediated induction of NQO-1 is increased in A431 cells adapted to 3.0% O_2 compared to A431 cells grown in 18.6% O_2 **(section 4.3.9)**. NQO-1 may therefore have detoxified more $O_2^{\bullet-}$ in A431 cells adapted to 3.0% O_2 compared to A431 cells grown in 18.6% O_2. For example, NQO-1 has been shown to scavenge $O_2^{\bullet-}$ produced by XO, which inhibited the oxidation of DHE [283]. Inhibition of NQO-1 by 5-methoxy-1,2-dimethyl-3-[(4-nitrophenoxy)methyl]indole-4,7-dione (ES936) attenuated NQO-1-mediated $O_2^{\bullet-}$ scavenging [283]. This may explain why there is an [auranofin]-mediated decrease in ROS detection by DHE in A431 cells adapted to 3.0% O_2 but not in A431 cells grown in 18.6% O_2 under the same treatment conditions [269]. The increased auranofin-mediated induction of NQO-1 in A431 cells adapted to 3.0% O_2 for 96 h compared to A431 cells grown in 18.6% O_2 may extend to other enzymes which may directly scavenge $O_2^{\bullet-}$ such as SOD **(section 1.2.7.2.1 and 1.2.7.2.2)**. Nrf-2 activation induces the expression of SOD for example [88]. As such, a differential induction of SOD in auranofin-treated A431 cells grown in 18.6% O_2 may directly affect the detoxification of ROS when compared to auranofin-treated A431 cells adapted to 3.0% O_2 for 96 h.

However, It cannot be assumed that DHE is specifically detecting $O_2^{\bullet-}$ due to the overlapping emission spectra of 2-OH-E^+ and E^+ **(section 1.2.3.2)**. Future work should determine the extent of the specificity of the DHE and MitoSOX probe for $O_2^{\bullet-}$ under 18.6% O_2 and 3.0% O_2 by separating the two DHE end products by HPLC in conjunction with fluorescence detection.

Overall, these data show that the DHE-mediated detection of ROS generation may be prone to artefact when tested in A431 cells grown chronically in standard cell culture [O_2] compared to A431 cells adapted to 3.0% O_2 for 96 h.

3.4.3.3. A431 cells grown in 18.6% O_2 generate more H_2O_2 than A431 cells adapted to 3.0% O_2

There was no difference in the basal production of ROS when comparing A431 cells grown in 18.6% O_2 to A431 cells adapted to 3.0% O_2 for 96 h as detected by DHE and MitoSOX. These probes are designed to detect $O_2^{\bullet-}$ (despite potential interferences as described in **section 1.2.3.2**), and so may not detect changes in H_2O_2 for example. As such, the Amplex Red probe **(section 1.2.3.1)** was utilised to measure differences in the generation of cellular H_2O_2 in A431 cells grown in 18.6% or 3.0% O_2 for 96 h. It was found that A431 cells grown in 18.6% O_2 for 96 h produced more H_2O_2 compared to A431 cells adapted to 3.0% O_2 for 96 h over a 2 h culture period **(section 3.3.7)**. If DHE and MitoSOX were detecting $O_2^{\bullet-}$, this suggests that not all ROS exhibit heightened levels in A431 cells grown in 18.6% O_2 compared to A431 cells adapted to 3.0% O_2 for 96 h.

In contrast, the DCFHDA probe did not show a difference in detected fluorescence when comparing untreated A431 cells grown in 18.6% O_2 to A431 cells adapted to 3.0% O_2 for 96 h **(section 3.3.6)**. DCFHDA is often used to measure H_2O_2 generation, but the use of the probe for measuring specific radicals and ROS has garnered criticism [284]. It has also been shown that the photo-reduction of DCF forms the DCF semiquinone free radical which is oxidized by O_2 to form $O_2^{\bullet-}$ in the process [285]. This phenomenon might in fact caution its use in highly oxygenated conditions such as that found in standard cell culture practise. As such the differences in the data generated when comparing the Amplex red study to the DCFHDA study are not surprising when one considers the number of artefacts the DCFHDA assay is prone to **(section 1.2.3.3).**

It has been reported that mammalian cells grown in 18.6% O_2 exhibit increased generation of ROS compared to those adapted to physioxia [17, 20, 76, 280, 281]. Some primary cells grown in 18.6% O_2 exhibited a decreased growth rate when compared to those adapted to physioxia, possibly due to increased ROS production [288]. For example, MEF grown in 18.6% O_2 exhibited higher instances of DNA damage and DNA mutagenesis, with G: C and T: A transversion mutations which are indicative of oxidative stress-induced damage [289]. This damage was associated with increasedH_2O_2 generation in MEF grown in 18.6% O_2 compared to 3.0% O_2 [280, 283].

The increased generation of H_2O_2 in 18.6% O_2 may be due to the heightened activity of NOX-4. The activity of NOX-4 has been reported to be sensitive to changes in [O_2] **(section 3.4.3.1).** As mentioned previously, the K_m (O_2%) of NOX-4 is high (16–20% O_2). The increased H_2O_2 generation in A431 cells grown in 18.6% O_2 compared to A431 cells adapted to 3.0% O_2 for 96 h may be due to higher NOX-4 activity [46]. NOX-4 is expressed in A431 cells and has been described as an O_2 sensor [60, 284]. In pulmonary artery smooth muscle cells, NOX4 mRNA levels doubled within 30 min of growth in 1% O_2 and increased five-fold after 8 h relative to smooth muscle cells grown in 18.6% O_2 [291]. In another report, the expression levels of NOX-4 and NOX-1 protein increased two-fold in C2C12 cells (mouse myoblast) adapted to 5.0% O_2 compared to C2C12 grown in 18.6% O_2 [46]. The [O_2]-dependent increase in H_2O_2 production in C2C12 cells was inhibited by GKT138731 (a potent inhibitor of NOX-1 and NOX-4) [46]. The heightened production of H_2O_2 in A431 cells grown in 18.6% O_2 compared to A431 cells adapted to 3.0% O_2 may be due to the heightened activity of H_2O_2-producing enzymes such as NOX-4.

3.4.4. A431 grown in 18.6% O_2 were resistant to carmustine-induced cell death compared to A431 cells adapted to 3.0% O_2

As mentioned earlier, carmustine inhibits (*inter alia*) GR **(section 1.2.6.5)**. As such, it was hypothesised that inhibition of this antioxidant enzyme would sensitise A431 cells to H_2O_2-induced cell death. However, carmustine did not sensitise A431 cells to further H_2O_2 treatment in either [O_2] group **(section 3.3.9)**. The concentration of H_2O_2 utilised for this sensitisation study was 0.5 mM which may not have been high enough to observe carmustine-mediated sensitisation to H_2O_2-induced cell death. Future work should utilise higher concentrations of H_2O_2 (0.75 mM – 1 mM) to induce cell death in carmustine pre-treated A431 cells grown in 18.6% O_2 or adapted to 3.0% O_2 for 96 h. However, A431 cells grown in 18.6% O_2 were resistant to direct carmustine-induced cell death compared to A431 cells adapted to 3.0% O_2 at higher carmustine concentrations (500 – 700 µM; **section 3.3.8**). This resistance was associated with an attenuation to carmustine-induced $\Delta\psi_m$ in A431 cells grown in 18.6% O_2 compared to A431 cells adapted to 3.0% O_2 for 96 h under the same treatment conditions **(section 3.3.13)**.

Carmustine is not currently used for the treatment of skin cancer, although a skin targeted topical carmustine delivery system was reported to be efficacious in a chemically-induced mouse model of skin cancer [273]. Carmustine was chosen as a test compound in this work based on a few observations: First: it inactivates the Nrf-2-target GR [292]; second: Nrf-2-overexpressing glioma cells (U87MG) were protected against carmustine-induced cell death compared to control cells expressing normal expression levels of Nrf-2 protein [189]; third: U87MG cells expressing a normal expression level of Nrf-2 protein could be protected against carmustine-induced cell death by first treating these cells with the Nrf-2 activator tBHQ [189]; and fourth, *NFE2L2* transcription was shown to be higher in A431 cells grown in 18.6% O_2 compared to A431 cells adapted to 2.0% O_2 for 48 h [21]. In this present work, it was shown that that the growth of A431 cells in 18.6% O_2 conferred resistance to carmustine-induced cell death compared to A431 cells adapted to 3.0% O_2 for 96 h under the same treatment conditions **(section 3.3.8)**. Later, A431 cells grown in 18.6% O_2 exhibited higher expression levels of nuclear Nrf-2 protein compared to A431 cells adapted to 3.0% O_2 for 96 h **(section 4.3.8)**. This may explain why A431 cells grown in 18.6% O_2 resisted carmustine-induced cell death compared to A431 cells adapted to 3.0% O_2 for 96 h. Unlike the interventions in U87MG cells [189], which genetically over expressed Nrf-2 to confer resistance to carmustine-induced cell death, this present work showed that the use standard cell culture [O_2] to grow cells long term is also sufficient to confer resistance to carmustine-induced cell death when compared to cells adapted to 3.0% O_2 for 96 h under the same treatment conditions. With Nrf-2 expression now associated with cancer cell resistance to 5-fluorouracil, carboplatin, cisplatin and temozolomide, the importance of designing *in vitro* systems which more closely model *in vivo* Nrf-2 signalling is now even more important [196–200].

3.4.5. A431 cells grown in 18.6% O_2 were resistant to H_2O_2, mercaptosuccinic acid and cumene hydroperoxide-induced lipid peroxidation compared to A431 cells adapted to 3.0% O_2

Based on the observations that A431 cells grown in 18.6% O_2 were resistant to oxidative stress-induced cell death compared to A431 cells adapted to 3.0% O_2 for 96 h, it was investigated whether this resistance extended to the induction of lipid peroxidation. As shown in **section 3.3.15 and 3.3.16**, A431 cells grown in 18.6% O_2 were resistant to H_2O_2 and CuOOH-induced lipid peroxidation

compared to A431 cells adapted to 3.0% O_2 for 96 h. A431 cells adapted to 3.0% O_2 slowly sensitised to CuOOH-induced lipid peroxidation over time when compared to CuOOH-treated A431 cells grown in 18.6% O_2, emerging first after a 24 h 3.0% O_2 adaptation period and further developing at a 96 h 3.0% O_2 adaptation period **(section 3.3.16)**.

CuOOH requires transition metal ion such as Fe^{2+} in order to initiate lipid peroxidation **(Figure 1.13)**. The availability of labile Fe^{2+} may have affected CuOOH-induced lipid peroxidation [118]. Ferritin is believed to be critical for the sequestration of Fe^{2+} ion, thereby limiting Fenton reaction-mediated generation of $^{\bullet}OH$ for example **(section 1.2.2.2)** [119, 287]. Mammalian tissue O_2 levels modulated iron-regulatory protein activities *in vivo* [294]. Additionally, ferritin expression is controlled by Nrf-2 [293]. Nrf-2 may modulate iron ion flux by controlling iron ion export and import via ferroportin 1 [293]. As discussed prior, A431 cells grown in 18.6% O_2 showed heightened transcription of *NFE2L2* compared to A431 cells adapted to 2.0% O_2 for 48 h [21]. In a later section, A431 cells grown in 18.6% O_2 exhibited about 2 times the expression levels of nuclear Nrf-2 protein compared to A431 cells adapted to 3.0% O_2 for 96 h **(section 4.3.8)**. The heightened expression levels of nuclear Nrf-2 protein in A431 cells grown in 18.6% O_2 may increase the expression levels of Nrf-2-target protein such as ferritin compared to A431 cells adapted to 3.0% O_2. This may protect against CuOOH and H_2O_2-induced lipid peroxidation which requires the formation of cumoxyl radical and $^{\bullet}OH$ (respectively) to initiate lipid peroxidation **(Figure 1.13).**

As discussed previously **(section 1.2.7.2.5)**, Gpx and GR enzyme systems are critical for cellular defence against lipid peroxidation. Girotti et al. [21] found that murine L1210 cells depleted of selenium (required for Gpx activity, **section 1.2.7.2.5**) were much more susceptible to photodynamic irradiation-induced lipid peroxidation compared to control cells. Additionally, the activity of Gpx was 60-fold lower in selenium deprived cells compared to control. Kirska et al. [295] showed that COH-BR1 overexpressing Gpx-4 were protected against lipid peroxidation relative to control cells. In a later section, A431 cells grown in 3.0% O_2 exhibited a time-dependent decrease in GR activity relative to the GR activity in A431 cells grown in 18.6% O_2 **(section 4.3.4)**. GR and Gpx operate in tandem to maintain the levels of GSH **(Figure 1.15)**. Decreased GR activity in A431 cells adapted to 3.0% O_2 may have sensitised these cells to CuOOH and H_2O_2-

induced lipid peroxidation compared to CuOOH and H_2O_2-treated A431 cells grown in 18.6% O_2.

MSA-mediated inhibition of Gpx was utilised to probe the mechanism through which A431 cells grown in 18.6% O_2 resisted CuOOH and H_2O_2-induced lipid peroxidation compared to CuOOH and H_2O_2-treated A431 cells adapted to 3.0% O_2 for 96 h. Treatment of A431 cells with 30–1000 µM MSA did not induce apoptosis, or affect the viability of A431 cells in either [O_2] group **(section 2.5.5)**. MSA did not induce lipid peroxidation in A431 cells grown in 18.6% O_2. However, MSA induced lipid peroxidation in A431 cells adapted to 3.0% O_2 for 96 h **(section 3.3.17)**. Inhibition of Gpx by MSA may be sufficient to induce lipid peroxidation in A431 cells adapted to 3.0% O_2, but not in A431 cells grown in 18.6% O_2. A431 cells grown in 18.6% O_2 may therefore possess altered antioxidant defence mechanisms to protect against lipid peroxidation even in the absence of active Gpx**.** If MSA were to be tested on A431 cells grown in 18.6% O_2, one may conclude MSA to be an ineffective inducer of lipid peroxidation in A431 cells. MSA can induce lipid peroxidation in A431 cells over the concentrations shown in this work. However, MSA-induced lipid peroxidation requires A431 cells to be adapted to physioxia prior to treatment over the tested concentrations studied in this work.

In order to build on this observation, MSA was utilised to sensitise A431 cells to further treatment with CuOOH **(section 3.3.18)**. The optimal concentration of CuOOH was determined to be 50 µM as it induced a similar level of lipid peroxidation in A431 cells grown in 18.6% O_2 and A431 cells adapted to 3.0% O_2 for 96 h. 50 µM CuOOH also lay in the centre of the concentration response curve where further increases or decreases in C_{11} BODIPY$^{581/591}$ fluorescence could be detected **(section 3.3.16)**. MSA sensitised A431 cells grown in both [O_2] conditions to CuOOH-induced lipid peroxidation. However, MSA was more effective at sensitising A431 cells adapted to 3.0% O_2 to CuOOH-induced lipid peroxidation compared to A431 cells grown in 18.6% O_2 under the same treatment conditions.

The transcription of the gene encoding Gpx is under the control of Nrf-2 **(section 1.2.7.3.1)** [155]. As mentioned previously, the transcription of the *NFE2L2* gene encoding Nrf-2 was increased in A431 cells grown in 18.6% O_2 compared to those

adapted to 2.0% O_2 for 48 h [21]. This increase in *NFE2L2* transcription was associated with increased transcription of *GPX1* in A431 cells grown in 18.6% O_2 compared to A431 cells adapted to 2.0% O_2 for 48 h [21]. This increase may have facilitated the resistance of A431 cells grown in 18.6% O_2 to inducers of lipid peroxidation compared to A431 cells adapted to 3.0% O_2 for 96 h. Evidence suggested that Gpx7 and Gpx8 expression are under the control of Nrf-2, however, these enzymes do not require selenocysteine for activity [296]. As such, these enzyme may continue to operate even in the presence of MSA [297].

NQO-1 may also be involved in the protection of A431 cells grown in 18.6% O_2 against lipid peroxidation compared to A431 cells adapted to 3.0% O_2 for 96 h. NQO-1-mediated vitamin E hydroquinone formation protected Chinese hamster ovary cells against CuOOH-mediated lipid peroxidation compared to non-pre-treated control cells [267, 292]. Later, it is shown that A431 cells grown in 18.6% O_2 exhibited a two-fold higher expression level of NQO-1 protein when compared to A431 cells adapted to 3.0% O_2 for 96 h **(section 4.3.9)**. A431 cells grown in 18.6% may therefore have possessed antioxidant defences which are better suited for the defence against lipid peroxidation compared to A431 cells adapted to 3.0% O_2 for 96 h. The work outlined in **section 3.3.17 and 3.3.18** cautions the testing of MSA *in vitro* on A431 cells grown chronically in standard cell culture [O_2].

Finally, the resistance of A431 cells grown in 18.6% O_2 to lipid peroxidation may also involve a resistance to an iron-dependent form of cell death such as ferroptosis when compared to A431 cells adapted to 3.0% O_2. The induction of ferroptosis is associated with lipid peroxidation [299]. The induction of ferroptosis was not investigated in this work however. Future work should investigate whether pathways involved in iron ion import (DMT1, TFR1), iron ion export (ferroportin, ceruloplasmin, and hephaestin), iron storage (ferritin), and inhibition of iron export (hepcidin) were involved in the resistance of A431 cells grown in 18.6% O_2 to lipid peroxidation compared to A431 cells adapted to 3.0% O_2 for 96 h. Future work should also determine whether the induction of other forms of cell death by redox-active compounds, such as pyroptosis and anoikis, are also altered by cellular growth in 18.6% O_2 compared to physioxia.

3.5. Chapter summary

In this chapter it is concluded that A431 cells grown in 18.6% O_2 are resistant to oxidative stress-induced cell death, $\Delta\psi_m$, ROS generation, and lipid peroxidation compared to A431 cells adapted to 3.0% O_2 for 96 h.

A431 cells grown in 18.6% O_2 were resistant to H_2O_2, auranofin and carmustine-induced cell death compared to A431 cells adapted to 3.0% O_2. The responses of A431 cells to H_2O_2 and auranofin-induced cell death appear to change until at least 96 h after placing the cells into 3.0% O_2 compared to A431 cells grown in 18.6% O_2 for 96 h under the same treatment conditions. Additionally, L-BSO-mediated depletion of GSH did not differentially sensitise A431 cells grown in 18.6% O_2 for 96 h to H_2O_2-induced cell death compared to A431 cells adapted to 3.0% O_2 for 96 h under the same treatment conditions. Not all aspects of cellular antioxidant defence may be prone to artefactual changes caused by long term cellular growth under standard cell culture [O_2]. Therefore, not all redox active compounds may be susceptible to artefactual efficacy (or lack thereof) when tested on mammalian cells grown in standard cell culture [O_2] compared to such testing on mammalian cells adapted to physioxia.

An acute switch in [O_2] during treatment was also sufficient to moderately affect auranofin-induced cell death in A431 cells previously grown in 18.6% O_2 or adapted to 3.0% O_2 for 48 h. Changing A431 cells grown in 18.6% for 48 h to 3.0% O_2 for 1 h during treatment sensitised these cells to auranofin-induced cell death compared to A431 cells cultured and treated in 18.6% O_2. In comparison, changing A431 cells previously adapted to 3.0% O_2 for 48 h into 18.6% O_2 during auranofin treatment partly protected against auranofin-induced cell death at sub lethal auranofin concentrations. This suggested that molecular O_2 itself may be required to protect A431 cells against auranofin-induced cell death.

A431 cells grown in 18.6% O_2 also exhibited altered treatment-induced ROS formation compared to A431 cells adapted to 3.0% O_2 for 96 h. A431 cells grown in 18.6% O_2 exhibited attenuated auranofin-induced mitochondria-derived ROS generation compared to A431 cells adapted to 3.0% O_2 for 96 h. A similar observation was made using the DCFHDA probe, where auranofin-induced oxidative stress was lower in A431 cells grown in 18.6% O_2 compared to A431

cells adapted to 3.0% O_2 for 96 h under the same treatment conditions. However, DHE-mediated detection of ROS formation showed no increase in auranofin-induced ROS formation in A431 cells grown in 18.6% O_2. However, DHE detected an [auranofin]-dependent decrease when used on A431 cells adapted to 3.0% O_2 for 96 h.

Finally, A431 cells grown in 18.6% O_2 were resistant to lipid peroxidation induced by H_2O_2, MSA and CuOOH compared to A431 cells adapted to 3.0% O_2 for 96 h under the same treatment conditions. MSA induced lipid peroxidation in A431 cells adapted to 3.0% O_2 for 96 h but not in A431 cells grown in 18.6% O_2. MSA was also less effective at sensitising A431 cells grown in 18.6% O_2 to CuOOH-induced lipid peroxidation compared to A431 cells adapted to 3.0% O_2 for 96 h under the same treatment conditions. This suggested that Gpx was critical for defending against lipid peroxidation in A431 cells adapted to 3.0% O_2, yet it was dispensable in A431 cells grown in 18.6% O_2.

It is concluded that A431 cells grown in 18.6% O_2 were resistant to oxidative stress-induced cell death, lipid peroxidation, and $\Delta\psi_m$ compared to A431 cells adapted to 3.0% O_2 for 96 h. Where ROS generation, cell death, lipid peroxidation or $\Delta\psi_m$ are chosen as endpoints to assay redox-active compound efficacy using the A431 cell line, it is concluded that such experiments should be performed on A431 cells adapted to 3.0% O_2 (for at least 4 days) and not A431 cells grown chronically in standard cell culture [O_2]. The *in vitro* testing of redox-active compounds on A431 cells grown in 18.6% O_2 may lead to an overestimation of how well such cells resist oxidative-stress-induced cell death *in vivo*.

CHAPTER 4: SQUAMOUS CELL CARCINOMA CELLS GROWN IN STANDARD CELL CULTURE OXYGEN CONCENTRATIONS EXHIBIT ALTERED CELLULAR ANTIOXIDANT DEFENCES COMPARED TO CELLS ADAPTED TO PHYSIOXIA.

4.1. Introduction

As discussed previously **(section 1.1)**, *in vitro* cell culture is largely performed in 18.6% O_2 which does not replicate the *in vivo* [O_2]. Evidence was earlier presented that the growth of mammalian cells in 18.6% O_2 alters the activity of the antioxidant defence regulatory transcription factor Nrf-2, as well as the induction of Nrf-2-target protein, by redox-active compounds **(section 1.3.1.1.1)**. As discussed previously **(section 1.3.1.1.1)**, A431 cells grown in 18.6% O_2 showed heightened gene expression of *NFE2L2* (encoding *de-novo* Nrf-2 protein) and of the Nrf-2-target genes such as *TRX* and *TRXR* (encoding Trx and TrxR) [21].

In chapter 3, it was shown that A431 cells grown in 18.6% O_2 were resistant to the effects of redox-active compounds such as H_2O_2 **(section 3.3.1)**, auranofin **(section 3.3.2)**, carmustine **(section 3.3.8)**, CuOOH **(section 3.3.16)**, and MSA **(section 3.3.17)**. The chapter set out to answer the following question: Are the previously observed resistances of A431 cells grown in 18.6% O_2 toward the effects of redox-active compounds due to the heightened activity and expression levels of Nrf-2-controlled antioxidant defence systems (i.e. catalase, SOD, GR, Gpx, GST, GSH) compared to A431 cells grown in 3.0% O_2? This research question addresses aim 4 and objective 7 outlined previously **(section 1.4)**.

To this end, A431 cells were grown in 18.6% O_2 or 3.0% O_2 for 24-96 h. The endpoints addressed involved measuring: the activity of Nrf-2-target enzyme including catalase, SOD, GR, Gpx, GST **(section 4.3.1 and sections 4.3.3-4.3.6)**; the levels of GSH and GSSG **(section 4.3.7)**; the expression levels of nuclear Nrf-2 protein **(section 4.3.8)** and Nrf-2-target protein (catalase and NQO-1; **sections 4.3.2 and 4.3.9**); and the expression levels of proteins containing the 3-NT protein modification **(section 4.3.10)**.

4.2. Methods

4.2.1. Measurement of catalase enzyme activity

A431 cells were seeded at a density of 9.5 x 10^3 cells/cm^2 in T75 flasks and were grown in 18.6% O_2 or 3.0% O_2 for 24-96 h (5% CO_2/37°C). Growth medium was changed every 24 h with appropriate [O_2]-equilibrated growth medium. A431 cells were then lysed under the appropriate [O_2] condition **(section 2.12.1-2.12.2)** and [protein] was determined by the BCA assay as described previously **(section 2.12.3)**.

To determine catalase activity a modified method described by Li and Schellhorn [300] was utilised by monitoring the decomposition of H_2O_2 at 240 nm. 150 µg sample protein was added to 5mM H_2O_2 in 55 mM phosphate buffer (31.8 mM Na_2HPO_4 and 23.2 mM NaH_2PO_4, pH 7.0) in a quartz cuvette. The solution was briefly mixed by pipetting. A_{240} was then monitored at intervals of 5 s for 1 min at 22 °C using an M_2e spectrophotometer **(Figure 4.1 a)**. This was then converted to the change in absorbance at 240 nm (ΔA_{240}). Known concentrations of catalase (0–100 U/mL) were also assayed, allowing interpolation of sample catalase activity against a standard curve, where the slope of the initial linear reaction (ΔA_{240} 0–1 min) was plotted against [catalase] **(Figure 4.1 b)**. The y axis of the standard curve is labelled as the reaction rate (a.u/s) **(Figure 4.1 b)**. The resulting sample activity, interpolated from the standard curve, was then normalised to sample [protein] **(section 4.3.1)**. One unit of catalase is defined as the amount of enzyme required to decompose 1 µM of H_2O_2 per minute at pH 7.0, at a temperature of 22ºC, and at a substrate concentration of 5 mM H_2O_2.

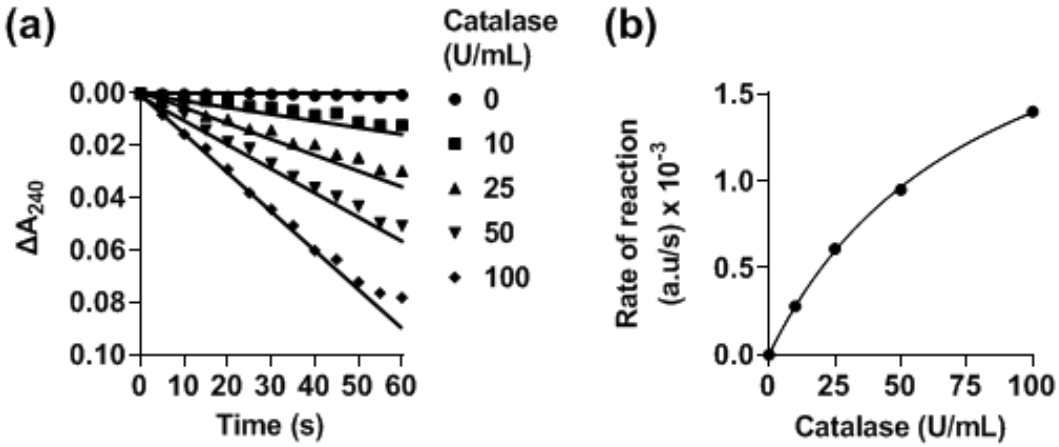

Figure 4.1. Representative absorbance time-course and standard curve for the measurement of catalase enzyme activity from cellular samples. Catalase enzyme from bovine liver was dissolved to the indicated final concentrations in assay buffer (55 mM phosphate buffer at pH 7) in a quartz cuvette. H_2O_2, from a stock solution dissolved in assay buffer, was added to a final concentration of 5 mM. **Panel (a),** ΔA_{240} of H_2O_2, in the presence of 0–100 U/mL catalase, was measured at intervals of 5 s for 60 s on a SpectraMax M_2e spectrophotometer at 22°C. **Panel (b),** the slope of the initial linear reaction (ΔA_{240} 0–1 min) plotted against [catalase] (0–100 U/mL) which represents the reaction rate (a.u./s), n=1. **ΔA:** change in absorbance.

4.2.2. Measurement of superoxide dismutase enzyme activity

A431 cells were seeded, grown and lysed as detailed before **(section 4.2.1)**. SOD activity was measured, using the method described by Peskin and Winterbourn [301], by monitoring the hypoxanthine and xanthine oxidase-generated $O_2^{\bullet-}$-dependent reduction of the tetrazolium dye, 2-(4-iodophenyl)-3-(4-nitrophenyl)-5-(2,4-disulfophenyl)-2H-tetrazolium sodium salt (WST-1). Assay buffer (47.8 mM Na_2HPO_4 and 7.2 mM NaH_2PO_4, pH 8.0) containing 0.1 mM diethylenetriaminepentaacetic acid, 0.1 mM hypoxanthine and 50 µM WST-1 was added to a clear bottom plastic 96 well plates containing 200 µg of sample protein. The reaction was initiated by adding 10 mU XO and the plate was shaken vigorously for 30 s. A_{438} of WST-1 was measured using a SpectraMax M_2e spectrophotometer (Molecular Devices) at 22°C **(Figure 4.2 a)**. Known concentrations of SOD (0–200 U/ ml) were also assayed, allowing interpolation of sample SOD activity from a standard curve, where the slope of the initial linear reaction (ΔA_{438} 0–1 min) was plotted against SOD activity **(Figure 4.2 b)**. The y axis of the standard curve is labelled as the reaction rate (a.u/s) **(Figure 4.2 b)**. The resulting activity was then normalised to sample [protein] **(section 4.3.3)**. One unit of SOD is defined as the amount of enzyme required to inhibit the $O_2^{\bullet-}$-dependent reduction of WST-1 by 50% at pH 7.0, at a temperature of 22ºC, and at a WST-1 concentration of 50 µM.

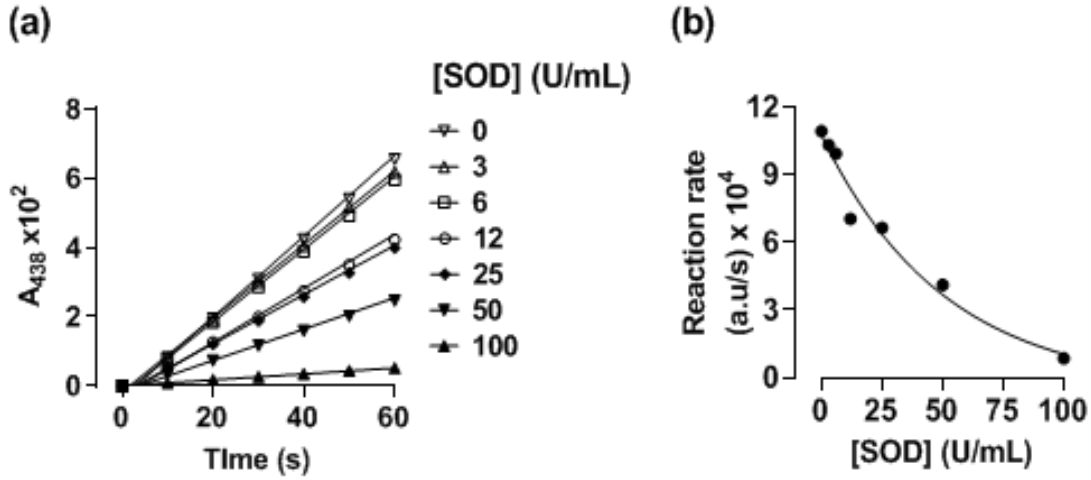

Figure 4.2. Representative absorbance time-course and standard curve for the measurement of superoxide dismutase enzyme activity from cellular samples. 0–100 U/mL bovine SOD was added to plastic 96 well plates in assay buffer (55 mM sodium phosphate (pH 8.0) containing 0.1 mM DTPA, 0.1 mM hypoxanthine, 50 µM WST-1 and 0–100 U/mL SOD). The reaction was initiated by adding XO to a final concentration of 10 mU/mL. The plate was shaken for 30 s and A_{438} was measured using a Spectramax M_2e spectrophotometer. **Panel (a),** A_{438} of WST-1 measured at intervals of 10 s for 60 s. **Panel (b),** the slope of the initial linear reaction (ΔA_{438} 0–1 min) plotted against [SOD] (0–100 U/mL), which represents the reaction rate (a.u./s). n=1. **ΔA:** change in absorbance; **SOD:** superoxide dismutase; **XO:** xanthine oxidase.

4.2.3. Measurement of glutathione reductase enzyme activity

A431 cells were seeded, grown and lysed as detailed before **(section 4.2.1)**. GR activity was measured utilising a modified version of the method described by Mannervik et al. [302] by monitoring the NADPH-dependent reduction of GSSG by GR. 20 µL of sample was added to plastic 96 well plates containing assay buffer (115.6 mM Na_2HPO_4 and 84.4 mM NaH_2PO_4 (pH 7.0), 2 mM EDTA, and 1 mM GSSG) [302]. The reaction was initiated by adding NADPH to a final concentration of 240 µM. The plate was shaken vigorously for 30 s on an orbital shaker and the oxidation of NADPH was monitored at 340 nm at intervals of 5 s for 1 min at 22°C **(Figure 4.3 a)**. Known concentrations of GR (0–10 mU/mL) were also assayed, allowing interpolation of sample GR activity from a standard curve, where slope of the initial linear reaction (ΔA_{340} 0–1 min) was plotted against GR activity **(Figure 4.3 b)**. The y axis of the standard curve is labelled as the reaction rate (a.u/s) **(Figure 4.3 b).** Sample activity was then normalised to sample [protein] **(section 4.3.4)**. One unit of GR is defined as the amount of enzyme which oxidized 1 µM of NADPH per minute at pH 7.0, at a temperature of 22°C, and at a substrate concentration of 1mM GSSG.

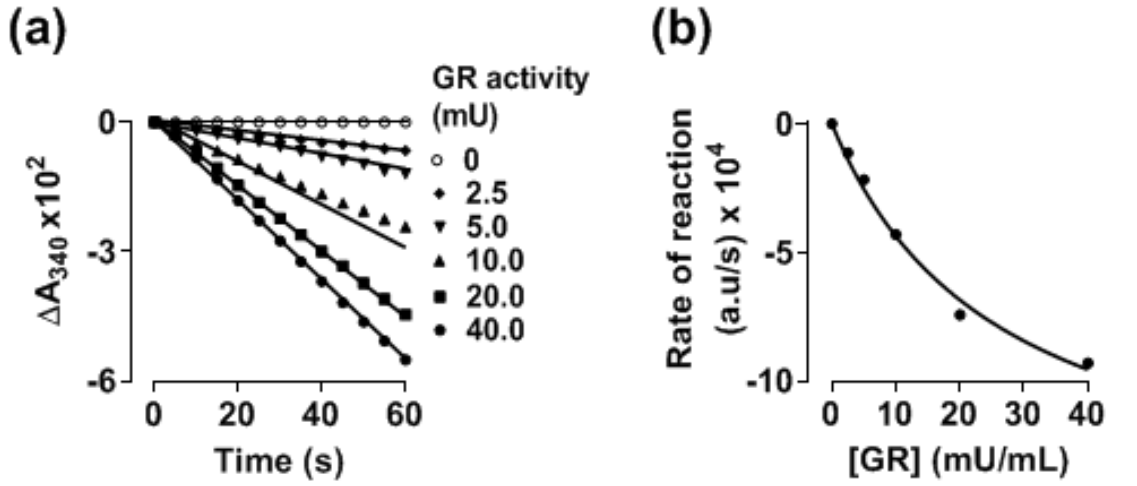

Figure 4.3. Representative absorbance time-course and standard curve for the measurement of glutathione reductase enzyme activity from cellular samples. Assay buffer (200 mM potassium phosphate (pH 7.0) containing 2 mM EDTA, 1 mM GSSG and 240 µM NADPH) was added to plastic 96 well plates. To this mixture, GR enzyme was added to the indicated final concentrations from a stock solution made up in assay buffer. The plate was shaken vigorously for 30 s and A_{340} was measured using a Spectramax M_2e spectrophotometer at 22°C. **Panel (a),** ΔA_{340} monitored at intervals of 5 s for 1 min. **Panel (b),** the slope of the initial linear reaction (ΔA_{340} 0–1 min) plotted against [GR] (0–40 mU/mL), which represents the reaction rate (a.u./s). n=1. **ΔA:** change in absorbance; **GR:** glutathione reductase.

4.2.4. Measurement of glutathione peroxidase enzyme activity

A431 cells were seeded, grown and lysed as before **(section 4.2.1)**. Gpx activity was measured, using a modified version of the method described by Mannervik et al. [302] by monitoring the NADPH-dependent reduction of GSSG. 20 µL of sample was added to plastic 96 well plates containing assay buffer (50 mM Tris-HCL (pH 7.0), 5 mM EDTA, and 1 mg/mL BSA). Co-substrate mixture containing 1 mM GSH, and 1 mU GR (dissolved in assay buffer) was added to equal volumes of Gpx sample in clear bottom plastic 96 well plates. 240 µM of NADPH, made up in assay buffer, was then added. The reaction was initiated by adding H_2O_2 to a final concentration of 100 µM. The plate was shaken vigorously for 30 s prior to montoring ΔA_{340} at intervals of 5 s for 55 s using a Spectramax M_2e spectrophotometer at 22°C **(Figure 4.4 a)**. Known concentrations of Gpx (0–1 mU/mL; Merck) were also assayed, allowing interpolation of sample Gpx activity from a standard curve, where the slope of the initial linear reaction (ΔA_{340} 0–55 s) was plotted against Gpx activity **(Figure 4.4 b)**. The y axis of the standard curve is labelled as the reaction rate (a.u/s) **(Figure 4.4 b)**. Sample activity was then normalised to sample [protein] **(section 4.3.5)**. One unit of Gpx is defined as the amount of enzyme which oxidised 1 µM of GSH per minute at pH 7.5, at a temperature of 22°C, and at a substrate concentration of 1mM GSH.

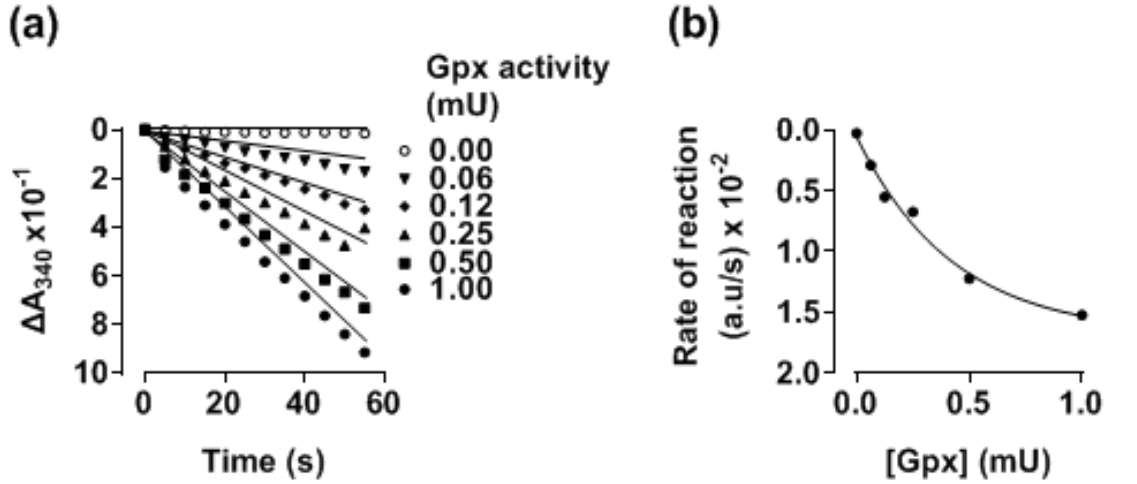

Figure 4.4. Representative absorbance time-course and standard curve for the measurement of glutathione peroxidase enzyme activity from cellular samples. Gpx from bovine erythrocyte (Merck) was diluted to the indicated concentrations in Gpx sample buffer (50 mM Tris-HCL containing 5 mM EDTA and 1 mg/mL BSA at pH 7.5). Co-substrate mixture (containing 1 mM GSH, and 1 mU GR dissolved in assay buffer (50 mM Tris-HCL with 5 mM EDTA at pH 7.5) was added to equal volumes of Gpx sample in clear bottom plastic 96 well plates. NADPH (made up in assay buffer) was added to a final concentration of 240 µM. The reaction was initiated by adding H_2O_2 to a final concentration of 100 µM. The plate was shaken for 30 s on an orbital shaker and A_{340} was measured using a Spectramax M_2e spectrophotometer at 22°C. **Panel (a),** ΔA_{340} monitored at intervals of 5 s for 55 s on a SpectraMax M_2e spectrophotometer. **Panel (b),** the slope of the initial linear reaction (ΔA_{340} 0–1 min) plotted against [Gpx] (0–1 mU/mL), which represents the reaction rate (a.u./s). n=1. **ΔA:** change in absorbance; **Gpx:** glutathione peroxidase; **GR:** glutathione reductase.

4.2.5. Measurement of glutathione S-transferase enzyme activity

A431 cells were seeded, grown and lysed as detailed before **(section 4.2.1)**. Measurement of GST enzyme activity was measured, using a modified method described by Pour et al. [303] by measuring the absorbance of the GSH-1-chloro-2,4-dinitrobenzene (CDNB) conjugate at 340 nm. 20 µL of sample was added to 50 µL of assay buffer (17.9 mM Na_2HPO_4 and 32.1 mM NaH_2PO_4, 1 mg/mL BSA, and 1 mM GSH at pH 6.5) in clear bottom plastic 96 well plates. The reaction was initiated by adding 10 µL of CDNB to a final concentration of 1 mM. The plate was shaken vigorously for 30 s on an orbital shaker prior to measuring A_{340} of the GSH-CDNB conjugate at intervals of 5 s for 1 min using a Spectramax m_2e spectrophotmeter at 22°C **(Figure 4.5 a)**. Known concentrations of GST (0–20 mU/mL; #G6511; Merck) were also assayed, allowing interpolation of sample GST activity from a standard curve, where the slope of the initial linear reaction (ΔA_{340} 0–1 min) was plotted against GST activity **(Figure 4.5 b)**. The y axis of the standard curve is labelled as the reaction rate (a.u/s) **(Figure 4.5 b)**. Sample activity was then normalised to sample [protein] **(section 4.3.6)**. One unit of GST is defined as the amount of enzyme which produced 1 µM of GS-DNB conjugate

per minute at pH 6.5, at a temperature of 22°C, and at a substrate concentration of 1mM GSH.

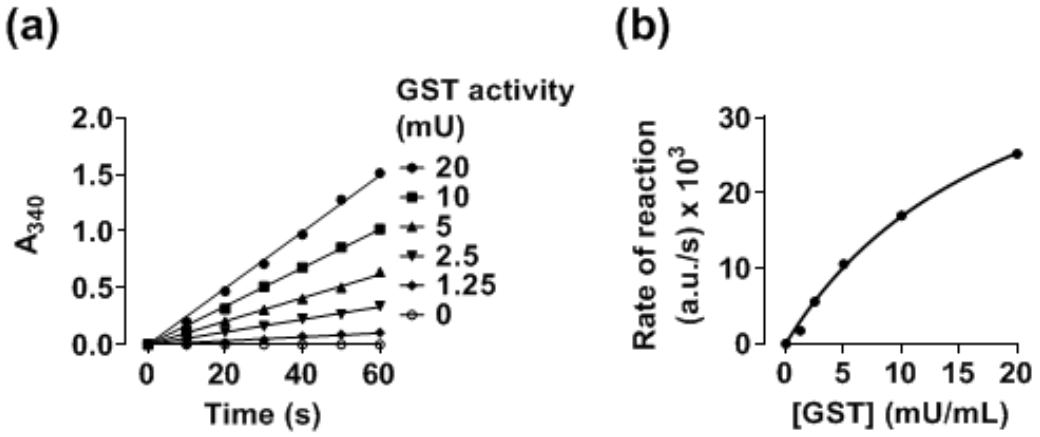

Figure 4.5. Representative absorbance time-course and standard curve for the measurement of glutathione S-transferase enzyme activity from cellular samples. GST was added to the indicated final concentrations in sample buffer (50 mM phosphate buffer and 1mg/mL BSA, pH 6.5). 20 µL of sample or standard was added to 50 µL of assay buffer (1mM GSH in 50 mM phosphate buffer, pH 6.5) in clear bottom plastic 96 well plates. The reaction was initiated by adding 10 µL of CDNB (made up in 50 mM phosphate buffer, pH 6.5) to each appropriate well to achieve a final concentration of 1 mM CDNB. The plate was shaken vigorously for 30 s and A_{340} was measured using a Spectramax M_2e spectrophotometer at 22°C. **Panel (a),** A_{340} monitored at intervals of 5 s for 1 min. **Panel (b),** the slope of the initial linear reaction (ΔA_{340} 0–1 min) plotted against [GST] (0–20 mU/mL), which represents the reaction rate (a.u./s). n=1. **ΔA:** change in absorbance; **CDNB:** 1-chloro-2,4-dinitrobenzene; **GSH:** glutathione **GST:** glutathione S-transferase.

4.2.6. Measurement of cellular oxidised and reduced glutathione

A431 cells were grown, seeded and lysed as detailed previously **(section 4.2.1)**. Measurement of GSH and GSSG from cellular samples was performed utilising the method of Rahman et al. [236]. GSH (0–100 µM) or 20 µL of sample were added to 20 µL of assay buffer (75.4 mM Na_2HPO_4 and 24.6 mM NaH_2PO_4 with 5 mM EDTA disodium salt, pH 7.4) to clear bottom plastic 96 well plates.120 µL of a DTNB and GR mixture was added (final concentration 1 mM and 2 U/mL respectively, made up in assay buffer). After 30 s, NADPH (from a stock solution made up in assay buffer) was added to achieve a final concentration of 240 µM. The plate was shaken for 10 s on an orbital shaker prior to measuring A_{412} at intervals of 10 s for 1 min utilising a SpectraMax M_2e spectrophotometer at 22°C **(Figure 4.6 a).** Known concentrations of GSH (0–200 µM) were also assayed to generate a standard curve where the slope of the initial linear reaction (ΔA_{412} 0–1 min) was plotted against [GSH] **(Figure 4.6 c)**. The y axis of the GSH standard curve is labelled as the reaction rate (a.u/s) **(Figure 4.6 c)**. Sample activity was then normalised to sample [protein] **(section 4.3.7)**.

Determination of [GSSG] was performed utilising the method of Rahmen et al. [236]. In brief, 2 µL of 2-vinylpyridine was added to 100 µL of cellular lysate. The samples were then vortexed briefly for 5 s and GSH was left to derivatise for 1 h in a fume hood. The reaction was then neutralised by adding 6 µL of tri-ethanolamine before vortexing for 5 s. The pH of the final reaction solution was about 6.5 (alkaline pH favours the formation of GSSG). The samples were then assayed exactly as detailed for the GSH samples **(Figure 4.6 b)**. Known concentrations of GSSG (0–20 µM) were also assayed, allowing interpolation of sample [GSSG] from a standard curve, where the slope of the initial linear reaction (ΔA_{412} 0–1 min) was plotted against [GSSG] **(Figure 4.6 d)**. The y axis of the GSH standard curve is labelled as the reaction rate (a.u/s) **(Figure 4.6 d)**. Sample activity was then normalised to sample [protein] **(section 4.3.7)**.

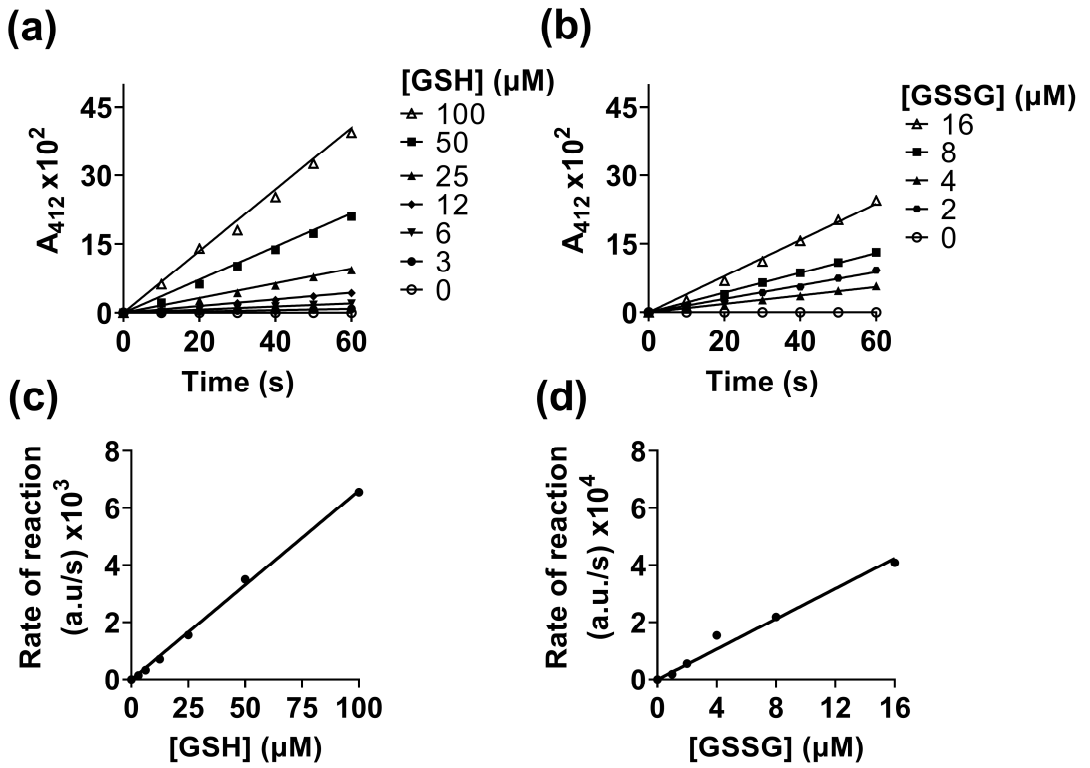

Figure 4.6. Representative absorbance time-course and standard curves for the measurement of cellular oxidised and reduced glutathione from cellular samples. 20 µL of GSH standards (0–100 µM) were added to clear bottom plastic 96 well plates in assay buffer (0.1M potassium phosphate buffer with 5 mM EDTA disodium salt, pH 7.5) at the indicated final concentrations. DTNB and GR (from stock solutions made up in assay buffer) were added together in equal volumes to achieve final concentrations of 1 mM and 2 U/mL respectively 120 µL of the DTNB and GR mixture was then added to sample or standards. After 30 s, NADPH (from a stock solution made up in assay buffer) was added to a final concentration of 240 µM. The plate was shaken for 10 s on an orbital shaker prior to measuring A_{412} at intervals of 10 s for 1 min using a SpectraMax M_2e spectrophotometer. For determination of [GSSG], 2 µL of 2-vinylpyridine was added to 20 µL of GSSG standards (0–20 µM). The samples were then vortex briefly for 5 s and GSH was left to derivatise for 1 h in a fume hood. The reaction was then neutralised by adding 6 µL of tri-ethanolamine before vortexing for 5 s. The samples were then assayed exactly as detailed for the GSH samples. **Panel (a),** GSH standard time-course monitoring A_{412}. **Panel (b),** GSSH standard time-course monitoring A_{412}. **Panel (c),** the slope of the initial linear reaction (ΔA_{412} 0–1 min) from the GSH time-course data plotted against [GSH] (0–100 µM) which represents the reaction rate (a.u./s). **Panel (d),** the slope of the initial linear reaction (ΔA_{412} 0–1 min) from GSSG time-course data plotted against [GSSG] (0–16 µM) which represents the reaction rate (a.u./s). n=1. **ΔA:** change in absorbance; **DTNB:** 5,5′-Dithiobis(2-nitrobenzoic acid); **GSH/GSSG:** reduced/oxidised glutathione.

4.2.7. Semi-quantitation of the levels of nuclear factor erythroid-2-related factor 2, NAD(P)H quinone oxidoreductase-1, catalase and 3-nitrotyrosine by western blotting

A431 cells were seeded at a density of 9.5 x 10^3 cells/cm^2 in 6 well plates. The cells were grown in 18.6% O_2 or 3.0% O_2 for 24-96 h (37°C/5% CO_2). A431 cells were fed every 24 h with respective (18.6% or 3.0% O_2) [O_2]-equilibrated growth medium. Multiple endpoints were then analysed. For the analysis of Nrf-2 and catalase expression, A431 cells were left untreated and basal protein expression

was analysed. For the analysis of NQO-1 and 3-NT, A431 cells were treated with 1–32 µM auranofin or vehicle (0.1% v/v DMSO) for 1 h under the appropriate [O_2] condition (37°C/5% CO_2). For the semi-quantitation of NQO-1, catalase, and 3-NT, whole cell lysis was performed **(section 2.12.1)**. For the semi-quantitation of nuclear Nrf-2 in cellular samples, nuclear extraction under the appropriate [O_2] condition was performed as described previously **(section 2.12.2)**. The BCA assay was used to measure [protein] **(section 2.12.3)**.

For the analysis of NQO-1, catalase, and 3-NT expression, 15 µg of whole cell sample protein was added to Laemmli buffer containing 50 mM DTT prior to boiling at 95°C/5 min **(section 2.12.4)**. For analysis of Nrf-2 expression, 50 µg of sample was added to Laemmli buffer containing 50 mM DTT prior to boiling at 95°C/5 min **(section 2.12.4)**. 2 µg of recombinant human NQO-1 or Nrf-2 protein was utilised as positive controls for NQO-1 or Nrf-2 expression (respectively). Nitrated albumin was made **(section 4.2.7.1.2.)** and used as a positive control for 3-NT formation**.** Each positive control protein was prepared for western blotting as detailed previously **(section 2.12.4)**.

Protein was separated by reducing SDS polyacrylamide gel electrophoresis, and transferred to a nitrocellulose membrane **(section 2.12.5)**. Total protein was measured to normalise Nrf-2 expression levels as detailed previously **(section 2.12.5).** The membrane was then blocked with protein free blocking buffer overnight at 4°C. After 16 h, the membrane was then probed with an anti-catalase (1:1000), anti-NQO-1 (1:1000), anti-Nrf-2 (1:500), or an anti-3-NT primary antibody (1:1000) for 1 h at room temperature. The NQO-1 and catalase membranes were probed respectively for anti-cytoskeletal actin (1:2000) or GAPDH (1:2000; respectively) to control for loading error. The membrane was then subsequently washed three times with PBS and one time with PBST **(section 2.12.7)** and stained with respective anti-mouse or anti-rabbit infrared dye-conjugated secondary antibody for 1 h at room temperature **(section 2.12.7)**. The membrane was then washed three times with PBS and one time with PBST and was imaged using a LI-COR Odyssey CLx imaging system **(section 2.12.9)**.

4.2.7.1. Positive control for 3-NT detection by western blotting: nitrated albumin.

For the positive detection of 3-NT, nitrated albumin was synthesised. This first required the synthesis of $ONOO^-$. As discussed previously, the reaction between tyrosine residues and $ONOO^-$ can form 3-NT **(section 1.2.4.2.1).**

4.2.7.1.1. Peroxynitrite synthesis

The method from Koppenol et al. [304] was used for the synthesis of $ONOO^-$. [H_2O_2] was measured by absorbance at 240 nm using ε = 43.6 $M^{-1}cm^{-1}$ at a 1 cm path length **(section 2.5.1)**. On ice, 50 mL of 0.7 M acidified ice cold H_2O_2 (made up in 0.6 M HCL) was added to equal an equal volume of ice cold 0.6 M $NaNO_2$. This was immediately followed by rapid addition of 50 mL of 1.2 M NaOH after 1 s. This formed a yellow solution of diluted $ONOO^-$. To this solution, 20 mg of granular MnO_2 was added to decompose the remaining H_2O_2. The resulting solution was then filtered and frozen immediately at -20°C. The most superficial surface of the frozen solution was $ONOO^-$ which thawed rapidly at room temperature. [$ONOO^-$] was measured by absorbance at 302 nm (ϵ = 1.7 × 10^3 M^{-1} s^{-1}) using the Beer-Lambert formula **(Eq. 2.2)** [305]. $ONOO^-$ was stored in aliquots of 100 mM. These aliquots were stored short-term (< 2 months) at -20°C, or long term (> 6 months) at -80°C.

4.2.7.1.2. Generation of nitrated albumin

BSA (which contains 19 tyrosine residues [306]), was nitrated for its use as a positive control in the 3-NT western blotting studies **(section 4.3.10)**. A 2 mg/ml BSA solution (Fisher Scientific, UK) was made up in a bicarbonate based nitration buffer (100 mM potassium phosphate (KH_2PO_4) and 25 mM sodium bicarbonate ($NaHCO_3$), pH 7.0). To this solution, $ONOO^-$ made previously **(section 4.2.7.1.1)** was added to the BSA solution to a final concentration of 1 mM (from a stock diluted to 30 mM with H_2O), whilst being gently vortexed every 15 s for 1 mins. After vortexing, the pH of the solution was checked using pH indicator paper (pH 0-14, Fisher Scientific, Loughborough UK). A pH of 7.0 was required for BSA nitration. The pH was titrated as required from a stock solution of 1 M HCL or 1M NaOH. After about 3-5 mins, the mixture turned a weak yellow colour. Nitration

was confirmed by absorbance at 430 nm using a Spectramax M_2e spectrophotometer. Nitrated albumin was generated immediately prior to its use as a positive control for the detection of 3-NT in western blotting **(section 4.3.10)**.

4.3. Results

4.3.1. The effect of growing A431 cells in 18.6% O_2 on catalase activity compared to A431 cells grown in 3.0% O_2

The effect of growing A431 cells in 18.6% O_2 on catalase enzyme activity compared to A431 cells grown in 3.0% O_2 for 24-96 h was measured by monitoring the absorbance of H_2O_2 at 240 nm **(section 4.2.1).** A representative example of an absorbance time-course scan is shown in **Figure 4.7 a.**

A two-way ANOVA was performed to analyse the effects of time, and the [O_2] a cell is grown in, on catalase activity. A multiple comparison *post-hoc* test showed no statistically significant differences in catalase enzymatic activity in A431 cells grown in 18.6% O_2 compared to A431 cells grown in 3.0% O_2 for 24–72 h (**Figure 4.7 b**). However, A431 cells grown in 18.6% O_2 showed a statistically significant increase in catalase enzyme activity compared to A431 cells grown in 3.0% O_2 for 96 h ($P < 0.01$; **Figure 4.7 b**), with means of 85.5 ± 7.1 U vs 61.8 ± 2.7 U, respectively. Additionally, A431 cells grown in 3.0% O_2 for 96 h exhibited lower catalase enzyme activity compared to catalase activity in A431 cells grown in 3.0% O_2 for 24 h group ($P < 0.05$, **Figure 4.7 b)**, with means of 81.9 ± 5.4 U vs 61.8 ± 3.1 U, respectively.

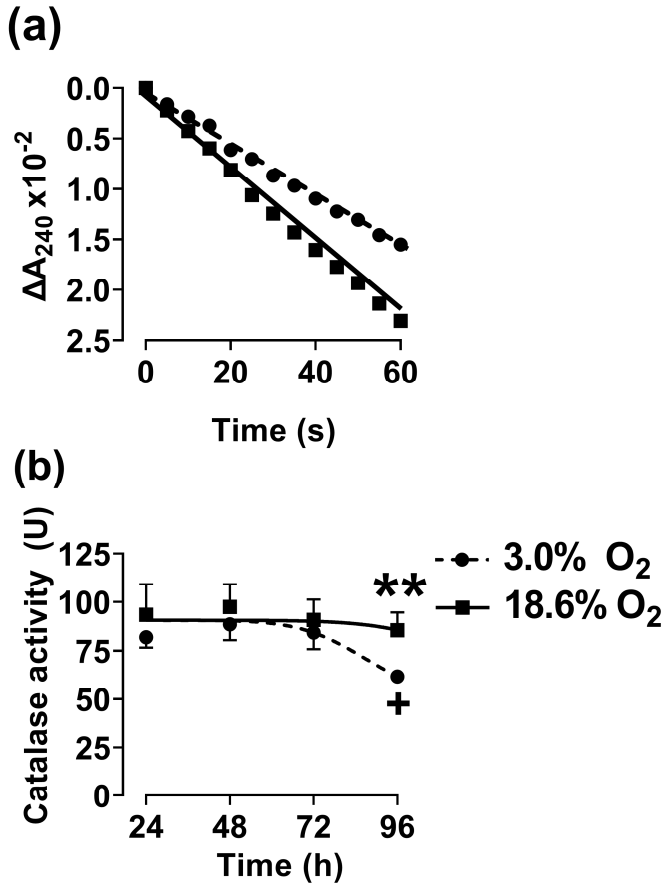

Figure 4.7. Effect of growing A431 cells in 18.6% O_2 on catalase enzyme activity compared to A431 cells grown in 3.0% O_2 for 24-96 h. A431 cells were seeded at a density of 9.5 x 10^3 cells/cm^2 in a six well plate and were grown in 18.6% O_2 or 3.0% O_2 for 24-96 h (37°C / 5% CO_2). After the indicated incubation times, A431 cells were lysed and [protein] was measured using the BCA assay (section 2.12.3). 100 µg of sample protein was added to assay buffer (50 mM phosphate buffer at pH 7). To this mixture, H_2O_2 was added to a final concentration of 5 mM. **Panel (a),** representative absorbance time course showing ΔA_{240} due to the decomposition of H_2O_2 in a solution containing cellular lysate derived from A431 cells previously grown in 18.6% or 3.0% O_2 for 96 h. The straight lines represent the initial linear reaction (solid line for the 18.6% O_2 group; dashed line for the 3.0% O_2 group) from which the slope was derived for standard curve interpolation. **Panel (b),** catalase activity in A431 cells grown in 18.6% or 3.0% O_2 for 24-96 h normalised to activity per mg of protein. + = $P < 0.05$ versus 3.0% O_2 24 h, ** = $P < 0.01$ versus 3.0% O_2 utilising a two-way ANOVA and a *post-hoc* multiple comparison test with Tukey correction. Data in panel (a) is representative of one experiment. Data in panel (b) is presented as the mean ± 1 SD. n = 4. Where error bars are not visible, this is because the error bar is smaller than the size of the data point. **ΔA:** change in absorbance.

4.3.2. The effect of growing A431 cells in 18.6% O_2 on the protein levels of catalase compared to A431 cells grown in 3.0% O_2

The effect of growing A431 cells in 18.6% O_2 on the expression levels of catalase protein compared to the catalase protein expression levels in A431 cells grown in 3.0% O_2 for 24-96 h was assessed by western blotting. The full length immunoblot images of the entire blot are shown in the Appendix **(Figure A.3)**

A two-way ANOVA was performed to analyse the effects of time, and the [O_2] a cell is grown in, on the expression levels of catalase protein. A multiple comparison *post-hoc* test showed that A431 cells grown in 18.6% O_2 exhibited a higher expression level of catalase protein compared A431 cells grown in 3.0% O_2 for 24 h ($P < 0.0001$, **Figure 4.8 b**), with means of 6.2 ± 0.9 vs 1.0 ± 0.2**.** Additionally, this higher expression level of catalase remained higher in A431 cells grown in 18.6% O_2 when compared to A431 cells grown in 3.0% O_2 for 48 hr ($P < 0.0001$), 72 hr ($P < 0.01$), and 96 hr ($P < 0.0001$; **Figure 4.8 b**).

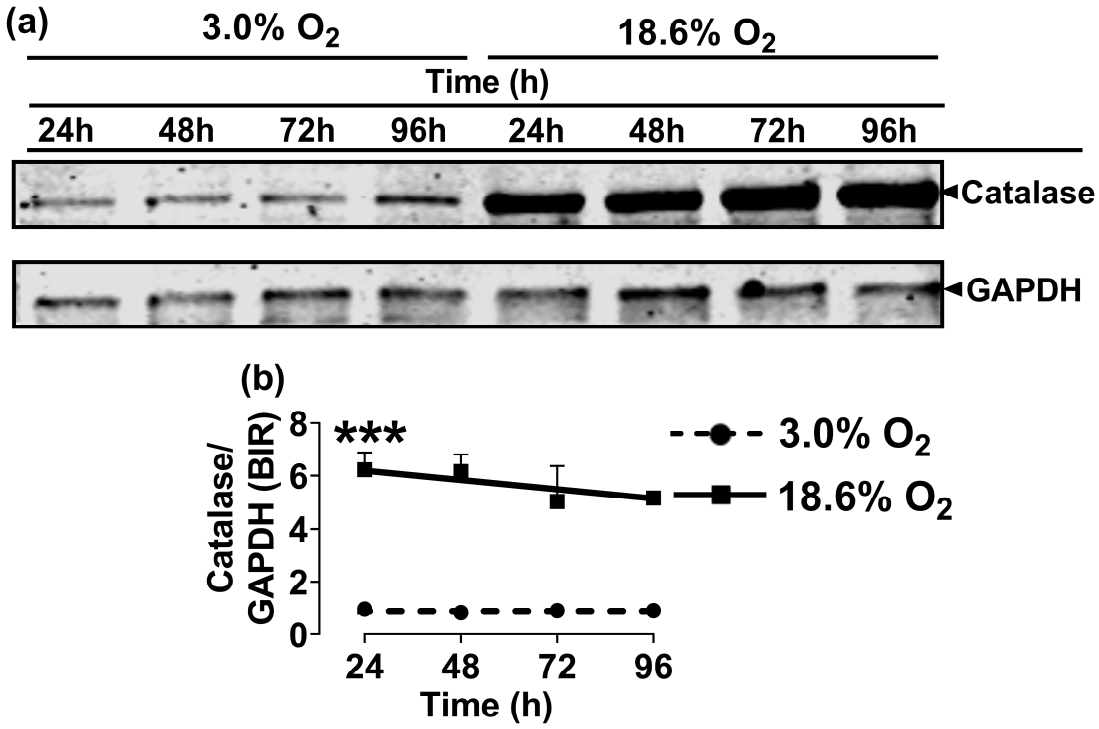

Figure 4.8. The effect of growing A431 cells in 18.6% O_2 on the level of basal catalase protein compared to A431 cells grown in 3.0% O_2 for 24-96 h. A431 cells were seeded at a density of 9.5 x 10^3 cells/cm^2 in 6 well plate and were grown in 18.6% O_2 or 3.0% O_2 for 24-96 h (37°C /5% CO_2). A431 cells were fed every 24 h with fresh respective (18.6% or 3.0% O_2) [O_2]-equilibrated growth medium. After treatment, cells were lysed (section 2.12.1) and [protein] was quantified by BCA assay (section 2.12.3). Proteins were then separated by reducing SDS PAGE, and transferred to a nitrocellulose membrane. Loading error was controlled for by staining for total protein utilising a LI-COR total protein stain kit (section 2.12.8). The membrane was then probed with an anti-catalase primary antibody for 1 h at room temperature. The membrane was then subsequently probed with an anti-rabbit infrared dye-conjugated secondary antibody for 1 h at room temperature (section 2.12.7). The immunoblot was then imaged using a LI-COR Odyssey CLx imaging system (section 2.12.9). **Panel (a),** representative immunoblot from one experiment showing the 60 kDa catalase band of interest denoting catalase protein expression in A431 cells grown in 18.6% O_2 or 3.0% O_2 for 24 – 96 h. The 36 kDa band is GAPDH (loading control). **Panel (b),** densitometry analysis (section 2.12.10) of catalase protein expression levels in A431 cells grown in 18.6% O_2 relative to the levels in A431 cells grown in 3.0% O_2 for 24 h. The blot from figure A.3 panel (b) was not included in the densitometric analysis due to the low antibody reactivity in the 3.0% O_2 sample lanes. *** = $P < 0.001$ versus 3.0% O_2 utilising a two-way ANOVA and a *post-hoc* multiple comparison test with Dunn-Šidák correction. Data in panel (b) is presented as the mean ± 1 SD. n = 3. Where error bars are not visible, this is because the error bar is smaller than the size of the data point. **BIR:** band intensity ratio; **GAPDH:** glyceraldehyde-3-phosphate dehydrogenase.

4.3.3. The effect of growing A431 cells in 18.6% O_2 on superoxide dismutase activity compared to A431 cells grown in 3.0% O_2

The effect of growing A431 cells in 18.6% O_2 on SOD enzyme activity compared to A431 cells grown in 3.0% O_2 for 24-96 h was measured by monitoring the XO-generated $O_2^{\bullet-}$-dependent reduction of the tetrazolium dye WST-1 **(section 4.2.2).** A representative example of an absorbance time-course scan is shown in **Figure 4.9 a.**

A two-way ANOVA was performed to analyse the effects of time, and the [O_2] a cell is grown in, on SOD activity. A multiple comparison *post-hoc* test showed no statistically significant differences in SOD activity when comparing A431 cells grown in 18.6% O_2 to A431 cells grown in 3.0% O_2 for 24 h–96 h **(Figure 4.9 b)**.

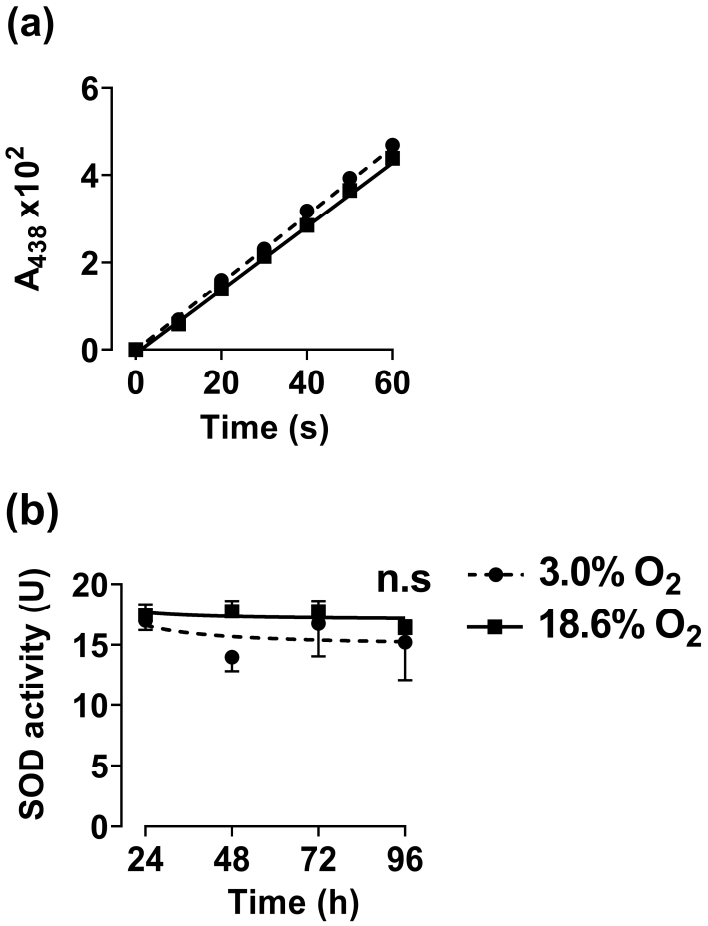

Figure 4.9. Effect of growing A431 cells in 18.6% O_2 on superoxide dismutase enzyme activity compared to A431 cells grown in 3.0% O_2 for 24-96 h. A431 cells were seeded at a density of 9.5 x 10^3 cells/cm^2 in a six well plate and grown in 18.6% O_2 or 3.0% O_2 for 24-96 h (37°C / 5% CO_2). After the indicated incubation times, cells were lysed and [protein] was measured using the BCA assay (section 2.12.3). 200 µg of sample protein was added to an equal volume of assay buffer (50 mM sodium phosphate (pH 8.5) containing 0.1 mM DTPA, 0.1 mM hypoxanthine and 50 µM WST-1). The reaction was initiated by adding xanthine oxidase to a final activity of 10mU. The plate was then shaken for 30 s on an orbital shaker and A_{438} was measured using a Spectramax M_2e spectrophotometer. **Panel (a),** representative absorbance time course showing A_{438} due to the $O_2^{\bullet-}$-dependent oxidation of WST-1 in a solution containing lysate derived from A431 cells previously grown in 18.6% or 3.0% O_2 for 96 h. Lines represent the initial linear reaction (solid line for the 18.6% O_2 group; dashed line for the 3.0% O_2 group) from which the slope was derived for standard curve interpolation. **Panel (b),** SOD activity in A431 cells previously grown in 18.6% or 3.0% O_2 for 24-96 h normalised to activity per mg of protein. n.s (not significant) versus 3.0% O_2 utilising a two-way ANOVA and a *post-hoc* multiple comparisons test with Dunn-Šidák correction. Data in panel (a) is representative of one experiment. Data in panel (b) is presented as the mean ± 1 SD. n = 4. Where error bars are not visible, this is because the error bar is smaller than the size of the data point. **A:** absorbance; **SOD:** superoxide dismutase.

4.3.4. The effect of growing A431 cells in 18.6% O_2 on glutathione reductase activity compared to A431 cells grown in 3.0% O_2

The effect of growing A431 cells in 18.6% O_2 on GR enzyme activity compared to A431 cells grown in 3.0% O_2 for 24-96 h was measured by monitoring the GR-dependent oxidation of NADPH at 340 nm **(section 4.2.3).** A representative example of an absorbance time-course scan is shown in **Figure 4.10 a.**

A two-way ANOVA was performed to analyse the effects of time and the [O_2] a cell is grown in on GR activity. A multiple comparison *post-hoc* test showed no statistically significant differences in GR enzyme activity when comparing A431 cells grown in 18.6% O_2 to A431 cells grown in 3.0% O_2 for 24 h or 48 h (**Figure 4.10 b**). However, A431 cells grown in 18.6% O_2 showed a statistically significant increase in GR activity compared to A431 cells grown in 3.0% O_2 for 72 or 96 h **(Figure 4.10 b)**, with means of 31.0 ±1.4 mU vs 21.2 ± 4.4 mU ($P < 0.05$), and 30.2 ± 1.9 mU vs 15.5 ± 3.3 mU ($P < 0.01$), respectively.

Additionally, A431 cells grown in 3.0% for 96 h exhibited decreased GR activity compared to A431 cells grown in 3.0% O_2 for 24 h, with means of 29.5 ± 9.5 mU vs 15.5 ± 3.3 mU ($P < 0.05$; **Figure 4.10 b**). The interaction between the effects of time, and the [O_2] cells were grown in, on GR activity was statistically significant (F (3, 44) = 3.825, P=0.0161).

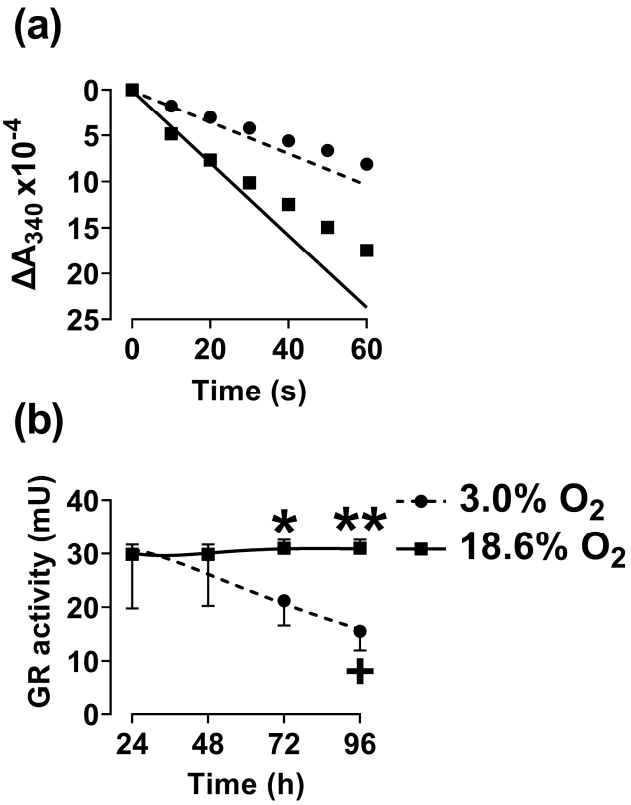

Figure 4.10. Effect of growing A431 cells in 18.6% O_2 on glutathione reductase enzyme activity compared to A431 cells grown in 3.0% O_2 for 24-96 h. A431 cells were seeded at a density of 9.5 x 10^3 cells/cm^2 in a six well plate and grown in 18.6% O_2 or 3.0% O_2 for 24-96 h (37°C / 5% CO_2). After the indicated incubation times, cells were lysed and [protein] was measured using the BCA assay (section 2.12.3). 100 µg of sample protein was added to an equal volume of assay buffer (200 mM potassium phosphate (pH 7.0) containing 2 mM EDTA, and 1 mM GSSG). To this mixture, NADPH was added to a final concentration of 240 µM. The plate was shaken on an orbital shaker for 30 s followed by measuring A_{340} using a Spectramax M_2e spectrophotometer. **Panel (a),** representative absorbance time course showing ΔA_{340} due to the GR-dependent oxidation of NADPH in a solution containing lysate derived from A431 cells previously grown in 18.6% or 3.0% O_2 for 96 h. Lines represent the initial linear reaction (solid line for the 18.6% O_2 group; dashed line for the 3.0% O_2 group) from which the slope was derived for standard curve interpolation. **Panel (b),** representative example showing GR activity in A431 cells previously grown in 18.6% or 3.0% O_2 for 24-96 h normalised to activity per mg protein. + = $P < 0.05$ versus 3.0% O_2 24 h, * = $P < 0.05$, ** = $P < 0.01$ versus 3.0% O_2 utilising a two-way ANOVA and a *post-hoc* multiple comparison test with Tukey correction. Data in panel (a) is representative of one experiment. Data in panel (b) is presented as the mean ± 1 SD. n = 4. Where error bars are not visible, this is because the error bar is smaller than the size of the data point. **ΔA:** change in absorbance; **GR:** glutathione reductase**.**

4.3.5. The effect of growing A431 cells in 18.6% O_2 on glutathione peroxidase activity compared to A431 cells grown in 3.0% O_2

The effect of growing A431 cells in 18.6% O_2 on Gpx enzyme activity compared to A431 cells grown in 3.0% O_2 for 24-96 h was measured by monitoring the NADPH-dependent reduction of GSSG by GR at 340 nm **(section 4.2.4).** A representative example of an absorbance time-course scan is shown in **Figure 4.11 a.**

A two-way ANOVA was performed to analyse the effects of time, and the [O_2] cells were grown in, on Gpx activity. A multiple comparison *post-hoc* test showed no statistically significant difference in Gpx enzyme activity when comparing A431 cells in 18.6% O_2 to A431 cells grown in 3.0% O_2 at any of the indicated time-points **(Figure 4.11 b)**.

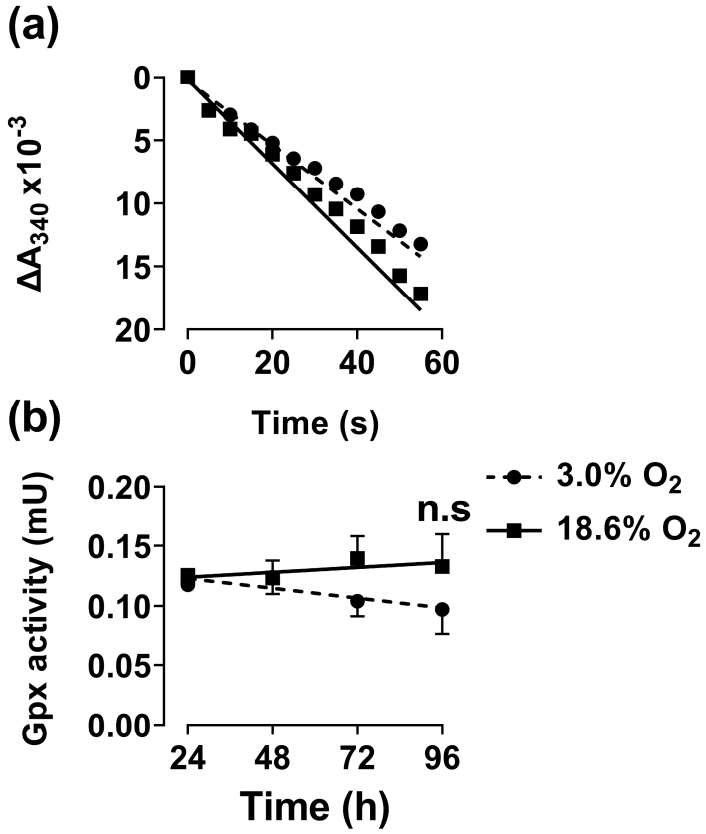

Figure 4.11. Effect of growing A431 cells in 18.6% O_2 on glutathione peroxidase enzyme activity compared to A431 cells grown in 3.0% O_2 for 24-96 h. A431 cells were seeded at a density of 9.5 x 10^3 cells/cm^2 in a six well plate and grown in 18.6% O_2 or 3.0% O_2 for 24-96 h (37°C / 5% CO_2). After the indicated incubation times, cells were lysed and [protein] was measured using the BCA assay (section 2.12.3). 200 µg of sample protein was added to 50 µL of co-substrate mixture (50 mM Tris-HCL, 5 mM EDTA, 1 mM GSH, 1 mU GR at pH 7.5) into a clear bottom plastic 96 well plates. NADPH was added to a final concentration of 240 µM. The reaction was initiated by adding H_2O_2 (made up in assay buffer) to a final concentration of 100 µM. The plate was then shaken on an orbital shaker for 30 s and A_{340} using a Spectramax M_2e spectrophotometer. **Panel (a),** representative absorbance time course showing ΔA_{340} due to the NADPH-dependent reduction of GSSG by GR in a solution containing cellular lysate derived from A431 cells previously grown in 18.6% or 3.0% O_2 for 24-96 h. Lines represent the initial linear reaction (solid line for the 18.6% O_2 group; dashed line for the 3.0% O_2 group) from which the slope was derived for standard curve interpolation. **Panel (b),** Gpx activity in A431 cells grown in 18.6% or 3.0% O_2 for 24-96 h normalised to activity per mg of protein. n.s = not significant versus 3.0% O_2 utilising a two-way ANOVA and a *post-hoc* multiple comparison test with Tukey correction. Data in panel (a) is representative of one experiment. Data in panel (b) is presented as the mean ± 1 SD. n = 3. Where error bars are not visible, this is because the error bar is smaller than the size of the data point. **ΔA:** change in absorbance; **Gpx:** glutathione peroxidase.

4.3.6. The effect of growing A431 cells in 18.6% O_2 on GST activity compared to A431 cells grown in 3.0% O_2

The effect of growing A431 cells in 18.6% O_2 on GST enzyme activity compared to A431 cells grown in 3.0% O_2 for 96 h was measured by monitoring the GST-dependent formation of the GSH-CDNB conjugate at 340 nm **(section 4.2.5).** A representative example of an absorbance time-course scan is shown in **Figure 4.12 a.**

A two-way ANOVA was performed to analyse the effects of time, and the [O_2] cells were grown in, on GST activity. A multiple comparison *post-hoc* test showed no statistically significant difference in GST enzyme activity when comparing A431 cells in 18.6% O_2 to A431 cells grown in 3.0% O_2 for 96 h **(Figure 4.12 b)**, with means of 0.9 ± 0.2 mU vs 0.9 ± 0.1 mU protein, respectively.

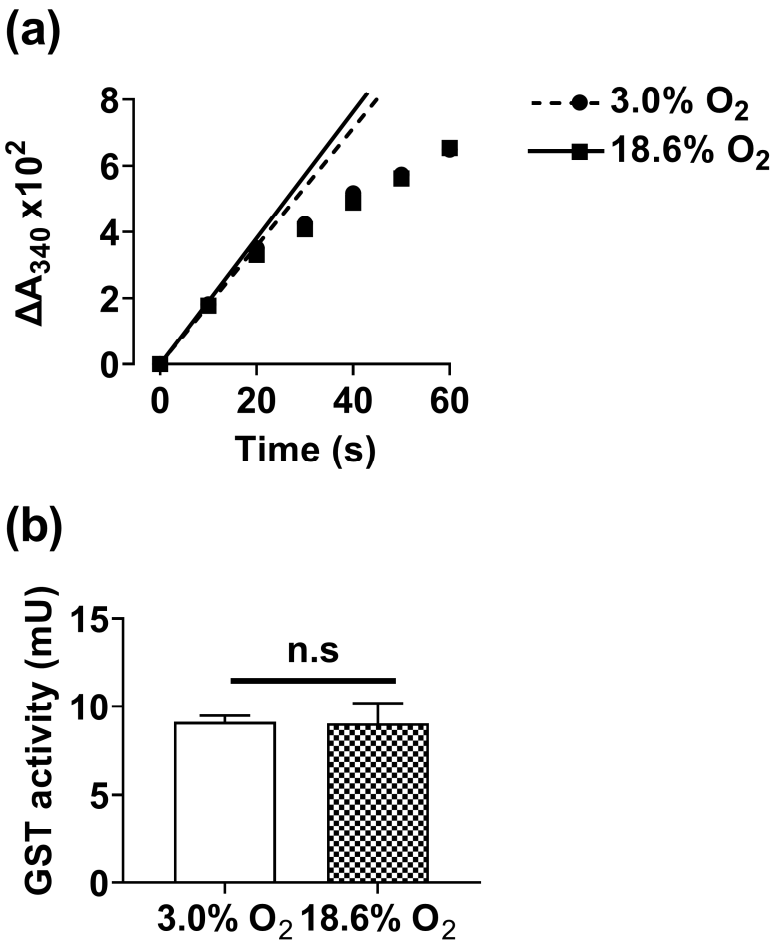

Figure 4.12. Effect of growing A431 cells in 18.6% O_2 on glutathione S-transferase enzyme activity compared to A431 cells grown in 3.0% O_2 for 24-96 h. A431 cells were seeded at a density of 9.5 x 10^3 cells/cm^2 in a six well plate and grown in 18.6% O_2 or 3.0% O_2 for 96 h (37°C / 5% CO_2). After the indicated incubation times, cells were lysed and [protein] was measured using the BCA assay (section 2.12.3). 100 µg of sample was added to an equal volume of assay buffer (1mM GSH in 50 mM phosphate buffer, pH 6.5) in clear bottom plastic 96 well plates. The reaction was initiated by adding 10 µL of CDNB (made up in 50 mM phosphate buffer, pH 6.5) to each appropriate well to achieve a final concentration of 1 mM CDNB. The plate was shaken vigorously for 30 s prior to measuring A_{340} using a Spectramax M_2e spectrophotometer**. Panel (a),** representative absorbance time course showing A_{340} due to the GST-dependent formation of the GSH-CDNB conjugate in a solution containing cellular lysate derived from A431 cells previously grown in 18.6% or 3.0% O_2 for 96 h. Lines represent the initial linear reaction (solid line for the 18.6% O_2 group; dashed line for the 3.0% O_2 group) from which the slope was derived for standard curve interpolation. **Panel (b),** GST activity in cellular lysate derived from A431 cells previously grown in 18.6% or 3.0% O_2 for 96 h normalised to activity per mg of protein. n.s = not significant versus 3.0% O_2 utilising a paired two-tailed Student's t-test. Data in panel (a) is representative of one experiment. Data in panel (b) is presented as the mean ± 1 SD. n = 3. Where error bars are not visible, this is because the error bar is smaller than the size of the data point. **A:** absorbance; **CDNB:** 1-chloro-2,4-dinitrobenzene; **GST:** glutathione S-transferase.

4.3.7. The effect of growing A431 cells in 18.6% O_2 on the concentration of reduced glutathione, oxidised glutathione and on the ratio of reduced: oxidised glutathione, compared to A431 cells grown in 3.0% O_2

The effect of growing A431 cells in 18.6% O_2 on [GSH], [GSSG] and GSH:GSSG compared to A431 cells grown in 3.0% O_2 for 24-96 h was measured by monitoring the GSH dependent formation of TNB at 412 nm **(section 4.2.6).** Representative absorbance time-course scans are shown in **Figure 4.13 a and b.**

A two way ANOVA was performed to test the effects of time, and the [O_2] cells were grown in, on [GSH]. A431 cells grown in 18.6% O_2 exhibited an apparent increase in [GSH] compared to A431 cells grown in 3.0% O_2 for 96 h (**Figure 4.13 c**), with means of 208.1 ± 25.6 µM vs 130.0 ± 2.6 µM, respectively. However, a multiple comparison *post-hoc* test showed that this apparent increase was not statistically significant ($P > 0.05$).

A two way ANOVA was performed to analyse the effects of time, and the [O_2] cells were grown in, on [GSSG]. A431 cells grown in 18.6% O_2 exhibited an apparent increase in [GSSG] compared to A431 cells grown in 3.0% O_2 for 96 h, with means of 26.1 ± 3.6 µM vs 13.9 ± 3.3 µM, respectively **(Figure 4.13 d)**. However, a *post-hoc* multiple comparison test showed that this apparent increase was not statistically significant.

A two way ANOVA was performed to test the effects of time, and the [O_2] cells were grown in, on total intracellular GSH. A431 cells grown in 18.6% O_2 exhibited an apparent increase in total glutathione compared to A431 cells grown in 3.0% O_2 for 96 h, with means of 234.2 ± 27.9 µM vs 144.7 ± 4.7 µM ($P < 0.001$; **Figure 4.13 e**). However, a *post-hoc* multiple comparison test showed that this apparent increase was not statistically significant. Additionally, there was no statistically significant difference in total [GSH] when comparing A431 cells grown in 3.0% O_2 for 96 h to A431 cells grown in 3.0% O_2 for 24 h **(Figure 4.13 e).**

Finally, there was no statistically significant difference in GSH:GSSG when comparing A431 cells grown in 18.6% O_2 to A431 cells grown in 3.0% O_2 at any of the indicated time points **(Figure 4.13 f)**.

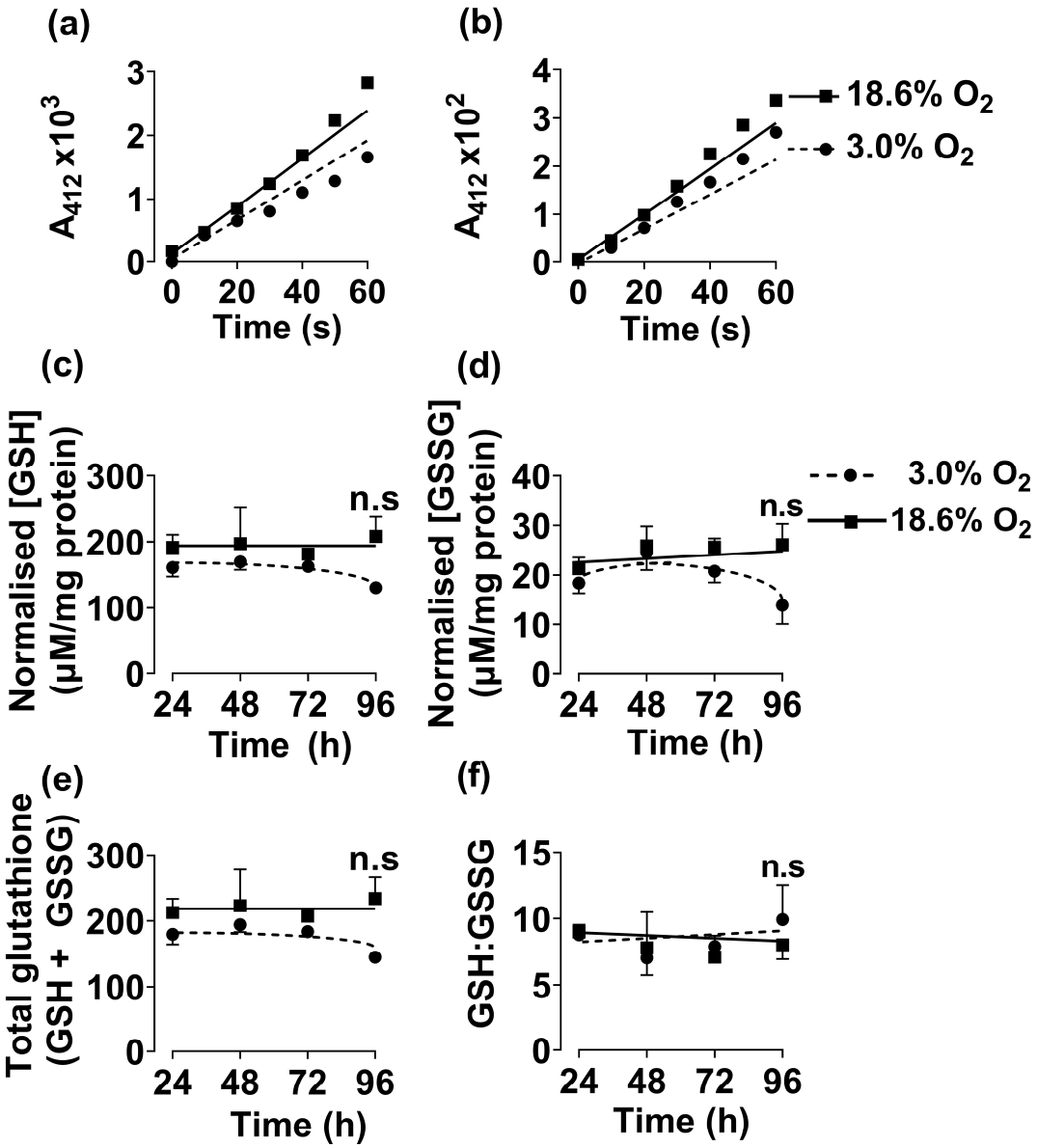
(a)
A_{412} x10^3
Time (s)
(b)
A_{412} x10^2
18.6% O_2
3.0% O_2
Time (s)
(c)
Normalised [GSH] (µM/mg protein)
n.s
Time (h)
(d)
Normalised [GSSG] (µM/mg protein)
3.0% O_2
18.6% O_2
n.s
Time (h)
(e)
Total glutathione (GSH + GSSG)
n.s
Time (h)
(f)
GSH:GSSG
n.s
Time (h)

Figure 4.13. Effect of growing A431 cells in 18.6% O_2 on the concentration of reduced and oxidised glutathione compared to A431 cells grown in 3.0% O_2 for 24-96 h. A431 cells were seeded at a density of 9.5 x 10^3 cells/cm^2 in a six well plate and grown in 18.6% O_2 or 3.0% O_2 for 24-96 h (37°C / 5% CO_2). After the indicated incubation times, cells were lysed and [protein] was measured using the BCA assay (section 2.12.3). For the measurement of [GSH], 50 µg of sample protein was added to an equal volume of assay buffer (0.1M potassium phosphate buffer with 5 mM EDTA disodium salt, pH 7.5) in clear bottom plastic 96 well plates. DTNB and GR (from stock solutions made up in assay buffer) were added together in equal volumes to achieve final concentrations of 1 mM and 2 U/mL, respectively. 120 µL of the DTNB/GR mixture was then added. After 30 s, NADPH (from a stock solution made up in assay buffer) was added to a final concentration of 240 µM. The plate was then shaken for 10 s on an orbital shaker prior to measuring A_{412} on a SpectraMax M_2e spectrophotometer at 22°C. For the determination of [GSSG], 2 µL of 2-vinylpyridine was added to 100 µg of cellular lysate sample. The samples were then vortexed for 5 s and GSH was left to derivatise for 1 h in a fume hood. The reaction was then neutralised by adding 6 µL of tri-ethanolamine before vortexing for 5 s. The samples were then assayed exactly as detailed for the GSH samples. Known concentrations of GSH (0–200 µM) or GSSG (0–20 µM) were assayed to allow interpolation of sample [GSH] or [GSSG] where the slope of the initial linear reaction (A_{412} 0–1 min) was plotted against [GSH] or [GSSG]. **Panel (a),** representative A_{412} time course for measuring GSH in a solution containing lysate derived from A431 cells grown in 18.6% or 3.0% O_2 for 96 h. The lines represent the initial linear reaction (solid line for the 18.6% O_2 group; dashed line for the 3.0% O_2 group) from which the slope was derived for standard curve interpolation. **Panel (b),** representative A_{412} time course for measuring GSSG in a solution containing cellular lysate derived from A431 cells grown in 18.6% or 3.0% O_2 for 96 h. The lines represent the initial linear reaction (solid line for the 18.6% O_2 group; dashed line for the 3.0% O_2 group) from which the slope was derived for standard curve interpolation. **Panel (c),** intracellular [GSH] in A431 cells grown in 18.6% O_2 or 3.0% O_2 for 24-96 h per mg of protein. **Panel (d),** intracellular [GSSG] in A431 cells grown in 18.6% O_2 or 3.0% O_2 for 24-96 h per mg of protein. **Panel (e),** total [GSH] (GSH + GSSG) in A431 cells grown in 18.6% O_2 or 3.0% O_2 for 24-96 h calculated by adding the [GSH] at each respective time-point in panel (a) to the [GSSG] at each respective time-point in panel (b). **Panel (f),** the ratio of GSH to GSSG in A431 cells grown in 18.6% O_2 or 3.0% O_2 for 24-96 h per mg of protein. n.s = not significant versus 3.0% O_2 utilising a two-way ANOVA and a *post-hoc* multiple comparison test with Tukey correction. Data in panels a-b are representative of single respective experiments. Data in panels c-f are presented as the mean ± 1 SD. n=4. Where error bars are not visible, this is because the error bar is smaller than the size of the data point. **A:** absorbance; **DTNB:** 5,5′-Dithiobis(2-nitrobenzoic acid); **GSH:** glutathione; **GSSG:** oxidised glutathione; **TNB:** 5'-thio-2-nitrobenzoic acid.

4.3.8. The effect of growing A431 cells in 18.6% O_2 on the levels of nuclear factor erythroid-2-related factor 2 compared to A431 cells grown in 3.0% O_2

The effect of growing A431 cells in 18.6% O_2 on the expression levels of nuclear Nrf-2 protein compared to A431 cells grown in 3.0% O_2 for 96 h was assessed by western blotting **(section 4.2.7)**. The full length immunoblot images of the entire blot are shown in the Appendix **(Figure A.2)**.

Figure 4.14 a shows representative examples of 95 kDa Nrf-2 immunoblot bands from the nuclear lysates of A431 cells grown in 18.6% or 3.0% O_2 for 96 h. **Figure 4.14 b** shows a representative example of the associated total protein stain from one experiment which was used for data normalisation. The nuclear Nrf-2 protein expression levels in A431 cells grown in 18.6% O_2 were 2.39 ± 0.39 times higher than the expression levels detected in A431 cells grown in 3.0% O_2 for 96 h ($P < 0.05$, **Figure 4.14 c**).

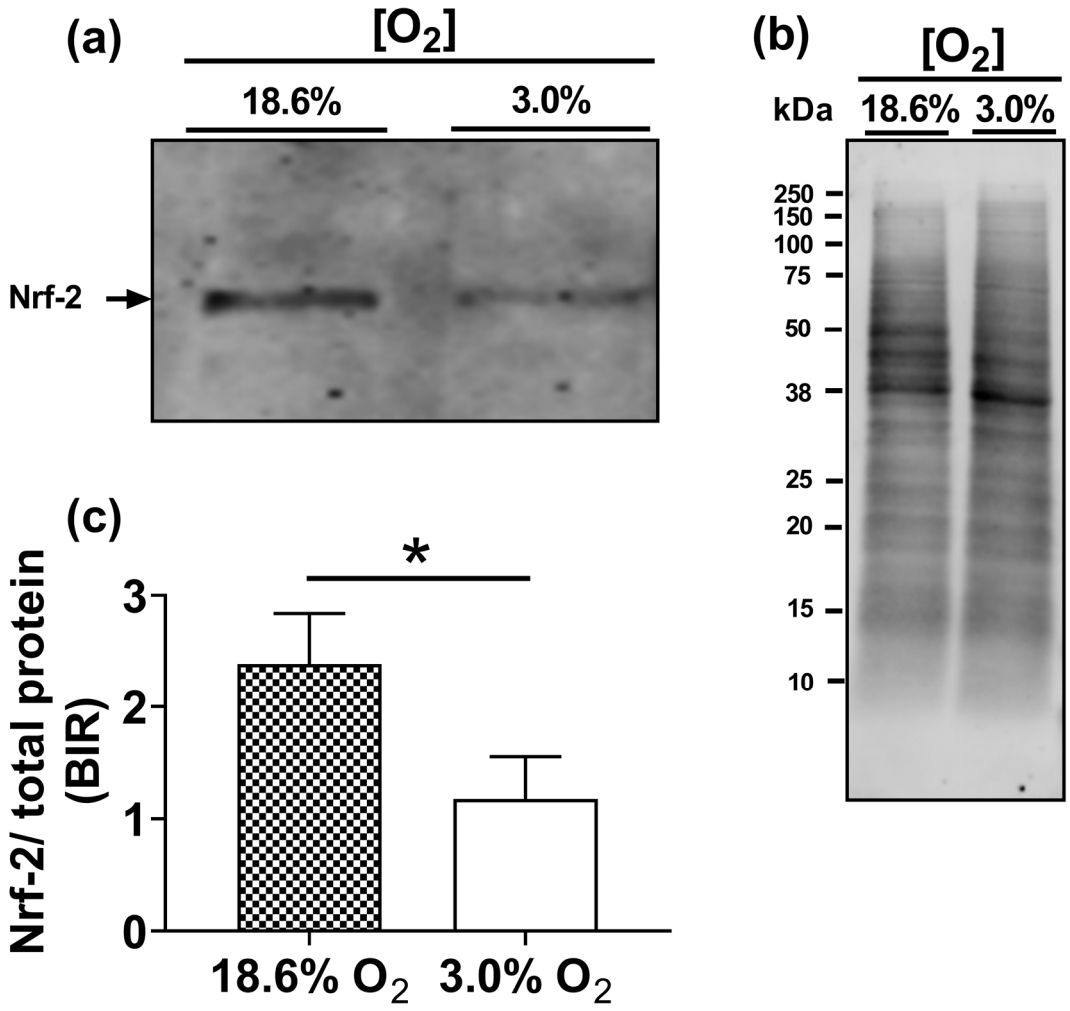

Figure 4.14. The effect of growing A431 cells in 18.6% O_2 on the level of nuclear factor erythroid-2-related factor 2 compared to A431 cells grown in 3.0% O_2 for 96 h. A431 cells were seeded at a density of 9.5 x 10^3 cells/cm^2 in 6 well plate and grown in 18.6% O_2 or 3.0% O_2 for 96 h (37°C /5% CO_2). A431 cells were fed every 24 h with fresh respective (18.6% or 3.0% O_2) [O_2]-equilibrated growth medium. A431 cells were then prepared for nuclear extraction (section 2.12.2). [Protein] was quantified by the BCA assay (section 2.12.3). Proteins were then separated by reducing SDS PAGE, transferred onto a nitrocellulose membrane, stained for total protein (section 2.12.8) and analysed for Nrf-2 expression by probing with an anti-Nrf-2 primary antibody and an anti-rabbit infrared dye-conjugated secondary antibody (section 2.12.7). The immunoblot was then imaged using a LI-COR Odyssey CLx imaging system (section 2.12.9). **Panel (a),** representative 95 kDa band of interest denoting nuclear Nrf-2 expression in A431 cells grown in 18.6% O_2 or 3.0% O_2 for 96 h. **Panel (b),** representative example of the associated total protein stain from one experiment. **Panel (c),** densitometry analysis (section 2.12.10) of nuclear Nrf-2 protein expression in A431 cells grown in 18.6% O_2 relative to levels in A431 cells grown in 3.0% O_2 for 96 h. * = $P < 0.05$ versus 3.0% O_2 utilising a two-tailed Student's t-test. Data in panel c is presented as the mean ± 1 SD. n=4. **BIR:** band intensity ratio; **kDa:** kilodalton.

4.3.9. The effect of growing A431 cells in 18.6% O_2 on auranofin-induced NAD(P)H quinone oxidoreductase induction compared to A431 cells grown in 3.0% O_2

The effect of growing A431 cells in 18.6% O_2 on auranofin-induced NQO-1 protein expression compared to auranofin-induced NQO-1 protein induction in A431 cells grown in 3.0% O_2 for 96 h was assessed by western blotting **(Figure 4.15 a and b)**. The full length immunoblot images of the entire blot are shown in the Appendix **(Figure A.4)**.

A two-way ANOVA was performed to analyse the effects of the [O_2] cells are grown in, and [auranofin], on the expression levels of NQO-1 protein. A multiple comparison *post-hoc* test showed that the expression levels of NQO-1 protein was higher in untreated A431 cells grown in 18.6% O_2 compared to untreated A431 cells grown in 3.0% O_2 ($P < 0.05$, **Figure 4.15 b**), with means of 1.8 ± 0.5 vs 1.0 ± 0.1. In A431 cells grown in 18.6% O_2, auranofin did not induce NQO-1 protein expression at any treatment concentration relative to the respective untreated control cells **(Figure 4.15 b)**. However, treatment of A431 cells grown in 3.0% O_2 for 96 h with 32 µM auranofin exhibited higher levels of NQO-1 protein expression compared to the respective untreated control cells **(Figure 4.15 b)**, with means of 1.8 ± 0.2 vs 1.0 ± 0.1.

Of note, the recombinant NQO-1 protein that was utilised as a positive control for NQO-1 expression ran to a different molecular weight (31 kDa band) relative to the target band detected in the samples (27 kDa; **Figure 4.16**). This was not due to sample preparation. Incubation of the recombinant NQO-1 protein with the sample during preparation for western blotting did not alter the molecular weight of the recombinant NQO-1 protein when compared to its molecular weight when run on its own **(Figure 4.16).** A possible explanation for the difference in the molecular weight of the recombinant NQO-1 protein compared to the molecular weight of the band detected in the A431 cell samples is discussed later in **section 4.4.4.**

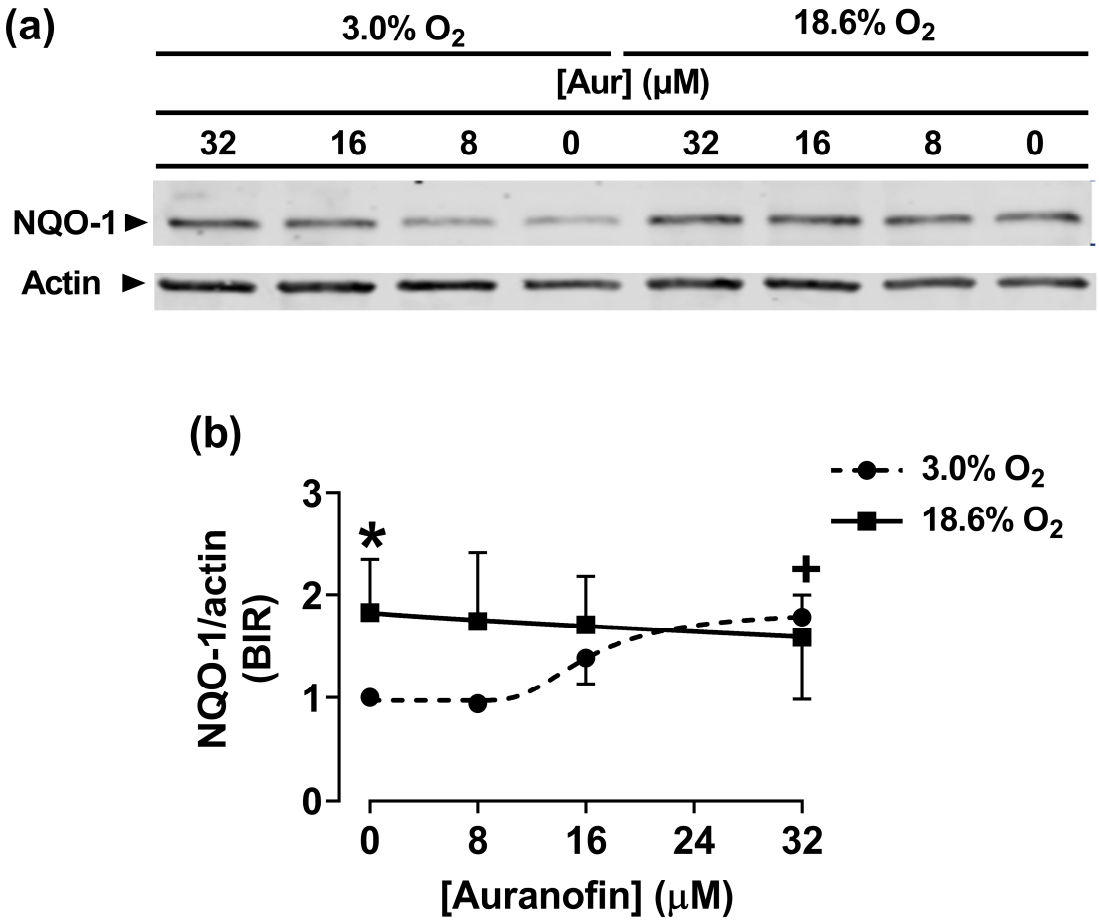

Figure 4.15. The effect of growing A431 cells in 18.6% O_2 on the auranofin-induced NAD(P)H quinone oxidoreductase-1 expression compared to A431 cells grown in 3.0% O_2 for 24-96 h. A431 cells were seeded at a density of 9.5 x 10^3 cells/cm^2 in 6 well plate and were grown in 18.6% O_2 or 3.0% O_2 for 96 h (37°C /5% CO_2). A431 cells were fed every 24 h with fresh respective (18.6% or 3.0% O_2) [O_2]-equilibrated growth medium. After 96 h of growth, cells were treated with 0–32 µM auranofin or vehicle (0.1% v/v DMSO) for 1 h in 3.0% or 18.6% O_2 (37°C /5% CO_2). After treatment, cells were lysed (section 2.12.1) and [protein] was quantified by the BCA assay (section 2.12.3). 2 µg of recombinant human NQO-1 protein was used as a positive control for NQO-1 detection (section 4.2.6). Proteins were then separated by reducing SDS PAGE, transferred to a nitrocellulose membrane, and probed with an anti-NQO-1 and anti-cytoskeletal actin antibody. The membrane was then probed with an anti-mouse/anti-rabbit infrared dye-conjugated secondary antibody for 1 h at room temperature (section 2.12.7). The immunoblot was then imaged using a LI-COR Odyssey CLx imaging system (section 2.12.9). **Panel (a),** representative immunoblot from one experiment showing the 27 kDa NQO-1 band of interest denoting NQO-1 protein expression in A431 cells grown in 18.6% or 3.0% O_2 for 96 h subsequently treated with 0-32 µM auranofin. The 42 kDa band is cytoskeletal actin (loading control). **Panel (b),** densitometry analysis (section 2.12.10) of auranofin-induced NQO-1-protein expression in A431 cells grown in 18.6% O_2 relative to levels in untreated A431 cells grown in 3.0% O_2 for 96 h**.** + = $P < 0.05$ versus the 3.0% O_2 untreated control, * = $P < 0.05$ versus 3.0% O_2 utilising a two-way ANOVA and a *post-hoc* multiple comparison test with Dunn-Šidák correction. Data in panel (b) is presented as the mean ± 1 SD. n=4. Where error bars are not visible, this is because the error bar is smaller than the size of the data point. **Aur**: auranofin; **BIR:** band intensity ratio; **kDa:** kilodalton; **NQO-1:** NAD(P)H quinone oxidoreductase 1.

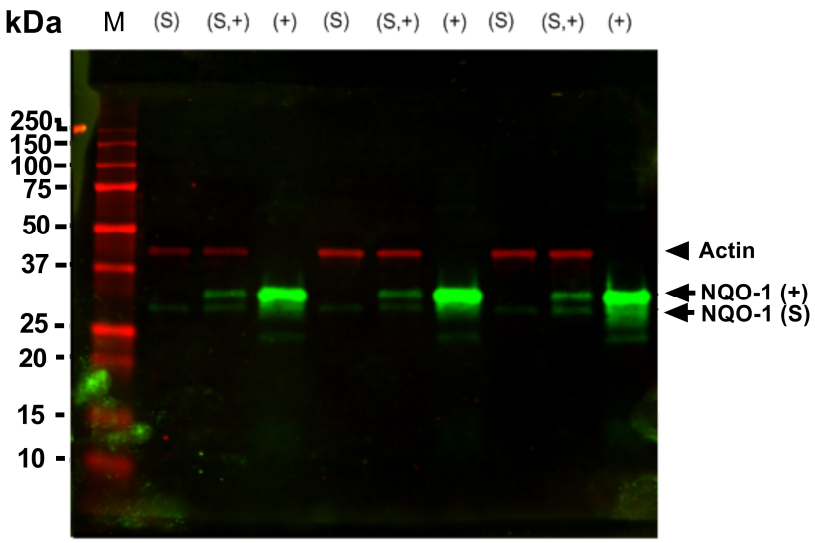

Figure 4.16: Incubation of NAD(P)H quinone oxidoreductase-1 recombinant protein with RIPA buffer containing lysed cellular sample. The following protein were then prepared for western blotting as detailed previously (section 2.12.4): 10 µg of A431 cellular lysate (S), 10 µg of A431 cellular lysate mixed with 1 µg of recombinant NQO-1 (S,+), or 5 µg of recombinant NQO-1 protein alone (+). Proteins were separated by SDS PAGE (section 2.12.5). Protein was transferred to a nitrocellulose membrane, and was subsequently stained with an anti-NQO-1 primary antibody for 1 h at room temperature. The membrane was then subsequently probed with an anti-mouse infrared dye-conjugated secondary antibody for 1 h at room temperature. The immunoblot was then imaged using a LI-COR Odyssey CLx imaging system (section 2.12.9). n=1. **kDa:** kilo Dalton; **M.W:** molecular weight; **NQO-1:** NAD(P)H quinone oxidoreductase-1.

4.3.10. The effect of growing A431 cells in 18.6% O_2 on auranofin induced protein expression containing the 3-nitrotyrosine protein modification compared to A431 cells grown in 3.0% O_2

The effect of growing A431 cells in 18.6% O_2 on auranofin-induced protein expression containing the 3-NT modification compared to A431 cells grown in 3.0% O_2 for 96 h was assessed by western blotting **(Figure 4.17 a)**. The full length immunoblot images of the entire blot are shown in the Appendix **(Figure A.5)**.

A two-way ANOVA was performed to analyse the effects of [auranofin], and the [O_2] cells were grown in, on the expression levels of protein containing the 3-NT protein modification. A multiple comparison *post-hoc* test showed that untreated A431 cells grown in 18.6% exhibited higher levels of 3-NT containing protein compared to untreated A431 cells grown in 3.0% O_2 for 96 h ($P < 0.05$, **Figure 4.17 b**), with means of 4.4 ± 2.1 vs 1.3 ± 0.1. However, auranofin treatment did not increase the levels of 3-NT containing protein in either [O_2] group compared to untreated control cells. **(Figure 4.17 b).**

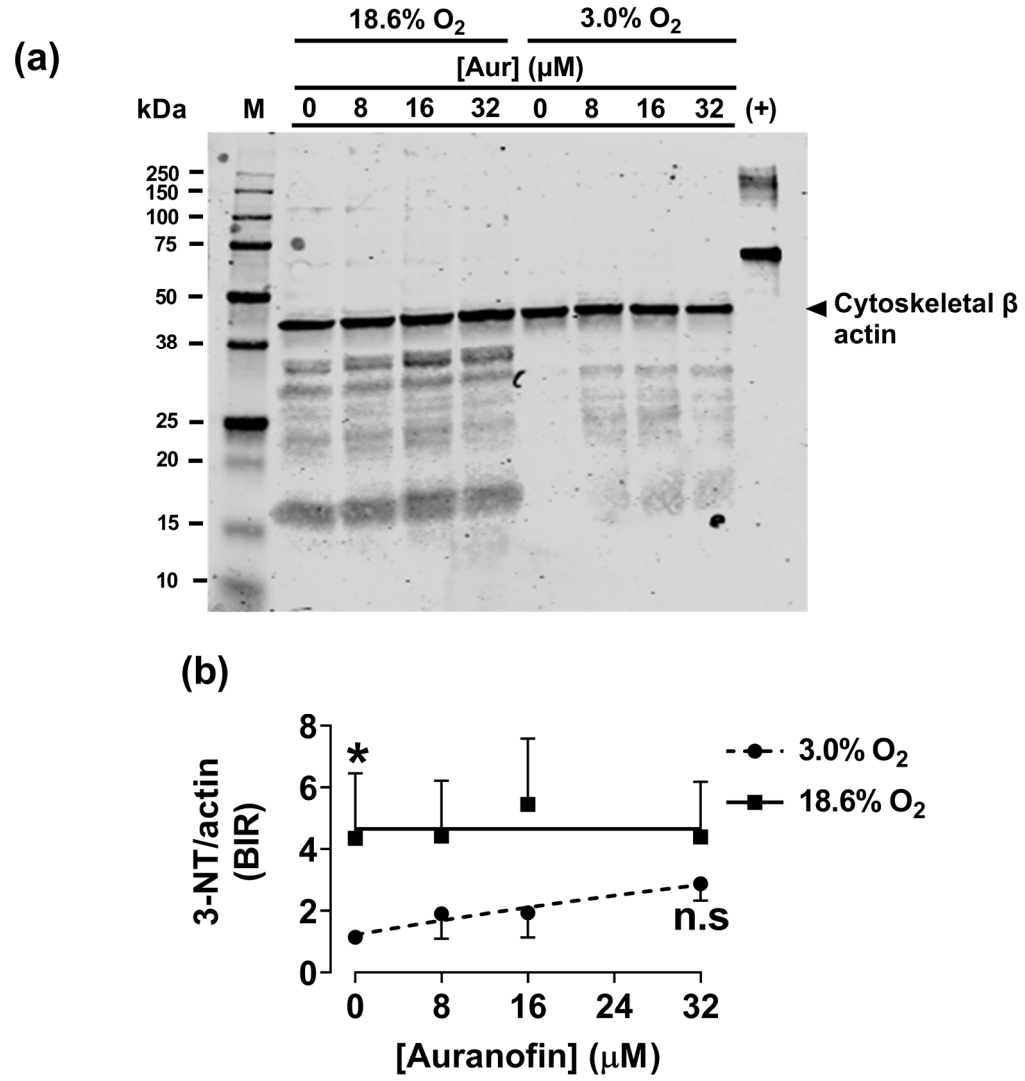

Figure 4.17. The effect of growing A431 cells grown in 18.6% O_2 on auranofin-induced 3-nitrotyrosine formation compared to A431 cells grown in 3.0% O_2 for 96 h. A431 cells were seeded at a density of 9.5 x 10^3 cells/cm^2 in 6 well plate and incubated in 18.6% O_2 or 3.0% O_2 for 96 h (37°C /5% CO_2). A431 cells were fed every 24 h with fresh respective (18.6% or 3.0% O_2) [O_2]-equilibrated growth medium. After 96 h of growth, cells were treated with 0–32 μM auranofin or vehicle (0.1% v/v DMSO) for 1 h in 3.0% or 18.6% O_2 (37°C /5% CO_2). After treatment, cells were lysed (section 2.12.1) and [protein] was quantified by BCA assay (section 2.12.3). Nitrated albumin was used as a positive control (+) for 3-NT detection (section 4.2.7.1.2). Proteins were then separated by reducing SDS PAGE, and transferred to a nitrocellulose membrane (section 2.12.4). The blot was then blocked overnight with PBS (see section 2.2.3 for concentration), stained with an anti-3-NT primary antibody or an anti-β cytoskeletal actin primary antibody (loading control) for 1 h at room temperature, and subsequently stained with an anti-mouse/rabbit infrared dye-conjugated secondary antibody for an additional 1 h at room temperature (section 2.12.7). The membrane was then imaged using a LI-COR Odyssey CLx imaging system (section 2.12.9).**Panel (a),** representative immunoblot from one experiment showing the levels of 3-NT containing protein from the lysates of auranofin-treated A431 cells grown in 18.6% or 3.0% O_2 for 96 h. The 42 kDa band is β cytoskeletal actin (loading control) **Panel (b),** densitometry analysis (section 2.12.10) of auranofin-induced 3-NT formation in A431 cells grown in 18.6% O_2 or 3.0% O_2 for 96 h relative to the levels of 3-NT formation in untreated A431 cells grown in 3.0% O_2 for 96 h. n.s = not significant versus respective untreated control, ** = P < 0.001 versus 3.0% O_2, utilising a two-way ANOVA and a *post-hoc* multiple comparison test with Dunn-Šidák correction. Data in panel (b) is presented as the mean ± 1 SD. n=3. Where error bars are not visible, this is because the error bar is smaller than the size of the data point. **3-NT:** 3-nitrotyrosine; **Aur**: auranofin; **BIR:** band intensity ratio; **kDa:** kilodalton; **MW:** molecular weight marker lane.

4.4. Discussion

The aim of this chapter was to determine whether growing A431 cells in 18.6% O_2 exhibited altered expression levels and activities of protein and enzyme (respectively) involved in cellular antioxidant defence compared to A431 cells grown in 3.0% O_2. The main experimental endpoints examined involved measuring the activities of Nrf-2-target enzymes (i.e. catalase, GR, Gpx, SOD, and GST), and the protein expression levels of Nrf-2-target protein (i.e. Nrf-2, catalase, and NQO-1). The expression levels of protein containing the 3-NT modification were also measured. These research endpoints were utilised to address aim 4 and objective 7 outlined in **section 1.4.**

4.4.1. A431 cells grown in 18.6% O_2 exhibited heightened catalase enzymatic activity compared to A431 cells adapted to 3.0% O_2

A431 cells grown in 18.6% O_2 exhibited increased catalase enzymatic activity compared to A431 cells adapted to 3.0% O_2 **(section 4.3.1)**. The increase in catalase activity in A431 cells grown in 18.6% O_2 was not statistically significant until compared with A431 cells which had adapted to 3.0% O_2 for 96 h **(Figure 4.7 b)**. These data showed that A431 cells required at least a 96 h adaptation period in 3.0% O_2 for catalase activity to decrease relative to the catalase activity of cells grown in 18.6% O_2. However, SOD activity was unchanged in A431 cells adapted to 3.0% O_2 for 96 h compared to A431 cells grown in 18.6% O_2 **(section 4.3.3)**. A431 cells may have required longer than 96 h in 3.0% O_2 for SOD activity to be affected relative to the SOD activity in A431 cells grown in 18.6% O_2.

The above data are partly consistent with Ferguson et al. [21] who showed an increase to the activity of both SOD and catalase in A431 cells grown in 18.6% O_2 compared to such activity in A431 cells adapted to 2.0% O_2 for 48 h. The data in this work did not show such an effect after a 48 h adaptation period in 3.0% O_2 **(section 4.3.1 and 4.3.3).** Fan et al. [307] showed that haematopoietic stem cells adapted to 5.0% O_2 for 7 days exhibited decreased transcription of the gene encoding catalase protein compared to hematopoietic stem cells grown in 18.6% O_2. However, only the activity of Gpx was lower in hematopoietic stem cells adapted to 5.0% O_2 compared to the Gpx activity in hematopoietic stem cells grown in 18.6% O_2, with the activities of catalase and SOD remaining unchanged [307]. The effect of growing mammalian cells in 18.6% O_2 on catalase and SOD

activity and expression is not uniform across all cell types. Whilst Ferguson et al [21] observed an increase in total SOD activity in A431 cells grown in 18.6% O_2 compared to physioxia, others have noted changes only in particular isoenzymes of SOD (i.e. SOD 1 or SOD 2, **(section 1.2.7.2.1-1.2.7.2.2)**) Bovine embryonic cells adapted to 5.0% O_2 for 7 days showed decreased expression of the SOD 2 isoenzyme compared to SOD 2 expression in bovine embryonic cells grown in 18.6% O_2 [77]. However, this observation did not extend to catalase activity or to SOD 1 activity [77]. Villeneuve et al. [75] observed that the expression level of SOD 2 protein was higher in SH-SY5Y neuroblastoma cells adapted to 5.0% O_2 compared to the expression levels of SOD 2 in SH-SY5Y grown in 18.6% O_2. The higher expression level of SOD 2 protein in SH-SY5Y adapted to 5.0% O_2 was associated with decreased mitochondrial ROS generation compared to the mitochondrial ROS formation in SH-SY5Y grown in 18.6% O_2. Human pulmonary arterial smooth muscle cells exhibited increased catalase activity when adapted to 10% O_2 compared to the catalase activity of pulmonary arterial smooth muscle cells grown in 18.6% O_2 [308].

Do all cells change their antioxidant defence systems in the same way when grown in 18.6% O_2 compared to cells adapted to physioxia? The above data suggested that this is likely not the case. There has been little work done (other than the work of Ferguson et al [21]) which investigated the effects of long term growth in standard cell culture [O_2] on skin cell antioxidant defences compared to skin cells adapted to physioxia. This makes it more difficult to determine how skin cells in general respond to growth in standard cell culture oxygenation conditions compared to when adapted to physioxia. Although cell type specific responses are likely involved, the length of the adaptation period to physioxia is also an important consideration. If the A431 cells used in this work had only been adapted to 3.0% for 24 h, a decrease in catalase activity would not have been observed relative to the catalase activity in A431 cells grown in 18.6% O_2. Only after A431 cells had adapted to 3.0% O_2 for 96 h was a statistically significant effect on catalase activity observed when compared to A431 cells grown in 18.6% O_2. This highlights the importance of adapting cells to physioxia for long enough in order for such differences to emerge. Some publications [303, 304] utilise short-term physioxia adaptation periods which may not be long enough for differences to emerge relative to cells grown in 18.6% O_2. This present data suggested that

catalase activity changes with time as A431 cells are adapted to physioxia. Overall, it is concluded that a physioxia adaptation period of 24 h is insufficient for maximal adaptation of catalase enzyme activity when compared to catalase enzyme activity in A431 cells grown in 18.6% O_2. However, the activity of catalase may continue to change even further after a 96 h adaptation period in A431 cells grown in 3.0% O_2 relative to the activity measured in A431 cells grown in 18.6% O_2. Future work should determine whether longer physioxia adaptation periods are required for the activity of catalase to change further relative to the catalase activity of A431 cells grown in 18.6% O_2.

Based on the slow decrease in the enzymatic activity of catalase, an associated slow decrease in the expression levels of catalase protein might be expected. However, when the protein expression levels of catalase protein were semi-quantified by western blotting, the expression levels of catalase lowered after just 24 h in 3.0% O_2 compared to 18.6% O_2. This catalase expression level remained low in A431 cells after 48 h, 72 h and 96 h in 3.0% O_2 when compared to the expression levels of catalase protein in A431 cells grown in 18.6% O_2. The expression levels of catalase protein were six times higher in A431 cells grown in 18.6% O_2 compared to A431 cells adapted to 3.0% O_2 for 24 h **(section 4.3.2)**. This observation was unexpected as there was no statistically significant difference in the activity of catalase when comparing A431 cells grown in 18.6% O_2 to A431 cells adapted to 3.0% O_2 for 24 h. The expression levels of catalase protein may adapt to physioxia faster than other proteins capable of detoxifying H_2O_2 (i.e. Trx, TrxR1, TrxR2, Prx, and GSH). It is likely that such enzymes were involved in the decomposition of H_2O_2 even as the catalase protein levels lowered in A431 cells adapted to 3.0% O_2 compared to A431 cells grown in 18.6% O_2. This suggested that the assay used in this work for measuring catalase enzyme activity was not specific to catalase alone. More likely, this assay was measuring a group of enzymes capable of detoxifying H_2O_2 such as the Prx family of proteins. This is likely the case as the treatment of A431 cells with 1 mM sodium azide further decreased the activity of catalase compared to A431 cells treated with 16 mM of 3-AT (a catalase-specific inhibitor; **section 2.10.1**). Sodium azide is a non-specific enzyme inhibitor, and can also inhibit other peroxidases (e.g. Gpx)[311]. Such peroxidases may have also decomposed H_2O_2 in the catalase activity assays. One might initially consider performing this previously described

catalase activity assay **(section 4.2.1)** in conjunction with a catalase-specific inhibitor (i.e. 3-AT) to determine the extent of H_2O_2 degradation that is due to catalase activity specifically. However, 3-AT inhibits only catalase complex I, which is formed when catalase reacts with H_2O_2 **(section 1.2.6.2.1)**. As such 3-AT-mediated inhibition of catalase is H_2O_2-dependent. As H_2O_2 generation was shown to be higher in A431 cells grown in 18.6% O_2 compared to A431 cells adapted to 3.0% O_2 for 96 h **(section 3.3.7)**, this may caution the use of 3-AT in cellular systems where cellular generation of H_2O_2 is dependent on the [O_2] a cell is adapted to growing in prior to assay. The non-specificity of the catalase assay used in this work for catalase in A431 cells is the most likely explanation for the discrepancy between the catalase activity data **(section 4.3.1)** and the catalase western blotting data **(section 4.3.2)**.

Despite the non-specificity of the catalase assay to catalase alone, the decomposition of H_2O_2 was greater when using lysates from A431 cells grown in 18.6% O_2 compared to A431 cells adapted to 3.0% O_2 for 96 h. A change in the activity of catalase might partially explain such a difference, but what molecular mechanisms might explain how A431 cells grown in 18.6% O_2 exhibit differences to the activity of catalase compared to A431 cells adapted to physioxia?

Changes to the active site in the catalase enzyme may have occurred in A431 cells grown in 18.6% O_2 compared to A431 cells adapted to 3.0% O_2. The formation of active catalase requires the insertion of one haem group per subunit [312]. Catalase is assembled within the peroxisome where it undergoes tetramerisation and haem insertion [308]. Trx1 supports haem insertion into the active side of catalase [313]. As discussed **(section 3.1)**, A431 cells grown in 18.6% O_2 exhibited heightened gene expression of *TRX1*, *TRX2,* and *TRXR1* compared to A431 cells adapted to 2.0% O_2 [21]. In A431 cells grown in 18.6% O_2, Trx1 may be increased thereby facilitating the heightened formation of active catalase compared to the active catalase expression levels in A431 cells adapted to 3.0% O_2 for 96 h. Catalase undergoes numerous post-translational modifications which can affect its activity, including S-nitrosation, chlorination, ubiquitination, and phosphorylation [312]. Whether the growth of A431 cells in 18.6% O_2 compared to physioxia affects the type, and extent, of post-translational modification in catalase is not yet unknown. Future work should investigate such outputs in A431 cells grown in 18.6% O_2 to better understand mechanistically

how cellular growth under standard cell culture [O_2] may affect the activity of antioxidant enzymes such as catalase when compared to A431 cells adapted to physioxia.

Additionally, NADPH is needed for catalase to function [194]. Four molecules of NADPH are found in tetrameric mature catalase protein [194]. NADPH slows the formation of inactive catalase by preventing the generation of the Fe^{4+} oxo-ligated porphyrin [194]. Diminished availability of NADPH might also affect the activity of other enzymes such as GR and NOS. NADPH is generated via the enzyme glucose-6-phosphate dehydrogenase (G6PD) through the reduction of $NADP^+$ to NADPH [371]. Nrf-2 supports NADPH generation in the cell by controlling the expression of enzymes such as G6PD, 6-phosphogluconate dehydrogenase, isocitrate dehydrogenase, and malic enzyme 1 [314]. Nrf-2 activation by sulforaphane in MEF showed preferential activation of the pentose phosphate pathway [315]. Inhibition of G6PD by dehydroandrostendione was also shown to decrease cellular detoxification of ROS [315]. As such, Nrf-2 may itself exert functional control over the activity of enzymes such as catalase, GR and NOS by modulating systems critical for energy production. In this present study it was shown that the expression levels of nuclear Nrf-2 protein were higher in A431 cells grown in 18.6% O_2 compared to the levels of Nrf-2 in A431 cells adapted to 3.0% O_2 **(section 4.3.8)**. The heightened expression levels of Nrf-2 protein in A431 cells grown in 18.6% O_2 compared to A431 cells adapted to 3.0% O_2 for 96 h may have modulated NADPH formation and thus increased the activity of enzymes which rely on NADPH for electrons and sequential catalytic activity [316].

Another possible explanation for the observed differences in catalase enzyme activity between the two [O_2] groups may involve the availability of labile transition metal ions. Copper and iron ions are found in the active site of both SOD and catalase **(section 1.2.7.2.1 and 1.2.7.2.3)**. Chelating agents such as desferrioxamine and tetraethylenepentamine inhibit the activities of catalase and SOD 1, respectively [365, 366]. However, the levels of labile iron may be sensitive to the [O_2] a cell is adapted to growing in. Labile iron ion levels are controlled through receptor-mediated endocytosis of Fe^{3+} ions via transferrin receptor 1 and 2 or by direct import of ferrous iron via divalent metal transporters [319]. Fe^{2+} ions are then oxidised and stored in ferritin as Fe^{3+} ions through a ferroxidation

reaction [319]. Ferritin expression is controlled by Nrf-2 [293] . As such, the availability of labile iron ions may be affected by cell culture under 18.6% O_2 compared to physioxia thus affecting the assembly of mature functional catalase. The levels of ferritin protein expression, as well as the availability of labile ferrous and ferric iron, should be measured in A431 cells grown in 18.6% or 3.0% O_2 to further elucidate the mechanism through which antioxidant enzymatic activity changes in response to long-term growth in standard cell culture [O_2]

4.4.2. A431 cells grown in 18.6% O_2 exhibited heightened activity of glutathione reductase compared to A431 cells adapted to 3.0% O_2.

In addition to catalase, the activity of GR was higher in A431 cells grown in 18.6% O_2 compared to the activity of GR in A431 cells adapted to 3.0% O_2 for 96 h **(section 4.3.4)**. However, as with the catalase activity investigations, the differences in GR activity only emerged relative to A431 cells grown in 18.6% O_2 after a 72 h adaptation period in 3.0% O_2. Some target enzyme activity (i.e. Gpx **(section 4.3.5)**, and GST **(section 4.3.6)**) did not show a statistically significant change when comparing A431 cells adapted to 3.0% O_2 for 96 h to A431 cells grown in 18.6% O_2. However, the Gpx activity investigations showed an apparent decrease in Gpx activity as A431 cells were adapted to 3.0% O_2 over the course of 4 days relative to A431 cells grown in 18.6% O_2. Although this difference was not statistically significant, a significant effect may be observed if performed on A431 cells adapted to 3.0% O_2 for longer than four days compared to A431 cells grown in 18.6% O_2. Future work should also aim to determine whether longer adaptation periods in 3.0% O_2 are required for the activity of GST to change when compared to GST enzyme activity in A431 cells grown in 18.6% O_2.

Additionally, A431 cells grown in 18.6% O_2 showed no statistically significant increase to the levels of GSH, GSSG, or to total GSH compared to A431 cells adapted to 3.0% O_2 for 96 h. Additionally, there were no differences to GSH:GSSG when comparing the two [O_2] groups **(section 4.3.7)**. In chapter 3, A431 cells grown in 18.6% O_2 exhibited heightened generation of H_2O_2 compared to cells adapted to 3.0% O_2 for 96 h **(section 3.3.7).** Thus, a lower GSH:GSSG ratio was hypothesised to exist in A431 cells grown in 18.6% O_2 compared to A431 cells adapted to 3.0% O_2 for 96 h. The increased activity of GR exhibited by A431 cells grown in 18.6% O_2 compared to the GR activity in A431 cells

adapted to 3.0% O_2 may have augmented the reduction of GSSG to GSH even in conditions of heightened H_2O_2 generation.

Although this present data showed that A431 cells grown in 18.6% O_2 exhibited heightened GR activity, and no change to the levels of intracellular GSH, when compared to A431 cells adapted to 3.0% O_2 for 96 h, other work investigating these endpoints in mammalian cells grown in 18.6% O_2 or physioxia have shown different cellular responses. Most applicable to this current work, A431 cells grown in 18.6% O_2 exhibited decreased levels of total GSH compared to the total GSH in A431 cells adapted to 2.0% O_2 for 48 h [21]. This decrease in total GSH was associated with an decrease in GSH:GSSG compared to GSH:GSSG in A431 cells grown in 18.6% O_2. Ferguson et al. [21] suggested that A431 cells grown in 18.6% O_2 were in a state of persistent oxidative stress compared to those adapted to 2.0% O_2 for 48 h. The observations of Ferguson et al. [21] contradict the associated data in this present work as no difference to the levels of intracellular GSH, GSSG, total GSH, or in GSH:GSSG were observed when comparing A431 cells grown in 18.6% O_2 to A431 cells adapted to 3.0% O_2 for 96 h. However, there are three key differences between the work of Ferguson et al. [21] and the work presented here: First, Ferguson et al. [21] utilised a physioxia set point of 2.0% O_2 whereas 3.0% O_2 was used in this present work; secondly, Ferguson et al. [21] adapted A431 cells to 2.0% O_2 for 48 h whereas A431 cells were adapted to 3.0% O_2 for as long as 96 h in this present work; third, Ferguson et al. [21] utilised an ortho-phthaldialdehyde GSH derivisation method to measure GSH whilst a GR enzyme recycling method was used in this present work. Although the GSH data shown in this work do not agree with Ferguson et al. [21], this present data suggested a potentially biologically significant effect of physioxia adaptation on the levels of intracellular GSH, GSSG, and total GSH should these endpoints be measured using A431 cells adapted to 3.0% O_2 for longer than 96 h. Future work should investigate changes to the levels of intracellular GSH, GSSG and total GSH in A431 cells adapted to 3.0% O_2 for longer than four days when compared to A431 cells grown in 18.6% O_2.

Investigations in other cell types have however shown an effect of physioxia adaptation on intracellular GSH levels when compared to cells grown in 18.6% O_2 Human peripheral blood mononuclear cells grown in 18.6% O_2 exhibited decreased intracellular GSH levels compared to such levels in human peripheral

blood mononuclear cells adapted to 5.0% O_2 [320]. Human primary T cells grown in 18.6% O_2 exhibited decreased total levels of intracellular GSH compared to those adapted to 5.0% O_2 [321]. However this decrease in total GSH in 18.6% O_2 was associated with an overall decrease in GSH:GSSG compared to GSH:GSSG in primary human T cells adapted to 5.0% O_2 [321]. The authors suggested that T cells adapted to physioxia exhibited a phenotype more reflective of *in vivo* T cell physiology compared to T cells grown in 18.6% O_2 [321]. Although GSH is associated with cancer cell resistance to chemotherapeutic agents [179, 199, 234], this resistance may be exacerbated when examined in mammalian cells grown chronically *in* vitro under a standard cell culture [O_2] compared to such resistances measured in mammalian cells adapted to physioxia.

4.4.3. A431 cells grown in 18.6% O_2 exhibited heightened levels of nuclear factor erythroid-2-related factor 2 protein compared to A431 cells adapted to 3.0% O_2

In this chapter, the expression levels of nuclear Nrf-2 protein were found to be about 2 times higher in A431 cells grown in 18.6% O_2 compared to A431 cells adapted to 3.0% O_2 for 96 h **(section 4.3.8)**. As discussed previously **(section 1.2.7.3.1.1)**, Nrf-2 regulates the expression of human antioxidant defence genes encoding catalase, GR, GPX, GST, NQO-1, HO-1, TRX, and TRXRD1. The higher expression levels of nuclear Nrf-2 protein in A431 cells grown in 18.6% O_2 compared to A431 cells adapted to 3.0% O_2 may in part explain the increased enzymatic activities of catalase, and GR. The observed two-fold higher expression level of nuclear Nrf-2 protein in A431 cells grown in 18.6% O_2 compared to the levels in A431 cells adapted to 3.0% O_2 for 96 h agrees with the previously reported [21] 1.2 fold increase of the gene transcription of NFE2L2 (encoding for Nrf-2 protein, **section 1.2.7.3.1**) in A431 cells grown in 18.6% O_2 compared to A431 cells adapted to 2.0% O_2 for 48 h.

Why might the expression levels of Nrf-2 nuclear protein be higher in A431 cells grown in 18.6% O_2 compared to those adapted to 3.0% O_2 for 96 h? As discussed previously, Keap-1 is a redox sensor which is susceptible to oxidation at critical cysteine residues on the IVF region **(Figure 4.18)**. The heightened expression levels of nuclear Nrf-2 protein in A431 cells grown in 18.6% O_2 may be caused by increased cellular generation of endogenous Nrf-2 activators such as NO, H_2O_2, 4-HNE, and 4 hydroxyestradiol. These inducers may activate Nrf-2 via

cysteine residues in the BTB and Kelch region of Keap-1 **(Figure 4.18)**. As previously described in **sections 3.4.3.2 and 3.4.3.3**, the activities of ROS producing enzymes, such as NOS and NOX4, exhibit K_m (%O_2) within the range of physioxia. Therefore, ROS-mediated activation of Nrf-2 may be heightened in cells grown in standard cell culture [O_2] compared to those adapted to physioxia. However, other aspects of cell culture experimental design may impact Nrf-2 activation. For example, estradiol, which can be found in some batches of FBS, can be hydroxylated by CYP450 to 4-hydroxyestradiol, an activator of Nrf-2 [223]. It is proposed that should Nrf-2 activation be used as an experimental endpoint during *in vitro* testing, this pathway may exhibit artefactual activity in mammalian cells grown chronically in standard cell culture [O_2] compared to such activity in such cells adapted to physioxia. As previously discussed **(section 1.3.1.1.1)**, altered Nrf-2 activity in cells grown in standard cell culture [O_2] has possible ramifications for the development of Nrf-2-activating compounds which use Nrf-2 activation as a primary assay endpoint in the early *in vitro* testing stage of lead compound development. However, it is not just the levels of Nrf-2 that are altered in A431 cells grown in 18.6% O_2 compared to physioxia; The ability of A431 cells to induce Nrf-2-target protein expression in response to oxidative stress is dependent on the [O_2] such cells are grown in long term. This will be discussed in the following section.

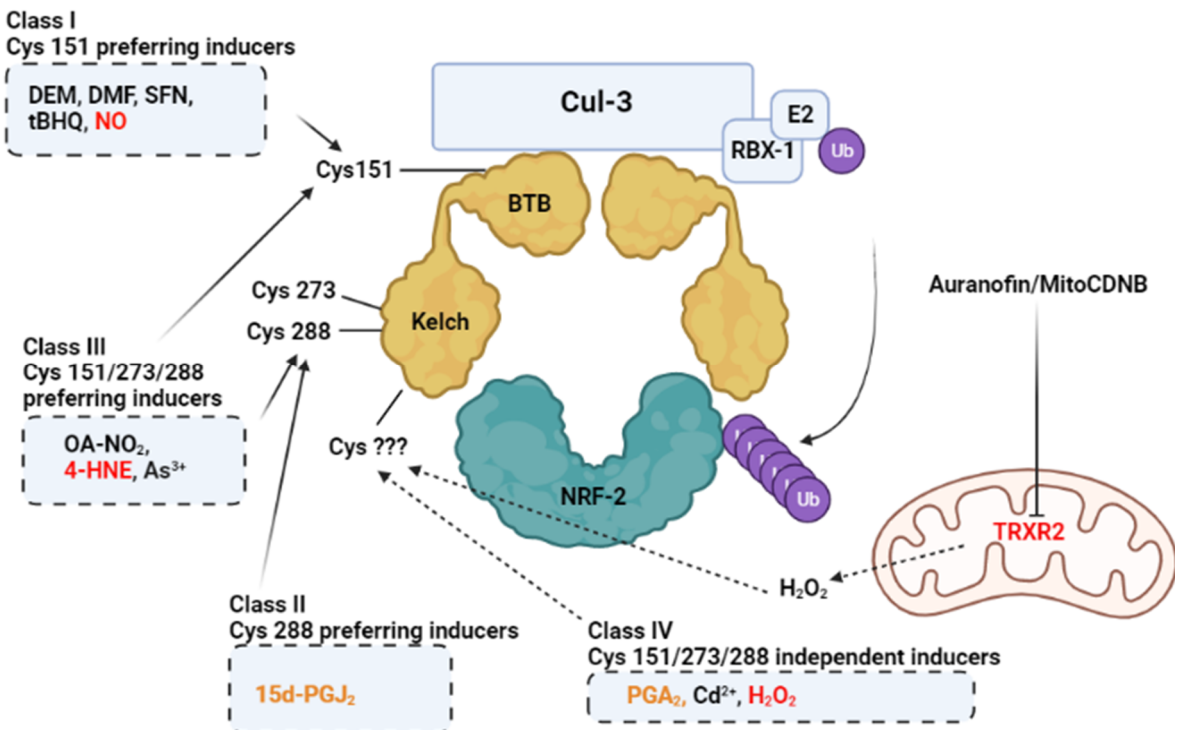

Figure 4.18. The activation of nuclear factor erythroid-2-related factor 2 under basal conditions by different classes of activating agents. There are four classes of Nrf-2 inducers, some are specific for the Cys151 residue on the BTB domain of Keap-1, whilst class II and III inducers target Cys151, Cys273 and Cys288. Class IV inducers activate Nrf-2 through a cysteine independent mechanism. **Listed in red** are inducers which show evidence of higher basal levels when measured in mammalian cells grown in 18.6% O_2 compared to mammalian cells adapted physioxia (see text). Higher basal levels of these inducers may activate Nrf-2 and consequently affect the expression of downstream Nrf-2-targets such as NQO-1 compared to physioxia. **Listed in orange** are Nrf-2 inducers which are produced endogenously by the cell, however, the effect of cell culture in 18.6% O_2 on the basal levels of such inducers compared to physioxia have not been studied in detail. Auranofin may activate Nrf-2 through H_2O_2-mediated oxidation of cysteine residues in the Keap-1 complex. Induction of Nrf-2-target genes by auranofin may be dependent on the levels of H_2O_2 induced by inhibition of TrxR2. **4-HNE:** 4-hydroxynoneal; **15d-PGJ$_2$:** 15-Deoxy-Delta-12,14-prostaglandin J2; **As^{3+}:** arsenic; **BTB:** broad complex/tramtrac/bric-a-brac; **Cd^{2+}:** cadmium; **Cul-3:** cullin 3; **Cys:** cysteine; **DEM:** diethylmaleate; **DMF:** dimethyl fumarate; **IVF:** intervening region; **Keap-1:** kelch-like ECH-associated protein 1; **Mito-CDNB:** mitochondria-targeted 1,5-dichloro-2,4-dinitrobenzene; **NO:** nitric oxide; **OA-NO$_2$:** Nitro oleic fatty acid; **PGA$_2$:** Prostaglandin; **Rbx-1:** E3-ubiquitin protein ligase; **SFN:** sulforaphane; **tBHQ:** tert-butyl hydroquinone; **TRXR2:** thioredoxin reductase 2; **Ub:** ubiquitin. Image adapted from [87] using www.Biorender.com.

4.4.4. Auranofin-induced induction of NAD(P)H quinone oxidoreductase-1 was blunted in A431 cells grown in 18.6% O_2 compared to A431 cells adapted to 3.0% O_2

In this chapter, the expression level of the Nrf-2-target protein NQO-1 was about 1.8 times higher in A431 cells grown in 18.6% O_2 compared to those adapted to 3.0% O_2 **(section 4.3.9)**. These data agree with the observations of Ferguson et al. [21] who showed that A431 cells grown in 18.6% O_2 exhibited about 2 fold higher transcription of the *NQO-1* gene compared to A431 cells adapted to 2.0% O_2 for 48 h. As discussed previously, the expression levels of nuclear Nrf-2 protein in A431 cells grown in 18.6% O_2 were two-fold higher than the Nrf-2 protein expression levels in A431 cells adapted to 3.0% O_2 for 96 h **(section 4.3.8)**. Such a difference may directly affect the expression levels of Nrf-2-target protein such as NQO-1. NQO-1 translation is induced during oxidative stress [269]. The present study showed that the induction of NQO-1 protein expression was dependent on the [O_2] utilised during the cell culture growth phase. Relative to an untreated control group, auranofin was incapable of inducing NQO-1 protein expression in A431 cells grown in 18.6% O_2. However, the induction of NQO-1 protein expression was observed in A431 cells adapted to 3.0% O_2 for 96 h. Only after treatment with 32 µM auranofin did the expression levels of NQO-1 protein in A431 cells adapted to 3.0% O_2 reach the expression levels observed in untreated A431 cells grown in 18.6% O_2. Although the expression levels of NQO-1 protein were unresponsive to auranofin-induced treatment in A431 cells grown in 18.6% O_2, the expression levels of NQO-1 protein were responsive to long term cellular growth in standard cell culture [O_2]. In this case, the 18.6% O_2 oxygenation condition can be viewed as an inducer of NQO-1 protein expression when measured relative to the expression levels of NQO-1 protein in A431 cells adapted to 3.0% O_2 for 96 h.

As shown previously **(section 3.3.2)**, A431 cells grown in 18.6% O_2 were resistant to auranofin-induced cell death compared to A431 cells adapted to 3.0% O_2 for 96 h. Despite this, a significant percentage of A431 cells still succumbed to apoptosis at 16 and 32 µM auranofin in 18.6% O_2. Auranofin-induced cell death induced mitochondrial ROS generation in both [O_2] conditions, although to a lesser extent in A431 cells grown in 18.6% O_2 compared to A431 cells adapted to 3.0% O_2 for 96 h **(section 3.3.4)**. One would expect therefore that NQO-1

(being a known target of Nrf-2) would be induced by auranofin in both [O_2] conditions where ROS is being produced. However, this was not observed **(section 4.3.9)**. Instead, the induction of NQO-1 by auranofin was blunted in A431 cells grown in 18.6% O_2 compared to A431 cells adapted to 3.0% O_2 for 96 h. In contrast, Chapple et al. [72] found that HUVEC grown in 18.6% O_2 showed increased induction of both HO-1 and NQO-1 after treatment with the Nrf-2 activator DEM compared to HUVEC adapted to 5.0% O_2. The findings of Chapple et al. [72] indicated that HUVEC grown in 18.6% O_2 could more easily recruit Nrf-2-target protein during oxidative stress compared to HUVEC adapted to 5.0% O_2. Similar findings have been reported in RAW 264.7 macrophages grown in 18.6% O_2 compared to macrophage adapted to 5.0% O_2 [78]. However, this present data suggested that the growth of A431 cells in 18.6% O_2 attenuated the ability of these cells to recruit Nrf-2-controlled target proteins such as NQO-1 when compared to A431 cells adapted to 3.0% O_2 for 96 h. A431 cells grown in 18.6% O_2 may, under basal conditions, have maintained a larger basal reservoir of antioxidant defence enzymes and proteins such as catalase, and NQO-1. This may be necessary to allow these cells to survive in the high O_2 conditions often utilised in standard cell culture practice. Despite the higher expression levels of NQO-1 protein under basal conditions in A431 cells grown in 18.6% O_2, the ability of these cells to further induce expression of NQO-1 protein in response to oxidative stress was blunted in comparison to A431 cells adapted to 3.0% O_2. This observation has possible implications for the *in vitro* efficacy testing of compounds which undergo bio-activation by NQO-1 such as β-lapachone [322].

What might explain such differences in the induction of NQO-1 protein expression in A431 cells grown under these two [O_2] conditions? The negative regulator of Nrf-2, Bach-1, may be involved. Bach-1 competes with Nrf-2 for Maf binding. Maf aids in Nrf-2 stabilisation, DNA binding, and transcriptional activation **(section 1.2.7.3.1.1**). Previously, it was shown that the knockdown of Bach-1 in HUVEC cells adapted to 5.0% O_2 restored DEM-mediated induction of both HO-1 and NQO-1 relative to the cellular responses in 18.6% O_2 [72]. The authors suggested that Bach-1 plays a uniquely suppressive role in HUVEC adapted to physioxia but not in HUVEC grown in 18.6% O_2 [72]. However, the observations in this present work suggest that Bach-1 may play a suppressive role in A431 cells grown in 18.6% O_2 but not in cells adapted to 3.0% O_2 for 96 h. As Nrf-2 regulates

the expression of Bach-1 [316, 317], the higher expression levels of Nrf-2 protein exhibited by A431 cells grown in 18.6% O_2 **(section 4.3.8)** may also increase the expression levels of Bach-1 protein compared to such levels in A431 cells adapted to 3.0% O_2 for 96 h. This may diminish the ability of A431 cells grown in 18.6% O_2 to recruit Nrf-2-target protein during oxidative stress. Bach-1 negative feedback on Nrf-2 signalling may detrimentally affect the ability of A431 cells grown in 18.6% O_2 to deal with further oxidative insult compared to A431 cells adapted to 3.0% O_2 for 96 h. The ways in which A431 cells adapt to physioxia are clearly different to HUVEC [72]. It should be noted that A431 cells are a cancer cell line and HUVEC are primary endothelial cells; secondly, mutations in the gene encoding Nrf-2 protein exist in many different types of cancers including squamous cell carcinoma [325]. This will be discussed presently.

Cutaneous squamous cell carcinomas (CSCC; from which A431 cells are derived) showed mutations in *NFE2L2*. Kim et al. [325] observed that these mutations were proximal to the DLG and ETGE motifs **(section 1.2.7.3.1.1, Figure 1.19)** which are critical for Nrf-2/Keap-1 interactions. All but one of these mutations in *NFE2L2* were found in CSCC, suggesting a key role of Nrf-2 in the pathogenesis of this cancer [325]. As DLG and ETGE are critical for Keap-1 binding, mutations in these sites may cause increased Nrf-2 activation. For example, human cells isolated from patients with Neh2 mutations exhibited a 2-60 fold upregulation in the expression of Nrf-2-target genes [326]. Oesophageal and skin CSCC with Nrf-2 mutations showed increased nuclear Nrf-2 expression and activity compared to non-cancerous tissue [325]. The increased Nrf-2 nuclear activity in some cancers may be due to the down-regulation of Nrf-2 degradation through hyper methylation of *KEAP-1,* or through mutations to Keap-1 itself [325]. Cancer cells have been shown to exhibit increased ROS generation [327]. Heightened Nrf-2 activity may facilitate cellular survival under such conditions [327]. These mutations to the gene encoding Nrf-2, widely prevalent in human cancers, may explain why the responses of A431 cells to redox-active compounds, after adaptation to physioxia, differ to those observed by Chapple et al. [72] in HUVEC and by Hass et al. [78] in macrophage. Although there are clear discrepancies between our investigations and those noted previously, there is one common underlying conclusion. The responses of mammalian cells grown in 18.6% O_2 to redox-active compounds show evidence of an artefactual cellular

response when compared to the responses noted in mammalian cells adapted to physioxia. As discussed previously, the altered induction of NQO-1 in cells grown chronically under 18.6% O_2 may impact on the development of novel Nrf-2-activating compounds where NQO-1 is utilised as a primary assay endpoint **(section 1.3.1.1.1)**.

However, the target immunoblot band for NQO-1 from the A431 cell samples migrated to 27 kDa which did not correspond to the molecular weight of the recombinant human NQO-1 protein in the positive control lane (31 kDa; **Figure A.4**). It was a concern that the NQO-1 protein in the sample may have been damaged during sample preparation resulting in the NQO-1 protein migrating to a lower molecular weight compared to recombinant NQO-1 protein. However, incubation of the recombinant NQO-1 protein with the cell lysis buffer, in the presence of the cellular sample, did not alter the molecular weight of the recombinant NQO-1 protein **(Figure 4.16)**. This suggested that a separate isoform of the NQO-1 protein had been detected. An *in silico* approach using UniProt revealed that NQO-1 has three separate isoforms, NQO-1*1 (31 kDa), NQO-1*2 (27-28 kDa), and NQO-1*3 (26 kDa). As the target sample band was migrating to 26-27 kDa, it was hypothesised that the NQO-1 protein detected in A431 cells may be either the NQO-1*2 or *3 isoform. Both NQO-1*2 and *3 are reported to have severely diminished enzymatic activity, with some evidence of total loss of enzymatic activity [328]. As such, the observed induction of NQO-1 in 3.0% O_2 may not lead to increased protection from oxidative stress if the isoform induced is NQO-1*2 or NQO-1*3. This may explain why A431 cells in 3.0% O_2 remain susceptible to auranofin-induced cell death despite the induction of the NQO-1 as this protein may be the NQO-1*2 or NQO-1*3 isoform. Mass spectrometry analysis should be performed to identify the isoform of NQO-1 detected in these studies. Additionally, an NQO-1 enzymatic activity assay should be performed to determine whether this protein exhibits functional activity in A431 cells grown in 18.6% O_2 or adapted to 3.0% O_2. Dicumorol, a potent inhibitor of NQO-1, should be used to test the selectivity of this assay for NQO-1. The lack of NQO-1 induction relative to control in 18.6% O_2 may involve Nrf-2 negative regulatory feedback (i.e. Keap-1, Bach-1 ATF6 and GSK6) [88]. The expression levels of such Nrf- negative regulators should be measured in A431 cells grown

in 18.6% O_2 or adapted to 3.0% O_2 under untreated conditions and after treatment with auranofin and/or an Nrf-2 activating electrophile (e.g. DMF).

Additionally, the full length western blotting immunoblots for NQO-1 showed additional banding at around 25 kDa and ~55-60 kDa in the 8 and 32 µM auranofin treatment lanes in **Figure A.4 panel (c)** and in the 16 and 32 µM auranofin treatment lanes in **Figure A.4 panel (d).** It was originally thought that such proteins were light and heavy chain immunoglobulin which have molecular weights of 25 and 50 kDa, respectively [329]. However, when the same lysate was immunoblotted separately with the anti-rabbit and anti-mouse secondary antibody alone, no reactivity was noted **Figure A.4 panel (e)**. As such, these bands at 25 kDa and ~55-60 kDa may not be light or heavy chain immunoglobulin. The higher 55-60 kDa band may represent the homo-dimer form of NQO-1 which normally migrates to 60-70 kDa. Protein Tech, which provide the #11451-1-AP anti-NQO-1 primary antibody, state that this antibody reacts with the NQO-1 homodimer. However, Abcam do not state whether #ab264434 (the antibody used in this work, **Figure A.4**) can detect the NQO-1 homodimer. The lower molecular weight form (25 kDa) may represent the products of partial proteolysis. Encarnación et al. [330] found that the cleavage of the N terminal region of NQO-1 by thermolysin yielded a 22.8 kDa band when separated on a reducing gel. It is possible that contamination of the sample by a protease (i.e. trypsin) may have caused partial proteolysis of native NQO-1. This is however unlikely, as the lysis solution used in this work contained a protease inhibitor **(section 2.12.1)**. If NQO-1 underwent partial proteolysis, this may have occurred prior to cell lysis by internal cellular proteases. Auranofin is known to inhibit deubiquitinase enzymes [148]. Therefore, the treatment of A431 cells with auranofin may allow such cleavage forms of NQO-1 to accumulate upon auranofin treatment. These 25 kDa bands are not found in all of the immunoblots, and are most prominent in **Figure A.4 (c)** and **Figure A.4 (d)** in the auranofin treatment lanes**.** Future work using the NQO-1 antibody (#ab87692) should identify the 25 kDa and 55-60 kDa protein products using mass spectrometry.

4.4.5. A431 cells grown in 18.6% O_2 exhibited higher levels of basal 3-nitrotyrosine modified proteins compared to A431 cells adapted to 3.0% O_2

Oxidative stress can induce protein damage and protein modifications. One of these modification is the 3-NT protein modification, a marker of $ONOO^-$-mediated damage **(section 1.2.4.2)**. In this chapter, A431 cells grown in 18.6% O_2 exhibited about 4.4 times the expression levels of protein containing the 3-NT protein modification compared to the levels detected in A431 cells adapted to 3.0% O_2 for 96 h. However, the expression levels of 3-NT modified proteins in A431 cells grown in both O_2 conditions were unresponsive to auranofin treatment compared to untreated control cells **(section 4.3.10)**. The heightened basal expression levels of 3-NT modified proteins in A431 cells grown in 18.6% O_2 suggested that these cells may be exposed to heightened levels of nitrative stress compared to A431 cells adapted to 3.0% O_2 for 96 h **(section 4.3.10)**. The specific identities of these nitrated proteins could not be determined using western blotting alone. Future work should utilise mass spectrometry to identify these 3-NT modified proteins in 18.6% O_2 and 3.0% O_2. An *in silico* analysis of what these proteins could be will be discussed below.

As described previously, $ONOO^-$ is formed through the reaction of $O_2^{\bullet-}$ with $^\bullet NO$ **(section 1.2.2.4)**. $^\bullet NO$ may diffuse into mitochondria from the cytosol due to its uncharged state and relatively long half-life (≥ 1s) [331]. Although $ONOO^-$ can potentially form anywhere within the cell, the very short half-life of $O_2^{\bullet-}$ under physiological conditions renders the production of $ONOO^-$ dependent on local concentrations of $O_2^{\bullet-}$. This renders many proteins in the mitochondria prone to nitration reactions where 1.0–5.0% of cellular O_2 is converted into $O_2^{\bullet-}$ [128]. $ONOO^-$ can also be produced from the reaction between O_2 and nitroxyl (HNO), the latter being the one electron reduction product of $^\bullet NO$ [305]. HNO can be formed through the incomplete reduction of L-arginine by NOS. The reaction between HNO and O_2 has a low rate constant (8×10^3 M^{-1} s^{-1}), and so its relevance to protein nitration reactions *in vivo* has been questioned, partly due to the low [O_2] in most tissues [305]. However, HNO-mediated $ONOO^-$ production may not be limited by [O_2] if measured in cells grown *in vitro* under 18.6% O_2.

The mitochondrial proteins most prone to nitration reactions include those involved in the TCA cycle (malate dehydrogenase, aconitase, glutamate

dehydrogenase), β-oxidation of fatty acids (acyl-CoA-dehydrogenase, enoyl-CoA hydratase, β-ketothiolase), and the respiratory chain (I and IV respiratory complexes, cytochrome c) [128]. Aldolase A, a key enzyme involved in the fourth step of glycolysis, is prone to a primary nitration reaction at Tyr363 in the C terminal domain, and also secondary nitration reactions at Tyr342 Tyr222 [125]. This results in the decreased enzymatic activity of aldolase A [125]. Succinyl-CoA:3-oxoacid CoA transferase, glyceraldehyde-3-phosphate dehydrogenase, and triose phosphate isomerase, are susceptible to nitration at Tyr34, Tyr68 and Tyr92 (respectively) causing decreased glycolytic flux [332]. Additionally, enzymes involved in the TCA cycle such as aconitase and malate dehydrogenase are susceptible to Tyr nitration [332].

What is the effect of protein nitration reactions on cellular phenotype, and could protein nitration affect the responses of cells to redox-active agents? Some enzymes involved in cellular antioxidant defences are altered directly by Tyr nitration **(Figure 4.19)**. SOD 2 is susceptible to nitration at Tyr34 which results in decreased enzyme activity and increased production of $ONOO^-$ within the mitochondria [125]. This may facilitate further Tyr nitration reactions [125]. Prx2, a key enzyme involved in peroxide degradation, can also undergo nitration at Tyr193 which facilitates Prx2 monomer disulfide formation and increased peroxidase activity [333]. GST, an enzyme involved in the conjugation of xenobiotics to GSH, undergoes nitration at Tyr92 resulting in increased enzymatic activity [334]. GR, which is involved in the reduction of GSSG to GSH, is directly inactivated by nitration at Tyr106 and Tyr114 [335].

As SOD 2, Prx2 and GST are critical for antioxidant defence, the growth of cells under 18.6% O_2 may (in part) affect the responses of A431 cells to redox-active compounds compared to physioxia through the modification of antioxidant enzyme activity **(Figure 4.19)**. The higher expression levels of 3-NT containing proteins in A431 cells grown in 18.6% O_2 compared to A431 cells adapted to 3.0% O_2 may be due to increased $ONOO^-$ formation or possibly decreased proteasomal activity. These outputs should be measured to provide a mechanism for the higher expression levels of 3-NT containing proteins in A431 cells grown in standard cell culture [O_2] compared to A431 cells adapted to 3.0% O_2 for 96 h.

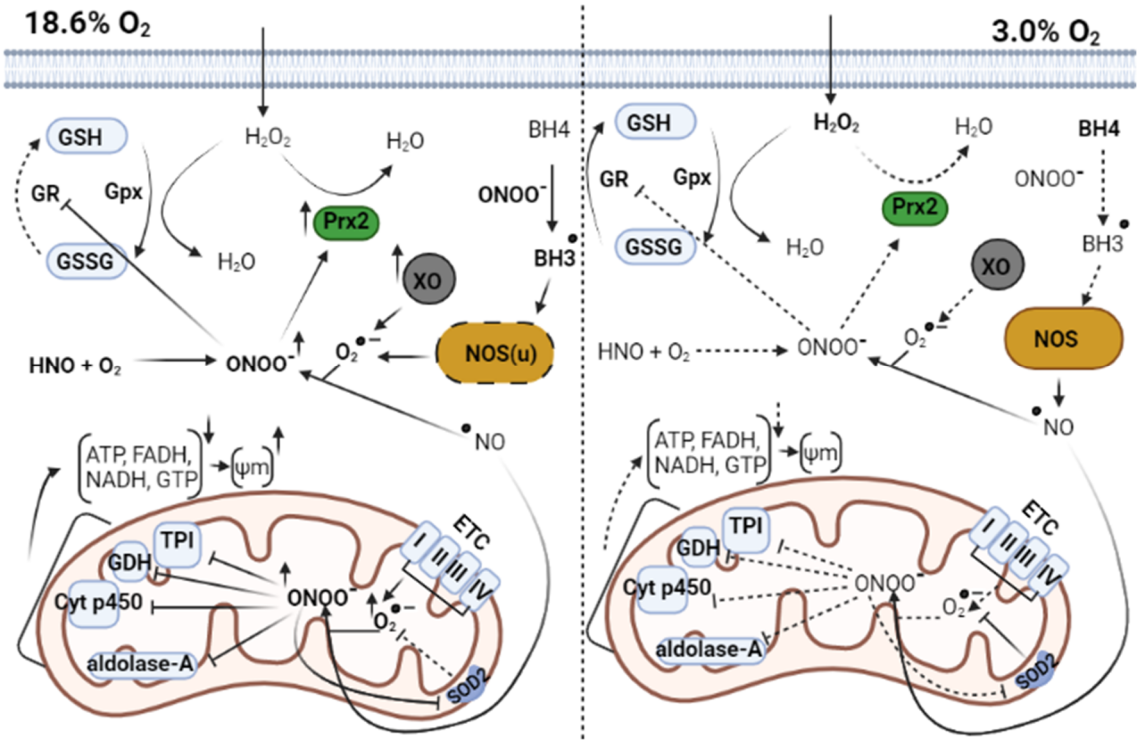

Figure 4.19. Proposed effect of the 3-nitrotyrosine protein modification on cellular antioxidant defence in A431 cells grown in 18.6% O_2 or adapted to 3.0% O_2. In mitochondria under 18.6% O_2 (left), $O_2^{\bullet-}$ produced by the ETC reacts with $^{\bullet}NO$ to form $ONOO^-$. $ONOO^-$ can inactive SOD 2 by nitrating Tyr34 leading to further increases in $O_2^{\bullet-}$ and $ONOO^-$ formation. $ONOO^-$ can also decrease the activity of GDH, TIP, cytochrome p450, and aldolase A which may decreased the production of ATP, FADH, $FADH_2$, NADH and GTP. This may cause hyperpolarisation of the mitochondrial membrane. The increased activity of XO under 18.6% O_2 may lead to increased $ONOO^-$ formation through the reaction of $O_2^{\bullet-}$ with $^{\bullet}NO$. Additionally, the oxidation of BH_4 to the $BH_3^{\bullet}$ by $ONOO^-$ may uncouple the production of $^{\bullet}NO$ by NOS to $O_2^{\bullet-}$. This overall increase in $O_2^{\bullet-}$ availability in 18.6% O_2 compared to 3.0% O_2 (right) may increase $ONOO^-$-mediated nitration reactions with antioxidant proteins such as prx-2, whose nitration at Tyr193 has been linked to increased peroxidase activity. Nitration of GR may also lead to decreased activity with attenuated GSSG reduction. Under 18.6% O_2, the increased availability of O_2 may augment the formation of $ONOO^-$ through nitroxyl-O_2 reactions. This could further propagate $ONOO^-$-mediated nitration reactions under 18.6% O_2 relative to physioxia. Solid arrows or bold font indicate increased activity/concentration compared to the opposing [O_2]. Dashed arrows indicate diminished activity compared to the opposing [O_2] concentration. **Ψm:** mitochondrial membrane potential; **I–IV:** electron transport chain complex I-V; **BH4/BH3•:** tetrahydrobiopterin/trihydrobiopterin radical; **Cyt P450:** cytochrome c p450; **ETC:** electron transport chain; **Gpx:** glutathione peroxidase; **GSH/GSSG:** reduced/oxidised glutathione; **GR:** glutathione reductase; **GDH:** glyceraldehyde-3-phosphate dehydrogenase; **HNO:** nitroxyl; **NOS/NOS (u):** Nitric oxide synthase/uncoupled nitric oxide synthase; **$O_2^{\bullet-}$:** superoxide; **$ONOO^-$:** peroxynitrite; **Prx-2:** peroxiredoxin 2; **TIP:** triose phosphate isomerase; **XO:** xanthine oxidase. Image made using www.BioRender.com.

4.5. Chapter summary

The aim of this chapter was to determine whether the growth of A431 cells in 18.6% O_2 affected the activity and expression levels of Nrf-2-target enzymes and proteins (respectively) compared to such activities and levels in A431 cells adapted to 3.0% O_2 for 96 h.

A431 cells grown in 18.6% O_2 exhibited heightened catalase and GR activities compared to A431 cells adapted to 3.0% O_2. The enzyme activities of catalase and GR changed until at least 96 h after placing A431 cells into 3.0% O_2 compared to the activity noted in A431 cells grown in 18.6% O_2. A431 cells grown in 18.6% O_2 exhibited higher expression levels of catalase and NQO-1 protein, compared to A431 cells adapted to 3.0% O_2 for 96 h. The higher expression levels of Nrf-2-target proteins in A431 cells grown in 18.6% O_2 was associated with higher expression levels of nuclear Nrf-2 protein compared to A431 cells adapted to 3.0% O_2 for 96 h. When treated with auranofin, A431 cells grown in 18.6% O_2 did not induce NQO-1 protein expression compared to untreated control cells. However, A431 cells adapted to 3.0% O_2 showed an [auranofin]-dependent induction of NQO-1 protein expression compared to untreated control cells. Additionally, A431 cells grown in 18.6% O_2 exhibited higher levels of proteins containing the 3-NT protein modification compared to A431 cells adapted to physioxia. This suggested that A431 cells grown in standard cell culture [O_2] were in a state of persistent nitrative stress compared to A431 cells adapted to 3.0% O_2.

It is concluded that A431 cells grown in 18.6% O_2 were resistant to cell death induced by redox-active compounds because they possess bolstered antioxidant defence systems compared to A431 cells adapted to physioxia. Despite this, A431 cells grown in 18.6% O_2 were unable to induce the expression of the NQO-1 antioxidant defence system in response to auranofin treatment in contrast to A431 cells adapted to physioxia. Should Nrf-2-target protein expression (e.g. NQO-1) be utilised as an efficacy endpoint for the *in vitro* development of Nrf-2 activating agents, it is suggested that the induction of NQO-1 should be measured in mammalian cells adapted to physioxia and not in mammalian cells grown chronically in standard cell culture oxygenation conditions.

CHAPTER 5: FINAL CONCLUSIONS

5.1. Final conclusions

Overall, this work showed that certain redox-active compounds demonstrate altered efficacy when tested on non-melanoma squamous cell carcinoma cells grown in standard cell culture [O_2] compared to such cells adapted to the [O_2] present in human skin under the same treatment conditions.

In chapter 3, A431 cells grown in 18.6% O_2 exhibited resistance to auranofin and H_2O_2-induced cell death compared to A431 cells adapted to 3.0% O_2 for 96 h. However, the cellular responses of A431 cells to auranofin, and H_2O_2 changed with time until at least 96 h after placing the cells into 3.0% O_2 compared to 18.6% O_2.

Although this work did not determine the physioxia adaptation period required for A431 cells to maximally adapt their response to auranofin and H_2O_2, it did reveal another point of consideration; the adaptation time period is a critical experimental parameter to consider when designing *in vitro* cell culture experiments under physioxia. Unfortunately, the adaptation time period for physioxic cell culture is often arbitrarily chosen, usually between 2–8 days [12]. The rationale for such choosing such time periods in the literature are usually not given, but such choices may be based (in part) on the doubling time of the cell (i.e. how quickly a parent population is replaced with daughter populations in the 'new' oxygen concentration). Others [80] have suggested that it allows adaptation of the cellular proteome, but the limited availability of data in this area do not support such claims. What are these large scale changes to the proteome that occur during physioxia adaptation? The levels of certain proteins change during physioxia adaptation in certain cell types (i.e. TrxR in A431 cells [21]), and the levels of others do not (GSH in HUVEC [72]). Such changes are likely cell-line and cell-type-dependent. As such, some adaptation time periods may be sufficient for some cells to adapt aspects of their phenotype to physioxia, but not for others.

The work in chapter 3 began by investigating changes to antioxidant enzyme systems in A431 cells grown in 18.6% O_2 compared to those adapted to 3.0% O_2 by using enzyme inhibitors like 3-AT, MSA, and L-BSO. Inhibition of catalase by 3-AT, and GSH by L-BSO, did not differentially sensitise A431 cells grown in

18.6% O_2 for 96 h to H_2O_2-induced cell death compared to A431 cells adapted to 3.0% O_2 for 96 h under the same treatment conditions. This suggested that certain elements of the antioxidant response may not change when A431 cells were grown in standard cell culture [O_2] compared to growth in physioxia. A431 cells grown in 18.6% O_2 were however resistant to other forms of oxidative stress-induced cell damage including CuOOH, MSA, and H_2O_2-induced lipid peroxidation compared to A431 cells adapted to 3.0% O_2 for 96 h. Similar to auranofin, the cellular responses of A431 cells to CuOOH-induced lipid peroxidation continued to change until at least 96 h after placing the cells into 3.0% O_2 compared to A431 cells grown in 18.6% O_2 for 96 h under the same treatment conditions. Overall, this suggested that phenotypic changes were occurring in A431 cells as they grew in 3.0% O_2 over time. These changes may have conferred sensitivity to the effects of redox-active compounds compared to A431 cells grown in 18.6% O_2 under the same treatment conditions.

In chapter 4, the molecular mechanism of this resistance was further investigated. A431 cells grown in 18.6% O_2 exhibited heightened activity of some Nrf-2-target protein and enzyme compared to A431 cells adapted to 3.0% O_2 for 96 h. A431 cells grown in 18.6% O_2 exhibited higher catalase, and GR enzymatic activity compared to A431 cells adapted to 3.0% O_2 for 96 h. Additionally, the expression levels of proteins exhibiting the 3-NT protein modification were higher in A431 cells grown in 18.6% O_2 compared to A431 cells adapted to 3.0% O_2 for 96 h. This suggested that squamous cell carcinoma cells grown in 18.6% O_2 were in a state of persistent nitrative stress compared to A431 cells adapted to physioxia.

The increased activities of Nrf-2-target enzymes in A431 cells grown in 18.6% O_2 were associated with higher expression levels of nuclear Nrf-2 protein compared to A431 cells adapted to 3.0% O_2 for 96 h. Additionally, the increased basal protein expression of Nrf-2 in A431 cells grown in 18.6% O_2 was associated with an increase in the basal protein expression of the Nrf-2-target proteins catalase and NQO-1 compared to A431 cells adapted to 3.0% O_2. The resistance of A431 cells grown in 18.6% O_2 to the effects of redox-active compounds was hypothesised to involve augmented induction of Nrf-2-target protein (i.e. NQO-1) during treatment. This was hypothesised due to the higher expression levels of nuclear Nrf-2 protein in 18.6% O_2 compared to A431 cells adapted to 3.0% O_2 for

96 h. However, A431 cells grown in 18.6% O_2 exhibited blunted auranofin-induced induction of NQO-1 protein compared to A431 cells adapted to 3.0% O_2 for 96 h under the same treatment conditions. The expression levels (and activity) of some Nrf-2-target protein/enzyme were higher in A431 cells grown in 18.6% O_2 compared to A431 cells adapted to 3.0% O_2. However, the induction of NQO-1 protein expression (Nrf-2-target) was blunted in A431 cells grown in 18.6% O_2 compared to A431 cells adapted to 3.0% O_2 for 96 h under the same treatment conditions. If these experiments had only been carried out in A431 cells grown in 18.6% O_2, the TrxR antioxidant system may have been deemed an invalid target for inducing NQO-1 protein expression through auranofin-mediated inhibition. It is concluded that the blunted auranofin-induced NQO-1 protein expression in A431 cells grown in 18.6% O_2 is artefactual when compared to A431 cells adapted to 3.0% O_2 under the same treatment conditions. This artefact was caused by growing these A431 cells in standard cell culture oxygenation conditions. As NQO-1 protein induction is used as an endpoint for validating potential 'hits' in the development of Nrf-2-activating agents [87, 329], it is suggested that the relevant cells should adapted to physioxia to ensure that the artefactual effects noted in A431 cells are not also present in other cell types.

Overall, the aims outlined in **section 1.4** were partially achieved. Aim 1 (to grow cells in 3.0% O_2 without inducing hypoxia), and aim 2 (to determine whether A431 cells grown in 18.6% O_2 conferred resistance to H_2O_2 and auranofin-induced cell death compared to 3.0% O_2) were achieved. Aim 3 however, to determine the optimal physioxia adaptation period for A431 cells, was not fully achieved. These data in this work suggest that A431 cells were not finished adapting to physioxia after a 96 h incubation period and may require longer adaptation times (i.e. > 4 days) to fully adapt their responses to auranofin and H_2O_2. Future work should determine whether the adaptation of A431 cells to physioxia beyond 4 days further sensitises these cells to auranofin and H_2O_2-induced cell death. Aim 4, to determine the molecular mechanism through which A431 cells grown in 18.6% O_2 resist oxidative stress-induced cell death compared to 3.0% O_2, was achieved as it identified Nrf-2-target protein expression levels and activity as being involved in said resistance.

However, the endpoints targeted to identify how A431 cells grown in 18.6% O_2 resisted oxidative stress-induced cell death (aim 4, **section 1.4**) were limited in scope (e.g. cell death, lipid peroxidation, $\Delta\psi_m$, ROS generation and Nrf-2-target protein expression levels/activity). Even if these endpoints were shown to maximally adapt at longer physioxia adaptation periods, other endpoints may require considerably longer to adapt (or may not adapt at all). These slow adapting mechanisms may involve epigenetic change. For example, enzymes such as ten-eleven translocation (instrumental in DNA demethylation) require both O_2 and Fe^{2+} to oxidise 5-methylcytosine in DNA to 5-hydroxymethylcytosine [337]. Although the K_m (O_2%) is quite low (1%), its activity is also dependent on the availability of Fe^{2+} which may be sensitive to Nrf-2 activity through the control of ferritin [33, 332]. This enzyme could be involved in slowly developing epigenetic changes during cellular adaptation to physioxia.

There is an argument that cell lines are not an appropriate cell type choice for testing the hypothesis outlined in **section 1.4**. Some cell lines, engineered (and selected) for growth in atmospheric O_2, may not ever fully adapt to physioxia. Some cell lines, including the A431 cell line used in this work, have likely already adapted to growth in 18.6% O_2 prior to experimentation. In fact, our use of the term ‘adaptation to physioxia’ might not be an appropriate term when utilising cell lines such as A431. The term ‘adaptation’ implies that a cell will, at some point, fully adapt to physioxia. However, it is unknown whether cell lines are capable of *fully* adapting their phenotype to a physiological [O_2] after many generations of growth in standard cell culture [O_2]. Some aspects of cell line cellular phenotype may have become irreversibly changed and so may not ever fully re-adapt to growth in physioxia. Future work should utilise primary skin cells (e.g. NHEK) to augment our observations in A431 cells. These primary cells should ideally be isolated in physioxia and be maintained in physioxia, with the other [O_2] group being switched into 18.6% O_2. Here, one would not be measuring cellular adaptation to physioxia, because presumably primary cells have already adapted to growth in physioxia. Instead a different question would be addressed: how do primary cells adapt to growth in standard cell culture [O_2] after they have fully adapted to growth in physioxia?

Leading on from this, free radical research journals should consider requiring all submitted manuscripts to report the average pO_2 of mammalian cell culture media across the culture period, and at the time of experimentation. This should be done even if the project at large is not performed under physioxia. This is due to the growing concern that the [O_2] used in standard cell culture represents a contributing factor toward the reproducibility problem in the life sciences [50, 71]. The problem of [O_2] in cell culture is however a general problem in the field of *in vitro* cell biology. Al-Ani et al. [71] examined two hundred papers from Cell, Nature, Science, and Nature Biotechnology (the most highly cited journals in cell biology) and found that only 6% of the examined papers provided all of the necessary experimental information needed to recreate the [O_2] in the appropriate work. Such experimental information involved reporting: culture vessel geometry, cell type, seeding density (both at the time of seeding and the cell density at the time of experimentation), and the medium volume. None of the papers examined from these journals measured the [O_2] in the cell culture medium, or measured the [O_2] within the cells [71]. Recently, there has been an urgent call to report, not just the [O_2] parameter, but a range of under-reported cell culture parameters such as medium pH, medium [CO_2], and passage number (at the time of experimentation) [339].

However, the effect of long term growth in standard cell culture [O_2] may not just affect redox biology related processes. Redox signalling pathways, such as Nrf-2, cross-talk with a large number of cell signalling pathways including xenobiotic stress, mitochondrial respiration, stem cell quiescence, mRNA translation, autophagy and the unfolded protein response [307, 329, 333–335]. Korcsmáros et al. [343] have developed an Nrf-2-ome, an integrated web resource containing information on Nrf-2 interacting factors, target genes, regulating transcription factors, and miRNAs. The interactions of Nrf-2 across these above categories number in the thousands [343]. It is therefore unlikely that *in vitro* [O_2] is a concern for redox biology alone **(Table 5.1)**.

Finally, one cannot discuss the practise of cell culture without mentioning the three R's of research (Replacement, Reduction and Refinement). These express the need to reduce and replace the number of animals used in clinical research with other forms of experimentation, or to refine said testing on animals so that

fewer animals need to be used (e.g. glass mouse models). *In-vitro* cell culture represents a method that, to some small extent, obviates the need for *in vivo* testing in animals. Unfortunately, our *in vitro* systems do not yet have the predictive power needed to make *in vivo* testing a redundancy. Biological scientists have a responsibility to improve the predictive power of *in vitro* models in order to reduce the number of animals used in pre-clinical testing. This present work does not imply that the issue of cell culture [O_2] is the biggest (or only) barrier in the way of such endeavours. There are many fundamental issues with *in vitro* cell culture **(section 1.1)**, though *all* will require addressing should animal experimentation be replaced further with a form of *in vitro* modelling. One criticism that is absolutely valid in this context, why should a laboratory put effort into accommodating *in vitro* physioxia cell culture in order to overcome just one of the many individual limitations that affect cell culture? Right now, there is limited information on the long term effects of mammalian cell culture on cellular phenotype, however the evidence that is available **(sections 1.3.1.1.1, 3.1, 4.1)** indicates that such changes should be noted in particular by those working in the field of redox biology. In essence, the [O_2] in cell culture may not affect all fields of research in the same way, however this issue may be of primary concern for those performing mammalian *in vitro* cell culture work in the field of redox biology.

To summarise, the ability of squamous cell carcinoma *in vivo* to resist oxidative stress-induced cell death may have been overestimated as such resistances have been largely studied in such cells grown long term in a non-physiological [O_2]. The responses of squamous cell carcinoma cells to the effects of redox-active compounds should be studied in such cells adapted to physioxia for at least 4 days and not standard cell culture [O_2].

Pathway	Targets	Reported redox interaction	Related disease
Apoptosis	Caspases	Caspase 3 was glutathiolated by glutaredoxin during TNF-α-induced cell death [344].	Cancer
	cGMP phosphodiesterase	Oxidative modification of caspase 9 modulated its interaction with apaf-1 [345]	
PI3K Signalling	Pi3K, SKT/PKB, PDK, PTEN, mTOR, GSK3β	Link between the PI3K/AKT pathway and redox homeostasis [346].	Cancer, rheumatoid arthritis/inflammation, respiratory disease.
		GSK3β was involved in the nuclear export of Nrf-2 [207].	
		Redox status regulated mTOR activity [347]	
MAPK	ERK, JNK, and p38	Oxidation of cysteine residues in JNK by H_2O_2 mediated redox regulation in chondrocytes [348]	Inflammation, rheumatoid arthritis, cancer
		Oxidative stress induced the JNK and p38 kinase pathways [349]	
		Pharmacological inhibition of ERK/AKT signalling pathways increased susceptibility to H_2O_2-mediated cell death [349]	
Angiogenesis	VEGF, VEGFR, RTK, FGF, FGFR, PDGF, PDGFR, FLT3, PKC, CXCR2, MMP2, HIF-1α.	NADPH oxidase-dependent ROS generation mediated HIF and VEGF signalling [212].	Cancer
		Oxidative stress inactivated VEGF survival signalling in retinal endothelial cells via Pi3K [350].	
		GSH depletion by L-BSO induced CXCR4 transcription [351].	

Pro-inflammatory pathways	TNF-α, TNF-α receptor, TACE, IKK-α, -β,- Ɣ, IL-1, IL-1R, IRAK1, IRAK2, IRAK 3, IL-6, IL-6R, Toll like receptors.	Exogenous ROS sensitised mammalian cells to TNF-mediated apoptosis [352]. Antioxidant treatment attenuated TNF-mediated apoptosis. [352] ROS mediated IKK-mediated inhibition of NFκB signalling [352]	Rheumatoid arthritis and inflammatory disorders.
Anti-inflammatory pathways	IL-2, IL-2R, IL-4, IL-4R, IL-10, IL-10R	Cytokine generated ROS inactivated IL-R associated PTP which modulates cytokine production [353]. IL associated PTPs regulated oxidation of catalytic cysteine residues [354].	Inflammation and cancer.
Glucose homeostasis	Glucagon, glucagon receptor, glucokinase, glycogen phosphorylase, glycogen synthase 1 and 2.	Extracellular redox state affected gluconeogenesis, and glycogen synthesis in hepatocyte [355]. H_2O_2 inhibited glucose metabolism in rat pancreatic islets which was reversed by catalase [356].	Diabetes and cancer.

Table 5.1: Non-exhaustive list of cellular pathways of interest to the pharmaceutical industry, with associated evidence of redox interaction. cGMP: cyclic guanine monophosphate; **CXCR:** α-chemokine receptor; **ERK:** extracellular signal-regulated kinase; **FGF/R:** fibroblast growth factor/receptor; **FLT:** tyrosine-protein kinase; **GSK:** glycogen synthase kinase; **HIF:** hypoxia-inducible factor; **IKK:** IκB kinase; **IL:** Interleukin; **IRAK:** Interleukin-1 receptor-associated kinases; **JNK:** c-Jun N terminal kinase; **MMP:** matrix metalloproteinase; **mTOR:** mammalian target of rapamycin; **PDGF/R:** platelet derived growth factor/receptor; **PDK:** pyruvate dehydrogenase kinase; **Pi3K:** phosphatidylinositol 3-kinase; **PKC:** protein kinase C; **PTEN:** phosphatase and tensin homolog deleted on chromosome 10; **PTP:** protein tyrosine phosphatase; **RTK:** receptor tyrosine kinase; **PBK:** protein kinase B; **SKT:** serine threonine kinase; **TACE:** tumour necrosis factor (TNF)-alpha converting enzyme; **TNF:** tumour necrosis factor; **VEGF/R:** vascular endothelial growth factor/receptor. Table adapted from [209].

REFERENCES

[1] **K. Sander**, “Wilhelm Roux and the rest: Developmental theories 1885-1895,” *Roux’s Arch. Dev. Biol.*, vol. 200, no. 6, pp. 297–299, Nov. 1991.

[2] **R. G. Harrison**, “An experimental study of the relation of the nervous system to the developing musculature in the embryo of the frog,” *Am. J. Anat.*, vol. 3, no. 2, pp. 197–220, Jun. 1904.

[3] **H. Zhu, A. Santo, M. Trush, and Y. R. Li**, “Oxygen and Oxygen Toxicity: The Birth of Concepts,” *React. Oxyg. Species*, vol. 1, no. 1, p. 1, Jan. 2016.

[4] **R. Gerschman, D. L. Gilbert, S. W. Nye, P. Dwyer, and W. O. Fenn**, “Oxygen poisoning and X-irradiation: A mechanism in common,” *Science (80-.).*, vol. 119, no. 3097, pp. 623–626, May 1954.

[5] **M. Richter, O. Piwocka, M. Musielak, I. Piotrowski, W. M. Suchorska, and T. Trzeciak**, “From Donor to the Lab: A Fascinating Journey of Primary Cell Lines,” *Front. Cell Dev. Biol.*, vol. 9, p. 1869, Jul. 2021.

[6] **A. Hernandez-Segura, S. Brandenburg, and M. Demaria**, “Induction and validation of cellular senescence in primary human cells,” *J. Vis. Exp.*, vol. 2018, no. 136, pp. 92–109, Jun. 2018.

[7] **J. W. Shay and W. E. Wright**, “Hayflick, his limit, and cellular ageing,” *Nat. Rev. Mol. Cell Biol.*, vol. 1, no. 1, pp. 72–76, Oct. 2000.

[8] **C. T. Ambrose**, “The Tissue Culture Laboratory of Dr. George Otto Gey 60 yrs ago as recalled by a former student,” *Vitr. Cell. Dev. Biol. - Anim.*, vol. 53, no. 5, pp. 467–473, May 2017.

[9] **C. Philippeos, R. D. Hughes, A. Dhawan, and R. R. Mitry**, “Introduction to cell culture,” *Methods Mol. Biol.*, vol. 806, pp. 1–13, 2012.

[10] **T. Yao and Y. Asayama**, “Animal□cell culture media: History, characteristics, and current issues,” *Reprod. Med. Biol.*, vol. 16, no. 2, p. 99, Apr. 2017.

[11] **R. Wenger, V. Kurtcuoglu, C. Scholz, H. Marti, and D. Hoogewijs**, “Frequently asked questions in hypoxia research,” *Hypoxia*, vol. 3, p. 35, 2015.

[12] **T. P. Keeley and G. E. Mann**, “Defining physiological normoxia for improved translation of cell physiology to animal models and humans,” *Physiol. Rev.*, vol. 99, no. 1, pp. 161–234, 2019.

[13] **Y. Li and K. A. Kilian**, “Bridging the Gap: From 2D Cell Culture to 3D Microengineered Extracellular Matrices,” *Adv. Healthc. Mater.*, vol. 4, no. 18, pp. 2780–2796, Dec. 2015.

[14] **V. Marx**, “Cell-line authentication demystified,” *Nat. Methods*, vol. 11, no. 5, pp. 483–488, 2014.

[15] **A. Capes-Davis *et al.***, “Check your cultures! A list of cross-contaminated or misidentified cell lines,” *Int. J. Cancer*, vol. 127, no. 1, pp. 1–8, 2010.

[16] **G. Gstraunthaler, T. Lindl, and J. Van Der Valk**, “A plea to reduce or replace fetal bovine serum in cell culture media,” *Cytotechnology*, vol. 65, no. 5, pp. 791–793, 2013.

[17] **J. Hodgson**, “Fetal bovine seram revisited: A year ago serum regulations were a hodgepodge. has anything changed?,” *Bio/Technology*, vol. 11, no. 1, pp. 49–53, 1993.

[18] **B. Halliwell**, “Cell culture, oxidative stress, and antioxidants: Avoiding pitfalls,” *Biomed. J.*, vol. 37, no. 3, pp. 99–105, 2014.

[19] **B. R. Weil, A. M. Abarbanell, J. L. Herrmann, Y. Wang, and D. R. Meldrum**, “High glucose concentration in cell culture medium does not acutely affect human mesenchymal stem cell growth factor production or proliferation,” *Am. J. Physiol. - Regul. Integr. Comp. Physiol.*, vol. 296, no. 6, p. R1735, Jun. 2009.

[20] **A. M. Greiner, B. Richter, and M. Bastmeyer**, “Micro-Engineered 3D Scaffolds for Cell Culture Studies,” *Macromol. Biosci.*, vol. 12, no. 10, pp. 1301–1314, Oct. 2012.

[21] **D. C. J. Ferguson *et al.***, “Altered cellular redox homeostasis and redox responses under standard oxygen cell culture conditions versus physioxia,” *Free Radic. Biol. Med.*, vol. 126, pp. 322–333, 2018.

[22] **J. O. C. Dunn, M. G. Mythen, and M. P. Grocott**, “Physiology of oxygen transport,” *BJA Educ.*, vol. 16, no. 10, pp. 341–348, Oct. 2016.

[23] **W. Wang**, “Oxygen partial pressure in outer layers of skin: Simulation using three-dimensional

multilayered models," *Microcirculation*, vol. 12, no. 2, pp. 195–207, Mar. 2005.

[24] **H. Baumgärtl, A. M. Ehrly, K. Saeger-Lorenz, and D. W. Lübbers**, "Initial Results of Intracutaneous Measurements of PO2 Profiles," *Antioxidants Redox Signal.*, vol. 9, no. 8, pp. 1169–1182, 1987.

[25] **R. Shulstad and S. Proper**, "Squamous Cell Carcinoma: A Review of Etiology, Pathogenesis, Treatment, and Variants," *J. Dermatol. Nurses. Assoc.*, vol. 2, no. 1, pp. 12–16, Jan. 2010.

[26] **P. Ebbesen *et al.***, "Hypoxia, normoxia and hyperoxia - Terminology for medical in vitro cell biology," *Acta Oncol. (Madr).*, vol. 39, no. 2, pp. 247–248, 2000.

[27] **S. R. McKeown**, "Defining normoxia, physoxia and hypoxia in tumours - Implications for treatment response," *Br. J. Radiol.*, vol. 87, no. 1035, p. 20130676, Mar. 2014.

[28] **M. Osrodek, M. L. Hartman, and M. Czyz**, "Physiologically relevant oxygen concentration (6% o2) as an important component of the microenvironment impacting melanoma phenotype and melanoma response to targeted therapeutics in vitro," *Int. J. Mol. Sci.*, vol. 20, no. 17, p. 4203, 2019.

[29] **Z. Ivanovic**, "Hypoxia or in situ normoxia: The stem cell paradigm," *J. Cell. Physiol.*, vol. 219, no. 2, pp. 271–275, May 2009.

[30] **Y.-Z. Jiang *et al.***, "Transcriptional and Functional Adaptations of Human Endothelial Cells to Physiological Chronic Low Oxygen," *Biol. Reprod.*, vol. 88, no. 5, p. 114, May 2013.

[31] **J. Sharkey**, "Effect of acute low oxygen exposure on the proliferation rate, viability and gene expression of C2C12 myoblasts in vitro," *bioRxiv*, 2020.

[32] **G. L. Semenza *et al.***, "Structural and functional analysis of hypoxia-inducible factor 1," *Kidney Int.*, vol. 51, no. 2, pp. 553–555, Feb. 1997.

[33] **D. Ferguson, A. Perry, M. E. Wood, P. G. Winyard, and M. Whiteman**, "Potentiation of Methyl Aminolevulinate (MAL)-Induced Photodynamic Therapy (PDT) Killing of Skin Cancer Cells by Mitochondria-Targeted Hydrogen Sulfide (H2S) Donors," *Free Radic. Biol. Med.*, vol. 76, no. 76, p. S135, Nov. 2014.

[34] **R. D. Stewart, V. K. Yu, A. G. Georgakilas, C. Koumenis, J. H. Park, and D. J. Carlson**, "Effects of radiation quality and oxygen on clustered DNA lesions and cell death," *Radiat. Res.*, vol. 176, no. 5, pp. 587–602, Nov. 2011.

[35] **S. Yoshiba, D. Ito, T. Nagumo, T. Shirota, M. Hatori, and S. Shintani**, "Hypoxia induces resistance to 5-fluorouracil in oral cancer cells via G1 phase cell cycle arrest," *Oral Oncol.*, vol. 45, no. 2, pp. 109–115, Feb. 2009.

[36] **J. A. Bertout, S. A. Patel, and M. C. Simon**, "The impact of O2 availability on human cancer," *Nat. Rev. Cancer*, vol. 8, no. 12, pp. 967–975, 2008.

[37] **P. J. Ratcliffe**, "Oxygen sensing and hypoxia signalling pathways in animals: The implications of physiology for cancer," *J. Physiol.*, vol. 591, no. 8, pp. 2027–2042, Apr. 2013.

[38] **C. Bayer, K. Shi, S. T. Astner, C. A. Maftei, and P. Vaupel**, "Acute versus chronic hypoxia: Why a simplified classification is simply not enough," *Int. J. Radiat. Oncol. Biol. Phys.*, vol. 80, no. 4, pp. 965–968, 2011.

[39] **T. Arnould, C. Michiels, I. Alexandre, and J. Remacle**, "Effect of hypoxia upon intracellular calcium concentration of human endothelial cells," *J. Cell. Physiol.*, vol. 152, no. 1, pp. 215–221, 1992.

[40] **S. Rodríguez-Enríquez *et al.***, "Oxidative phosphorylation is impaired by prolonged hypoxia in breast and possibly in cervix carcinoma," *Int. J. Biochem. Cell Biol.*, vol. 42, no. 10, pp. 1744–1751, Oct. 2010.

[41] **M. R. Duchen**, "Mitochondria and calcium: From cell signalling to cell death," *J. Physiol.*, vol. 529, no. 1, pp. 57–68, 2000.

[42] **S. W. Chang, T. J. Stelzner, J. V. Weil, and N. F. Voelkel**, "Hypoxia increases plasma glutathione disulfide in rats," *Lung*, vol. 167, no. 1, pp. 269–276, Dec. 1989.

[43] **V. Savransky *et al.***, "Chronic intermittent hypoxia and acetaminophen induce synergistic liver injury in

mice: Experimental Physiology - Research Paper," *Exp. Physiol.*, vol. 94, no. 2, pp. 228–239, 2009.

[44] **J. Y. Yin *et al.***, "Characterization and analyses of multidrug resistance-associated protein 1 (MRP1/ABCC1) polymorphisms in Chinese population," *Pharmacogenet. Genomics*, vol. 19, no. 3, pp. 206–216, Mar. 2009.

[45] **G. L. Wang and G. L. Semenza**, "General involvement of hypoxia-inducible factor 1 in transcriptional response to hypoxia," *Proc. Natl. Acad. Sci. U. S. A.*, vol. 90, no. 9, pp. 4304–4308, May 1993.

[46] **J. A. Stuart *et al.***, "How supraphysiological oxygen levels in standard cell culture affect oxygen-consuming reactions," *Oxid. Med. Cell. Longev.*, vol. 2018, p. 8238459, 2018.

[47] **D. Lando, D. J. Peet, J. J. Gorman, D. A. Whelan, M. L. Whitelaw, and R. K. Bruick**, "FIH-1 is an asparaginyl hydroxylase enzyme that regulates the transcriptional activity of hypoxia-inducible factor," *Genes Dev.*, vol. 16, no. 12, pp. 1466–1471, Jun. 2002.

[48] **M. Ivan *et al.***, "HIFα targeted for VHL-mediated destruction by proline hydroxylation: Implications for O2 sensing," *Science (80-.).*, vol. 292, no. 5516, pp. 464–468, 2001.

[49] **M. M. Hickey and M. C. Simon**, "Regulation of Angiogenesis by Hypoxia and Hypoxia-Inducible Factors," *Curr. Top. Dev. Biol.*, vol. 76, pp. 217–257, 2006.

[50] **T. L. Place, F. E. Domann, and A. J. Case**, "Limitations of oxygen delivery to cells in culture: An underappreciated problem in basic and translational research," *Free Radic. Biol. Med.*, vol. 113, pp. 311–322, 2017.

[51] **E. L. Bell, T. A. Klimova, J. Eisenbart, P. T. Schumacker, and N. S. Chandel**, "Mitochondrial Reactive Oxygen Species Trigger Hypoxia-Inducible Factor-Dependent Extension of the Replicative Life Span during Hypoxia," *Mol. Cell. Biol.*, vol. 27, no. 16, pp. 5737–5745, Aug. 2007.

[52] **P. Pollard, M. Yang, H. Su, T. Soga, and K. Kranc**, "Prolyl hydroxylase domain enzymes: important regulators of cancer metabolism," *Hypoxia*, vol. 2, p. 127, Aug. 2014.

[53] **D. R. Mole**, "Iron Homeostasis and Its Interaction with Prolyl Hydroxylases," *Antioxidants Redox Signal.*, vol. 12, no. 4, pp. 445–458, Feb. 2010.

[54] **Y. Pan *et al.***, "Multiple Factors Affecting Cellular Redox Status and Energy Metabolism Modulate Hypoxia-Inducible Factor Prolyl Hydroxylase Activity In Vivo and In Vitro," *Mol. Cell. Biol.*, vol. 27, no. 3, pp. 912–925, Feb. 2007.

[55] **L. Eberson**, "Moses gomberg and the nobel prize," *Cult. Chem. Best Artic. Hum. Side 20th-Century Chem. from Arch. Chem. Intell.*, pp. 283–289, Jan. 2015.

[56] **N. Haugaard**, "Cellular mechanisms of oxygen toxicity.," *Physiol. Rev.*, vol. 48, no. 2, pp. 311–373, Apr. 1968.

[57] **D. C. Gautheron**, "Mitochondrial oxidative phosphorylation and respiratory chain: Review," *J. Inherit. Metab. Dis.*, vol. 7, no. 1, pp. 57–61, 1984.

[58] **E. Rosini, G. Molla, S. Ghisla, and L. Pollegioni**, "On the reaction of d-amino acid oxidase with dioxygen: O2 diffusion pathways and enhancement of reactivity," *FEBS J.*, vol. 278, no. 3, pp. 482–492, Feb. 2011.

[59] **C. H. Wang, C. Zhang, and X. H. Xing**, "Xanthine dehydrogenase: An old enzyme with new knowledge and prospects," *Bioengineered*, vol. 7, no. 6, pp. 395–405, Nov. 2016.

[60] **Y. Nisimoto, B. A. Diebold, D. Constentino-Gomes, and J. D. Lambeth**, "Nox4: A hydrogen peroxide-generating oxygen sensor," *Biochemistry*, vol. 53, no. 31, pp. 5111–5120, Aug. 2014.

[61] **S. C. Daubner, T. Le, and S. Wang**, "Tyrosine hydroxylase and regulation of dopamine synthesis," *Arch. Biochem. Biophys.*, vol. 508, no. 1, pp. 1–12, Apr. 2011.

[62] **L. R. F. Backman, M. A. Funk, C. D. Dawson, and C. L. Drennan**, "New tricks for the glycyl radical enzyme family," *Crit. Rev. Biochem. Mol. Biol.*, vol. 52, no. 6, pp. 674–695, Nov. 2017.

[63] **X. Fang *et al.***, "Loss of Cardiac Ferritin H Facilitates Cardiomyopathy via Slc7a11-Mediated

Ferroptosis," *Circ. Res.*, vol. 127, no. 4, pp. 486–501, Jul. 2020.

[64] **Z. Lu and J. A. Imlay**, "When anaerobes encounter oxygen: mechanisms of oxygen toxicity, tolerance and defence," *Nat. Rev. Microbiol.*, vol. 19, no. 12, pp. 774–785, Jun. 2021.

[65] **N. Urao and M. Ushio-Fukai**, "Redox regulation of stem/progenitor cells and bone marrow niche," *Free Radic. Biol. Med.*, vol. 54, pp. 26–39, Jan. 2013.

[66] **A. Tiwari *et al.***, "Impact of oxygen levels on human hematopoietic stem and progenitor cell expansion," *Stem Cells Dev.*, vol. 25, no. 20, pp. 1604–1613, Oct. 2016.

[67] **M. Jež, P. Rožman, Z. Ivanović, and T. Bas**, "Concise Review: The Role of Oxygen in Hematopoietic Stem Cell Physiology," *J. Cell. Physiol.*, vol. 230, no. 9, pp. 1999–2005, Sep. 2015.

[68] **H. Le, N. Vishwanathan, N. M. Jacob, M. Gadgil, and W. S. Hu**, "Cell line development for biomanufacturing processes: recent advances and an outlook," *Biotechnol. Lett.*, vol. 37, no. 8, pp. 1553–1564, Aug. 2015.

[69] **A. Castan, P. Schulz, T. Wenger, and S. Fischer**, "Cell Line Development," *Biopharm. Process. Dev. Des. Implement. Manuf. Process.*, vol. 22, no. 3, pp. 131–146, Jan. 2018.

[70] **H. J. Forman and K. J. A. Davies**, "Commentary on 'bach1 differentially regulates distinct Nrf2-dependent genes in human venous and coronary artery endothelial cells adapted to physiological oxygen levels' by Chapple et al.," *Free Radic. Biol. Med.*, vol. 92, pp. 163–164, Mar. 2016.

[71] **A. Al-Ani, D. Toms, D. Kondro, J. Thundathil, Y. Yu, and M. Ungrin**, "Oxygenation in cell culture: Critical parameters for reproducibility are routinely not reported," *PLoS One*, vol. 13, no. 10, p. e0204269, Oct. 2018.

[72] **S. J. Chapple *et al.***, "Bach1 differentially regulates distinct Nrf2-dependent genes in human venous and coronary artery endothelial cells adapted to physiological oxygen levels," *Free Radic. Biol. Med.*, vol. 92, pp. 152–162, Mar. 2016.

[73] **A. Kumar *et al.***, "Quantifying the magnitude of the oxygen artefact inherent in culturing airway cells under atmospheric oxygen versus physiological levels," *FEBS Lett.*, vol. 590, no. 2, pp. 258–269, Jan. 2016.

[74] **X. Liu *et al.***, "Oxygen regulates the effective diffusion distance of nitric oxide in the aortic wall," *Free Radic. Biol. Med.*, vol. 48, no. 4, pp. 554–559, Feb. 2010.

[75] **L. Villeneuve, L. M. Tiede, B. Morsey, and H. S. Fox**, "Quantitative proteomics reveals oxygen-dependent changes in neuronal mitochondria affecting function and sensitivity to rotenone," *J. Proteome Res.*, vol. 12, no. 10, pp. 4599–4606, Oct. 2013.

[76] **Y. M. Lages, J. M. Nascimento, G. A. Lemos, A. Galina, L. R. Castilho, and S. K. Rehen**, "Low oxygen alters mitochondrial function and response to oxidative stress in human neural progenitor cells," *PeerJ*, vol. 2015, no. 12, p. e1486, 2015.

[77] **G. A. Corrêa, R. Rumpf, T. C. D. Mundim, M. M. Franco, and M. A. N. Dode**, "Oxygen tension during in vitro culture of bovine embryos: Effect in production and expression of genes related to oxidative stress," *Anim. Reprod. Sci.*, vol. 104, no. 2–4, pp. 132–142, Mar. 2008.

[78] **B. Haas *et al.***, "Permanent culture of macrophages at physiological oxygen attenuates the antioxidant and immunomodulatory properties of dimethyl fumarate," *J. Cell. Physiol.*, vol. 230, no. 5, pp. 1128–1138, May 2015.

[79] **S. Parrinello, E. Samper, A. Krtolica, J. Goldstein, S. Melov, and J. Campisi**, "Oxygen sensitivity severely limits the replicative lifespan of murine fibroblasts," *Nat. Cell Biol.*, vol. 5, no. 8, pp. 741–747, Aug. 2003.

[80] **T. P. Keeley, R. C. M. Siow, R. Jacob, and G. E. Mann**, "A PP2A-mediated feedback mechanism controls Ca2+-dependent NO synthesis under physiological oxygen," *FASEB J.*, vol. 31, no. 12, pp. 5172–5183, 2017.

[81] **B. Sahaf *et al.***, “Culturing of human peripheral blood cells reveals unsuspected lymphocyte responses relevant to HIV disease,” *Proc. Natl. Acad. Sci. U. S. A.*, vol. 105, no. 13, pp. 5111–5116, Apr. 2008.

[82] **L. M. Tiede, E. A. Cook, B. Morsey, and H. S. Fox**, “Oxygen matters: Tissue culture oxygen levels affect mitochondrial function and structure as well as responses to HIV viroproteins,” *Cell Death Dis.*, vol. 2, no. 12, p. 246, Dec. 2011.

[83] **I. Martinez *et al.***, “The influence of oxygen tension on the structure and function of isolated liver sinusoidal endothelial cells,” *Comp. Hepatol.*, vol. 7, p. 4, May 2008.

[84] **D. C. J. Ferguson *et al.***, “Altered cellular redox homeostasis and redox responses under standard oxygen cell culture conditions versus physioxia,” *Free Radic. Biol. Med.*, vol. 126, pp. 322–333, Oct. 2018.

[85] **H. M. Yan, A. Ramachandran, M. L. Bajt, J. J. Lemasters, and H. Jaeschke**, “The oxygen tension modulates acetaminophen-induced mitochondrial oxidant stress and cell injury in cultured hepatocytes,” *Toxicol. Sci.*, vol. 117, no. 2, pp. 515–523, Jul. 2010.

[86] **V. T. V. Dao *et al.***, “Pharmacology and clinical drug candidates in redox medicine,” *Antioxidants Redox Signal.*, vol. 23, no. 14, pp. 1113–1129, Nov. 2015.

[87] **A. Cuadrado *et al.***, “Transcription factor NRF2 as a therapeutic target for chronic diseases: A systems medicine approach,” *Pharmacol. Rev.*, vol. 70, no. 2, pp. 348–383, Apr. 2018.

[88] **A. Cuadrado *et al.***, “Therapeutic targeting of the NRF2 and KEAP1 partnership in chronic diseases,” *Nat. Rev. Drug Discov.*, vol. 18, no. 4, pp. 295–317, Jan. 2019.

[89] **B. Halliwell and J. M. C. Gutteridge**, “Role of free radicals and catalytic metal ions in human disease: An overview,” *Methods Enzymol.*, vol. 186, no. C, pp. 1–85, Jan. 1990.

[90] **G. R. Buettner**, “The Pecking Order of Free Radicals and Antioxidants: Lipid Peroxidation, α-Tocopherol, and Ascorbate,” *Arch. Biochem. Biophys.*, vol. 300, no. 2, pp. 535–543, Feb. 1993.

[91] **A. Ayala, M. F. Muñoz, and S. Argüelles**, “Lipid peroxidation: Production, metabolism, and signaling mechanisms of malondialdehyde and 4-hydroxy-2-nonenal,” *Oxid. Med. Cell. Longev.*, vol. 2014, p. 360438, 2014.

[92] **B. Halliwell and J. M. Gutteridge**, “Chapter 3: Antioxidant defences synthesized in vivo,” in *Free Radicals in Biology and Medicine.*, 5th editio., B. Halliwell and J. M. Gutteridge, Eds. Oxford University Press, 2015, pp. 77–153.

[93] **B. Halliwell and J. M. Gutteridge**, “Chapter 2: Redox chemistry, the essentials,” in *Free Radicals in Biology and Medicine*, 5th editio., B. Halliwell and J. M. Gutteridge, Eds. Oxford University Press, 2015, pp. 30–77.

[94] **A. N. Pham, G. Xing, C. J. Miller, and T. D. Waite**, “Fenton-like copper redox chemistry revisited: Hydrogen peroxide and superoxide mediation of copper-catalyzed oxidant production,” *J. Catal.*, vol. 301, pp. 54–64, May 2013.

[95] **B. A. Jurkiewicz and G. R. Buettner**, “Ultraviolet Light□Induced Free Radical Formation in Skin: an Electron Paramagnetic Resonance Study,” *Photochem. Photobiol.*, vol. 59, no. 1, pp. 1–4, Jan. 1994.

[96] **P. Wardman and L. P. Candeias**, “Fenton chemistry: An introduction,” *Radiat. Res.*, vol. 145, no. 5, pp. 523–531, 1996.

[97] **S. D. Aust, L. A. Morehouse, and C. E. Thomas**, “Role of metals in oxygen radical reactions,” *J. Free Radicals Biol. Med.*, vol. 1, no. 1, pp. 3–25, 1985.

[98] **B. Balasubramanian, W. K. Pogozelski, and T. D. Tullius**, “DNA strand breaking by the hydroxyl radical is governed by the accessible surface areas of the hydrogen atoms of the DNA backbone,” *Proc. Natl. Acad. Sci. U. S. A.*, vol. 95, no. 17, pp. 9738–9743, Aug. 1998.

[99] **J. F. Turrens**, “Mitochondrial formation of reactive oxygen species,” *J. Physiol.*, vol. 552, no. 2, pp. 335–344, Oct. 2003.

[100] **F. Haber and J. Weiss**, “Über die Katalyse des Hydroperoxydes,” *Naturwissenschaften*, vol. 20, no. 51, pp. 948–950, Dec. 1932.

[101] **M. J. Burkitt**, “Chemical, biological and medical controversies surrounding the Fenton reaction,” *Prog. React. Kinet. Mech.*, vol. 28, no. 1, pp. 75–103, 2003.

[102] **R. Radi**, “Oxygen radicals, nitric oxide, and peroxynitrite: Redox pathways in molecular medicine,” *Proc. Natl. Acad. Sci. U. S. A.*, vol. 115, no. 23, pp. 5839–5848, Jun. 2018.

[103] **B. Görg, N. Qvartskhava, P. Voss, T. Grune, D. Häussinger, and F. Schliess**, “Reversible inhibition of mammalian glutamine synthetase by tyrosine nitration,” *FEBS Lett.*, vol. 581, no. 1, pp. 84–90, Jan. 2007.

[104] **D. Francescutti, J. Baldwin, L. Lee, and B. Mutus**, “Peroxynitrite modification of glutathione reductase: Modeling studies and kinetic evidence suggest the modification of tyrosines at the glutathione disulfide binding site,” *Protein Eng.*, vol. 9, no. 2, pp. 189–194, Feb. 1996.

[105] **J. A. Swain, V. Darley-Usmar, and J. M. C. Gutteridge**, “Peroxynitrite releases copper from caeruloplasmin: implications for atherosclerosis,” *FEBS Lett.*, vol. 342, no. 1, pp. 49–52, Mar. 1994.

[106] **A. Gomes, E. Fernandes, and J. L. F. C. Lima**, “Fluorescence probes used for detection of reactive oxygen species,” *J. Biochem. Biophys. Methods*, vol. 65, no. 2–3, pp. 45–80, Dec. 2005.

[107] **K. Tanaka *et al.***, “Rational design of fluorescein-based fluorescence probes. Mechanism-based design of a maximum fluorescence probe for singlet oxygen,” *J. Am. Chem. Soc.*, vol. 123, no. 11, pp. 2530–2536, 2001.

[108] **N. Soh, Y. Katayama, and M. Maeda**, “A fluorescent probe for monitoring nitric oxide production using a novel detection concept,” *Analyst*, vol. 126, no. 5, pp. 564–566, Jan. 2001.

[109] **M. Zhou, Z. Diwu, N. Panchuk-Voloshina, and R. P. Haugland**, “A stable nonfluorescent derivative of resorufin for the fluorometric determination of trace hydrogen peroxide: Applications in detecting the activity of phagocyte NADPH oxidase and other oxidases,” *Anal. Biochem.*, vol. 253, no. 2, pp. 162–168, Nov. 1997.

[110] **J. G. Mohanty, J. S. Jaffe, E. S. Schulman, and D. G. Raible**, “A highly sensitive fluorescent micro-assay of H2O2 release from activated human leukocytes using a dihydroxyphenoxazine derivative,” *J. Immunol. Methods*, vol. 202, no. 2, pp. 133–141, Mar. 1997.

[111] **F. A. Summers, B. Zhao, D. Ganini, and R. P. Mason**, “Photooxidation of amplex red to resorufin: Implications of exposing the amplex red assay to light,” *Methods Enzymol.*, vol. 526, pp. 1–17, 2013.

[112] **H. Zhao *et al.***, “Superoxide reacts with hydroethidine but forms a fluorescent product that is distinctly different from ethidium: Potential implications in intracellular fluorescence detection of superoxide,” *Free Radic. Biol. Med.*, vol. 34, no. 11, pp. 1359–1368, Jun. 2003.

[113] **B. Halliwell and J. M. Gutteridge**, “Chapter 6: Measurement of Reactive Species,” in *Free Radicals in Biology and Medicine*, 5th editio., B. Halliwell and J. M. Gutteridge, Eds. Oxford University Press, 2015, pp. 284–354.

[114] **C. Rota, Y. C. Fann, and R. P. Mason**, “Phenoxyl free radical formation during the oxidation of the fluorescent dye 2’,7’-dichlorofluorescein by horseradish peroxidase. Possible consequences for oxidative stress measurements,” *J. Biol. Chem.*, vol. 274, no. 40, pp. 28161–28168, Oct. 1999.

[115] **H. SIES**, “Strategies of antioxidant defense,” *Eur. J. Biochem.*, vol. 215, no. 2, pp. 213–219, 1993.

[116] **H. Sies, C. Berndt, and D. P. Jones**, “Oxidative stress,” *Annu. Rev. Biochem.*, vol. 86, pp. 715–748, Jun. 2017.

[117] **M. M. Gaschler and B. R. Stockwell**, “Lipid peroxidation in cell death,” *Biochem. Biophys. Res. Commun.*, vol. 482, no. 3, pp. 419–425, Jan. 2017.

[118] **A. Ayala, M. F. Muñoz, and S. Argüelles**, “Lipid peroxidation: Production, metabolism, and signaling mechanisms of malondialdehyde and 4-hydroxy-2-nonenal,” *Oxid. Med. Cell. Longev.*, vol. 2014, 2014.

[119] **W. H. Koppenol**, “Oxyradical reactions: from bond-dissociation energies to reduction potentials,” *FEBS Lett.*, vol. 264, no. 2, pp. 165–167, May 1990.

[120] **H. W. Gardner**, “Oxygen radical chemistry of polyunsaturated fatty acids,” *Free Radic. Biol. Med.*, vol. 7, no. 1, pp. 65–86, 1989.

[121] **W. Wang, H. Yang, D. Johnson, C. Gensler, E. Decker, and G. Zhang**, “Chemistry and biology of ω-3 PUFA peroxidation-derived compounds,” *Prostaglandins Other Lipid Mediat.*, vol. 132, pp. 84–91, Sep. 2017.

[122] **B. Halliwell and J. M. C. Gutteridge**, “Free Radicals in Biology and Medicine,” *Free Radicals Biol. Med.*, 2015.

[123] **Y. Ji, Z. Dai, G. Wu, and Z. Wu**, “4-Hydroxy-2-nonenal induces apoptosis by activating ERK1/2 signaling and depleting intracellular glutathione in intestinal epithelial cells,” *Sci. Rep.*, vol. 6, no. 1, pp. 1–13, Sep. 2016.

[124] **V. M. V. Costa, M. A. Amorim, A. Quintanilha, and P. Moradas-Ferreira**, “Hydrogen peroxide-induced carbonylation of key metabolic enzymes in Saccharomyces cerevisiae: The involvement of the oxidative stress response regulators Yap1 and Skn7,” *Free Radic. Biol. Med.*, vol. 33, no. 11, pp. 1507–1515, Dec. 2002.

[125] **J. Kanski, A. Behring, J. Pelling, and C. Schöneich**, “Proteomic identification of 3-nitrotyrosine-containing rat cardiac proteins: Effects of biological aging,” *Am. J. Physiol. - Hear. Circ. Physiol.*, vol. 288, no. 1 57-1, pp. 371–381, Jan. 2005.

[126] **M. W. Duncan**, “A review of approaches to the analysis of 3-nitrotyrosine,” *Amino Acids*, vol. 25, no. 3–4, pp. 351–361, 2003.

[127] **B. Halliwell, K. Zhao, and M. Whiteman**, “Nitric oxide and peroxynitrite. The ugly, the uglier and the not so good: A personal view of recent controversies,” *Free Radic. Res.*, vol. 31, no. 6, pp. 651–669, 1999.

[128] **S. Greenacre and H. Ischiropoulos**, “Tyrosine nitration: Localisation, quantification, consequences for protein function and signal transduction,” *Free Radic. Res.*, vol. 34, no. 6, pp. 541–581, 2001.

[129] **P. F. Good, A. Hsu, P. Werner, D. P. Perl, and C. Warren Olanow**, “Protein nitration in Parkinson’s disease,” *J. Neuropathol. Exp. Neurol.*, vol. 57, no. 4, pp. 338–342, 1998.

[130] **J. A. Hinson, S. L. Michael, S. G. Ault, and N. R. Pumford**, “Western blot analysis for nitrotyrosine protein adducts in livers of saline-treated and acetaminophen-treated mice,” *Toxicol. Sci.*, vol. 53, no. 2, pp. 467–473, Feb. 2000.

[131] **L. Galluzzi *et al.***, “Molecular mechanisms of cell death: Recommendations of the Nomenclature Committee on Cell Death 2018,” *Cell Death Differ.*, vol. 25, no. 3, pp. 486–541, Jan. 2018.

[132] **J. F. R. Kerr, A. H. Wyllie, and A. R. Currie**, “Apoptosis: A basic biological phenomenon with wide-ranging implications in tissue kinetics,” *Br. J. Cancer*, vol. 26, no. 4, pp. 239–257, Aug. 1972.

[133] **S. Elmore**, “Apoptosis: A Review of Programmed Cell Death,” *Toxicol. Pathol.*, vol. 35, no. 4, pp. 495–516, Jun. 2007.

[134] **J. Savill and V. Fadok**, “Corpse clearance defines the meaning of cell death,” *Nature*, vol. 407, no. 6805, pp. 784–788, Oct. 2000.

[135] **M. Raffray and G. M. Cohen**, “Apoptosis and necrosis in toxicology: A continuum or distinct modes of cell death?,” *Pharmacol. Ther.*, vol. 75, no. 3, pp. 153–177, Sep. 1997.

[136] **B. F. Trump, I. K. Berezesky, S. H. Chang, and P. C. Phelps**, “The pathways of cell death: Oncosis, apoptosis, and necrosis,” *Toxicol. Pathol.*, vol. 25, no. 1, pp. 82–88, Jan. 1997.

[137] **A. K. Bhuyan, A. Varshney, and M. K. Mathew**, “Resting membrane potential as a marker of apoptosis: Studies on Xenopus oocytes microinjected with cytochrome c,” *Cell Death Differ.*, vol. 8, no. 1, pp. 63–69, Mar. 2001.

[138] **N. D. Lakin and S. P. Jackson**, “Regulation of p53 in response to DNA damage,” *Oncogene*, vol. 18, no. 53, pp. 7644–7655, Dec. 1999.

[139] **J. Walters *et al.***, “A constitutively active and uninhibitable caspase-3 zymogen efficiently induces apoptosis,” *Biochem. J.*, vol. 424, no. 3, pp. 335–345, Dec. 2009.

[140] **M. O. Hengartner**, “The biochemistry of apoptosis,” *Nature*, vol. 407, no. 6805, pp. 770–776, Oct. 2000.

[141] **T. C. Karlenius and K. F. Tonissen**, “Thioredoxin and cancer: A role for thioredoxin in all states of tumor oxygenation,” *Cancers (Basel).*, vol. 2, no. 2, pp. 209–232, Jun. 2010.

[142] **A. Gallegos *et al.***, “Transfection with human thioredoxin increases cell proliferation and a dominant-negative mutant thioredoxin reverses the transformed phenotype of human breast cancer cells,” *Cancer Res.*, vol. 56, no. 24, pp. 5765–5770, 1996.

[143] **S. J. Kim *et al.***, “High thioredoxin expression is associated with resistance to docetaxel in primary breast cancer,” *Clin. Cancer Res.*, vol. 11, no. 23, pp. 8425–8430, Dec. 2005.

[144] **T. Sasada *et al.***, “Redox control of resistance to cis-diamminedichloroplatinum (II) (CDDP): Protective effect of human thioredoxin against CDDP-induced cytotoxicity,” *J. Clin. Invest.*, vol. 97, no. 10, pp. 2268–2276, May 1996.

[145] **A. Yokomizo *et al.***, “Cellular Levels of Thioredoxin Associated with Drug Sensitivity to Cisplatin, Mitomycin C, Doxorubicin, and Etoposide,” *Cancer Res.*, vol. 55, no. 19, pp. 4293–4296, 1995.

[146] **C. Roder and M. J. Thomson**, “Auranofin: repurposing an old drug for a golden new age,” *Drugs R D*, vol. 15, no. 1, pp. 13–20, Mar. 2015.

[147] **S. Jackson-Rosario *et al.***, “Auranofin disrupts selenium metabolism in Clostridium difficile by forming a stable Au-Se adduct,” *J. Biol. Inorg. Chem.*, vol. 14, no. 4, pp. 507–519, May 2009.

[148] **N. Liu *et al.***, “Clinically used antirheumatic agent auranofin is a proteasomal deubiquitinase inhibitor and inhibits tumor growth,” *Oncotarget*, vol. 5, no. 14, pp. 5453–5471, 2014.

[149] **P. Sabatier, C. M. Beusch, R. Gencheva, Q. Cheng, R. Zubarev, and E. S. J. Arnér**, “Comprehensive chemical proteomics analyses reveal that the new TRi-1 and TRi-2 compounds are more specific thioredoxin reductase 1 inhibitors than auranofin,” *Redox Biol.*, vol. 48, p. 102184, Dec. 2021.

[150] **J. M. Madeira, C. J. Renschler, B. Mueller, S. Hashioka, D. L. Gibson, and A. Klegeris**, “Novel protective properties of auranofin: Inhibition of human astrocyte cytotoxic secretions and direct neuroprotection,” *Life Sci.*, vol. 92, no. 22, pp. 1072–1080, Jun. 2013.

[151] **A. G. Cox, K. K. Brown, E. S. J. Arner, and M. B. Hampton**, “The thioredoxin reductase inhibitor auranofin triggers apoptosis through a Bax/Bak-dependent process that involves peroxiredoxin 3 oxidation,” *Biochem. Pharmacol.*, vol. 76, no. 9, pp. 1097–1109, Oct. 2008.

[152] **Mayo Clinic**, “Auranofin and Sirolimus in Treating Participants With Ovarian Cancer,” *ClinicalTrials.gov*, 2021.

[153] **T. Mokudai, K. Nakamura, T. Kanno, and Y. Niwano**, “Presence of Hydrogen Peroxide, a Source of Hydroxyl Radicals, in Acid Electrolyzed Water,” *PLoS One*, vol. 7, no. 9, p. e46392, Sep. 2012.

[154] **M. Giorgio, M. Trinei, E. Migliaccio, and P. G. Pelicci**, “Hydrogen peroxide: A metabolic by-product or a common mediator of ageing signals?,” *Nat. Rev. Mol. Cell Biol.*, vol. 8, no. 9, pp. 722–728, Sep. 2007.

[155] **A. Cuadrado *et al.***, “Therapeutic targeting of the NRF2 and KEAP1 partnership in chronic diseases,” *Nat. Rev. Drug Discov.*, vol. 18, no. 4, pp. 295–317, Apr. 2019.

[156] **J. Xiang, C. Wan, R. Guo, and D. Guo**, “Is hydrogen peroxide a suitable apoptosis inducer for all cell types?,” *Biomed Res. Int.*, vol. 2016, 2016.

[157] **E. MARGOLIASH, A. NOVOGRODSKY, and A. SCHEJTER**, “Irreversible reaction of 3-amino-1:2:4-triazole and related inhibitors with the protein of catalase.,” *Biochem. J.*, vol. 74, no. 2, pp. 339–348, 1960.

[158] **H. Yuan, T. Kaneko, and M. Matsuo**, “Relevance of oxidative stress to the limited replicative capacity of

cultured human diploid cells: the limit of cumulative population doublings increases under low concentrations of oxygen and decreases in response to aminotriazole," *Mech. Ageing Dev.*, vol. 81, no. 2–3, pp. 159–168, Jul. 1995.

[159] **T. V. Bagnyukova, O. Y. Vasylkiv, K. B. Storey, and V. I. Lushchak**, "Catalase inhibition by amino triazole induces oxidative stress in goldfish brain," *Brain Res.*, vol. 1052, no. 2, pp. 180–186, Aug. 2005.

[160] **D. Birnbaum, S. Csukas, A. Costarides, E. Forbes, and K. Green**, "3-amino-triazole effects on the Eye of young and adult rabbits in the presence and absence of hydrogen peroxide," *Curr. Eye Res.*, vol. 6, no. 12, pp. 1403–1414, 1987.

[161] **N. Ueda, B. Guidet, and S. V. Shah**, "Measurement of intracellular generation of hydrogen peroxide by rat glomeruli in vitro," *Kidney Int.*, vol. 45, no. 3, pp. 788–793, 1994.

[162] **K. Ono and D. C. Shrieve**, "Enhancement of EMT6/SF tumor cell killing by mitomycin C and cyclophosphamide following in vivo administration of buthionine sulfoximine," *Int. J. Radiat. Oncol. Biol. Phys.*, vol. 12, no. 7, pp. 1175–1178, 1986.

[163] **A. L. Ortega, S. Mena, and J. M. Estrela**, "Glutathione in cancer cell death," *Cancers (Basel).*, vol. 3, no. 1, pp. 1285–1310, Mar. 2011.

[164] **G. Gokce *et al.***, "Glutathione depletion by buthionine sulfoximine induces oxidative damage to DNA in organs of rabbits in vivo," *Biochemistry*, vol. 48, no. 22, pp. 4980–4987, Jun. 2009.

[165] **S. X. Skapek *et al.***, "Melphalan-induced toxicity in nude mice following pretreatment with buthionine sulfoximine," *Cancer Chemother. Pharmacol.*, vol. 28, no. 1, pp. 15–21, Jan. 1991.

[166] **L. Révész, M. R. Edgren, and A. A. Wainson**, "Selective toxicity of buthionine sulfoximine (BSO) to melanoma cells in vitro and in vivo," *Int. J. Radiat. Oncol. Biol. Phys.*, vol. 29, no. 2, pp. 403–406, May 1994.

[167] **A. Tagde, H. Singh, M. H. Kang, and C. P. Reynolds**, "The glutathione synthesis inhibitor buthionine sulfoximine synergistically enhanced melphalan activity against preclinical models of multiple myeloma," *Blood Cancer J.*, vol. 4, no. 7, p. 229, Jul. 2014.

[168] **J. Wang *et al.***, "Protective effect of N-acetylcysteine against oxidative stress induced by zearalenone via mitochondrial apoptosis pathway in SIEC02 cells," *Toxins (Basel).*, vol. 10, no. 10, p. 407, Oct. 2018.

[169] **A. S. Tan and M. V. Berridge**, "Evidence for NAD(P)H:quinone oxidoreductase 1 (NQO1)-mediated quinone-dependent redox cycling via plasma membrane electron transport: A sensitive cellular assay for NQO1," *Free Radic. Biol. Med.*, vol. 48, no. 3, pp. 421–429, Feb. 2010.

[170] **V. N. Bochkov, O. V. Oskolkova, K. G. Birukov, A. L. Levonen, C. J. Binder, and J. Stöckl**, "Generation and biological activities of oxidized phospholipids," *Antioxidants Redox Signal.*, vol. 12, no. 8, pp. 1009–1059, Apr. 2010.

[171] **Y. A. Kim, M. Y. Kim, and Y. S. Jung**, "Glutathione depletion by l-buthionine-s,r-sulfoximine induces apoptosis of cardiomyocytes through activation of pkc-δ," *Biomol. Ther.*, vol. 21, no. 5, pp. 358–363, 2013.

[172] **S. G. Kimani, J. B. Phillips, J. I. Bruce, A. J. MacRobert, and J. P. Golding**, "Antioxidant inhibitors potentiate the cytotoxicity of photodynamic therapy," *Photochem. Photobiol.*, vol. 88, no. 1, pp. 175–187, Jan. 2012.

[173] **R. H. Weiss and R. W. Estabrook**, "The mechanism of cumene hydroperoxide-dependent lipid peroxidation: The function of cytochrome P-450," *Arch. Biochem. Biophys.*, vol. 251, no. 1, pp. 348–360, Nov. 1986.

[174] **S. J. Han *et al.***, "Redox regulation of the tumor suppressor PTEN by the thioredoxin system and cumene hydroperoxide," *Free Radic. Biol. Med.*, vol. 112, pp. 277–286, Nov. 2017.

[175] **S. Behnisch-Cornwell, G. Laubenstein, and P. J. Bednarski**, "Studies of the inhibitory activities of tiopronin and mercaptosuccinic acid on glutathione peroxidase and their cytotoxic and antioxidant

properties," *Pharmazie*, vol. 74, no. 9, pp. 536–542, 2019.

[176] **J. Chaudiere, E. C. Wilhelmsen, and A. L. Tappel**, "Mechanism of selenium-glutathione peroxidase and its inhibition by mercaptocarboxylic acids and other mercaptans," *J. Biol. Chem.*, vol. 259, no. 2, pp. 1043–1050, 1984.

[177] **W. S. Yang *et al.***, "Regulation of ferroptotic cancer cell death by GPX4," *Cell*, vol. 156, no. 1–2, pp. 317–331, 2014.

[178] **S. J. Hopkins, M. I. V. Jayson, and P. Van der Zeil**, "Inhibition of lymphocyte activation by gold sodium thiomalate," *Br. J. Pharmacol.*, vol. 79, no. 2, pp. 617–622, 1983.

[179] **D. Amantea *et al.***, "Oxidative Stress in Stroke Pathophysiology. Validation of Hydrogen Peroxide Metabolism as a Pharmacological Target to Afford Neuroprotection," *Int. Rev. Neurobiol.*, vol. 85, no. 9, pp. 363–374, Jan. 2009.

[180] **C. Ene *et al.***, "Safety and efficacy of carmustine (BCNU) wafers for metastatic brain tumors," *Surg. Neurol. Int.*, vol. 7, no. Suppl 11, pp. 295–299, Oct. 2016.

[181] **R. McKenna, T. Ahmad, C. H. Ts'ao, and H. Frischer**, "Glutathione reductase deficiency and platelet dysfunction induced by 1,3-bis(2-chloroethyl)-1-nitrosourea," *J. Lab. Clin. Med.*, vol. 102, no. 1, pp. 102–115, 1983.

[182] **H. Frischer and T. Ahmad**, "Severe generalized glutathione reductase deficiency after antitumor chemotherapy with BCNU [1,3-bis(chloroethyl)-1-nitrosourea]," *J. Lab. Clin. Med.*, vol. 89, no. 5, pp. 1080–1091, 1977.

[183] **H. Frischer**, "Erythrocytic glutathione reductase deficiency in a hospital population in the united states," *Am. J. Hematol.*, vol. 2, no. 4, pp. 327–334, 1977.

[184] **K. Li, C. Zhong, B. Wang, J. He, and J. Bi**, "Nrf2 expression participates in growth and differentiation of endometrial carcinoma cells in vitro and in vivo," *J. Mol. Histol.*, vol. 45, no. 2, pp. 161–167, 2014.

[185] **T. Shibata *et al.***, "Genetic Alteration of Keap1 Confers Constitutive Nrf2 Activation and Resistance to Chemotherapy in Gallbladder Cancer," *Gastroenterology*, vol. 135, no. 4, pp. 363–374, 2008.

[186] **A. Singh *et al.***, "RNAi-mediated silencing of nuclear factor erythroid-2-related factor 2 gene expression in non-small cell lung cancer inhibits tumor growth and increases efficacy of chemotherapy," *Cancer Res.*, vol. 68, no. 19, pp. 7975–7984, Oct. 2008.

[187] **P. Zhang *et al.***, "Loss of kelch-like ECH-associated protein 1 function in prostate cancer cells causes chemoresistance and radioresistance and promotes tumor growth," *Mol. Cancer Ther.*, vol. 9, no. 2, pp. 336–346, Feb. 2010.

[188] **Z. X. Cong *et al.***, "Temozolomide and irradiation combined treatment-induced Nrf2 activation increases chemoradiation sensitivity in human glioblastoma cells," *J. Neurooncol.*, vol. 116, no. 1, pp. 41–48, Jan. 2014.

[189] **S. Sukumari-Ramesh, N. Prasad, C. H. Alleyne, J. R. Vender, and K. M. Dhandapani**, "Overexpression of Nrf2 attenuates Carmustine-induced cytotoxicity in U87MG human glioma cells," *BMC Cancer*, vol. 15, no. 1, Dec. 2015.

[190] **K. Uchida and S. Kawakishi**, "Identification of oxidized histidine generated at the active site of Cu,Zn-superoxide dismutase exposed to H2O2. Selective generation of 2-oxo- histidine at the histidine 118," *J. Biol. Chem.*, vol. 269, no. 4, pp. 2405–2410, 1994.

[191] **T. Fukai and M. Ushio-Fukai**, "Superoxide dismutases: Role in redox signaling, vascular function, and diseases," *Antioxidants Redox Signal.*, vol. 15, no. 6, pp. 1583–1606, Sep. 2011.

[192] **A. R. Cyr, M. J. Hitchler, and F. E. Domann**, "Regulation of SOD 2 in cancer by histone modifications and CpG Methylation: Closing the loop between redox biology and epigenetics," *Antioxidants Redox Signal.*, vol. 18, no. 15, pp. 1946–1955, May 2013.

[193] **M. Moradi, A. Divsalar, A. A. Saboury, B. Ghalandari, and A. R. Harifi**, "Inhibitory effects of

deferasirox on the structure and function of bovine liver catalase: A spectroscopic and theoretical study," *J. Biomol. Struct. Dyn.*, vol. 33, no. 10, pp. 2255–2266, Oct. 2015.

[194] **M. M. Goyal and A. Basak**, "Human catalase: Looking for complete identity," *Protein Cell*, vol. 1, no. 10, pp. 888–897, 2010.

[195] **N. Couto, J. Wood, and J. Barber**, "The role of glutathione reductase and related enzymes on cellular redox homoeostasis network," *Free Radic. Biol. Med.*, vol. 95, pp. 27–42, Jun. 2016.

[196] **L. Moine, M. Rivoira, G. D. de Barboza, A. Pérez, and N. T. de Talamoni**, "Glutathione depleting drugs, antioxidants and intestinal calcium absorption," *World J. Gastroenterol.*, vol. 24, no. 44, pp. 4979–4988, Nov. 2018.

[197] **C. C. Winterbourn**, "Revisiting the reactions of superoxide with glutathione and other thiols," *Arch. Biochem. Biophys.*, vol. 595, pp. 68–71, Apr. 2016.

[198] **R. Brigelius-Flohé and L. Flohé**, "Basic principles and emerging concepts in the redox control of transcription factors," *Antioxidants Redox Signal.*, vol. 15, no. 8, pp. 2335–2381, Oct. 2011.

[199] **T. Ramming, H. G. Hansen, K. Nagata, L. Ellgaard, and C. Appenzeller-Herzog**, "GPx8 peroxidase prevents leakage of H2O2 from the endoplasmic reticulum," *Free Radic. Biol. Med.*, vol. 70, pp. 106–116, May 2014.

[200] **R. Prabhakar, T. Vreven, K. Morokuma, and D. G. Musaev**, "Elucidation of the mechanism of selenoprotein glutathione peroxidase (GPx)-catalyzed hydrogen peroxide reduction by two glutathione molecules: A density functional study," *Biochemistry*, vol. 44, no. 35, pp. 11864–11871, Sep. 2005.

[201] **E. Lubos, J. Loscalzo, and D. E. Handy**, "Glutathione peroxidase-1 in health and disease: From molecular mechanisms to therapeutic opportunities," *Antioxidants Redox Signal.*, vol. 15, no. 7, pp. 1957–1997, Oct. 2011.

[202] **J. F. Collet and J. Messens**, "Structure, function, and mechanism of thioredoxin proteins," *Antioxidants Redox Signal.*, vol. 13, no. 8, pp. 1205–1216, Oct. 2010.

[203] **G. Spyrou, E. Enmark, A. Miranda-Vizuete, and J. Å. Gustafsson**, "Cloning and expression of a novel mammalian thioredoxin," *J. Biol. Chem.*, vol. 272, no. 5, pp. 2936–2941, Jan. 1997.

[204] **D. Mustacich and G. Powis**, "Thioredoxin reductase," *Biochem. J.*, vol. 346, no. 1, pp. 1–8, 2000.

[205] **K. I. Tong, A. Kobayashi, F. Katsuoka, and M. Yamamoto**, "Two-site substrate recognition model for the Keap1-Nrf2 system: A hinge and latch mechanism," *Biol. Chem.*, vol. 387, no. 10–11, pp. 1311–1320, Oct. 2006.

[206] **W. Li, S. W. Yu, and A. N. T. Kong**, "Nrf2 possesses a redox-sensitive nuclear exporting signal in the Neh5 transactivation domain," *J. Biol. Chem.*, vol. 281, no. 37, pp. 27251–27263, Sep. 2006.

[207] **C. A. Umscheid, D. J. Margolis, and C. E. Grossman**, "Key concepts of clinical trials: A narrative review," *Postgrad. Med.*, vol. 123, no. 5, pp. 194–204, Sep. 2011.

[208] **M. J. Waring *et al.***, "An analysis of the attrition of drug candidates from four major pharmaceutical companies," *Nat. Rev. Drug Discov.*, vol. 14, no. 7, pp. 475–486, Jul. 2015.

[209] **D. Brown and G. Superti-Furga**, "Rediscovering the sweet spot in drug discovery," *Drug Discov. Today*, vol. 8, no. 23, pp. 1067–1077, Dec. 2003.

[210] **M. P. Gleeson, A. Hersey, D. Montanari, and J. Overington**, "Probing the links between in vitro potency, ADMET and physicochemical parameters," *Nat. Rev. Drug Discov.*, vol. 10, no. 3, pp. 197–208, Mar. 2011.

[211] **L. Rochette *et al.***, "Nitric oxide synthase inhibition and oxidative stress in cardiovascular diseases: Possible therapeutic targets?," *Pharmacol. Ther.*, vol. 140, no. 3, pp. 239–257, 2013.

[212] **E. Chan, G.-S. Liu, and G. Dusting**, "Redox mechanisms in pathological angiogenesis in the retina: roles for NADPH oxidase," *Curr. Pharm. Des.*, vol. 21, no. 41, pp. 5988–5998, Oct. 2015.

[213] **T. M. Paravicini and R. M. Touyz**, "Redox signaling in hypertension," *Cardiovasc. Res.*, vol. 71, no. 2,

pp. 247–258, Jul. 2006.

[214] **J. D. Lambeth, K. H. Krause, and R. A. Clark**, “NOX enzymes as novel targets for drug development,” *Semin. Immunopathol.*, vol. 30, no. 3, pp. 339–363, Jul. 2008.

[215] **L. Prosperini and S. Pontecorvo**, “Dimethyl fumarate in the management of multiple sclerosis: Appropriate patient selection and special considerations,” *Ther. Clin. Risk Manag.*, vol. 12, no. 2, pp. 339–350, Mar. 2016.

[216] **J. T. Phillips, S. Agrella, and R. J. Fox**, “Dimethyl fumarate: A review of efficacy and practical management strategies for common adverse events in patients with multiple sclerosis,” *Int. J. MS Care*, vol. 19, no. 2, pp. 74–83, 2017.

[217] **J. Brück, R. Dringen, A. Amasuno, I. Pau-Charles, and K. Ghoreschi**, “A review of the mechanisms of action of dimethylfumarate in the treatment of psoriasis,” *Exp. Dermatol.*, vol. 27, no. 6, pp. 611–624, Jun. 2018.

[218] **Y. Nakagami *et al.***, “Novel Nrf2 activators from microbial transformation products inhibit blood-retinal barrier permeability in rabbits,” *Br. J. Pharmacol.*, vol. 172, no. 5, pp. 1237–1249, 2015.

[219] **L. Hu *et al.***, “Discovery of a small-molecule inhibitor and cellular probe of Keap1-Nrf2 protein-protein interaction,” *Bioorganic Med. Chem. Lett.*, vol. 23, no. 10, pp. 3039–3043, May 2013.

[220] **C. Higashi *et al.***, “The novel Nrf2 inducer TFM-735 ameliorates experimental autoimmune encephalomyelitis in mice,” *Eur. J. Pharmacol.*, vol. 802, pp. 76–84, 2017.

[221] **T. G. Davies *et al.***, “Monoacidic inhibitors of the kelch-like ECH-associated protein 1: Nuclear Factor Erythroid 2-Related Factor 2 (KEAP1:NRF2) protein-protein interaction with high cell Potency Identified by Fragment-Based Discovery,” *J. Med. Chem.*, vol. 59, no. 8, pp. 3991–4006, Apr. 2016.

[222] **O. C. Attucks *et al.***, “Induction of heme oxygenase I (HMOX1) by HPP-4382: A novel modulator of bach1 activity,” *PLoS One*, vol. 9, no. 7, p. e101044, Jul. 2014.

[223] **X. J. Wang, J. D. Hayes, L. G. Higgins, C. R. Wolf, and A. T. Dinkova-Kostova**, “Activation of the NRF2 Signaling Pathway by Copper-Mediated Redox Cycling of Para- and Ortho-Hydroquinones,” *Chem. Biol.*, vol. 17, no. 1, pp. 75–85, 2010.

[224] **A. Aroun, J. L. Zhong, R. M. Tyrrell, and C. Pourzand**, “Iron, oxidative stress and the example of solar ultraviolet A radiation,” *Photochem. Photobiol. Sci.*, vol. 11, no. 1, pp. 118–134, 2012.

[225] **C. L. MacLeod, A. Luk, J. Castagnola, M. Cronin, and J. Mendelsohn**, “EGF induces cell cycle arrest of A431 human epidermoid carcinoma cells,” *J. Cell. Physiol.*, vol. 127, no. 1, pp. 175–182, Apr. 1986.

[226] **D. E. Brash *et al.***, “A role for sunlight in skin cancer: UV-induced p53 mutations in squamous cell carcinoma,” *Proc. Natl. Acad. Sci. U. S. A.*, vol. 88, no. 22, pp. 10124–10128, 1991.

[227] **H. N. Ananthaswamy *et al.***, “Inhibition of solar simulator-induced p53 mutations and protection against skin cancer development in mice by sunscreens,” *J. Invest. Dermatol.*, vol. 112, no. 5, pp. 763–768, 1999.

[228] **W. Strober**, “Trypan blue exclusion test of cell viability.,” *Curr. Protoc. Immunol.*, vol. Appendix 3, p. Appendix 3B, May 2001.

[229] **M. Ivan *et al.***, “HIFα targeted for VHL-mediated destruction by proline hydroxylation: Implications for O2 sensing,” *Science (80-.).*, vol. 292, no. 5516, pp. 464–468, Apr. 2001.

[230] **B. H. Jiang, G. L. Semenza, C. Bauer, and H. H. Marti**, “Hypoxia-inducible factor 1 levels vary exponentially over a physiologically relevant range of O2 tension,” *Am. J. Physiol. - Cell Physiol.*, vol. 271, no. 4, pp. 40–4, 1996.

[231] **A. V. Razygraev *et al.***, “Activity of catalase in surgically induced endometrial-like lesions in rats,” *J. Obstet. women’s Dis.*, vol. 68, no. 6, pp. 57–63, Dec. 2019.

[232] **S. T. Smiley *et al.***, “Intracellular heterogeneity in mitochondrial membrane potentials revealed by a J-aggregate-forming lipophilic cation JC-1,” *Proc. Natl. Acad. Sci. U. S. A.*, vol. 88, no. 9, pp. 3671–3675,

1991.

[233] **Y. Miyazono, S. Hirashima, N. Ishihara, J. Kusukawa, K. I. Nakamura, and K. Ohta**, “Uncoupled mitochondria quickly shorten along their long axis to form indented spheroids, instead of rings, in a fission-independent manner,” *Sci. Rep.*, vol. 8, no. 1, pp. 1–14, Jan. 2018.

[234] **P. A. Johnston *et al.***, “Development of a 384-well colorimetric assay to quantify hydrogen peroxide generated by the redox cycling of compounds in the presence of reducing agents,” *Assay Drug Dev. Technol.*, vol. 6, no. 4, pp. 505–518, Aug. 2008.

[235] **B. Zhitomirsky, H. Farber, and Y. G. Assaraf**, “LysoTracker and MitoTracker Red are transport substrates of P-glycoprotein: implications for anticancer drug design evading multidrug resistance,” *J. Cell. Mol. Med.*, vol. 22, no. 4, pp. 2131–2141, Apr. 2018.

[236] **I. Rahman, A. Kode, and S. K. Biswas**, “Assay for quantitative determination of glutathione and glutathione disulfide levels using enzymatic recycling method,” *Nat. Protoc.*, vol. 1, no. 6, pp. 3159–3165, Jan. 2007.

[237] **E. Schreiber, P. Matthias, M. M. Müller, and W. Schaffner**, “Rapid detection of octamer binding proteins with ‘mini extracts’, prepared from a small number of cells,” *Nucleic Acids Res.*, vol. 17, no. 15, p. 6419, Aug. 1989.

[238] **K. Kakuta, K. Orino, S. Yamamoto, and K. Watanabe**, “High Levels of Ferritin and its Iron in Fetal Bovine Serum,” *Comp. Biochem. Physiol. Part A Physiol.*, vol. 118, no. 1, pp. 165–169, Sep. 1997.

[239] **S. L. Hempel, G. R. Buettner, D. A. Wessels, G. M. Galvan, and Y. Q. O’Malley**, “Extracellular iron(II) can protect cells from hydrogen peroxide,” *Arch. Biochem. Biophys.*, vol. 330, no. 2, pp. 401–408, Jun. 1996.

[240] **U. Sivagnanam, S. K. Palanirajan, and S. N. Gummadi**, “The role of human phospholipid scramblases in apoptosis: An overview,” *Biochim. Biophys. Acta - Mol. Cell Res.*, vol. 1864, no. 12, pp. 2261–2271, Dec. 2017.

[241] **K. Ono and D. C. Shrieve**, “Effect of glutathione depletion by L-buthionine sulfoximine on the cytotoxicity of cyclophosphamide in single and fractionated doses to EMT6/SF mouse tumors and bone marrow,” *J. Natl. Cancer Inst.*, vol. 79, no. 4, pp. 811–815, 1987.

[242] **A. Kholmukhamedov, J. M. Schwartz, and J. J. Lemasters**, “Mitotracker probes and mitochondrial membrane potential,” *Shock*, vol. 39, no. 6, p. 543, 2013.

[243] **K. C. Das**, “Thioredoxin-deficient mice, a novel phenotype sensitive to ambient air and hypersensitive to hyperoxia-induced lung injury,” *Am. J. Physiol. - Lung Cell. Mol. Physiol.*, vol. 308, no. 5, pp. 429–442, Mar. 2015.

[244] **A. E. Finkelstein, D. T. Walz, V. Batista, M. Mizraji, F. Roisman, and A. Misher**, “Auranofin. New oral gold compound for treatment of rheumatoid arthritis,” *Ann. Rheum. Dis.*, vol. 35, no. 3, pp. 251–257, Jun. 1976.

[245] **R. Behrens, M. Devereaux, B. Hazleman, K. Szaz, J. Calvin, and G. Neale**, “Investigation of Auranofin-induced diarrhoea,” *Gut*, vol. 27, no. 1, pp. 59–65, 1986.

[246] **J. M. Madeira, C. J. Renschler, B. Mueller, S. Hashioka, D. L. Gibson, and A. Klegeris**, “Novel protective properties of auranofin: Inhibition of human astrocyte cytotoxic secretions and direct neuroprotection,” *Life Sci.*, vol. 92, no. 22, pp. 1072–1080, Jun. 2013.

[247] **L. Feng *et al.***, “Repurposing Auranofin and Evaluation of a New Gold(I) Compound for the Search of Treatment of Human and Cattle Parasitic Diseases: From Protozoa to Helminth Infections,” *Molecules*, vol. 25, no. 21, pp. 50–75, Nov. 2020.

[248] **A. Caroli, S. Simeoni, R. Lepore, A. Tramontano, and A. Via**, “Investigation of a potential mechanism for the inhibition of SmTGR by Auranofin and its implications for Plasmodium falciparum inhibition,” *Biochem. Biophys. Res. Commun.*, vol. 417, no. 1, pp. 576–581, Jan. 2012.

[249] **A. R. Sannella *et al.***, “New uses for old drugs. Auranofin, a clinically established antiarthritic metallodrug, exhibits potent antimalarial effects in vitro: Mechanistic and pharmacological implications,” *FEBS Lett.*, vol. 582, no. 6, pp. 844–847, Mar. 2008.

[250] **B. Zhang, Y. Liu, X. Li, J. Xu, and J. Fang**, “Small Molecules to Target the Selenoprotein Thioredoxin Reductase,” *Chem. - An Asian J.*, vol. 13, no. 23, pp. 3593–3600, Dec. 2018.

[251] **S. Urig and K. Becker**, “On the potential of thioredoxin reductase inhibitors for cancer therapy,” *Semin. Cancer Biol.*, vol. 16, no. 6, pp. 452–465, Dec. 2006.

[252] **S. Li *et al.***, “Inhibition of both thioredoxin reductase and glutathione reductase may contribute to the anticancer mechanism of TH-302,” *Biol. Trace Elem. Res.*, vol. 136, no. 3, pp. 294–301, Sep. 2010.

[253] **I. Ozgencli, D. Kilic, U. Guller, M. Ciftci, O. I. Kufrevioglu, and H. Budak**, “A Comparison of the Inhibitory Effects of Anti-Cancer Drugs on Thioredoxin Reductase and Glutathione S-Transferase in Rat Liver,” *Anticancer. Agents Med. Chem.*, vol. 18, no. 14, pp. 2053–2061, Sep. 2018.

[254] **X. Zhu, C. Huang, and B. Peng**, “Overexpression of thioredoxin system proteins predicts poor prognosis in patients with squamous cell carcinoma of the tongue,” *Oral Oncol.*, vol. 47, no. 7, pp. 609–614, Jul. 2011.

[255] **J. Jurado, M. J. Prieto-Álamo, J. Madrid-Rísquez, and C. Pueyo**, “Absolute Gene Expression Patterns of Thioredoxin and Glutaredoxin Redox Systems in Mouse,” *J. Biol. Chem.*, vol. 278, no. 46, pp. 45546–45554, Nov. 2003.

[256] **B. H. Jiang, G. L. Semenza, C. Bauer, and H. H. Marti**, “Hypoxia-inducible factor 1 levels vary exponentially over a physiologically relevant range of O2 tension,” *Am. J. Physiol. - Cell Physiol.*, vol. 271, no. 4, pp. 4–40, Oct. 1996.

[257] **Y. Nisimoto, B. A. Diebold, D. Constentino-Gomes, and J. D. Lambeth**, “Nox4: A hydrogen peroxide-generating oxygen sensor,” *Biochemistry*, vol. 53, no. 31, pp. 5111–5120, Aug. 2014.

[258] **E. C. Vaquero, M. Edderkaoui, S. J. Pandol, I. Gukovsky, and A. S. Gukovskaya**, “Reactive oxygen species produced by NAD(P)H oxidase inhibit apoptosis in pancreatic cancer cells,” *J. Biol. Chem.*, vol. 279, no. 33, pp. 34643–34654, Aug. 2004.

[259] **G. Chang, L. Chen, H. M. Lin, Y. Lin, and J. K. Maranchie**, “Nox4 inhibition enhances the cytotoxicity of cisplatin in human renal cancer cells,” *J. Exp. Ther. Oncol.*, vol. 10, no. 1, pp. 9–18, 2012.

[260] **K. Shimada, T. Fujii, S. Anai, K. Fujimoto, and N. Konishi**, “ROS generation via NOX4 and its utility in the cytological diagnosis of urothelial carcinoma of the urinary bladder,” *BMC Urol.*, vol. 11, no. 1, pp. 1–12, Oct. 2011.

[261] **K. Shanmugasundaram, B. K. Nayak, W. E. Friedrichs, D. Kaushik, R. Rodriguez, and K. Block**, “NOX4 functions as a mitochondrial energetic sensor coupling cancer metabolic reprogramming to drug resistance,” *Nat. Commun.*, vol. 8, no. 1, pp. 1–16, Oct. 2017.

[262] **J. R. Hickok, D. Vasudevan, K. Jablonski, and D. D. Thomasn**, “Oxygen dependence of nitric oxide-mediated signaling,” *Redox Biol.*, vol. 1, no. 1, pp. 203–209, 2013.

[263] **R. J. G. Cardnell and R. B. Mikkelsen**, “Nitric oxide synthase inhibition enhances the antitumor effect of radiation in the treatment of squamous carcinoma xenografts,” *PLoS One*, vol. 6, no. 5, pp. 140–157, 2011.

[264] **A. W. Girotti**, “Modulation of the anti-tumor efficacy of photodynamic therapy by nitric oxide,” *Cancers (Basel).*, vol. 8, no. 10, p. 96, Oct. 2016.

[265] **E. R. Gomes, R. D. Almeida, A. P. Carvalho, and C. B. Duarte**, “Nitric oxide modulates tumor cell death induced by photodynamic therapy through a cGMP-dependent mechanism¶,” *Photochem. Photobiol.*, vol. 76, no. 4, pp. 423–430, Oct. 2007.

[266] **R. Bhowmick and A. W. Girotti**, “Cytoprotective induction of nitric oxide synthase in a cellular model of 5-aminolevulinic acid-based photodynamic therapy,” *Free Radic. Biol. Med.*, vol. 48, no. 10, pp. 1296–

1301, May 2010.

[267] **M. Niziolek, W. Korytowski, and A. W. Girotti**, “Nitric oxide-induced resistance to lethal photooxidative damage in a breast tumor cell line,” *Free Radic. Biol. Med.*, vol. 40, no. 8, pp. 1323–1331, Apr. 2006.

[268] **M. Niziolek-Kierecka, W. Korytowski, and A. W. Girotti**, “Tumor cell hyperresistance to photodynamic killing arising from nitric oxide preconditioning,” *Opt. Methods Tumor Treat. Detect. Mech. Tech. Photodyn. Ther. XVI*, vol. 6427, p. 642705, Feb. 2007.

[269] **D. Ross and D. Siegel**, “Functions of NQO1 in cellular protection and CoQ10 metabolism and its potential role as a redox sensitive molecular switch,” *Front. Physiol.*, vol. 8, no. 2, pp. 595–607, Aug. 2017.

[270] **N. Watanabe, D. A. Dickinson, R. M. Liu, and H. J. Forman**, “Quinones and Glutathione Metabolism,” *Methods Enzymol.*, vol. 378, pp. 319–340, 2004.

[271] **Y. Song and G. R. Buettner**, “Thermodynamic and kinetic considerations for the reaction of semiquinone radicals to form superoxide and hydrogen peroxide,” *Free Radic. Biol. Med.*, vol. 49, no. 6, p. 919, Sep. 2010.

[272] **J. P. Kehrer, J. D. Robertson, and C. V. Smith**, “Free Radicals and Reactive Oxygen Species,” *Compr. Toxicol. Second Ed.*, vol. 1–14, pp. 277–307, Jan. 2010.

[273] **V. Roginsky and T. Barsukova**, “Kinetics of oxidation of hydroquinones by molecular oxygen. Effect of superoxide dismutase,” *J. Chem. Soc. Perkin Trans. 2*, vol. 2, no. 7, pp. 1575–1582, 2000.

[274] **B. Singh, A. M. Ronghe, A. Chatterjee, N. K. Bhat, and H. K. Bhat**, “MicroRNA-93 regulates NRF2 expression and is associated with breast carcinogenesis,” *Carcinogenesis*, vol. 34, no. 5, pp. 1165–1172, May 2013.

[275] **W. Li *et al.***, “MicroRNA-93 Regulates Hypoxia-Induced Autophagy by Targeting ULK1,” *Oxid. Med. Cell. Longev.*, vol. 2017, 2017.

[276] **Y. Chen, J. Cai, T. J. Murphy, and D. P. Jones**, “Overexpressed human mitochondrial thioredoxin confers resistance to oxidant-induced apoptosis in human osteosarcoma cells,” *J. Biol. Chem.*, vol. 277, no. 36, pp. 33242–33248, Sep. 2002.

[277] **T. Tanaka *et al.***, “Thioredoxin-2 (TRX-2) is an essential gene regulating mitochondria-dependent apoptosis,” *EMBO J.*, vol. 21, no. 7, pp. 1695–1703, Apr. 2002.

[278] **Y. Wang *et al.***, “SLC25A39 is necessary for mitochondrial glutathione import in mammalian cells,” *Nature*, vol. 599, no. 7883, pp. 136–140, Oct. 2021.

[279] **B. R. You, H. R. Shin, B. R. Han, S. H. Kim, and W. H. Park**, “Auranofin induces apoptosis and necrosis in HeLa cells via oxidative stress and glutathione depletion,” *Mol. Med. Rep.*, vol. 11, no. 2, pp. 1428–1434, Feb. 2015.

[280] **N. Saba *et al.***, “The Gold Compound Auranofin Induces Oxidative Stress and Apoptosis in Primary CLL Cells Independent of Classic Prognostic Markers and the Protective Effect of the Tissue Microenvironment,” *Blood*, vol. 120, no. 21, pp. 865–865, Nov. 2012.

[281] **H. Wang *et al.***, “Auranofin radiosensitizes tumor cells through targeting thioredoxin reductase and resulting overproduction of reactive oxygen species,” *Oncotarget*, vol. 8, no. 22, pp. 35728–35742, 2017.

[282] **R. W. Miller**, “Reactions of superoxide anion, catechols, and cytochrome c.,” *Can. J. Biochem.*, vol. 48, no. 8, pp. 935–939, 1970.

[283] **D. Siegel *et al.***, “NAD(P)H:quinone oxidoreductase 1: Role as a superoxide scavenger,” *Mol. Pharmacol.*, vol. 65, no. 5, pp. 1238–1247, May 2004.

[284] **H. Sies *et al.***, “Defining roles of specific reactive oxygen species (ROS) in cell biology and physiology,” *Nat. Rev. Mol. Cell Biol.*, pp. 1–17, Feb. 2022.

[285] **E. Marchesi, C. Rota, Y. C. Fann, C. F. Chignell, and R. P. Mason**, “Photoreduction of the fluorescent

dye 2'-7'-dichlorofluorescein: a spin trapping and direct electron spin resonance study with implications for oxidative stress measurements," *Free Radic. Biol. Med.*, vol. 26, no. 1–2, pp. 148–161, Jan. 1999.

[286] **L. Jagannathan, S. Cuddapah, and M. Costa**, "Oxidative Stress Under Ambient and Physiological Oxygen Tension in Tissue Culture," *Curr. Pharmacol. Reports*, vol. 2, no. 2, pp. 64–72, Apr. 2016.

[287] **J. A. Krieger, J. C. Landsiedel, and D. A. Lawrence**, "Differential in vitro effects of physiological and atmospheric oxygen tension on normal human peripheral blood mononuclear cell proliferation, cytokine and immunoglobulin production," *Int. J. Immunopharmacol.*, vol. 18, no. 10, pp. 545–552, Oct. 1996.

[288] **S. Parrinello, E. Samper, A. Krtolica, J. Goldstein, S. Melov, and J. Campisi**, "Oxygen sensitivity severely limits the replicative lifespan of murine fibroblasts," *Nat. Cell Biol.*, vol. 5, no. 8, pp. 741–747, Jul. 2003.

[289] **S. Bashir, G. Harris, M. A. Denman, D. R. Blake, and P. G. Winyard**, "Oxidative DNA damage and cellular sensitivity to oxidative stress in human autoimmune diseases," *Ann. Rheum. Dis.*, vol. 52, no. 9, pp. 659–666, Sep. 1993.

[290] **A. Juhasz *et al.***, "Expression of NADPH oxidase homologues and accessory genes in human cancer cell lines, tumours and adjacent normal tissues," *Free Radic. Res.*, vol. 43, no. 6, pp. 523–532, 2009.

[291] **I. Diebold, A. Petry, J. Hess, and A. Görlach**, "The NADPH oxidase subunit NOX4 is a new target gene of the hypoxia-inducible factor-1," *Mol. Biol. Cell*, vol. 21, no. 12, pp. 2087–2096, Jun. 2010.

[292] **M. B. Cohen and D. L. Duvel**, "Characterization of the inhibition of glutathione reductase and the recovery of enzyme activity in exponentially growing murine leukemia (11210) cells treated with 1,3-bis(2-chloroethyl)-1-nitrosourea," *Biochem. Pharmacol.*, vol. 37, no. 17, pp. 3317–3320, Sep. 1988.

[293] **M. J. Kerins and A. Ooi**, "The Roles of NRF2 in Modulating Cellular Iron Homeostasis," *Antioxidants Redox Signal.*, vol. 29, no. 17, pp. 1756–1773, Dec. 2018.

[294] **E. G. Meyron-Holtz, M. C. Ghosh, and T. A. Rouault**, "Mammalian tissue oxygen levels modulate iron-regulatory protein activities in vivo," *Science (80-.).*, vol. 306, no. 5704, pp. 2087–2090, Dec. 2004.

[295] **J. P. Thomas and A. Girotti**, "Role of Lipid Peroxidation in Hematoporphyrin Derivative-sensitized Photokilling of Tumor Cells: Protective Effects of Glutathione Peroxidase," *Cancer Res.*, vol. 49, no. 7, pp. 1682–1686, 1989.

[296] **V. Granatiero, C. Konrad, K. Bredvik, G. Manfredi, and H. Kawamata**, "Nrf2 signaling links ER oxidative protein folding and calcium homeostasis in health and disease," *Life Sci. Alliance*, vol. 2, no. 5, p. e201900563, Oct. 2019.

[297] **M. D. Hall *et al.***, "Inhibition of glutathione peroxidase mediates the collateral sensitivity of multidrug-resistant cells to tiopronin," *J. Biol. Chem.*, vol. 289, no. 31, pp. 21473–21489, Aug. 2014.

[298] **D. Siegel, E. M. Bolton, J. A. Burr, D. C. Liebler, and D. Ross**, "The reduction of α-tocopherolquinone by human NAD(P)H: Quinone oxidoreductase: The role of α-tocopherolhydroquinone as a cellular antioxidant," *Mol. Pharmacol.*, vol. 52, no. 2, pp. 300–305, Aug. 1997.

[299] **Y. Yu *et al.***, "Ferroptosis: a cell death connecting oxidative stress, inflammation and cardiovascular diseases," *Cell Death Discov.*, vol. 7, no. 1, pp. 1–10, Jul. 2021.

[300] **M. Berggren, A. Gallegos, J. R. Gasdaska, P. Y. Gasdaska, J. Warneke, and G. Powis**, "Thioredoxin and thioredoxin reductase gene expression in human tumors and cell lines, and the effects of serum stimulation and hypoxia," *Anticancer Res.*, vol. 16, no. 6 B, pp. 3459–3466, 1996.

[301] **A. V. Peskin and C. C. Winterbourn**, "Assay of superoxide dismutase activity in a plate assay using WST-1," *Free Radic. Biol. Med.*, vol. 103, pp. 188–191, Feb. 2017.

[302] **B. Mannervik**, "Chapter 7, unit 7.2: Measurement of glutathione reductase activity," in *Current Protocols in Toxicology*, vol. 0, no. 1, M. D. Maines, Ed. John Wiley & Sons, Inc., 1999.

[303] **L. Moatamedi Pour, A. Farahnak, M. Molaei Rad, T. Golmohamadi, and M. Eshraghian**, "Activity assay of glutathione S-Transferase (GSTs) enzyme as a diagnostic biomarker for liver Hydatid cyst in vitro,"

Iran. J. Public Health, vol. 43, no. 7, pp. 994–999, 2014.

[304] **W. H. Koppenol, R. Kissner, and J. S. Beckman**, “Syntheses of peroxynitrite: To go with the flow or on solid grounds?,” *Methods Enzymol.*, vol. 269, pp. 296–302, 1996.

[305] **R. Smulik *et al.***, “Nitroxyl (HNO) reacts with molecular oxygen and forms peroxynitrite at physiological ph: Biological implications,” *J. Biol. Chem.*, vol. 289, no. 51, pp. 35570–35581, Dec. 2014.

[306] **J. P. Crow and H. Ischiropoulos**, “Detection and quantitation of nitrotyrosine residues in proteins: In vivo marker of peroxynitrite,” *Methods Enzymol.*, vol. 269, pp. 185–194, 1996.

[307] **J. Fan, H. Cai, S. Yang, L. Yan, and W. S. Tan**, “Comparison between the effects of normoxia and hypoxia on antioxidant enzymes and glutathione redox state in ex vivo culture of CD34+ cells,” *Comp. Biochem. Physiol. - B Biochem. Mol. Biol.*, vol. 151, no. 2, pp. 153–158, 2008.

[308] **H. Awad, N. Nolette, M. Hinton, and S. Dakshinamurti**, “AMPK and FoxO1 regulate catalase expression in hypoxic pulmonary arterial smooth muscle,” *Pediatr. Pulmonol.*, vol. 49, no. 9, pp. 885–897, 2014.

[309] **H. Onozuka, K. Tsuchihara, and H. Esumi**, “Hypoglycemic/hypoxic condition in vitro mimicking the tumor microenvironment markedly reduced the efficacy of anticancer drugs,” *Cancer Sci.*, vol. 102, no. 5, pp. 975–982, May 2011.

[310] **I. S. Wood, T. Stezhka, and P. Trayhurn**, “Modulation of adipokine production, glucose uptake and lactate release in human adipocytes by small changes in oxygen tension,” *Pflugers Arch. Eur. J. Physiol.*, vol. 462, no. 3, pp. 469–477, Sep. 2011.

[311] **Y. C. Awasthi, E. Beutler, and S. K. Srivastava$**, “Purification and Properties of Human Erythrocyte Glutathione Peroxidase*,” *J. Biol. Chem.*, vol. 250, no. 13, pp. 5144–5149, 1975.

[312] **E. Middelkoop, E. A. C. Wiemer, D. E. T. Schoenmaker, A. Strijland, and J. M. Tager**, “Topology of catalase assembly in human skin fibroblasts,” *BBA - Mol. Cell Res.*, vol. 1220, no. 1, pp. 15–20, Dec. 1993.

[313] **R. Chakravarti and D. J. Stuehr**, “Thioredoxin-1 regulates cellular heme insertion by controlling S-nitrosation of glyceraldehyde-3-phosphate dehydrogenase,” *J. Biol. Chem.*, vol. 287, no. 20, pp. 16179–16186, May 2012.

[314] **C. Tonelli, I. I. C. Chio, and D. A. Tuveson**, “Transcriptional Regulation by Nrf2,” *Antioxidants Redox Signal.*, vol. 29, no. 17, pp. 1727–1745, Dec. 2018.

[315] **E. H. Heiss, D. Schachner, K. Zimmermann, and V. M. Dirsch**, “Glucose availability is a decisive factor for Nrf2-mediated gene expression,” *Redox Biol.*, vol. 1, no. 1, pp. 359–365, Jan. 2013.

[316] **O. Apanasets *et al.***, “PEX5, the Shuttling Import Receptor for Peroxisomal Matrix Proteins, Is a Redox-Sensitive Protein,” *Traffic*, vol. 15, no. 1, pp. 94–103, Jan. 2014.

[317] **S. S. Percival and M. Layden-Patrice**, “HL-60 cells can be made copper deficient by incubating with tetraethylenepentamine,” *J. Nutr.*, vol. 122, no. 12, pp. 2424–2429, 1992.

[318] **A. Hahn and M. Keler-Bačoka**, “The Effect of Desferrioxamine B upon the Enzymatic Catalase and PPD-Oxydase Activity in Plasma and Serum,” *Acta Med. Scand.*, vol. 179, no. 445 S, pp. 276–283, 1966.

[319] **H. Kawabata, R. S. Germain, P. T. Vuong, T. Nakamaki, J. W. Said, and H. P. Koeffler**, “Transferrin receptor 2-α supports cell growth both in iron-chelated cultured cells and in vivo,” *J. Biol. Chem.*, vol. 275, no. 22, pp. 16618–16625, Jun. 2000.

[320] **J. Fan, H. Cai, S. Yang, L. Yan, and W. S. Tan**, “Comparison between the effects of normoxia and hypoxia on antioxidant enzymes and glutathione redox state in ex vivo culture of CD34+ cells,” *Comp. Biochem. Physiol. - B Biochem. Mol. Biol.*, vol. 151, no. 2, pp. 153–158, Oct. 2008.

[321] **K. R. Atkuri, L. A. Herzenberg, A. K. Niemi, T. Cowan, and L. A. Herzenberg**, “Importance of culturing primary lymphocytes at physiological oxygen levels,” *Proc. Natl. Acad. Sci. U. S. A.*, vol. 104, no. 11,

pp. 4547–4552, Mar. 2007.

[322] **L. Torrente *et al.***, “Inhibition of TXNRD or SOD 1 overcomes NRF2-mediated resistance to β-lapachone,” *Redox Biol.*, vol. 30, p. 101440, Feb. 2020.

[323] **H. K. Jyrkkänen *et al.***, “Novel insights into the regulation of antioxidant-response-element-mediated gene expression by electrophiles: Induction of the transcriptional repressor BACH1 by Nrf2,” *Biochem. J.*, vol. 440, no. 2, pp. 167–174, Dec. 2011.

[324] **X. Zhang *et al.***, “Bach1: Function, regulation, and involvement in disease,” *Oxid. Med. Cell. Longev.*, vol. 2018, 2018.

[325] **Y. R. Kim *et al.***, “Oncogenic NRF2 mutations in squamous cell carcinomas of oesophagus and skin,” *J. Pathol.*, vol. 220, no. 4, pp. 446–451, Mar. 2010.

[326] **P. Huppke *et al.***, “Activating de novo mutations in NFE2L2 encoding NRF2 cause a multisystem disorder,” *Nat. Commun.*, vol. 8, no. 1, pp. 1–10, Oct. 2017.

[327] **G. Y. Liou and P. Storz**, “Reactive oxygen species in cancer,” *Free Radic. Res.*, vol. 44, no. 5, pp. 479–496, 2010.

[328] **R. D. Traver *et al.***, “Characterization of a polymorphism in NAD(P)H: quinone oxidoreductase (DT-diaphorase),” *Br. J. Cancer 1997 751*, vol. 75, no. 1, pp. 69–75, 1997.

[329] **X. Zhang, M. Li, B. Zhang, K. Chen, and K. H. He**, “Development of a Sandwich ELISA for EHEC O157:H7 Intimin γ1,” *PLoS One*, vol. 11, no. 9, p. e0162274, Sep. 2016.

[330] **M. C. Encarnación *et al.***, “Conformational dynamics is key to understanding loss-of-function of NQO1 cancer-associated polymorphisms and its correction by pharmacological ligands,” *Sci. Reports 2016 61*, vol. 6, no. 1, pp. 1–14, Feb. 2016.

[331] **M. Sabadashka, M. Nagalievska, and N. Sybirna**, “Tyrosine nitration as a key event of signal transduction that regulates functional state of the cell,” *Cell Biol. Int.*, vol. 45, no. 3, pp. 481–497, Mar. 2021.

[332] **P. Picón-Pagès, J. Garcia-Buendia, and F. J. Muñoz**, “Functions and dysfunctions of nitric oxide in brain,” *Biochim. Biophys. Acta - Mol. Basis Dis.*, vol. 1865, no. 8, pp. 1949–1967, Aug. 2019.

[333] **L. Randall, B. Manta, K. J. Nelson, J. Santos, L. B. Poole, and A. Denicola**, “Structural changes upon peroxynitrite-mediated nitration of peroxiredoxin 2; Nitrated Prx2 resembles its disulfide-oxidized form,” *Arch. Biochem. Biophys.*, vol. 590, pp. 101–108, Jan. 2016.

[334] **Y. Ji and B. M. Bennett**, “Activation of microsomal glutathione S-transferase by peroxynitrite,” *Mol. Pharmacol.*, vol. 63, no. 1, pp. 136–146, Jan. 2003.

[335] **S. N. Savvides *et al.***, “Crystal structure of the antioxidant enzyme glutathione reductase inactivated by peroxynitrite,” *J. Biol. Chem.*, vol. 277, no. 4, pp. 2779–2784, Jan. 2002.

[336] **M. Pajares, A. Cuadrado, and A. I. Rojo**, “Modulation of proteostasis by transcription factor NRF2 and impact in neurodegenerative diseases,” *Redox Biol.*, vol. 11, pp. 543–553, Apr. 2017.

[337] **J. An, A. Rao, and M. Ko**, “TET family dioxygenases and DNA demethylation in stem cells and cancers,” *Exp. Mol. Med.*, vol. 49, no. 4, pp. 323–323, Apr. 2017.

[338] **W. M. Skiles, A. Kester, J. H. Pryor, M. E. Westhusin, M. C. Golding, and C. R. Long**, “Oxygen-induced alterations in the expression of chromatin modifying enzymes and the transcriptional regulation of imprinted genes,” *Gene Expr. Patterns*, vol. 28, pp. 1–11, Jun. 2018.

[339] **S. G. Klein *et al.***, “A prevalent neglect of environmental control in mammalian cell culture calls for best practices,” *Nat. Biomed. Eng.*, vol. 5, no. 8, pp. 787–792, Aug. 2021.

[340] **S. Murakami, T. Suzuki, H. Harigae, P.-H. Romeo, M. Yamamoto, and H. Motohashi**, “NRF2 Activation Impairs Quiescence and Bone Marrow Reconstitution Capacity of Hematopoietic Stem Cells,” *Mol. Cell. Biol.*, vol. 37, no. 19, pp. e00086-17, Oct. 2017.

[341] **A. T. Dinkova-Kostova and A. Y. Abramov**, “The emerging role of Nrf2 in mitochondrial function,” *Free*

Radic. Biol. Med., vol. 88, no. Part B, pp. 179–188, 2015.

[342] **A. Lau *et al.***, “A Noncanonical Mechanism of Nrf2 Activation by Autophagy Deficiency: Direct Interaction between Keap1 and p62,” *Mol. Cell. Biol.*, vol. 30, no. 13, pp. 3275–3285, Jul. 2010.

[343] **D. Türei *et al.***, “NRF2-ome: An integrated web resource to discover protein interaction and regulatory networks of NRF2,” *Oxid. Med. Cell. Longev.*, vol. 13, no. 1, p. 737591, 2013.

[344] **M. C. Sykes, A. L. Mowbray, and H. Jo**, “Reversible glutathiolation of caspase-3 by glutaredoxin as a novel redox signaling mechanism in tumor necrosis factor-α-induced cell death,” *Circ. Res.*, vol. 100, no. 2, pp. 152–154, Feb. 2007.

[345] **Y. Zuo *et al.***, “Oxidative modification of caspase-9 facilitates its activation via disulfide-mediated interaction with Apaf-1,” *Cell Res.*, vol. 19, no. 4, pp. 449–457, Apr. 2009.

[346] **N. Koundouros and G. Poulogiannis**, “Phosphoinositide 3-Kinase/Akt signaling and redox metabolism in cancer,” *Front. Oncol.*, vol. 15, no. 8, p. 160, May 2018.

[347] **S. Yoshida *et al.***, “Redox regulates mammalian target of rapamycin complex 1 (mTORC1) activity by modulating the TSC1/TSC2-Rheb GTPase pathway,” *J. Biol. Chem.*, vol. 286, no. 37, pp. 32651–32660, Sep. 2011.

[348] **K. J. Nelson *et al.***, “H2O2 oxidation of cysteine residues in c-Jun N-terminal kinase 2 (JNK2) contributes to redox regulation in human articular chondrocytes,” *J. Biol. Chem.*, vol. 293, no. 42, pp. 16376–16389, Oct. 2018.

[349] **S. O. Yoon, C. H. Yun, and A. S. Chung**, “Dose effect of oxidative stress on signal transduction in aging,” *Mech. Ageing Dev.*, vol. 123, no. 12, pp. 1597–1604, Nov. 2002.

[350] **A. B. El-Remessy, M. Bartoli, D. H. Platt, D. Fulton, and R. B. Caldwell**, “Retraction: Oxidative stress inactivates VEGF survival signaling in retinal endothelial cells via PI 3-kinase tyrosine nitration.,” *J. Cell Sci.*, vol. 129, no. 16, p. 3203, Jan. 2016.

[351] **A. Saccani *et al.***, “Redox regulation of chemokine receptor expression,” *Proc. Natl. Acad. Sci. U. S. A.*, vol. 97, no. 6, pp. 2761–2766, Mar. 2000.

[352] **D. Han, M. D. Ybanez, S. Ahmadi, K. Yeh, and N. Kaplowitz**, “Redox regulation of tumor necrosis factor signaling,” *Antioxidants Redox Signal.*, vol. 11, no. 9, pp. 2245–2263, Sep. 2009.

[353] **M. Singh, H. Sharma, and N. Singh**, “Hydrogen peroxide induces apoptosis in HeLa cells through mitochondrial pathway,” *Mitochondrion*, vol. 7, no. 6, pp. 367–373, Dec. 2007.

[354] **S. G. Rhee, Y. S. Bae, S. R. Lee, and J. Kwon**, “Hydrogen peroxide: a key messenger that modulates protein phosphorylation through cysteine oxidation.,” *Sci. STKE*, vol. 2000, no. 53, p. pe1, Oct. 2000.

[355] **L. Nocito, A. S. Kleckner, E. J. Yoo, A. R. Jones, M. Liesa, and B. E. Corkey**, “The extracellular redox state modulates mitochondrial function, gluconeogenesis, and glycogen synthesis in murine hepatocytes,” *PLoS One*, vol. 10, no. 3, p. e0122818, Mar. 2015.

[356] **E. Rebelato, F. Abdulkader, R. Curi, and A. R. Carpinelli**, “Control of the intracellular redox state by glucose participates in the insulin secretion mechanism,” *PLoS One*, vol. 6, no. 8, p. e24507, 2011.

APPENDIX CONTAINING FULL-LENGTH WESTERN BLOTS AND TOTAL PROTEIN STAINS.

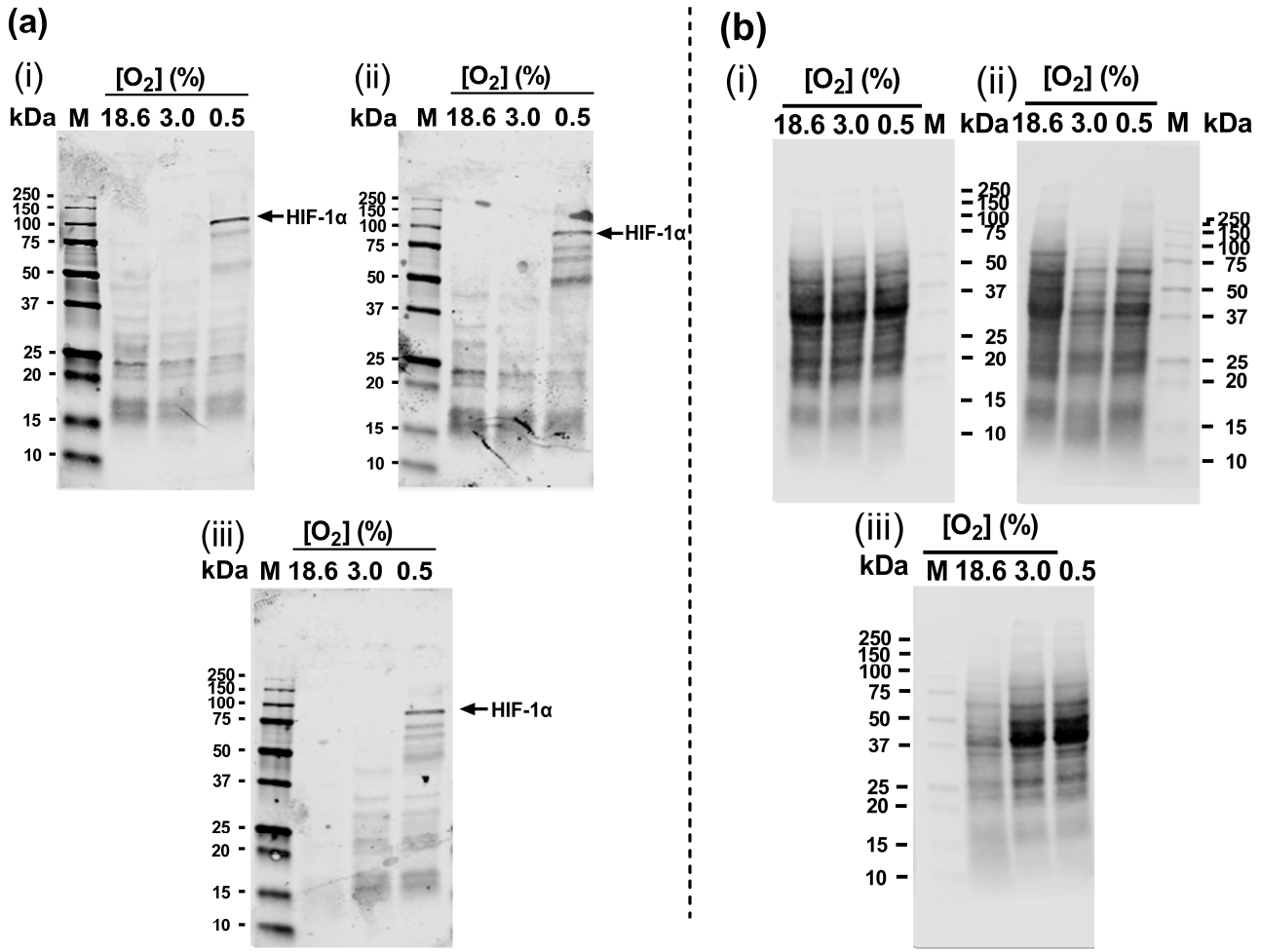

Figure A.1. Full length anti-hypoxia-inducible factor-1α immunoblots and associated total protein stains. A431 cells grown in 18.6% or 3.0% O_2 for 96 h were analysed for HIF-1α protein expression by western blotting (section 2.12). For positive expression of HIF-1α, A431 cells were grown in 0.5% O_2 for 1 h. **Panel (a),** full length immunoblot replicates for HIF-1 α (i–iii, n = 3; band of interest 93 kDa which is HIF-1α). Densitometry analysis was not performed on the 93 kDa band due to the low antibody reactivity in this section of the blot in the 18.6% and 3.0% O_2 sample lanes (section 2.12.10). **Panel (b),** associated total protein stain replicates (i–iii) originally intended to normalise HIF-1α protein levels from cellular samples. **HIF:** hypoxia-inducible factor; **kDa:** kilodalton; **M:** molecular weight marker lane.

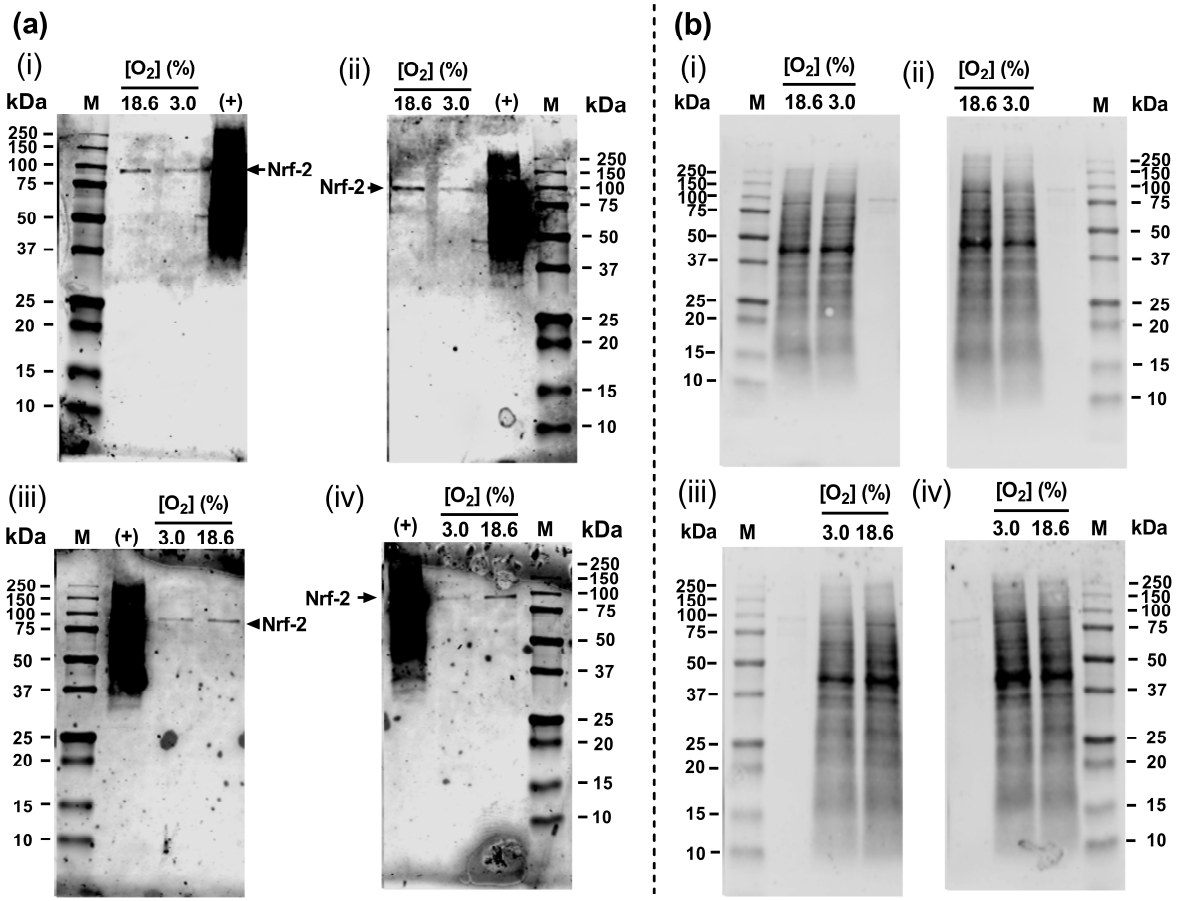

Figure A.2. Full length anti-nuclear factor erythroid-2-related factor 2 immunoblots and associated total protein stains. A431 cells grown in 18.6% or 3.0% O_2 for 96 h were analysed for nuclear Nrf-2 protein expression by western blotting (section 2.12). The (+) symbol represents the positive control which comprises recombinant human Nrf-2 protein. **Panel (a),** full length immunoblot replicates for Nrf-2 (i–iv, n = 4; band of interest 95 kDa which is Nrf-2). Densitometry analysis (section 2.12.10) was performed on the Nrf-2 95 kDa band which was normalised to total protein. The result of this analysis is shown in Figure 4.14. **Panel (b),** associated total protein stain replicates (i–iv, n = 4) used for normalising the levels of Nrf-2 in cellular samples. **kDa:** kilodalton; **M:** molecular weight marker lane; **Nrf-2:** nuclear factor erythroid-2-related factor 2.

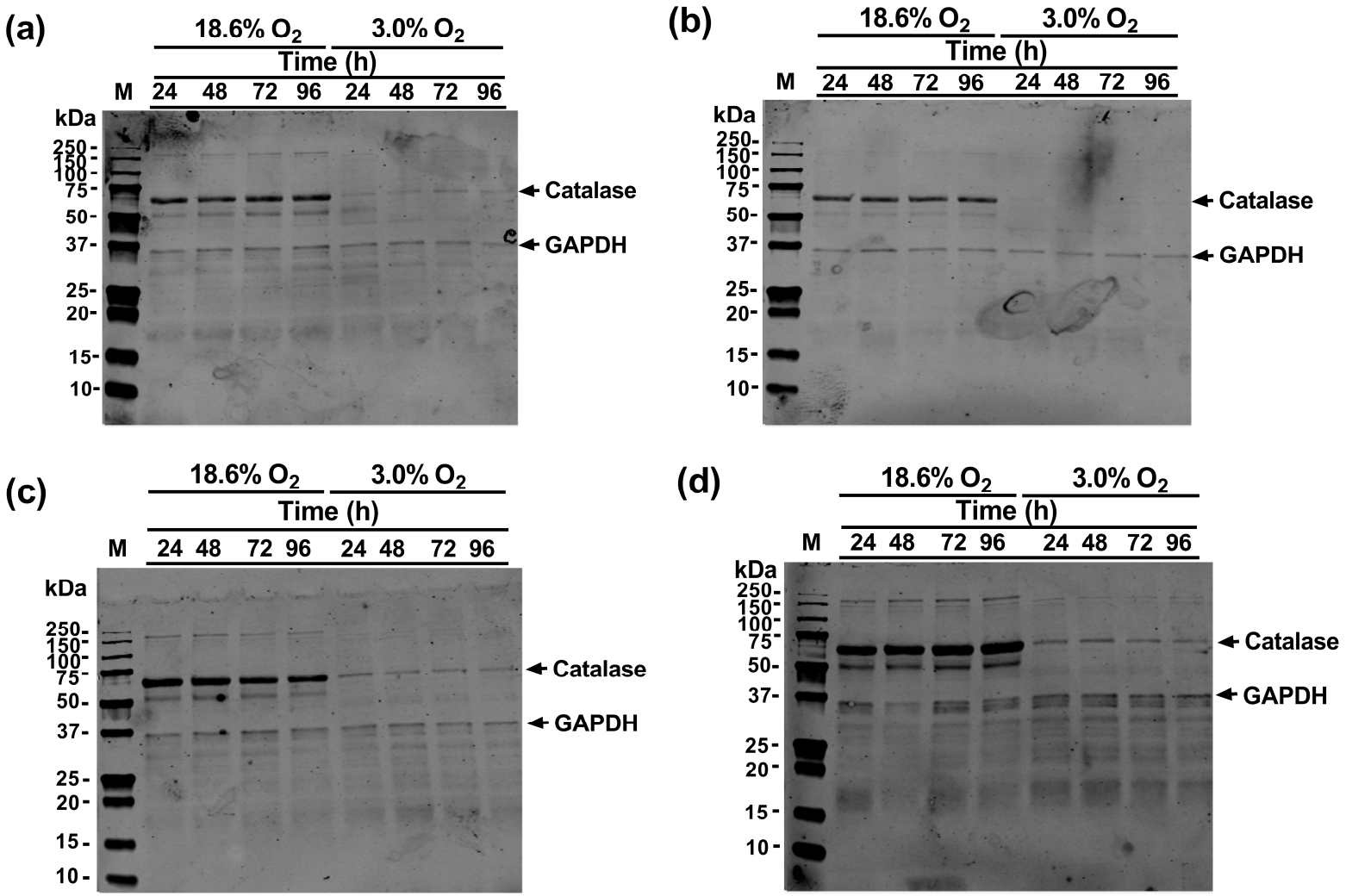

Figure A.3. Full length anti-catalase immunoblots. A431 cells were grown in 18.6% or 3.0% O_2 for 24-96 h and were analysed for catalase protein expression by western blotting (section 2.12). **Panels (a–d),** full length immunoblot replicates for catalase (n = 4; band of interest 60 kDa which is catalase). Densitometry analysis (section 2.12.10) was performed on the 60 kDa catalase bands which was normalised to GAPDH (36 kDa). The results of this analysis is shown in . **GAPDH**: glyceraldehyde-3-phosphate dehydrogenase; **kDa:** kilodalton; **M:** molecular weight marker lane.

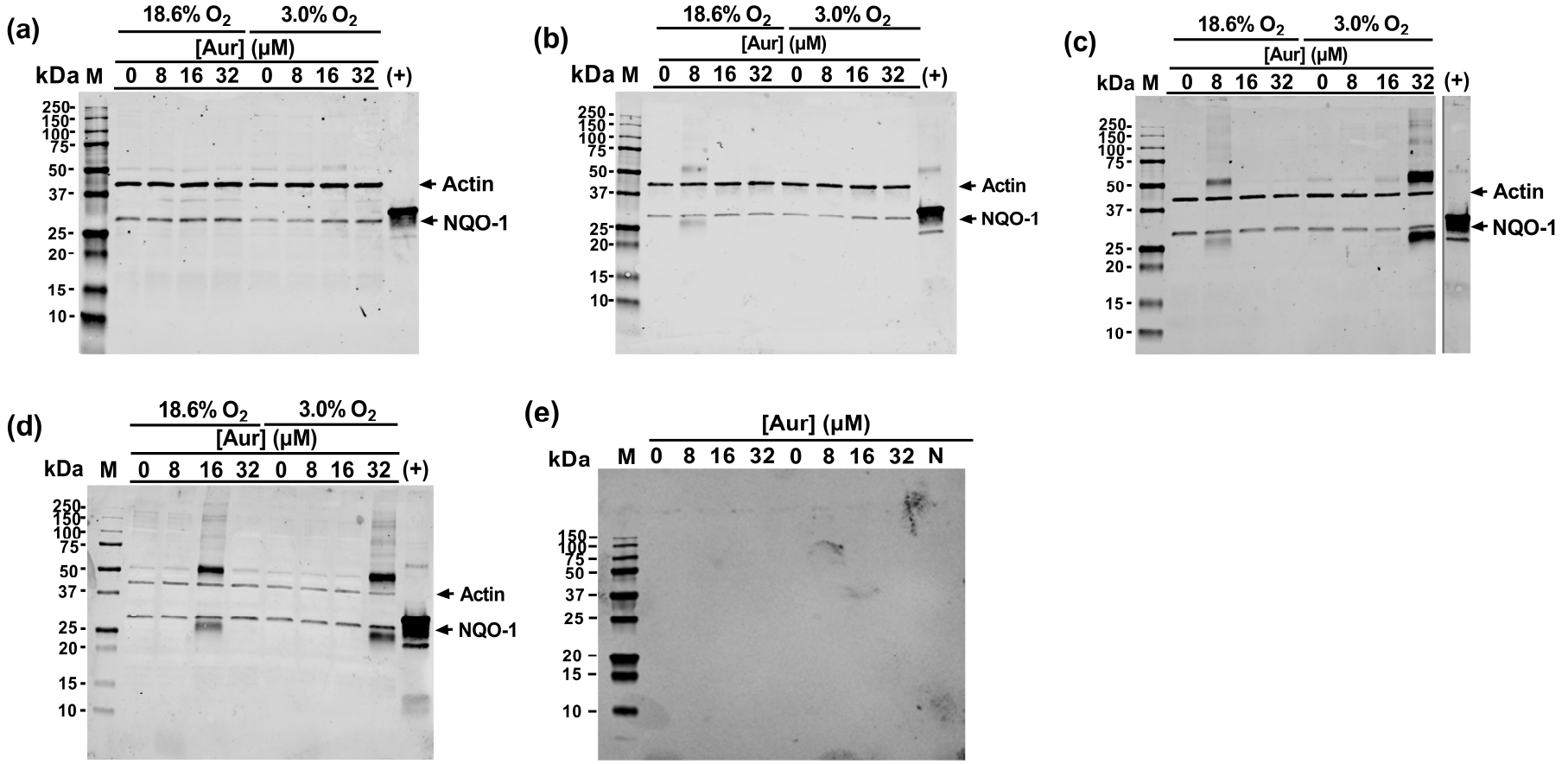

Figure A.4. Full length anti-NQO-1 immunoblots. A431 cells were grown in 18.6% or 3.0% O_2 for 96 h prior to treatment with 0–32 µM auranofin for 1 h in 3.0% or 18.6% O_2. NQO-1 expression was then analysed by western blotting (section 2.12). The (+) symbol represents the positive control lane which comprises recombinant human NQO-1 protein. **Panels (a–d),** full length immunoblot replicates for NQO-1 (n = 4; band of interest 27 kDa which is NQO-1). Densitometry analysis (section 2.12.10) was performed on the NQO-1 27 kDa band which was normalised to respective β cytoskeletal actin (42 kDa). The result of this analysis is shown in Figure 4.15. The (+) lane in panel c was spliced to readjust the lane order as indicated by the vertical white line separating the (+) lane and the 3.0% O_2/32 µM auranofin lane. **Panel (e),** secondary control immunoblot where a different aliquot from the same lysate sample used for immunoblotting in panel d, having undergone electrophoresis and membrane transfer, underwent reaction with an IRDye 800CW goat anti-mouse polyclonal secondary antibody alone (1:10,000; #926-32210). The lane labelled (N) was loaded with lysis buffer alone without sample protein. **Aur:** auranofin; **kDa:** kilodalton; **M:** molecular weight marker lane; **NQO-1:** NAD(P)H quinone oxidoreductase-1.

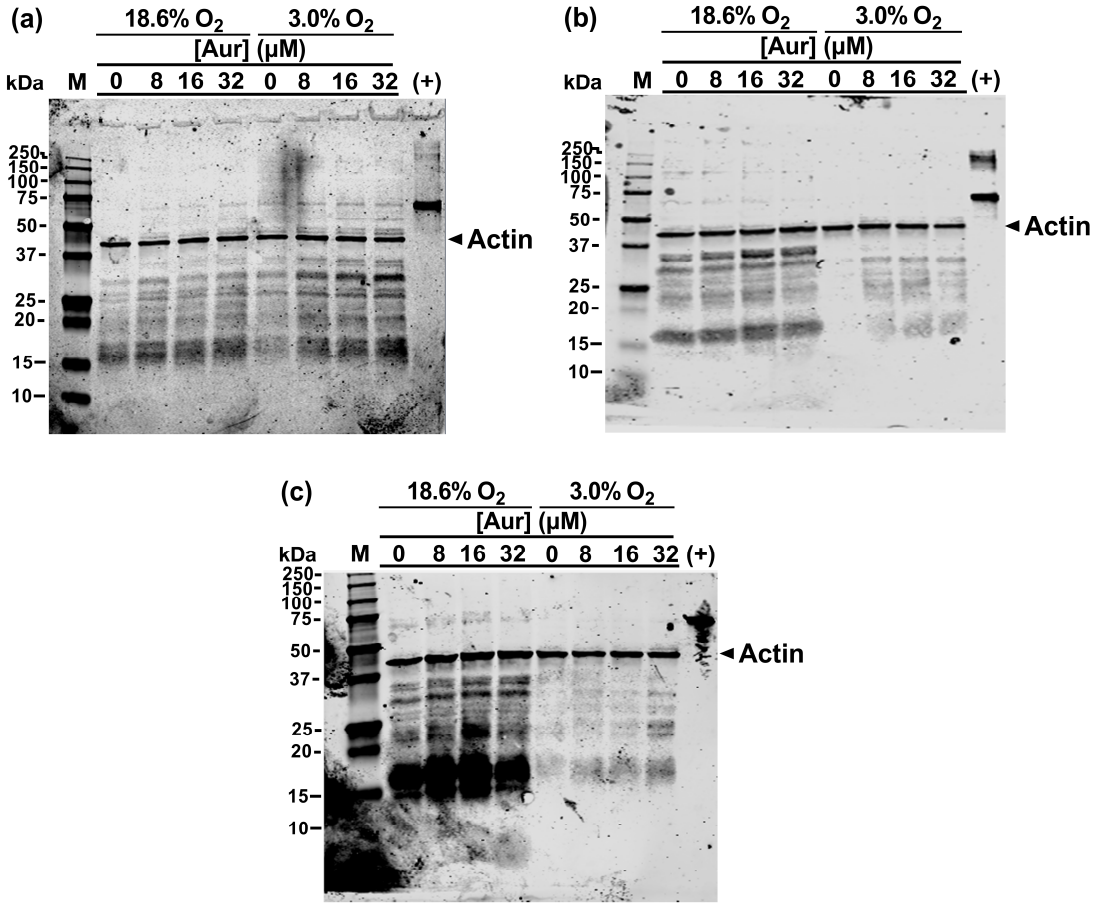

Figure A.5. Full length anti-3 nitrotyrosine immunoblots and associated total protein stains. A431 cells grown in 18.6% or 3.0% O_2 for 96 h were treated with 0–32 μM auranofin for 1 h. The levels of 3-NT modified protein were assessed by western blotting (section 2.12). The (+) symbol represents the positive control lane which comprises nitrated albumin (66 kDa). **Panels (a–c),** full length immunoblots for 3-NT with a 42 kDa band denoting cytoskeletal actin staining (n = 3). Densitometry analysis (section 2.12.10) was performed on the total 3-NT band intensity in each lane which was normalised to respective β cytoskeletal actin (42 kDa). The results of this analysis is shown in Figure 4.17. **3-NT:** 3-nitrotyrosine; **Aur**: auranofin, **kDa:** kilodalton; **M:** molecular weight marker lane.